

Cover page_dedication.pdf

Table of contents.pdf

Certificate.PDF

Declaration.PDF

Acknowledgement_Preface.pdf

1st Chapter.pdf

2nd Chapter.pdf

3rd Chapter.pdf

4th Chapter.pdf

5th Chapter.pdf

6th Chapter.pdf

List of Publications.pdf

Development of Novel Molecular Probes for Metal Ions and Small Biomolecules

A Thesis Submitted for the Degree of
Doctor of Philosophy

By

Debabrata Maity



Bioorganic Chemistry Laboratory, New Chemistry Unit
Jawaharlal Nehru Centre for Advanced Scientific Research
(A Deemed University)

Bangalore-560 064, India

June 2013

Dedicated to Maa and Baba

TABLE OF CONTENTS

CERTIFICATE.....	I
DECLARATION.....	III
ACKNOWLEDGEMENTS.....	V
PREFACE.....	VII
Chapter 1: Introduction	1
Useful optical window for <i>in vitro</i> or <i>in vivo</i> molecular imaging and spectroscopy.....	5
Different analytes.....	6
Common dyes used to design fluorescent probes.....	7
Conventional signal mechanisms.....	15
Approaches for designing fluorescent molecular probes.....	25
References.....	34
Chapter 2: Fluorescent molecular probes for Al³⁺	45
1. Introduction.....	47
2. Rationality for designing molecular probes for aluminium.....	48
3.1 Pyrrolidine constrained bipyridyl-dansyl (BD) click molecular probe for Al ³⁺	51
3.1.1 Synthesis.....	51
3.1.2 Photophysical properties of BD click molecular probe and its Al ³⁺ detection.....	52
3.1.3 Competitive study for fluorometric detection of Al ³⁺ using BD	55
3.1.4 Determination of binding stoichiometry and binding mode of BD with Al ³⁺	56
3.1.5 Conclusion.....	60
3.2 Pyrrolidine constrained coumarin-bipyridyl (CB) click molecular probe for Al ³⁺ detection.....	61
3.2.1 Synthesis.....	61

3.2.2	Photophysical properties of CB click molecular probe and Al ³⁺ detection.....	62
3.2.3	Competitive study for fluorometric detection of Al ³⁺ using CB	66
3.2.4	Determination of binding stoichiometry and binding mode of CB with Al ³⁺	67
3.2.5	Conclusion.....	70
3.3	Pyrrolidine constrained quinoline-coumarin (QC) click molecular probe for dual-mode ratiometric detection of Al ³⁺	71
3.3.1	Synthesis.....	71
3.3.2	Photophysical properties of QC click molecular probe and dual-mode ratiometric detection of Al ³⁺	72
3.3.3	Competitive study for fluorometric detection of Zn ²⁺ and Al ³⁺	76
3.3.4	Determination of binding stoichiometry and binding mode of QC with Zn ²⁺ and Al ³⁺	78
3.3.5	Conclusion.....	84
3.4	Naphthaldehyde–urea/thiourea conjugates as turn on fluorescent probes for Al ³⁺ based on restricted C=N isomerization.....	85
3.4.1	Synthesis.....	85
3.4.2	Photophysical properties of naphthaldehyde-carbonohydrazone (NC) and naphthaldehyde-thiocarbonohydrazone (NTC) Schiff bases and fluorometric turn on detection of Al ³⁺	86
3.4.3	Competitive study for Al ³⁺ detection.....	91
3.4.4	Determination of binding stoichiometry and binding mode of NTC and NC with Al ³⁺	93
3.4.5	Conclusion.....	98
4.	Experimental.....	99
4.1	General experimental procedure.....	99
4.2	Detailed synthetic procedure.....	99
4.3	General method of UV-Vis and fluorescence titration.....	106
4.4	Job plot by UV-Vis method.....	107
4.5	Determination of binding constant.....	107
4.6	Calculation of detection limit for CB	108
4.7	Calculation of quantum yields for NC/NTC	108

4.8 Appendix.....	109
5. References.....	120
Chapter 3: Visible–near-infrared colorimetric copper selective molecular probe.....	125
1. Introduction.....	127
2. Rationale for designing visible and near-infrared colorimetric molecular probes for copper.....	129
3. Visible and near-infrared colorimetric molecular probes for copper.....	130
3.1 Synthesis.....	130
3.2 Photophysical study of Schiff base molecular probes and Cu ²⁺ detection.....	132
3.3 Competitive study for NIR colorimetric detection of Cu ²⁺	141
3.4 Determination of binding stoichiometry and binding constant.....	142
3.5 pH dependent study.....	148
3.6 Fluorometric detection of Cu ²⁺ using Julolidine-thiocarbonohydrazone 4	150
3.7 Theoretical investigation.....	152
3.8 Bioimaging.....	159
4. Conclusion.....	161
5. Experimental.....	162
5.1 General experimental procedure.....	162
5.2 General procedure for the synthesis of Schiff base ligands.....	162
5.3 General method of UV-Vis titration.....	166
5.4 Job plot by UV-Vis method.....	166
5.5 Determination of binding constant.....	166
5.6 Bioimaging.....	167
5.7 Appendix.....	168
6. References.....	179
Chapter 4: Visible–near-infrared fluorescent copper selective molecular probes.....	185
1. Introduction.....	187
2. Rationale for designing fluorescent molecular probes for copper.....	188

3.1 A highly selective reaction-based two-photon probe (XanCu) for Cu ⁺ in aqueous media.....	191
3.1.1 Synthesis.....	191
3.1.2 Photophysical property of molecular probe XanCu and Cu ⁺ detection.....	192
3.1.3 pH dependent study.....	195
3.1.4 Product analysis and proposed mechanism.....	196
3.1.5 Two photon experiment for Cu ⁺ detection.....	200
3.1.6 Conclusion.....	201
3.2 Reactive probe (HBTCu) for ratiometric detection of Cu ⁺ based on excited-state intramolecular proton transfer mechanism	202
3.2.1 Synthesis.....	202
3.2.2 Photophysical property of HBTCu and ratiometric detection of Cu ⁺	203
3.2.3 Competitive study for ratiometric detection of Cu ⁺	206
3.2.4 pH dependent effects for ratiometric detection of Cu ⁺	206
3.2.5 Proposed reaction mechanism.....	207
3.2.6 Conclusion.....	210
3.3 Resorufin-based reactive probe (ResCu) for Cu ⁺ with dual output (colorimetric and fluorometric) modes.....	211
3.3.1 Synthesis.....	211
3.3.2 Photophysical property of ResCu and selective colorimetric and fluorometric detection of Cu ⁺	212
3.3.3 pH dependent study.....	218
3.3.4 Competitive study for detection of Cu ⁺	218
3.3.5 Product analysis.....	219
3.3.6 Conclusion.....	221
3.4 Switch on near infrared fluorescent reactive probe (TPACy) for Cu ⁺	222
3.4.1 Synthesis.....	222
3.4.2 Photophysical properties of TPACy and NIR fluorometric detection of Cu ⁺	224
3.4.3 pH dependent study.....	227
3.4.4 Conclusion.....	228
3.5 FRET-based rational strategy for ratiometric detection of Cu ²⁺ and live cell imaging..	229

3.5.1 Synthesis.....	229
3.5.2 Spectral properties of CRO	230
3.5.3 Spectral properties of CRS	234
3.5.4 Competitive binding experiment.....	238
3.5.5 Stoichiometry of binding, response parameter and binding constant determination.....	240
3.5.6 pH dependence study.....	244
3.5.7 Bioimaging.....	246
3.5.8 Conclusion.....	247
4. Experimental.....	248
4.1 General experimental procedure.....	248
4.2 Detailed synthetic procedure.....	248
4.3 General method for measurements of photophysical properties.....	255
4.4 Job plot by UV-Vis method.....	256
4.5 Determination of binding constant.....	256
4.6 Appendix.....	257
5. References.....	270
Chapter 5: Colorimetric and fluorometric molecular probes for Co²⁺	277
1. Introduction.....	279
2. Rationale for designing colorimetric and fluorometric molecular probes for cobalt.....	280
3.1 Highly selective colorimetric molecular probe (CTC) for Co ²⁺	283
3.1.1 Synthesis.....	283
3.1.2 Photophysical property of coumarin-thiocarbonohydrazone (CTC) and colorimetric detection of Co ²⁺	284
3.1.3 Competitive study for colorimetric detection of Co ²⁺ using CTC	286
3.1.4 Determination of binding stoichiometry of CTC with Co ²⁺ and pH dependent study.....	287
3.1.5 Colorimetric kit for Co ²⁺ detection.....	290
3.1.6 CTC as colorimetric reagent for the detection of Co ²⁺ in microbe.....	291
3.1.7 Conclusion.....	292

3.2 Reactive probe (HBTCo) for ratiometric fluorescence detection of Co^{2+} based on excited-state intramolecular proton transfer (ESIPT) mechanism.....	293
3.2.1 Synthesis.....	293
3.2.2 Photophysical property of HBTCo and ratiometric detection of Co^{2+}	294
3.2.3 Competitive study for ratiometric detection of Cu^{2+}	297
3.2.4 pH dependent effects for ratiometric detection of Cu^{2+}	297
3.2.5 Proposed reaction mechanism.....	298
3.2.6 Conclusion.....	302
3.3 Resorufin-based reactive probe (ResCo) for Co^{2+} with dual output (colorimetric and fluorometric) modes.....	303
3.3.1 Synthesis.....	303
3.3.2 Photophysical property of ResCo and selective colorimetric and fluorometric detection of Co^{2+}	304
3.3.3 pH dependent study.....	309
3.3.4 Competitive study for detection of Co^{2+}	310
3.3.5 Product analysis.....	311
3.3.6 Conclusion.....	314
4. Experimental.....	315
4.1 General experimental procedure.....	315
4.2 Detailed synthetic procedure.....	315
4.3 General method for measurements of photophysical properties.....	320
4.4 Job plot by UV-Vis method.....	320
4.5 Determination of binding constant.....	320
4.6 Appendix.....	322
4.7 HRMS data.....	331
5. References.....	332

Chapter 6: Near-infrared fluorometric and colorimetric molecular probes for thiol and H_2S 337

Part A

1. Turn on NIR fluorescence and colorimetric cyanine probe (DNBSCy) for thiol.....	339
---	-----

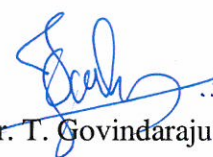
1.1 Introduction.....	339
1.2 Design strategy.....	340
1.3 Synthesis of molecular probe DNBSCy	341
1.4 Photophysical studies of DNBSCy in presence of thiol.....	342
1.5 Competitive study.....	345
1.6 Product analysis after reaction with GSH.....	346
1.7 pH dependent study.....	347
1.8 Reduced thiol detection in fetal bovine serum (FBS).....	348
1.9 Selective detection of the reduced GSH over oxidized GSSG using a combination of glutathione reductase and DNBSCy	349
1.10 Conclusion.....	353

Part B

2. Ratiometric NIR fluorescence and colorimetric cyanine probe (DNPOCy) for H ₂ S.....	354
2.1 Introduction.....	354
2.2 Design strategy.....	356
2.3 Synthesis.....	357
2.4 Photophysical studies of DNPOCy and H ₂ S detection.....	358
2.5 pH dependent study.....	363
2.5 Product analysis.....	363
2.6 Theoretical investigation.....	365
2.7 Conclusion.....	367
3. Experimental.....	368
3.1 General experimental procedure.....	368
3.2 Detailed synthetic procedure.....	368
3.3 General method for measurements of photophysical properties.....	371
3.4 Appendix.....	372
4. References.....	383
List of publications	391

CERTIFICATE

I hereby certify that the work described in this thesis entitled “**Development of Novel Molecular Probes for Metal Ions and Small Biomolecules**” has been carried out by Mr. Debabrata Maity under my supervision at the Bioorganic Chemistry Laboratory, New Chemistry Unit, Jawaharlal Nehru Centre for Advanced Scientific Research, Bangalore, India and that it has not been submitted elsewhere for the award of any degree or diploma.



Dr. T. Govindaraju

(Research Supervisor)

DECLARATION

I hereby declare that the matter embodied in the thesis entitled “**Development of Novel Molecular Probes for Metal Ions and Small Biomolecules**” is the result of investigations carried out by me at the Bioorganic Chemistry Laboratory, New Chemistry Unit, Jawaharlal Nehru Centre for Advanced Scientific Research, Bangalore, India under the supervision of **Dr. T. Govindaraju** and that it has not been submitted elsewhere for the award of any degree or diploma.

In keeping with the general practice in reporting the scientific observations, due acknowledgement has been made whenever the work described is based on the findings of other investigators. Any omission that might have occurred due to oversight or error in judgement is regretted.



Debabrata Maity

ACKNOWLEDGEMENTS

First and foremost, I would like to express my sincere gratitude to my research supervisor Dr. T. Govindaraju, Faculty Fellow, Bioorganic Chemistry Laboratory, New Chemistry Unit, JNCASR, who right from the beginning provided me kind support, valuable guidance, criticism and consistent encouragement all through the course of these investigations. I have learnt so much by interacting with him both professionally and personally. I am thankful to him for giving me an opportunity to work under his guidance.

I would like to thank Professor C. N. R. Rao, FRS, the Chairman, New Chemistry Unit for his generous support and encouragement throughout my stay in JNCASR. His presence has given me immense inspiration to indulge in active research. I also thank him for providing the infrastructure and facilities to carry out my research work.

I am thankful to the faculty members of JNCASR and Indian Institute of Science for the course that have been extremely beneficial to this study. In particular, I would like to thank Prof. P. Balaram and Prof. Siddhartha P. Sarma of IISc and Dr. T. Govindaraju, Dr. Subi George, Prof. M. Eswaramoorthy and Prof. Tapas K Maji of JNCASR for their courses.

I would like to thank Prof. Swapan Pati (TSU) and Prof. Tapas Kundu (MBGU) and Prof. Sudipta maiti (TIFR) for fruitful collaborations.

I thank the technical staff namely Mr. Vasu, Mrs. Suma, Mr. Mahesh, Ms. Sonia and Mr. Shivakumar for their help with the various characterization techniques. I also thank Mrs. Shashi, Mr. Hanume Gowda Mr. Suresh, Mr. Naveen and Mr. Mune Gowda for their help in various ways.

I would like to thank Academics staff, Administration staff and NCU office staff for their constant help.

I thank JNCASR Library, Comp Lab, Hostel, and Health Center for providing and maintaining the various facilities that have helped me immensely.

I also thank my wonderful lab mates Mr. Avinash, Mr. Pandeewar, Mr. Nagarjun, Mr. Shivaprasad, Mr. Rajasekhar, Ms. Suseela, Mr. Anand for their kind cooperation and help. Also I acknowledge all the visiting scientists and students (POCE and SRF) for their contributions. In particular, I would like to thank Subha, Arindom Deepa, Ramya, Vikash, Divya G, Naik and Divya V.

I would like to thank all my teachers from childhood to MSc. In particular, I would like to thank all the faculty members of Chemistry Department, Jadavpur University and teachers of Kolaghat Thermal Power Plant High School.

My cordial thanks are due to my friends Pika, Subha, Som, Mantu, Surath, Pam, Ujjal, Tushar, Sushmita, Srijita, Sutonuka, Sauvik, Piyal, Suvendu, Banu, Suman, Jyoti, Abhishek, Satrajit, Saptaswa, Someswar, Sharmistha, Nabanita, Tista, Nabamita, Sovan, Subirda, Kanishkada, Sandeepda, Barun, Debasish, Saptarshi, Pralayda, Subhendu, Sumanta, Raju, Dibyendu, Arun, Debasisda, Shubhoda, Arupda, Ritesh, Arpan, Pralok, Arun, Rana, Sabyasachi, Sudip, Prakash, Partha, Gautam, Sudeshna, Dibyajyoti, Jiaul, Amrit, Pranab, Soumik, Anupama, Babhru, Bivas, Koushik, Somananda, Arkamita, Swastika, Somnath, Saikat, Subhajit, Abhijit, Rajib, Anirban, Abhijeet, Chandradhish, Syamantak, Moumita, Tarak, Tanmoy, Sumanta, Jayaram, Venkat, Srinu, Dheeraj, Satya, Lattuda, Tintin. Their support and encouragement have been an indispensable in my academic life.

Last but not least, my heartfelt thanks to my family members for being there for me always. Their love and care has been the greatest strength for me. This thesis is a humble offering to my parents.

PREFACE

The thesis entitled “**Development of Novel Molecular Probes for Metal Ions and Small Biomolecules**” is divided into six chapters as follows

1st chapter deals with introduction and basic requirement for designing a molecular probe selective for a particular bioanalyte in living cells. Living cells communicate each other and with their environments through several elementary chemical pathways. Understanding the molecular interactions not only a major challenge but also provide unique opportunity and motivation for researchers to generate new molecular tools to study dynamic intracellular biological relationships. Molecular imaging has been defined as the in vivo characterization and measurement of biological phenomena at the cellular and molecular level, by combining synergistic advances in synthetic molecular probe design and biological imaging instrumentation. Molecular probe contains a recognition site with a signaling reporter. The main aim of the binding unit is to recognize a target analyte. This molecular recognition process accompanies the electronic or optical changes in the reporting unit, displays colorimetric, fluorometric alterations.

In **2nd chapter**, five Al^{3+} selective fluorescence-based molecular probes are reported. The pyrrolidine-triazole linker was used as constrained spacer between ionophore and fluorophore in three Al^{3+} selective molecular probes. The pyrrolidine-triazole constrained bipyridyl-dansyl probe (**BD**) serves as a selective ratiometric and colorimetric molecular probe for Al^{3+} based on internal charge transfer (ICT). Similarly, ICT based coumarin-bipyridyl probe (**CB**) serves as ‘turn on’ molecular probe for Al^{3+} . The third probe is conjugate of quinoline-coumarin (**QC**) exhibited differential dual selectivity for Zn^{2+} and Al^{3+} in mixed aqueous media. The last two probes naphthaldehyde–carbonohydrazone (**NC**) and naphthaldehyde–thiocarbonohydrazone (**NTC**) showed turn-on fluorescence in the presence of Al^{3+} , as a result of a restricted C=N isomerization mechanism.

In **3rd chapter**, four Cu^{2+} selective colorimetric molecular probes are reported. Simple carbonohydrazone and thiocarbonohydrazone systems are developed for selective detection of paramagnetic Cu^{2+} by visible color changes with a characteristic NIR absorbance band in aqueous medium. Moreover julolidine–thiocarbonohydrazone was used for the detection of

Cu²⁺ fluorometrically, as it overall increases the sensitivity of the probe. The julolidine–thiocarbohydrazone ligand was also successfully used for bioimaging of Cu²⁺ in HEK293T cells.

In **4th chapter**, different mechanism based fluorochrome are exploited to design reaction based molecular probes for Cu²⁺ and Cu⁺. FRET based probes **CRS** and **CRO** probes have been effectively used for ratiometric bioimaging of Cu²⁺ in HEK293T cells. Another four probes are designed using Cu⁺ catalyzed oxidative cleavage of the benzylic ether (C–O) bond. ESIPT active 2-(2'-hydroxyphenyl)benzothiazole, ICT based resorufin, xanthone and cyanine fluorophores are combined with tri-picolylamine moiety to design molecular probes **HBTCu**, **ResCu**, **XanCu** and **TPACy** for the selective ratiometric, switch-on detection of Cu⁺ in the UV-Vis-NIR region under reducing aqueous environment. Cu⁺ catalyzed oxidative cleavage of the benzylic ether bond in the probes releases unbound fluorophore in the presence of O₂.

In **5th chapter**, a new highly selective colorimetric molecular probe **CTC** for paramagnetic Co²⁺ was developed based on coumarin-conjugated thiocarbohydrazone. This ligand detects Co²⁺ in solution by changing its visible color from light yellow to deep pink. The molecular probe has been used in the development of practically viable colorimetric kits and as a staining agent for Co²⁺ in microorganisms. Another two fluorescent probes are designed using Co²⁺ catalyzed oxidative cleavage of the benzylic ether (C–O) bond strategy varying different mechanism based fluorophore. ESIPT active 2-(2'-hydroxyphenyl)benzothiazole, ICT based resorufin fluorophore are combined with hydroxy-di-picolyl amine moiety to design molecular probes **HBTCo** and **ResCo** for the selective ratiometric, switch-on detection of Co²⁺ under reducing aqueous environment. Co²⁺ catalyzed oxidative cleavage of the benzylic ether bond in the probes releases unbound fluorophore in the presence of O₂.

In **6th chapter**, two novel reaction-based NIR fluorescence and colorimetric cyanine probes have been developed for selective detection of small molecule thiol and hydrogen sulfide. GSH reacted efficiently with the electron withdrawing sulfonyl ester moiety of **DNBSCy**, releasing the quinone embedded heptamethine cyanine with extended π -electron conjugation responsible for the turn-on NIR fluorescence. This probe was effectively employed to monitor the thiols in fetal bovine serum and also capable of monitoring the oxidized glutathione

(GSSG)/GSH redox process in the presence of glutathione reductase and NADPH. Thiolysis of dinitrophenylphenyl ether reaction-based approach has been used to develop **DNPOCy** probe for NIR ratiometric fluorescence and colorimetric detection of H₂S. H₂S reacted efficiently with the electron withdrawing dinitrophenyl ether moiety of **DNPOCy**.

Chapter 1

Introduction

The universe is a complex collection of elements, ions and molecules that continuously experience a network of chemical interactions. Living organisms and their environments communicate each other through several elementary chemical pathways like electron transfer, acid–base chemistry and metal–ligand interactions as well as stoichiometric and catalytic transformations. Understanding the molecular interactions present in these processes not only a major challenge, but also provides unique opportunity and motivation for chemists to develop new tools to study dynamic intracellular biological relationships. In this context, the chemists are trying to create novel analytical methods that allow real-time studies of intact biological systems with spatial resolution. Molecular imaging has been defined as the *in vivo* characterization and measurement of biological phenomena at the cellular and molecular level, by combining synergistic advances in synthetic molecular probe design and imaging instrumentation.¹ This technology enables visualization of biomolecules and ions in cells, tissues and organisms with the aim of acquiring information about the biological effects of these analytes. Molecular probe contains a recognition site with a signaling subunit/reporter.² The main purpose of the binding unit is to recognize a particular target analyte. This molecular recognition process accompanied by the electronic or optical changes in the reporting unit which display colorimetric, fluorometric or electrochemical alterations.³ An efficient molecular probe must be highly selective and sensitive for a particular target analyte among others. To achieve this goal, it is essential to combine the recognition process with smart photophysical behavior from a reporting unit. Generally, suitable molecular probes have been designed based on the different receptor-analyte noncovalent interactions which include hydrogen bonding, π – π , donor–acceptor, electrostatic, hydrophobic, and hydrophilic interactions. Similarly, metal-coordination based molecular probes have been developed to work in the physiological media.⁴ Fluorescent probes have become very useful tool owing to their simplicity and high sensitivity, for sensing biologically important species such as metal ions, anions and other biomolecules *in vitro* and *in vivo*.⁵ The advanced spectroscopy and bioimaging techniques such as fluorescence light microscopy, two-photon and confocal microscopy have motivated the chemists to develop novel functional fluorescent probes that can be employed to monitor intra- and extracellular events with high chemoselectivity.^{6–9} Colorimetric molecular probes have attracted much attention for allowing “naked-eye” detection in an uncomplicated and inexpensive manner, offering

qualitative and quantitative information.^{10,11} A fluorescent or colorimetric molecular probe/chemosensor is defined as a compound which recognizes an analyte with concomitant fluorescent or colorimetric signal transduction.

The major underlying principle of molecular probe design is to optimize signal to background ratio. This can be achieved either by maximizing signal from the target, minimizing signal from the background, or both. Improving the signal to background ratio increases the sensitivity and specificity for detecting target analyte *in vivo*. Strategies for optimizing signal to background ratio can be considered from the whole organism level to the atomic level. For the organism level optical imaging, the size of the animal (e.g. mouse vs. human) should be considered, as the depth of signal penetration varies with the probe types. Therefore the depth of target tissue from the organism surface is an important component of detected signal strength. At the organ level, physiology should be considered, given that probe pharmacokinetics, uptake, breakdown, clearance, and excretion, all affect signals to background ratio. At cellular level, target expression, binding affinity, on and off targets, intracellular processing and catabolism can affect the probe signal.¹²⁻¹⁴ The physical interaction with target and chemical or enzymatic processing alter the probe signal at molecular level. Finally, at the atomic level the inter- or intra-molecular energy transfer, photon-induced electron transfer, and conjugation are significant means of achieving signal activation and/or signal amplification (Figure 1).

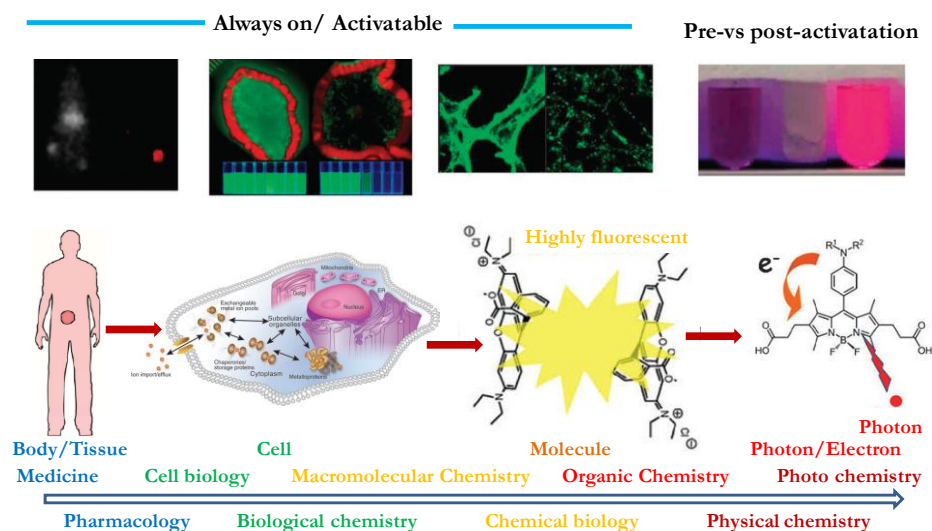


Figure 1. A schematic of rational strategies for target specific imaging in all physical levels. Reprinted with permission from reference 9, copyright 2008, by the Nature Publishing Group.

Useful optical window for *in vitro* or *in vivo* molecular imaging and spectroscopy

Optical detection and imaging relies on photons ranging in wavelength from the visible to the near infrared (NIR) (450 to 1500 nm wavelength).^{15,16} Charge coupled device (CCD) detectors, which are used for optical sensing and imaging, generally show better sensitivity for photons at shorter wavelengths, ranging from 650 to 800 nm. This range provides the best visualization of samples deeper structures, up to several centimeters, from the surface, as this range is less readily absorbed by living tissue. Shorter wavelength (400- 600) photons are limited to imaging the surface or immediate subsurface phenomena of samples because of near complete absorbance of light for example by oxy- and deoxyhemoglobin (Figure 2). Of course, depth of penetration is partly related to the strength of the light source as it can penetrate tissue more deeply and fluorophores with strong emission facilitate better signal collection. Numerous visible-NIR emitting probes are used for optical sensing and imaging and such fluorophores show picomolar sensitivity without employing ionizing radiation.

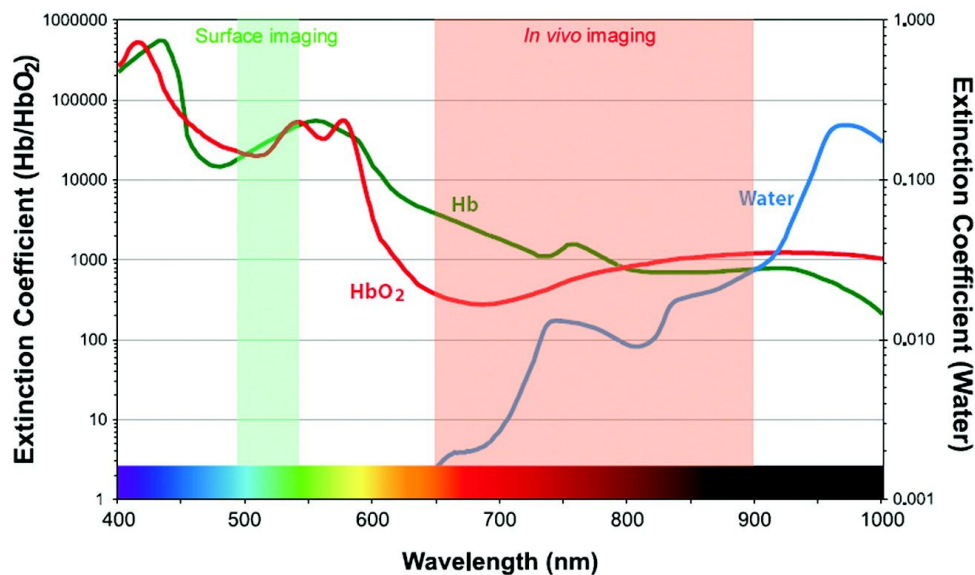


Figure 2. The *in vivo* NIR window and the extinction coefficient value of water, oxy- and deoxy-hemoglobin are plotted ranging from visible to near infrared wavelength. Reprinted with permission from reference 16, copyright 2011, by the Nature Publishing Group.

Different analytes

There are several chemosensors have been developed to track following analytes in their bioavailable/environmental forms.

Metal ions: Zn^{2+} , Cu^+ , Fe^{2+} , Pb^{2+} , Cd^{2+} , Hg^{2+} , Ag^+ , Au^{3+} , Al^{3+} , Ca^{2+} , Co^{2+} , Mg^{2+} , Ni^{2+} , Pd^{2+} , K^+ , Mn^{2+}

Anions: F^- , SO_3^- , CN^- , N_3^- , HSO_3^- , I^- , Br^- , Cl^- , HSO_4^- , AsO_4^{3-}

Reactive nitrogen species (RNS): NO^{2-} , $ONOO^-$, NO_2 , N_2O_3 , HNO , NO_3^-

Reactive oxygen species (ROS): H_2O_2 , $\cdot OH$, $HOCl$

Nucleotides: ATP, GTP, AMP, ADP, GMP, UTP, UDP, TMP, TDP, TTP, DNA, FAD, NADH, NAD^+

Aliphatic amines: Histamine, Tyramine, Dopamine, Epinephrine, Morphine, Quinine, Nicotine, Cocaine, Strychnine, Coniine

Amino acids: Lysine, Histidine, Tryptophan, Cysteine, Glutathione

Neurotransmitter agent: NO, H_2S , CO

Intracellular pH, Cellular redox status

Chemical Warfare Agents, Chemical explosives

Common dyes used to design fluorescent probes

Selection of suitable chromophore is very much important. An ideal chromophore must have the following characteristics to work as reporter in a probe:

- High optical brightness to reduce the amount of probe needed for bioimaging experiments. This also minimizes the interference generated from endogenous cellular analytes and reactions.
- Non-toxic and biocompatible.
- Excitation and emission profiles in the visible or near-infrared region, or be suitable for two-photon excitation, in order to minimize sample damage or interference from autofluorescence.
- Finally, the balance between hydrophobicity and hydrophilicity should be considered in the context of membrane permeability, cellular retention and water solubility.

Ideally, an optical probe must allow monitoring of specific intra- and/or extracellular regions.¹⁷

Here are few common dyes used to design fluorescent probes *in vitro* or *in vivo* molecular imaging and spectroscopy:

Naphthalene based fluorophores: Chersie and coworkers used dansyl chloride for direct “in synthesis” to label peptides.^{18,19} Fluorescently labeled proteins are very useful in a large number of bioanalytical applications including *in vivo* imaging, high throughput screening, diagnostics, proteomics, and single biomolecules spectroscopy.²⁰⁻²² Summerer *et al.* report a strategy for the selective and efficient biosynthetic incorporation of a low molecular weight

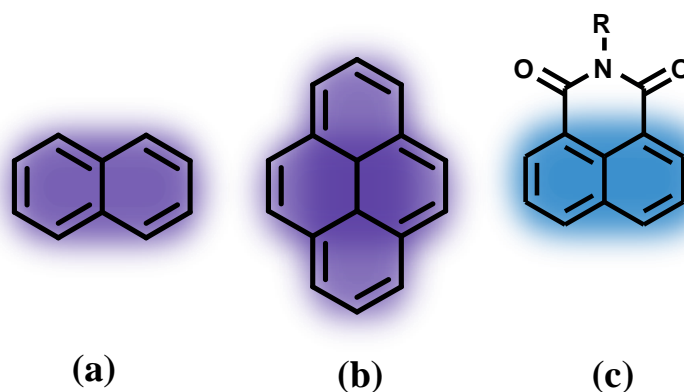
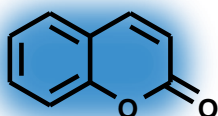


Figure 3. Naphthalene based Fluorophores:(a) naphthalene; (b) pyrene; and (c) 1,8-naphthalimide.

fluorophore into proteins at defined sites.²³ Dansyl chloride was used in the synthesis of fluorescent amino acid 2-amino-3-[5-(dimethylamino)naphthalene-1-sulfonamide] propanoic acid (dansylalanine), which was then incorporated into protein in yeast at genetically specified sites in response to the nonsense codon TAG. Molecular probes incorporating environmentally sensitive fluorophores, which alter their spectral properties in response to changes in their environment are of great importance in the study of biological processes. 6-Propionyl-2-(dimethylamino)naphthalene (PRODAN) is an example of environmentally sensitive fluorophore. In hydrophobic environments PRODAN shows marked blue shift in the emission maximum with increased fluorescence quantum yield. Due to unique photophysical properties, the naphthalimide molecular platform has found application in many areas of chemistry. Its absorption and fluorescence emission lie within the UV and visible regions, and the photophysical properties can be easily fine-tuned through judicious structural design. Synthetic modifications are readily accommodated on either the aromatic ‘naphthalene’ core, or at the ‘N-imide site’, allowing variety of functional groups and structural motifs to be incorporated. Consequently, the 1,8-naphthalimide has been extensively used within the dye industry as strongly absorbing and colorful dyes in the construction of novel therapeutics as well as in the construction of molecular probes, particularly for sensing of biologically relevant cations.^{24,25} These are typical fluorophores with intramolecular charge transfer (ICT) characteristics, an important design feature and sensitive to changes in the microenvironment. These probes possess relatively simple structural features for which facile and straightforward syntheses have been established. In

addition, most importantly, they can be derivatized with two or more separate side chains in sequence e.g. derivation sites for the 4,5- or 3,4-positions and the imide position.²⁶

Fluorophores based on oxygen heterocycles: 3-Oxo-3H-benzopyrans, commonly designated as coumarins are one of the most sensitive and commercially accepted categories of reagents for fluorescent derivatization.²⁷ Modified fluorogenic amino acids with



Coumarin

oxobenzopyrans appear to be interesting molecules due to their extended spectral range, high emission quantum yield, photostability, and good solubility in several solvents.^{28,29} Several natural and synthetic coumarins and their derivatives such as coumarin glycosides possess potent biological activities. Coumarin scaffolds are found in antibiotic, antimetabolic, immune modulating, antiviral, anticancer, anti-inflammatory, anticoagulant, antifungal, antioxidant and cytotoxic agents, as well as in some biological assays. The fluorescent coumarin such as 7-hydroxycoumarin is widely used as a research tool in polymer based science. Coumarins are used as laser dye-sensitized photoinitiators, for incorporation into polymer chains by co-polymerization, in the estimation of polymer solvent effects, for various structural characterizations, in monitoring of releasing properties of poly(methylmethacrylate) nanospheres, and for polymeric fluorescent solar collectors. Benzofurans and naphthofurans are other polycyclic oxygen heterocycles which have been reported as fluorescent markers for biomolecules.

Fluorophores based on nitrogen heterocycles: The large Stokes shift is a desired feature for fluorophores to avoid the self-absorption or the inner filter effect. The sensitivity and selectivity of fluorescence analysis can be improved with excited state intramolecular proton transfer (ESIPT) fluorophores.³⁰ It is difficult to increase the Stokes shift of the conventional fluorophores by chemical modification. One of the commonly adopted ESIPT chromophores is 2-(2'-hydroxyaryl)benzazole (Figure 4a). Another category of fluorophores, benzooxadiazoles (Figure 4b) substituted at positions 4 and 7, namely, the 4-chloro-7-nitrobenzooxadiazole (NBD-Cl), have been used as derivatization reagents for amino acids in HPLC analysis and also for proteins in electrophoresis.^{31,32} It emits in the green region ($\lambda_{em} = 530$ nm) upon 470 nm excitation. The amino acid tryptophan has been widely used as an

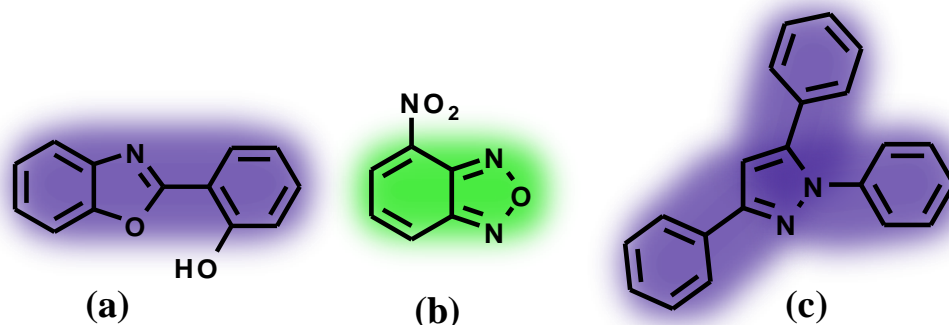


Figure 4. Naphthalene based Fluorophores: (a) 2-(2'-hydroxyaryl)benzazole; (b) 4-chloro-7-nitrobenzoxadiazole; (c) 1,3,5-triaryl-2-pyrazoline.

intrinsic fluorescent probe to study protein dynamics and ligand binding in solution.³³ The structural flexibility of 1,3,5-triaryl pyrazoline (Figure 4c) allows for facile tuning of the photophysical properties.³⁴ The substituents on the aromatic groups influence the photoinduced electron transfer (PET) thermodynamics of the investigated donor-substituted fluorophores in distinctly different ways. The pyrazoline fluorophores works as a versatile platform for the development of PET-based fluorescence ‘on-off’ chemosensors for different analytes.³⁵

Spiro-ring opening of xanthenes: Xanthene dye, fluorescein was first synthesized by von Bayer in 1871 by condensing resorcinol and phthalic anhydride via Friedel Crafts acylation/cyclodehydration.²⁶ Fluorescein, a polycyclic fluorophore with absorption and emission maxima in the visible region of the electromagnetic spectra ($\lambda_{\text{abs}} = 490 \text{ nm}$ and $\lambda_{\text{em}} = 512 \text{ nm}$, in water), is one of the most commonly employed labels in biological applications. The amine-reactive fluorescein derivatives are the most common fluorescent derivatization reagents for covalent labeling of proteins.³⁶ In addition to its relatively high absorptivity, excellent fluorescence quantum yield and good water solubility, fluorescein has an excitation maximum closely matches the 488 nm spectral line of the argon-ion laser, making it an important fluorophore for confocal laser-scanning microscopy and flow cytometry applications. Fluorescein derivatives are nonfluorescent when they exist in the lactone form, while the ring opened form can induce color changes and fluorescence enhancements.³⁷ Spirocyclic fluorescein dyes are useful sensing platforms because the ring-opening process leads to a turn on fluorescence change.³⁸

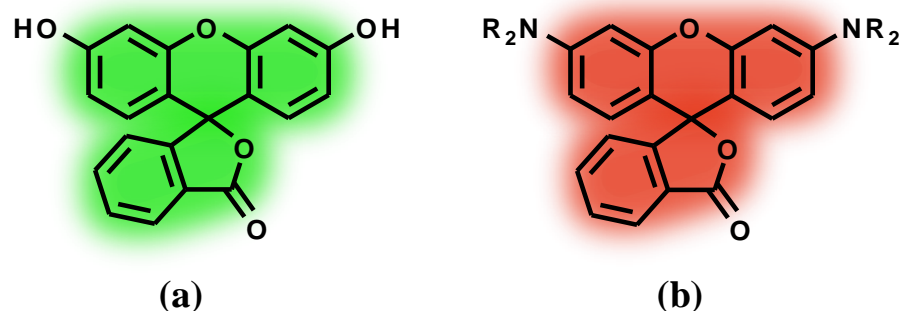


Figure 5. Xanthene dyes (a) fluorescein; (b) rhodamine.

Rhodamine was first synthesized by Noelting and Dziewonsky in 1905 and has been widely used in many research fields including the lasing medium in dye lasers and fluorescent markers in biological studies.³⁷ However, it was only in 1997 that the rhodamine B derivative and its ring-opening reaction received a great deal of attention from organic chemists.³⁹ Rhodamine spirolactam or spirolactone derivatives are nonfluorescent and colorless, whereas ring-opening of the corresponding spirolactam/lactone gives rise to strong fluorescence emission and colorometric change. In general, rhodamine derivatives display red color change and strong fluorescence in acidic solutions by activation of carbonyl group in the spirolactone or spirolactam moiety. Similarly, an appropriate ligand on the spirolactam ring can induce visible color change as well as a fluorescence change upon addition of metal ions, even though this process is somewhat dependent on the solvent system. They generally have high molar absorptivities in the visible region, and its many derivatives are strongly fluorescent. The absorption and emission properties are strongly influenced by substituent in the xanthene nucleus.⁴⁰

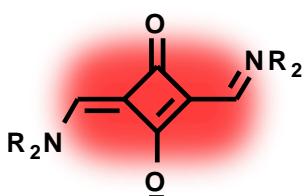
BODIPY: 4,4-Difluoro-4-bora-3*a*,4*a*-diazas-*s*-indacene better known as BODIPY (difluoroborondipyromethene) shows perhaps the highest potential and has spectacularly



risen in popularity. The first member of this set was reported as early as 1968 by Treibs and Kreuzer.⁴¹ The uses of BODIPY-based dyes for biological labeling, for electroluminescent devices, as tunable laser dyes, as potential candidates for solid-state solar concentrators, as fluorescent

switches, and fluorophores in chemosensors were totally recognized only in the mid-1990s. These dyes are mainly used as fluorescent markers and sensors, owing to their very sharp emissions, high fluorescent quantum yield, good photostability and insensitivity to pH. The typical BODIPY compounds emit strong green light.⁴² Modification of its core to achieve red-shifts has attracted considerable interest, as the long wavelength emission can avoid the interference of inherent biological fluorescence in the short wavelength region.⁴³ The conjugation length can be extended via introducing phenylethene groups at 2,6 positions to obtain strong red-emissive derivatives. BODIPY derivatives have the disadvantage of very small Stokes shifts which leads to self-quenching and measurement errors by excitation light and scattering light. Modification of the core with an electron donor functionality to form donor–acceptor system is an efficient way to increase the Stokes shifts of BODIPY system due to very strong ICT characteristics.

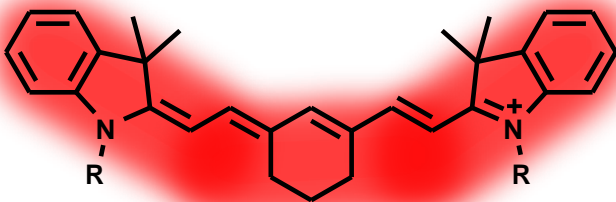
Squaraine: Squaraines, a subclass of polymethine dyes with zwitterionic structure are one of the most interesting classes of dyes which can be used as fluorescent probes in the near-



Squaraine

infrared.^{44,45} Squaraines have been used in applications such as optical recording, solar-energy conversion, electro-photography, nonlinear optics, photodynamic therapy, biochemical labeling, chromo/fluorogenic probes, pH responsive probes, cation/anion/neutral molecule recognition, and self-assembled aggregates. These compounds possess unique physico-chemical properties such as extremely intense and sharp absorption and emission bands that can be in the visible and near-infrared regions.⁴⁶ They are also known to be unusual in exhibiting photoconductivity.⁴⁷ Structural modifications in these compounds can be done by introducing substituents on the aromatic ring or on the N-atom of the terminal heterocyclic moiety. It is difficult to modify the squaraine ring but possible. Such changes can be used to produce a red shift of the absorption and fluorescence bands.

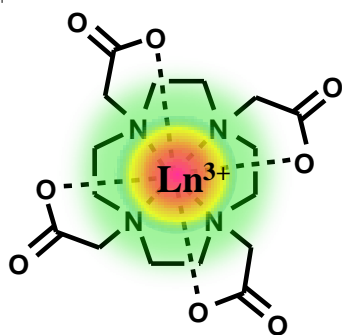
Cyanine: Cyanine dyes are fluorescent compounds, have numerous technical applications since their discovery including their use as photographic sensitizers, nonlinear optical materials,⁴⁸ and more recently fluorescent probes for biomolecular labeling.^{49,50} Applications



Cyanine

of these dyes in genetic analysis, DNA sequencing,⁵¹ *in vivo* imaging,⁵² and proteomics⁵³ are increasing dramatically. The basic structure of cyanine dyes includes two aromatic or heterocyclic rings linked by a polymethine chain with conjugated carbon-carbon double bonds. Nowadays, these compounds can be considered to be the main source of organic long-wavelength fluorophores and provide excitation bands in the range 600-900 nm. A further large bathochromic shift can be obtained by addition of a vinyl group (-CH=CH-) to the polymethine chain. Much of the interest on cyanine dyes stems from their straightforward synthesis,⁵⁴ broad wavelength tunability in particular, high NIR absorption and emission, and large molar absorptivities. Some drawbacks in the analytical use of cyanine dyes are also known. For example, the number of these dyes available as probes for labeling is very limited at present. In addition, most cyanine dyes have short fluorescence lifetimes and low fluorescence quantum yields and undergo extensive aggregation in aqueous solution leading to low fluorescence intensities.⁵⁵ Nevertheless, the photophysical properties of these dyes can be improved in solutions containing macromolecules or when organic solvents are present. Alteration of the molecular structure of the dye, for example through introduction of alkyl sulfonate groups help improves water solubility, fluorescence quantum yield, and photochemical stability. Use of precursors with a labile chlorine atom at the central meso position facilitate the easy substitution by various nucleophiles (such as metal alcoholates, amines, and thiols) which allow the synthesis of new markers with appropriate reactivity and optical properties for *in vivo* imaging.

Luminescent lanthanide complexes: Luminescent lanthanide complexes are particularly advantageous for application in sensing and bioimaging due to long emission lifetime, large Stokes shift and sharp emission profile.³⁷ Especially the long emission lifetimes of lanthanide ions allow the use of time-resolved luminescence detection to eliminate scattering excitation lights and short-lived autofluorescence from both biological samples and optical



Lanthanide complex components.⁵⁶ Because lanthanide ions exhibit low molar extinction coefficients, they often require sensitization with organic ligand capable of providing energy transfer to lanthanide excited states. Thus, the luminescence of lanthanide complexes depends on the energy transfer efficiencies from ligand sensitizers to lanthanide ions, which are determined by the chemical structures and triplet energy levels of ligands.⁵⁷ If the reaction of ligand with the analyte changes its chemical structure and triplet energy level, the energy transfer efficiency from ligand to lanthanide ions will be changed, which results in the variation in luminescence properties of lanthanide ions. Thus, luminescent chemodosimeters based on lanthanide complexes can be realized.^{37,58-60}

Conventional signal mechanisms

Integrating an organic fluorophore (reporter) with specific chelator (receptor) is the common approach to design fluorescent probes for metal ions. Metal coordination to the receptor will alter the fluorescence intensity, lifetime or excitation/emission maxima, reporting the presence of metal cations. The intramolecular interaction between the fluorophore and receptor is essential for the design of these fluorescent probes. A turn on emission or a shift in excitation/emission profiles is preferred over a turn off quenching response. A turn on response gives a bright signal against a dark background, which maximizes spatial resolution. Likewise, a shift in excitation/emission maxima can be used for ratiometric imaging which allows for internal calibration of reacted and unreacted probe to minimize artifacts that may arise from variations in light intensity, sample thickness and heterogeneity, and dye distribution. Conventional mechanisms such as PET, ICT, fluorescence resonance energy transfer (FRET) and photoinduced excimer/exciple formation have been frequently adopted for the construction of probe molecules. On the other hand, a number of new rationales, such as metal ion coordination inhibited ESIPT and aggregation-induced emission (AIE), have also been explored to devise probes.

Photoinduced electron transfer (PET): PET is the most widely employed signaling mechanism for the design of fluorescence based molecular probes.⁶¹ Generally PET probe contain three parts i) fluorophore, ii) spacer and iii) ionophore (Figure 6).⁴ Ionophores are generally electron donors (e.g. amino-containing group), while fluorophores are electron acceptors. In the free molecular probe, the electron occupying the highest occupied molecular orbital (HOMO) of the fluorophore can be promoted to the lowest unoccupied molecular orbital (LUMO) by absorbing an excitation photon. If energy of the ionophore HOMO is just higher than that of the fluorophore, the electron in this molecular orbital will transfer to the HOMO of the excited fluorophore through space, which blocks the emission transition of the excited electron occupying the fluorophore LUMO to fluorophore HOMO. This fluorescence quenching effect is termed as photoinduced electron transfer (PET). When the ionophore coordinates to the target metal ion, the energy gap between the two HOMO orbitals is changed from positive to negative due to the decreasing level of the ionophore HOMO via

metal coordination. The emission transition of the excited electron occupying the fluorophore LUMO to fluorophore HOMO is allowed and hence fluorescence of the probe is recovered. This metal coordination enhanced fluorescence is also defined as chelation enhanced fluorescence (CHEF) effect. In this case, emission of the formed metal complex is ascribed mainly to the relaxation of the π - π^* excited state of the organic fluorophore. Protonation of the ionophore may also lead to the blockage of the PET process.⁷

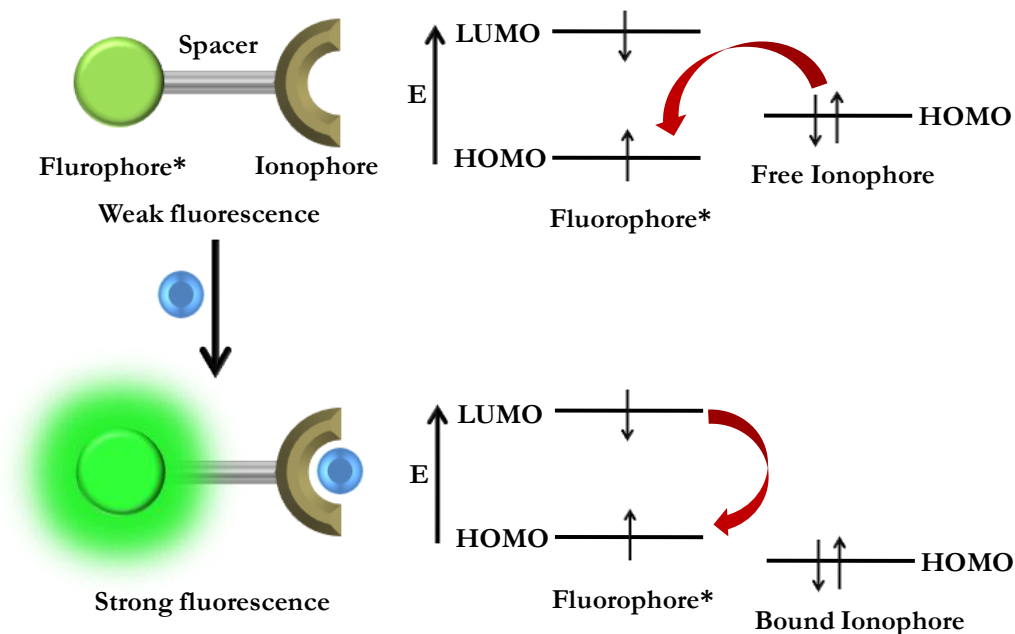


Figure 6. PET fluorescent probes for metal cations and their “turn on” sensing mechanism.

Internal Charge Transfer (ICT): When a fluorophore contains an electron-donating group (often an amino group) conjugated to an electron-withdrawing group, it undergoes intramolecular charge transfer from the donor to the acceptor upon excitation by light.^{3,4,7} The consequent change in dipole moment results in a Stokes shift that depends on the microenvironment of the fluorophore; polarity probes have been designed on this basis. It can thus be anticipated that cations in close interaction with the donor or the acceptor moiety will change the photophysical properties of the fluorophore because the complexed cation affects the efficiency of ICT. When a group (amino group) playing the role of an electron donor within the fluorophore interacts with a cation, the latter reduces the electron-donating character of this group owing to resulting reduction of conjugation, a blue shift in the

absorption spectrum is expected together with decreased extinction coefficient. Conversely, a cation interacting with the acceptor group enhances the electron-withdrawing character of this group; the absorption spectrum is thus red-shifted and the molar absorption coefficient is increased. The fluorescence spectra are in principle shifted in the same direction as those of

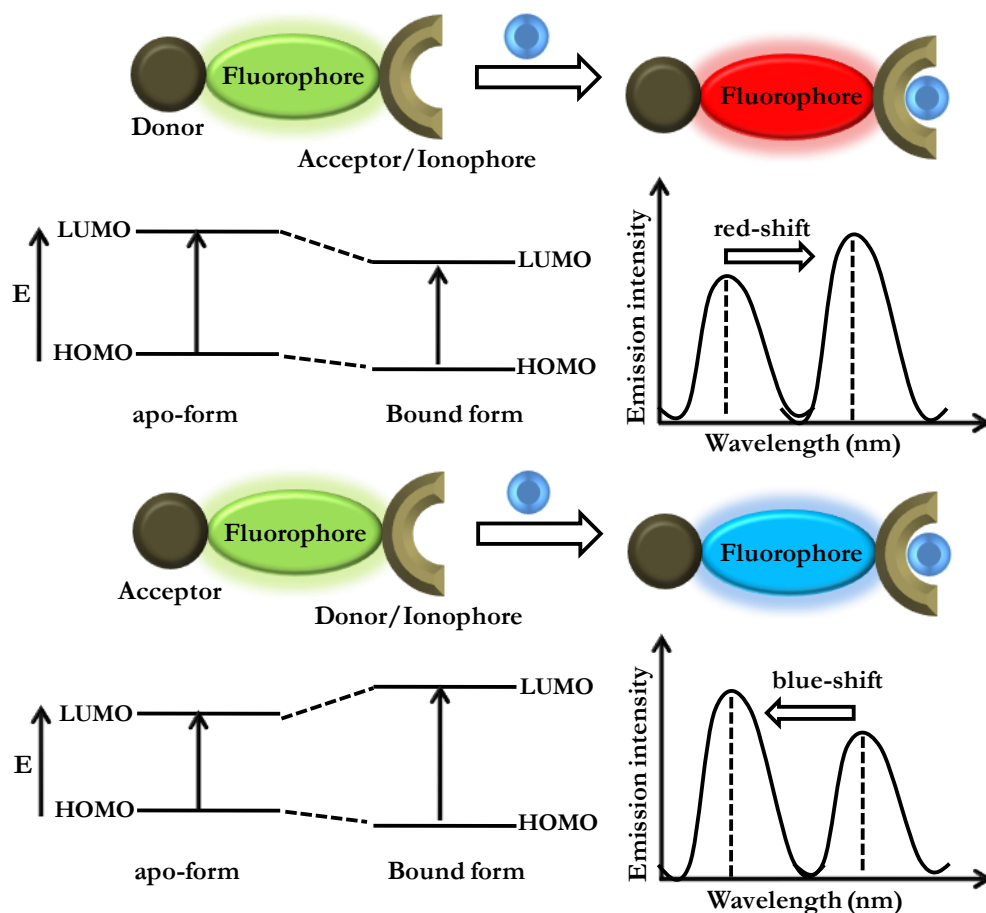
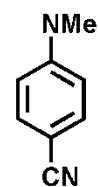


Figure 7. ICT fluorescent probes for metal cations and their ratiometric sensing mechanisms.

the absorption spectra. The photophysical changes upon cation binding can also be described in terms of charge dipole interaction. Let us consider only the case where the dipole moment in the excited state is larger than that in the ground state. Then, the cation interaction with the donor group strongly destabilizes the excited state compared to the ground state, and a blue shift of the absorption and emission spectra is expected. Conversely, when the cation interacts with the acceptor group, the excited state is more stabilized than the ground state, and this leads to a red shift of the absorption and emission spectra.

Twisted Internal Charge Transfer (TICT): Twisted intramolecular charge transfer (TICT) process in various organic molecules containing electron acceptor and donor groups separated by aromatic moieties has received considerable attention.⁷ Dual fluorescence behavior is observed in a number of such cases, for example excitation of such systems results in an excited state in which electron donor group is coplanar with the acceptor group and this state is known as locally excited (LE or B*) state. Formation of the second state, known as TICT state is due to the intramolecular rotation of the electron donor group from within the whole molecular plane to a position perpendicular to the other moiety of the molecule, accompanying the intramolecular charge transfer from the electron donor to the acceptor group during the excited state lifetime of the LE state. In most of these studies, formation and stabilization of the TICT state is attributed to viscosity and mainly to the polarity of the medium suggesting the energy barrier for TICT state process decreases with increase in polarity of the medium. However some authors have suggested that the specific hydrogen bonding between the electron donor group and the solvent molecules also plays a role in stabilizing the twisted conformer to facilitate the formation of the TICT state. On the other hand, Kim *et al.* have shown that the hydrogen bonding between electron acceptor group and solvent molecules play major role in the stabilization of TICT state and enhancement in the TICT emission. 4-Cyano-N,N'-dimethylaniline is perhaps the most celebrated of these systems and gives emission from its TICT excited state along with a shorter wavelength emission from a ICT-type excited state. The latter has the more delocalized excitation even though it was formerly referred to as a LE (locally excited) state. It has a planar skeleton and hence a well conjugated π -system. The ICT-type excited state is similarly planar, whereas the TICT excited state has the dimethyl amino unit orthogonalized from the rest of the π -system. The result is a dimethylamino radical cation and an adjacent benzonitrile radical anion.



Fluorescence resonance energy transfer (FRET): Fluorescence resonance energy transfer (FRET) relies on the distance-dependent transfer of energy from a donor molecule to an acceptor molecule.^{5,7,26} FRET is the radiationless transmission of energy from a donor molecule to an acceptor molecule.^{62,63} The donor molecule is the dye or chromophore that initially absorbs energy and acceptor is the chromophore to which energy is subsequently

transferred.⁶⁴ This resonance interaction occurs over greater than inter atomic distances without conversion to thermal energy and without any molecular collision. The transfer of energy leads to a reduction in the donor's fluorescence intensity and excited state lifetime, and concomitant increase in the acceptor's emission intensity. A pair of molecules the interaction result in FRET is often referred to as a donor/acceptor pair. While there are many factors that influence FRET, the primary conditions that need to be met in order for FRET to occur are relatively few. The donor and acceptor molecules must be in close proximity to one another (typically 10-100 Å). The absorption or excitation spectrum of the acceptor must overlap fluorescence emission spectrum of the donor (Figure 8). Genetically encoded fluorophores, such as green fluorescent protein (GFP) and related blue, cyan, yellow and red fluorescent proteins have provided the ability to perform FRET *in vitro* and *in vivo*, particularly in living cells. These proteins form FRET pairs with each other as well as with conventional dyes.

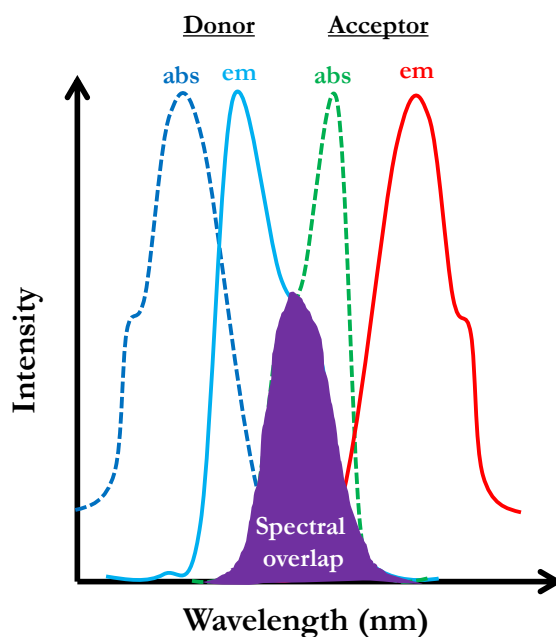


Figure 8. Schematic representation of the spectral overlap integral.

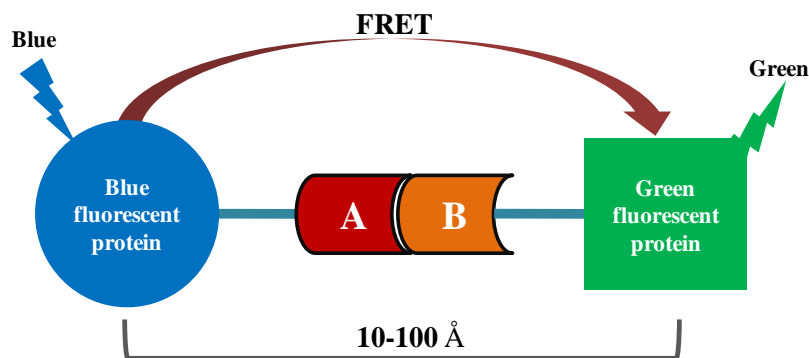


Figure 9. Schematic representation of the interaction of two different fluorescent protein. Protein-protein interactions between proteins labeled A and B bring blue fluorescent protein and green fluorescent proteins in close enough proximity to allow for FRET to occur. In this example, excitation of blue fluorescent protein results in the emission of fluorescence by green fluorescent protein.

Excited state intramolecular proton transfer (ESIPT) mechanism: ESIPT process requires a preformed intramolecular hydrogen bond (H-bond) between proton donor (-OH or -NH₂) and proton acceptor (-C=O or -N=) groups in close proximity to each other in a molecule.^{30,65} In the electronic ground state, typical ESIPT molecules exist exclusively as an enol (E) form, which is better stabilized by intramolecular H-bond (Figure 10). However, upon photoexcitation redistribution of electronic charge occurs causing an increase in the

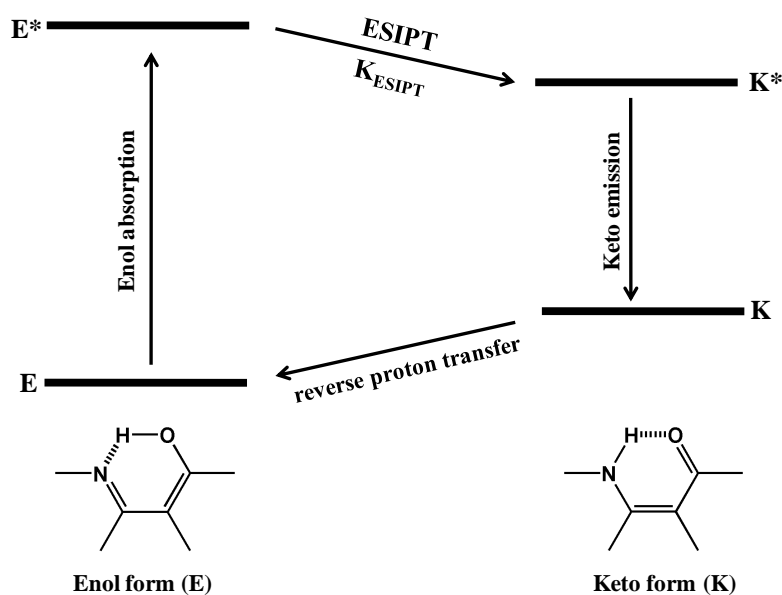


Figure 10. ESIPT sensing mechanism.

acidity of the proton donor and the basicity of the proton acceptor.⁶⁶ As a result, fast proton transfer from the proton donor to the proton acceptor takes place along the excited-state potential energy surface via the intramolecular H-bond leading to a tautomeric transformation from the excited enol form (E*) to the excited keto form (K*) in sub-picosecond time scale. After decaying radiatively to the ground state, reverse proton transfer occurs to their initial E form. Different absorbing (E) and emitting (K) molecular species in this intrinsic four-level photocycle often give rise to the total exclusion of self-absorption and the large Stokes' shifted emission. In addition, this process brings about the transient chemical change from E to K tautomer, resulting in the transient alternation of the electronic properties such as electron density distribution, energies of electronic state, and dipole moments. Due to the complicated photophysical process and transient changes involved in its four-level photocycle, ESIPT is to be easily affected by its environmental conditions leading to intricate spectral responses.

Monomer/Excimer: An excimer is formed by a fluorophore in the excited state with another fluorophore molecule in the ground state via weak interactions (e.g. π - π^* stacking).^{5,7,26} A typical metal ion probe functioning via excimer formation consists of two identical fluorophore moieties spaced by a flexible spacer which is also an ionophore. After coordinating with metal ion, the altered spacer brings the fluorophore moieties in close proximity (within van der Waals contact) which results in effective weak interactions between the two fluorophores.⁶⁷ In this way, electronic excitation of one fluorophore causes an enhanced interaction with its neighbor leading to the formation of an excimer. Compared to the monomer, the excimer typically affords a red-shifted and broad emission band. In most cases, both emission bands of the monomer and excimer can be observed simultaneously. Therefore, the metal coordination to the spacer ionophore can effectively alter the ratio between monomer emission and excimer emission. Thus excimer formation becomes an approach to design ratiometric probes for metal cations (Figure 11). Several probes based on this mechanism have been reported by Kim's group for the detection of Cu^{2+} . These probes generally require highly π -delocalized planar systems such as pyrene as the monomer. Therefore, they normally display poor aqueous solubility. Moreover, the excimer formation is highly dependent on the distance resulting from metal coordination.

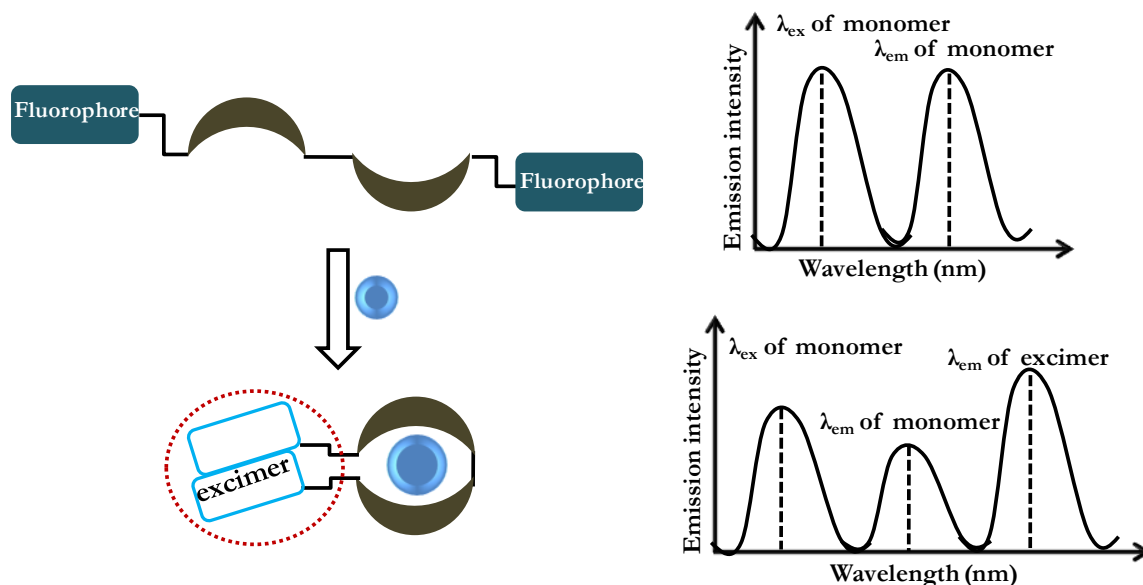
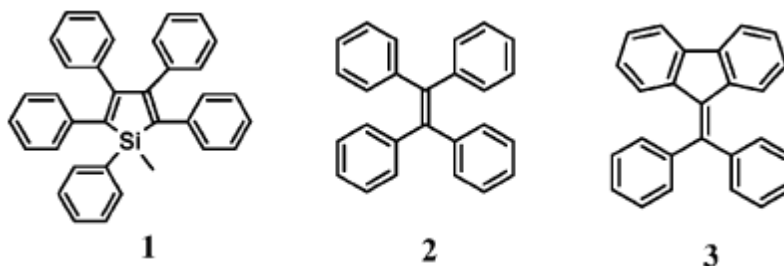


Figure 11. Excimer formation-based fluorescent sensing.

Aggregation-induced emission (AIE): It is well known that fluorescent emission of organic fluorophores is often quenched in aggregated form; this effect is denoted as aggregation-caused quenching (ACQ).⁶⁸ Because of the ACQ effect, the application of many organic fluorophores in organic light-emitting diodes (OLEDs) and as sensing materials (chemosensors, biosensors) has been greatly restricted. To



overcome the ACQ effect, branched chains, bulky cyclic species and dendritic segments have been covalently attached to the fluorophores to suppress the formation of aggregates.^{69,70} In contrast, some organic molecules that are nonfluorescent in solution were shown to become fluorescent upon aggregation, which is an unusual behavior. This unusual fluorescence phenomenon was noted by Tang *et al.* in 2001 from a solution of 1-methyl-1,2,3,4,5-pentaphenylsilole (**1**),⁷¹ and termed as aggregation-induced emission (AIE). The fluorescence quantum yield (Φ_F) of **1** in pure ethanol is 0.63×10^{-3} , but rose to 0.21 when the water fraction is increased to 90%. The AIE effect greatly boosts the fluorescence quantum yield of **1** by 333 times, turning it from essentially nonfluorescent to strongly fluorescent. The same group

subsequently reported that a variety of tetraphenylethene (**2**), diphenyldibenzofulvenes (**3**), substituted olefins, and pyran derivatives also showed AIE phenomena. Tang *et al.* studied AIE phenomenon using a series of experimental investigations. They identified that the restriction of intramolecular rotation in the aggregates was the main cause of AIE phenomenon.^{72,73} Unhindered intramolecular rotation in AIE molecules in the free-state leads to efficient nonradiative decay of the corresponding excited states, making them nonemissive. Upon aggregation in a suitable environment, intramolecular rotation is restricted and emission is thus greatly enhanced. For instance, in silole **1** and tetraphenylethene (**2**), the propeller-like molecular conformation induces free intramolecular rotation. In view of such strange fluorescence behavior, AIE phenomena have been successfully utilized to design sensitive and selective bio-/chemo-sensors. The aggregation of AIE molecules can be altered by guest molecules through electrostatic interaction, coordination interaction, hydrophobic interaction, steric hindrance, particular mercapto reaction, or the influence of polarity and viscosity. As a result, a variety of new AIE-active fluorescent bio-/chemo-sensors have been developed to detect ionic species (Hg^{2+} , Ag^+ , CN^-), biomolecules (protein, heparin, ATP and DNA), and gases and explosives (CO_2 , TNT, picric acid), as well as assay to study nuclease activities.

C=N isomerization: C=N isomerization as a signaling mechanism was reported in 2007. This idea initiated from the study on photophysical properties of conformationally restricted compounds. It was found that C=N isomerization is the predominant decay process of excited states in compounds with an unbridged C=N structure and those compounds are often nonfluorescent.⁷⁴⁻⁷⁶ In contrast, the fluorescence of their analogs containing a covalently bridged C=N structure increases dramatically due to the suppression of C=N isomerization in the excited states (Figure 12a). Thus it is reasonable to expect that C=N isomerization can also be suppressed through complexation of a guest species to a sophisticatedly designed fluorescent-sensing molecule rather than the covalently bridged C=N bond. Based on this hypothesis, coumarin-derived imine was designed as a novel fluorescent chemosensor that used C=N isomerization as a signal system (Figure 12b).⁷⁷ The free ligand is nonfluorescent because of rapid isomerization of the C=N double bond in the excited state. However, solution of ligand in CH_3CN shows 200-fold enhancement in fluorescence quantum yield

upon complexation with zinc ions, along with a red shift in the emission maxima from 500 to 522 nm. As the first molecular probe based on C=N isomerization mechanism, some problems exist, for example, interference from other competitive ions, and the need to use organic solvents. Further modifications are required to improve the design of molecular probes that operate based on C=N isomerization.

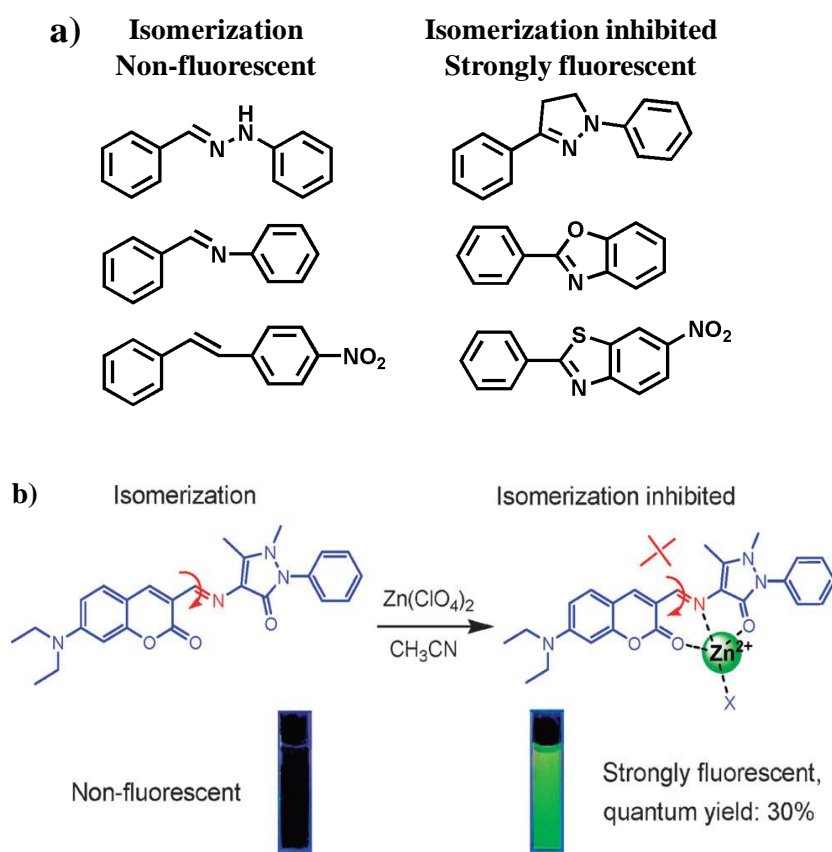


Figure 12. C=N isomerization mechanism based fluorescence sensing. Reprinted with permission from reference 77, copyright 2007, by the American Chemical Society.

Approaches for designing Fluorescent molecular probes

Molecular probes (chemosensors) are highly valuable tools for selective recognition of chemical and biological species. Host-guest interactions making use of hydrogen bonding, electrostatic force, metal-ligand coordination, hydrophobic and van der Waals interactions have been employed to develop chemosensors. Fluorescent molecular probes can be categorized based on two different approaches.

(i) Classic combination of fluorophore and ionophore: The classic fluorescence-based molecular probes (fluoroionophore) contains a receptor/ionophore (the recognition site) connected via spacer (linker) to a fluorophore (the reporter) which displays differential fluorescence response as a consequence of recognition process.^{7,61} This is the most common approach adopted for designing a fluorescent molecular sensor (Figure 13). Receptor/ionophore are generally electron donors (e.g. amino-containing group), while fluorophores are electron acceptors.^{2,4} In normal ‘off’ state condition, excitation of the fluoroionophore produces an electron transfer from the receptor to the fluorophore. The thermodynamic condition, first derived by Weller, is the excited state energy of the fluorophore needs to be sufficient to provide both the reduction potential of the fluorophore and the oxidation potential of the receptor. In ‘on’ state, excitation of the fluoroionophore results in fluorescence only because the PET process is arrested by the arrival of the analyte at the receptor site. The arresting PET process can be easily comprehended by considering H^+ as the analyte. H^+ electrostatically attracts the electron which increases the oxidation

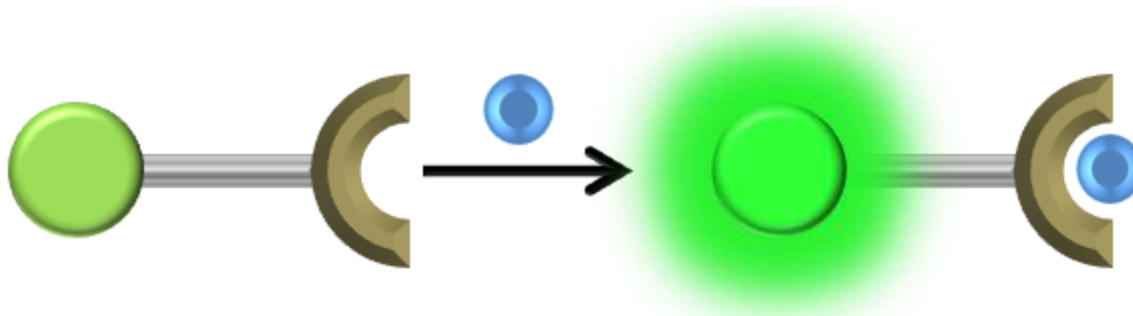


Figure 13. Classic approach: chemosensor bearing a signaling subunit as well as a binding site.

potential of the analyte-bound receptor to the point that the thermodynamics for PET are no longer favourable. These ideas can also be expressed with the aid of molecular orbital energy diagrams. PET occurs if the oxidation potential of the receptor is smaller in magnitude than that of the fluorophore and in opposite case PET does not occur. This rule of thumb is very useful practically, even though several approximations are involved. Quantitative design of fluorescent PET chemosensors is a rare example of molecular engineering design. Molecular PET chemosensors can now be designed and built for a variety of individual purposes. Each of the three components in the ‘fluorophore–spacer–receptor’ format deserves the designer’s attention. The analyte to be sensed determines the choice of receptor. The reciprocal of the binding constant for the receptor–analyte interaction determines the median analyte concentration to be sensed. Consideration needs to be given at this stage to the selectivity of the receptor towards the analyte and against anticipated levels of potential interferences.

(ii) Reaction based probes: The host–guest interactions between receptor and analyte undergo dynamic molecular transformations by making or breaking of covalent bonds rather than forming supramolecular complexes in the biological milieu.⁷⁸ Reactive probes undergo structural changes after chemical conversion show maximum spectroscopic changes compared to normal noncovalent interactions based chemical probes. The reactive probes are designed in such way that the analyte can perform typical chemical reactions like nucleophilic additions and substitutions with the probe moiety. The analyte can also undergo tandem reaction in the probe to generate electronically different final product.⁸

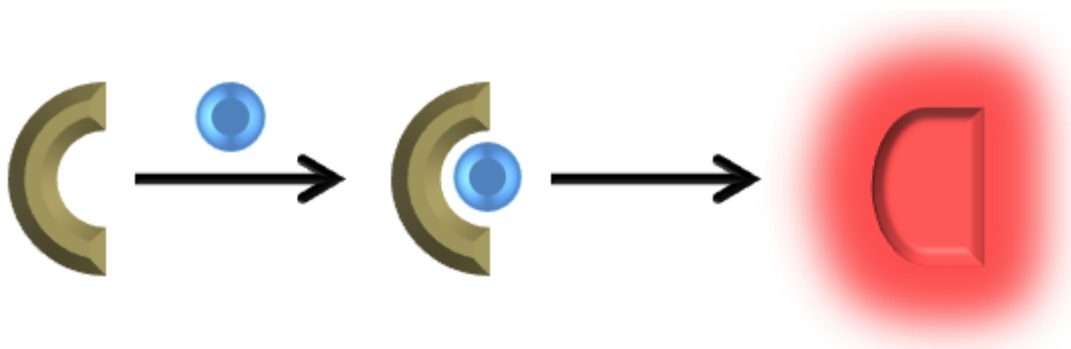


Figure 14. Analyte assisted reaction based approach and their detection.

Oxidative cycloaddition reaction: Cycloaddition reaction offers a broadly useful set of potential reactions for chemoselective sensing and bioimaging, as the formation of new heterocycles conjugated to a fluorophore can readily alter its optical properties. Aromatic vicinal diamines can react with nitric oxide (NO) in the presence of O₂ to form triazole ring. Diaminofluoresceins are weakly fluorescent because of PET quenching from the electron-rich amino functional group. However, conversion to the triazole functionality results in turn on emission because the extent of PET quenching is reduced.⁷⁹ Well-known cycloaddition reaction between singlet oxygen (¹O₂) and anthracene to form an endoperoxide has been used for sensing of ¹O₂.⁸⁰

Oxidative cleavage reaction: Another strategy for reaction-based detection of small molecules is to use a pro-fluorophore approach, where reaction of a small molecule selectively releases nonfluorescent or weakly fluorescent pro-fluorophore to produce the parent dye. Chang and coworkers have reported hydrogen peroxide-mediated conversion of arylboronates to phenols for H₂O₂ detection.⁸¹ Dicarbonyl cleavage reactions offer another attractive strategy for selective H₂O₂ detection.⁸² Peroxynitrite (ONOO⁻) can selectively oxidize a trifluoroketone functionality to form a labile dioxirane intermediate, which decompose and oxidize a proximal anisole ring to the corresponding dienone functionality with concomitant release of an alcohol.^{83,84} Hypochlorous acid (HOCl)-mediated oxidation and cleavage of a p-methoxyphenol can serve as a selective trigger for detecting this highly reactive oxygen species.⁸⁵ Selenoether oxidations have also been reported to show some specificity for ONOO⁻ detection.⁸⁶ Finally, ozonolysis reaction oxidatively fragment an olefin into two carbonyl products and has been elegantly used to create a probe for chemoselective ozone sensing.⁸⁷

Reductive cleavage reaction: A prime example of reductive transformations is the hydrogen sulfide-mediated reduction of azides to amines as a means of monitoring of analyte (H₂S).⁸⁸ This strategy has been elegantly implemented for detecting H₂S using different azido-fluorophores. First Chang and coworkers reported selective conversion of azides to amines for H₂S detection over biologically relevant thiols.⁸⁹ Similarly, H₂S mediated reduction of

nitro and hydroxylamine to amino group has been used to design several probes for detection of this small molecule.^{90,91}

Oxidative and reductive transformations have been used together to design fluorescent probe for the redox cycle process utilizing the redox property of the versatile selenium. Selenium containing fluorescent probe monitors cellular redox change induced by peroxynitrite and glutathione or hydrogen sulfide in solution. Upon addition of HClO, an increase in the fluorescence was observed as the PET process is blocked by the formation of “selenoxide”. Then the “selenoxide” was reduced to “selenide” by H₂S or GSH, switches off the fluorescence.⁹²

Nucleophilic reaction and tandem process: Generally, sensing of anionic or neutral analytes is achieved by exploiting their nucleophilicity in the nucleophilic addition or substitution reactions. Nucleophilicity of cyanide (CN⁻) or carboxylates (RCOO⁻) is sufficient enough to react with highly electrophilic carbonyl functionality and has been successfully implemented in the design of fluorescent probes for these analytes.⁹³⁻⁹⁵ Neutral bifunctional analytes such as amino-thiols (cysteine, homocysteine) reacts with aldehyde group to form corresponding heterocyclic thiazolines and has been used for the development of fluorescent probes for their sensing.⁹⁶ The soft nucleophilic thiols (RSH) also readily undergo 1,4-addition (Michael or conjugate addition) to α , β -unsaturated carbonyl compounds.⁹⁷ This kind of reaction based approach has been extensively used in designing various fluorescent probes for thiols. The thiol assisted nucleophilic aromatic substitution removes 2,4-dibenzenesulfonyl moiety from the hydroxyl or amine group of a fluorophore and this chemical transformation has been found to have excellent selectivity towards thiol detection with off–on fluorescence signaling. Biogenic thiols such as glutathione can undergo sulfide exchange reaction.⁹⁸ Inclusion of disulfide bond in the molecular probe has been extensively used for designing thiol selective probes. Boranes as anion receptors form covalent bond with the nucleophilic anions CN⁻ and F⁻. A number of molecular probes containing borane have been reported for the detection of these toxic anions.⁹⁹

Displacement reaction by metal–ligand substitution: Coordinated chemosensor can undergo exchange reaction with the target analyte resulting change in fluorometric response.

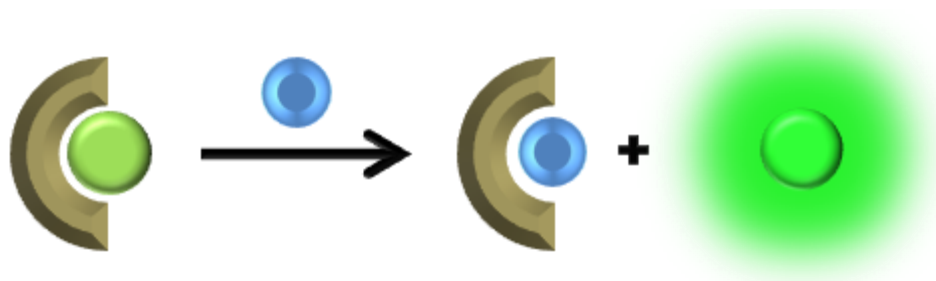


Figure 15. Displacement reaction based approach for chemosensors.

Introduction of a nucleophile to the solution of coordinated chemosensor, can release the unbound probe which also results restoration of fluorometric behavior (Figure 15). Metal–ligand substitution and reaction of small molecule with flexible pendant dyes offers a versatile approach to tune fluorescence properties. Generally, metal ions are strong quenchers of fluorescent excited states because of their unpaired electrons or partially filled orbitals, as well as heavy-atom effects that can turn off emission by electron- or energy transfer quenching pathways. The general approach relies on quenching of pendant fluorophores by coordination to a paramagnetic and/or heavy-metal ion like Cu^{2+} or Hg^{2+} .^{100,101} Turn on fluorescent sensing can be achieved from displacement of this metal ion by some other metal ions such as Zn^{2+} or Cd^{2+} which has more affinity towards the coordination sphere of dye scaffolds.¹⁰² Metal ions of same group like $\text{Mg}^{2+}/\text{Ca}^{2+}$ or $\text{Zn}^{2+}/\text{Cd}^{2+}$ exhibit similar chemical properties.¹⁰³ It is a difficult task to develop chemosensors for these analytes as they interferes each other recognition process. The minute change in the fluoroionophore coordination site varies the cation binding affinity, giving rise to variations either in its fluorescence intensity (turn on-off) or/and in emission wavelength (ratiometric).¹⁰⁴ In this context, reactive biological small molecule NO can be detected directly by displacement of ligand-fluorophores from chelated metal centres. This general approach relies on fluorescence quenching of pendant fluorophores by coordination to a paramagnetic and/or heavy-metal ion, then NO can selectively displace and release the fluorophore with concomitant emission turn on response.¹⁰⁵ Detection of biologically relevant anionic phosphates has been achieved using variety of Zn^{2+} -coordinated di-2-picolyamine derivatives of different dyes, where the fluorophore can coordinate with the bimetallic Zn^{2+} ion and quench fluorescence.¹⁰⁶ Upon binding of a phosphorylated substrate such as ATP to

the Zn^{2+} -DPA moiety, the pendant fluorophore is displaced from the metal first-coordination spheres to generate an emission turn-on response. Metal displacement strategy is also used for H_2S detection employing the classic gravimetric precipitation of CuS from Cu^{2+} complexes. Cu^{2+} binding to the fluorophore-ionophore conjugate quenches its emission. Addition of H_2S triggers displacement of bound metal to precipitate CuS and release the free dye, resulting in fluorescence enhancement.^{107,108} CN^- forms stable $[\text{Cu}(\text{CN})_x]^{n-}$ complex reacting with copper ions. Fluorescence of a chemosensor is generally quenched by complexing with paramagnetic Cu^{2+} . Quenched fluorescence can be recovered mixing with CN^- as it forms stable complex with copper to release free chemosensor which give rise to turn on detection for cyanide ions.⁹³

Metal-mediated redox addition or cleavage reaction: Simple Lewis acid-base metal-ligand substitution chemistry and metal-induced redox processes also provide a wealth of opportunities for small molecule sensing and bioimaging. The reductive N-nitrosylation and release of metal quenchers from fluorophore scaffolds emerged as a versatile and general method for direct NO detection.^{109,110} The probe consists of a copper-bound fluoroionophore conjugate where the paramagnetic Cu^{2+} ion quenches dye fluorescence. Upon direct reaction with NO, a metal-mediated reductive nitrosylation reaction releases the bound metal ion with a concomitant increase in emission. Mechanistic study reveals the secondary amine as the site of NO modification and show that this mechanism gives high selectivity for NO over a variety of RNS and ROS analytes.¹¹⁰ Oxidative reactivity at metal centres can also provide a path to chemoselective sensing and bioimaging applications. This approach has been used for chemoselective monitoring of H_2O_2 , inspired by the heme-mediated horseradish peroxidase-Amplex red (N-acetyl-3,7-dihydroxyphenoxazine) assay that has been used extensively to indirectly quantify the activity of various H_2O_2 -producing enzymes.¹¹¹ Reaction between H_2O_2 and probe leads to iron-mediated oxidation, cleavage and release of a fluorescent dye. Cationic triarylstibine-palladium complex and tetraarylstibonium act as fluoride anion receptor.^{112,113} Formation of hypervalent fluorostiboranyl motif results in photophysical property change of the complex ensuing fluoride sensing.¹¹⁴ Fluoride (F^-) has strong affinity toward silicon atom; hence fluoride mediated desilylation reactions have been used in designing fluoride selective fluorescent probes.^{115,116}

Lewis acid hydrolysis and related non-redox reaction: The inherent Lewis acidity of metal ions promoted hydrolysis and related non-redox reactions, hard–soft acid base chemistry, and a variety of such strategies can emerge for chemoselective turn on or ratiometric detection. Two classic examples by Czarnik and colleagues have inspired a host of subsequent elegant chemical designs for imaging metal ion. One reaction-based system established that the strong thiophilic nature of Hg^{2+} can selectively enhance the activation and desulfurization/hydrolysis of thiocarbonyl compounds, such as the conversion of thioamides to carboxylates.¹¹⁷ The second study, on the Cu^{2+} -catalyzed hydrolysis of hydrazines to carboxylates with concomitant ring-opening of a non-fluorescent spirorhodamine to its fluorescent open form, highlights this platform as a general and versatile sensing molecular scaffold.¹¹⁸ The mercury-promoted cycloaddition of thiourea substrates has developed as a universal reaction-based strategy for detection of this toxic heavy metal.^{63,119} The conversion of thioacetals to carbonyls has also been applied to monitoring biological and environmental mercury.^{120,121} Finally, several copper- and silver-promoted hydrolysis reactions have been reported for fluorescent *in vivo* detection of these metal ions in aqueous media.^{122,123}

Organometallic reaction: Metal-mediated organometallic reactions can be used for metal ion detection. Copper-accelerated alkyne click (CuAAC) chemistry offers an ideal reaction-based mechanism for detection of this essential biological metal.¹²⁴ Tsuji–Trost¹²⁵ and Claisen¹²⁶ chemistry of metal–allyl complexes offers another versatile approach to metal ion sensing, particularly for palladium and platinum. The Tsuji–Trost probes operate through hydrolysis of allyl ether by an electrophilic metal–allyl intermediate, whereas other conditions favor aromatic Claisen rearrangements. Adjustments in pH, ligand additives and other experimental conditions can promote specificity for palladium or platinum with oxidation state selectivity. O-Propargylated fluorescein derivatives that can monitor palladium in a variety of oxidation states (for example Pd^0 , Pd^{2+} , and Pd^{4+}).¹²⁷ Fluorescent probes for Hg^{2+} have also developed based on the oxymercuration of alkynes and alkenes, where the phenolic hydroxyl group of a fluorescent dye is caged with a terminal butyne or a vinyl ether moiety.¹²⁸ The Hg^{2+} -catalyzed hydration and oxidation of the alkyne or alkene to the corresponding ketone triggers facile β -elimination to yield the latent dye. Aryl vinyl ether

probes are used for assaying mercury in fish, and alkynes with thioamide directing groups are used to achieve mercury imaging in live cells. Au³⁺ selective fluorescent probes have been developed by activating the fluorophore by reactive and alkynophilic Au³⁺ ion.¹²⁹⁻¹³¹ Au³⁺ induced intramolecular cyclization changes the PET process towards fluorophore thus allowing its detection.

Metal ion detection through small molecule reactivity: Reaction-based strategy for metal ion detection is achieved through metal-mediated activation of small molecules. In an elegant study, Taki and coworkers reported the Cu(I)-responsive fluorescent probe FluTPA2.¹³² In the absence of Cu(I), FluTPA2 is inert to oxygen and weakly fluorescent owing to reduction of the xanthenone ring and alkylation of its phenolic oxygen. Aerobic C–O bond cleavage promoted by Cu(I) followed by air oxidation releases the free Tokyo Green dye. Similarly, selective fluorescence probe for cobalt was reported by Chang and coworkers combining a Tokyo Green scaffold alkylated with a N₃O ligand.¹³³ Binding of Co²⁺ in the presence of air triggers oxidative C–O bond cleavage and a roughly 18-fold increase in turn on emission.

An ideal molecular probe must fulfill following basic requirements:

- (i) The receptor must have strong affinity towards the relevant target which shows selective binding or reactivity.
- (ii) The signal should not be disturbed from environmental interference, such as probe concentration, pH, polarity, temperature, and so forth.
- (iii) Fluorometric/colorimetric optical response must be quick over a wide dynamic range of analyte concentrations.
- (iv) Biocompatibility of the probe in terms of toxicity, solubility, and stability.

The ultimate goal in developing a molecular probe is to detect and image the target of interest in living cellular systems. Though, live cell imaging has been carried out to understand the biological effects of particular analyte and this process is not yet attained the total perfection. Images obtained from inside the living organisms are highly informative which emphasizes the need for development of novel and efficient molecular probes.

References

1. Ueno, T.; Nagano, T., Fluorescent probes for sensing and imaging. *Nat. Meth.* **2011**, *8*, 642-645.
2. Lemke, E. A.; Schultz, C., Principles for designing fluorescent sensors and reporters. *Nat. Chem. Biol.* **2011**, *7*, 480-483.
3. New, E. J., Tools to study distinct metal pools in biology. *Dalton Trans.* **2013**, *42*, 3210-3219.
4. Liu, Z.; He, W.; Guo, Z., Metal coordination in photoluminescent sensing. *Chem. Soc. Rev.* **2013**, *42*, 1568-1600.
5. Terai, T.; Nagano, T., Fluorescent probes for bioimaging applications. *Curr. Opin. Chem. Biol.* **2008**, *12*, 515-521.
6. Kim, H. M.; Cho, B. R., Two-photon probes for intracellular free metal ions, acidic vesicles, and lipid rafts in live tissues. *Acc. Chem. Res.* **2009**, *42*, 863-872.
7. de Silva, A. P.; Gunaratne, H. Q. N.; Gunnlaugsson, T.; Huxley, A. J. M.; McCoy, C. P.; Rademacher, J. T.; Rice, T. E., Signaling recognition events with fluorescent sensors and switches. *Chem. Rev.* **1997**, *97*, 1515-1566.
8. Chan, J.; Dodani, S. C.; Chang, C. J., Reaction-based small-molecule fluorescent probes for chemoselective bioimaging. *Nat. Chem.* **2012**, *4*, 973-984.
9. Domaille, D. W.; Que, E. L.; Chang, C. J., Synthetic fluorescent sensors for studying the cell biology of metals. *Nat. Chem. Biol.* **2008**, *4*, 168-175.
10. Merino, E., Synthesis of azobenzenes: the coloured pieces of molecular materials. *Chem. Soc. Rev.* **2011**, *40*, 3835-3853.
11. Zhou, Y.; Xu, Z.; Yoon, J., Fluorescent and colorimetric chemosensors for detection of nucleotides, FAD and NADH: highlighted research during 2004-2010. *Chem. Soc. Rev.* **2011**, *40*, 2222-2235.
12. Urano, Y.; Asanuma, D.; Hama, Y.; Koyama, Y.; Barrett, T.; Kamiya, M.; Nagano, T.; Watanabe, T.; Hasegawa, A.; Choyke, P. L.; Kobayashi, H., Selective molecular imaging of viable cancer cells with pH-activatable fluorescence probes. *Nat. Med.* **2009**, *15*, 104-109.
13. Kamiya, M.; Kobayashi, H.; Hama, Y.; Koyama, Y.; Bernardo, M.; Nagano, T.; Choyke, P. L.; Urano, Y., An enzymatically activated fluorescence probe for targeted tumor imaging. *J. Am. Chem. Soc.* **2007**, *129*, 3918-3929.
14. Hama, Y.; Urano, Y.; Koyama, Y.; Bernardo, M.; Choyke, P. L.; Kobayashi, H., A comparison of the emission efficiency of four common green fluorescence dyes after internalization into cancer cells. *Bioconjugate Chem.* **2006**, *17*, 1426-1431.

15. Kobayashi, H.; Longmire, M. R.; Ogawa, M.; Choyke, P. L., Rational chemical design of the next generation of molecular imaging probes based on physics and biology: mixing modalities, colors and signals. *Chem. Soc. Rev.* **2011**, *40*, 4626-4648.
16. Mitsunaga, M.; Ogawa, M.; Kosaka, N.; Rosenblum, L. T.; Choyke, P. L.; Kobayashi, H., Cancer cell-selective in vivo near infrared photoimmunotherapy targeting specific membrane molecules. *Nat. Med.* **2011**, *17*, 1685-1691.
17. Qian, X.; Xiao, Y.; Xu, Y.; Guo, X.; Qian, J.; Zhu, W., "Alive" dyes as fluorescent sensors: fluorophore, mechanism, receptor and images in living cells. *Chem. Commun.* **2010**, *46*, 6418-6436.
18. Chersi, A.; di Modugno, F.; Rosanò, L., Selective 'in synthesis' labelling of peptides by fluorochromes. *Biochim Biophys Acta.* **1997**, *1336*, 83-88.
19. Chersi, A.; Sezzi, M. L.; Romano, T. F.; Evangelista, M.; Nista, A., Preparation and utilization of fluorescent synthetic peptides. *Biochim Biophys Acta.* **1990**, *1034*, 333-336.
20. Zhang, J.; Campbell, R. E.; Ting, A. Y.; Tsien, R. Y., Creating new fluorescent probes for cell biology. *Nat. Rev. Mol. Cell. Biol.* **2002**, *3*, 906-918.
21. Gaietta, G.; Deerinck, T. J.; Adams, S. R.; Bouwer, J.; Tour, O.; Laird, D. W.; Sosinsky, G. E.; Tsien, R. Y.; Ellisman, M. H., Multicolor and electron microscopic imaging of connexin trafficking. *Science* **2002**, *296*, 503-507.
22. MacBeath, G.; Schreiber, S. L., Printing proteins as microarrays for high-throughput function determination. *Science* **2000**, *289*, 1760-1763.
23. Summerer, D.; Chen, S.; Wu, N.; Deiters, A.; Chin, J. W.; Schultz, P. G., A genetically encoded fluorescent amino acid. *Proc. Natl. Acad. Sci. USA* **2006**, *103*, 9785-9789.
24. Bhosale, S. V.; Bhosale, S. V.; Bhargava, S. K., Recent progress of core-substituted naphthalenediimides: highlights from 2010. *Org. Biomol. Chem.* **2012**, *10*, 6455-6468.
25. Sakai, N.; Mareda, J.; Vauthey, E.; Matile, S., Core-substituted naphthalenediimides. *Chem. Commun.* **2010**, *46*, 4225-4237.
26. Gonçalves, M. S. T., Fluorescent labeling of biomolecules with organic probes. *Chem. Rev.* **2008**, *109*, 190-212.
27. Toyooka, T., Fluorescent tagging of physiologically important carboxylic acids, including fatty acids, for their detection in liquid chromatography. *Anal. Chim. Acta* **2002**, *465*, 111-130.
28. Gikas, E.; Parissi-Poulou, M.; Kazanis, M.; Vavagianis, A., BrMOZPhC, a novel coumarin type reagent for the fluorescent derivatisation of carboxylic acids. *Anal. Chim. Acta* **2003**, *489*, 153-163.
29. Ammar, H.; Fery-Forgues, S.; El Gharbi, R., UV/vis absorption and fluorescence spectroscopic study of novel symmetrical biscoumarin dyes. *Dyes Pigm.* **2003**, *57*, 259-265.

30. Kwon, J. E.; Park, S. Y., Advanced organic optoelectronic materials: harnessing excited-state intramolecular proton transfer (ESIPT) process. *Adv. Mater.* **2011**, *23*, 3615-3642.
31. Uchiyama, S.; Takehira, K.; Kohtani, S.; Imai, K.; Nakagaki, R.; Tobita, S.; Santa, T., Fluorescence on-off switching mechanism of benzofurazans. *Org. Biomol. Chem.* **2003**, *1*, 1067-1072.
32. Dufau, I.; Mazarguil, H., Design of a fluorescent amino acid derivative usable in peptide synthesis. *Tetrahedron Lett.* **2000**, *41*, 6063-6066.
33. Eftink, M. R.; Shastry, M. C. R., Fluorescence methods for studying kinetics of protein-folding reactions. In *Methods Enzymol.*, Ludwig Brand, M. L. J., Ed. Academic Press: **1997**; *278*, 258-286.
34. Cody, J.; Mandal, S.; Yang, L.; Fahrni, C. J., Differential tuning of the electron transfer parameters in 1,3,5-triarylpyrazolines: A rational design approach for optimizing the contrast Ratio of fluorescent probes. *J. Am. Chem. Soc.* **2008**, *130*, 13023-13032.
35. Qian, Y.; Karpus, J.; Kabil, O.; Zhang, S.-Y.; Zhu, H.-L.; Banerjee, R.; Zhao, J.; He, C., Selective fluorescent probes for live-cell monitoring of sulphide. *Nat. Commun.* **2011**, *2*, 495.
36. Wu, S.; Dovichi, N. J., High-sensitivity fluorescence detector for fluorescein isothiocyanate derivatives of amino acids separated by capillary zone electrophoresis. *J. Chromatogr. A* **1989**, *480*, 141-155.
37. Yang, Y.; Zhao, Q.; Feng, W.; Li, F., Luminescent chemodosimeters for bioimaging. *Chem. Rev.* **2012**, *113*, 192-270.
38. Chen, X.; Pradhan, T.; Wang, F.; Kim, J. S.; Yoon, J., Fluorescent chemosensors based on spiroring-opening of xanthenes and related derivatives. *Chem. Rev.* **2011**, *112*, 1910-1956.
39. Dujols, V.; Ford, F.; Czarnik, A. W., A long-wavelength fluorescent chemodosimeter selective for Cu(II) ion in water. *J. Am. Chem. Soc.* **1997**, *119*, 7386-7387.
40. Arbeloa, I. L.; Ojeda, P. R., Molecular forms of rhodamine B. *Chem. Phys. Lett.* **1981**, *79*, 347-350.
41. Treibs, A.; Kreuzer, F.-H., Difluorboryl-komplexe von di- und tripyrrylmethenen. *Liebigs Ann. Chem.* **1968**, *718*, 208-223.
42. Boens, N.; Leen, V.; Dehaen, W., Fluorescent indicators based on BODIPY. *Chem. Soc. Rev.* **2012**, *41*, 1130-1172.
43. Ulrich, G.; Ziessel, R.; Harriman, A., The chemistry of fluorescent Bodipy dyes: Versatility unsurpassed. *Angew. Chem. Int. Ed.* **2008**, *47*, 1184-1201.
44. Oswald, B.; Lehmann, F.; Simon, L.; Terpetschnig, E.; Wolfbeis, O. S., Red laser-induced fluorescence energy transfer in an immunosystem. *Anal. Biochem.* **2000**, *280*, 272-277.

45. Kukrer, B.; Akkaya, E. U., Red to near IR fluorescent signalling of carbohydrates. *Tetrahedron Lett.* **1999**, *40*, 9125-9128.
46. Kim, S.-H.; Kim, J.-H.; Cui, J.-Z.; Gal, Y.-S.; Jin, S.-H.; Koh, K., Absorption spectra, aggregation and photofading behaviour of near-infrared absorbing squarylium dyes containing perimidine moiety. *Dyes Pigm.* **2002**, *55*, 1-7.
47. Hyodo, Y.; Nakazumi, H.; Yagi, S., Synthesis and light absorption/emission properties of novel squarylium dimers bearing a ferrocene spacer. *Dyes Pigm.* **2002**, *54*, 163-171.
48. Williams, D. J., Organic polymeric and non-polymeric materials with large optical nonlinearities. *Angew. Chem. Int. Ed.* **1984**, *23*, 690-703.
49. Gómez-Hens, A.; Aguilar-Caballos, M. P., Long-wavelength fluorophores: new trends in their analytical use. *TrAC, Trends Anal. Chem.* **2004**, *23*, 127-136.
50. Patonay, G.; Salon, J.; Sowell, J.; Streckowski, L., Noncovalent labeling of biomolecules with red and near- infrared dyes. *Molecules* **2004**, *9*, 40-49.
51. Mitra, R. D.; Shendure, J.; Olejnik, J.; Edyta Krzymanska, O.; Church, G. M., Fluorescent in situ sequencing on polymerase colonies. *Anal. Biochem.* **2003**, *320*, 55-65.
52. Weissleder, R.; Ntziachristos, V., Shedding light onto live molecular targets. *Nat. Med.* **2003**, *9*, 123-128.
53. Tonge, R.; Shaw, J.; Middleton, B.; Rowlinson, R.; Rayner, S.; Young, J.; Pognan, F.; Hawkins, E.; Currie, I.; Davison, M., Validation and development of fluorescence two-dimensional differential gel electrophoresis proteomics technology. *Proteomics* **2001**, *1*, 377-396.
54. Mason, S. J.; Balasubramanian, S., Solid-phase catch, activate, and release synthesis of cyanine dyes. *Org. Lett.* **2002**, *4*, 4261-4264.
55. McCorquodale, E. M.; Colyer, C. L., Indocyanine green as a noncovalent, pseudofluorogenic label for protein determination by capillary electrophoresis. *Electrophoresis* **2001**, *22*, 2403-2408.
56. Eliseeva, S. V.; Bunzli, J.-C. G., Lanthanide luminescence for functional materials and bio-sciences. *Chem. Soc. Rev.* **2010**, *39*, 189-227.
57. Shi, M.; Li, F.; Yi, T.; Zhang, D.; Hu, H.; Huang, C., Tuning the triplet energy levels of pyrazolone ligands to match the 5D0 level of europium(III). *Inorg. Chem.* **2005**, *44*, 8929-8936.
58. Lippert, A. R.; Gschneidtnr, T.; Chang, C. J., Lanthanide-based luminescent probes for selective time-gated detection of hydrogen peroxide in water and in living cells. *Chem. Commun.* **2010**, *46*, 7510-7512.
59. McMahon, B. K.; Gunnlaugsson, T., Selective detection of the reduced form of glutathione (GSH) over the oxidized (GSSG) form using a combination of glutathione reductase and a Tb(III)-cyclen

- maleimide based lanthanide luminescent ‘Switch On’ assay. *J. Am. Chem. Soc.* **2012**, *134*, 10725-10728.
60. Pershagen, E.; Nordholm, J.; Borbas, K. E., Luminescent lanthanide complexes with analyte-triggered antenna formation. *J. Am. Chem. Soc.* **2012**, *134*, 9832-9835.
61. de Silva, A. P.; Moody, T. S.; Wright, G. D., Fluorescent PET (Photoinduced Electron Transfer) sensors as potent analytical tools. *Analyst* **2009**, *134*, 2385-2393.
62. Othman, A. B.; Lee, J. W.; Wu, J.-S.; Kim, J. S.; Abidi, R.; Thuéry, P.; Strub, J. M.; Van Dorsselaer, A.; Vicens, J., Calix[4]arene-based, Hg²⁺-induced intramolecular fluorescence resonance energy transfer chemosensor. *J. Org. Chem.* **2007**, *72*, 7634-7640.
63. Zhang, X.; Xiao, Y.; Qian, X., A ratiometric fluorescent probe based on FRET for imaging Hg²⁺ ions in living cells. *Angew. Chem. Int. Ed.* **2008**, *47*, 8025-8029.
64. Jisha, V. S.; Thomas, A. J.; Ramaiah, D., Fluorescence ratiometric selective recognition of Cu²⁺ ions by dansyl–naphthalimide dyads. *J. Org. Chem.* **2009**, *74*, 6667-6673.
65. Zhao, J.; Ji, S.; Chen, Y.; Guo, H.; Yang, P., Excited state intramolecular proton transfer (ESIPT): from principal photophysics to the development of new chromophores and applications in fluorescent molecular probes and luminescent materials. *PCCP* **2012**, *14*, 8803-8817.
66. Demchenko, A. P.; Tang, K.-C.; Chou, P.-T., Excited-state proton coupled charge transfer modulated by molecular structure and media polarization. *Chem. Soc. Rev.* **2013**, *42*, 1379-1408.
67. Jung, H. S.; Park, M.; Han, D. Y.; Kim, E.; Lee, C.; Ham, S.; Kim, J. S., Cu²⁺ ion-induced self-assembly of pyrenylquinoline with a pyrenyl excimer formation. *Org. Lett.* **2009**, *11*, 3378-3381.
68. Wu, J.; Liu, W.; Ge, J.; Zhang, H.; Wang, P., New sensing mechanisms for design of fluorescent chemosensors emerging in recent years. *Chem. Soc. Rev.* **2011**, *40*, 3483-3495.
69. Kraft, A.; Grimsdale, A. C.; Holmes, A. B., Electroluminescent conjugated polymers—seeing polymers in a new light. *Angew. Chem. Int. Ed.* **1998**, *37*, 402-428.
70. Fan, C.; Wang, S.; Hong, J. W.; Bazan, G. C.; Plaxco, K. W.; Heeger, A. J., Beyond superquenching: Hyper-efficient energy transfer from conjugated polymers to gold nanoparticles. *Proc. Natl. Acad. Sci. USA* **2003**, *100*, 6297-6301.
71. Chen, J.; Law, C. C. W.; Lam, J. W. Y.; Dong, Y.; Lo, S. M. F.; Williams, I. D.; Zhu, D.; Tang, B. Z., Synthesis, light emission, nanoaggregation, and restricted intramolecular rotation of 1,1-substituted 2,3,4,5-tetraphenylsiloles. *Chem. Mater.* **2003**, *15*, 1535-1546.
72. Hong, Y.; Lam, J. W. Y.; Tang, B. Z., Aggregation-induced emission: phenomenon, mechanism and applications. *Chem. Commun.* **2009**, *0*, 4332-4353.

73. Wang, M.; Zhang, G.; Zhang, D.; Zhu, D.; Tang, B. Z., Fluorescent bio/chemosensors based on silole and tetraphenylethene luminogens with aggregation-induced emission feature. *J. Mater. Chem.* **2010**, *20*, 1858-1867.
74. Yang, G.; Morlet-Savary, F.; Peng, Z.; Wu, S.; Fouassier, J.-P., Triplet-triplet absorption of 2-(2'-hydroxyphenyl) benzoxazole (HBO) in polar solvents. *Chem. Phys. Lett.* **1996**, *256*, 536-542.
75. Li, Z.; Wu, S., The effect of molecular structure on the photophysical behavior of substituted styryl pyrazine derivatives. *Journal of Fluorescence* **1997**, *7*, 237-242.
76. Wang, P.; Wu, S., Spectroscopy and photophysics of bridged enone derivatives: effect of molecular structure and solvent. *J. Photochem. Photobiol., A* **1995**, *86*, 109-113.
77. Wu, J.-S.; Liu, W.-M.; Zhuang, X.-Q.; Wang, F.; Wang, P.-F.; Tao, S.-L.; Zhang, X.-H.; Wu, S.-K.; Lee, S.-T., Fluorescence turn on of coumarin derivatives by metal cations: a new signaling mechanism based on C=N isomerization. *Org. Lett.* **2006**, *9*, 33-36.
78. Eun Jun, M.; Roy, B.; Han Ahn, K., "Turn-on" fluorescent sensing with "reactive" probes. *Chem. Commun.* **2011**, *47*, 7583-7601.
79. Kojima, H.; Nakatsubo, N.; Kikuchi, K.; Kawahara, S.; Kirino, Y.; Nagoshi, H.; Hirata, Y.; Nagano, T., Detection and imaging of nitric oxide with novel fluorescent indicators: diamino fluoresceins. *Anal. Chem.* **1998**, *70*, 2446-2453.
80. Song, B.; Wang, G.; Tan, M.; Yuan, J., A europium(III) complex as an efficient singlet oxygen luminescence probe. *J. Am. Chem. Soc.* **2006**, *128*, 13442-13450.
81. Lippert, A. R.; Van de Bittner, G. C.; Chang, C. J., Boronate oxidation as a bioorthogonal reaction approach for studying the chemistry of hydrogen peroxide in living systems. *Acc. Chem. Res.* **2011**, *44*, 793-804.
82. Abo, M.; Urano, Y.; Hanaoka, K.; Terai, T.; Komatsu, T.; Nagano, T., Development of a highly sensitive fluorescence probe for hydrogen peroxide. *J. Am. Chem. Soc.* **2011**, *133*, 10629-10637.
83. Yang, D.; Wang, H.-L.; Sun, Z.-N.; Chung, N.-W.; Shen, J.-G., A highly selective fluorescent probe for the detection and imaging of peroxynitrite in living cells. *J. Am. Chem. Soc.* **2006**, *128*, 6004-6005.
84. Sun, Z.-N.; Wang, H.-L.; Liu, F.-Q.; Chen, Y.; Tam, P. K. H.; Yang, D., BODIPY-based fluorescent probe for peroxynitrite detection and imaging in living cells. *Org. Lett.* **2009**, *11*, 1887-1890.
85. Zhang, W.; Guo, C.; Liu, L.; Qin, J.; Yang, C., Naked-eye visible and fluorometric dual-signaling chemodosimeter for hypochlorous acid based on water-soluble p-methoxyphenol derivative. *Org. Biomol. Chem.* **2011**, *9*, 5560-5563.

86. Yu, F.; Li, P.; Li, G.; Zhao, G.; Chu, T.; Han, K., A Near-IR reversible fluorescent probe modulated by selenium for monitoring peroxyxynitrite and imaging in living cells. *J. Am. Chem. Soc.* **2011**, *133*, 11030-11033.
87. Garner, A. L.; St Croix, C. M.; Pitt, B. R.; Leikauf, G. D.; Ando, S.; Koide, K., Specific fluorogenic probes for ozone in biological and atmospheric samples. *Nat. Chem.* **2010**, *2*, 422-422.
88. Lin, V. S.; Chang, C. J., Fluorescent probes for sensing and imaging biological hydrogen sulfide. *Curr. Opin. Chem. Biol.* **2012**, *16*, 595-601.
89. Lippert, A. R.; New, E. J.; Chang, C. J., Reaction-based fluorescent probes for selective imaging of hydrogen sulfide in living cells. *J. Am. Chem. Soc.* **2011**, *133*, 10078-10080.
90. Montoya, L. A.; Pluth, M. D., Selective turn-on fluorescent probes for imaging hydrogen sulfide in living cells. *Chem. Commun.* **2012**, *48*, 4767-4769.
91. Das, S. K.; Lim, C. S.; Yang, S. Y.; Han, J. H.; Cho, B. R., A small molecule two-photon probe for hydrogen sulfide in live tissues. *Chem. Commun.* **2012**, *48*, 8395-8397.
92. Xu, K.; Qiang, M.; Gao, W.; Su, R.; Li, N.; Gao, Y.; Xie, Y.; Kong, F.; Tang, B., A near-infrared reversible fluorescent probe for real-time imaging of redox status changes in vivo. *Chem. Sci.* **2013**, *4*, 1079-1086.
93. Xu, Z.; Chen, X.; Kim, H. N.; Yoon, J., Sensors for the optical detection of cyanide ion. *Chem. Soc. Rev.* **2010**, *39*, 127-137.
94. Kubo, Y.; Tsukahara, M.; Ishihara, S.; Tokita, S., A simple anion chemosensor based on a naphthalene-thiuronium dyad. *Chem. Commun.* **2000**, *0*, 653-654.
95. Chung, Y. M.; Raman, B.; Kim, D.-S.; Ahn, K. H., Fluorescence modulation in anion sensing by introducing intramolecular H-bonding interactions in host-guest adducts. *Chem. Commun.* **2006**, *0*, 186-188.
96. Chen, X.; Zhou, Y.; Peng, X.; Yoon, J., Fluorescent and colorimetric probes for detection of thiols. *Chem. Soc. Rev.* **2010**, *39*, 2120-2135.
97. Jung, H. S.; Chen, X.; Kim, J. S.; Yoon, J., Recent progress in luminescent and colorimetric chemosensors for detection of thiols. *Chem. Soc. Rev.* **2013**.
98. Lee, M. H.; Yang, Z.; Lim, C. W.; Lee, Y. H.; Dongbang, S.; Kang, C.; Kim, J. S., Disulfide-Cleavage-Triggered Chemosensors and Their Biological Applications. *Chem. Rev.* **2013**.
99. Guo, Z.; Shin, I.; Yoon, J., Recognition and sensing of various species using boronic acid derivatives. *Chem. Commun.* **2012**, *48*, 5956-5967.
100. Wu, Z.; Zhang, Y.; Ma, J. S.; Yang, G., Ratiometric Zn²⁺ sensor and strategy for Hg²⁺ selective recognition by central metal ion replacement. *Inorg. Chem.* **2006**, *45*, 3140-3142.

101. Yu, M.-M.; Li, Z.-X.; Wei, L.-H.; Wei, D.-H.; Tang, M.-S., A 1,8-naphthyridine-based fluorescent chemodosimeter for the rapid detection of Zn^{2+} and Cu^{2+} . *Org. Lett.* **2008**, *10*, 5115-5118.
102. Xue, L.; Liu, Q.; Jiang, H., Ratiometric Zn^{2+} fluorescent sensor and new approach for sensing Cd^{2+} by ratiometric displacement. *Org. Lett.* **2009**, *11*, 3454-3457.
103. Xue, L.; Liu, C.; Jiang, H., Highly sensitive and selective fluorescent sensor for distinguishing cadmium from zinc ions in aqueous media. *Org. Lett.* **2009**, *11*, 1655-1658.
104. Lee, J. W.; Jung, H. S.; Kwon, P. S.; Kim, J. W.; Bartsch, R. A.; Kim, Y.; Kim, S.-J.; Kim, J. S., Chromofluorescent indicator for intracellular $\text{Zn}^{2+}/\text{Hg}^{2+}$ dynamic exchange. *Org. Lett.* **2008**, *10*, 3801-3804.
105. Lim, M. H.; Lippard, S. J., Fluorescence-based nitric oxide detection by ruthenium porphyrin fluorophore complexes. *Inorg. Chem.* **2004**, *43*, 6366-6370.
106. Pires, M. M.; Chmielewski, J., Fluorescence imaging of cellular glutathione using a latent rhodamine. *Org. Lett.* **2008**, *10*, 837-840.
107. Choi, M. G.; Cha, S.; Lee, H.; Jeon, H. L.; Chang, S.-K., Sulfide-selective chemosignaling by a Cu^{2+} complex of dipicolylamine appended fluorescein. *Chem. Commun.* **2009**, *0*, 7390-7392.
108. Sasakura, K.; Hanaoka, K.; Shibuya, N.; Mikami, Y.; Kimura, Y.; Komatsu, T.; Ueno, T.; Terai, T.; Kimura, H.; Nagano, T., Development of a highly selective fluorescence probe for hydrogen sulfide. *J. Am. Chem. Soc.* **2011**, *133*, 18003-18005.
109. Tsuge, K.; DeRosa, F.; Lim, M. D.; Ford, P. C., Intramolecular reductive nitrosylation: Reaction of nitric oxide and a copper(II) complex of a cyclam derivative with pendant luminescent chromophores. *J. Am. Chem. Soc.* **2004**, *126*, 6564-6565.
110. Lim, M. H.; Xu, D.; Lippard, S. J., Visualization of nitric oxide in living cells by a copper-based fluorescent probe. *Nat. Chem. Biol.* **2006**, *2*, 375-380.
111. Hitomi, Y.; Takeyasu, T.; Funabiki, T.; Kodera, M., Detection of enzymatically generated hydrogen peroxide by metal-based fluorescent probe. *Anal. Chem.* **2011**, *83*, 9213-9216.
112. Wade, C. R.; Gabbai, F. o. P., Fluoride anion chelation by a bidentate stibonium–borane lewis acid. *Organometallics* **2011**, *30*, 4479-4481.
113. Wade, C. R.; Ke, I.-S.; Gabbai, F. P., Sensing of aqueous fluoride anions by cationic stibine–palladium complexes. *Angew. Chem. Int. Ed.* **2012**, *51*, 478-481.
114. Ke, I.-S.; Myahkostupov, M.; Castellano, F. N.; Gabbai, F. P., Stibonium ions for the fluorescence turn-on sensing of F^- in drinking water at parts per million concentrations. *J. Am. Chem. Soc.* **2012**, *134*, 15309-15311.
115. Zhang, J. F.; Lim, C. S.; Bhuniya, S.; Cho, B. R.; Kim, J. S., A highly selective colorimetric and ratiometric two-photon fluorescent probe for fluoride ion detection. *Org. Lett.* **2011**, *13*, 1190-1193.

116. Kim, S. Y.; Hong, J.-I., Chromogenic and fluorescent chemodosimeter for detection of Fluoride in aqueous solution. *Org. Lett.* **2007**, *9*, 3109-3112.
117. Chae, M. Y.; Czarnik, A. W., Fluorometric chemodosimetry. Mercury(II) and silver(I) indication in water via enhanced fluorescence signaling. *J. Am. Chem. Soc.* **1992**, *114*, 9704-9705.
118. Kim, H. N.; Lee, M. H.; Kim, H. J.; Kim, J. S.; Yoon, J., A new trend in rhodamine-based chemosensors: application of spirolactam ring-opening to sensing ions. *Chem. Soc. Rev.* **2008**, *37*, 1465-1472.
119. Ko, S.-K.; Yang, Y.-K.; Tae, J.; Shin, I., In vivo monitoring of mercury ions using a Rhodamine-based molecular probe. *J. Am. Chem. Soc.* **2006**, *128*, 14150-14155.
120. Kim, J. H.; Kim, H. J.; Kim, S. H.; Lee, J. H.; Do, J. H.; Kim, H.-J.; Lee, J. H.; Kim, J. S., Fluorescent coumarinyldithiane as a selective chemodosimeter for mercury(II) ion in aqueous solution. *Tetrahedron Lett.* **2009**, *50*, 5958-5961.
121. Rao, A. S.; Kim, D.; Wang, T.; Kim, K. H.; Hwang, S.; Ahn, K. H., Reaction-based two-photon probes for mercury ions: fluorescence imaging with dual optical windows. *Org. Lett.* **2012**, *14*, 2598-2601.
122. Kierat, R. M.; Krämer, R., A fluorogenic and chromogenic probe that detects the esterase activity of trace copper(II). *Bioorg. Med. Chem. Lett.* **2005**, *15*, 4824-4827.
123. Chatterjee, A.; Santra, M.; Won, N.; Kim, S.; Kim, J. K.; Kim, S. B.; Ahn, K. H., Selective fluorogenic and chromogenic probe for detection of silver ions and silver nanoparticles in aqueous media. *J. Am. Chem. Soc.* **2009**, *131*, 2040-2041.
124. Zhou, Z.; Fahrni, C. J., A fluorogenic probe for the copper(I)-catalyzed azide-alkyne ligation reaction: modulation of the fluorescence emission via $3(n,\pi^*)-1(\pi,\pi^*)$ inversion. *J. Am. Chem. Soc.* **2004**, *126*, 8862-8863.
125. Garner, A. L.; Koide, K., Studies of a fluorogenic probe for palladium and platinum leading to a palladium-specific detection method. *Chem. Commun.* **2009**, *0*, 86-88.
126. Garner, A. L.; Koide, K., Oxidation state-specific fluorescent method for Palladium(II) and Platinum(IV) based on the catalyzed aromatic claisen rearrangement. *J. Am. Chem. Soc.* **2008**, *130*, 16472-16473.
127. Santra, M.; Ko, S.-K.; Shin, I.; Ahn, K. H., Fluorescent detection of palladium species with an O-propargylated fluorescein. *Chem. Commun.* **2010**, *46*, 3964-3966.
128. Song, F.; Watanabe, S.; Floreancig, P. E.; Koide, K., Oxidation-resistant fluorogenic probe for mercury based on alkyne oxymercuration. *J. Am. Chem. Soc.* **2008**, *130*, 16460-16461.
129. Do, J. H.; Kim, H. N.; Yoon, J.; Kim, J. S.; Kim, H.-J., A rationally designed fluorescence turn-on probe for the Gold(III) ion. *Org. Lett.* **2010**, *12*, 932-934.

130. Patil, N. T.; Shinde, V. S.; Thakare, M. S.; Hemant Kumar, P.; Bangal, P. R.; Barui, A. K.; Patra, C. R., Exploiting the higher alkynophilicity of Au-species: development of a highly selective fluorescent probe for gold ions. *Chem. Commun.* **2012**, *48*, 11229-11231.

131. Jung Jou, M.; Chen, X.; Swamy, K. M. K.; Na Kim, H.; Kim, H.-J.; Lee, S.-g.; Yoon, J., Highly selective fluorescent probe for Au³⁺ based on cyclization of propargylamide. *Chem. Commun.* **2009**, *0*, 7218-7220.

132. Taki, M.; Iyoshi, S.; Ojida, A.; Hamachi, I.; Yamamoto, Y., Development of highly sensitive fluorescent probes for detection of intracellular copper(I) in living systems. *J. Am. Chem. Soc.* **2010**, *132*, 5938-5939.

133. Au-Yeung, H. Y.; New, E. J.; Chang, C. J., A selective reaction-based fluorescent probe for detecting cobalt in living cells. *Chem. Commun.* **2012**, *48*, 5268-5270.

Chapter 2

Fluorescent molecular probes for Al³⁺

Papers based on this chapter have been published in *Chem. Commun.*, **2010**, 46, 4499-4501([Link](#)); *Inorg. Chem.*, **2010**, 49, 7229-7231 ([Link](#)); *Eur. J. Inorg. Chem.*, **2011**, 5479-5489 ([Link](#)); *Chem. Commun.*, **2012**, 48, 1039-1041 ([Link](#)).
Reproduced by permission of the Royal Society of Chemistry and John Wiley and Sons.

1. Introduction

Aluminium is used excessively in the modern world with diverse applications due to its many unusual combinations of properties.¹ It is the third most prevalent element and the most abundant metal in the biosphere accounting for approximately 8% of its mass. Such wide spread applications of aluminium lead to its presence across variety of domains such as in home, transportation, on land, sea, air, and industry. High concentrations of aluminium are known to cause toxicity in plants, fish, algae, bacteria and other species in aquatic ecosystems.² Environmental acidification due to increased solubility of aluminium minerals at lower pH increases the amount of available Al^{3+} which is deadly to growing plants.² Aluminium in its ionic form (Al^{3+}) has the ability to react with biological species by changing or suppressing their function leading to harmful effects. Aluminium can be toxic to humans in excessive amounts and even in small amounts if deposited in the brain.³⁻⁵ Excess aluminium is acquired by the use of antiperspirants, aluminium cookware, cans, bleached flour, antacids and drinking water supplies. According to WHO report the average daily human intake of aluminium is approx. 3-10 mg/day. Tolerable weekly aluminium intake in the human body is estimated to be 7 mg/kg body weight.^{6,7} The superfluous ingestion of aluminium influence the absorption of calcium in the bowel, causing the bone to soften, atrophy, even aberrance and also affect the absorption of iron in blood causing anaemia. Al^{3+} exerts several neurotoxic effects such as neurofibrillary, enzymatic and neurotransmitter changes in the central nervous system. The toxicity of aluminium exhibits damage of the central nervous system and suspected to be involved in neurodegenerative diseases such as Alzheimer's, Parkinson's, and responsible for intoxication in haemodialysis patients.^{4,8,9} Therefore the detection of Al^{3+} is crucial to control its concentration levels in the biosphere and direct impact on maintaining human health. At present, the main methods for aluminium detection are graphite furnace atomic absorption spectrometry and inductively coupled plasma atomic emission spectrometry. These techniques are relatively complex and involve expensive instrumentation. The design of fluorescent molecular probes for selective recognition and sensing of specific cations has attracted considerable interests due to their importance in biological and environmental applications. Detection of Al^{3+} has always been problematic due to the lack of spectroscopic characteristics and poor coordination ability

comparing to other transition metals. The presence of H⁺, alkali and alkaline earth metal ions do not allow the reduction of Al³⁺.¹⁰ Therefore, the development of fluorescent probes is critical in environmental and biological monitoring of aluminium ion. Probably a few fluorescent molecular probes have been reported for the detection of Al³⁺ with moderate success.^{8,11-14}

2. Rationality for designing molecular probes for aluminium

Chemical sensing¹⁵ involves the interaction between a target molecule (analyte) and a receptor (chemosensor) that is signalled by an easily detectable change.^{16,17} Most molecular probes rely on a binding event or a chemical reaction to change the optical characteristics of an appended chromophore reporter.^{18,19} Other molecular probes utilise changes in redox potential or conformation as a means of detection. The major challenge in the design of molecular probes is how to discriminate different metal ions with similar chemical properties.²⁰ Hard and soft acids and bases theory (HSAB) and Irving–Williams rule are general guiding principles for the design of related metal ionophores.²¹ Coordination atom, coordination number, coordination geometry or cavity size are some of the key factors in designing an ionophore.²² Additional non-covalent interactions may play synergetic roles in differentiating similar metal cations. For example, ancillary π –ligand and π –cation interactions favour the enhancement of the binding ability for soft transition metal cations from the second and third rows in the periodic table. Bidentate heteroaromatic ligands 2,2'-bipyridine and 1,10-phenanthroline are among the best known coordination agents for many metal ions.²³ These multidentate nitrogen ligands generally afford high binding affinities for metal ions due to the chelation effect. Since the advent of click chemistry in 2001, the 1,4-disubstituted triazole has become an increasingly common motif in chemical sensors.²⁴ Although these click-derived triazoles are generally used as a convenient method of ligation, their prevalence in molecular probes can be attributed to their ability to bind both cations and anions.²⁵ They may (1) contribute to the binding of the target analyte, (2) act as a linker between the binding site and the reporter, or (3) contribute to the reporter, usually as part of a conjugated fluorophore. Constrained pyrrolidinyl-triazolyl backbone in a molecular probe can induces right balance of conformational rigidity for binding particular metal ion.

Fluorophore dansyl moiety shows dual characteristic behavior as reporting and binding unit to a metal ion. Keeping this in mind, a novel **BD** based ionophore-fluorophore (fluoroionophore) conjugate has been designed for the selective detection of Al^{3+} .²⁶ Coumarin and its derivatives have been heavily used as fluorophores because of their tunable photophysical properties and significant fluorescent behavior in the visible region.²⁷ Coumarin-moiety can display a dual behavior i.e. reporting as well as binding to a metal ion.²⁸ Based on these design principles a new conformationally constrained **CB** conjugate with pyrrolidinyl-triazolyl backbone has been developed.²⁹ It is highly desirable to design molecular probe that shows differential optical response for multiple metal ions based on single emission mechanism. Later a novel fluoroionophore **QC** by conjugating two fluorophores (coumarin-hydroxyquinoline) by means of triazolyl-pyrrolidinyl linker is synthesized.³⁰ The oxygen atom and methylene groups in the linker backbone were expected to impart water-solubility.

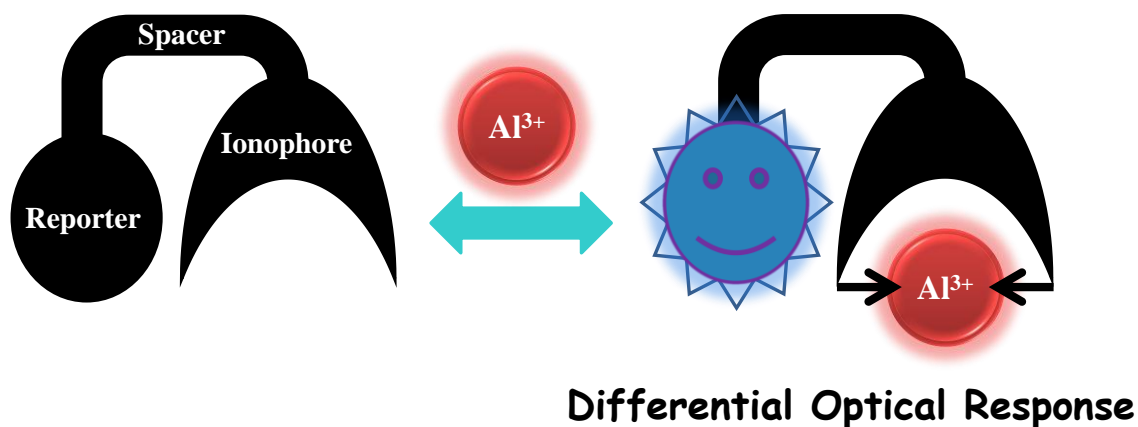


Figure 1. Basic structure of Al^{3+} selective molecular probe.

Synthesis of these three probes was achieved through very simple and high yielding click chemistry. Triazole moiety formed during click reaction served as both spacer and cation binding site. Fluorophore plays a dual role as reporting unit and cation binding site. These molecular probes can detect the Al^{3+} ion with differential optical response on the basis of ICT with high sensitivity and selectivity.³¹ This study opens up the new possibility of

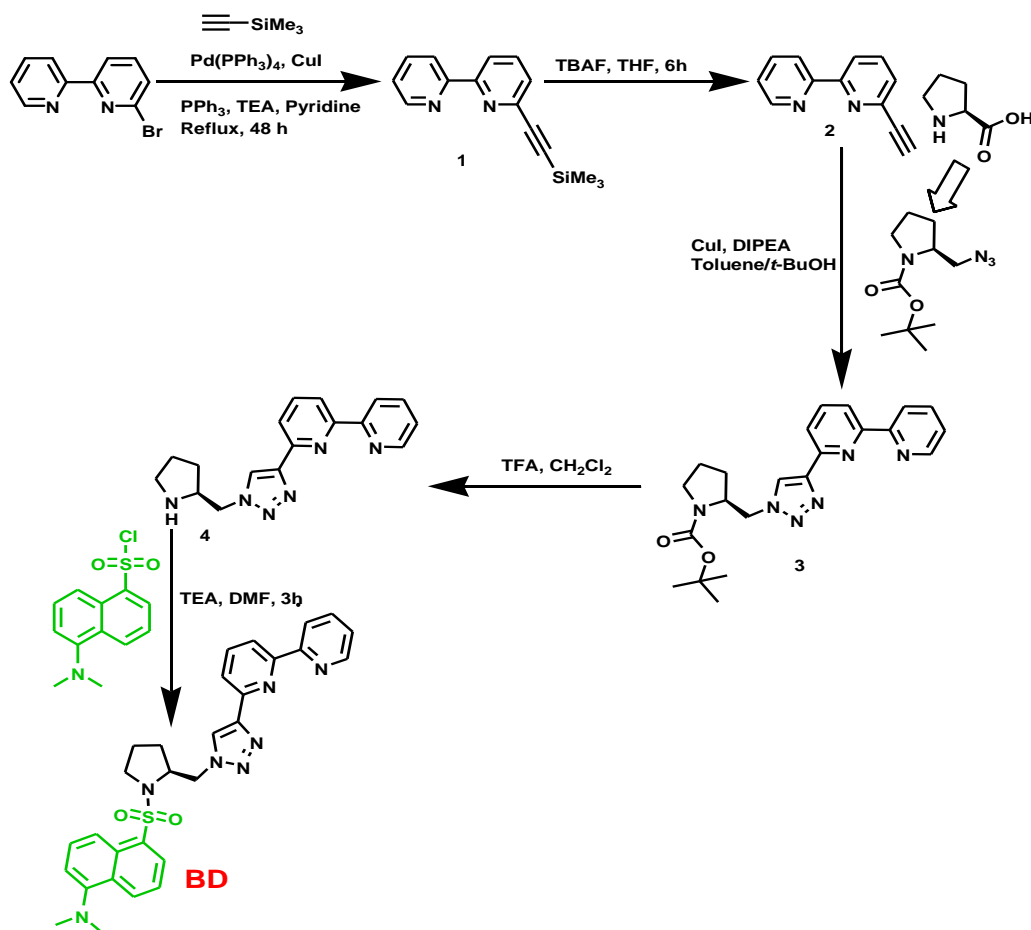
designing new family of highly selective probes for Al³⁺ based on fluorophore-ionophore click conjugates.

C=N isomerization as a new signaling mechanism was reported in 2007 based on the photophysical properties of conformationally restricted compounds.³² It was found that C=N isomerization is the predominant decay process of excited states in compounds with an unbridged C=N structure so those compounds are often nonfluorescent.²⁸ In contrast, the fluorescence of their analogs containing a covalently bridged C=N structure increases dramatically due to the suppression of C=N isomerization in the excited states.³³ Thus it is reasonable expected that C=N isomerization may also be inhibited through complexation of a metal ion to a suitably designed fluorescent-sensing molecule.^{34,35} Based on this hypothesis, naphthaldehyde-carbonohydrazone (**NC**) and naphthaldehyde-thiocarbonohydrazone (**NTC**) Schiff base ligands are designed as novel fluorescent chemosensors for Al³⁺ that use C=N isomerization as a signal system.³⁶ Probably these are the first examples where C=N isomerization has been exploited as a signal transduction mechanism for the recognition of the Al³⁺.

3.1 Pyrrolidine constrained bipyridyl-dansyl (BD) click molecular probe for Al³⁺

3.1.1 Synthesis

The synthesis of bipyridyl-dansyl based ligand **BD** was achieved through click chemistry approach (Scheme 1). The 1,2,3-triazole framework formed by the click reaction between alkyne and azide have been reported with anion and cation binding properties.²⁴ 6-Bromo-2,2'-bipyridine was converted to 6-trimethylsilylethynyl-2, 2'-bipyridine (**1**) via Sonogashira coupling.³⁷ Then it was reacted with tetra-*n*-butylammonium fluoride (TBAF) to form 6-ethynyl-2,2'-bipyridine (**2**). Boc-protected azido-pyrrolidine was synthesized from proline.³⁸ Boc-protected azido-pyrrolidine was subjected to click reaction with 6-ethynyl-2,2'-bipyridine to obtain click compound Boc-protected pyrrolidinyl-triazolyl-bipyridine (**3**).



Scheme 1. Synthesis of molecular probe **BD**.

After removal of Boc group using trifluoroacetic acid, free amine (pyrrolidinyl-triazolyl-bipyridine) (4) was condensed with dansyl chloride to obtain final probe **BD** in good yield.

3.1.2 Photophysical properties of bipyridyl-dansyl (**BD**) click molecular probe and its Al^{3+} detection

The photophysical properties of **BD** were investigated with fluorescence and absorption studies upon addition of several metal ions such as Li^+ , Na^+ , K^+ , Ag^+ , Mg^{2+} , Co^{2+} , Ba^{2+} , Sr^{2+} , Mn^{2+} , Fe^{2+} , Ni^{2+} , Cu^{2+} , Hg^{2+} , Pb^{2+} , Cd^{2+} , Zn^{2+} , In^{3+} and Al^{3+} in CH_3CN (Figure 2). The emission spectrum of free **BD** exhibit a band with maxima positioned around 532 nm upon excitation at 350 nm in CH_3CN . The examined alkali and alkaline earth metals exhibited no changes relative to **BD**, whereas d^{10} transition metal ions Zn^{2+} , Cd^{2+} , Ag^+ , Hg^{2+} , Pb^{2+} quench the emission intensity to different extent and rest of the transition metal ions used, completely quench the emission intensity. Interestingly Al^{3+} showed distinct behavior with quenching of emission intensity at 532 nm and appearance of new peak at 446 nm. This blue shift was accompanied by enhanced fluorescence intensity. Next change in fluorescence

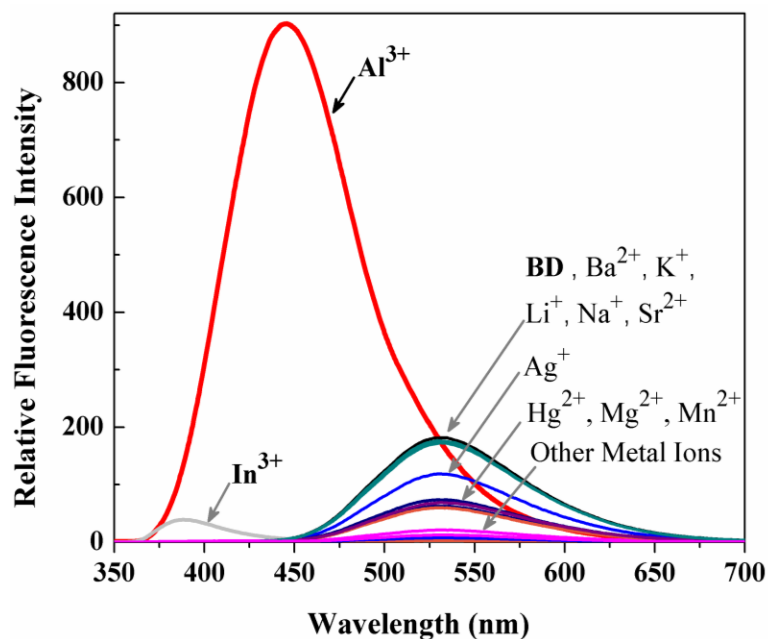


Figure 2. Fluorescence spectra of **BD** (100.0 μ M) and on addition of salts of Li^+ , Na^+ , K^+ , Ag^+ , Mg^{2+} , Co^{2+} , Ba^{2+} , Sr^{2+} , Mn^{2+} , Fe^{2+} , Ni^{2+} , Cu^{2+} , Hg^{2+} , Pb^{2+} , Cd^{2+} , Zn^{2+} , In^{3+} and Al^{3+} (1.0 equiv) in CH_3CN .

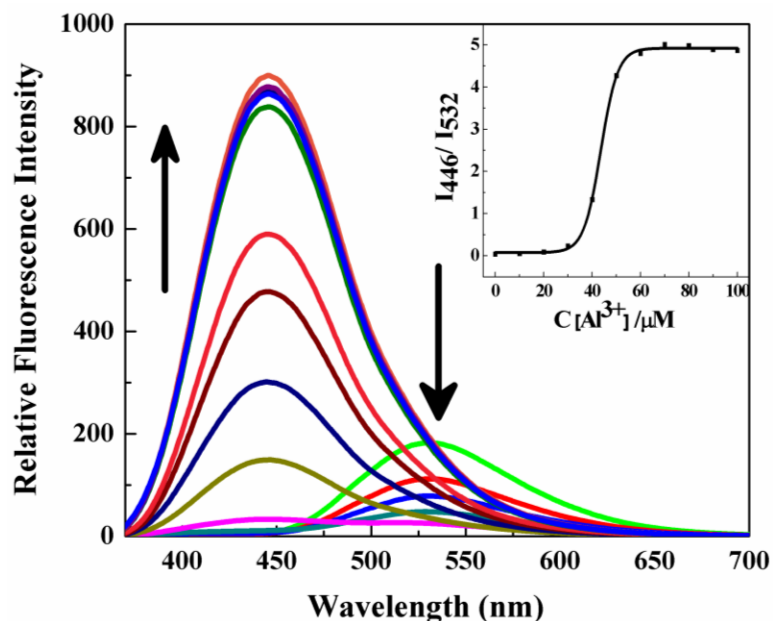


Figure 3. Fluorescence spectra of **BD** (100.0 μM) in CH_3CN upon addition of Al^{3+} (0, 10, 20, 30, 40, 50, 60, 70, 80, 90 and 100 μM). Inset: Ratiometric fluorescence intensity [I_{446}/I_{532}] as a function of [Al^{3+}].

behavior of **BD** was studied as a function of Al^{3+} concentration (Figure 3). Initially, quenching of the emission intensity around 532 nm due to binding of Al^{3+} to $-\text{N}(\text{CH}_3)_2$ of dansyl moiety reduce the electron transfer, thus suppressing the ICT process and causing the blue shift in emission spectra.³⁹ Further coordination of Al^{3+} to nitrogen atoms on the bipyridyl-triazole moiety suppress the PET quenching process, thus leading to an enhancement in the emission intensity.¹⁷ Emission intensity around 446 nm increased and attains saturation on reaching 1:1 ratio of **BD**: Al^{3+} . The host-guest complex formation via coordination of Al^{3+} with **BD** occurs through two N-atoms on bipyridyl, one each from triazole and dansyl rings.

The absorption study of **BD** was performed in presence of different metal ions at low concentrations (μM). This study showed no proper selectivity for a particular metal ion (Figure 4). The change in the emission color of **BD** was visible to naked eye under UV light at low concentrations (μM) of Al^{3+} . At higher concentration (mM) of Al^{3+} **BD** gave color changes in the visible light, which is corresponding to a new peak, positioned around 520 nm in the absorption spectrum (Figure 5). Higher concentrations of Al^{3+} can be easily detected by observing the change in color of **BD** solution by the naked eye in visible light. A similar

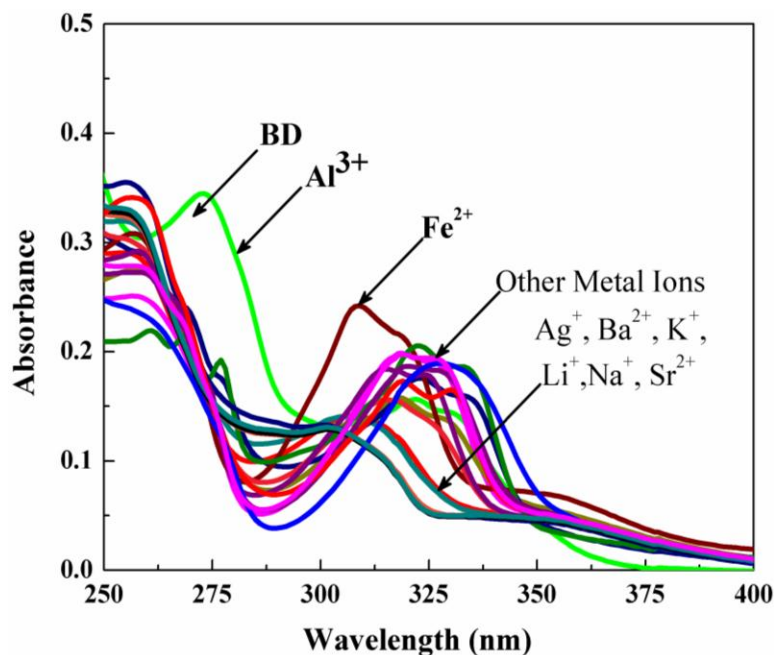


Figure 4. UV-Vis absorption spectra of **BD** [100.0 μ M] in the presence of different metal ions [100.0 μ M] in CH_3CN .

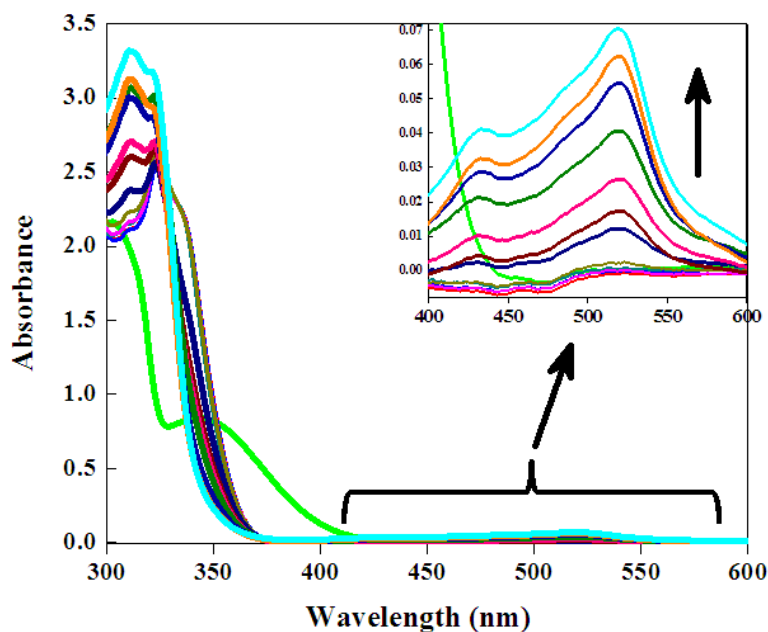


Figure 5. UV-Vis absorption spectra of **BD** (2.5 mM) in CH_3CN upon adding various concentrations of $Al(ClO_4)_3$ (0, 1.25, 2.5, 5, 12.5, 25, 62.5, 125, 187.5, 250, 500, 750 and 1000 mM). Inset: absorption intensity in range 400-600 nm as a function of $[Al^{3+}]$.

absorption band in the range of 400-600 nm was not observed in the absorption spectra of different concentrations of Al(ClO₄)₃ recorded in the absence of ligand. **BD** as chemosensor thus combines the sensitivity of fluorescence with the convenience and the aesthetic appeal of a colorimetric assay.

3.1.3 Competitive study for fluorometric detection of Al³⁺ using **BD**

To utilize **BD** as ion-selective fluorescence chemosensor for Al³⁺, the effect of competing metal ions was studied. For this purpose, **BD** was treated with 1 equiv of Al³⁺ in presence of other metal ions of the same concentration. Relatively low interference was observed for the detection of Al³⁺ in the presence of other metal ions (Figure 6). The **BD** responses for Al³⁺ in presence of Fe²⁺, Co²⁺, Ni²⁺, Zn²⁺, Cd²⁺ and Pb²⁺ are relatively low but clearly detectable. In case of Cu²⁺ and In³⁺, quenching of the fluorescence signal was observed. Thus **BD** can be used as a selective fluorescent sensor for Al³⁺ in the presence of most competing metal ions.

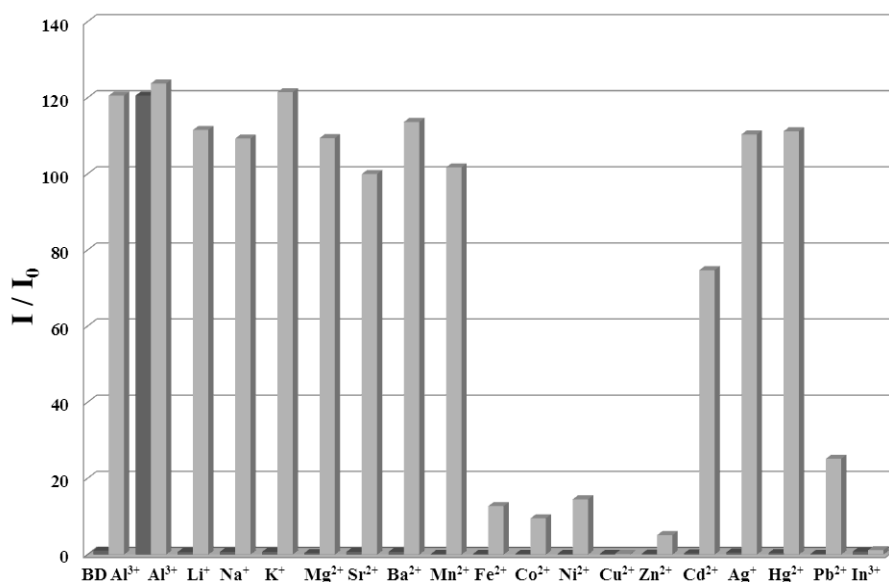


Figure 6. Relative fluorescence intensities of **BD** and its complexation with Al³⁺ in presence of various other metal ions. Dark grey bar: **BD** (100.0 μM) with 1 equiv of metal ion stated. Light grey bar: 100.0 μM of **BD** and 1 equiv of Al³⁺ with 1 equiv of metal ions stated. (for Al³⁺ effect 2 equiv of Al³⁺) ($E_{\lambda} = 446$ nm). The responses of the **BD** to Al³⁺, in the absence of competing ions, is included as controls, dark bar, no metal ion added, light bar, 100.0 μM of ligand **BD** with 1 equiv of Al³⁺.

3.1.4 Determination of binding stoichiometry and binding mode of **BD** with Al^{3+}

1H NMR spectra of **BD** on addition of various concentrations of Al^{3+} in CD_3CN were recorded to determine the mode of complexation. Significant spectral changes observed upon addition of Al^{3+} to **BD** are depicted in Figure 7. The main peaks considered for assigning the binding mode of **BD**: Al^{3+} are methyl protons (H_a) of dansyl moiety, triazole ring (H_b) and ortho position of the bipyridyl ring (H_c). Methyl protons undergo overall large downfield shift of 0.61 ppm upon addition of 1.0 equiv of Al^{3+} salt. This is a clear indication of the

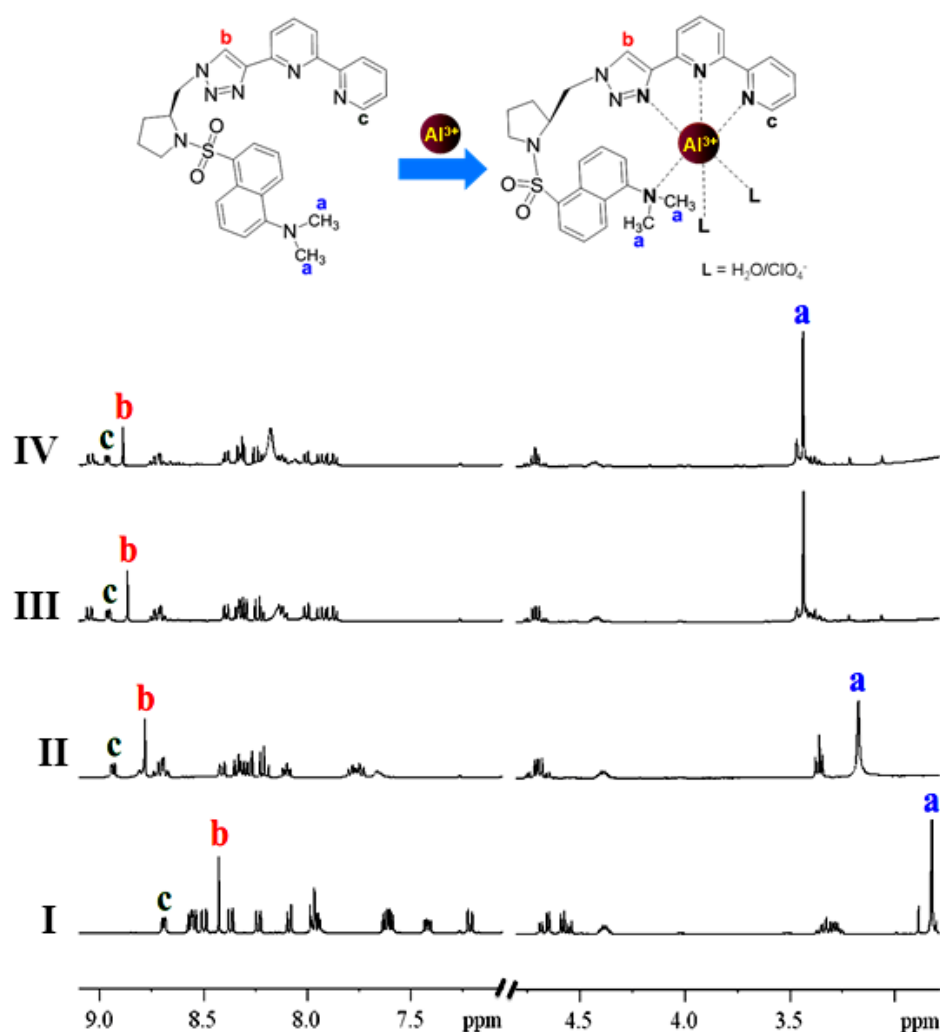


Figure 7. Binding mode of **BD**· Al^{3+} and 1H NMR spectra of **BD** with $Al(ClO_4)_3$ in CD_3CN . **BD** with (I) 0.0 equiv, (II) 0.5 equiv, (III) 1.0 equiv and (IV) 1.5 equiv of Al^{3+} .

direct involvement of $-\text{N}(\text{CH}_3)_2$ in coordinating with Al^{3+} . Similarly, peaks corresponding to triazole ring (H_b) and ortho-proton of bipyridyl ring (H_c) were downfield shifted by 0.44 and 0.27 ppm respectively. Downfield shift of other aromatic protons from bipyridyl and dansyl rings were also observed. There was no appreciable change observed in the peak positions on addition of > 1.0 equiv of Al^{3+} to **BD**. These observed downfield shifts of various protons suggest 1:1 binding stoichiometry for **BD**: Al^{3+} and tetra-coordination of Al^{3+} to **BD** through four nitrogens, two from bipyridyl, one from triazole ring and another one being the $-\text{N}(\text{CH}_3)_2$ of dansyl moiety. The hexa-coordination of Al^{3+} can be satisfied by two solvent molecules (or H_2O) or counter ions.

Job plot (Figure 8) showed 1:1 stoichiometric complexation between **BD** and Al^{3+} . The association constant ($\log K_a$) of **BD** for Al^{3+} was calculated to be 3.94 based on the fluorescence changes of **BD** upon gradual addition of the Al^{3+} (Figure 9).⁴⁰ The 1:1 binding stoichiometry determined from ^1H NMR, absorption and emission spectral studies, was also confirmed by CHNS elemental analysis. Elemental analysis data matched with the 1:1 complex of **BD**: Al^{3+} and two molecules of coordinated water. The 1:1 binding stoichiometry and overall hexa-coordination was further confirmed by mass data of **BD**: Al^{3+} complex (Figure 10). MALDI-MS showed exclusively the formation of **BD**· Al^{3+} · $2\text{H}_2\text{O}$ complex

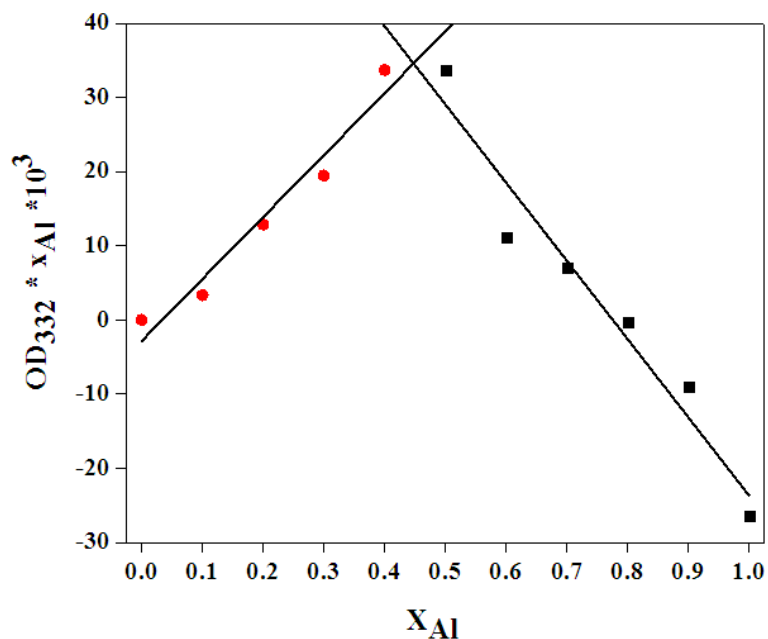


Figure 8. Job plot for the determination of the stoichiometry of **BD** and Al^{3+} in the complex.

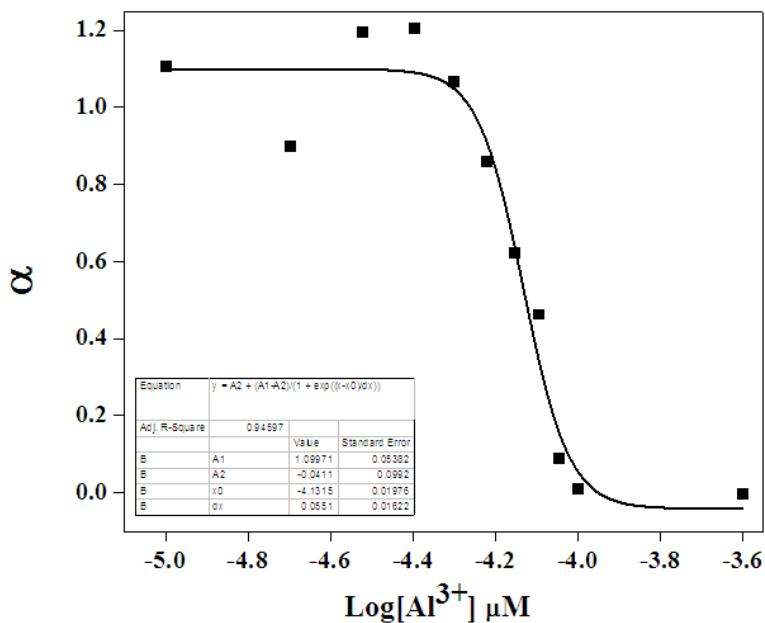


Figure 9. Response parameter values (α) as a function of the logarithm of Al^{3+} concentration. α is defined as the ratio between the free ligand (**BD**) concentration and the initial concentration of the ligand.

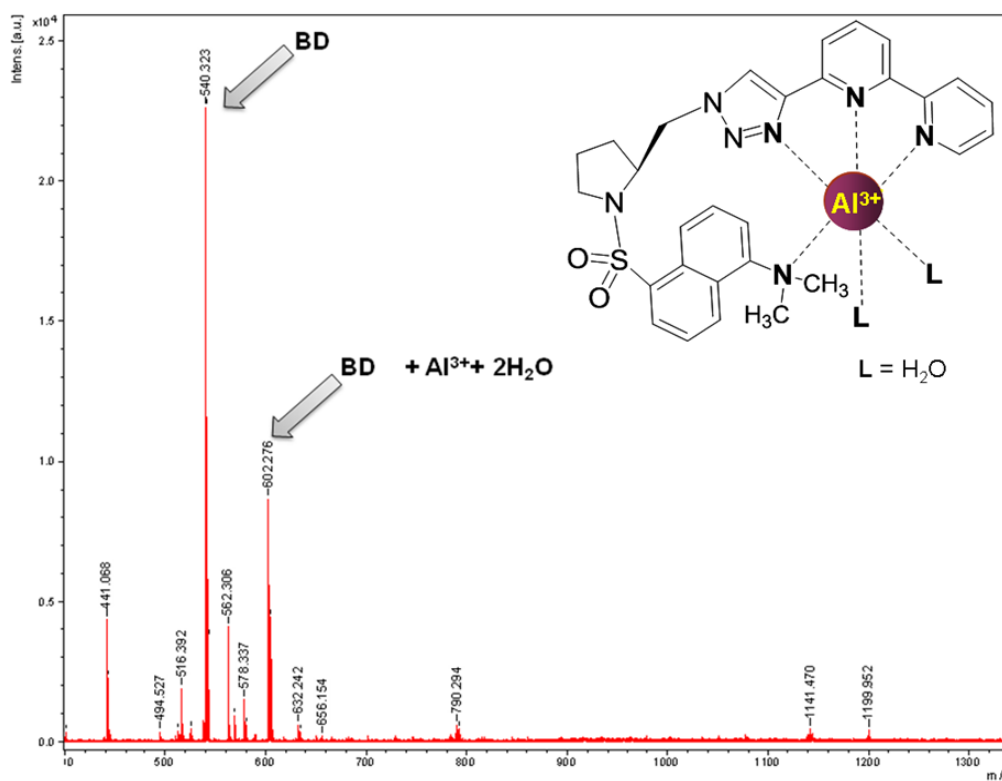


Figure 10. MALDI-TOF mass spectrum of complex $BD \cdot Al^{3+} \cdot 2H_2O$ in acetonitrile.

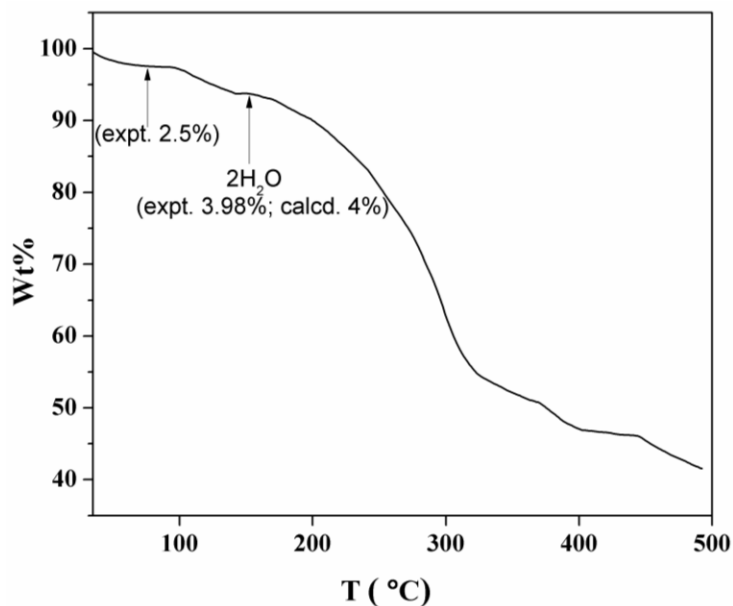


Figure 11. Thermogravimetric analysis of $\text{BD}\cdot\text{Al}^{3+}$ Complex. Experimentally 3.98% water loss is corresponding to two water molecules.

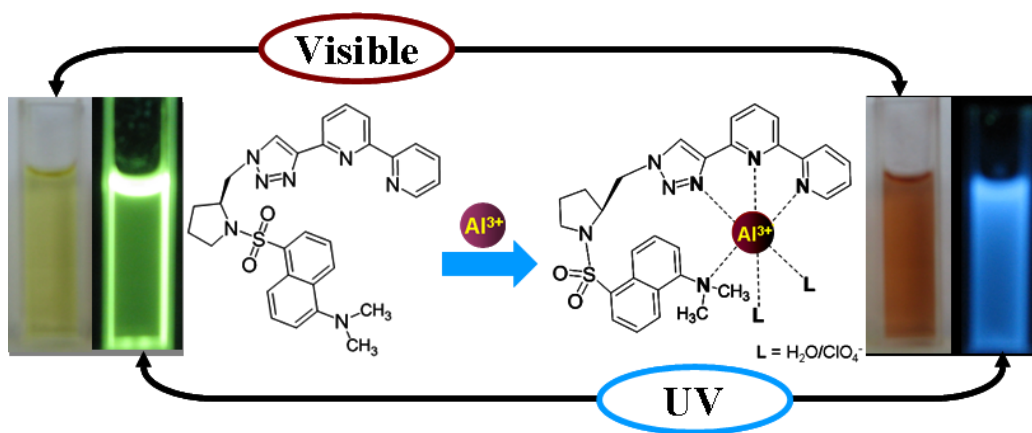


Figure 12. Color changes on addition of Al^{3+} to **BD** solution. Visible color change shown corresponding to addition of excess of Al^{3+} salt.

[MW: 602.27; calcd, 602.21 for $\text{C}_{29}\text{H}_{33}\text{AlCl}_3\text{N}_7\text{O}_{16}\text{S}$]. Coordination of two water molecules in the **BD**: Al^{3+} was also confirmed by thermogravimetric analysis (Figure 11).

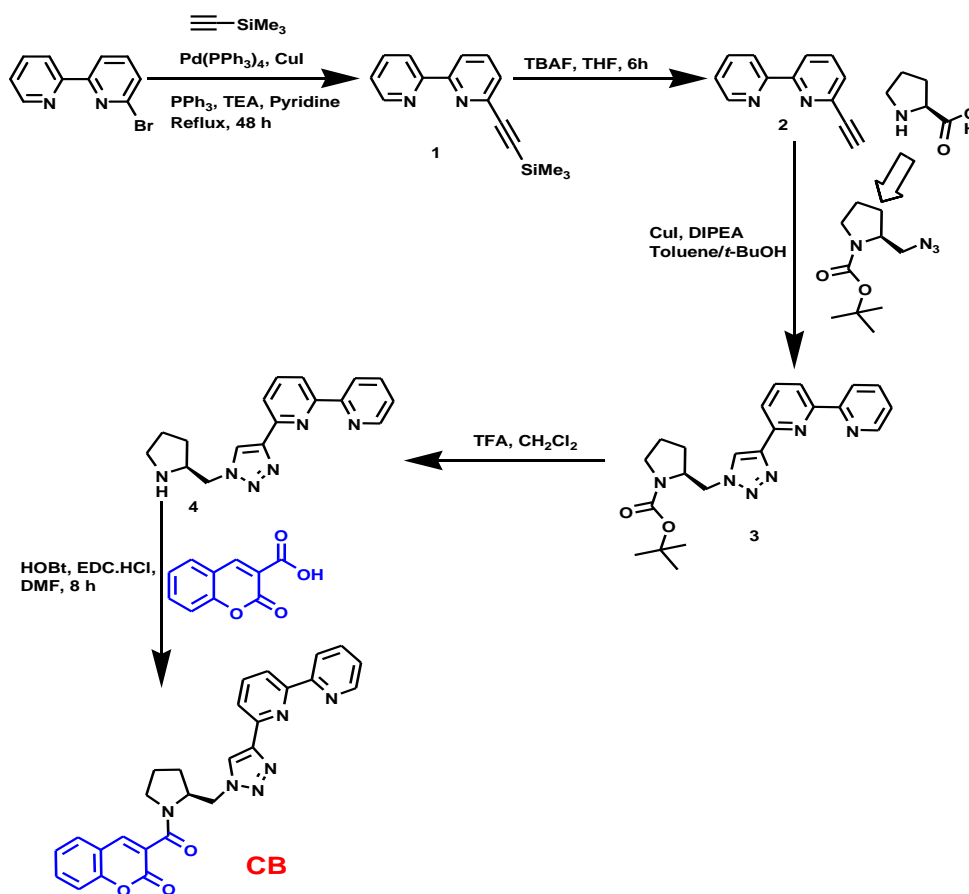
3.1.5 Conclusion

On the basis of rational designing of fluoroionophore, a new pyrrolidine constrained bipyridyl-dansyl (**BD**) molecular probe was synthesized through very simple and high yielding click chemistry. Triazole moiety formed during click reaction served as both spacer and cation binding site. Dansyl moiety also plays a dual role as reporting unit and cation binding site. Fluoroionophore **BD** can detect the Al³⁺ ion on the basis of ICT with high sensitivity and selectivity. **BD** can be used as a selective fluorescent sensor for Al³⁺ in the presence of most competing metal ions. **BD** binds Al³⁺ in 1:1 stoichiometry manner, determined from ¹H NMR, absorption and emission spectral studies and also confirmed by CHNS elemental analysis. This study opens up the new possibility of designing new family of highly selective chemosensors for a range of cations based on bipyridyl-fluorophore click conjugates.

3.2 Pyrrolidine constrained coumarin-bipyridyl (CB) click molecular probe for Al³⁺ detection

3.2.1 Synthesis

The synthesis of coumarin-pyrrolidinyl-triazolyl-bipyridyl **CB** conjugate was achieved through azide-alkyne click transformation as one of the key intermediate reaction. The 1,2,3-triazole frameworks formed by the click reaction have been widely investigated for its coordination properties.⁴¹⁻⁴⁶ **CB** was obtained through a straight forward synthetic route as shown in Scheme 2. 6-Bromo-2,2'-bipyridine was converted to 6-trimethylsilylethynyl-2,2'-bipyridine (1) via Sonogashira coupling.³⁷ Then it was treated with tetra-*n*-butylammonium fluoride (TBAF) to give 6-ethynyl-2,2'-bipyridine (2). Boc-protected azido-pyrrolidine synthesized from proline³⁸ was subjected to click reaction with 6-ethynyl-2,2'-bipyridine to



Scheme 2. Synthesis of molecular probe **CB**.

obtain click compound Boc-protected pyrrolidinyl-triazolyl-bipyridine (3). Free-amine (4) generated from the Boc-deprotection, was coupled to coumarin-3-carboxylic acid to obtain **CB** in excellent yield.

3.2.2 Photophysical properties of coumarin-bipyridyl (**CB**) click molecular probe and Al^{3+} detection

The photophysical properties of **CB** were investigated by monitoring absorption and fluorescence behavior upon addition of several metal ions in CH_3CN . **CB** exhibits an absorption band centered around 301 nm, which remains unchanged on addition of Li^+ , Na^+ , K^+ , Ag^+ , Ba^{2+} and Sr^{2+} . On addition of Mg^{2+} , Mn^{2+} , Co^{2+} , Hg^{2+} , Pb^{2+} , Cd^{2+} , Cu^{2+} , Zn^{2+} , In^{3+} and Al^{3+} slight red shift in the absorption maxima to different extents was observed (Figure 13). In case of Al^{3+} , the absorption maximum was red shifted to 324 nm (Figure 14). A clear isobestic point was observed at 312 nm on recording the spectra with varying concentrations of Al^{3+} .¹² The observed changes in fluorescence emission are shown in Figure 15. At 320 nm

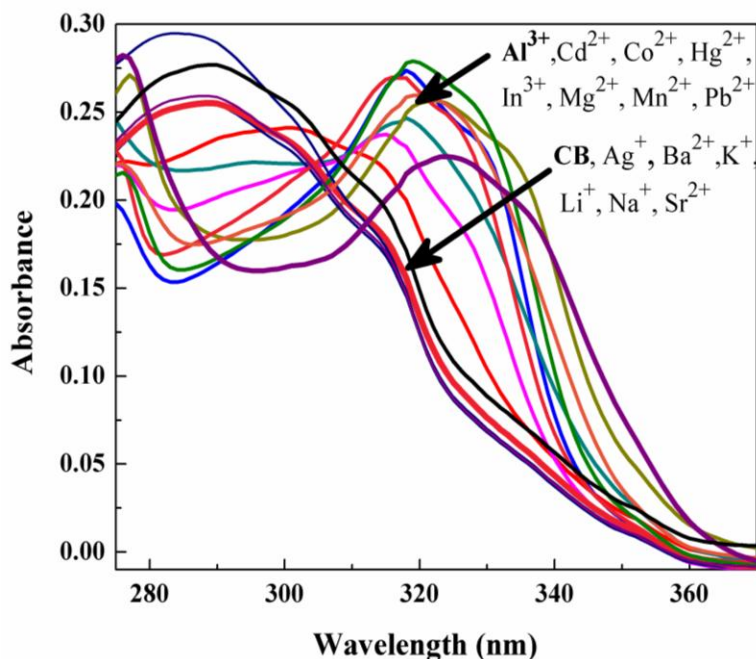


Figure 13. UV-Vis absorption spectra of **CB** (50 μ M) in the presence of 50 equiv of different metal ions in CH_3CN .

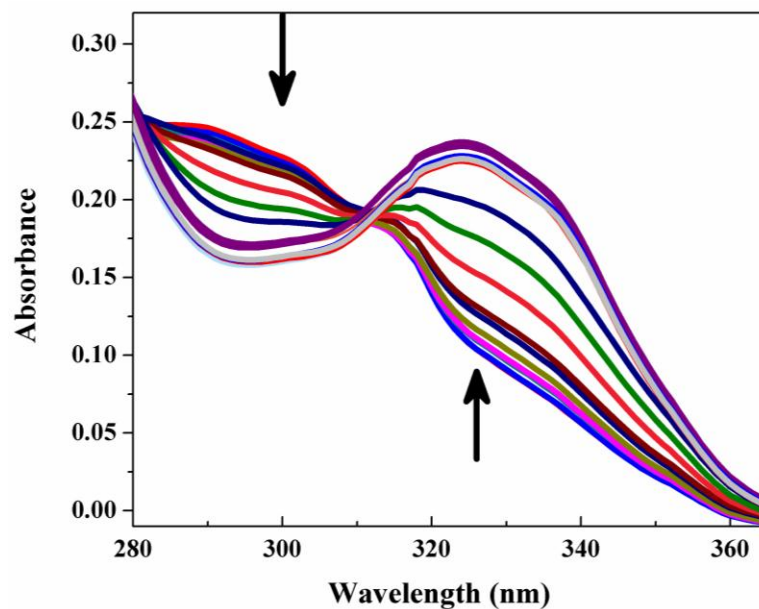


Figure 14. UV-Vis absorption spectra of CB (50 μ M) upon addition of 0.0, 0.5, 1, 2, 4, 6, 8, 10, 15, 20, 30, 40, 50, 60, 80, 100, 150, 200 μ M of Al^{3+} in CH_3CN .

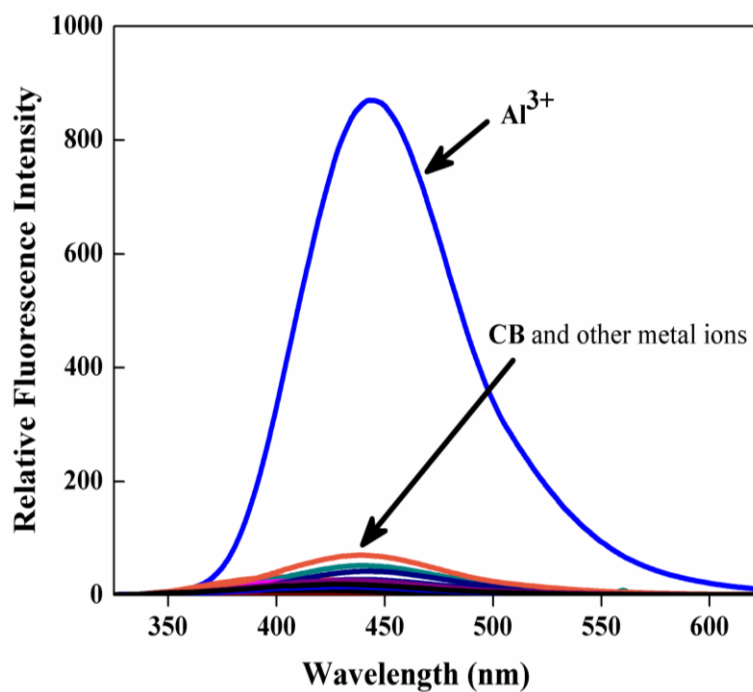


Figure 15. Fluorescence spectra of CB (25.0 μ M) and on addition of salts (50.0 equiv) of Li^+ , Na^+ , K^+ , Ag^+ , Mg^{2+} , Co^{2+} , Ba^{2+} , Sr^{2+} , Hg^{2+} , Pb^{2+} , Cd^{2+} , Mn^{2+} , Cu^{2+} , Zn^{2+} , In^{3+} and Al^{3+} in CH_3CN .

excitation, **CB** alone did not show any significant fluorescence. Coumarin fluorescence is quenched due to photoinduced electron transfer (PET) from pyrrolidine-triazolyl-bipyridyl moiety. When the ionophore coordinates to the target metal ion, the energy gap between the two HOMO orbitals is changed from positive to negative due to the decreasing level of the ionophore HOMO via metal coordination, and the fluorescence of the probe is recovered.²¹ Addition of Li^+ , Na^+ , K^+ , Ag^+ , Ba^{2+} and Sr^{2+} have no effect on the fluorescence emission whereas Mg^{2+} , Mn^{2+} , Co^{2+} , Hg^{2+} , Pb^{2+} , Cd^{2+} , Cu^{2+} , Zn^{2+} and In^{3+} responded with very little enhancement in fluorescent intensity. In contrast, the addition of Al^{3+} resulted in large enhancement of emission intensity positioned around 443 nm, as shown in Figure 16. Furthermore, Al^{3+} can be detected at least down to 1.0×10^{-7} M when **CB** was employed at 25 μ M concentration (Figure 17). Enhancement of the fluorescence intensity of CB is presumably due to metal binding to bipyridyl-triazolyl moiety followed by PET suppression. There were no obvious changes in the fluorescence response to Al^{3+} with different counter ions (Figure 18).

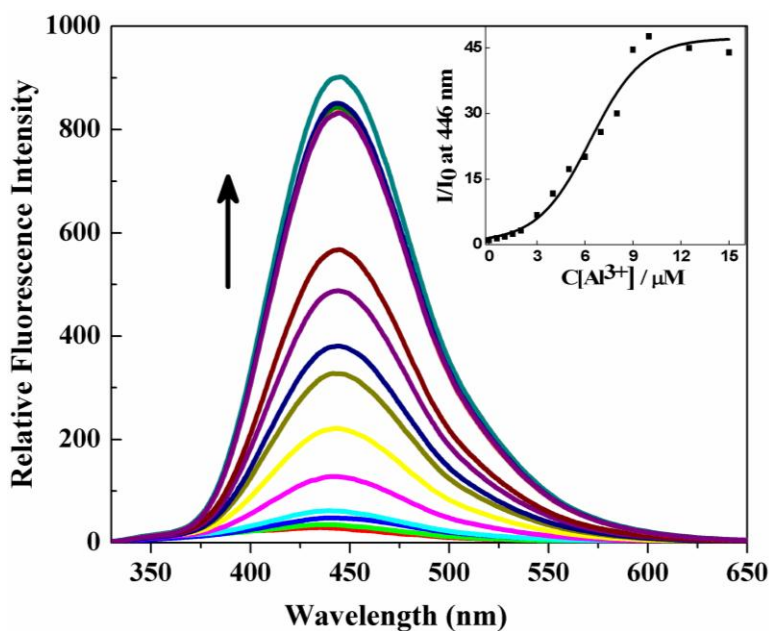


Figure 16. Fluorescence spectra of **CB** (25 μ M) in CH_3CN upon addition of $Al(ClO_4)_3$ (0, 0.5, 1, 1.5, 2, 3, 4, 5, 6, 7, 8, 9, 10, 12.5, 15 and 25 μ M) with an excitation of 320 nm. Inset: Fluorescence intensity at 443 nm as a function of $[Al^{3+}]$.

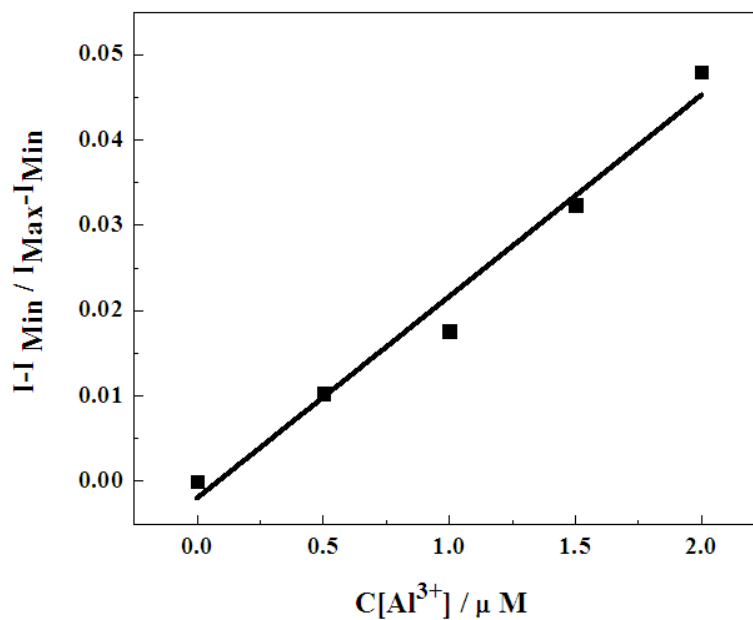


Figure 17. Emission (at 443 nm) of **CB** at different concentrations of Al^{3+} (0, 0.5, 1.0, 1.5, 2.0 μM) added, normalized between the minimum emission (0.0 μM Al^{3+}) and the maximum emission intensity. The detection limit was determined to be 1×10^{-7} μM .

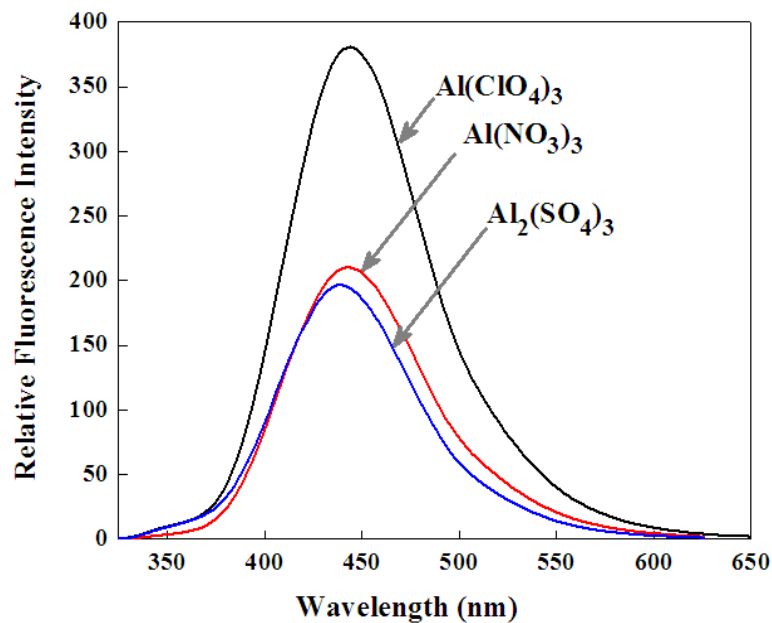


Figure 18. The fluorescence responses of **CB** (25.0 μM) to 5 equiv Of $\text{Al}(\text{ClO}_4)_3$, $\text{Al}(\text{NO}_3)_3$, $\text{Al}_2(\text{SO}_4)_3$ in CH_3CN .

3.2.3 Competitive study for fluorometric detection of Al³⁺ using CB

Al³⁺ selectivity of fluorescence chemosensor **CB** was studied in presence of various competing metal ions. For this purpose, 25.0 μM of **CB** was treated with 1 equiv of Al³⁺ in presence of 20 equiv of other metal ions. Data in Figure 19 show that there is no interference for the detection of Al³⁺ in presence of most of the metal ions used in the competitive binding studies. In case of In³⁺, quenching of the fluorescence signal was observed. The response of **CB** for Al³⁺ detection in presence of Co²⁺ and Pb²⁺ are relatively low but clearly detectable. Thus **CB** can be used as a selective fluorescent sensor for Al³⁺ detection in the presence of most competing metal ions.

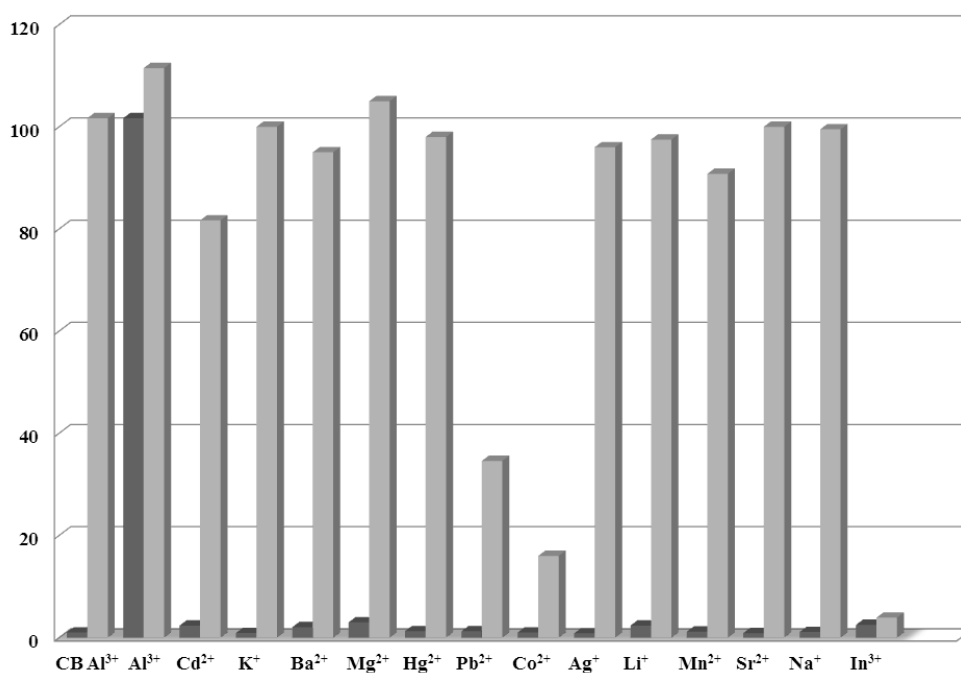


Figure 19. Relative fluorescence of **CB** and its complexation with Al³⁺ in presence of various metal ions. Dark grey bar: **CB** (25.0 μM) with 20 equiv of metal ion stated. Light grey bar: 25.0 μM of **CB** and 20 equiv of Al³⁺ with 20 equiv of metal ions stated. (for Al³⁺ effect, 40 equiv of Al³⁺) ($E_{\lambda} = 443$ nm). The response of the **CB** is included as controls, dark bar: no metal ion added, light bar: 25.0 μM of **CB** with 20 equiv of Al³⁺.

3.2.4 Determination of binding stoichiometry and binding mode of **CB** with Al^{3+}

For determination of stoichiometry of complexation and binding mode of **CB** with Al^{3+} , NMR spectroscopy was used. 1H NMR spectra of **CB** were recorded in CD_3CN on addition of various concentrations of Al^{3+} . The main peaks considered for assigning the binding mode of **CB**: Al^{3+} are β -proton (H_a) of coumarin-moiety, triazole ring (H_b) and ortho-proton of the bipyridyl ring (H_c). Significant spectral changes were observed upon addition of Al^{3+} as shown in Figure 20. Coumarin β -proton (H_a) undergoes overall large downfield shift of 0.51 ppm upon addition of 1.0 equiv of Al^{3+} salt. This is a clear indication of the direct involvement of coumarin-moiety in coordinating with Al^{3+} . Similarly, peaks corresponding

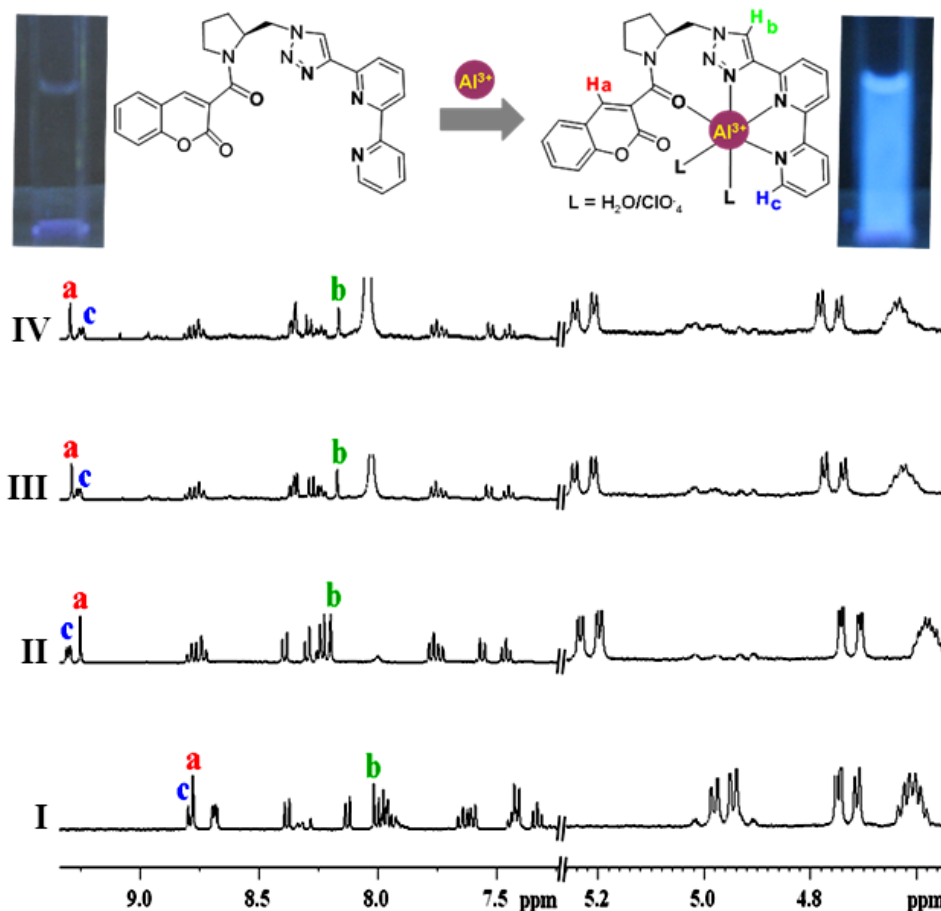


Figure 20. Binding mode of **CB**• Al^{3+} and 1H NMR spectra of **CB** with $Al(ClO_4)_3$ in CD_3CN . I) **CB**, II) **CB** with 0.5 equiv of Al^{3+} , III) **CB** with 1.0 equiv of Al^{3+} and IV) **CB** with 1.5 equiv of Al^{3+} .

to triazole ring (H_b) and ortho-proton of bipyridyl ring (H_c) were downfield shifted by 0.16 and 0.47 ppm respectively. There were no appreciable changes with any of the proton signals on addition of > 1.0 equiv of Al^{3+} to **CB** suggesting 1:1 binding stoichiometry for **CB**: Al^{3+} .

Job plot obtained from emission data showed the 1:1 stoichiometric complexation between **CB** and Al^{3+} (Figure 21). Response parameter α which is defined as the ratio of free ligand concentration to the initial concentration of ligand is plotted as a function of Al^{3+} concentration (Figure 22). This plot can serve as the calibration curve for the detection of Al^{3+} . The association constant ($\log K_a$) of **CB** for Al^{3+} was calculated to be 5.08.⁴⁰ The 1:1

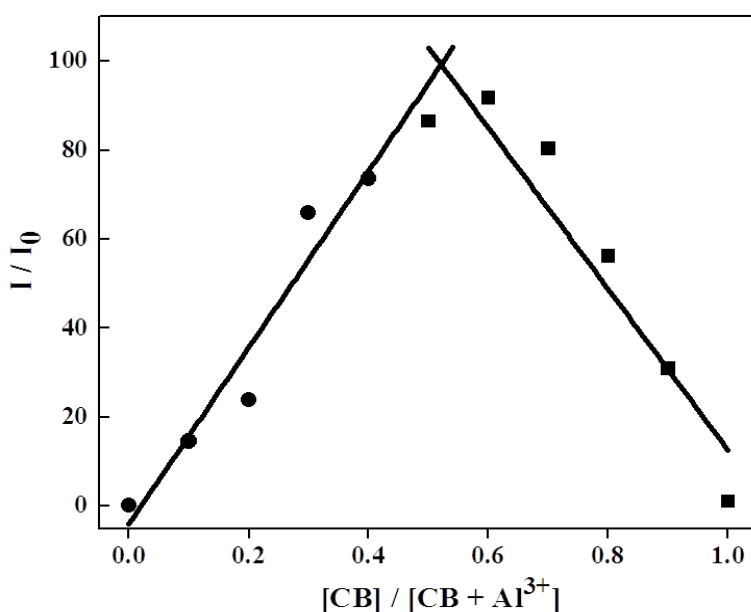


Figure 21. Job plot for the determination of the stoichiometry of **CB** and Al^{3+} in the complex.

binding stoichiometry determined from 1H NMR and emission spectral studies was further confirmed by elemental analysis data which matches with the 1:1 complex of **CB**• $Al(ClO_4)_3$ and two coordinating water molecules. This data was also supported by mass data of **CB**: Al^{3+} complex. MALDI/TOF-MS shows the formation of **CB**• Al^{3+} • $2H_2O$ complex [MW: 541.14; calcd, 541.18 for $C_{27}H_{26}AlN_6O_5$ (Figure 23). In IR spectra, stretching frequency of amide carbonyl of coumarin-moiety was significantly decreased by $\sim 26\text{ cm}^{-1}$ upon Al^{3+} binding and suggests coordination to amide carbonyl-oxygen (Figure 24). Thus Al^{3+} binding to **CB** through three nitrogens (two from bipyridyl, one from triazole ring) and amide carbonyl-

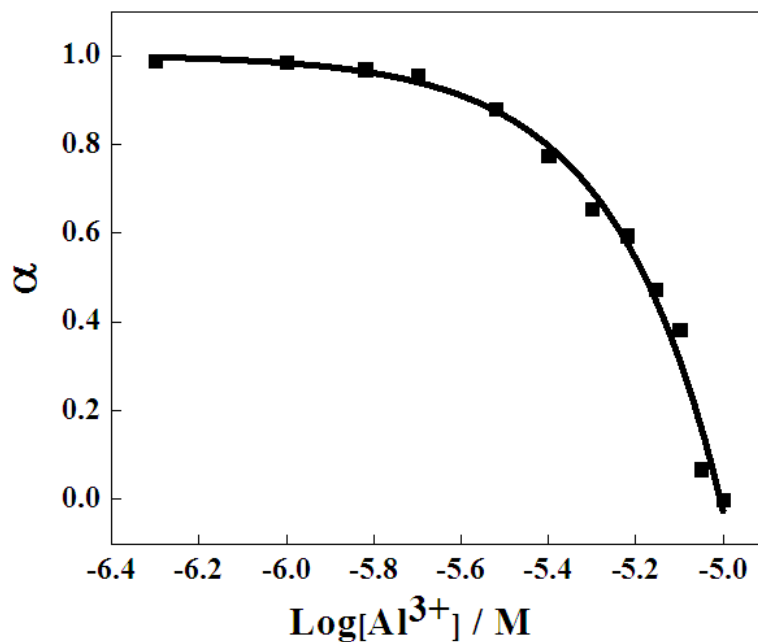


Figure 22. Response parameter values (α) as a function of the logarithm of Al^{3+} concentration. α is defined as the ratio between the free ligand concentration and the initial concentration of ligand.

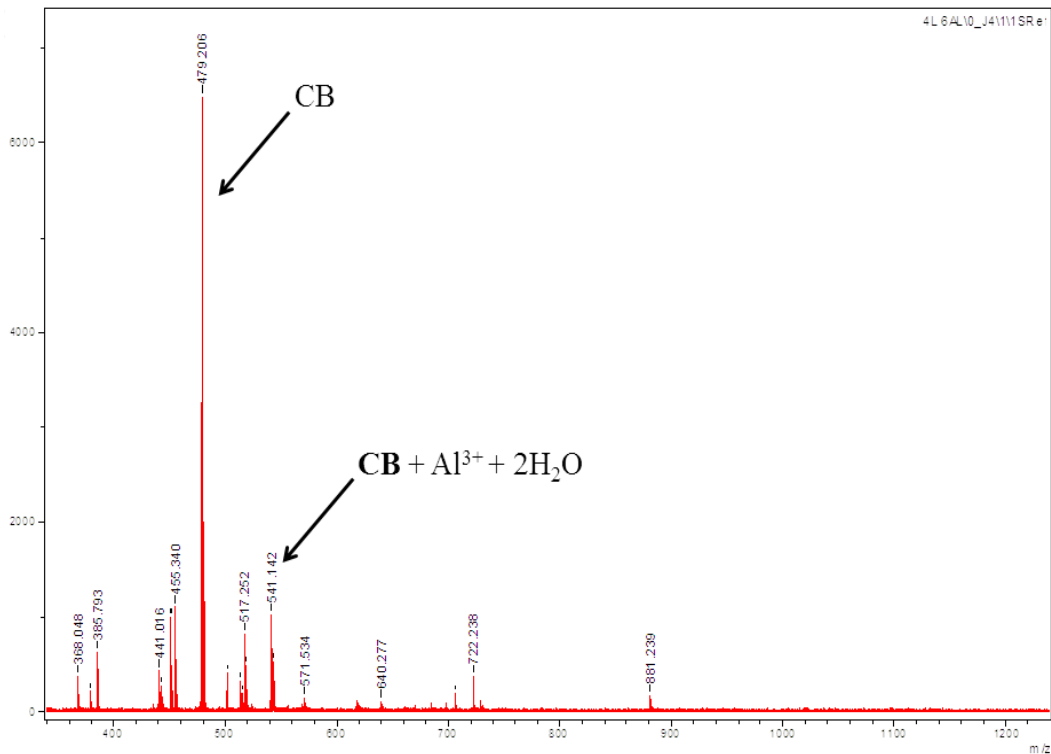


Figure 23. MALDI-TOF mass spectrum of complex $CB \cdot Al^{3+} \cdot 2H_2O$ in CH_3CN .

oxygen (Figure 20). The hexa-coordination of Al³⁺ can be satisfied by water molecules or counter ions. From the above spectroscopic studies, it can be concluded that metal binding to the amide carbonyl-oxygen leads to a red shift in the absorption band of **CB** by ICT.⁴⁷

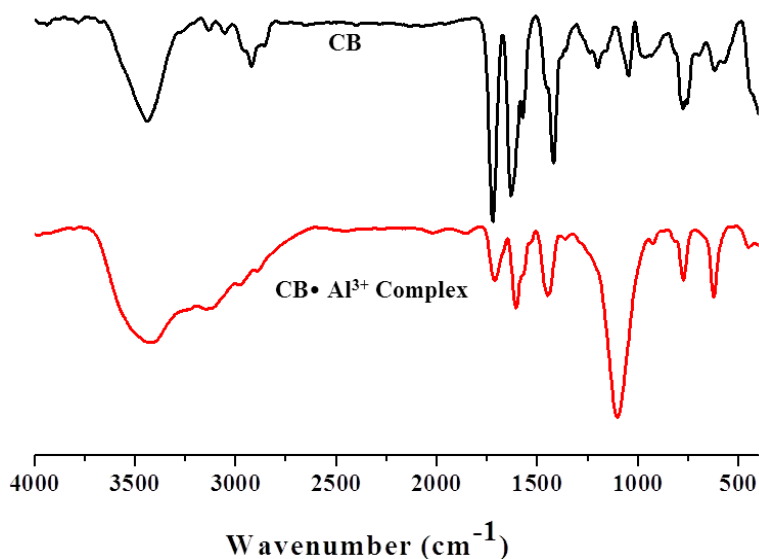


Figure 24. IR spectra of **CB** and **CB·Al³⁺** complex.

3.2.5 Conclusion

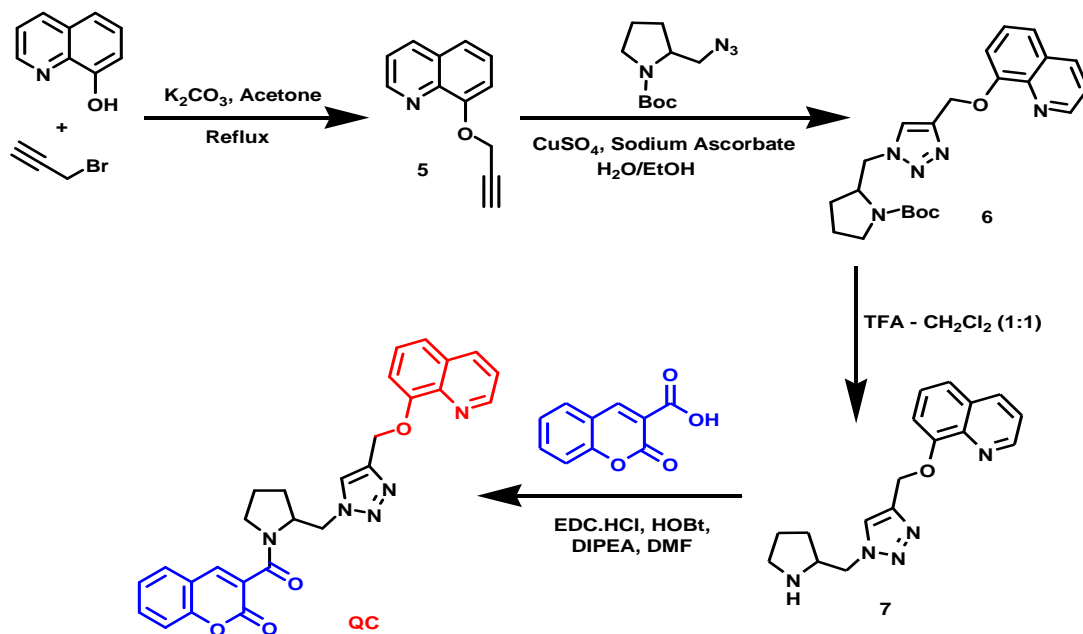
In conclusion, a conformationally constrained coumarin-bipyridyl (**CB**) chemosensor was developed utilizing click chemistry protocols. The triazole spacer serves as cation binding site and coumarin-moiety plays a dual role as reporting unit as well as cation binding site. **CB** detects the Al³⁺ ion with high sensitivity and selectivity on the basis of suppression of photoinduced electron transfer (PET) upon metal ion coordination. **CB** shows enhanced fluorescence in presence of Al³⁺, allowing its detection in presence of most competing metal ions. **CB** binds Al³⁺ in 1:1 stoichiometry manner, determined from ¹H NMR, absorption and emission spectral studies and also confirmed by CHNS elemental analysis. **CB** can be used as a selective fluorescent chemosensor for Al³⁺ detection in the presence of other most competing metal ions.

3.3 Pyrrolidine constrained quinoline-coumarin (QC) click molecular probe for dual-mode ratiometric detection of Al³⁺

Molecular probes with differential response towards multiple analytes are cost effective and would be highly desirable from the point of practical applications. Photoinduced electron transfer (PET)-based molecular probes exhibit changes in emission intensity with little or no spectral shift, whereas internal charge transfer (ICT) sensors exhibit both intensity changes and spectral shifts. However, developing such sensors with multiple analyte recognition capability is a challenging task. Investigating the concentration levels of free metal ions such as Zn²⁺ and Al³⁺ in analyte samples is difficult due to lack of spectroscopic properties.^{48,49} It is highly desirable to design molecular probe that shows differential optical response for multiple metal ions based on single emission mechanism. A novel quinoline-coumarin (QC) fluorescent molecular probe was designed. Quinoline and coumarin moieties were combined through pyrrolidine-triazolyl spacer for multiple ion selectivity. Quinoline and coumarin individually show dual behavior of reporting as well as chelation to a metal ion.^{50,51}

3.3.1 Synthesis

The QC molecular probe was synthesized for fluorometric detection of Zn²⁺ and Al³⁺ based on ICT mechanism. Azide-alkyne click addition was employed as one of the key intermediate reactions in the synthesis of QC conjugate.²⁴ Ligand QC was accessed through a high yielding synthetic route shown in Scheme 3. 8-Hydroxyquinoline was alkylated under basic condition with propargyl bromide to give 8-(propargyloxy)quinoline (5). Boc-protected azido-pyrrolidine was synthesized from proline.³⁸ Quinoline-alkyne was subjected to Cu(I) catalyzed 1,3-cycloaddition with Boc-protected pyrrolidinyl-azide to obtain Boc-pyrrolidinyl-triazolyl-quinoline (6). After Boc group deprotection of triazole intermediate, free amine (7) was coupled to coumarin carboxylic acid to obtain quinoline-coumarin (QC) molecular probe in excellent yield. The oxygen atom and methylene groups in the linker backbone were expected to impart water-solubility and multiple ion selectivity through right balance of conformational rigidity.



Scheme 3. Synthesis of molecular probe QC.

3.3.2 Photophysical properties of quinoline-coumarin (QC) click molecular probe and dual-mode ratiometric detection of Al^{3+}

The photophysical property of QC was investigated upon addition of different metal ions such as Li^+ , Na^+ , K^+ , Ba^{2+} , Sr^{2+} , Mg^{2+} , Ca^{2+} , Mn^{2+} , Fe^{2+} , Co^{2+} , Ni^{2+} , Cu^{2+} , Zn^{2+} , Cd^{2+} , Ag^+ , Hg^{2+} , Pb^{2+} and Al^{3+} in mixed solvent media (acetonitrile/water =9/1) (Figure 25). The emission spectrum of free QC ligand showed a weak band with emission maxima positioned around 400 nm upon excitation at 340 nm. The examined alkali and alkaline earth metals exhibited no changes relative to emission spectrum of QC. While transition metal ions Mn^{2+} , Co^{2+} , Ni^{2+} , Cu^{2+} , Zn^{2+} , Ag^+ and Hg^{2+} quenched the emission intensity of ligand to a different extent. Cd^{2+} showed little enhancement in emission, whereas Fe^{2+} and Pb^{2+} red shifted ligand emission band to 480 nm. In case of Zn^{2+} , the spectra is red shifted to 418 nm with four fold enhancement in the fluorescence intensity of QC as a typical of ICT based optical response. Blue emission intensity increased with the concentration of Zn^{2+} in titration experiment (Figure 26). In contrast, Al^{3+} exhibited distinct behavior by quenching of emission intensity of the ligand at 400 nm with the appearance of a new band at 484 nm (green emission). The red shift in emission band was accompanied by four fold enhancement in the fluorescence

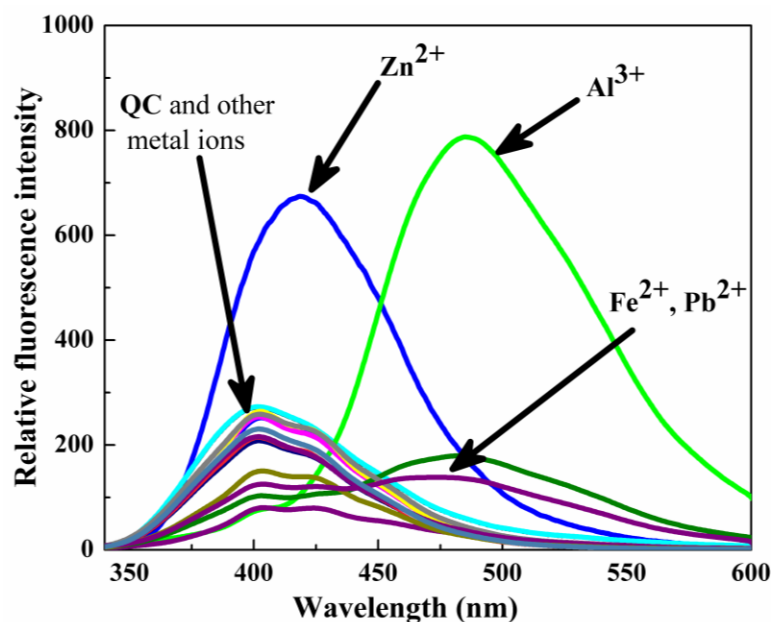


Figure 25. Fluorescence spectra of QC (20 μM) and on addition of salts of different metal ions (25 equiv) in mixed solvent media (acetonitrile/water = 9/1).

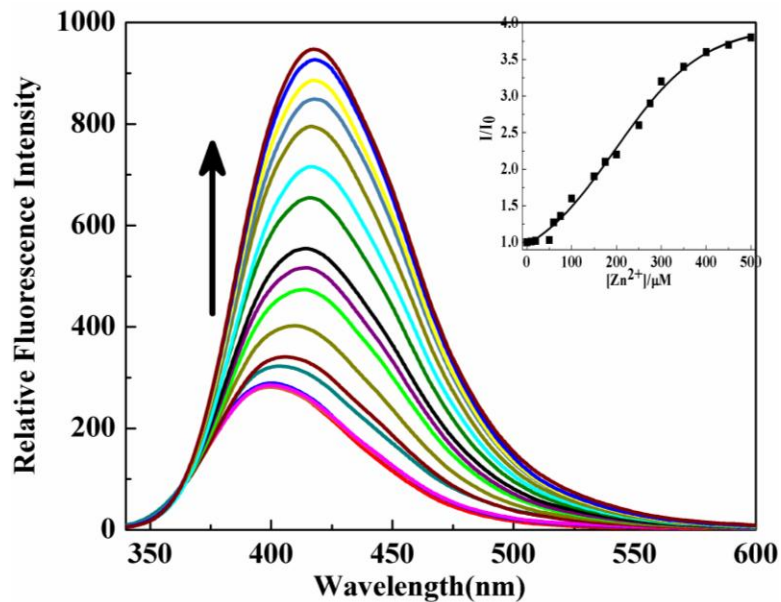


Figure 26. Fluorescence spectra of QC (20 μM) upon addition of Zn^{2+} (0, 10, 20, 50, 60, 75, 100, 150, 175, 200, 250, 275, 300, 350, 400, 450 and 500 μM) in mixed media (acetonitrile/water = 9/1). Inset: Fluorescence intensity as a function of $[Zn^{2+}]$.

intensity around 484 nm. This ratiometric behavior leads to the formation of a clear isobestic point at 430 nm (Figure 27). Minimum 20 μM concentration of Al^{3+} can be easily detected by this ratiometric study employing 20 μM QC. Thus QC can be used as fluorometric sensor for Zn^{2+} and Al^{3+} by means of ‘turn on’ and ‘ratiometric’ fluorescence responses respectively. Interestingly, another ratiometric fluorescent signal output for Al^{3+} was exploited using [QC+ Zn^{2+}] complex. Al^{3+} exhibited higher affinity for QC and displace ligand bound Zn^{2+} to form more stable [QC+ Al^{3+}] complex (Figure 28). A competitive experiment has been performed by titrating Al^{3+} into a solution of [QC+ Zn^{2+}] complex. Addition of Al^{3+} resulted in change in the fluorescence emission from blue to green. The emission maximum of [QC+ Zn^{2+}] gradually quenched and red shifted from 418 to 484 nm as function of Al^{3+} with the formation of a clear isobestic point at 449 nm implying that [QC+ Zn^{2+}] can be used as second optical response for sensing Al^{3+} with improved detection limit of at least down to 10 μM . These results demonstrate that QC can be employed as dual-mode Al^{3+} sensor via two ratiometric processes exploited through ICT mechanism and competitive metal ion displacement approach.^{7,21,39} Dual-mode ratiometric optical responses

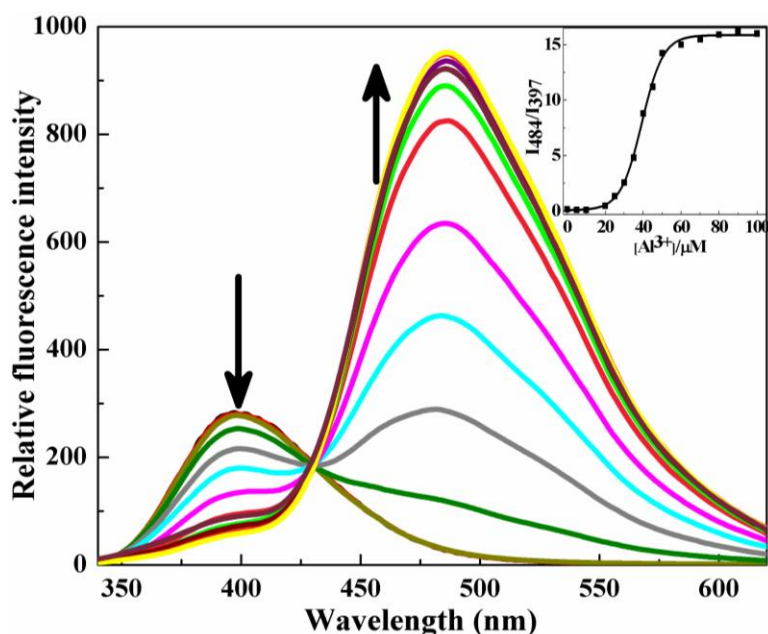


Figure 27. Fluorescence spectra of QC (20 μM) upon addition of Al^{3+} (0, 5, 10, 20, 25, 30, 35, 40, 45, 50, 60, 70, 80, 90 and 100 μM) in mixed solvent media (acetonitrile/water =9/1). Inset: Ratiometric fluorescence intensity [I_{484}/I_{397}] as a function of [Al^{3+}].

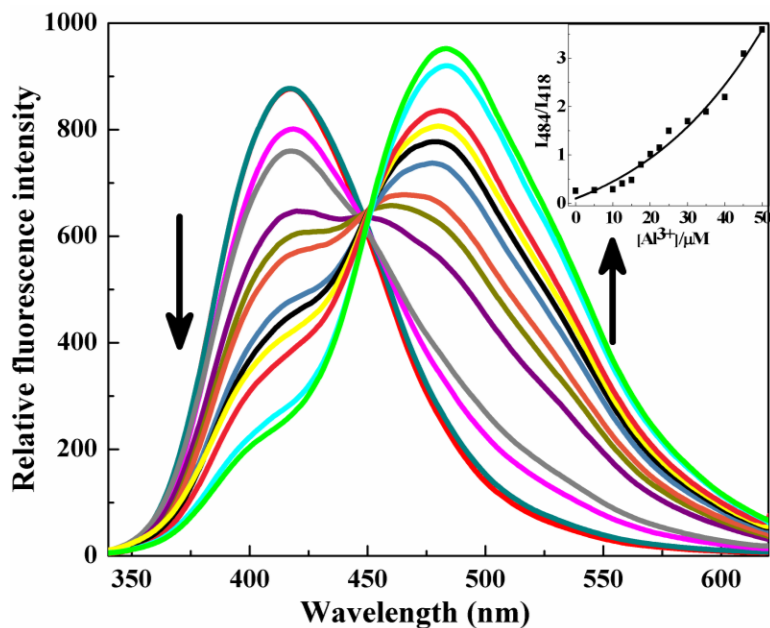


Figure 28. Fluorescence spectra of $[QC+Zn^{2+}]$ ($20 \mu M$ QC mixed with $250 \mu M$ Zn^{2+}) upon addition of Al^{3+} ($0, 5, 10, 12.5, 15, 17.5, 20, 22.5, 25, 30, 35, 40, 45$ and $50 \mu M$) in mixed solvent media (acetonitrile/water = 9/1). Inset: Ratiometric fluorescence intensity $[I_{484}/I_{418}]$ as a function of $[Al^{3+}]$.

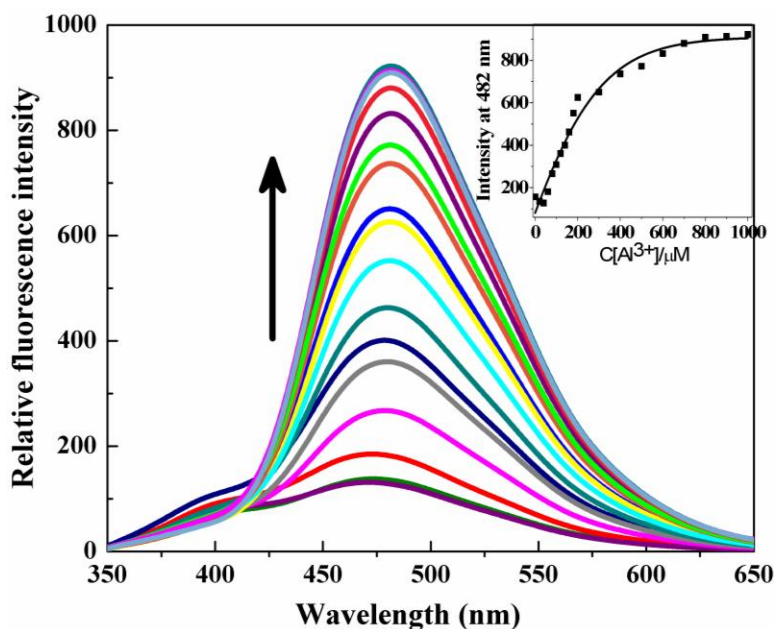


Figure 29. Fluorescence spectra of QC ($20 \mu M$) upon addition of Al^{3+} ($0, 20, 40, 60, 80, 100, 120, 140, 160, 180, 200, 300, 400, 500, 600, 700, 800, 900$ and $1000 \mu M$) in water. Inset: Fluorescence intensity at 482 nm as a function of $[Al^{3+}]$.

effectively increased the dynamic range by signal rationing and provide built-in-correction to environmental effects for the detection of Al^{3+} using **QC**.

Next, the fluorescence behavior of **QC** in presence of various metal ions has been studied in water. **QC** showed weak and broad emission band around 440 nm. Some of the metal ions tested have no effect on the emission behavior of **QC** whereas others show little quenching or enhancement in the fluorescence intensity of **QC** in water. On the other hand fluorescence intensity increased remarkably in presence of Al^{3+} with E_{max} around 482 nm (Figure 29). **QC** can also sense Al^{3+} in the most common pH ranges (pH = 5.0-8.0) (Figure 30).

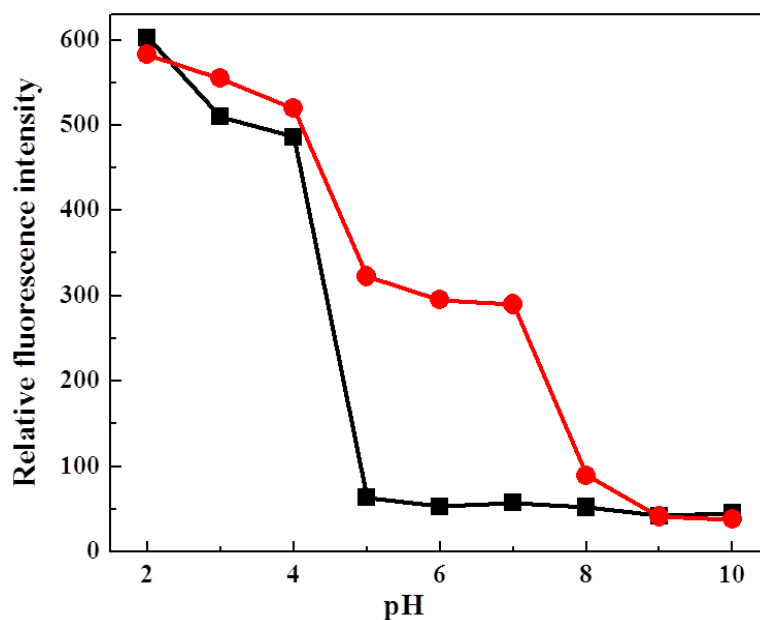


Figure 30. Dependence of the fluorescence intensity at 482 nm of **QC** on pH. Black trace: **QC** (20 μ M) and red trace: **QC** with 20.0 equivalents of Al^{3+} in aqueous medium.

3.3.3 Competitive study for fluorometric detection of Zn^{2+} and Al^{3+}

To utilize **QC** as selective chemosensor for Zn^{2+} and Al^{3+} , the effect of competing metal ions was studied. Zn^{2+} can be easily detected in presence of most competing metal ions from fluorescence ‘turn on’ behavior using molecular probe **QC** in mixed solvent media (acetonitrile/water = 9/1) (Figure 31). In presence of Al^{3+} , Fe^{2+} and Cu^{2+} quenching of

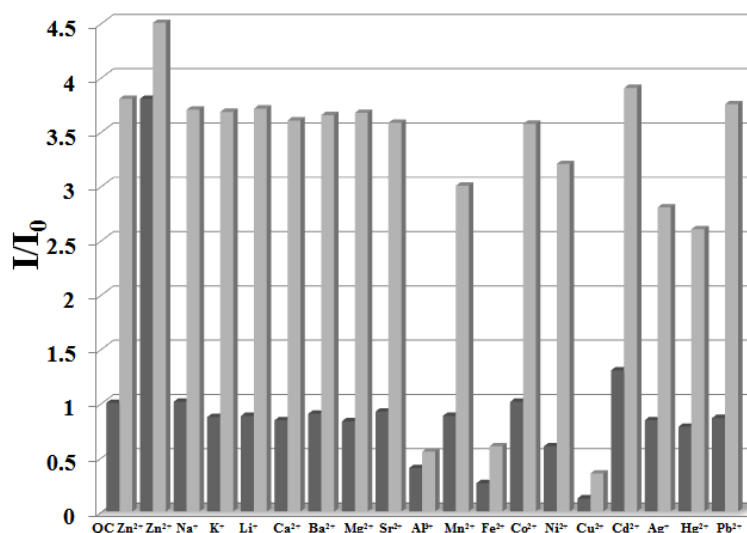


Figure 31. Relative fluorescence intensities of **QC** and its complexation with Zn^{2+} in the presence of various other metal ions. Dark grey bar: **QC** (20 μ M) with 20 equiv of metal ion stated. Light grey bar: 20 μ M of **QC** and 20 equiv of Zn^{2+} with 20 equiv of metal ions stated (for Zn^{2+} effect 40 equiv of Zn^{2+}). The response of the **QC** to Zn^{2+} , in the absence of competing ions, is included as controls. Extreme left dark bar: 20 μ M of **QC** with no metal ion; light bar, 20 μ M of **QC** with 20 equiv of Zn^{2+} . Solvent: mixed media (acetonitrile/water = 9/1).

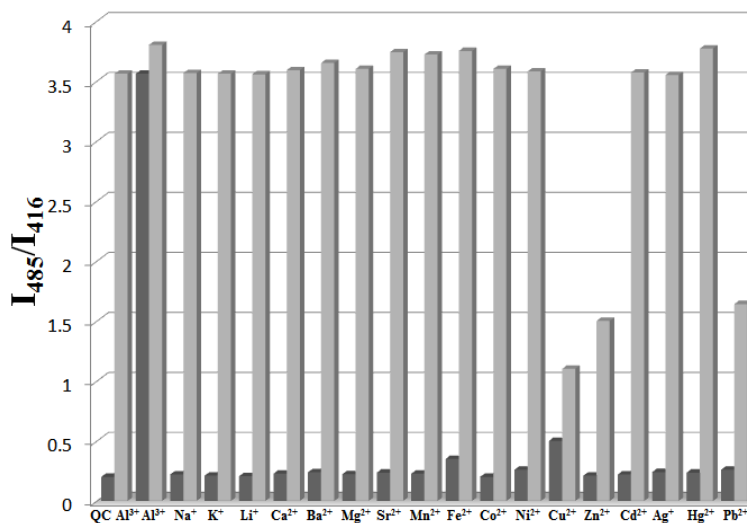


Figure 32. Relative fluorescence intensities of **QC** and its complexation with Al^{3+} in the presence of various other metal ions. Dark grey bar: **QC** (20 μ M) with 20 equiv of metal ion stated. Light grey bar: 20 μ M of **QC** and 20 equiv of Al^{3+} with 20 equiv of metal ions stated (for Al^{3+} effect 40 equiv of Al^{3+}). The response of the **QC** to Al^{3+} , in the absence of competing ions, is included as controls. Extreme left dark bar: 20 μ M of **QC** with no metal ion; light bar, 20 μ M of **QC** with 20 equiv of Al^{3+} . Solvent: mixed media (acetonitrile/water = 9/1).

fluorescence was observed. **QC** detects Al^{3+} selectively in presence of all other metal ions by means of ‘ratiometric’ phenomenon in mixed solvent media (acetonitrile/water = 9/1) (Figure 32). There was no interference for the detection of Al^{3+} from other metal ions as confirmed from competitive experiment in pure aqueous media (Figure 33). Thus, **QC** exclusively detects Al^{3+} in presence of all other ions in water.

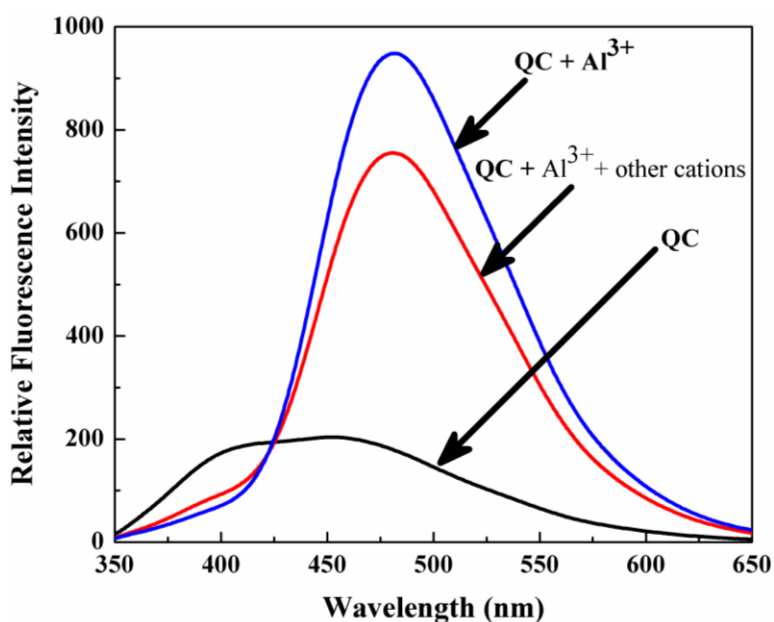


Figure 33. Relative fluorescence intensities of **QC** and its complexation with Al^{3+} in the presence of various other metal ions in water. **QC** (20 μ M) is mixed with 20 equiv of Al^{3+} in presence of 20 equiv of all other metal ions.

3.3.4 Determination of binding stoichiometry and binding mode of **QC** with Zn^{2+} and Al^{3+}

Job plot obtained from emission data showed 1:1 stoichiometric complexation of **QC** with Zn^{2+} and Al^{3+} (Figure 34 & 35). The response parameter α , which is defined as the ratio of free ligand concentration to the initial concentration of the ligand, is plotted as a function of both Zn^{2+} and Al^{3+} concentration. This plot can serve as the calibration curve for detection of Zn^{2+} and Al^{3+} respectively (Figure 36 & 37). The association constants ($\log K_a$) of **QC** for Zn^{2+} and Al^{3+} were found to be 8.07 and 13.98 respectively in mixed media. The association constant ($\log K_a$) of **QC** for Al^{3+} is 13.04 in water.

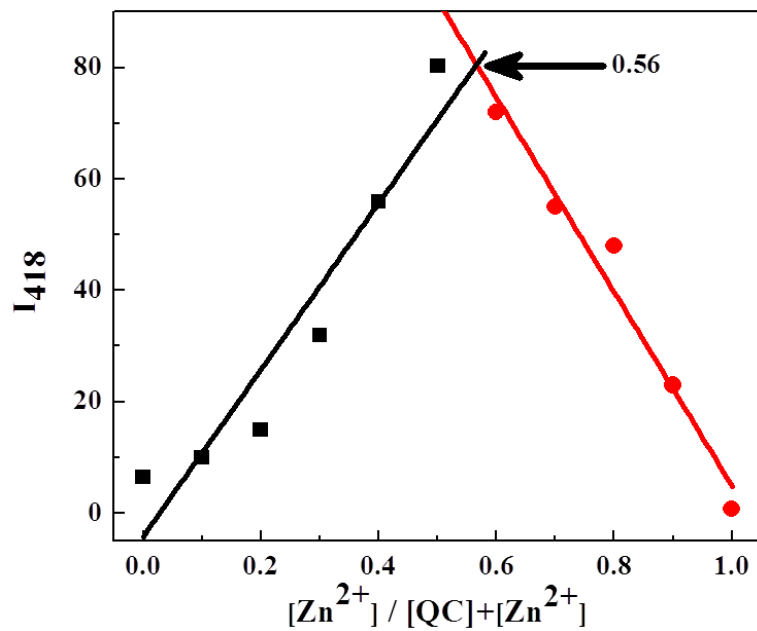


Figure 34. Job plot for the determination of the stoichiometry of QC and Zn^{2+} in the complex.

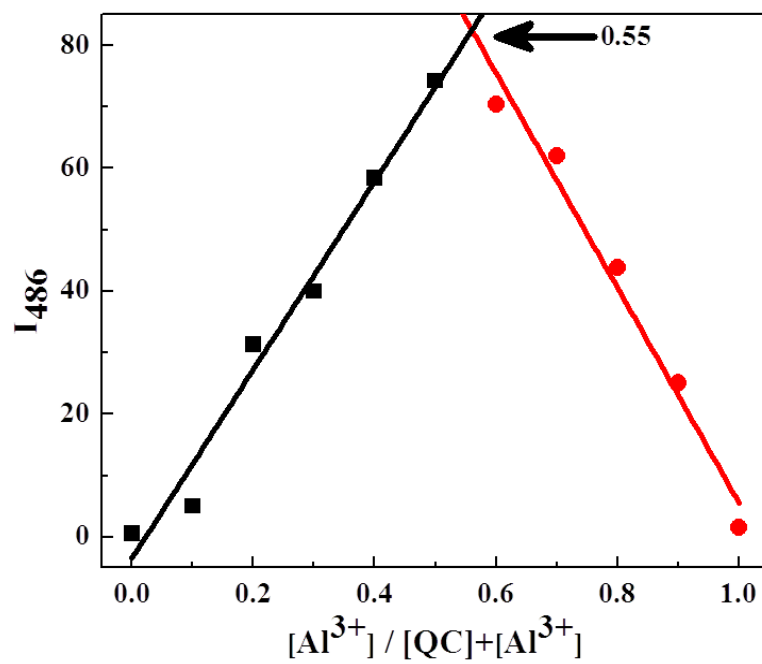


Figure 35. Job plot for the determination of the stoichiometry of QC and Al^{3+} in the complex.

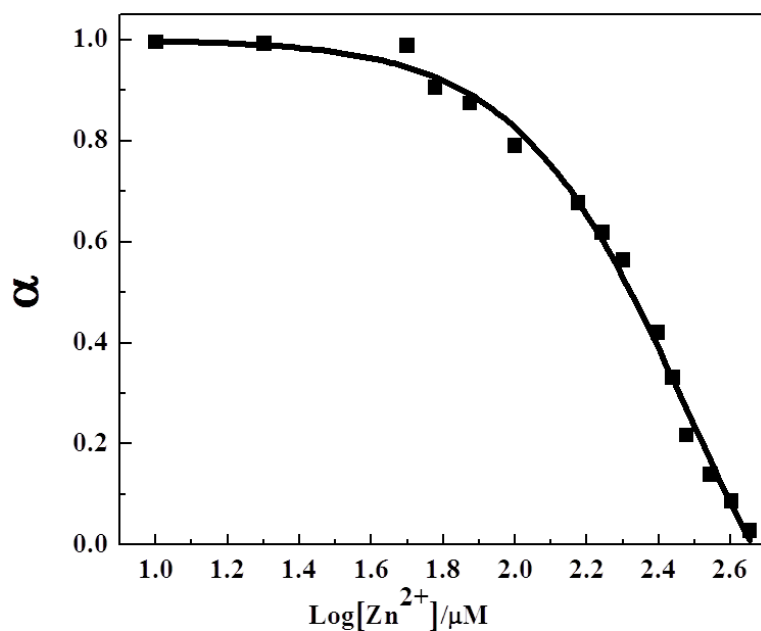


Figure 36. Response parameter values (α) of QC as a function of the logarithm of $[Zn^{2+}]$. α is defined as the ratio between the free ligand concentration and the initial concentration of ligand.

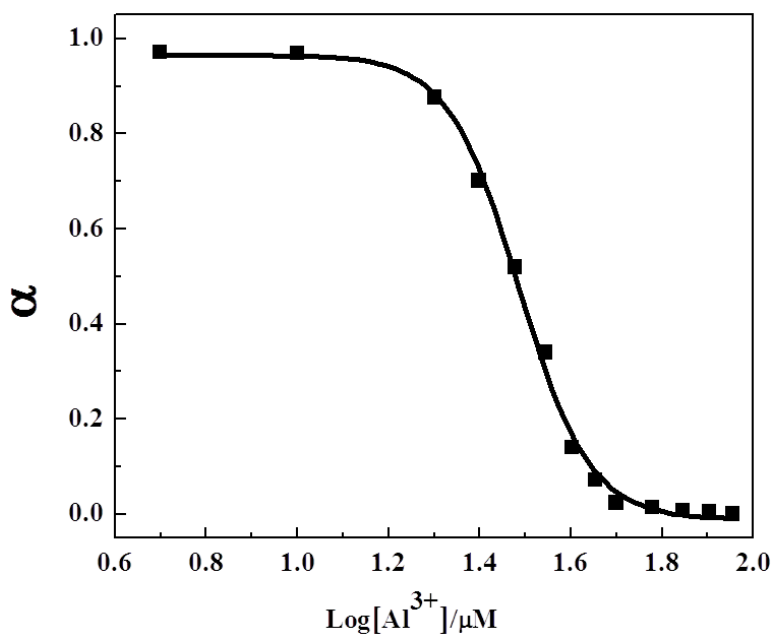


Figure 37. Response parameter values (α) of QC as a function of the logarithm of $[Al^{3+}]$. α is defined as the ratio between the free ligand concentration and the initial concentration of ligand.

To understand the nature of interaction between probe **QC** and Al³⁺/Zn²⁺, ¹H NMR titration experiments were carried out (Figure 38) independently with Al³⁺ and Zn²⁺. Upon complexation with metal ions the *ortho*-proton (H_a) of quinoline moiety in **QC** downfield shifted from 8.78 to 9.12 ppm for Al³⁺ and to 8.97 ppm for Zn²⁺. Similarly *meta*-proton (H_b) downfield shifted from 8.16 to 9.10 and 8.66 ppm for Al³⁺ and Zn²⁺ respectively, suggested N-metal coordination. Coumarin β-proton (H_c) also experienced downfield shift (Δδ_{Al} = 0.39 ppm and Δδ_{Zn} = 0.20 ppm) indicating the involvement of coumarin moiety in metal-ligand

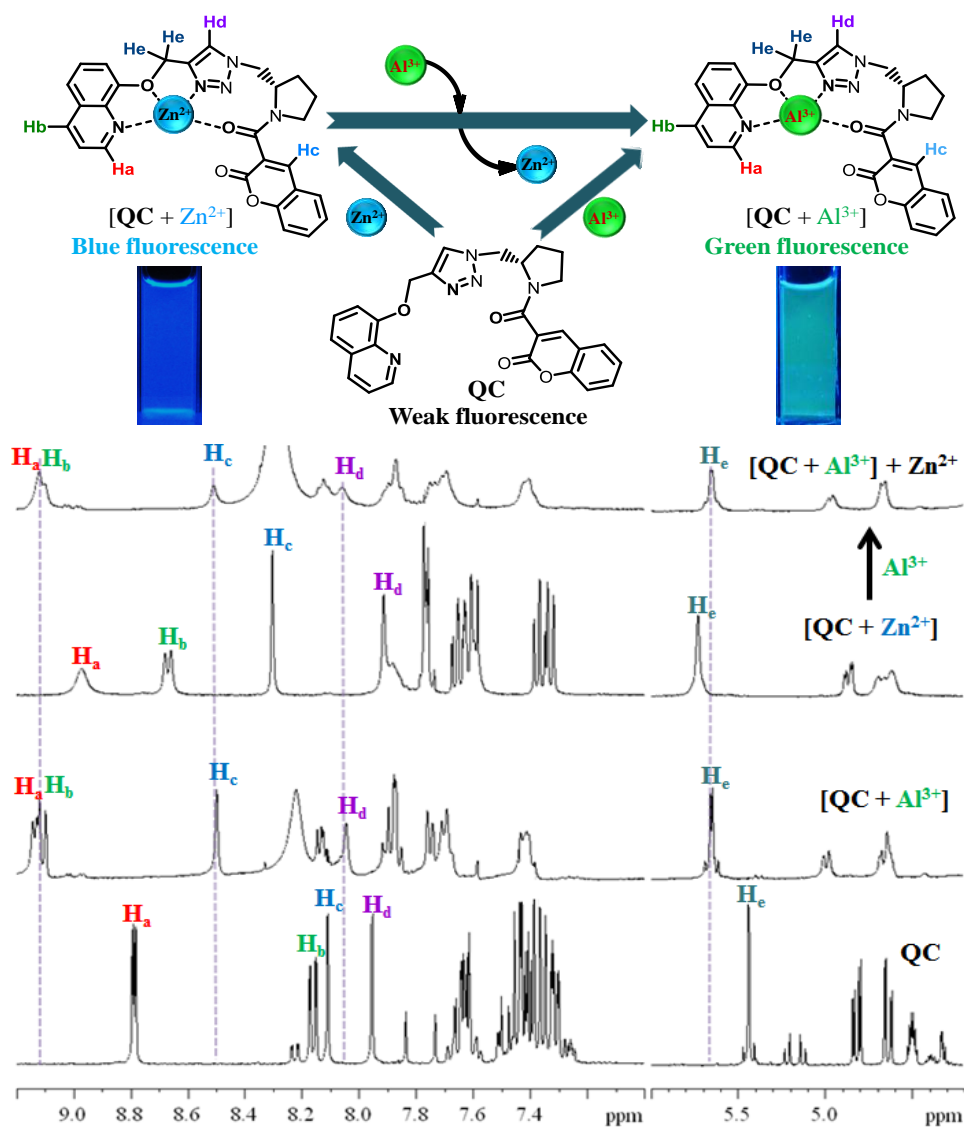


Figure 38. Top: Sensing process and binding mode of **QC** for Zn²⁺ and Al³⁺. Bottom: ¹H NMR spectra of **QC** in CD₃CN: (a) free **QC**; (b) **QC**+ 1 equiv of Al³⁺; (c) **QC**+ 1 equiv of Zn²⁺ and (d) [**QC**+Zn²⁺] + 1 equiv of Al³⁺.

coordination. Relatively small downfield shifts were observed for triazolyl-proton (H_d) for Al³⁺ and Zn²⁺. The significant downfield shifts of quinolinyl-oxy-methylene (H_e) protons ($\Delta\delta_{\text{Al}} = 0.22$; $\Delta\delta_{\text{Zn}} = 0.30$ ppm) suggest strong coordination of oxygen atom with metal ion (Al³⁺/Zn²⁺). These overall shifts in the proton signals were observed upon addition of 1.0 equiv of metal ion to the solution of QC. There was no shift in the position of proton signals on further addition of metal ion (> 1.0 equiv) which confirms 1:1 complexation between Al³⁺/Zn²⁺ and QC (Figure 39 & 40). Relatively high proton downfield shifts observed during Al³⁺ titration suggested stronger [QC+Al³⁺] complex formation. In a subsequent measurement, the NMR spectrum of [QC+Zn²⁺] complex was acquired by adding 1.0 equiv of Al³⁺. Interestingly, proton signals of QC in [QC+Zn²⁺] complex undergo significant change to match the proton NMR spectrum of [QC+Al³⁺] complex (Figure 38). This finding clearly indicated higher affinity of QC towards Al³⁺ in comparison to Zn²⁺. This result is in agreement with the displacement process observed in emission study (Figure 28) and NMR titration experiment.

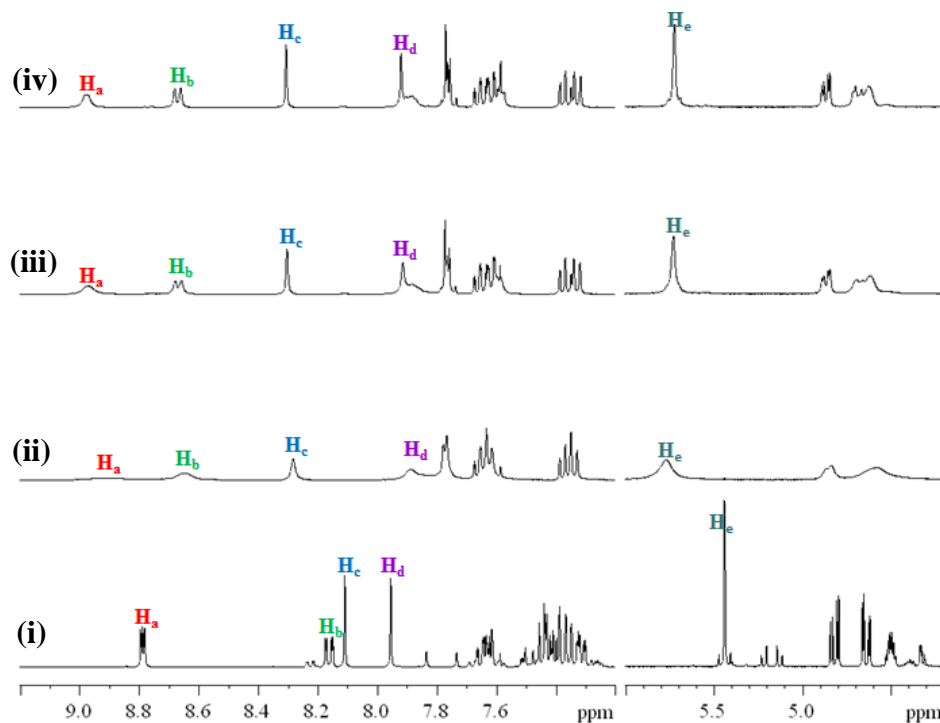


Figure 39. ¹H NMR spectra of QC with Zn²⁺ in CD₃CN. (i) QC, (ii) QC with 0.5 equiv of Zn²⁺, (iii) QC with 1.0 equiv of Zn²⁺ and (iv) QC with 1.5 equiv of Zn²⁺.

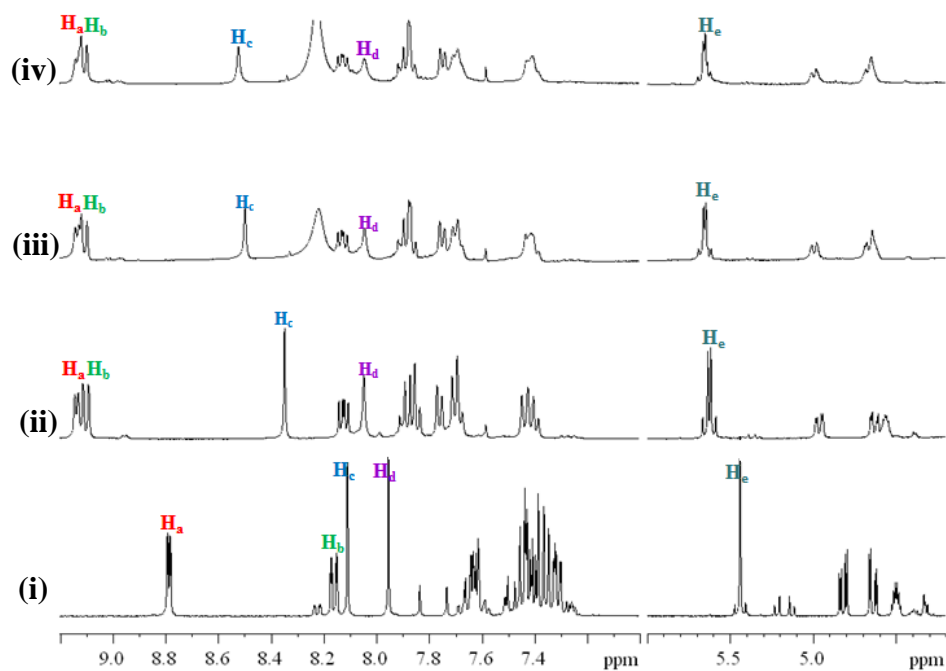


Figure 40. 1H NMR spectra of QC with Al^{3+} in CD_3CN . (i) QC, (ii) QC with 0.5 equiv of Al^{3+} , (iii) QC with 1.0 equiv of Al^{3+} and (iv) QC with 1.5 equiv of Al^{3+} .

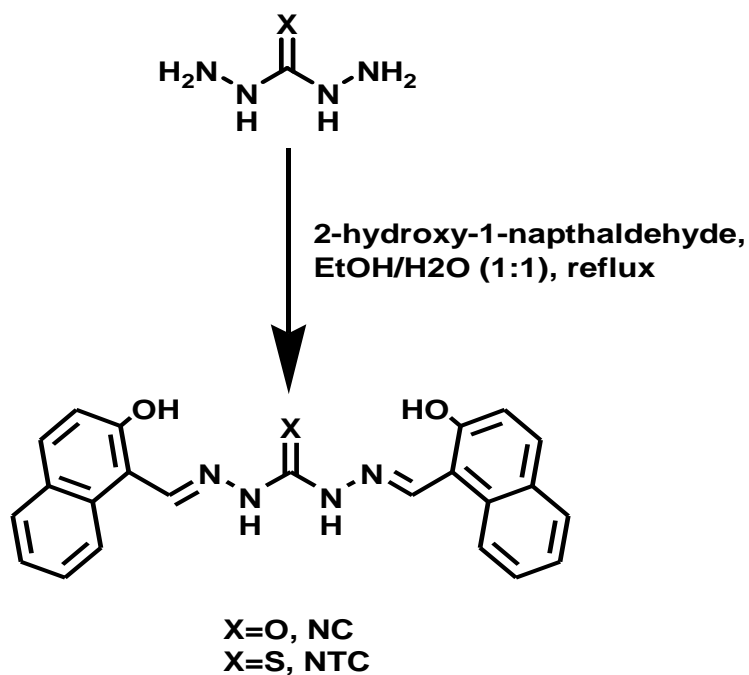
3.3.5 Conclusion

On the basis of rational design a novel differentially selective quinoline-coumarin (**QC**) fluorescent molecular probe was synthesized. **QC** shows fluorescence turn on response to Zn²⁺, while ratiometric response to Al³⁺ based on ICT mechanism in mixed solvent media. **QC** binds Zn²⁺ and Al³⁺ in 1:1 stoichiometry manner, determined from ¹H NMR and emission spectral studies. Moreover, Al³⁺ displaces Zn²⁺ from [**QC**+Zn²⁺] complex with red shifted second fluorescence ratiometric signature. This is further confirmed by ¹H NMR competitive study. Thus, dual-mode **QC** sensor can be employed to detect Al³⁺ through two distinct ratiometric processes based on ICT and competitive metal ion displacement approach. Furthermore, **QC** can exclusively detect Al³⁺ in presence of all other competing metal ions in water. This design concept can serve as platform to develop molecular probes with differential selectivity for various metal ions employing single signalling mechanism.

3.4 Naphthaldehyde–urea/thiourea conjugates as turn on fluorescent probes for Al³⁺ based on restricted C=N isomerization

3.4.1 Synthesis

Solution of 2-hydroxy-1-naphthaldehyde in ethanol was added slowly to a solution of thiocarbohydrazide or carbohydrazide in water. The reaction mixture was refluxed with stirring for 24 h. Reaction mixture was cooled to room temperature and the precipitated was filtered. The precipitate was washed with ethanol and dried under vacuo to obtain naphthaldehyde-carbohydrazone (NC) or naphthaldehyde-thiocarbohydrazone (NTC) in quantitative yield (Scheme 4).



Scheme 4. Synthesis of ligands NC and NTC.

3.4.2 Photophysical properties of naphthaldehyde-carbonohydrazone (NC) and naphthaldehyde-thiocarbonohydrazone (NTC) Schiff bases and fluorometric turn on detection of Al^{3+}

The photophysical properties of NC and NTC were investigated by monitoring absorption and emission spectral behavior upon addition of metal ions such as Li^+ , Na^+ , K^+ , Ba^{2+} , Sr^{2+} , Mg^{2+} , Ca^{2+} , Mn^{2+} , Fe^{2+} , Co^{2+} , Ni^{2+} , Cu^{2+} , Zn^{2+} , Cd^{2+} , Ag^+ , Hg^{2+} , Pb^{2+} , In^{3+} and Al^{3+} in $CH_3CN/DMSO$ (99.5/0.5). NTC exhibits an absorption band centered around 380 nm, which remains unchanged for Li^+ , Na^+ , K^+ , Ba^{2+} , Sr^{2+} , Mg^{2+} , Ca^{2+} , Mn^{2+} and Pb^{2+} . Addition of Fe^{2+} , Co^{2+} , Ni^{2+} , Cu^{2+} , Zn^{2+} , Cd^{2+} , Ag^+ , Hg^{2+} , In^{3+} and Al^{3+} leads red shift in the absorption maxima to different extents (Figure 41). In case of Al^{3+} , the absorption intensity slightly decreases around 380 nm and a new band appeared 440 nm (Figure 42). NC showed an absorption band centered around 370 nm, which remains unchanged upon addition of Li^+ , Na^+ , K^+ , Ba^{2+} , Sr^{2+} , Mg^{2+} , Ca^{2+} , Mn^{2+} , Ag^+ and Pb^{2+} . Addition of Fe^{2+} , Co^{2+} , Ni^{2+} , Cu^{2+} , Zn^{2+} , Cd^{2+} , Hg^{2+} , In^{3+} and Al^{3+} leads to red shifts in the absorption maxima to different extents (Figure 43). The absorption band gradually decreases around 370 nm on addition of

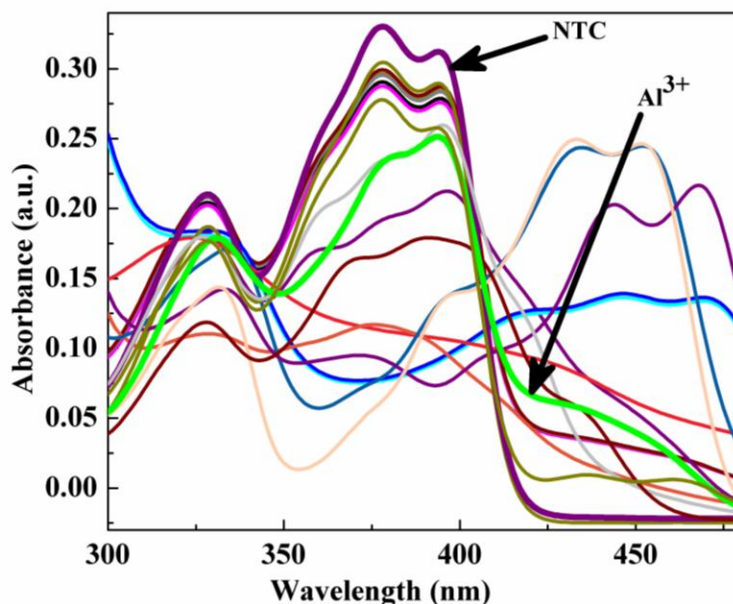


Figure 41. UV-Vis absorption spectra of NTC (10 μM) in the presence of 50 equiv of different metal ions (Li^+ , Na^+ , K^+ , Ba^{2+} , Sr^{2+} , Mg^{2+} , Ca^{2+} , Mn^{2+} , Fe^{2+} , Co^{2+} , Ni^{2+} , Cu^{2+} , Zn^{2+} , Cd^{2+} , Ag^+ , Hg^{2+} , Pb^{2+} , In^{3+} and Al^{3+}) in $CH_3CN/DMSO$ (99.5/0.5).

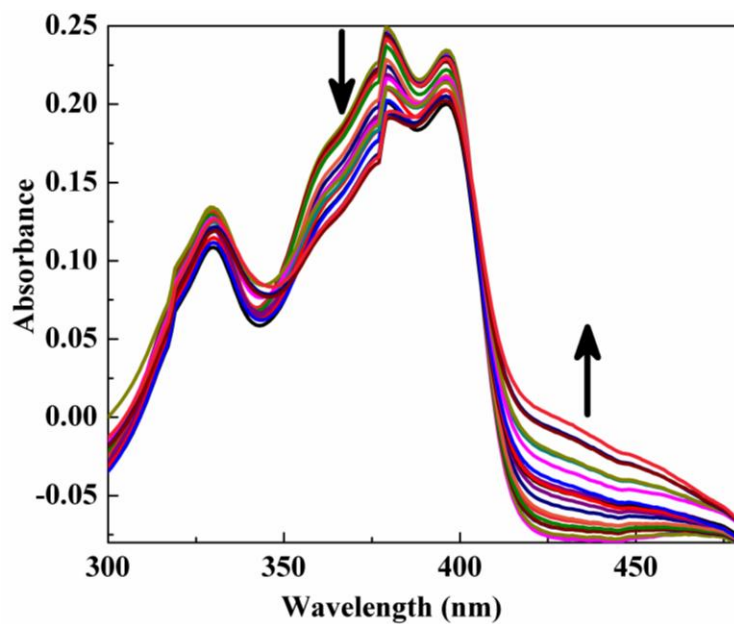


Figure 42. UV-Vis absorption spectra of NTC (10 μ M) upon addition of 0, 10, 20, 30, 40, 50, 60, 70, 80, 90, 100, 120, 140, 160, 180, 200, 300 and 400 μ M of Al^{3+} in $CH_3CN/DMSO$ (99.5/0.5).

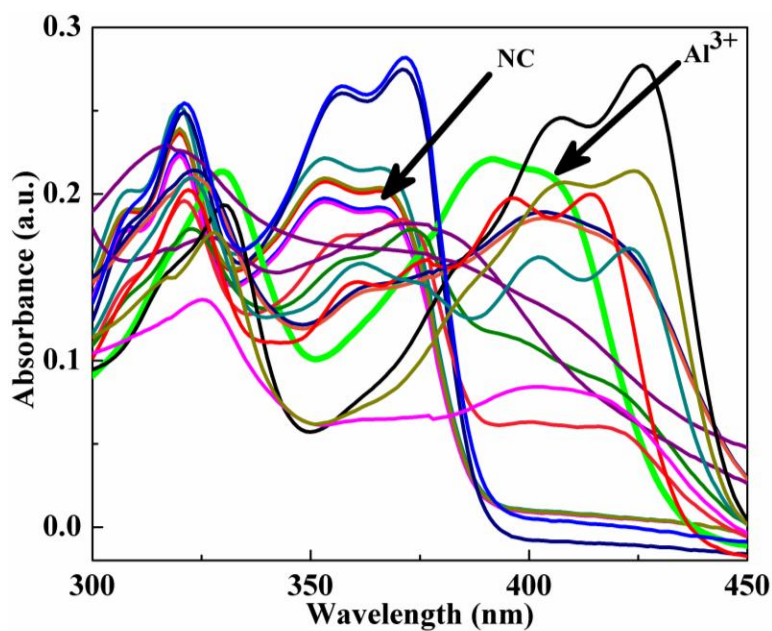


Figure 43. UV-Vis absorption spectra of NC (10 μ M) in the presence of 50 equiv of different metal ions (Li^+ , Na^+ , K^+ , Ba^{2+} , Sr^{2+} , Mg^{2+} , Ca^{2+} , Mn^{2+} , Fe^{2+} , Co^{2+} , Ni^{2+} , Cu^{2+} , Zn^{2+} , Cd^{2+} , Ag^+ , Hg^{2+} , Pb^{2+} , In^{3+} and Al^{3+}) in $CH_3CN/DMSO$ (99.5/0.5).

one equivalent of Al³⁺. Absorbance at 370 nm decreases sharply on addition of one more equiv of Al³⁺ to its limiting value and a new prominent peak appears at 400 nm with an isobestic point at 378 nm (Figure 44). The color of the solution changes from colorless to light green.

With 395 nm excitation, NTC did not show any significant fluorescence emission (quantum yield $\Phi = 0.00035$). The addition of Li⁺, Na⁺, K⁺, Ba²⁺, Sr²⁺, Mg²⁺, Ca²⁺, Mn²⁺, Fe²⁺, Co²⁺, Ni²⁺, Cu²⁺, Ag⁺, Hg²⁺ and Pb²⁺ has no effect on the fluorescence emission,

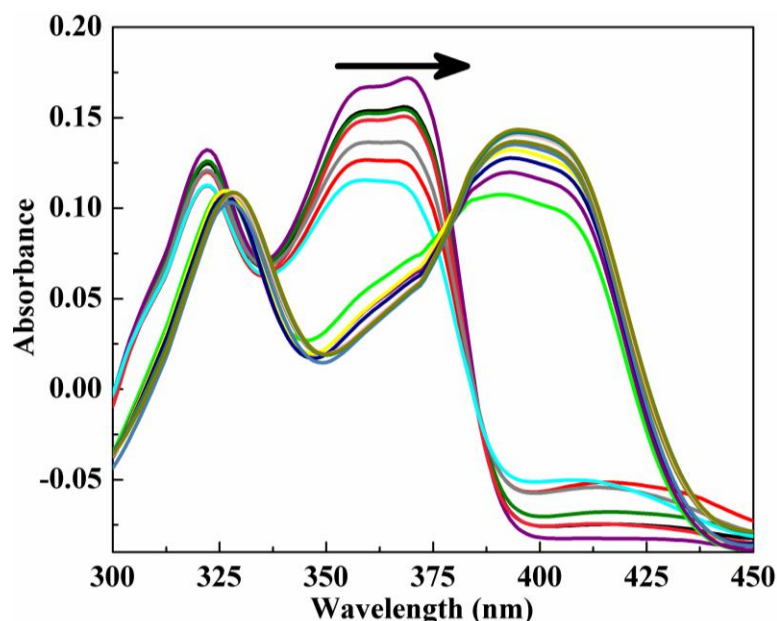


Figure 44. UV-Vis absorption spectra of NC (10 μM) upon addition of 0, 1, 5, 10, 15, 20, 30, 40, 50, 60, 70, 80, 90, 100, 150 and 200 μM of Al³⁺ in CH₃CN/DMSO (99.5/0.5).

whereas Zn²⁺, Cd²⁺ and In³⁺ shows little enhancement with red shift in the fluorescence spectra. In contrast, addition of Al³⁺ resulted in turn on fluorescence with 33 fold enhancement (quantum yield $\Phi = 0.0115$) of emission intensity positioned around 458 nm, as shown in Figure 45. Fluorometric titration was performed by adding different concentration of Al³⁺ to the solution appreciable fluorescence emission (quantum yield $\Phi = 0.00026$) with 390 nm excitation (Figure 46). Addition of Li⁺, Na⁺, K⁺, Ba²⁺, Sr²⁺, Mg²⁺, Ca²⁺, Mn²⁺, Fe²⁺, Co²⁺, Ni²⁺, Cu²⁺, Zn²⁺, Cd²⁺, Ag⁺, Hg²⁺, Pb²⁺ and In³⁺ has no effect on the fluorescence emission (Figure 47) of NC. In contrast, addition of Al³⁺ resulted in turn on fluorescence with 700 fold enhancement in the emission intensity (quantum yield $\Phi = 0.1813$) positioned

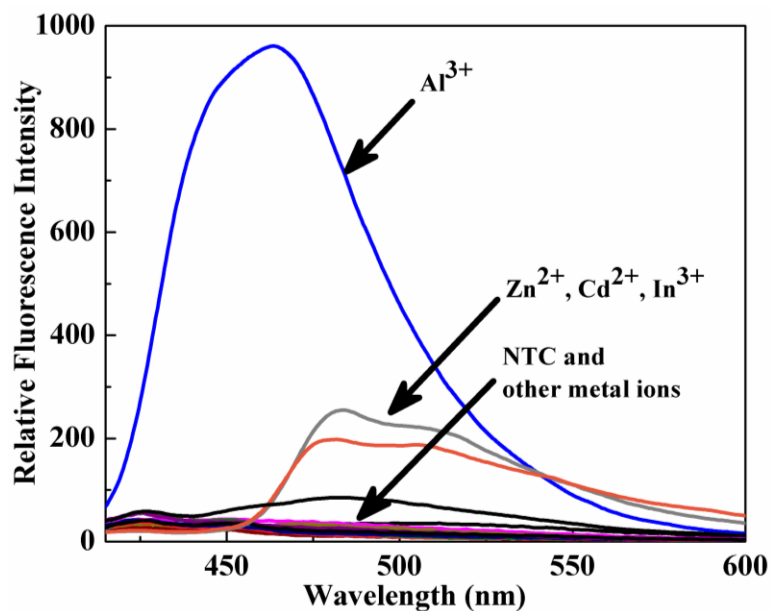


Figure 45. Fluorescence spectra of NTC (10.0 μM) and upon the addition of metal ions (50.0 equiv) Li^+ , Na^+ , K^+ , Ba^{2+} , Sr^{2+} , Mg^{2+} , Ca^{2+} , Mn^{2+} , Fe^{2+} , Co^{2+} , Ni^{2+} , Cu^{2+} , Zn^{2+} , Cd^{2+} , Ag^+ , Hg^{2+} , Pb^{2+} , In^{3+} and Al^{3+} with excitation at 395 nm.

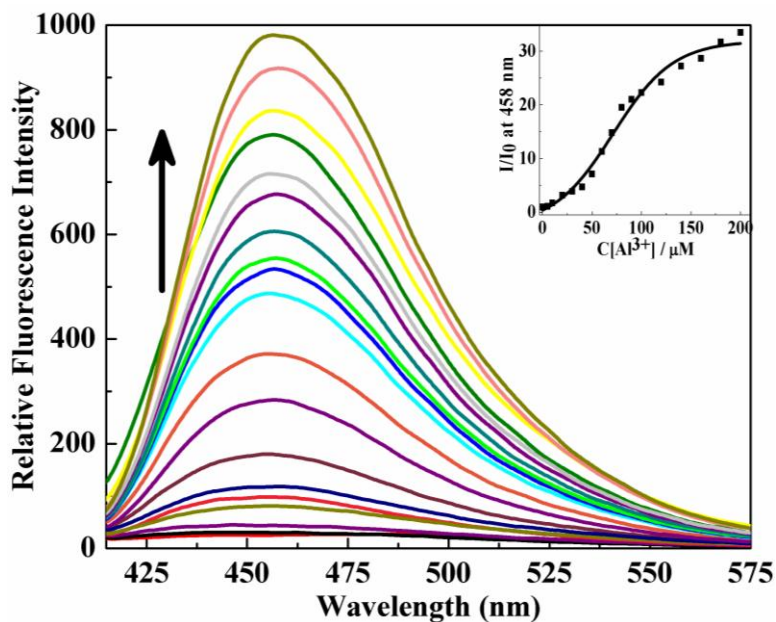


Figure 46. Fluorescence spectra of NTC (10.0 μM) upon the addition of Al^{3+} (0, 10, 20, 30, 40, 50, 60, 70, 80, 90, 100, 120, 140, 160, 180, 200, 300 and 400 μM) with excitation of 395 nm. Inset: Fluorescence intensity at 458 nm as a function of $[Al^{3+}]$.

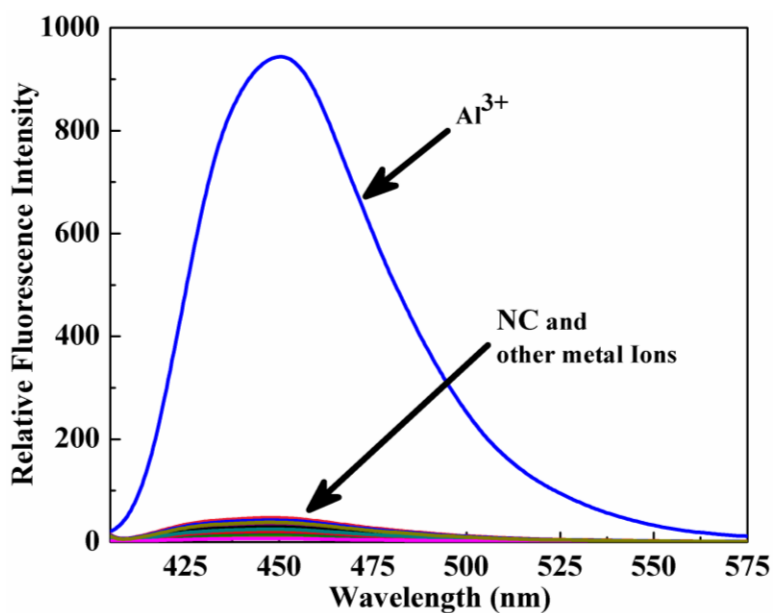


Figure 47. Fluorescence spectra of NC (10.0 μ M) and upon the addition of metal ions (50.0 equiv) Li^+ , Na^+ , K^+ , Ba^{2+} , Sr^{2+} , Mg^{2+} , Ca^{2+} , Mn^{2+} , Fe^{2+} , Co^{2+} , Ni^{2+} , Cu^{2+} , Zn^{2+} , Cd^{2+} , Ag^+ , Hg^{2+} , Pb^{2+} , In^{3+} and Al^{3+} .

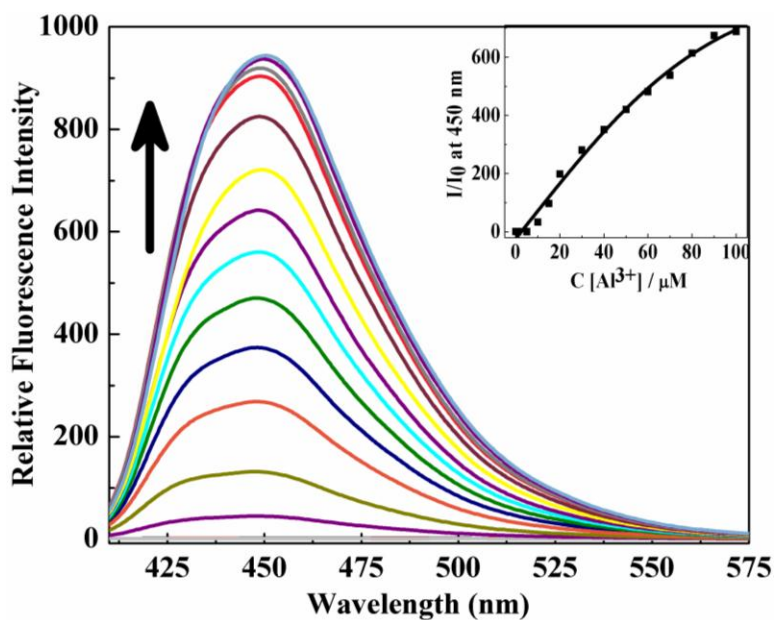


Figure 48. Fluorescence spectra of NC (10.0 μ M) upon the addition of Al^{3+} (0, 1, 5, 10, 15, 20, 30, 40, 50, 60, 70, 80, 90, 100, 150 and 200 μ M) with an excitation of 390 nm. Inset: Emission intensity at 450 nm as a function of $[Al^{3+}]$.

around 450 nm. Fluorescence emission of **NC** with sequential addition of increasing concentrations of Al³⁺ is shown in Figure 48. Minimum 20.0 μM and 10.0 μM of Al³⁺ can be easily detected by using 10.0 μM of **NTC** and **NC** respectively.

NC and **NTC** ligands have no appreciable fluorescence emission in their free form and show bright fluorescence on complexation with Al³⁺. This phenomenon of turn on fluorescence can be explained by considering the restricted C=N isomerisation mechanism. Rapid C=N isomerisation of imine double bonds in ligands **NC** and **NTC** responsible for non-radiative deactivation of the fluorophore in the excited state.³² Hence these ligands exhibit very poor fluorescence quantum yield in unbound form.³³⁻³⁴ To support this mechanistic proposal, two control compounds condensing 1-naphthaldehyde with thiocarbohydrazide or carbohydrazide in water have been synthesized. Then fluorescence spectra of these two Schiff bases in presence of Al³⁺ have been studied. Both compounds are non-fluorescent and have not shown any fluorescent turn on behavior in presence of Al³⁺. This is due to absence of phenolic –OH in these compounds and are not able to coordinate properly with Al³⁺, therefore the free rotation around C=N is not restricted. Hence these ligands exhibit very poor fluorescence quantum yield in unbound form as well as in presence of Al³⁺. This control study confirmed turn on fluorescent behavior of **NC** and **NTC** in presence of Al³⁺ attributed to restricted C=N isomerization. There are some reports in the recent past describing the specific detection of metal ions through Schiff base receptors based on the C=N isomerization mechanism.^{28,35}

3.4.3 Competitive study for Al³⁺ detection

Selectivity of **NC** and **NTC** as fluorescent chemosensor for the detection of Al³⁺ was studied in presence of various competing metal ions. For this purpose, **NTC** was treated with 10 equiv of Al³⁺ in the presence of 10 equiv of other metal ions (Figure 49a). There was no interference for the detection of Al³⁺ in presence of Li⁺, Na⁺, K⁺, Ba²⁺, Sr²⁺, Ca²⁺, Mg²⁺, Mn²⁺, Cd²⁺, Ag⁺ and Pb²⁺. Relatively low but clearly detectable response was observed in presence of Fe²⁺, Co²⁺, Ni²⁺, Cu²⁺, Zn²⁺, Hg²⁺ and In³⁺. Similarly **NC** was treated with 10 equiv of Al³⁺ in presence of the same concentrations of other metal ions. Data in Figure 49b show that there is no interference for detection of Al³⁺ in the presence of all other metal ions

except Cu²⁺, Hg²⁺, Fe²⁺, Co²⁺, Ni²⁺ and Zn²⁺. In case of Cu²⁺ and Hg²⁺, quenching of the fluorescence signal was observed. The NC responses for Al³⁺ in the presence of Fe²⁺, Co²⁺, Ni²⁺ and Zn²⁺ are relatively low but clearly detectable. Thus, NC can be used as a selective fluorescent probe for Al³⁺ detection in the presence of most competing metal ions except Cu²⁺ and Hg²⁺.

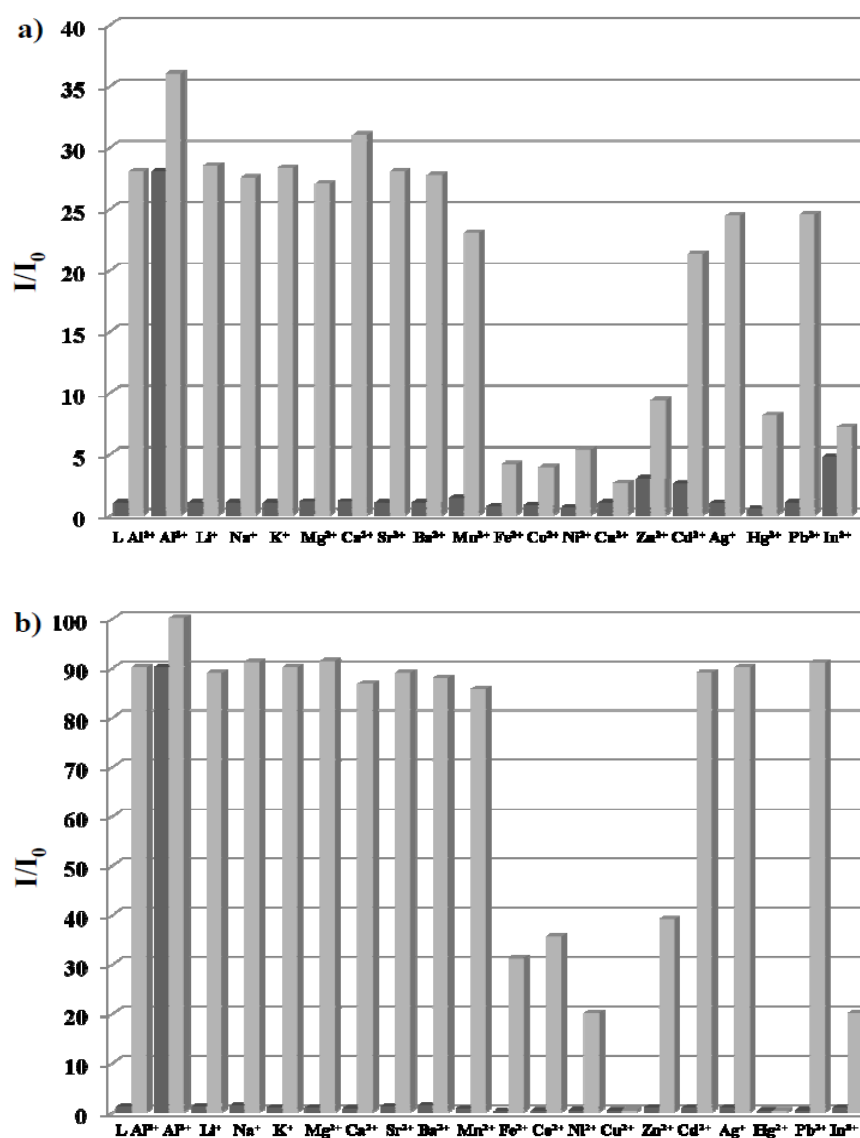


Figure 49. Relative fluorescence of a) NTC ($E_{\lambda}=458$ nm) and b) NC ($E_{\lambda}=450$ nm) and its complexation with Al³⁺ in the presence of various metal ions. Dark-gray bar: a) NTC (10.0 μ M) and b) NC (10.0 μ M) with 10 equiv of metal ion stated. Light-gray bar: 10.0 μ M of a) NTC and b) NC and 10 equiv of Al³⁺ with 10 equiv of metal ions stated (for an Al³⁺ effect, 20 equiv of Al³⁺). The response of 10.0 μ M of a) NTC and b) NC is included as controls (dark grey bar, L) and NTC/NC with 10 equiv of Al³⁺ (light grey bar).

3.4.4 Determination of binding stoichiometry and binding mode of NTC and NC with Al^{3+}

Job's plot obtained from the absorbance data showed 1:1 stoichiometric complexation for both NC and NTC with Al^{3+} (Figure 50 and 51). The 1:1 binding stoichiometry of NC with

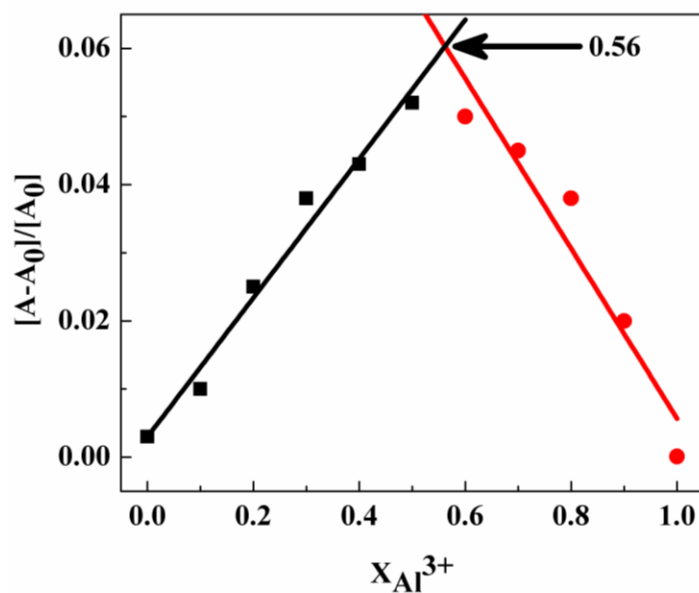


Figure 50. Job plot for the determination of the stoichiometry of NTC and Al^{3+} in the complex.

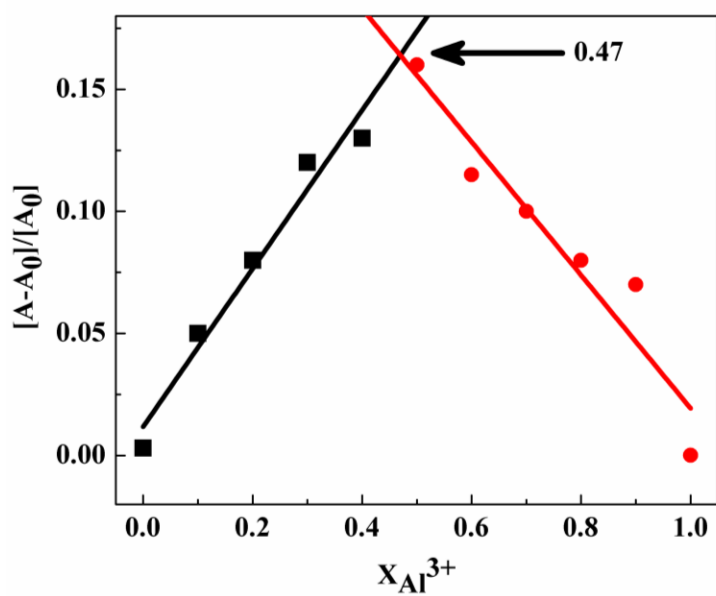


Figure 51. Job plot for the determination of the stoichiometry of NC and Al^{3+} in the complex.

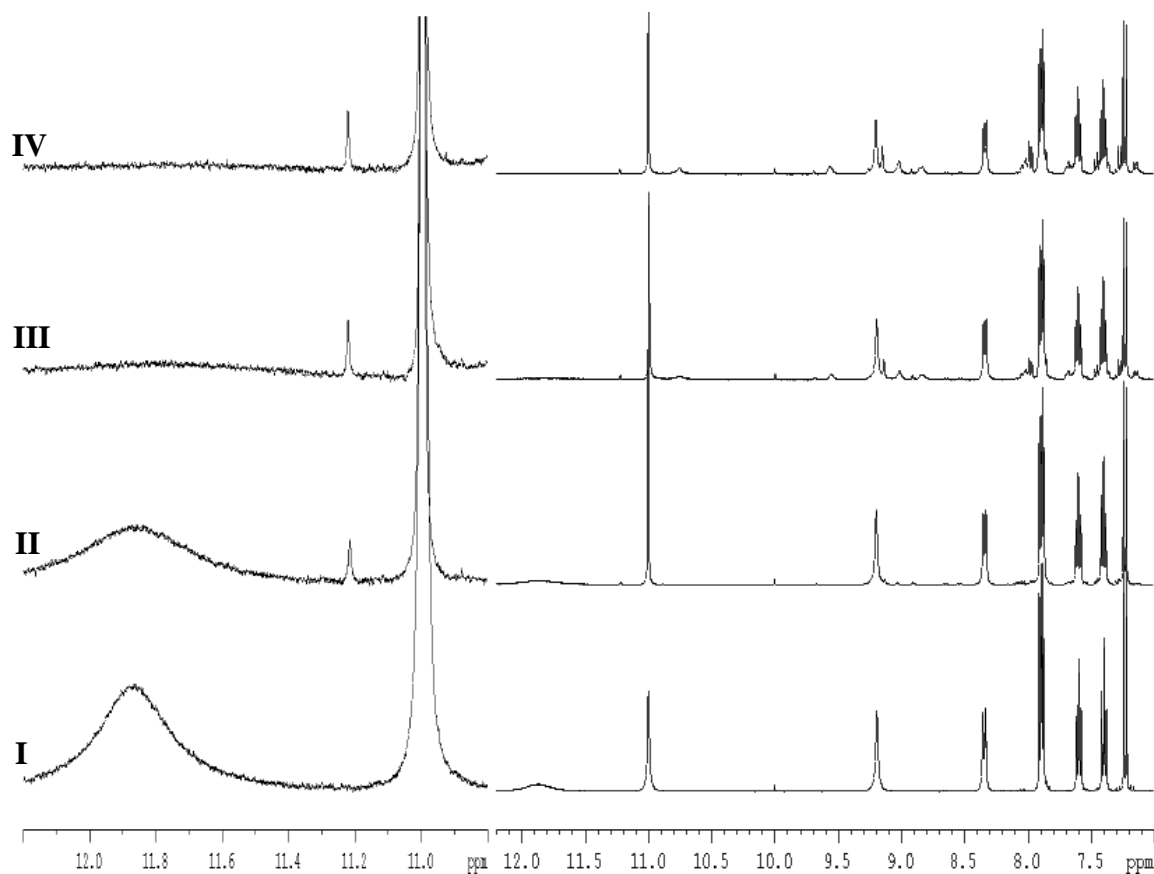
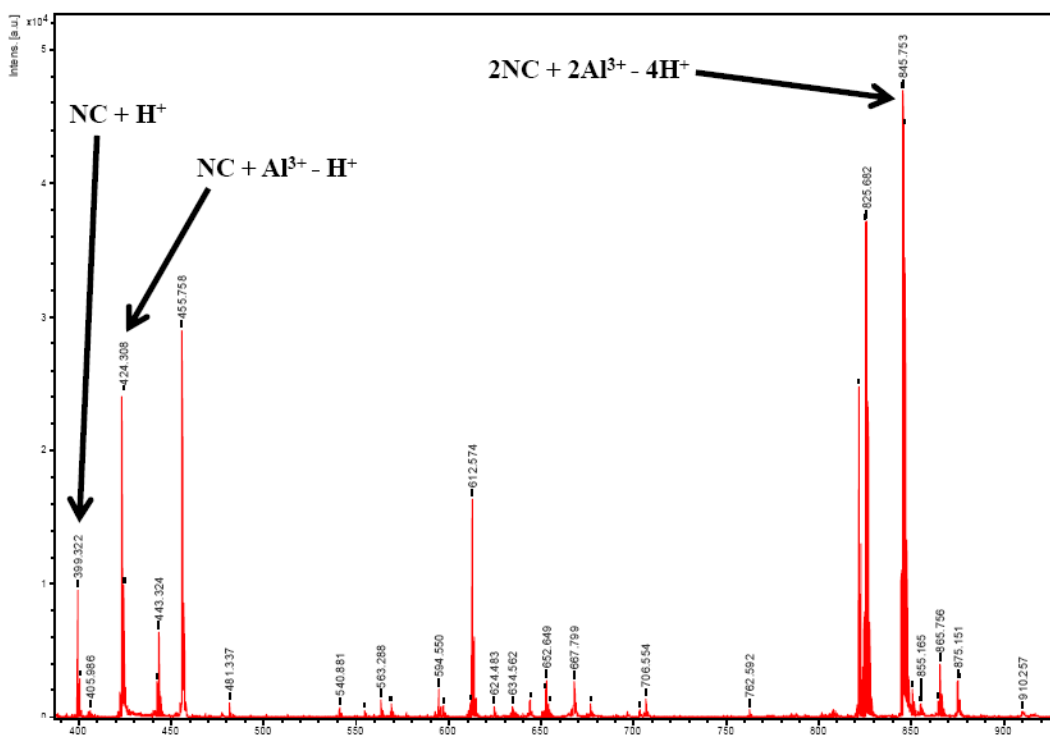
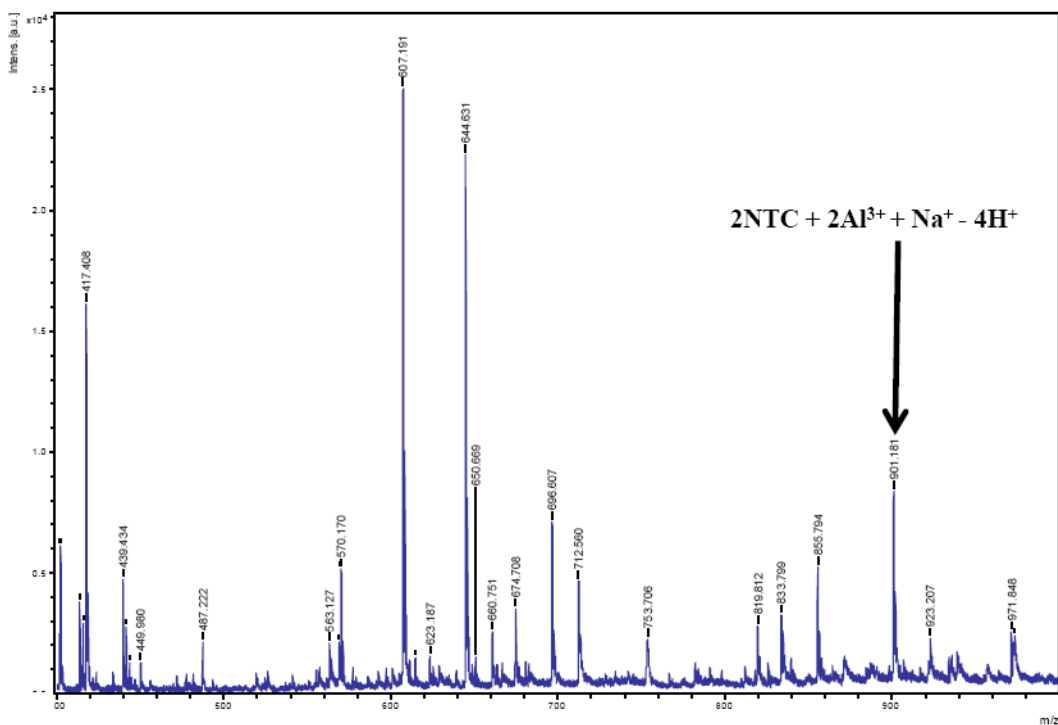
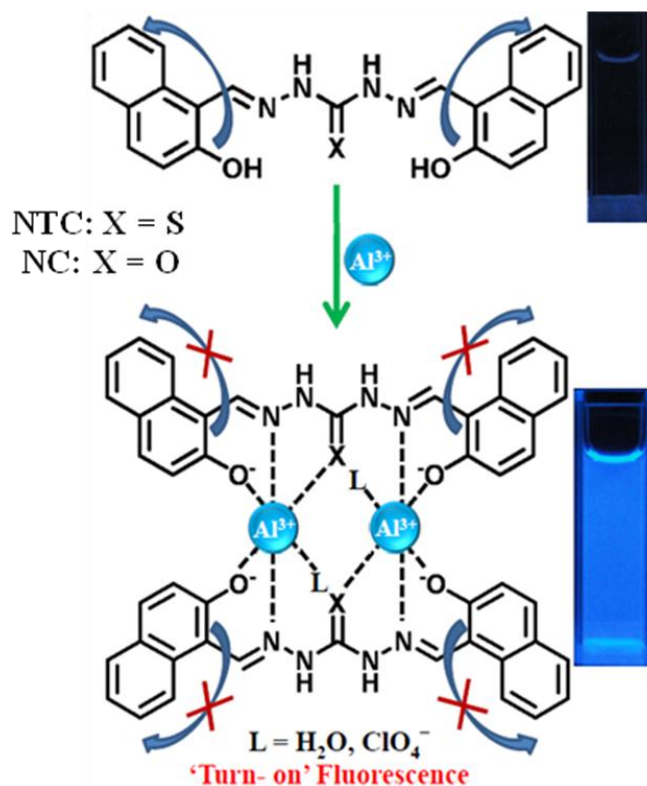


Figure 52. ^1H NMR spectrum of Bis[[2-hydroxynaphthyl]methylene]-carbonic dihydrazide [naphthaldehyde-carbonohydrazone (NC)] with $\text{Al}(\text{ClO}_4)_3$ in CD_3CN : (I) NC; (II) NC with 0.5 equiv of Al^{3+} ; (III) NC with 1.0 equiv of Al^{3+} ; (IV) NC with 1.5 equiv of Al^{3+} . [full Spectra (right), magnified spectra (10.8-12.2 ppm) to show double deprotonation of alcohol group at 11.87 ppm upon addition of 1.0 equiv of Al^{3+} (left)].

Al^{3+} was also supported by ^1H NMR spectra of NC on addition of various concentrations of Al^{3+} in CD_3CN (Figure 52). Both naphthol groups lose their protons at 11.87 ppm upon addition of 1.0 equiv of Al^{3+} . After coordination of NC with Al^{3+} , all the protons of the NC- Al^{3+} complex resonate slightly in the downfield region. A series of new peaks appear upon addition of 1.0 equiv Al^{3+} salt and those new peaks almost become constant after further addition of Al^{3+} . Deprotonation of naphthol followed by the coordination of naphthoxy group with Al^{3+} as depicted in Scheme 5. This data is further confirmed by mass spectroscopic analysis of double deprotonated NC: Al^{3+} complex (Figure 53). MALDI/TOF-MS data showed the formation of complex involving two molecules of double deprotonated NC and two aluminium ions [MW: 845.75; calcd.845.75 for $\text{C}_{46}\text{H}_{32}\text{Al}_2\text{N}_8\text{O}_6$ ($2\text{NC} + 2\text{Al}^{3+} - 4\text{H}^+$)].

Figure 53. MALDI-TOF mass spectrum of NC- Al^{3+} complex in CH_3CN .Figure 54. MALDI-TOF mass spectrum of NTC- Al^{3+} complex in CH_3CN .

Similarly MALDI/TOF-MS data (Figure 54) also showed the formation of 2:2 stoichiometric complex between two molecules of double deprotonated **NTC** and two aluminium ions [MW: 901.18; calcd. 901.15 for $C_{46}H_{32}Al_2N_8NaO_4S_2$ ($2\text{NTC} + 2Al^{3+} + Na^+ - 4H^+$)].



Scheme 5. Proposed mechanism of formation of $2[\text{NTC/NC}]:2Al^{3+}$ complex. Restricted isomerisation of $C=N$ is indicated by crossed arrows. Turn on fluorescence emission of ligands upon complexation with Al^{3+} is shown (right). $L = H_2O/ClO_4^-$.

The response parameter α , which is defined as the ratio of the free ligand concentration to the initial concentration of the ligand, is plotted as a function of the Al^{3+} concentration (Figure 55). This plot can serve as the calibration curve for detection of Al^{3+} . The association constant ($\log K_a$) of **NC** and **NTC** for Al^{3+} was calculated to be 14.5 and 14.1 respectively.

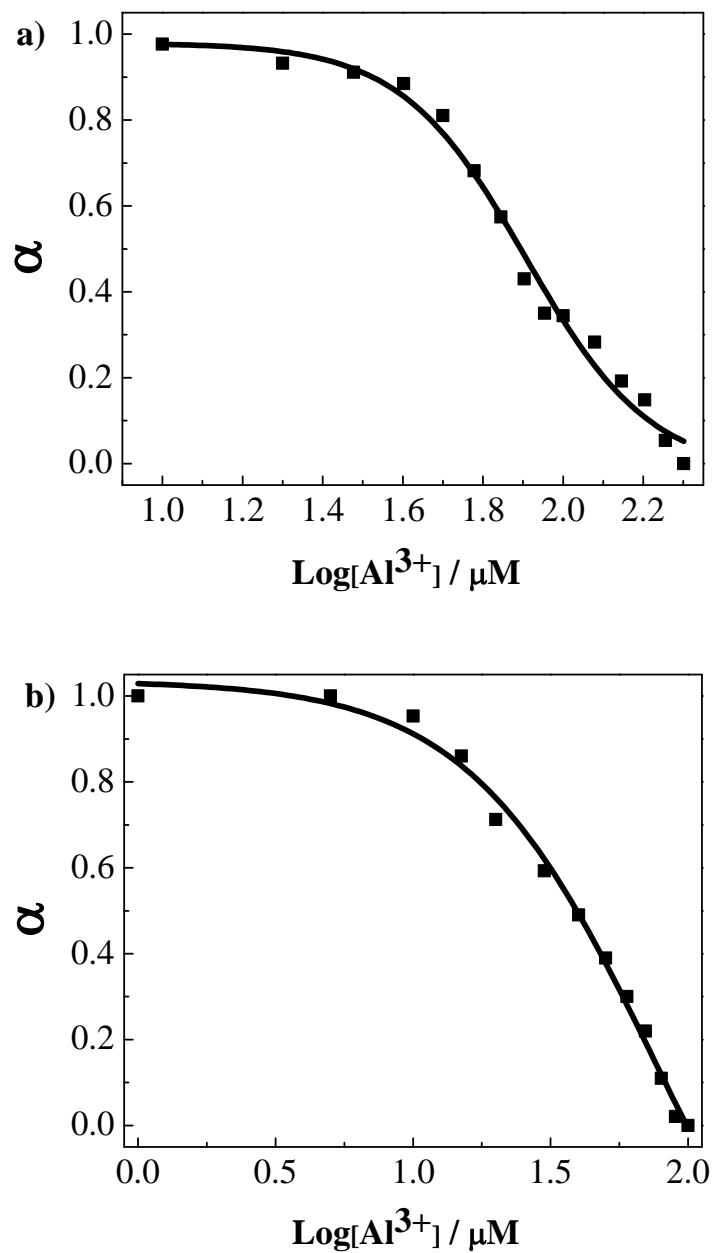


Figure 55. Response parameter values (α) as a function of the logarithm of the Al^{3+} concentration. α is defined as the ratio between the free ligand concentration and the initial concentration of the ligand. a) NTC and b) NC.

3.4.5 Conclusion

Schiff base derivatives naphthaldehyde-carbonohydrazone (**NC**) and naphthaldehyde-thiocarbonohydrazone (**NTC**) has been demonstrated as selective fluorometric chemosensors of Al^{3+} . The strength of the work presented here is the ability to access Al^{3+} probe through highly economical, simple and straight forward synthetic route. Here, two signal transduction mechanisms namely chelation-enhanced fluorescence and restricted C=N isomerization has been exploited to design **NC** and **NTC** ligands as turn on fluorescence chemosensors for aluminium ion. Al^{3+} can be detected in the presence of most of the competing metal ions using **NC** and **NTC**. Both **NC** and **NTC** undergo 1:1 stoichiometric complexation with Al^{3+} , confirmed from emission spectra, as clearly indicated by 1H NMR and mass analysis. This design concept can serve as platform to develop molecular probes for various metal ions based on restricted C=N isomerisation mechanism.

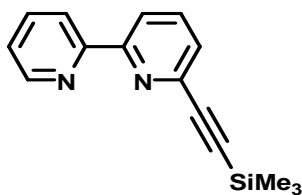
4. Experimental

4.1 General experimental procedure

All the solvents and reagents (analytical grade and spectroscopic grade) were obtained from Sigma-Aldrich and used as received unless otherwise mentioned. The solutions of metal ions were prepared from Al(ClO₄)₃·9H₂O, LiClO₄·3H₂O, NaClO₄, KClO₄, Mg(ClO₄)₂, Sr(NO₃)₂, Ba(ClO₄)₂, Mn(ClO₄)₂·6H₂O, Fe(ClO₄)₂, Co(ClO₄)₂·6H₂O, Ni(ClO₄)₂·6H₂O, Cu(ClO₄)₂·6H₂O, Zn(ClO₄)₂·6H₂O, Cd(ClO₄)₂·H₂O, Ag(ClO₄)₂, HgCl₂, Pb(ClO₄)₂, In(NO₃)₃ respectively in CH₃CN. ¹H and ¹³C NMR were measured on a Bruker AV-400 spectrometer with chemical shifts reported as *ppm* (in CDCl₃, CD₃CN and DMSO-*d*₆, tetramethylsilane as internal standard). Mass spectra are measured on Shimadzu 2020 LC-MS and Bruker Ultraflex II MALDI/TOF spectrometers. Melting points were determined on hot oil-bath melting point apparatus in an open-mouth capillary and were uncorrected. IR spectra are recorded on a Bruker IFS 66/V spectrometer, using KBr discs. Thermal gravimetric analysis was carried out on a TGA 850 Mettler Toledo instrument. Elemental analysis was carried out on Thermo Scientific FLASH 2000 Organic Element Analyzer and specific rotation [α]_D²⁵ was recorded on a JASCO P-2000 polarimeter. UV spectra were recorded on a Perkin Elmer Model Lambda 900 spectrophotometer and fluorescence spectra were recorded on a Perkin Elmer model LS 55 spectrophotometer.

4.2 Detailed synthetic procedure

6-Trimethylsilylethynyl-2,2'-bipyridine (1): 6-Bromo-2,2'-bipyridine (1g, 4.25 mmol), CuI

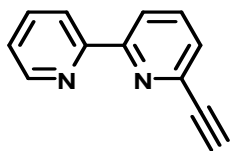


(0.202g, 1.06 mmol) and PPh₃ (1.5g, 5.74 mmol) were added to a mixture of 37.5 mL pyridine and 75 mL trimethylamine. The mixture was degassed for several times, followed by addition of ethynyltrimethylsilane (5.9 mL, 42.54 mmol). The reaction mixture

was degassed one more time. Pd(PPh₃)₄ (0.39g, 0.34 mmol) was added, and the reaction flask was evacuated and flushed with argon. The reaction mixture was refluxed for 48 hrs at 85°C under an argon atmosphere. After cooling to room temperature the precipitated salt was

filtered off and washed with triethylamine. The filtrate was evaporated and 100 mL of water were added. The mixture was extracted with diethyl ether until the aqueous phase was colorless. The combined organic phases were dried over Na₂SO₄, and the solvent was evaporated. The crude product was purified by column chromatography on silica gel with ethyl acetate/pet ether (2:100) as an eluent to afford 1.06g of a dark yellow oily product (99 % yield). ¹H NMR (400 MHz, CDCl₃) δ 0.295 (9H, s), 7.260-7.316 (1H, ddd, *J* = 3.6 Hz, 1.6 Hz, 0.8Hz), 7.468-7.490 (1H, dd, *J* = 6.8 Hz, 1.2 Hz), 7.741-7.819 (2H, m), 8.338-8.361 (1H, dd, *J* = 6.8Hz, 1.2Hz), 8.454-8.479 (1H, ddd, *J* = 6Hz, 1.2Hz, 0.8Hz), 8.643-8.660 (1H, ddd, *J* = 2.8Hz, 1.2Hz, 0.8Hz). ¹³C NMR (100 MHz) δ 94.69, 104.24, 120.76, 121.83, 124.17, 127.75, 137.06, 137.15, 142.67, 149.26, 155.63, 156.67. MS (EI): *m/z* = 252 (M⁺). Elemental analysis: Calcd: C, 79.98; H, 4.47; N, 15.55. Found: C, 79.28; H, 4.47; N, 14.07.

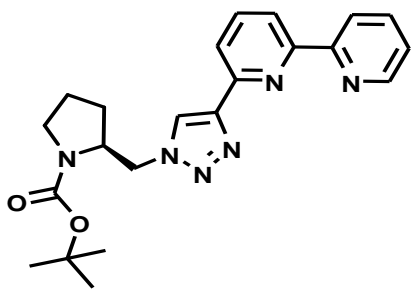
6-Ethynyl-2,2'-bipyridine (2): 6-Trimethylsilylethynyl-2,2'-bipyridine (1g, 3.96 mmol) was dissolved in 60 mL dry THF. A solution of TBAF (1.12g, 4.28 mmol) in 4.3 mL of THF was



added, and the reaction mixture was stirred at room temperature for 6 hrs. Then THF was evaporated under vacuum and residue was dissolved in 20 mL DCM. This organic layer was washed with 15 mL of water three times. The organic phase was dried over Na₂SO₄ and solvent was evaporated. The crude product was purified by column chromatography on silica gel with ethyl acetate/pet ether (1:10) as an eluent to afford 0.65g of brown crystalline product (92% yield). Mp 82-84°C. ¹H NMR (400 MHz, CDCl₃) δ 3.182 (1H, s), 7.294-7.328 (1H, ddd, *J* = 3.6 Hz, 1.6 Hz, 1.2 Hz), 7.489-7.511 (1H, dd, *J* = 6.4Hz, 1.2 Hz), 7.769-7.825 (2H, m), 8.393-8.416 (1H, dd, *J* = 7.2 Hz, 1.2 Hz), 8.454-8.479 (1H, ddd, *J* = 6 Hz, 1.2 Hz, 0.8 Hz), 8.652-8.657 (1H, ddd, *J* = 2 Hz, 1.2 Hz, 0.8Hz). ¹³C NMR (100 MHz, CDCl₃) δ 76.78, 83.04, 120.92, 121.48, 124.04, 127.44, 136.90, 137.08, 141.64, 149.08, 155.25, 156.58. MS (EI): *m/z* = 180 (M⁺). Elemental analysis: Calcd: C, 79.98; H, 4.47; N, 15.55. Found: C, 79.28; H, 4.47; N, 14.07.

Boc-pyrrolidinyl-triazolyl-bipyridine (3): To a solution of Boc-protected azido-pyrrolidine³⁸ (1g, 4.42 mmol) in toluene and *tert*-butanol (4:1), 6-ethynyl-2,2'-bipyridine³⁷ (0.8g, 4.42 mmol), CuI (0.042g, 0.221 mmol) and N,N'-diisopropylethylamine (DIPEA) (1.54 mL, 8.84 mmol) were added. The reaction mixture was stirred at room temperature for

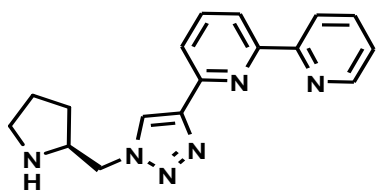
overnight. After removal of the solvent under vacuo, the residue was diluted with 20 mL



CH₂Cl₂ and washed with water (15 mL X 3). The organic phase was dried over Na₂SO₄ and solvent was evaporated to dryness. The crude product was purified by column chromatography on silica gel using chloroform-methanol (10:1) as an eluent to afford white product in good yield (1.72 g, 96%). M.P. 122-124°C.

$[\alpha]_D^{25} +79.5$ (c 1.0, CH₃OH). ¹H NMR (400 MHz, CDCl₃) δ 1.52 (9H, s), 1.72-1.75 (2H, m), 1.98-2.00 (2H, m), 3.18-3.43 (2H, m), 4.19 (1H, m), 4.50-4.78 (2H, m), 7.31-7.34 (1H, dd, *J* = 5.2 Hz, 1.6 Hz), 7.80-7.84 (1H, t, *J* = 7.4 Hz), 7.88-7.92 (1H, t, *J* = 7.6 Hz), 8.17-8.25 (2H, m), 8.35-8.37 (1H, d, *J* = 8.0 Hz), 8.48-8.50 (1H, d, *J* = 7.2 Hz), 8.68-8.69 (1H, d, *J* = 3.6 Hz). ¹³C NMR (100 MHz, CDCl₃) δ 23.3, 28.2, 28.5, 47.1, 51.4, 57.2, 136.6, 137.7, 148.8, 149.1, 149.6, 154.7, 155.6, 155.9. MS (EI): *m/z* = 406.30 [M⁺] for C₂₂H₂₆N₆O₂. Elemental analysis: Found: C, 65.16; H, 6.47; N, 20.62, Calcd: C, 65.01; H, 6.45; N, 20.68 for C₂₂H₂₆N₆O₂.

Pyrolidinyl-triazolyl-bipyridine (4): To Boc-protected product (406 mg, 1.0 mmol),

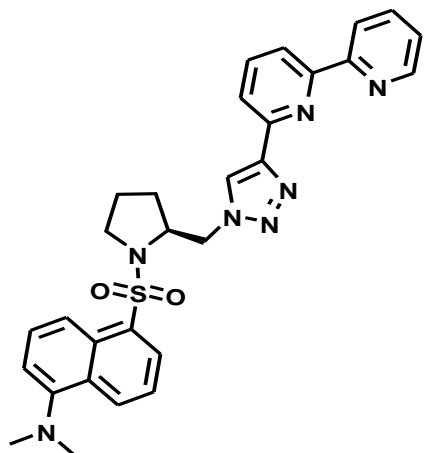


CH₂Cl₂-TFA (30 mL, 50:50) was added slowly at ice temperature. The mixture was warmed to room temperature and stirred for 2 hrs. After evaporating reaction mixture to dryness under vacuo, the residue was dissolved in CH₂Cl₂ (15

mL) and then treated with a saturated NaHCO₃ solution (30 mL) for 1h at room temperature. The aqueous layer was extracted with CH₂Cl₂ (10 mL x 3) and combined extracts were dried over anhydrous Na₂SO₄. After filtration the CH₂Cl₂ was evaporated to obtain light yellowish solid of free-amine (300 mg, Yield 98 %). ¹H NMR (400 MHz, CDCl₃) δ 1.54-1.61 (1H, m), 1.74-1.86 (2H, m), 1.97-2.05 (2H, m), 2.97-3.03 (2H, m), 3.68-3.75 (1H, m), 4.30-4.54 (2H, m), 7.31-7.34 (1H, ddd, *J* = 1.6 Hz, 3.6 Hz, 1.2 Hz), 7.81-7.85 (1H, td, *J* = 6.0 Hz, 1.6 Hz), 7.88-7.93 (1H, t, *J* = 7.6 Hz), 8.17- 8.19 (1H, dd, *J* = 7.2 Hz, 0.8 Hz), 8.33- 8.35 (1H, dd, *J* = 7.2 Hz, 0.8 Hz), 8.39 (1H, s), 8.48-8.50 (1H, d, *J* = 8.0 Hz), 8.69- 8.70 (1H, dd, *J* = 4.0 Hz, 0.8 Hz). ¹³C NMR (100 MHz, CDCl₃) δ 25.3, 28.9, 46.4, 55.4, 57.8, 119.8, 119.9, 120.9, 122.8, 123.6, 136.6, 137.6, 148.2, 148.9, 149.6, 155.5, 155.8. MS (EI): *m/z* = 306.50 [M⁺] for

C₁₇H₁₈N₆. Elemental analysis: Found: C, 66.72; H, 5.94; N, 27.34, Calcd: C, 66.65; H, 5.92; N, 27.43 for C₁₇H₁₈N₆.

Dansylatedpyrrolidine methylene triazolebipyridine (BD): To a solution of free amine (300 mg, 0.98 mmol) and dansyl chloride (264 mg, 0.98 mmol) in dry DMF (15 mL)

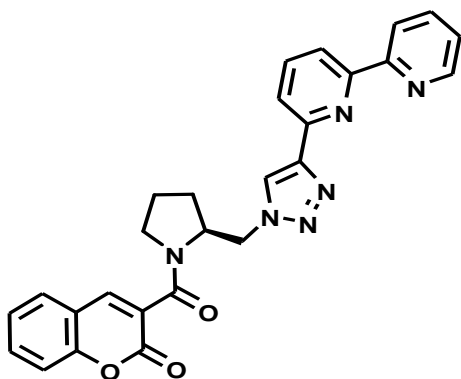


triethylamine (TEA) (0.27 mL, 1.96 mmol) was added drop wise over 30 min. The reaction mixture was stirred for 3 hrs at room temperature. After removal of solvent in vacuo, the residue was dissolved in CH₂Cl₂ (15 mL) and was washed with water (10 mL x 3). The organic phase was dried over Na₂SO₄ and solvent was evaporated on rotavap. The crude product was purified by column chromatography on silica gel using chloroform-methanol (10:1) as an eluent to afford green fluorescent solid **BD** in

good yield (520 mg, 98 %). M.P. 76-78 °C. $[\alpha]_D^{25} +71.25$ (c 1.0, CH₃OH). ¹H NMR (400 MHz, CDCl₃) δ 1.35-1.46 (1H, m), 1.54-1.63 (1H, m), 1.73-1.82 (1H, m), 1.98-2.04 (1H, m), 2.78 (1H, s), 3.24-3.33 (2H, m), 4.26-4.31 (1H, m), 4.64-4.77 (2H, m), 7.17-7.19 (1H, d, *J* = 7.6 Hz), 7.33-7.36 (1H, m), 7.54-7.62 (1H, m), 7.89-7.93 (2H, m), 8.14-8.17 (1H, dd, *J* = 6.8 Hz, 0.8 Hz), 8.27-8.29 (1H, dd, *J* = 6.4 Hz, 0.8 Hz), 8.36- 8.38 (1H, dd, *J* = 6.8 Hz, 0.8 Hz), 8.41 (1H, s), 8.53-8.60 (3H, m), 8.69-8.71 (1H, ddd, *J* = 2.4 Hz, 0.8 Hz, 0.8 Hz, 0.8 Hz). ¹³C NMR (100 MHz, CDCl₃) δ 23.8, 29.1, 45.3, 49.2, 54.0, 58.9, 115.4, 119.2, 120.0, 120.1, 121.2, 123.2, 123.4, 123.8, 128.4, 130.1, 130.2, 130.6, 131.0, 133.1, 136.9, 137.7, 148.8, 149.1, 149.5, 151.8, 155.7, 155.9. LCMS: *m/z* = 540.28 [M⁺ + H] for C₂₉H₂₉N₇O₂S. Elemental analysis: Found: C, 64.43; H, 5.52; N, 17.88; S, 5.42, Calcd: C, 64.54; H, 5.42; N, 18.17; S, 5.94. for C₂₉H₂₉N₇O₂S. Elemental analysis for **BD**•Al(ClO₄)₃•2H₂O: Found, C, 38.74; H, 3.95; N, 10.43; S, 3.36; Calcd, C, 38.66; H, 3.69; N, 10.88; S, 3.56. for C₂₉H₃₃AlCl₃N₇O₁₆S.

Coumarin-pyrrolidinyl-triazolyl-bipyridine (CB): The free-amine (300 mg, 0.98 mmol) was dissolved in dry DMF (15 mL). To this solution coumarin-3-carboxylic acid (205 mg, 1.08 mmol) was added. Then HOBt (158 mg, 1.17 mmol) and EDC.HCl (224.3 mg, 1.17

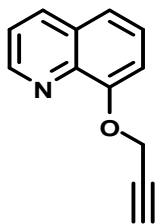
mmol) were added to this solution followed by dropwise addition of DIPEA (0.51 mL, 2.94



mmol) at 0°C. The reaction mixture was stirred at room temperature for 8 hrs. After removal of solvent in vacuo, the residue was dissolved in 15 mL CH₂Cl₂. This organic layer was washed with 10 mL of water three times (10 mL x 3). The organic phase was dried over Na₂SO₄ and solvent was evaporated. The crude product was purified by column chromatography on

silica gel with methanol/chloroform (1:10) as an eluent to afford 460 mg of white crystalline product **CB** (98 % yield). Mp 108-110°C. [α]_D²⁵ +68.35 (c 1.0, CH₃OH). ¹H NMR (400 MHz, CDCl₃) δ 1.46-1.54 (1H, M), 1.69-1.79 (1H, m), 1.98-2.07 (1H, m), 2.13-2.20 (1H, m), 3.26-3.41 (2H, m), 4.61-4.67 (1H, m), 4.76-4.80 (1H, dd, *J* = 14.0 Hz, 2.8 Hz), 5.10-5.14 (1H, dd, *J* = 14.0 Hz, 4.8 Hz), 7.24-7.28 (1H, m), 7.32-7.42 (3H, m), 7.56-7.61 (1H, m), 7.86-7.94 (2H, m), 7.99 (1H, s), 8.18-8.20 (1H, dd, *J* = 7.6 Hz, 0.8 Hz), 8.38-8.41 (1H, dd, *J* = 8.0 Hz, 0.8 Hz), 8.70-8.71 (1H, d, *J* = 4.0 Hz), 8.76 (1H, s), 8.78-8.80 (1H, d, *J* = 8.0 Hz). ¹³C NMR (100 MHz, CDCl₃) δ 24.15, 27.52, 48.85, 50.60, 57.44, 116.76, 118.13, 119.96, 120.00, 121.75, 123.80, 124.11, 124.93, 125.70, 128.75, 133.01, 137.06, 137.80, 142.94, 148.86, 149.16, 149.65, 154.16, 155.66, 155.96, 157.86, 164.38. MS (EI): *m/z* = 478.40 (M⁺) for C₂₇H₂₂N₆O₃. Elemental analysis: Found. C, 67.62; H, 4.65; N, 17.52. Calcd. C, 67.77; H, 4.63; N, 17.56 for C₂₇H₂₂N₆O₃. Elemental analysis for the complex **CB**·Al(ClO₄)₃·2H₂O; Found. C, 38.55; H, 3.13; N, 9.98. Calcd. C, 38.61; H, 3.12; N, 10.01 for C₂₇H₂₆AlCl₃N₆O₁₇. MALDI/TOF-MS for **CB**·Al³⁺·2H₂O complex. MW found, 541.14; calcd, 541.18 for C₂₇H₂₆AlN₆O₅.

8-(propargyloxy)quinoline (5): To a solution of 8-hydroxyquinoline (5.0 g, 34 mmol) in dry

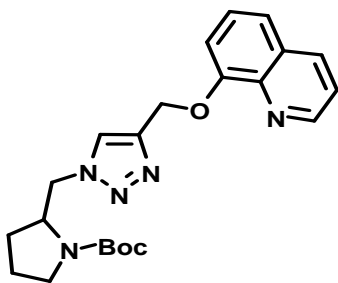


acetone (200 mL) excess anhydrous K₂CO₃ (28.15 g, 204 mmol) was added and the mixture was refluxed for 30 min. To the mixture propargyl bromide (4.09 g, 34 mmol) was added over a period of 5 h using a pressure equalizing funnel. The resulting mixture was refluxed over a period of 17 h. The reaction mixture was then cooled, filtered and filtrate was evaporated. The brown oily

residue was dissolved in CHCl₃ and then solution was washed twice with water (50 mL)

followed by saturated brine solution (50 mL). Organic layer was dried over anhydrous Na₂SO₄ and the solvent was evaporated under vacuo. The crude product was purified using column chromatography on silica gel using EtOAc /Pet Ether (4:6) as eluent to afford 5.16 g brown solid product (yield 88%). ¹H NMR (400 MHz, CDCl₃) δ 2.54 (1H, t, J = 2.4), 5.05 (2H, d, J = 2.4), 7.27 (1H, dd, J = 5.6 Hz, 1.6 Hz), 7.42-7.51 (3H, m), 8.14 (1H, dd, J = 6.8 Hz, 1.6 Hz), 8.94 (1H, dd, J = 2.4 Hz, 1.6 Hz). LCMS (EI): m/z = 184 (M+H⁺). Elemental analysis: Found. C, 78.65; H, 4.95; N, 7.66. Calcd. C, 78.67; H, 4.95; N, 7.65 for C₁₂H₉NO.

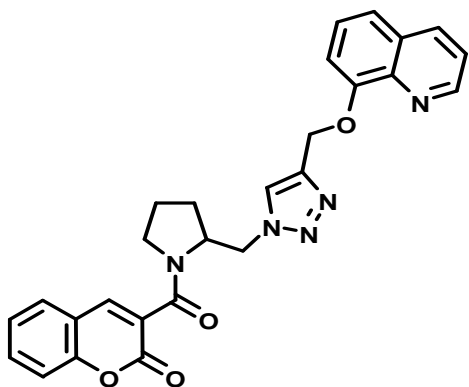
Boc-pyrrolidinyl-triazolyl-quinoline (6): To a mixture of N-Boc-2-azidomethyl pyrrolidine (1.5 g, 6.63 mmol) and 8-(propargyloxy)quinoline (1.21 g, 6.63 mmol) in water/ethanol (160 mL, v/v = 1:1), sodium ascorbate (1.3 mL, 1.32 mmol) of freshly prepared 1 M solution in water was added, followed by the addition of copper(II) sulfate 7.5 % in water (0.705 mL, 0.332 mmol). The heterogeneous mixture was stirred vigorously overnight in the dark at room temperature. The ethanol was removed under vacuo and the residue was diluted with water, cooled in ice, and then the precipitate was



collected by filtration. After washing the precipitate with cold water (10 mL), it was dried under vacuum and the crude product was purified using column chromatography on silica gel with CHCl₃/MeOH (9:1) as eluent to afford brown oily product (2.26 g, yield 96%). ¹H NMR (400 MHz, CDCl₃) δ 1.3 (11H, m), 1.82 (2H, m), 2.77-3.23 (2H, m), 4 (1H, m), 4.46 (2H, m), 5.54 (2H, s), 7.19 (1H, m), 7.33 (3H, m), 7.57 (1H, m), 8.07 (1H, d, J = 8 Hz), 8.88 (1H, d, J = 2.8 Hz). LCMS (ED): m/z = 410 (M+H⁺). Elemental analysis: Found. C, 64.49; H, 6.65; N, 17.12. Calcd. C, 64.53; H, 6.65; N, 17.10 for C₂₂H₂₇N₅O₃.

Quinoline-triazolyl-pyrrolidinyl-coumarin (QC): To Boc-protected product **6** (0.5 g, 1.22 mmol), CH₂Cl₂-TFA (30 mL, 50:50) was added slowly at ice temperature. The mixture was warmed to room temperature and stirred for 2 h. After evaporating reaction mixture to dryness under vacuo, the residue was dissolved in CH₂Cl₂ (15 mL) and then treated with a saturated NaHCO₃ solution (30 mL) for 1 h at room temperature. The aqueous layer was extracted with CHCl₃ (10 mL x 3) and combined extracts were dried over anhydrous Na₂SO₄.

After filtration the CH₂Cl₂ was evaporated to obtain dark brown oily Boc-protected amine

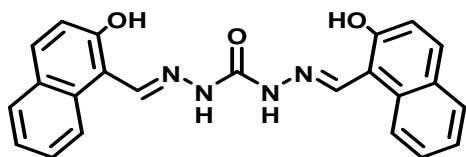


(7) (0.35 g, Yield 92 %). This amine (7) (0.35 g, 85.6 mmol) was dissolved in dry DMF (15 mL) and coumarin-carboxylic acid (0.163 g, 85.6 mmol) was added. Then HOBt (0.14 g, 1.027 mmol) and EDC.HCl (0.197 g, 1.027 mmol) were added to this solution followed by dropwise addition of DIPEA (0.5 mL, 2.56 mmol) at ice temperature. The reaction mixture was stirred at room temperature for 10 h.

After removal of solvent in vacuo, the residue was dissolve in 15 mL CH₂Cl₂. This organic layer was washed with 10 mL of water (10 mL x 3). The organic phase was dried over Na₂SO₄ and solvent was evaporated under vacuo. The crude product was purified by column chromatography on silica gel with methanol/chloroform (1:10) as an eluent to afford crystalline light pink product quinoline-triazolyl-pyrrolidinyl-coumarin (**QC**) (0.52 g, 93 % yield). ¹H NMR (400 MHz, CDCl₃) 1.25 (1H, m), 1.62 (1H, m), 1.92 (1H, m), 2.05 (1H, m), 3.02 (1H, m), 3.25 (1H, m), 4.52 (1H, m), 4.63 (1H, m), 4.91 (1H, dd, *J* = 9.2 Hz, 4.8 Hz), 5.59 (2H, s), 7.39 (6H, m), 7.53 (1H, dd, *J* = 6.4 Hz, 1.2 Hz), 7.60 (1H, m), 7.95 (1H, s), 8.09 (2H, m), 8.88 (1H, dd, *J* = 2.8 Hz, 1.6 Hz). ¹³C NMR (100 MHz, CDCl₃) δ 23.9, 27.5, 48.3, 50.7, 57.4, 62.7, 110.3, 116.8, 118.1, 120.1, 121.5, 124.9, 125.0, 125.5, 126.6, 128.8, 129.4, 133.0, 135.9, 140.3, 143.1, 144.2, 149.2, 153.8, 154.1, 157.7, 164.2. LCMS (EI): *m/z* = 482 (M+H⁺). Elemental analysis: Found. C, 65.36; H, 4.81; N, 14.52. Calcd. C, 65.35; H, 4.81; N, 14.54 for C₂₇H₂₃N₅O₄.

Naphthaldehyde-carbonohydrazone (NC) or naphthaldehyde-thiocarbonohydrazone (NTC): A solution of 2-hydroxy-1-naphthaldehyde (1.0 g, 6.0 mmol) in ethanol (40 mL) was added slowly to a solution of thiocarbonylhydrazide or carbonylhydrazide (3.0 mmol) in water (40 mL). Initially the solution turned turbid and after complete addition the solution became clear. The reaction mixture was refluxed with stirring for 24 h. Reaction mixture was cooled to room temperature and the precipitated was filtered. The precipitate was washed with ethanol and dried under vacuo to obtain naphthaldehyde-carbonohydrazone (**NC**) or naphthaldehyde-thiocarbonohydrazone (**NTC**) in quantitative yield.

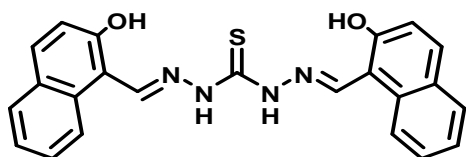
Bis[[2-hydroxynaphthyl]methylene]-carbonic dihydrazide [naphthaldehyde-carbonohydrazone (NC)]: Yield 94%. ¹H NMR (400 MHz, DMSO-*d*₆) δ_{ppm} 7.22-7.24 (2H,



d, *J* = 8.8 Hz), 7.38-7.42 (2H, m), 7.58-7.62 (2H, m), 7.87-7.90 (4H, m), 8.33-8.35 (2H, d, *J* = 8.4 Hz), 9.19 (2H, s), 11.00 (2H, s), 11.87 (2H, br). ¹³C NMR (100 MHz, DMSO-*d*₆) δ_{ppm} 109.4, 118.6, 121.6, 123.3,

127.6, 127.9, 128.7, 131.5, 131.9, 143.2, 151.6, 156.7. MS (EI): *m/z* = 399.2 [M+H]⁺, calcd. 398.14 for C₂₃H₁₈N₄O₃. Elemental analysis: Found C, 69.37; H, 4.57; N, 13.99; Calcd. C, 69.34; H, 4.55; N, 14.06 for C₂₃H₁₈N₄O₃.

Bis[[2-hydroxynaphthyl]methylene]-carbonothioic dihydrazide dihydrazide [naphthaldehyde-thiocarbonohydrazone (NTC)]: Yield 94%. ¹H NMR (400 MHz,



DMSO-*d*₆) δ_{ppm} 7.23-7.25 (2H, d, *J* = 9.2 Hz), 7.39-7.43 (2H, m), 7.59-7.63 (2H, m), 7.88-7.95 (4H, m), 8.24-8.52 (2H, br), 9.16-9.64 (2H, br), 10.61 (1H, br), 12.07 (2H, s), 12.88 (1H, br). ¹³C NMR (100 MHz,

DMSO-*d*₆) δ_{ppm} 109.3, 118.7, 121.0, 123.5, 127.8, 127.9, 128.7, 131.7, 132.6, 145.8, 157.1, 174.0. MS (EI): *m/z* = 415.4 [M+H]⁺, calcd. For 414.12 C₂₃H₁₈N₄O₂S. Elemental analysis: Found C, 66.7; H, 4.39; N, 13.51; S, 7.72; Calcd. C, 66.65; H, 4.38; N, 13.52; S, 7.74 for C₂₃H₁₈N₄O₂S.

4.3 General method of UV-Vis and fluorescence titration

UV-Vis spectra were recorded on Perkin Elmer Lambda 900 spectrophotometer and fluorescence spectra were recorded on a Perkin Elmer model LS 55 spectrophotometer. 1 cm cells were used for absorption and emission titration. For UV-Vis and fluorescence titrations stock solution of probes (**BD 1**, **CB 1** and **QC**) were prepared (*c* = 2000 μM) in CH₃CN. For UV-Vis and fluorescence titrations stock solution of ligands (**NC** and **NTC**) were prepared (*c* = 2000 μM) in DMSO. The solutions of guest cations were prepared in CH₃CN in the order of 10⁻³ M. Working solutions of probes and metal ions were prepared from the stock solutions 10 nm excitation and 10 nm emissions slit widths are used for study.

4.4 Job plot by UV-Vis method

A series of solutions containing **BD** and Al(ClO₄)₃ were prepared such that the sum of the total metal ion and **BD** concentration remained constant (100 μM). The mole fraction (X) of Al³⁺ was varied from 0.1 to 1.0. The corrected absorbance (OD₃₃₂*X_{Al³⁺}*10³) at 332 nm was plotted against the molar fraction of the Al³⁺ solution.

A series of solutions containing **CB** and Al(ClO₄)₃ were prepared such that the sum of the total metal ion and **CB** concentration remained constant (100 μM). The mole fraction (X) of **CB** was varied from 0.1 to 1.0. The fluorescence intensity at 443 nm was plotted against the molar fraction of the ligand (**CB**) solution.

A series of solutions containing **QC** and Zn²⁺/ Al³⁺ were prepared such that the sum of the total concentration of **QC** and Zn²⁺/ Al³⁺ remained constant (100 μM). The mole fraction (X) of Zn²⁺ /Al³⁺ was varied from 0.1 to 1.0.

A series of solutions containing **NC/NTC** and Al(ClO₄)₃ were prepared such that the sum of the total concentration of metal ion and **NC/NTC** remained constant (100 μM). The mole fraction (X) of Al³⁺ was varied from 0.1 to 1.0. The corrected absorbance ([A-A₀] / [A₀]) at 440 nm for **NTC** and at 400 nm for **NC** were plotted against the molar fraction of the Al³⁺ solution.

4.5 Determination of binding constant

The response parameter α is defined as the ratio of the free ligand concentration to the initial concentration of the ligand. α defined as the ratio between the free ligand concentration ([L]) and the total concentration of ligand [L_T]:

$$\alpha = \frac{[L]}{[L_T]}$$

α can be determined from the emission changes in the presence of different concentrations of Mⁿ⁺:

$$\alpha = \frac{[I - I_0]}{[I_1 - I_0]}$$

where I_1 and I_0 are the limiting emission values for $\alpha = 1$ (in the absence of M^{n+}) and $\alpha = 0$ (probe is completely complexes with M^{n+}), respectively.

Li *et al.*⁴⁰ derived the Tsein equation⁵² to the following equations that can be used in any stoichiometric ratio between the ligand and analyte.

$$[M^{n+}]^m = \frac{1}{n \cdot K} \cdot \frac{1}{[L]_T^{n-1}} \cdot \frac{1-\alpha}{\alpha^n}$$

Where K is complex equilibrium constant, M_mL_n is metal-ligand, L is ligand, $[L]$, $[M^{n+}]$, and $[M_mL_n]$ are the concentrations of respective species.

4.6 Calculation of detection limit for CB

The detection limit was determined from the fluorescence titration data based on a reported and broadly used method.^{53,54} According to the result of titrating experiment, the fluorescent intensity data at 443 nm were normalized between the minimum intensity (0.0 equiv. free Al³⁺) and the maximum intensity. A linear regression curve was then fitted to these normalized fluorescent intensity data, and the point at which this line crossed the ordinate axis was considered as the detection limit (1×10^{-7} M).

4.7 Calculation of quantum yields for NC/NTC

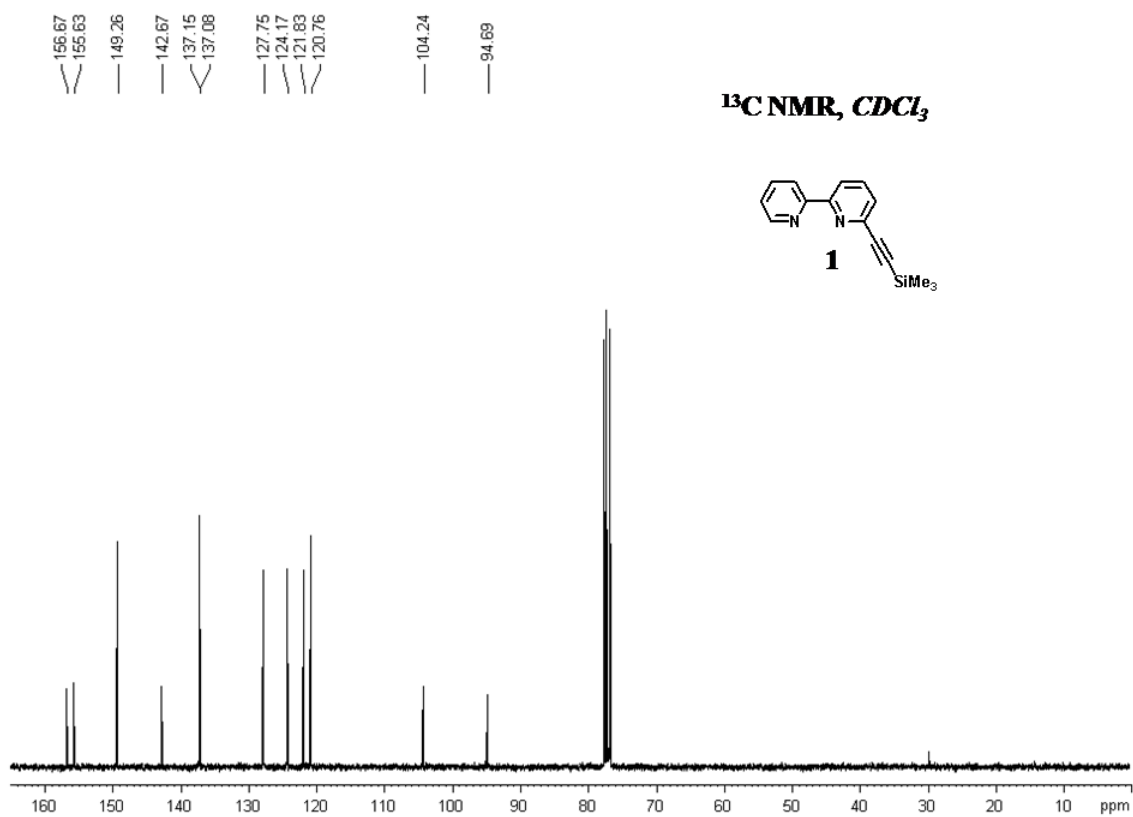
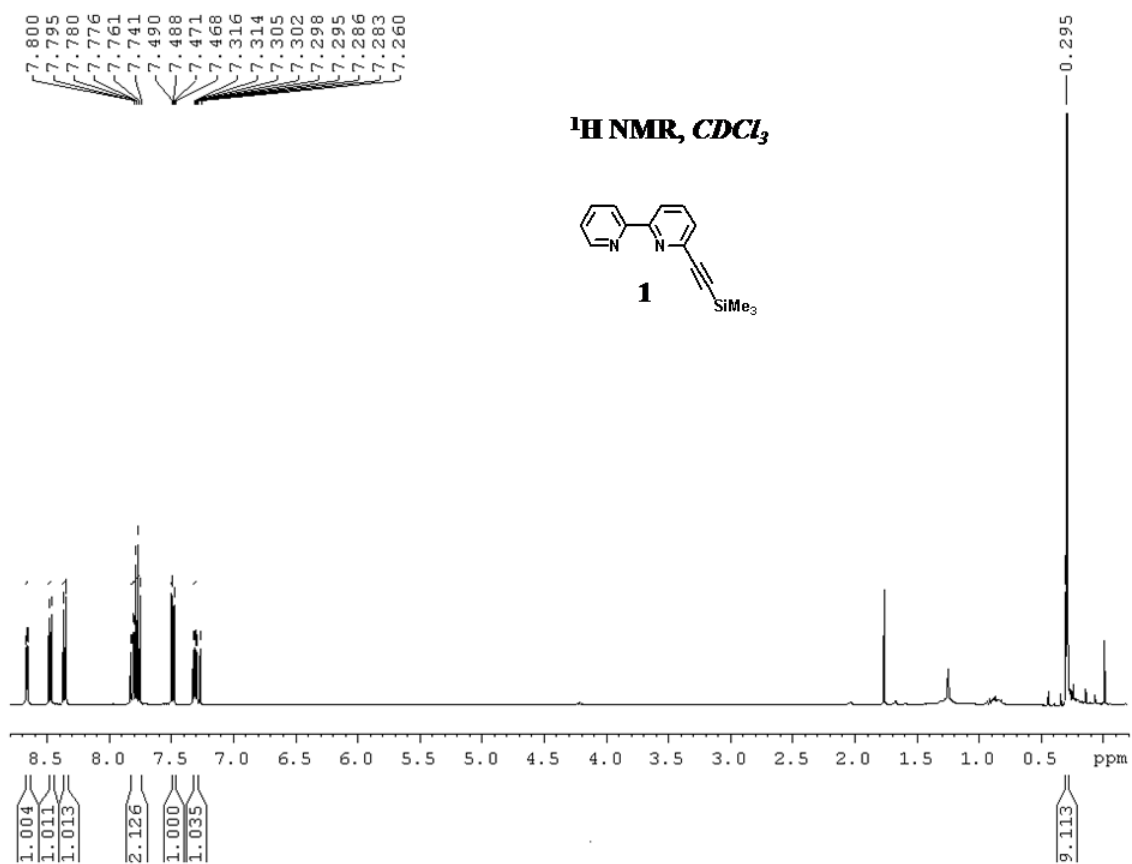
Fluorescence quantum yields were determined using the reference of perylene ($\Phi = 0.94$) in cyclohexane.⁵⁵ The quantum yields of NC/NTC and its Al³⁺ complex are calculated according to following equation at 395 nm excitation.

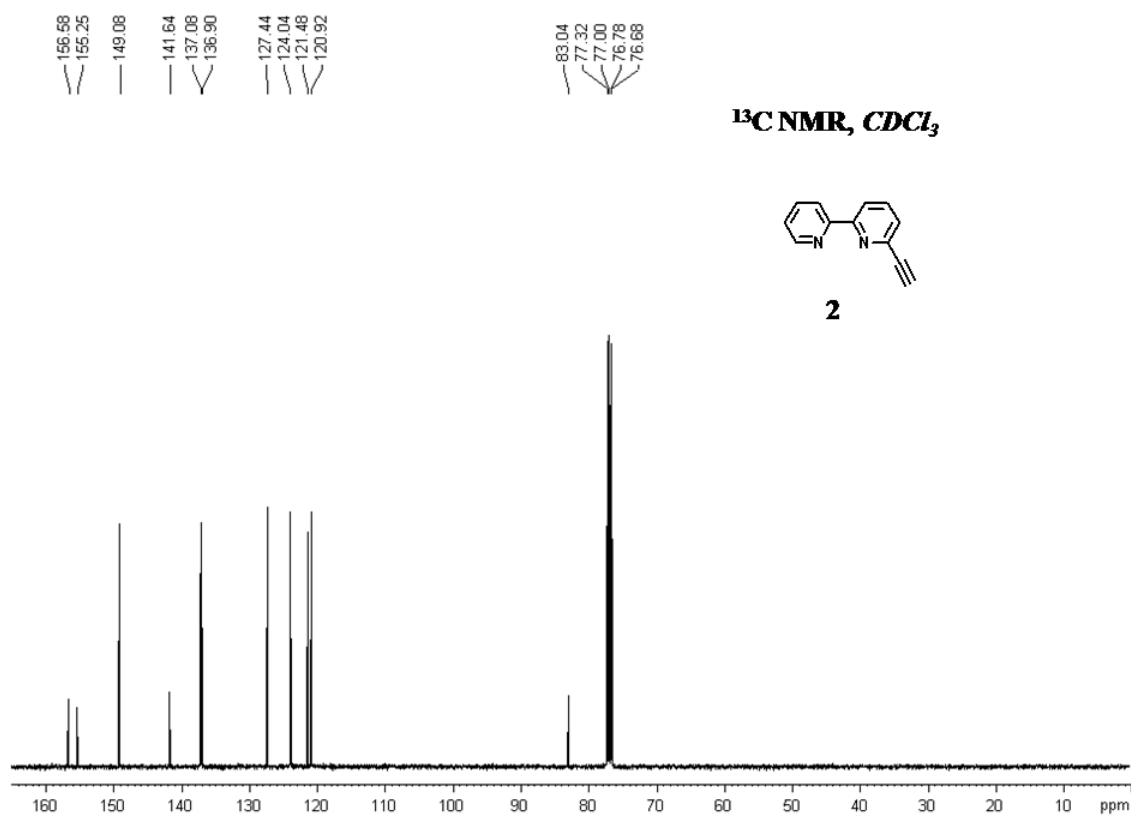
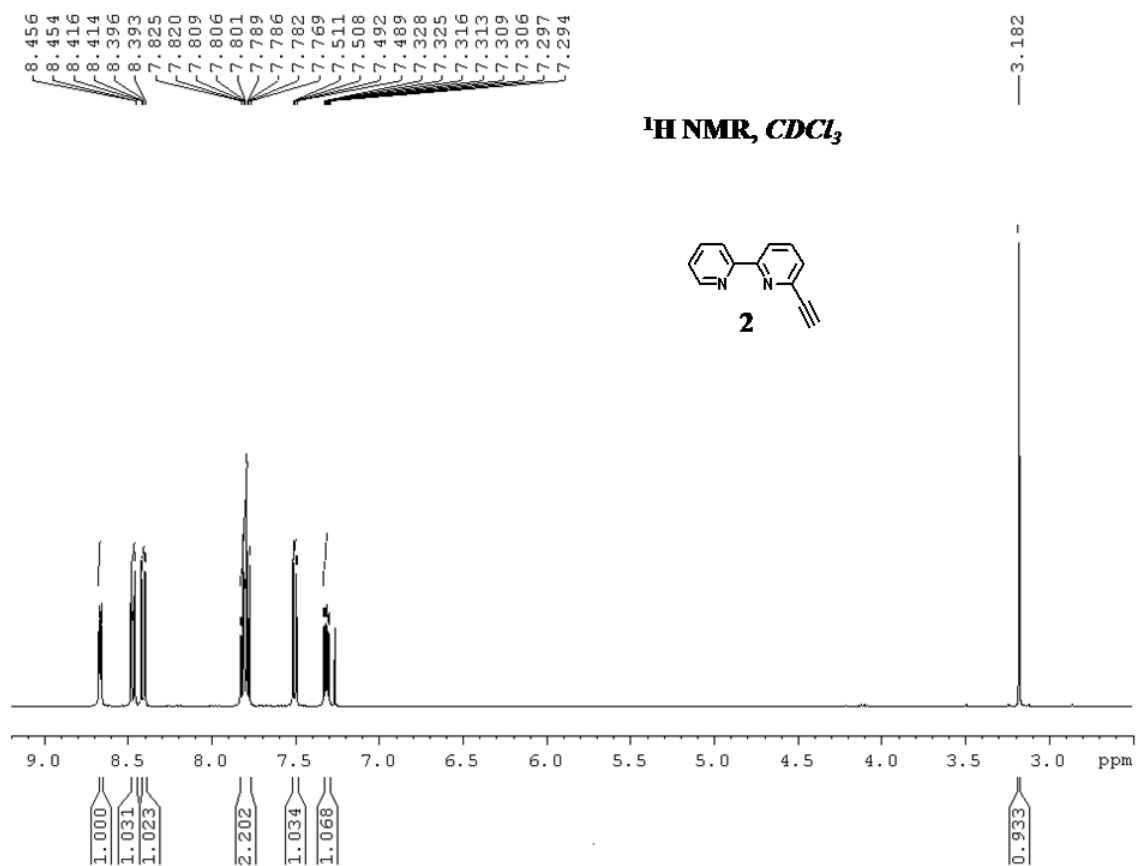
$$\Phi_x = \Phi_s (A_s S_x) / (A_x S_s) (n_x / n_s)$$

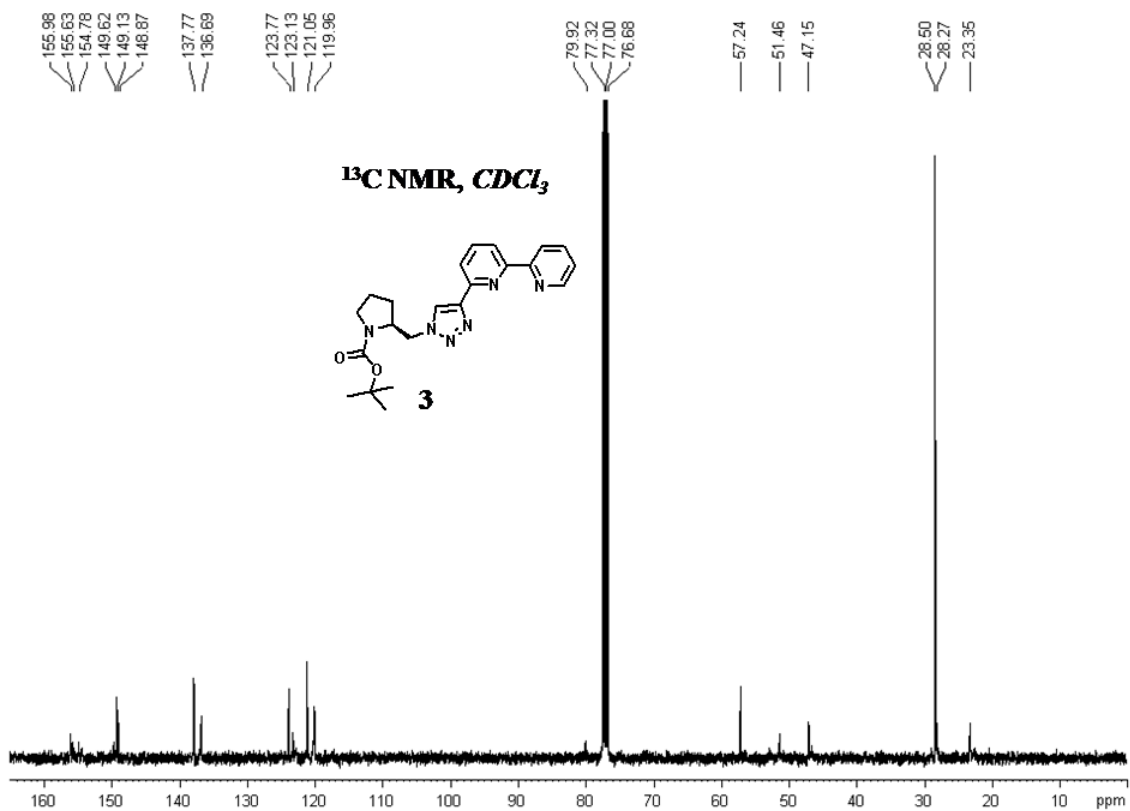
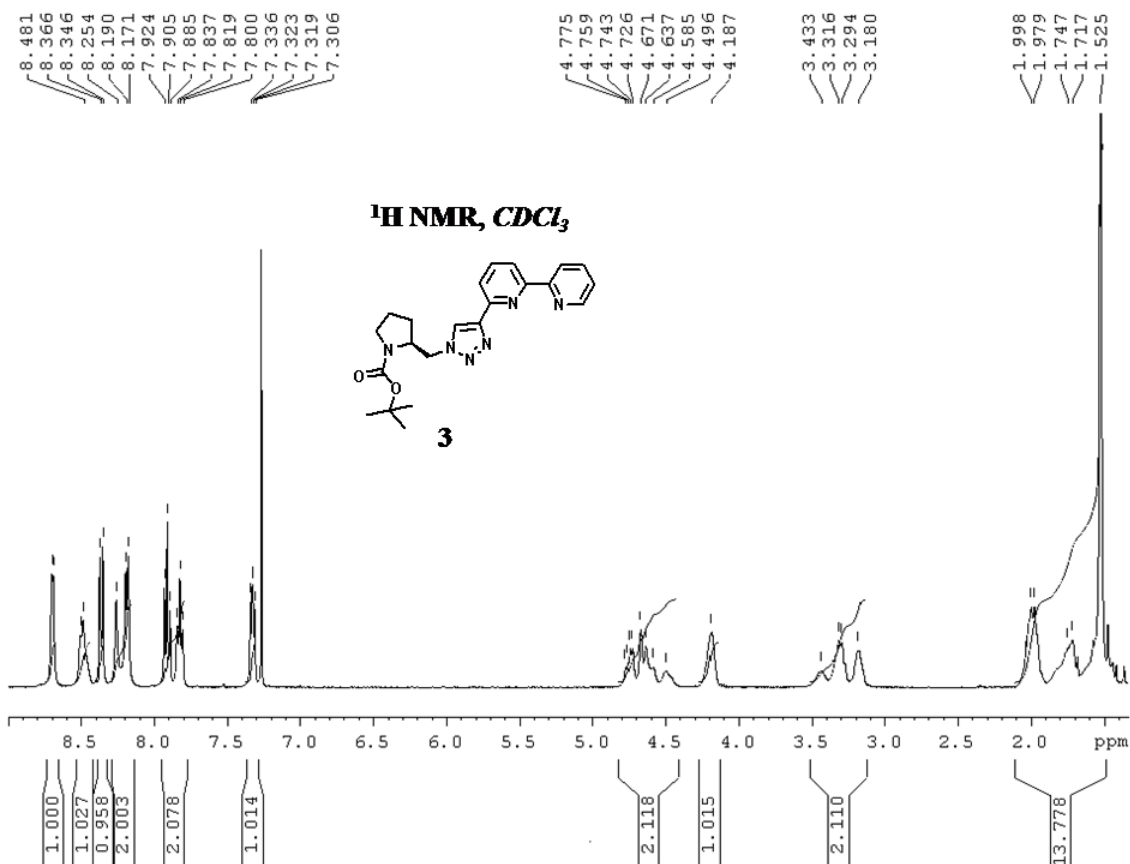
where A_x is the absorbance of NC/NTC-Al³⁺ complex and A_s of the standard perylene. S_x is the integrated fluorescence emission corresponding to NC/NTC-Al³⁺ complex and S_s of the standard perylene. n_x and n_s are the refractive index of the solvents used for complex and standard sample measurements.

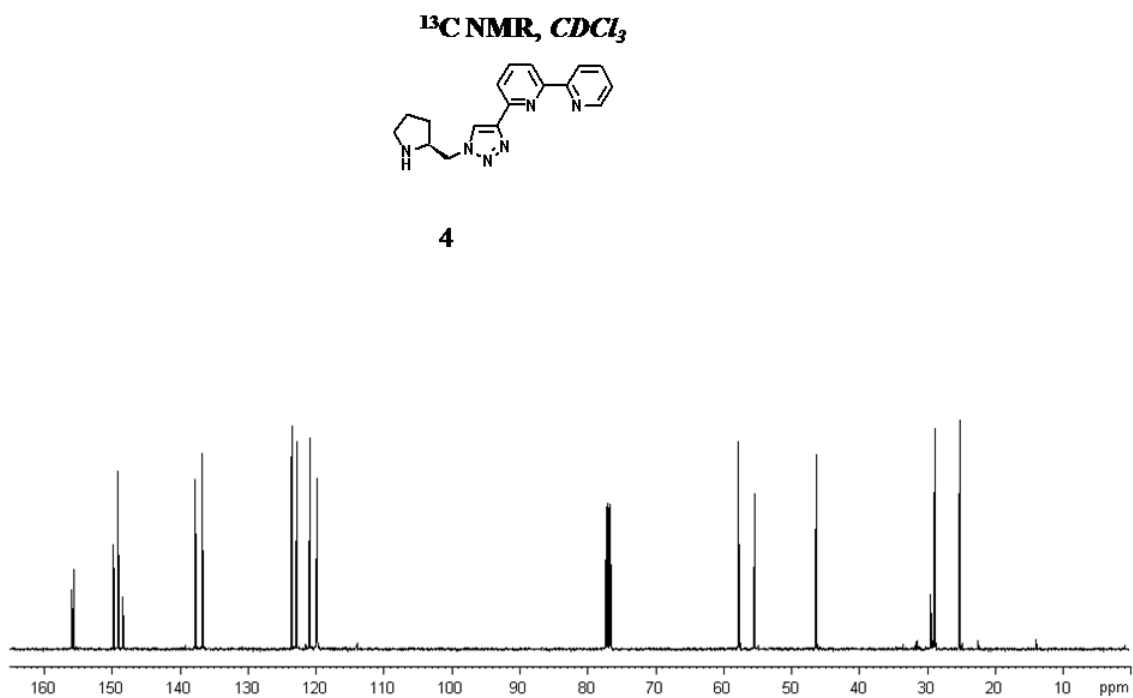
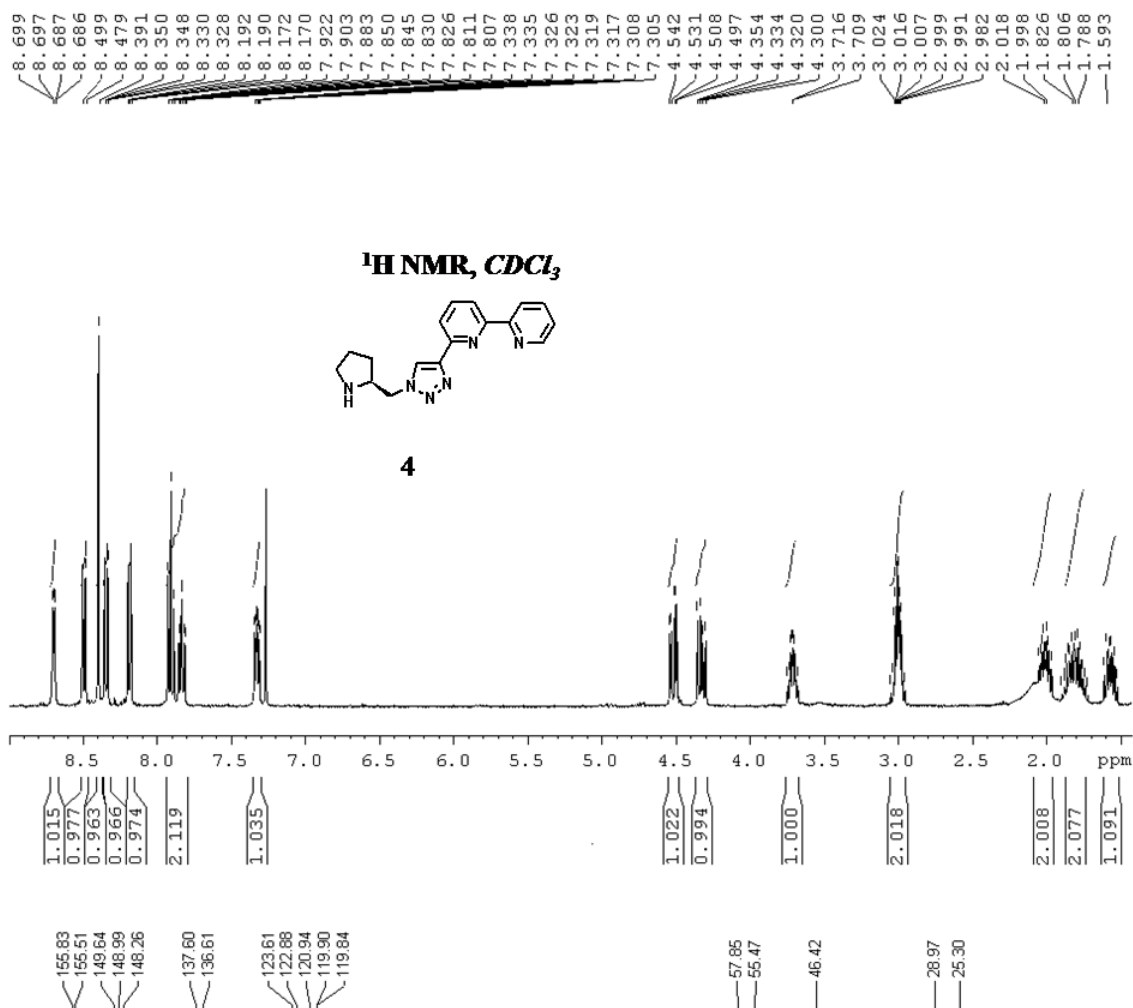
4.8 Appendix

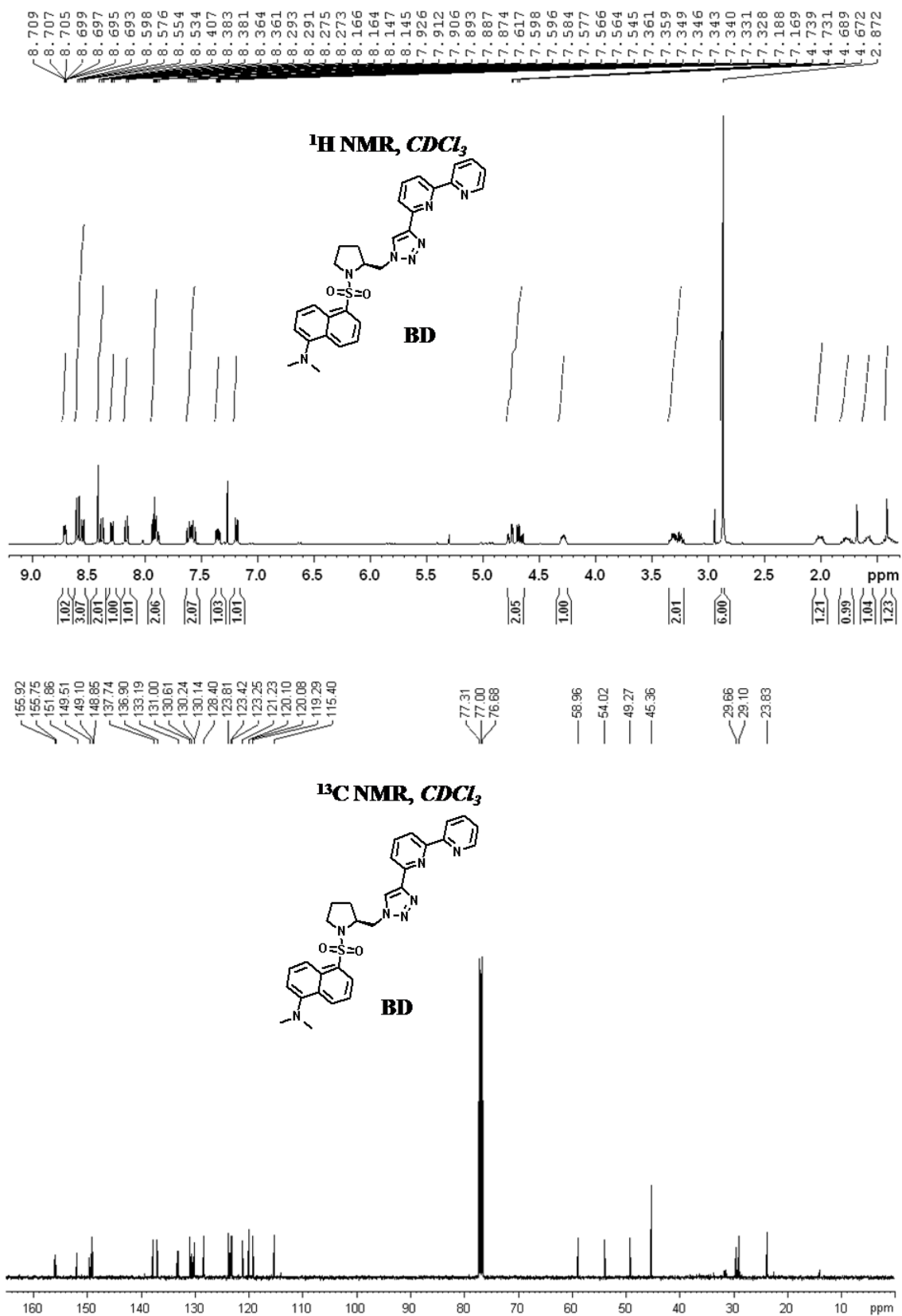
- ❖ Compound 1, ¹H and ¹³C NMR
- ❖ Compound 2, ¹H and ¹³C NMR
- ❖ Compound 3, ¹H and ¹³C NMR
- ❖ Compound 4, ¹H and ¹³C NMR
- ❖ Compound BD, ¹H and ¹³C NMR
- ❖ Compound CB, ¹H and ¹³C NMR
- ❖ Compound 5 and 6, ¹H NMR
- ❖ Compound QC, ¹H and ¹³C NMR
- ❖ Compound NC, ¹H and ¹³C NMR
- ❖ Compound NTC, ¹H and ¹³C NMR

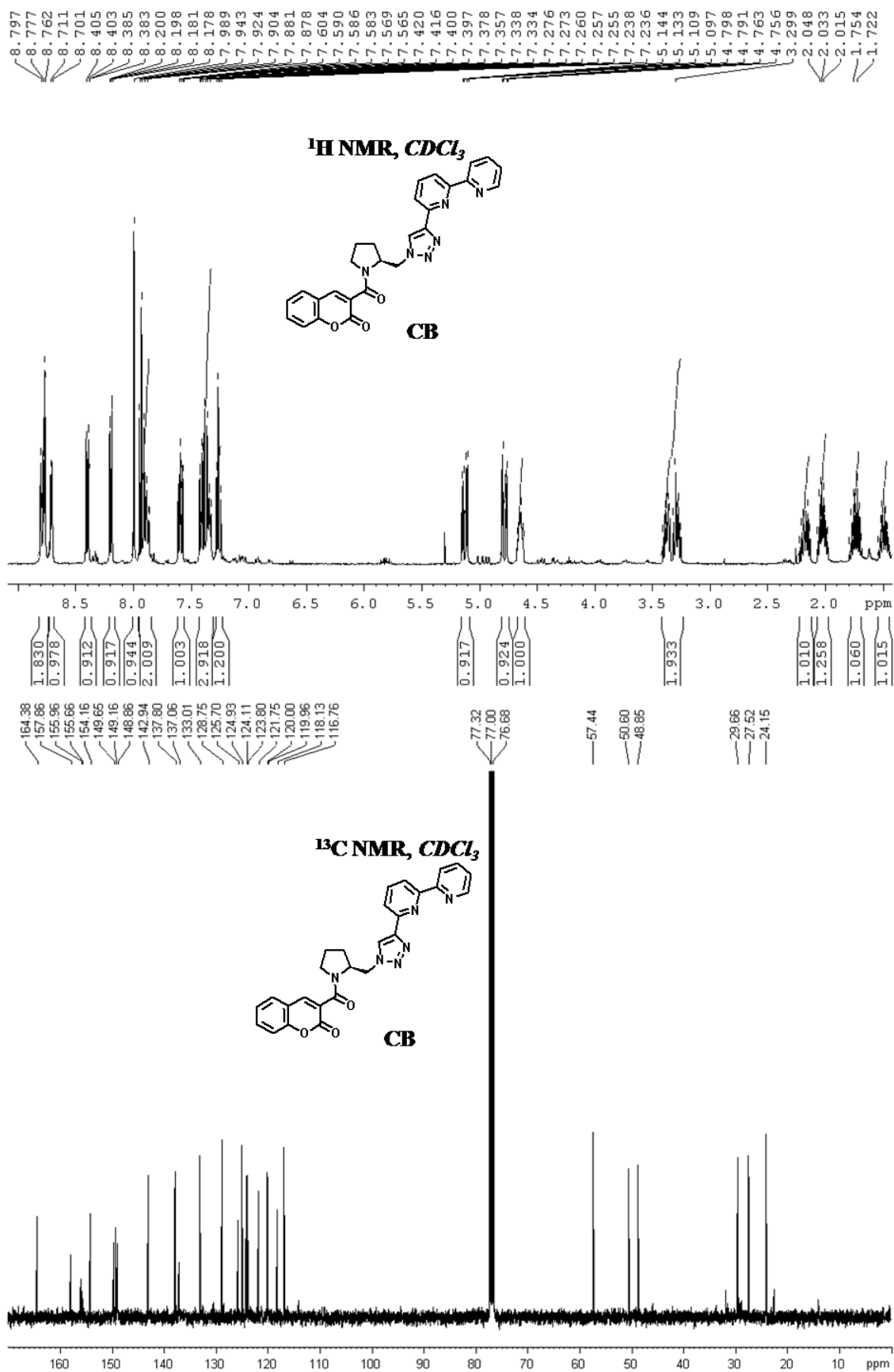


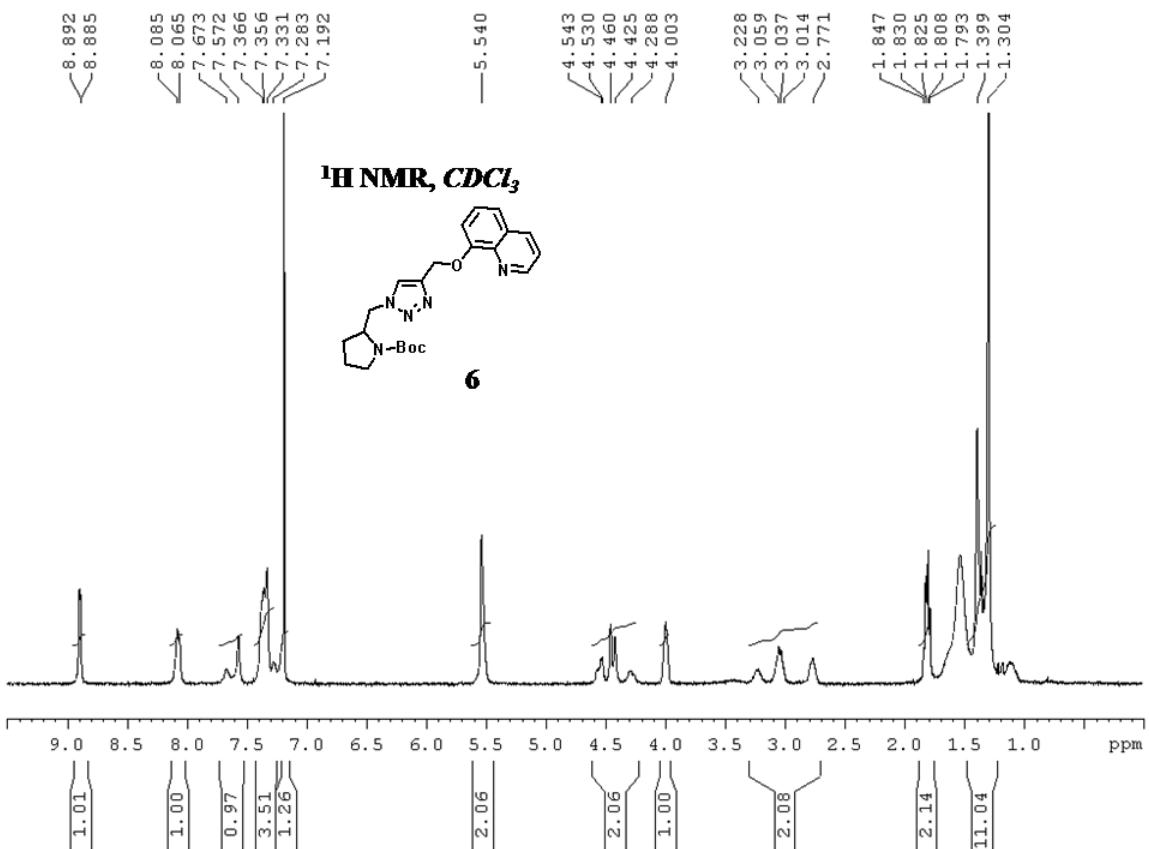
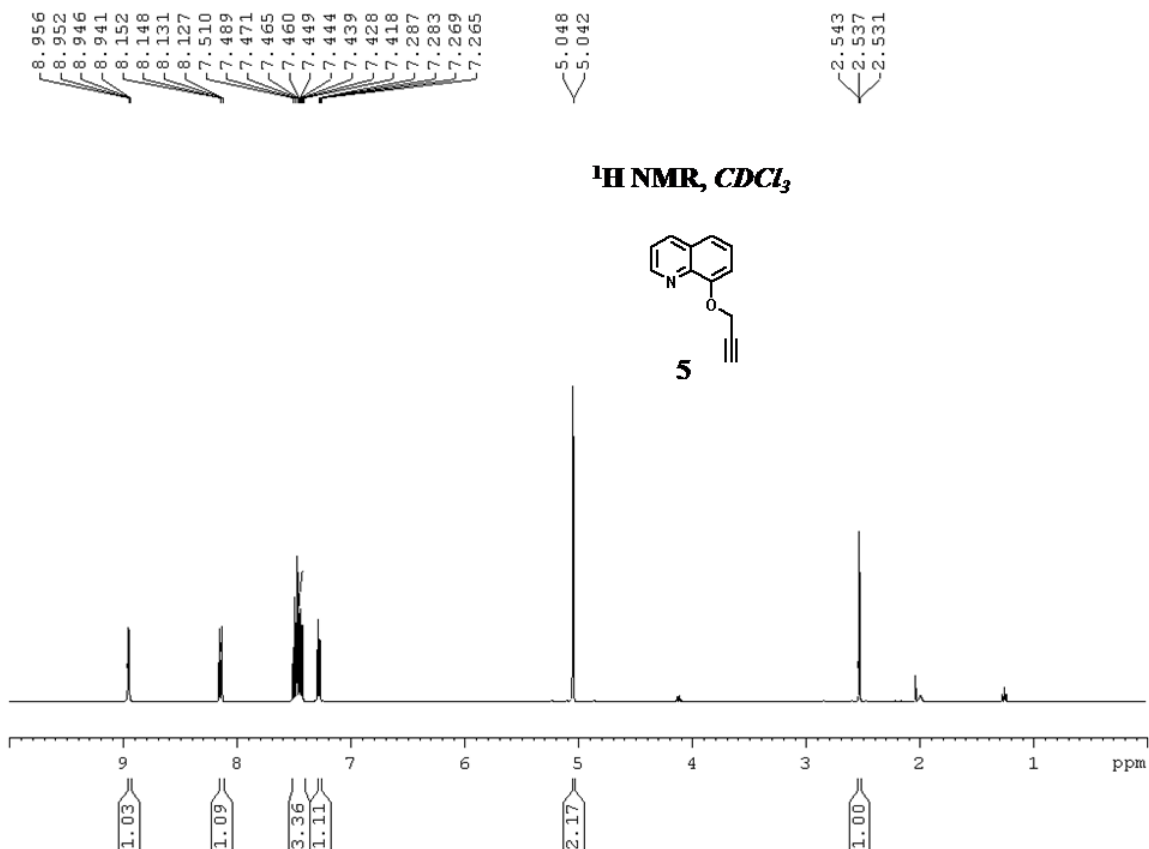


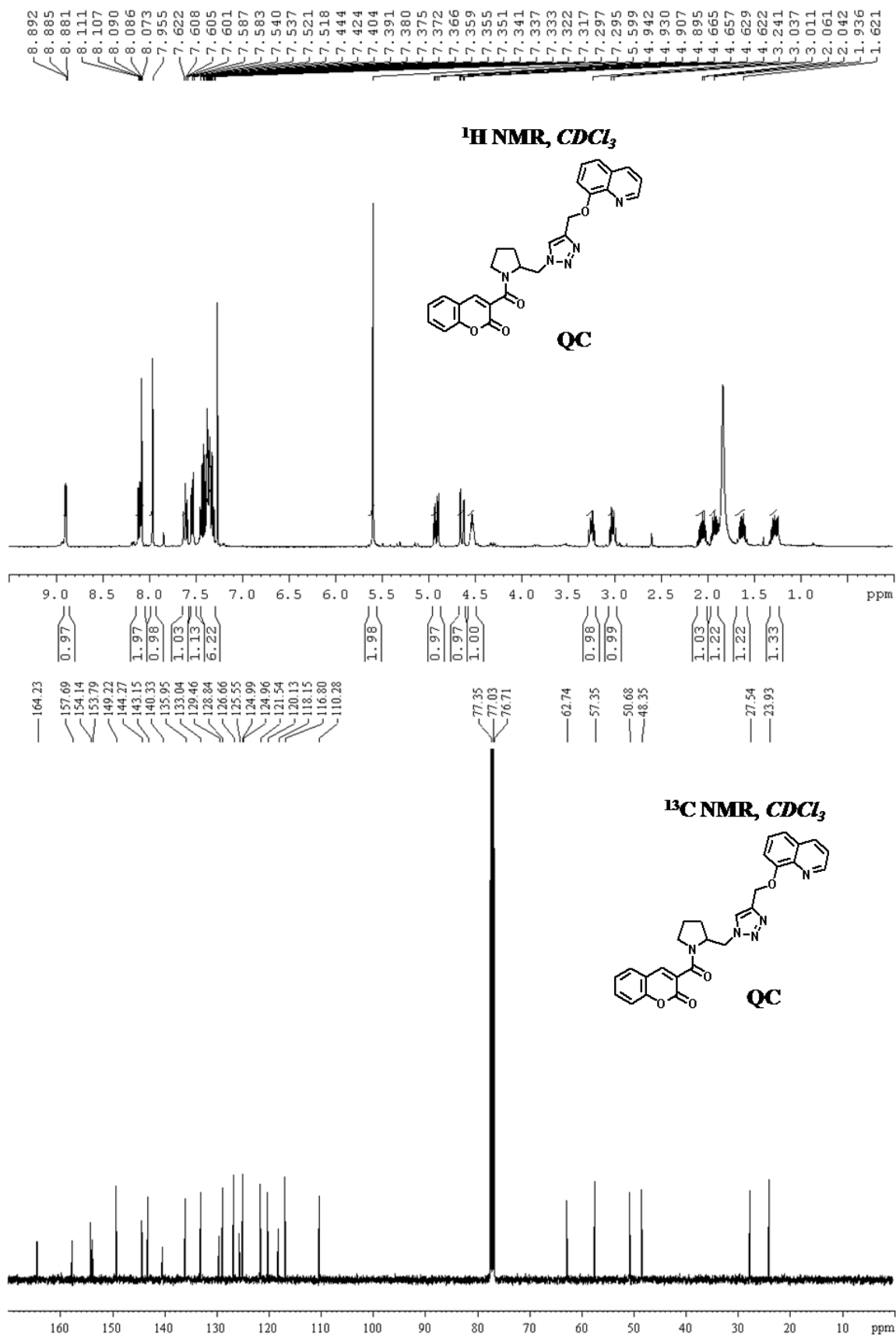


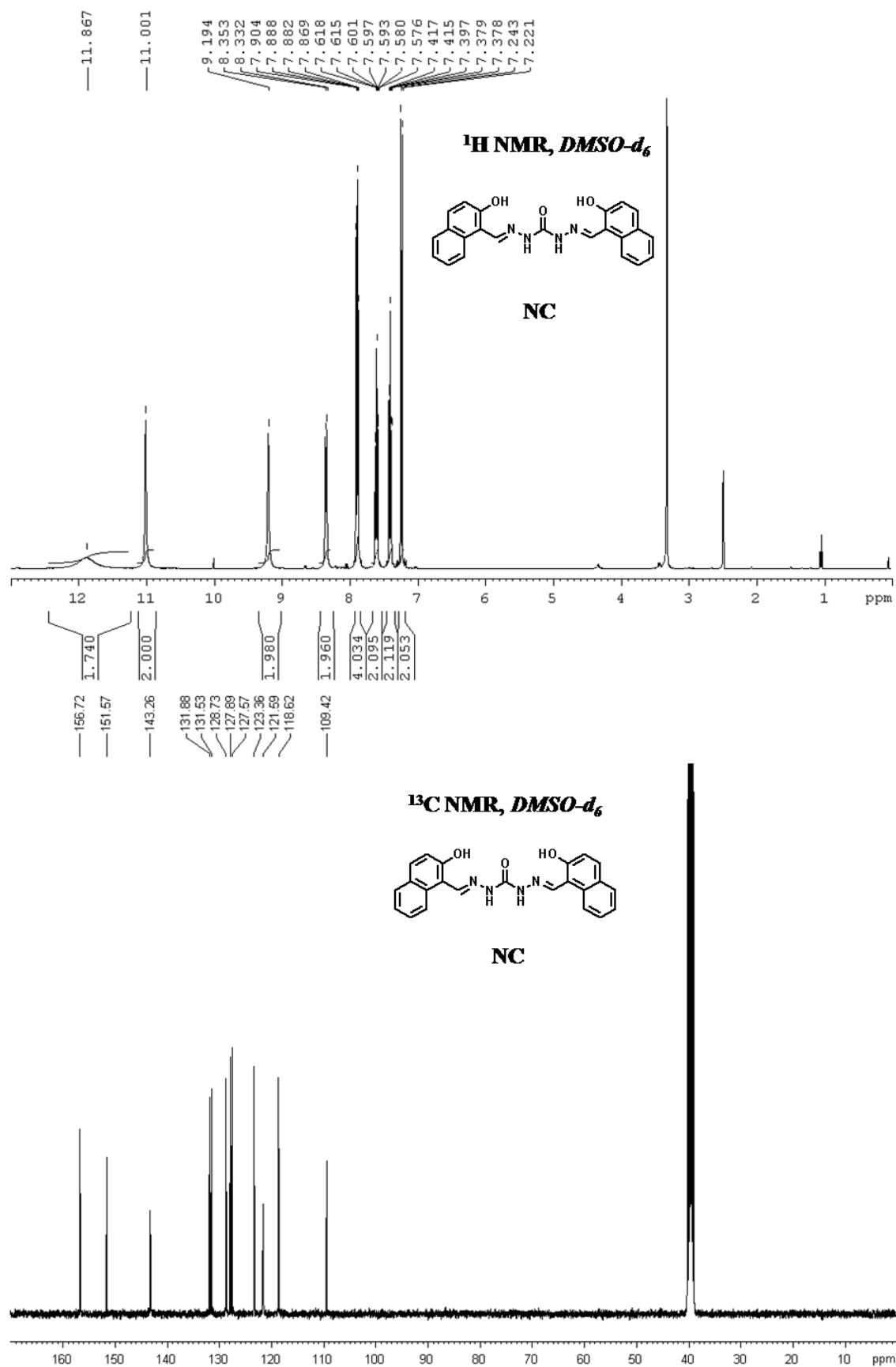


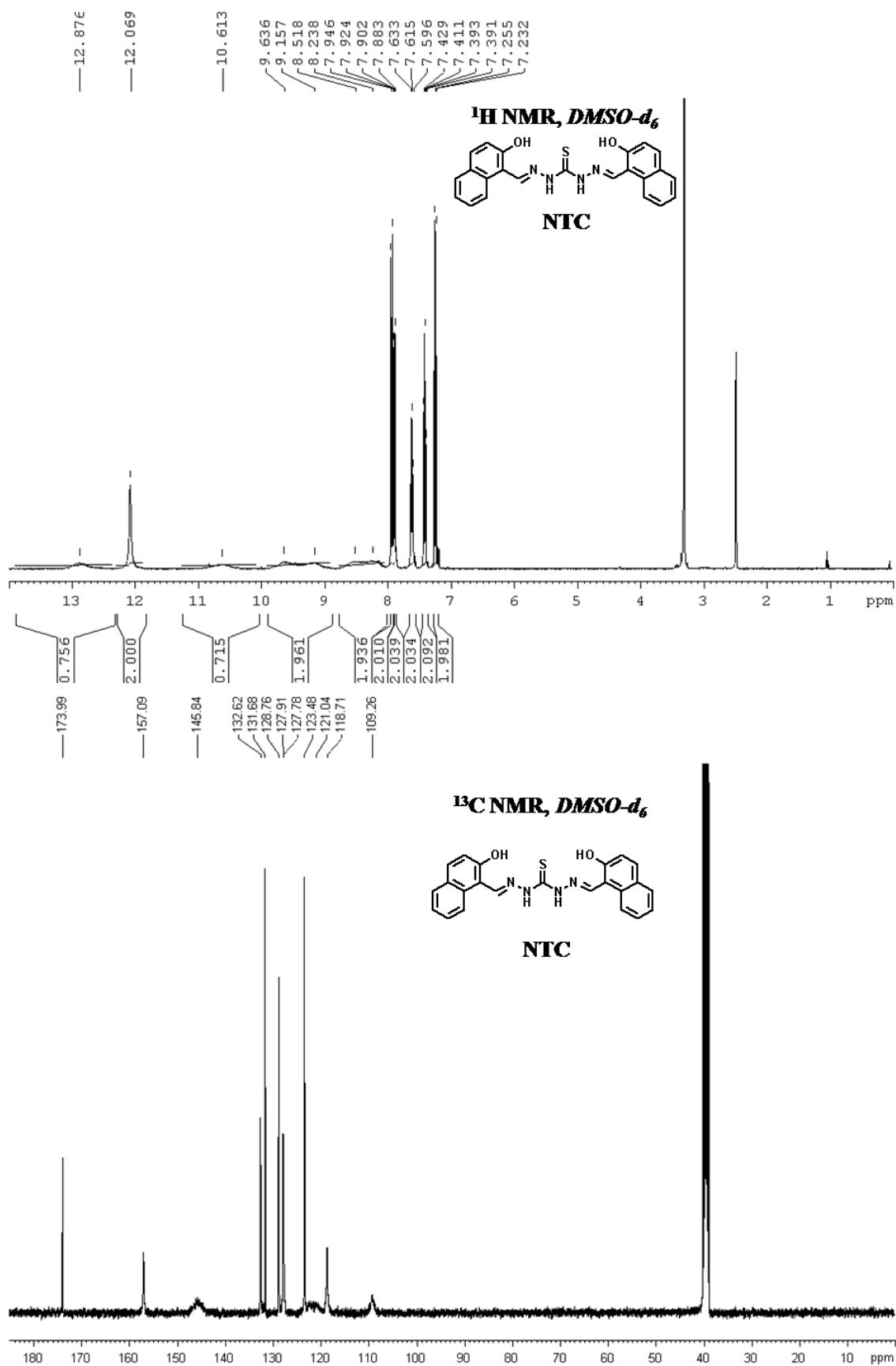












5. References

1. Burgess, J., Man and the elements of Group 3 and 13. *Chem. Soc. Rev.* **1996**, *25*, 85-92.
2. Godbold, D. L.; Fritz, E.; Hüttermann, A., Aluminum toxicity and forest decline. *Proc. Natl. Acad. Sci. USA* **1988**, *85*, 3888-3892.
3. Berthon, G., Aluminium speciation in relation to aluminium bioavailability, metabolism and toxicity. *Coord. Chem. Rev.* **2002**, *228*, 319-341.
4. Fasman, G. D., Aluminum and alzheimer's disease: model studies. *Coord. Chem. Rev.* **1996**, *149*, 125-165.
5. Martin, R. B., Aluminum: a neurotoxic product of acid rain. *Acc. Chem. Res.* **1994**, *27*, 204-210.
6. Barceló, J.; Poschenrieder, C., Fast root growth responses, root exudates, and internal detoxification as clues to the mechanisms of aluminium toxicity and resistance: a review. *Environ. Exp. Bot.* **2002**, *48*, 75-92.
7. Valeur, B.; Leray, I., Design principles of fluorescent molecular sensors for cation recognition. *Coord. Chem. Rev.* **2000**, *205*, 3-40.
8. Kim, S. H.; Choi, H. S.; Kim, J.; Lee, S. J.; Quang, D. T.; Kim, J. S., Novel optical/electrochemical selective 1,2,3-triazole ring-appended chemosensor for the Al³⁺ ion. *Org. Lett.* **2009**, *12*, 560-563.
9. Nayak, P., Aluminum: impacts and disease. *Environ. Res.* **2002**, *89*, 101-115.
10. Soroka, K.; Vithanage, R. S.; Phillips, D. A.; Walker, B.; Dasgupta, P. K., Fluorescence properties of metal complexes of 8-hydroxyquinoline-5-sulfonic acid and chromatographic applications. *Anal. Chem.* **1987**, *59*, 629-636.
11. Arduini, M.; Felluga, F.; Mancin, F.; Rossi, P.; Tecilla, P.; Tonellato, U.; Valentinuzzi, N., Aluminium fluorescence detection with a FRET amplified chemosensor. *Chem. Commun.* **2003**, *0*, 1606-1607.
12. Othman, A. B.; Lee, J. W.; Huh, Y.-D.; Abidi, R.; Kim, J. S.; Vicens, J., A novel pyrenyl-appended tricalix[4]arene for fluorescence-sensing of Al(III). *Tetrahedron* **2007**, *63*, 10793-10800.
13. Zhou, Y.; Wang, F.; Kim, Y.; Kim, S.-J.; Yoon, J., Cu²⁺-selective ratiometric and "off-on" sensor based on the rhodamine derivative bearing pyrene group. *Org. Lett.* **2009**, *11*, 4442-4445.
14. Zhao, Y.; Lin, Z.; Liao, H.; Duan, C.; Meng, Q., A highly selective fluorescent chemosensor for Al³⁺ derivated from 8-hydroxyquinoline. *Inorg. Chem. Commun.* **2006**, *9*, 966-968.
15. Hung, T.-C.; Lin, C.-W.; Hsu, T.-L.; Wu, C.-Y.; Wong, C.-H., Investigation of SSEA-4 binding protein in breast cancer cells. *J. Am. Chem. Soc.* **2013**, *135*, 5934-5937.
16. Domaille, D. W.; Que, E. L.; Chang, C. J., Synthetic fluorescent sensors for studying the cell biology of metals. *Nat. Chem. Biol.* **2008**, *4*, 168-175.

17. de Silva, A. P.; Moody, T. S.; Wright, G. D., Fluorescent PET (Photoinduced Electron Transfer) sensors as potent analytical tools. *Analyst* **2009**, *134*, 2385-2393.
18. Ueno, T.; Nagano, T., Fluorescent probes for sensing and imaging. *Nat. Meth.* **2011**, *8*, 642-645.
19. Xu, Z.; Chen, X.; Kim, H. N.; Yoon, J., Sensors for the optical detection of cyanide ion. *Chem. Soc. Rev.* **2010**, *39*, 127-137.
20. Waldron, K. J.; Rutherford, J. C.; Ford, D.; Robinson, N. J., Metalloproteins and metal sensing. *Nature* **2009**, *460*, 823-830.
21. Liu, Z.; He, W.; Guo, Z., Metal coordination in photoluminescent sensing. *Chem. Soc. Rev.* **2013**, *42*, 1568-1600.
22. McRae, R.; Bagchi, P.; Sumalekshmy, S.; Fahrni, C. J., In situ imaging of metals in cells and tissues. *Chem. Rev.* **2009**, *109*, 4780-4827.
23. Hancock, R. D., The pyridyl group in ligand design for selective metal ion complexation and sensing. *Chem. Soc. Rev.* **2013**, *42*, 1500-1524.
24. Lau, Y. H.; Rutledge, P. J.; Watkinson, M.; Todd, M. H., Chemical sensors that incorporate click-derived triazoles. *Chem. Soc. Rev.* **2011**, *40*, 2848-2866.
25. Hua, Y.; Flood, A. H., Click chemistry generates privileged CH hydrogen-bonding triazoles: the latest addition to anion supramolecular chemistry. *Chem. Soc. Rev.* **2010**, *39*, 1262-1271.
26. Maity, D.; Govindaraju, T., Pyrrolidine constrained bipyridyl-dansyl click fluoroionophore as selective Al³⁺ sensor. *Chem. Commun.* **2010**, *46*, 4499-4501.
27. Trenor, S. R.; Shultz, A. R.; Love, B. J.; Long, T. E., Coumarins in polymers: from light harvesting to photo-cross-linkable tissue scaffolds. *Chem. Rev.* **2004**, *104*, 3059-3078.
28. Ray, D.; Bharadwaj, P. K., A coumarin-derived fluorescence probe selective for magnesium. *Inorg. Chem.* **2008**, *47*, 2252-2254.
29. Maity, D.; Govindaraju, T., Conformationally constrained (coumarin-triazolyl-bipyridyl) click fluoroionophore as a selective Al³⁺ sensor. *Inorg. Chem.* **2010**, *49*, 7229-7231.
30. Maity, D.; Govindaraju, T., A differentially selective sensor with fluorescence turn-on response to Zn²⁺ and dual-mode ratiometric response to Al³⁺ in aqueous media. *Chem. Commun.* **2012**, *48*, 1039-1041.
31. Zhang, J. F.; Zhou, Y.; Yoon, J.; Kim, J. S., Recent progress in fluorescent and colorimetric chemosensors for detection of precious metal ions (silver, gold and platinum ions). *Chem. Soc. Rev.* **2011**, *40*, 3416-3429.
32. Wu, J.; Liu, W.; Ge, J.; Zhang, H.; Wang, P., New sensing mechanisms for design of fluorescent chemosensors emerging in recent years. *Chem. Soc. Rev.* **2011**, *40*, 3483-3495.

33. Martínez, R.; Espinosa, A.; Tárraga, A.; Molina, P., New Hg²⁺ and Cu²⁺ Selective chromo- and fluoroionophore based on a bichromophoric azine. *Org. Lett.* **2005**, *7*, 5869-5872.
34. Wu, J.-S.; Liu, W.-M.; Zhuang, X.-Q.; Wang, F.; Wang, P.-F.; Tao, S.-L.; Zhang, X.-H.; Wu, S.-K.; Lee, S.-T., Fluorescence turn on of coumarin derivatives by metal cations: a new signaling mechanism based on C=N isomerization. *Org. Lett.* **2006**, *9*, 33-36.
35. Liu, W.; Xu, L.; Sheng, R.; Wang, P.; Li, H.; Wu, S., A water-soluble “switching on” fluorescent chemosensor of selectivity to Cd²⁺. *Org. Lett.* **2007**, *9*, 3829-3832.
36. Maity, D.; Govindaraju, T., Naphthaldehyde–urea/thiourea conjugates as turn-on fluorescent probes for Al³⁺ based on restricted C=N isomerization. *Eur. J. Inorg. Chem.* **2011**, 5479-5485.
37. Baier, M. C.; Huber, J.; Mecking, S., Fluorescent conjugated polymer nanoparticles by polymerization in miniemulsion. *J. Am. Chem. Soc.* **2009**, *131*, 14267-14273.
38. Govindaraju, T.; Kumar, V. A., Backbone-extended pyrrolidine peptide nucleic acids (bepPNA): design, synthesis and DNA/RNA binding studies. *Chem. Commun.* **2005**, *0*, 495-497.
39. de Silva, A. P.; Gunaratne, H. Q. N.; Gunlaugsson, T.; Huxley, A. J. M.; McCoy, C. P.; Rademacher, J. T.; Rice, T. E., Signaling recognition events with fluorescent sensors and switches. *Chem. Rev.* **1997**, *97*, 1515-1566.
40. Li, C.-Y.; Zhang, X.-B.; Dong, Y.-Y.; Ma, Q.-J.; Han, Z.-X.; Zhao, Y.; Shen, G.-L.; Yu, R.-Q., A porphyrin derivative containing 2-(oxymethyl)pyridine units showing unexpected ratiometric fluorescent recognition of Zn²⁺ with high selectivity. *Anal. Chim. Acta* **2008**, *616*, 214-221.
41. Brombosz, S. M.; Appleton, A. L.; Zappas Ii, A. J.; Bunz, U. H. F., Water-soluble benzo- and naphtho-thiadiazole-based bistriazoles and their metal-binding properties. *Chem. Commun.* **2010**, *46*, 1419-1421.
42. Li, Y.; Flood, A. H., Pure C-H Hydrogen Bonding to Chloride Ions: A preorganized and rigid macrocyclic receptor. *Angew. Chem. Int. Ed.* **2008**, *47*, 2649-2652.
43. Tamanini, E.; Katewa, A.; Sedger, L. M.; Todd, M. H.; Watkinson, M., A synthetically simple, click-generated cyclam-based zinc(II) sensor. *Inorg. Chem.* **2008**, *48*, 319-324.
44. Rosenthal, J.; Lippard, S. J., Direct detection of nitroxyl in aqueous solution using a tripodal copper(II) BODIPY complex. *J. Am. Chem. Soc.* **2010**, *132*, 5536-5537.
45. Tamanini, E.; Rigby, S. E. J.; Motevalli, M.; Todd, M. H.; Watkinson, M., Responsive metal complexes: a click-based “Allosteric Scorpionate” complex permits the detection of a biological recognition event by EPR/ENDOR spectroscopy. *Chem. Eur. J.* **2009**, *15*, 3720-3728.
46. Lee, S.; Hua, Y.; Park, H.; Flood, A. H., Intramolecular hydrogen bonds preorganize an aryl-triazole receptor into a crescent for chloride binding. *Org. Lett.* **2010**, *12*, 2100-2102.

47. Kim, H. N.; Lee, M. H.; Kim, H. J.; Kim, J. S.; Yoon, J., A new trend in rhodamine-based chemosensors: application of spirolactam ring-opening to sensing ions. *Chem. Soc. Rev.* **2008**, *37*, 1465-1472.
48. Du, P.; Lippard, S. J., A highly selective turn-on colorimetric, red fluorescent sensor for detecting mobile zinc in living cells. *Inorg. Chem.* **2010**, *49*, 10753-10755.
49. Xu, Z.; Baek, K.-H.; Kim, H. N.; Cui, J.; Qian, X.; Spring, D. R.; Shin, I.; Yoon, J., Zn²⁺-triggered amide tautomerization produces a highly Zn²⁺-selective, cell-permeable, and ratiometric fluorescent sensor. *J. Am. Chem. Soc.* **2009**, *132*, 601-610.
50. Fahrni, C. J.; O'Halloran, T. V., Aqueous coordination chemistry of quinoline-based fluorescence probes for the biological chemistry of zinc. *J. Am. Chem. Soc.* **1999**, *121*, 11448-11458.
51. Lim, N. C.; Bruckner, C., DPA-substituted coumarins as chemosensors for zinc(ii): modulation of the chemosensory characteristics by variation of the position of the chelate on the coumarin. *Chem. Commun.* **2004**, *0*, 1094-1095.
52. Grynkiewicz, G.; Poenie, M.; Tsien, R. Y., A new generation of Ca²⁺ indicators with greatly improved fluorescence properties. *J. Biol. Chem.* **1985**, *260*, 3440-3450.
53. Shortreed, M.; Kopelman, R.; Kuhn, M.; Hoyland, B., Fluorescent fiber-optic calcium sensor for physiological measurements. *Anal. Chem.* **1996**, *68*, 1414-1418.
54. Caballero, A.; Martínez, R.; Lloveras, V.; Ratera, I.; Vidal-Gancedo, J.; Wurst, K.; Tárraga, A.; Molina, P.; Veciana, J., Highly selective chromogenic and redox or fluorescent sensors of Hg²⁺ in aqueous environment based on 1,4-disubstituted azines. *J. Am. Chem. Soc.* **2005**, *127*, 15666-15667.
55. Lentijo, S.; Miguel, J. A.; Espinet, P., Cyclopalladated complexes of perlene imine: formation of acetato-bridged dinuclear complexes with 6,6- and 5,6-membered metallacycles. *Organometallics* **2011**, *30*, 1059-1066.

Chapter 3

Visible–near-infrared colorimetric copper selective molecular probe

Papers based on this chapter have been published in *Chem. Eur. J.*, **2011**, *17*, 1410-1414 ([Link](#)); *Chem. Eur. J.*, **2011**, *17*, 11152-11161 (**Frontispiece**) ([Link](#)). Reproduced by permission of the John Wiley and Sons.

1. Introduction

Copper is required by all living organisms owing in large part to its potent redox activity and propensity to engage in catalytic chemistry.¹ The soft transition metal copper is the third most abundant essential trace element in human body. However, copper has to be supplemented through human diet in regular amounts for absorption.² The adult human body contains between 1.4 – 2.1 mg of copper per kilogram of body weight under normal conditions. Copper dependent enzymes act as catalysts to help a number of body functions to provide energy for biochemical reactions, transform melanin for pigmentation of the skin, assist the formation of cross-links in collagen and elastin, and thereby maintain and repair connective tissues.² This is especially important for the heart and arteries³⁻⁷ and research suggests that copper deficiency is one of the factors leading to an increased risk of developing coronary heart disease.^{8,9} In general most human diets contain enough copper (2–5 mg/day) to prevent a deficiency, but not sufficient to cause toxicity. The World Health Organization (WHO) and the Food and Agricultural Administration (FAA) reports suggest that the population mean intake of copper should not exceed 10-12 mg/day for adults. Excessive copper in the human body is highly dangerous and in general toxicity is progressing day by day due to the widespread use of copper in industry, agriculture, household utensils, and hot water pipes etc. The common nutritional deficiencies in zinc, manganese and other trace minerals also help the accumulation of copper to very high levels. However, if unregulated, copper can cause exacerbate oxidative stress and damage events connected with aging and disease,¹⁰⁻¹² including serious neurodegenerative disorders such as Menkes and Wilson's diseases,¹³ amyotrophic lateral sclerosis¹⁰ and Alzheimer's disease¹². Free solvated copper ions catalyze the formation of reactive organic species including radical and non-radical species that participate in initiation and/or propagation of radical chain reactions which can damage biomolecules. Because of its dual essential but toxic nature, cells exert exquisite control over cellular copper pools through an elegant array of uptake, trafficking and storage mechanisms to maintain a low concentration of thermodynamically free copper ions^{3,4,6,7}, while concurrently maintaining excellent kinetic lability of cellular copper stores for function. Along these lines, supplementation of cells with micromolar extracellular copper can increase intracellular copper levels by up to 20-fold within 1 h.¹⁴ In humans and higher

eukaryotes, particularly in specialized cell types within brain, heart, intestine and liver tissue, paradigms of how kinetically labile copper pools are regulated at the subcellular level and consequences of copper misregulation in aging and disease remain insufficiently understood. Therefore, it is crucial to detect trace amounts of copper for maintaining good human health. In this regard, many efforts have been focused on developing Cu^{2+} sensors involving chromogenic sensors, fluorescent sensors and electrochemical devices for sensitive, selective and convenient detection. Live-cell imaging with copper-specific fluorescent sensors offers a potentially powerful method for studying copper cell biology. Designing fluorometric molecular probe is practically difficult because of the fluorescence quenching nature of paramagnetic Cu^{2+} . Colorimetric techniques are widely accepted due to low cost and easy detection without requiring the costly instrumental set-up. In the past few years, many synthetic receptors have been reported for sensing of copper ion which shows visible color changes in presence of this ion.¹⁵⁻²⁰ Chemosensors with near-infrared (NIR) optical response (700-1000 nm) are useful probes for *in vitro* and *in vivo* biological sensing and imaging of metal ions. Main advantages of sensors with NIR response over UV-Vis probes include a) low background to signal ratio, b) low absorption and light scattering of biological samples facilitate deeper penetration of the NIR-radiation into biological matrices and helps obtaining the information from inner regions of the tissues, c) no interference of the autofluorescence generate from endogenous biomolecules and d) NIR-optical measurements do not require expensive instrumentation.²¹⁻²³ There have been few reports on UV-Vis-NIR sensing of cation and anions.²⁴⁻³⁷ Designing novel and efficient NIR chemosensors necessitates the need for understanding detailed molecular mechanism involved in the origin of such interesting phenomenon. The studies aimed at understanding the underlying mechanism of origin of NIR response are scarce and hence the theoretical calculations would be of great help in order to understand the microscopic details of such changes in the photophysical characteristics.

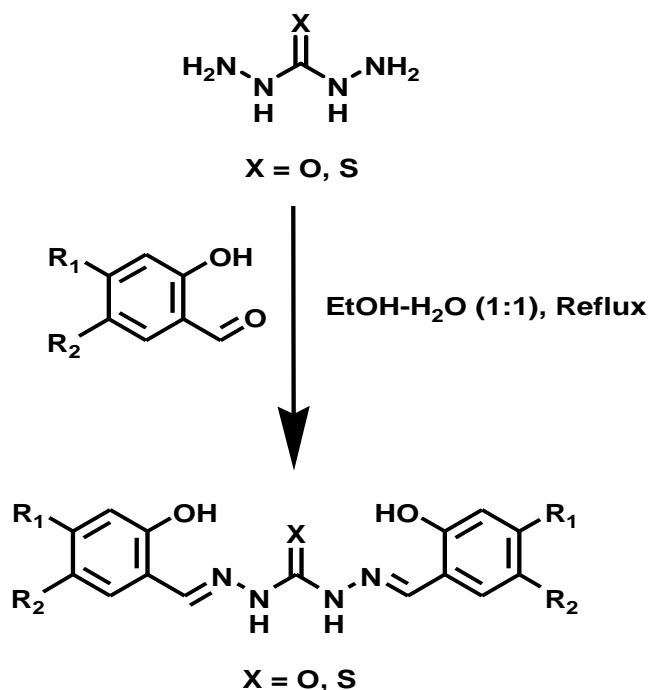
2. Rationale for designing visible and near-infrared colorimetric molecular probes for copper

Colorimetric chemosensors of cations can be generated based on right combination of a receptor and chromophore. Colorimetric sensing of Cu^{2+} reported through coordination of conjugated imine and deprotonation of amide.^{24,38,39} One such combination would be a conjugate of an amine and aldehyde carrying $-\text{CONH}$ and $-\text{OH}$ functionalities formed through Schiff base linkage. In these sensors π -electron delocalization and amide or alcohol deprotonation are mainly responsible for the signal generation as a consequence of cation binding events. A simple design approach has been undertaken by conjugating urea/thiourea with salicylaldehyde-derivative to form biscarbonohydrazone/bisthiocarbonohydrazone system as efficient colorimetric sensor that can selectively detect Cu^{2+} by visible color change with a characteristic near-infrared (NIR) absorbance band at > 800 nm in aqueous medium. In these probes, the tertiary amine group functionalized phenolic moiety serves as the chromophore core. An intramolecular charge transfer (ICT) is thus enhanced as a result of the extended π -conjugation and the stronger electron-withdrawing ability of the ketone/thioketone group.⁴⁰⁻⁴² The extended ICT usually exhibits high sensitivity to external perturbations such as the polarity of solution and the electric field in its vicinity, often showing as remarkable color changes. The imine and alcohol groups in those probes serve as chelating sites for metal cations, in particular, transition- and post-transition-metal cations. All atoms in these probes are almost in one plane upon metal ion coordination. The planarity of these molecular probes is not disturbed upon deprotonation, which instead supports the maximum delocalization of the negative charges over the entire molecule. Additional stability is gained through conjugation and coordination with Cu^{2+} which is reflected as the characteristic NIR signature in the UV-Vis spectrum in presence of Cu^{2+} . To the best of our knowledge these molecular probes are the first set of examples shows huge red-shifted NIR signal in presence of only Cu^{2+} .

3. Visible and near-infrared colorimetric molecular probes for copper

3.1 Synthesis

A series of Schiff base ligands have been synthesized via one step condensation reaction (Scheme 1). The ethanol solution different salicylaldehyde was added slowly to a solution of carbohydrazide or thiocarbohydrazide in water. Different salicylaldehyde derivatives were taken varying the electron donating and withdrawing functional groups. The reaction mixture was refluxed for 24 h with constant stirring. Reaction mixture was cooled to room temperature and the precipitate was filtered. The precipitate was washed with ethanol and dried under vacuo to obtain Schiff base ligands (**1-10**) in quantitative yield (Figure 1). All the synthesized Schiff base ligands (**1-10**) were characterized by NMR, mass spectrometry and elemental analysis.



Scheme 1. Synthesis of different Schiff base molecular probes (**1-10**).

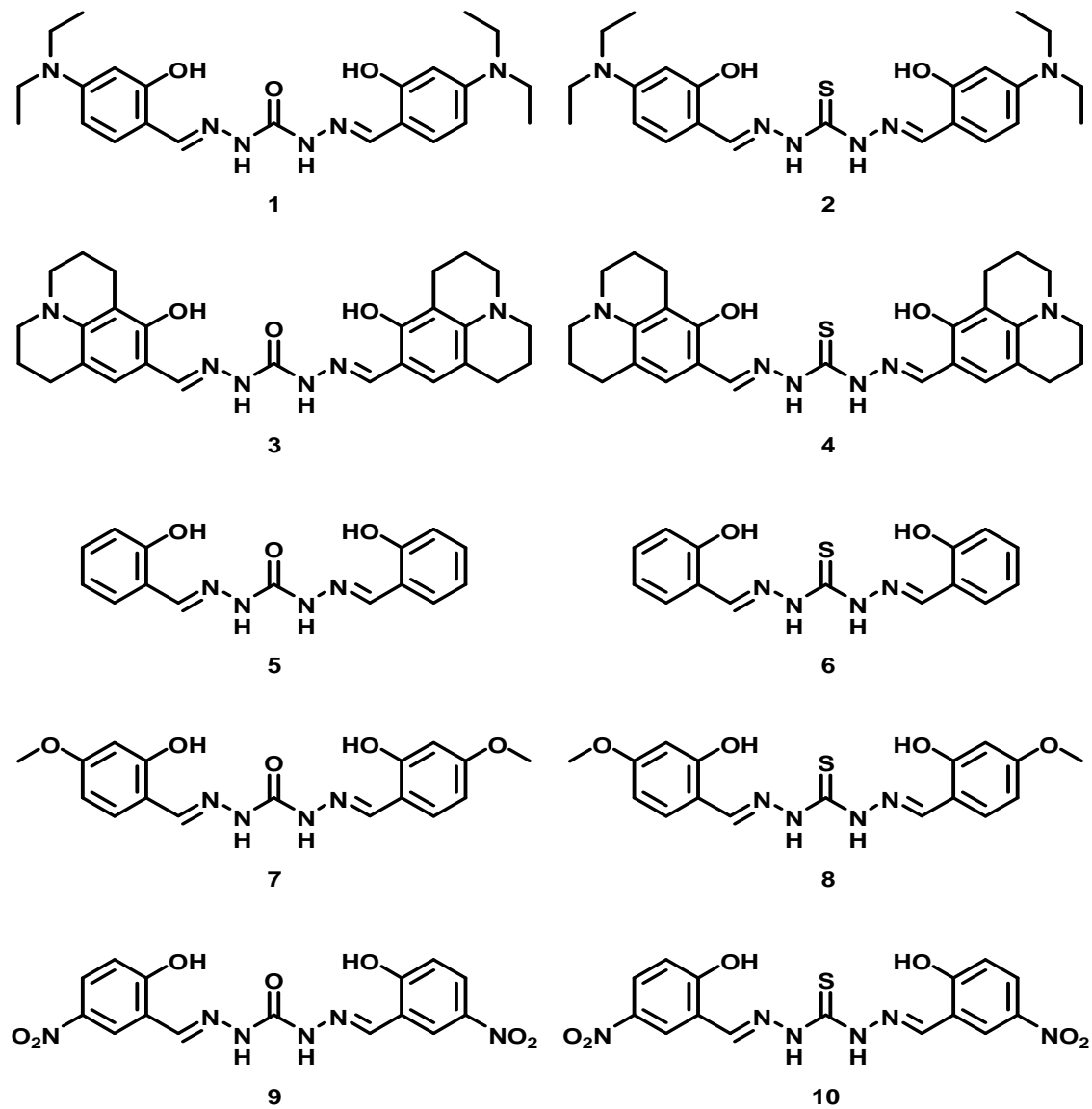


Figure 1. Different Schiff base molecular probes (1-10).

3.2 Photophysical study of Schiff base molecular probes and Cu²⁺ detection

The photophysical properties of different Schiff base ligands carrying electron withdrawing and electron donating functional groups have been studied upon addition of several metal ions such as Li⁺, Na⁺, K⁺, Ba²⁺, Sr²⁺, Mg²⁺, Al³⁺, Ca²⁺, Mn²⁺, Fe²⁺, Co²⁺, Ni²⁺, Zn²⁺, Ag⁺, Cd²⁺, Hg²⁺, Pb²⁺ and Cu²⁺. Biscarbonohydrazone **1** showed an absorption band centered around 365 nm, which remains unchanged upon addition of 25 equiv of Li⁺, Na⁺, K⁺, Ba²⁺, Sr²⁺, Mg²⁺, Al³⁺ and Ca²⁺ in CH₃CN (Figure 2). Upon addition of 25 equiv of Mn²⁺, Fe²⁺, Co²⁺, Ni²⁺, Zn²⁺, Ag⁺, Cd²⁺, Hg²⁺ and Pb²⁺ the absorption maxima was slightly red shifted to different extents. On addition of 2 equiv of Cu²⁺ to the solution of **1**, the absorbance at 365 nm decreases gradually. After addition of one more equiv of Cu²⁺, absorbance at 365 nm decreases sharply to its limiting value, while a new prominent peak was observed at 450 nm and color changed from light green to primrose yellow. A clear isobestic point is observed at 390 nm upon recording the spectra with varying concentrations of 2 to 3 equiv of Cu²⁺ (Figure 3). Furthermore, addition of Cu²⁺, the absorbance at 450 nm decreases gradually, and

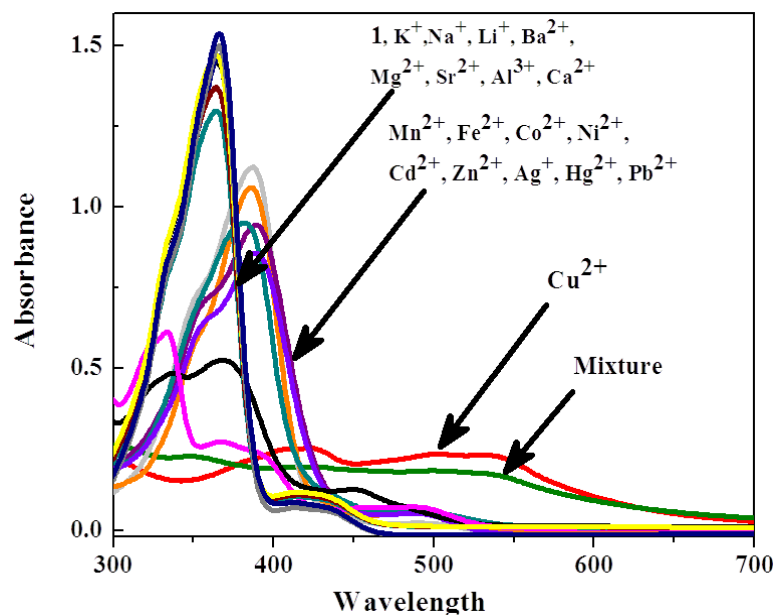


Figure 2. UV-Vis absorption spectra of **1** (20.0 μM) and on addition of salts (25.0 equiv) of Li⁺, Na⁺, K⁺, Ba²⁺, Sr²⁺, Mg²⁺, Al³⁺, Ca²⁺, Mn²⁺, Fe²⁺, Co²⁺, Ni²⁺, Zn²⁺, Ag⁺, Cd²⁺, Hg²⁺, Pb²⁺ and Cu²⁺ in CH₃CN.

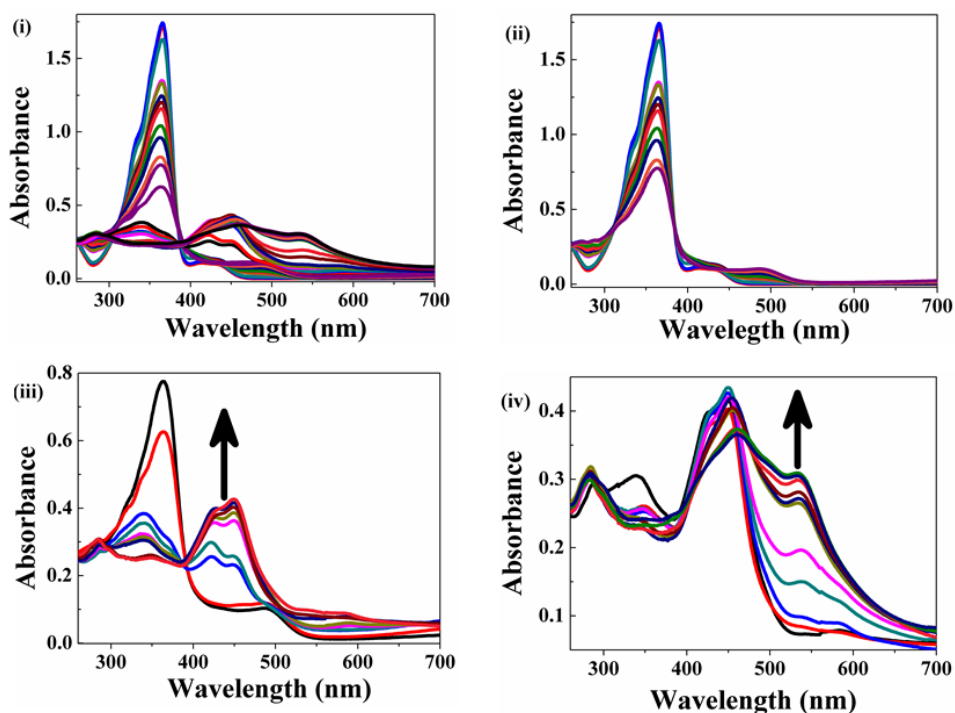


Figure 3. (i) UV-Vis absorption spectra of **1** (20.0 μM) on addition of different concentrations of Cu^{2+} (0-100.0 μM) in CH_3CN . (ii) Cu^{2+} = 0-40.0 μM , [**1**] = 20.0 μM . (iii) Cu^{2+} = 40.0-60.0 μM , [**1**] = 20.0 μM . (iv) Cu^{2+} = 60.0-100.0 μM , [**1**] = 20.0 μM .

an absorption band at 535 nm appears and reaches maxima upon addition of 5 equiv of Cu^{2+} , which induces a color change from primrose yellow to pink. However, addition of more than 5 equiv of Cu^{2+} leads to no significant changes in the UV-Vis spectra.

Bisthiocarbonohydrazone **2** showed excellent photophysical response in aqueous medium (20% CH_3CN , 50 mM HEPES at pH = 7.2). **2** can selectively detect Cu^{2+} colorimetrically with a NIR signature (Figure 4). **2** shows an absorption band centered around 395 nm, which remains unchanged upon addition of 25 equiv of Li^+ , Na^+ , K^+ , Ba^{2+} , Sr^{2+} , Mg^{2+} , Al^{3+} and Ca^{2+} . Upon addition of 25 equiv of Mn^{2+} , Fe^{2+} , Co^{2+} , Ni^{2+} , Zn^{2+} , Ag^+ , Cd^{2+} , Hg^{2+} and Pb^{2+} the absorbance decreases and slightly red shifted to different extents. There was no significant change in absorption spectra of **2** on addition of 1.75 equiv of Cu^{2+} . After adding 2 equiv of Cu^{2+} to the solution of **2**, color was changed to purple. The maximum peak shift is observed at 936 nm (541 nm red shift) along with a peak in the visible region at 535 nm. The absorbance at 535 and 936 nm reaches maximum upon addition of 5 equiv of

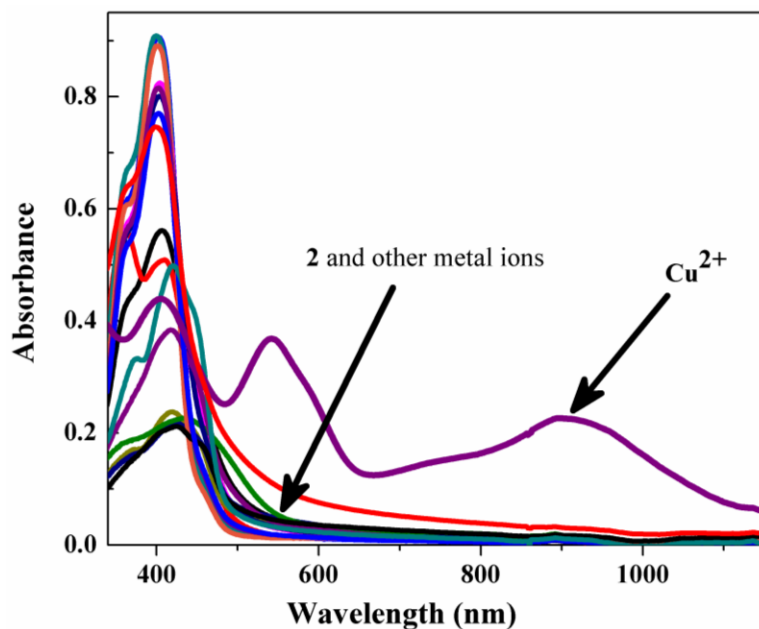


Figure 4. UV-Vis absorption spectra of **2** (20.0 μM) and on addition of salts (25.0 equiv) of Li^+ , Na^+ , K^+ , Ba^{2+} , Sr^{2+} , Mg^{2+} , Al^{3+} , Ca^{2+} , Mn^{2+} , Fe^{2+} , Co^{2+} , Ni^{2+} , Zn^{2+} , Ag^+ , Cd^{2+} , Hg^{2+} , Pb^{2+} and Cu^{2+} in aqueous medium (20% CH_3CN , 50 mM HEPES at $\text{pH} = 7.2$).

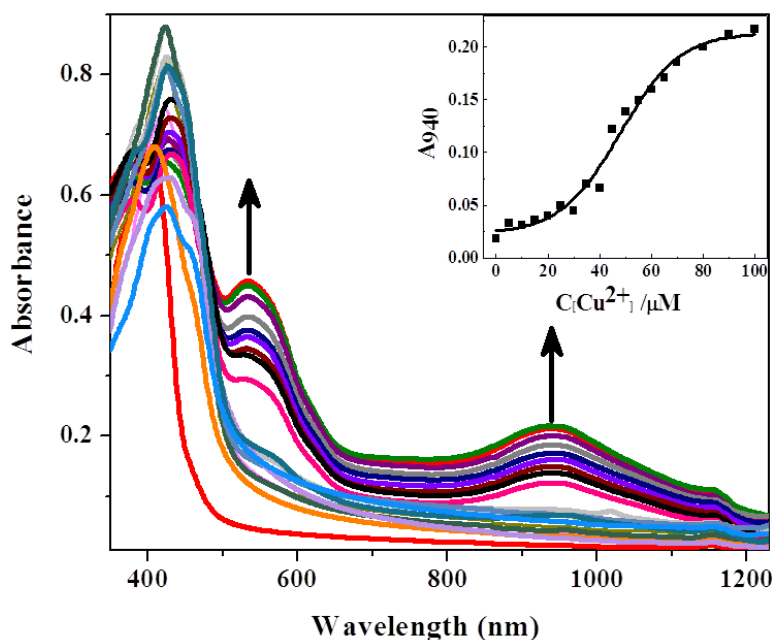


Figure 5. UV-Vis absorption spectra of **2** (20.0 μM) on addition of different concentrations of Cu^{2+} (0, 5, 10, 15, 20, 25, 30, 35, 40, 45, 50, 60, 65, 70, 80, 90, 100 μM) in aqueous medium (20% CH_3CN , 50 mM HEPES at $\text{pH} = 7.2$). Inset: Absorbance at 940 nm as a function of $[\text{Cu}^{2+}]$.

Cu^{2+} as shown in Figure 5. Accordingly, 2 equiv of Cu^{2+} can be set as the colorimetric threshold for determination using **2** in aqueous medium. Such a peak at the NIR region would be useful for sensing of Cu^{2+} in the system from unwanted interference of endogenous chromophores in the visible region. The observed large redshift in the absorption peak of **2** is presumed to arise from conjugation and planarity of the probe which allows maximum distribution of negative charge of the deprotonated receptor. The structure of biscarbonohydrazone **1** and bithiocarbonohydrazone **2** clearly shows that all atoms associated in this receptor are almost in one plane. Planarity of these molecules will not be disturbed upon deprotonation which supports the maximum delocalization of the negative charge. The thioketones ($\text{C}=\text{S}$) are less stable than ketones ($\text{C}=\text{O}$) because of poor overlap between the 2sp^2 orbital on carbon and the 3sp^2 orbital on sulfur as well as the more or less similar electronegativity values of the two elements. In case of **2**, thioamide undergoes conjugation with nitrogen to stabilize weak $\text{C}=\text{S}$ bond providing extra conjugation and coordination with Cu^{2+} which is reflected in its UV-Vis spectrum in presence of Cu^{2+} as NIR signature.

Bithiocarbonohydrazone have been recently reported for colorimetric sensors for

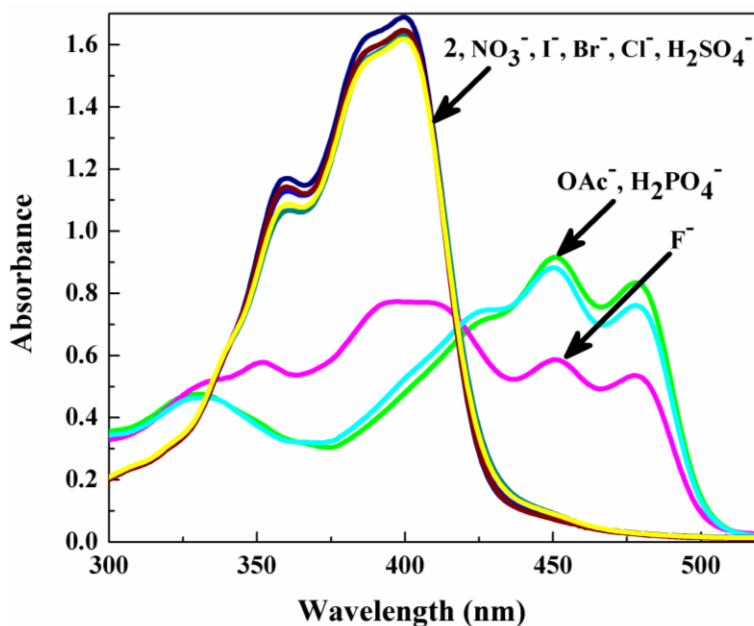


Figure 6. UV-Vis absorption spectra of **2** (20.0 μM) and on addition of salts (25.0 equiv) of tetrabutylammonium salts of F^- , Cl^- , Br^- , I^- , NO_3^- , H_2SO_4^- , OAc^- and H_2PO_4^- in CH_3CN .

anions.^{33,43,44} The absorption spectra of **2** in presence of different anions i.e. tetrabutylammonium salts of halides, acetate, nitrate, hydrogen sulfate and hydrogen phosphate have been studied in CH_3CN (Figure 6). Absorbance spectra remain unchanged upon addition of 25 equiv of Cl^- , Br^- , I^- , H_2SO_4^- and NO_3^- . But for F^- , OAc^- and H_2PO_4^- absorption spectra are red shifted and two new peaks have been appeared at 450 nm and 478 nm. Thus all these anions can be classified colorimetrically into two classes using bisthiocarbonohydrazone **2**.

Next, the photophysical properties of julolidinal based Schiff base ligands **3** and **4** were investigated by monitoring the absorption spectral behaviour upon addition of several metal ions such as Li^+ , Na^+ , Ba^{2+} , Sr^{2+} , Mg^{2+} , Al^{3+} , Ca^{2+} , Mn^{2+} , Fe^{2+} , Co^{2+} , Ni^{2+} , Zn^{2+} , Ag^+ , Cd^{2+} , Hg^{2+} , Pb^{2+} and Cu^{2+} in aqueous buffer medium (50 mM HEPES: CH_3CN , 6:4, v/v; pH=7.2). Ligands **3** and **4** have exhibited characteristic absorbance in the visible (460-600 nm) and NIR (700-1100 nm) regions in presence of Cu^{2+} as shown in Figure 7 and Figure 8. The presence of other metal ions did not lead to appearance of any such visible and NIR absorbance of ligands **3** and **4**. In contrast, other Schiff base ligands (**5-10**) did not exhibit

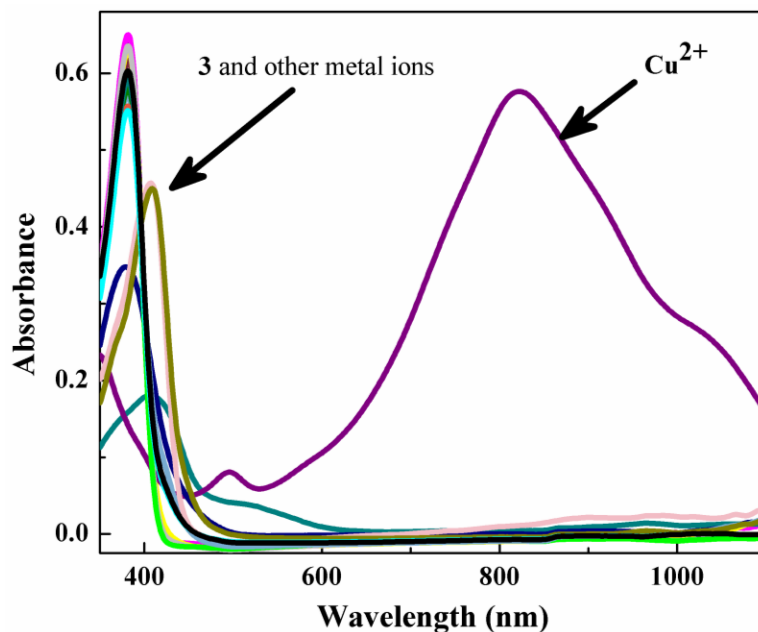


Figure 7. UV-Vis absorption spectra of julolidine-carbonohydrazone **3** (10.0 μM) and on addition of salts (50.0 equivalents) of Li^+ , Na^+ , Ba^{2+} , Sr^{2+} , Mg^{2+} , Al^{3+} , Ca^{2+} , Mn^{2+} , Fe^{2+} , Co^{2+} , Ni^{2+} , Zn^{2+} , Ag^+ , Cd^{2+} , Hg^{2+} , Pb^{2+} and Cu^{2+} in aqueous medium (50 mM HEPES: CH_3CN , 6:4, v/v; pH=7.2).

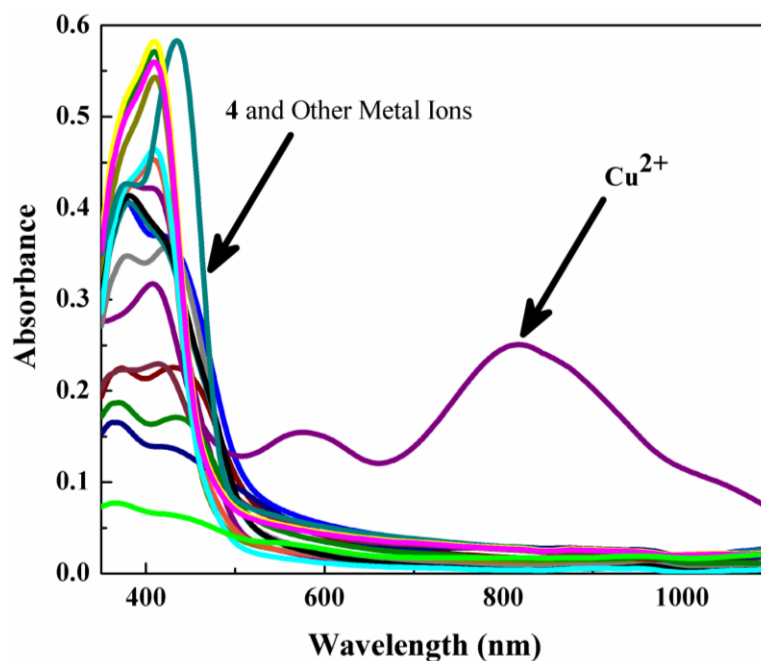


Figure 8. UV-Vis absorption spectra of julolidine-thiocarbonohydrazone **4** (10.0 μM) and on addition of salts (50.0 equiv) of Li^+ , Na^+ , Ba^{2+} , Sr^{2+} , Mg^{2+} , Al^{3+} , Ca^{2+} , Mn^{2+} , Fe^{2+} , Co^{2+} , Ni^{2+} , Zn^{2+} , Ag^+ , Cd^{2+} , Hg^{2+} , Pb^{2+} and Cu^{2+} in aqueous medium (50 mM HEPES: CH_3CN , 6:4, v/v; pH=7.2).

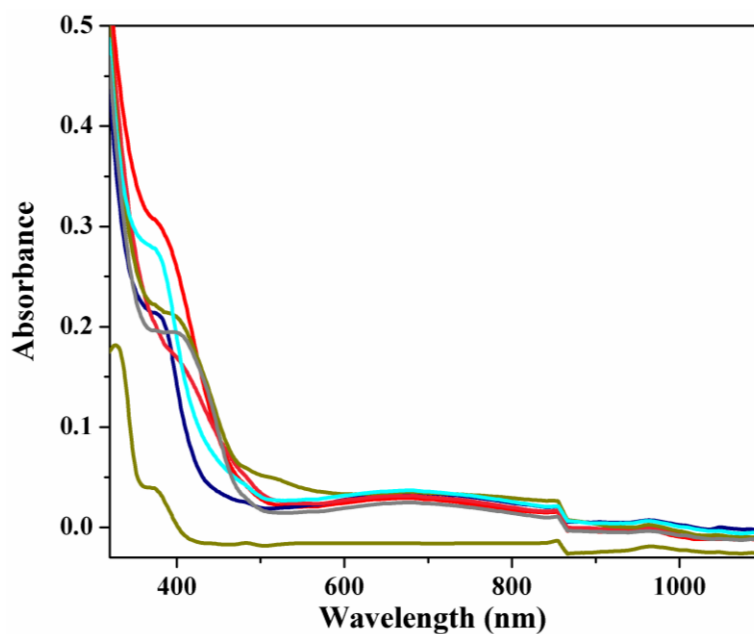


Figure 9. UV-Vis absorption spectra of Schiff base ligands (10.0 μM) and on addition of 50.0 equiv of Cu^{2+} in aqueous medium (50 mM HEPES: CH_3CN , 6:4, v/v; pH=7.2).

any characteristic optical response in presence of Cu^{2+} (Figure 9). Julolidine-carbonohydrazone (**3**) showed an absorption band centered around 380 nm, which remains unchanged upon addition of 50.0 equiv of Li^+ , Na^+ , Ba^{2+} , Sr^{2+} , Mg^{2+} , Al^{3+} , Ca^{2+} , Mn^{2+} , Fe^{2+} , Ag^+ , Cd^{2+} and Pb^{2+} . With the addition of 50.0 equiv of Co^{2+} , Ni^{2+} , Zn^{2+} and Hg^{2+} the absorbance intensity decreases and is slightly red shifted to different extents as shown in Figure 7. At similar concentration of Cu^{2+} (50.0 equiv), ligand **3** showed characteristic absorbance in the visible (495 nm) and NIR (823 nm) regions. During sequential titration the absorption spectra of ligand **3** in the visible region gradually red shifted to 412 nm with the addition of 1.5 equiv of Cu^{2+} and the colorless solution turns to light green (Figure 10). Increasing concentration of Cu^{2+} in the solution of ligand **3** from 1.5 to 2.0 equiv leads to change in the solution color from light green to light purple. A new absorption band ($\lambda_{\text{max}} = 570 \text{ nm}$) was appeared in the visible region accompanied by a distinguishable NIR band with λ_{max} centered at 930 nm. The absorbance at 570 nm reaches to maximum upon addition of 6.0 equiv of Cu^{2+} with extinction coefficient (ϵ) of $2 \times 10^4 \text{ M}^{-1} \text{ cm}^{-1}$ and then decreases with

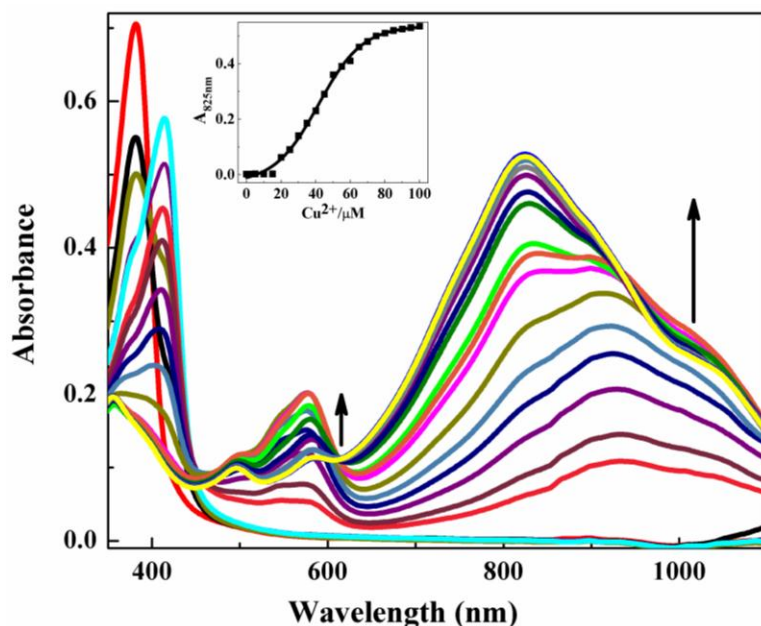


Figure 10. UV-Vis absorption spectra of julolidine-carbonohydrazone **3** ($10.0 \mu\text{M}$) on addition of different concentrations of Cu^{2+} (0, 2.5, 5, 10, 15, 20, 25, 30, 35, 40, 45, 50, 55, 60, 65, 70, 75, 80, 85, 90, 95, $100 \mu\text{M}$) in aqueous medium (50 mM HEPES: CH_3CN , 6:4, v/v; pH=7.2). Inset: Absorbance at 825 nm as a function of $[\text{Cu}^{2+}]$.

further addition of Cu²⁺. The absorbance in the NIR region reaches maximum ($\epsilon = 5.2 \times 10^4 \text{ M}^{-1} \text{ cm}^{-1}$) upon addition of total 8.0 equiv of Cu²⁺ with gradual blue shift of λ_{max} from 930 nm to 825 nm and that remains unchanged upon further addition of Cu²⁺. The final solution color of ligand **3** becomes aqua colored. The complete colorimetric titration of ligand **3** with sequential addition of Cu²⁺ is shown in Figure 10. Cu²⁺ can be detected by NIR response at least down to 20 μM when 10 μM of **3** is employed in aqueous medium (50 mM HEPES:CH₃CN, 6:4, v/v; pH=7.2). An absorbance peak in the NIR region would be useful for sensing Cu²⁺ in systems that contains unwanted interference of endogenous chromophores in the visible region. Ligand **4** (10 μM) exhibited absorption band in the visible region ($\lambda_{\text{max}} = 570 \text{ nm}$) accompanied by a well distinguished NIR absorption band around 820 nm as shown in Figure 8. During sequential titration, two absorption bands were appeared at 570 nm and 980 nm corresponds to visible and NIR region respectively after addition of 1.0 equiv of Cu²⁺ (Figure 11). At this concentration of added Cu²⁺ the color of the ligand **4** solution changes from greenish to light purple. The absorbance at 570 nm and 980

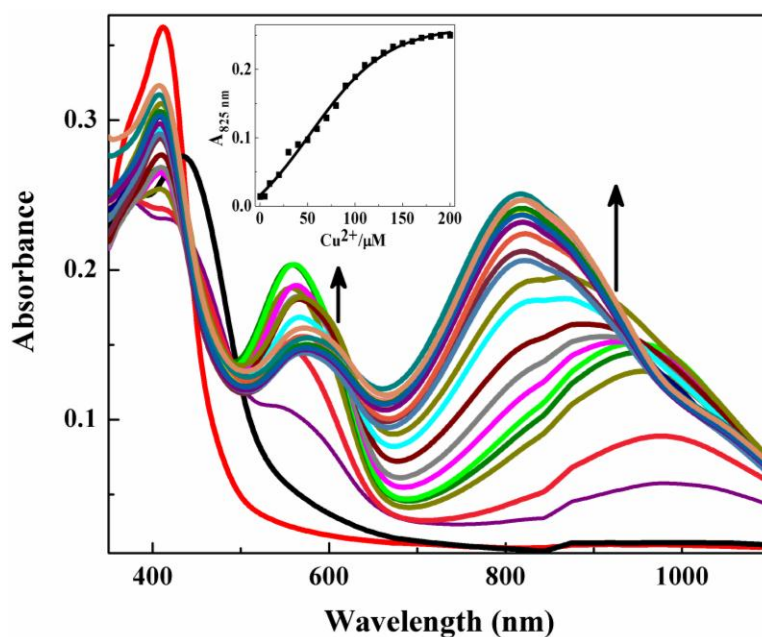


Figure 11. UV-Vis absorption spectra of julolidine-thiocarbonohydrazone **4** (10.0 μM) on addition of different concentrations of Cu²⁺ (0, 5, 10, 20, 30, 40, 50, 60, 70, 80, 90, 100, 110, 120, 130, 140, 150, 160, 170, 180, 190, 200 μM) in aqueous medium (50 mM HEPES:CH₃CN, 6:4, v/v; pH=7.2). Inset: Absorbance at 825 nm as a function of [Cu²⁺].

nm enhances by increasing the concentration of added of Cu²⁺ from 1.5 to 2.0 equivalents and the purple colored solution turns to light violet. The absorbance at 570 nm reaches the maximum at 5.0 equiv of Cu²⁺ with extinction coefficient (ϵ) of $2 \times 10^4 \text{ M}^{-1} \text{ cm}^{-1}$ and consequent increase in the intensity of NIR absorption band was observed. At this composition of ligand **4** and Cu²⁺ the solution color changed from light violet to blue. Further addition of Cu²⁺ resulted in the gradual decrease in the absorbance at 570 nm as shown in Figure 11 whereas the absorbance in the NIR region increases and band was gradually blue shifted to 820 nm and reaches maximum with $\epsilon = 2.5 \times 10^4 \text{ M}^{-1} \text{ cm}^{-1}$ upon overall addition of 15.0 equiv of Cu²⁺ (Figure 11). The final solution color of ligand **4** becomes greenish aqua. Employing 10 μM concentration of ligand **4**, Cu²⁺ can be detected by NIR response at least down to 10 μM in aqueous medium. Apart from selective detection of Cu²⁺ using ligands **3** and **4**, different concentrations of Cu²⁺ can also be detected (Figure 12). The specific micromolar concentrations of added Cu²⁺ gave distinct coloration to aqueous solutions of ligands **3** and **4** (Figure 12a and 12b respectively). These colorimetric changes correspond to well distinguishable visible absorbance spectra with characteristic NIR signature in Figure 10 and Figure 11.

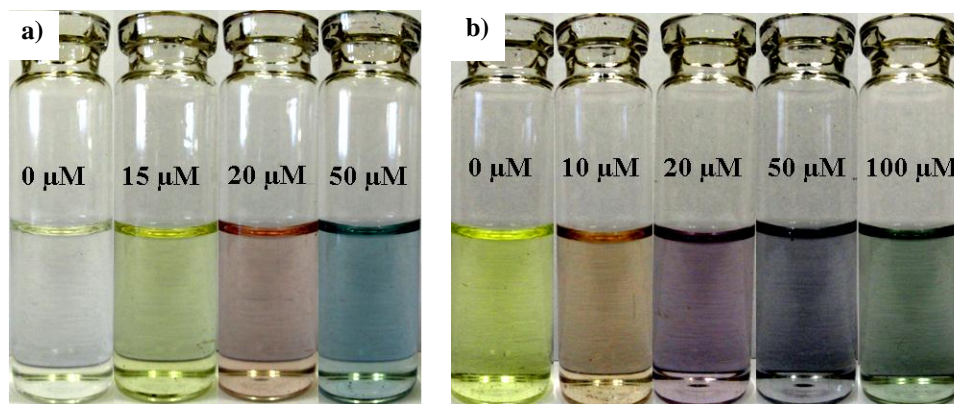


Figure 12. Detectable colorimetric change with increasing concentration of Cu²⁺ to the solution of a) julolidine-carbonohydrazone **3** (10.0 μM) and b) julolidine-thiocarbonohydrazone **4** (10.0 μM) in aqueous medium (50 mM HEPES:CH₃CN, 6:4, v/v; pH=7.2). The values indicated on the vials correspond to [Cu²⁺].

3.3 Competitive study for NIR colorimetric detection of Cu^{2+}

Selectivity of probe **1** and **2** as colorimetric sensors for Cu^{2+} was studied in presence of different other metal ions. Figure 2 shows Cu^{2+} can be detected in presence of different metal ions by significant color change in CH_3CN . For ligand **2**, all samples containing various other metal ions exhibited a very distinguished color change after being exposed to Cu^{2+} (Figure 13) except Ag^+ . It reveals that **2** can discriminate Cu^{2+} from other all metal ions (except Ag^+) in a colorimetric manner in aqueous medium.

Selectivity of ligands **3** and **4** as Vis-NIR chemosensors for Cu^{2+} was also studied in the presence of various competing metal ions. For these purpose ligands **3** and **4** were treated with mixture of 5.0 equiv of Cu^{2+} and 10.0 equiv of all other metal ions. Data shown in Figure 14 confirms that there is no interference for the detection of Cu^{2+} in presence of all other metal ions tested. The aqua colour of the solutions of ligands **3** and **4** persist even in the presence of other metal ions in excess. Thus, ligands **3** and **4** can serve as highly selective colorimetric as well as NIR sensors for Cu^{2+} in the presence of most competing metal ions.

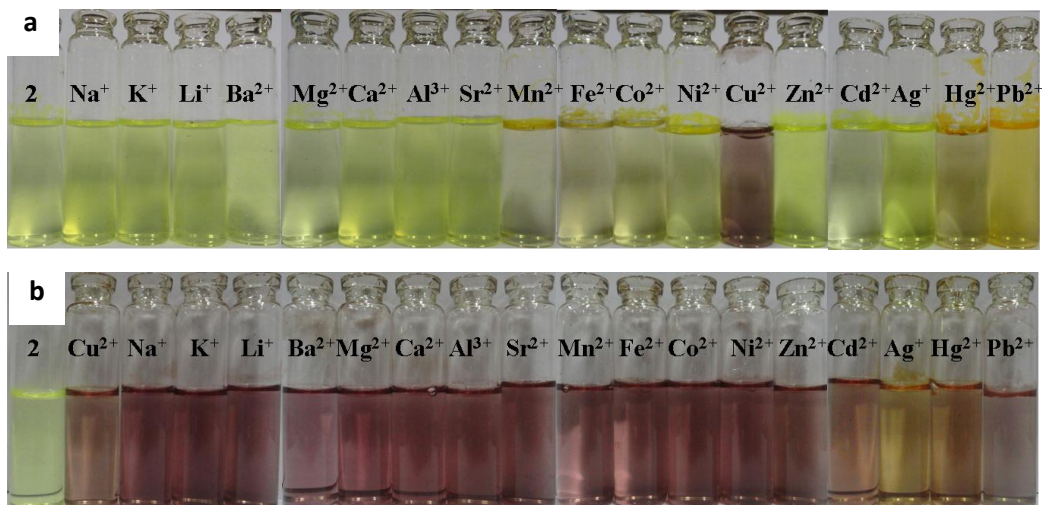


Figure 13. (a) The color changes of **2** (20.0 μM) upon adding 5 equiv of different metal ions in aqueous medium (20% CH_3CN , 50 mM HEPES at pH = 7.2). (b): The color change of **2** (20.0 μM) upon adding 5 equiv of Cu^{2+} in the presence of various metal ions in aqueous medium (20% CH_3CN , 50 mM HEPES at pH = 7.2).

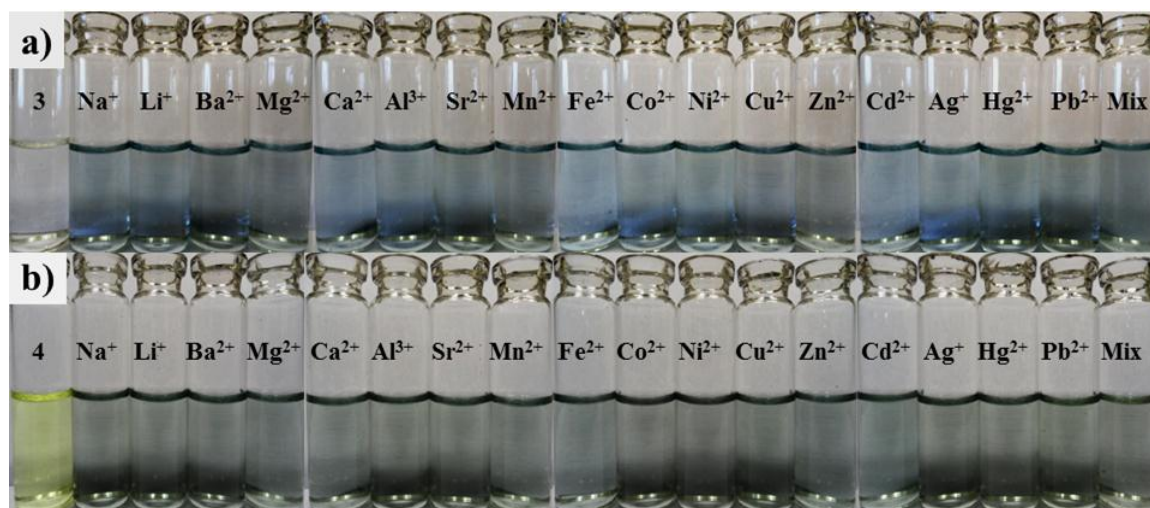


Figure 14. Competitive study of a) julolidine-carbonohydrazone **3** (10.0 μM) and b) julolidine-thiocarbonohydrazone **4** (10.0 μM) with Cu^{2+} in the presence of various metal ions in aqueous medium (50 mM HEPES: CH_3CN , 6:4, v/v; pH=7.2). **3** and **4** were treated with 5.0 equiv of Cu^{2+} in the presence of 10.0 equiv of other metal ions. Visible colors of ligand **3** and **4** solutions with Cu^{2+} in presence of other metal ions as indicated. Persistence of aqua blue (a) and greenish blue (b) colors corresponding to $[\mathbf{3} + 2\text{Cu}^{2+}]$ and $[\mathbf{4} + 2\text{Cu}^{2+}]$ complexes respectively in presence of all other metal ions indicate the high selectivity of sensor ligands towards copper ions.

3.4 Determination of binding stoichiometry and binding constant

The stoichiometry of binding of Cu^{2+} to molecular probes (**2-4**) was studied by various analytical techniques. Job plot study shows (Figure 15-17) 1:2 stoichiometric complexation between probes (**2-4**) and Cu^{2+} respectively.

This data was further supported by mass spectrometry analysis. MALDI/TOF-MS shows the formation of double deprotonated $2:2\text{Cu}^{2+}$ complex [MW: 580.122; calcd., 580.074 for $\text{C}_{23}\text{H}_{30}\text{Cu}_2\text{N}_6\text{O}_2\text{S}$] (Figure 18). The addition of Cu^{2+} to ligands **3** and **4** resulted in deprotonation of hydroxyl functional groups of julolidine-moieties followed by complex formation. MALDI/TOF-MS shows the formation of a complex between deprotonated ligands and two copper ions [$(\text{C}_{27}\text{H}_{32}\text{Cu}_2\text{N}_6\text{O}_3 + \text{Na}^+ - 2\text{H}^+)$, m/z: 635.17; calcd. for $\text{C}_{27}\text{H}_{32}\text{Cu}_2\text{N}_6\text{O}_3 + \text{Na}^+$, 637.1] and [$\text{C}_{27}\text{H}_{32}\text{Cu}_2\text{N}_6\text{O}_2\text{S} + \text{Na}^+ - 3\text{H}^+$, m/z: 650.07; calcd. for $\text{C}_{27}\text{H}_{31}\text{Cu}_2\text{N}_6\text{O}_2\text{S} + \text{Na}^+$, 653.07] (Figure 19 and 20).

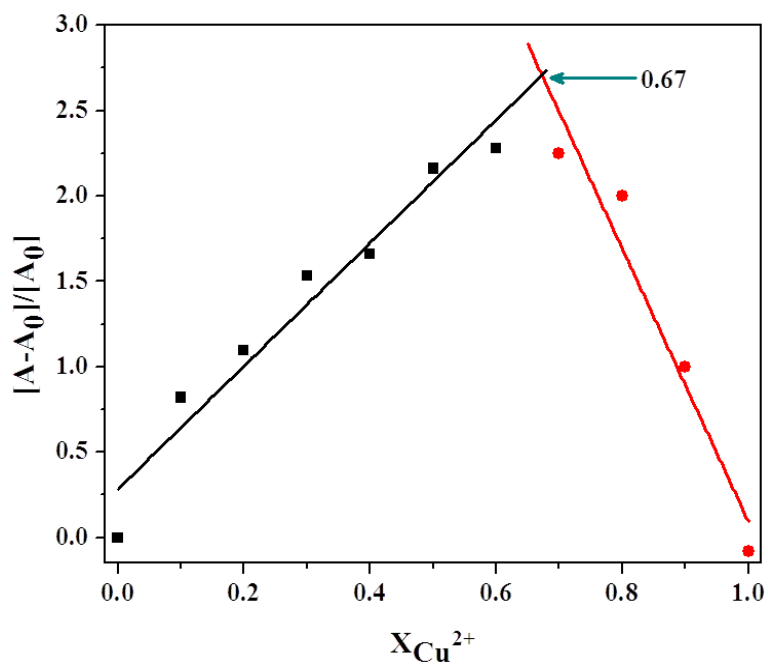


Figure 15. Job plot for the determination of the stoichiometry of **2** and Cu^{2+} in the complex.

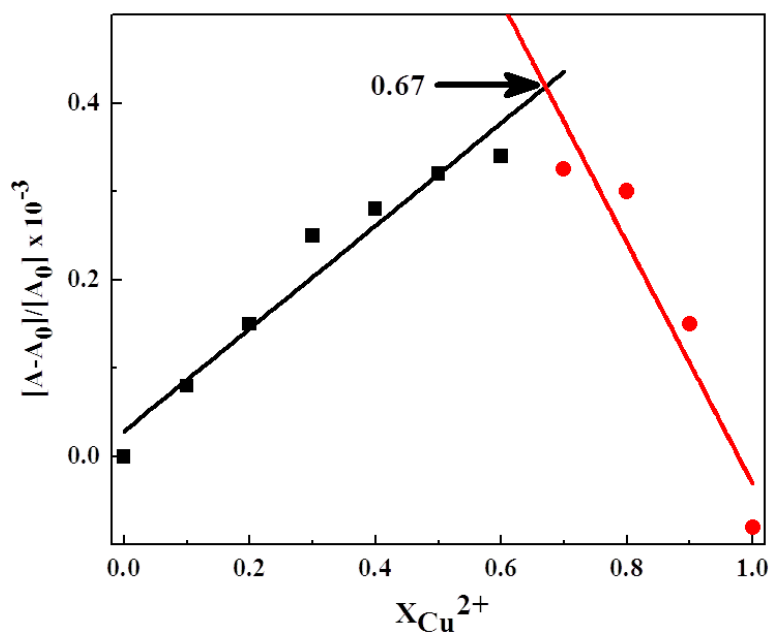


Figure 16. Job plot for the determination of the stoichiometry of julolidine-carbonohydrazone **3** and Cu^{2+} in the complex.

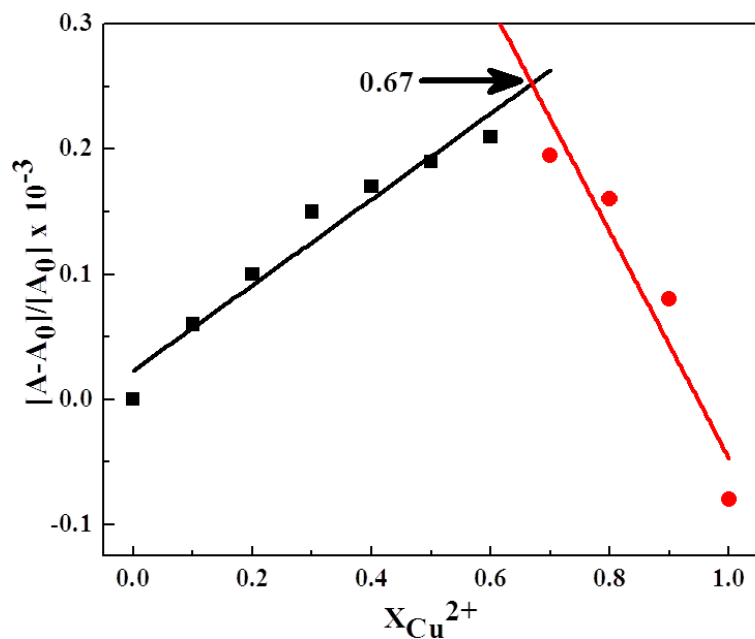


Figure 17. Job plot for the determination of the stoichiometry of julolidine-thiocarbohydrazone **4** and Cu^{2+} in the complex.

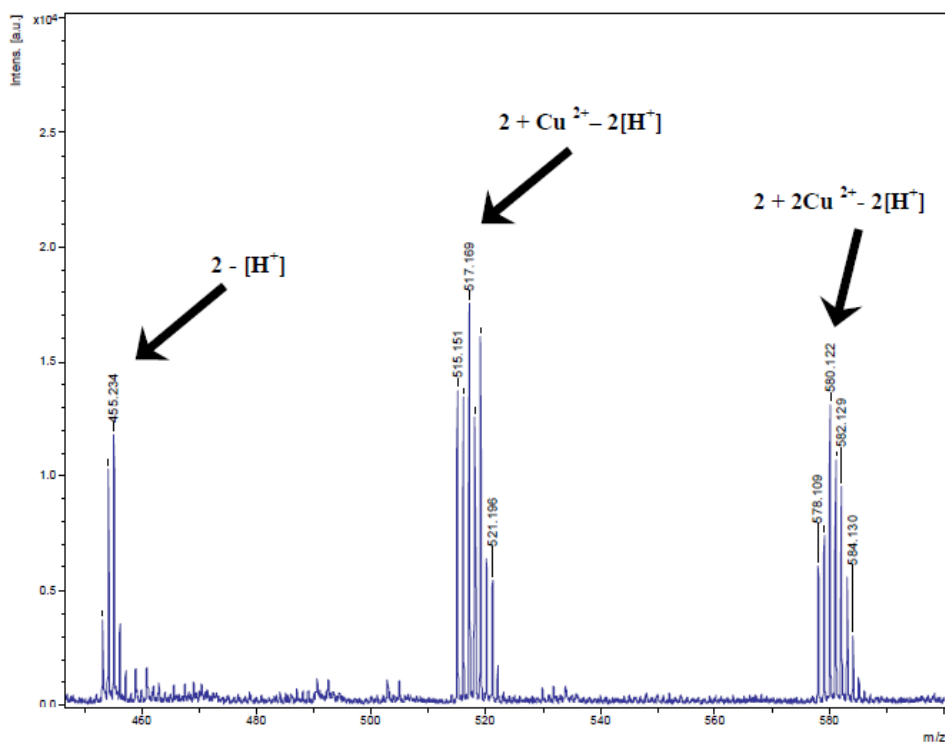


Figure 18. MALDI-TOF mass spectrum of bithiocarbohydrazone **2**: 2Cu^{2+} complex in CH_3CN .

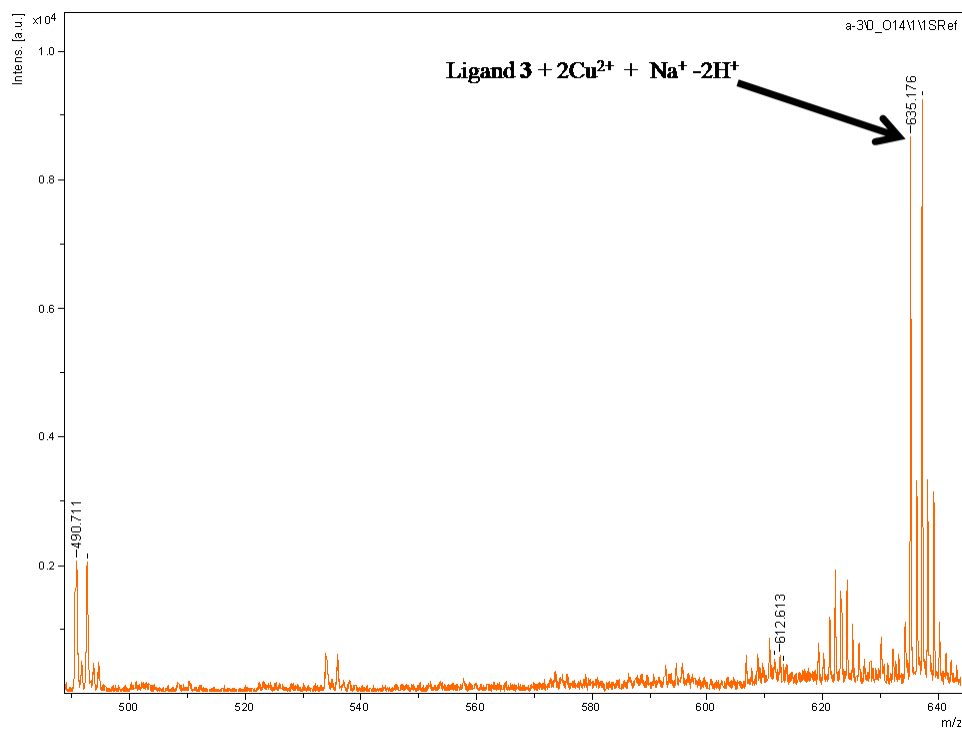


Figure 19. MALDI-TOF mass spectrum of julolidine-carbonohydrazone **3**- Cu^{2+} complex in CH_3CN .

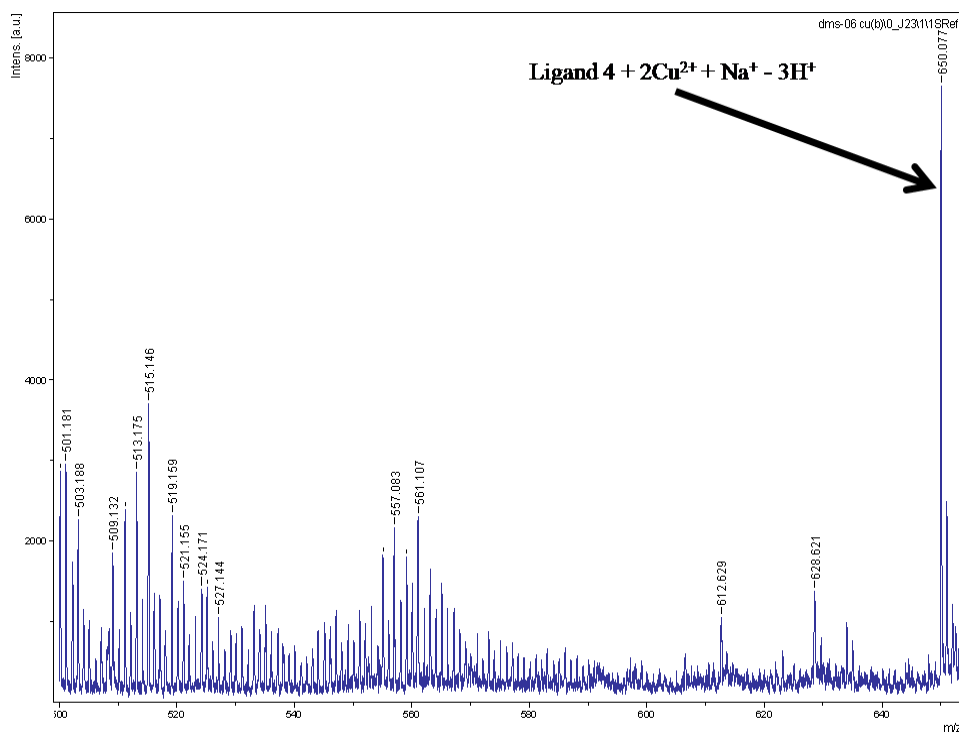


Figure 20. MALDI-TOF mass spectrum of julolidine-thiocarbonohydrazone **4**- Cu^{2+} complex in CH_3CN .

Response parameter α which is defined as the ratio of free ligand concentration to the initial concentration of ligand is plotted as a function of Cu^{2+} concentration (Figure 21). This plot can serve as the calibration curve for the detection of Cu^{2+} . The association constant ($\log K_a$) of **2** for Cu^{2+} was calculated to be 13.63 M^{-1} . The response parameter (α) is plotted as a function of Cu^{2+} concentration (Figure 22 and 23). This plot can serve as the calibration curve for the detection of Cu^{2+} . The association constant ($\log K_a$) of ligands **3** and **4** with Cu^{2+} was calculated to 13.52 and 14.36 M^{-1} respectively.

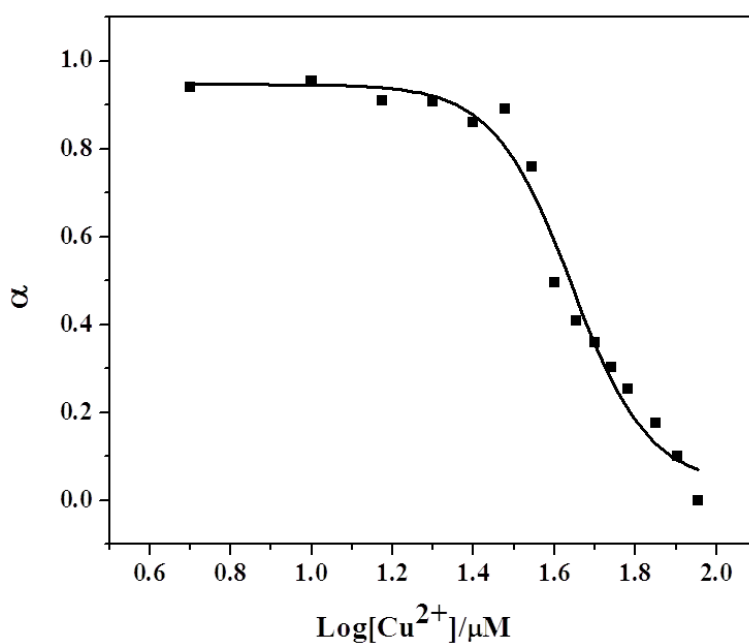


Figure 21. Response parameter values (α) of ligand **2** as a function of the logarithm of Cu^{2+} concentration. α is defined as the ratio between the free ligand concentration and the initial concentration of ligand.

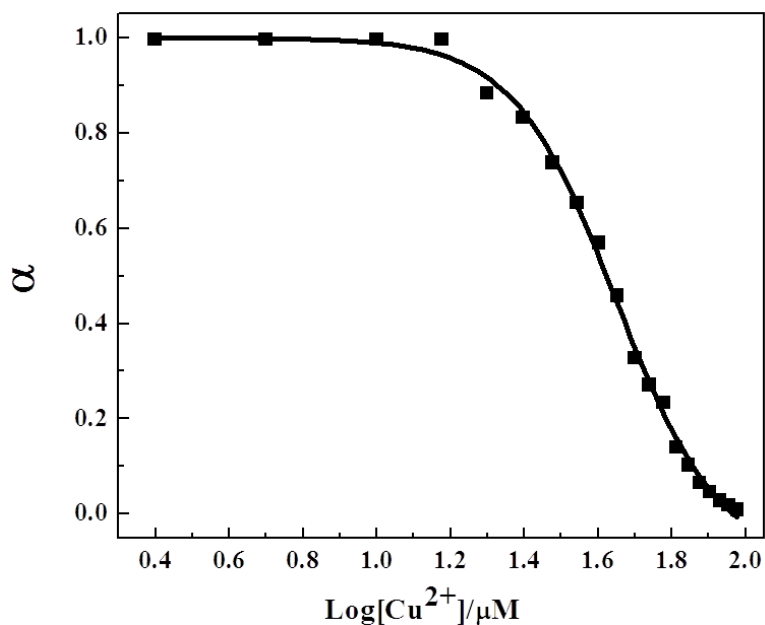


Figure 22. Response parameter values (α) of julolidine-carbonohydrazone **3** as a function of the logarithm of $[\text{Cu}^{2+}]$. α is defined as the ratio between the free ligand concentration and the initial concentration of ligand.

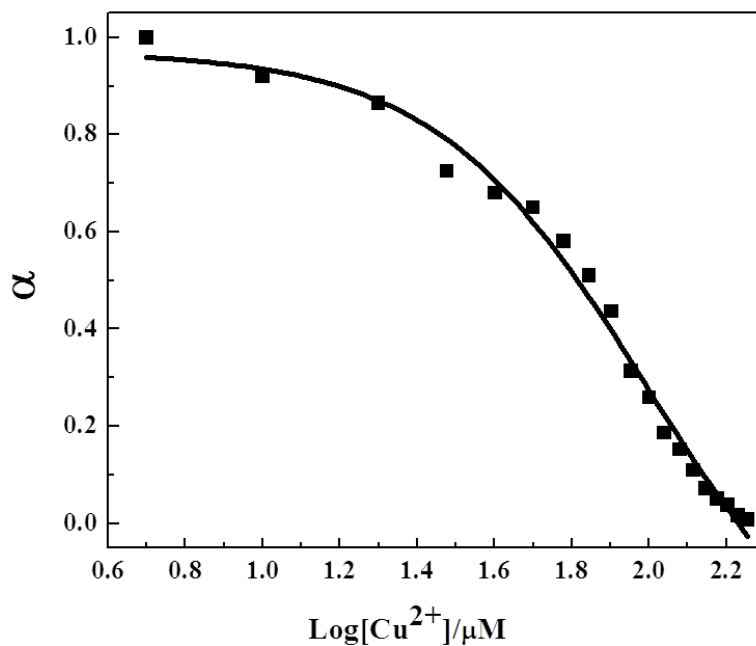


Figure 23. Response parameter values (α) of julolidine-thiocarbonohydrazone **4** as a function of the logarithm of $[\text{Cu}^{2+}]$. α is defined as the ratio between the free ligand concentration and the initial concentration of ligand.

3.5 pH dependent study

The influence of pH on the absorbance of molecular probes (**2-4**) upon complexation with Cu^{2+} was studied in aqueous medium.⁴⁵ Absorbance of **2**- Cu^{2+} complex at 535 and 936 nm slowly decreases between pH 12.0 and 2.5 leading to a sigmoid curve as shown in Figure 24. But Cu^{2+} can be clearly detected by UV-Vis method using probe **2** in both acidic as well as in basic medium. Cu^{2+} can be clearly detected from the visible and NIR absorbance measurements using ligands **3** and **4** over pH range of 2–11 (Figure 25 and 26). Therefore ligands **3** and **4** can be used for environmental monitoring and biological detection of copper in most of the commonly encountered pH ranges.

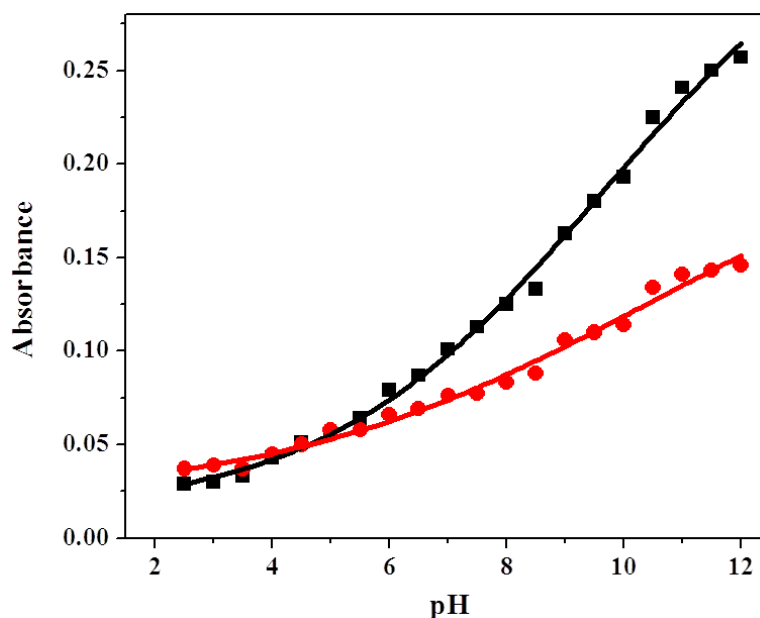


Figure 24. Dependence of the absorbance of the band at 535 nm (black line) and 936 nm (red line) on pH for a solution of 1 equiv of **2** and 5 equiv of Cu^{2+} in aqueous medium (20% CH_3CN , 50 mM HEPES).

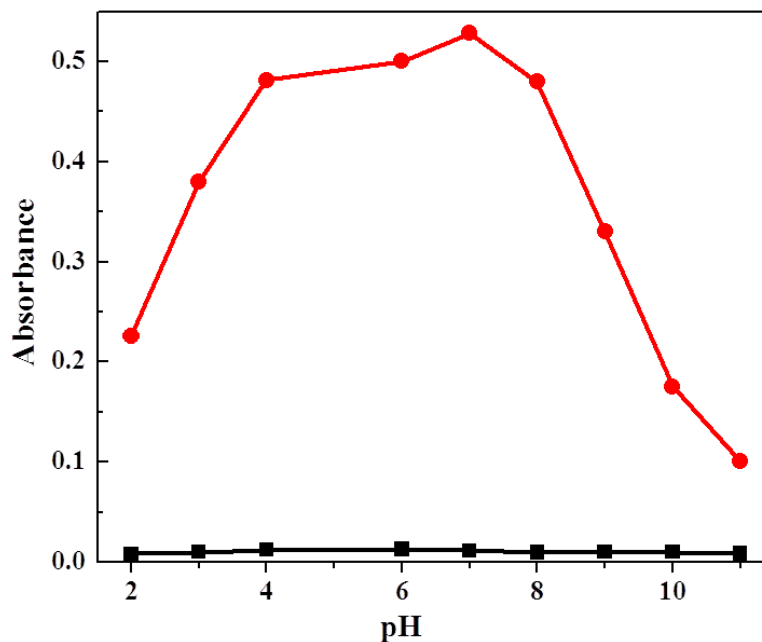


Figure 25. Dependence of the absorbance at 825 nm of julolidine-carbonohydrazone **1** on pH. Black trace: ligand (10 μM) and red trace: ligand with 10.0 equiv of Cu^{2+} in aqueous medium (50 mM HEPES: CH_3CN , 6:4, v/v; pH=7.2).

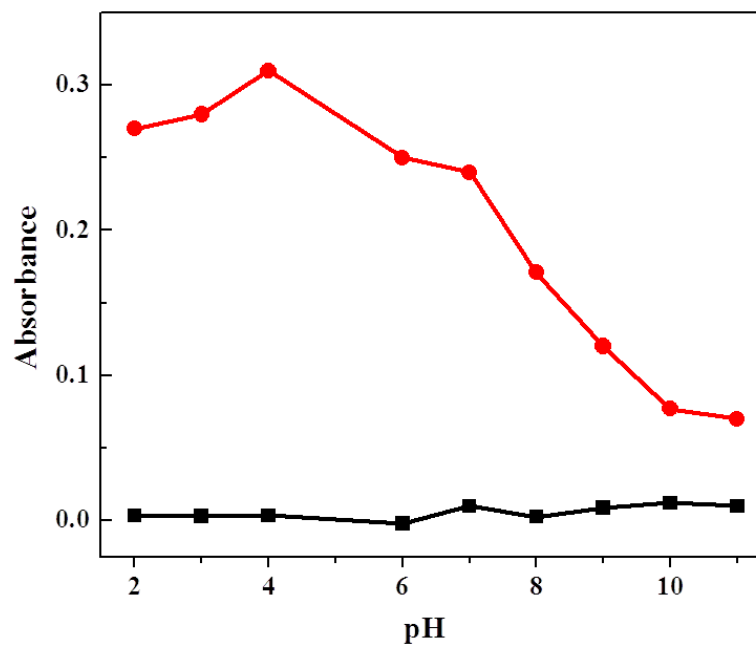


Figure 26. Dependence of the absorbance at 820 nm of julolidine-thiocarbonohydrazone **2** respectively on pH. Black trace: ligand (10 μM) and red trace: ligand with 10.0 equiv of Cu^{2+} in aqueous medium (50 mM HEPES: CH_3CN , 6:4, v/v; pH=7.2).

3.6 Fluorometric detection of Cu^{2+} using Julolidine-thiocarbonohydrazone **4**

Fluorometric behaviour of both the ligands **3** and **4** were studied upon addition of 20.0 equiv of Li^+ , Na^+ , Ba^{2+} , Sr^{2+} , Mg^{2+} , Al^{3+} , Ca^{2+} , Mn^{2+} , Fe^{2+} , Co^{2+} , Ni^{2+} , Zn^{2+} , Ag^+ , Cd^{2+} , Hg^{2+} , Pb^{2+} and Cu^{2+} in aqueous medium (50 mM HEPES: CH_3CN , 6:4, v/v; pH=7.2). Ligand **3** did not show any specific changes in the fluorescence emission in presence of Cu^{2+} and other metal ions used upon excitation at 402 nm (Figure 27). On the other hand, ligand **4** showed strong fluorescence emission around 535 nm upon excitation at 430 nm. The fluorescence intensity around 535 nm was quenched in presence of Cu^{2+} with 430 nm excitation, whereas no significant changes were observed in the fluorescence emission of ligand **3** in presence of other metal ions under similar conditions (Figure 28a). The quenched fluorescence of ligand **4** was restored upon treating the ligand **4**: 2Cu^{2+} complex with EDTA (Inset: Figure 28a). Fluorescence emission of ligand **4** with sequential addition of increasing concentrations (0 to 50 μM) of Cu^{2+} is shown in Figure 28b. This data shows that ligand **4** can easily detect copper ions at least down to 1.0 μM in aqueous medium. The reason behind the fluorescence quenching of **4** upon complexation with Cu^{2+} was understood by theoretical study as

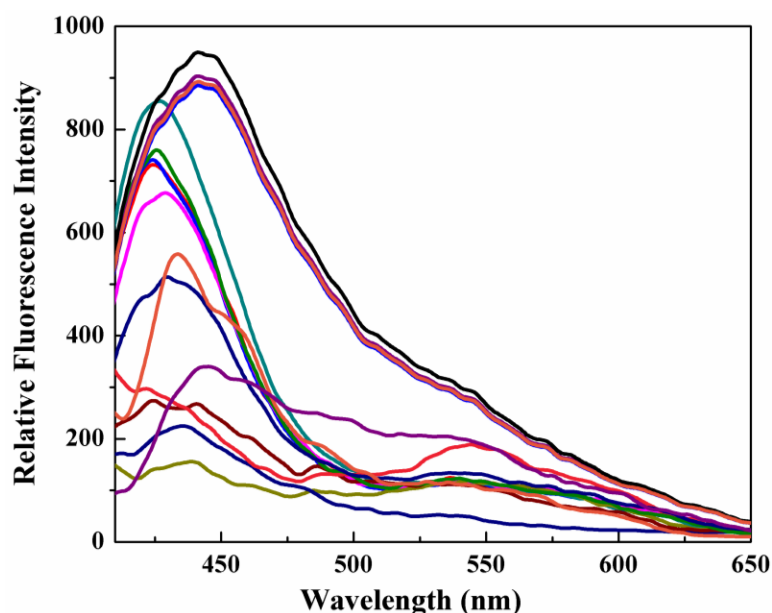


Figure 27. Fluorescence spectra of julolidine-carbonohydrazone **3** (10.0 μM) and on addition of salts (20.0 equivalents) of Li^+ , Na^+ , Ba^{2+} , Sr^{2+} , Mg^{2+} , Al^{3+} , Ca^{2+} , Mn^{2+} , Fe^{2+} , Co^{2+} , Ni^{2+} , Zn^{2+} , Ag^+ , Cd^{2+} , Hg^{2+} , Pb^{2+} and Cu^{2+} in aqueous medium (50 mM HEPES: CH_3CN , 6:4, v/v; pH=7.2).

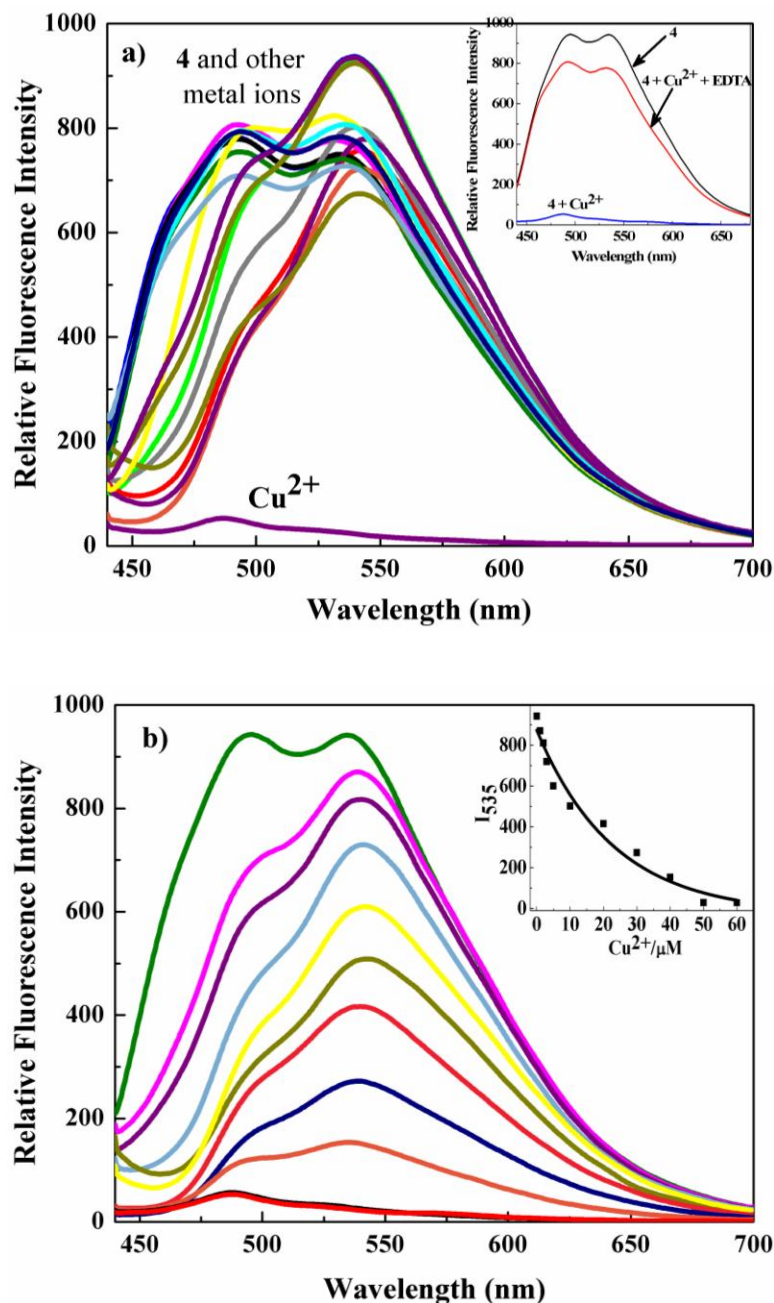


Figure 28. a) Fluorescence spectra of julolidine-thiocarbonohydrazone **4** (10.0 μM) and on addition of salts (20.0 equivalents) of Li^+ , Na^+ , Ba^{2+} , Sr^{2+} , Mg^{2+} , Al^{3+} , Ca^{2+} , Mn^{2+} , Fe^{2+} , Co^{2+} , Ni^{2+} , Zn^{2+} , Ag^+ , Cd^{2+} , Hg^{2+} , Pb^{2+} and Cu^{2+} in aqueous medium (50 mM HEPES: CH_3CN , 6:4, v/v; pH=7.2). Inset: fluorescence spectra of ligand **4** (10.0 μM), [**4** + Cu^{2+}] and [**4** + Cu^{2+} + EDTA (10.0 μM)]. b) Fluorescence spectra of julolidine-thiocarbonohydrazone **4** (10.0 μM) on addition of different concentrations of Cu^{2+} (0, 1, 2, 3, 5, 10, 20, 30, 40, 50 and 60 μM) in aqueous medium. Inset: Intensity at 535 nm as a function of [Cu^{2+}].

discussed in theoretical calculations Section. Ligand **4** can be used for detection of Cu^{2+} by fluorescence “on-off” phenomena over wide pH (2-11) range in aqueous medium (Figure 29).

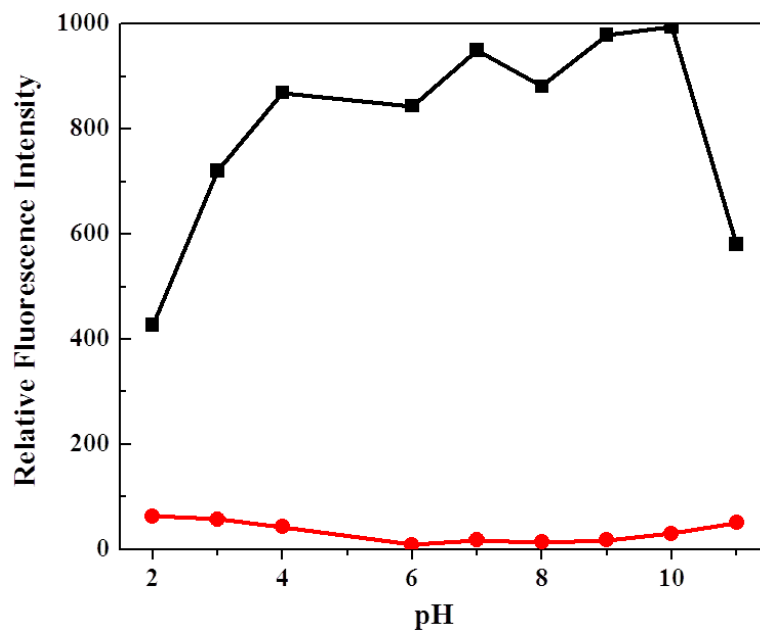


Figure 29. Dependence of the fluorescence intensity at 535 nm on pH. Black trace: julolidine-thiocarbonohydrazone **4** (10 μM) and red trace: julolidine-thiocarbonohydrazone **4** (10 μM) with 5.0 equiv of Cu^{2+} in aqueous (50 mM HEPES: CH_3CN , 6:4, v/v; pH=7.2).

3.7 Theoretical investigation

To understand the molecular mechanism underlying the experimentally observed photophysical characteristics of ligands **3** and **4** upon complexation with Cu^{2+} , the structural, electronic and optical properties have been investigated using *ab initio* density functional theory (DFT) combined with time dependent density functional theory (TDDFT) calculations as implemented in Gaussian 03 package.⁴⁶ Hybrid B3LYP⁴⁷⁻⁴⁹ exchange and correlation function have been adopted using an effective core potential with LANL2DZ⁵⁰⁻⁵² basis set for transition metal Cu and 6-31+g(d,p) basis set for all the other elements in the calculations. Job's plots and mass spectrometry analysis showed that ligand **3** and **4** form complexes with Cu^{2+} in 1:2 stoichiometric ratio. Consequently, two magnetic Cu^{2+} ($S_z^t = 1/2$) complexed with **3** and **4** have been considered for the DFT calculations. In order to find out the minimum

energy magnetic ground state, unrestricted DFT calculations were performed considering both the high-spin ($S_z^{\uparrow} = 1$) and low-spin ($S_z^{\downarrow} = 0$) states within the broken symmetry (BS) approach.⁵³⁻⁵⁵ Vibrational energy calculations have also been conducted to confirm the local energy minimum structures. All the DFT optimised geometries are shown in Figure 30.

Our calculated results showed that the two magnetic Cu²⁺ centers are coupled with ferromagnetic (FM) spin alignments while forming complexes with both the ligands **3** and **4**. The FM state is stabilised over anti-ferromagnetic (AFM) state by 5.61 kcal mol⁻¹ for ligand **3** + 2Cu²⁺ and 3.58 kcal mol⁻¹ for ligand **4** + 2Cu²⁺ complex (Table 1). To focus on the strength of magnetic coupling constant (J), the simple 1D Heisenberg Hamiltonian have been used for the interaction of two spins⁵⁶ and have obtained the FM coupling constants for both the complexes using the energy of low-spin state calculated within BS approach (Table 1). As can be seen from Table 1, the relatively higher J value of **3** + 2Cu²⁺ complex results from the strong super exchange interaction between two magnetic Cu²⁺ ions mediated by the

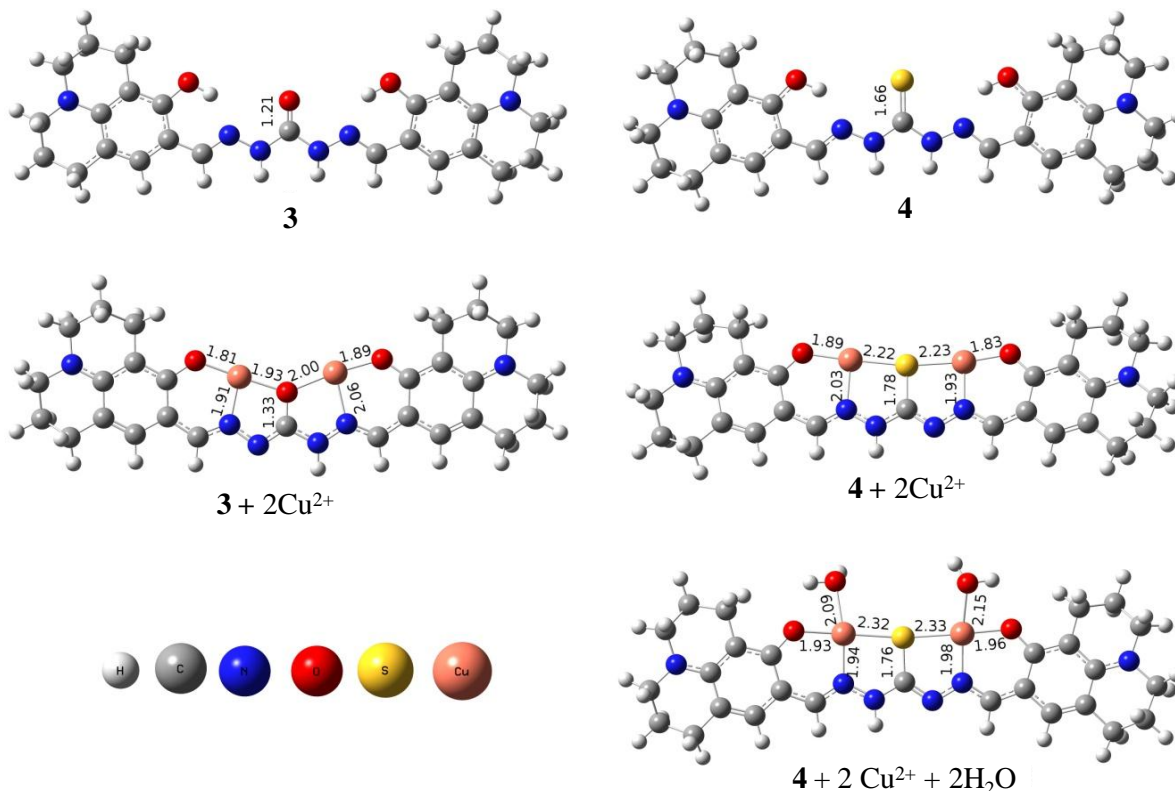


Figure 30. The optimised structures of julolidine-carbonohydrazone **3**, julolidine-thiocarbonohydrazone **4** and their Cu²⁺ complexes. The numbers in each structure show the selected important bond length parameters in Å unit.

Table 1: Relevant electronic energy terms for **3**, **4**, and their Cu²⁺ ion complexes. $\Delta E_{\text{FM-AFM}}$, J, $\Delta E_{\text{H-L}}$, CT represent energy difference between ferromagnetic (FM) and anti-ferromagnetic (AFM) state, FM coupling constant, HOMO-LUMO energy gap, and charge transfer, respectively. The experimental transition energies are given within bracket. The symbols α and β represent two set of spin orbital.

System	$\Delta E_{\text{FM-AFM}}$ (kcal mol ⁻¹)	J (kcal mol ⁻¹)	$\Delta E_{\text{H-L}}$ (eV)	CT (e)	Transition energy (nm)
3	-		3.60		381.50 (382.00)
3 + 2Cu ²⁺	-5.61	11.22	3.35 (α) 1.08 (β)	0.92	1231.48, 455.83, 429.58, 420.30 (933, 558, 412)
4	-		3.35		411.49 (411)
4 + 2Cu ²⁺	-3.58	7.16	3.28 (α) 1.07 (β)	0.98	1126.01, 993.86, 526.80, 472.15, 453.95 (980, 560, 414)
4 + 2Cu ²⁺ + 2H ₂ O	-2.11	4.22	0.12 (α) 0.04 (β)	0.92	916.45, 518.61, 464.10, 447.68, 428.04, 403.42 (980, 560, 414)

oxygen bridge compared to the sulphur bridge in **4** + 2Cu²⁺ complex. The spin density distribution (Figure 31) for both complexes also confirmed the FM spin alignments of two copper ions. It should be noted that a significant amount of spin density is distributed over

the delocalised conjugated π -orbital in both the complexes. To obtain insight on the charge density profile and bonding aspects, the natural bond orbital (NBO) and natural electronic configuration have been calculated. A significant amount of charge transfer from ligand **3** and **4** to the Cu^{2+} center was observed (Table 1). This excess transferred electronic charge was found to be mainly localized on the d-orbital of the two Cu^{2+} centers.

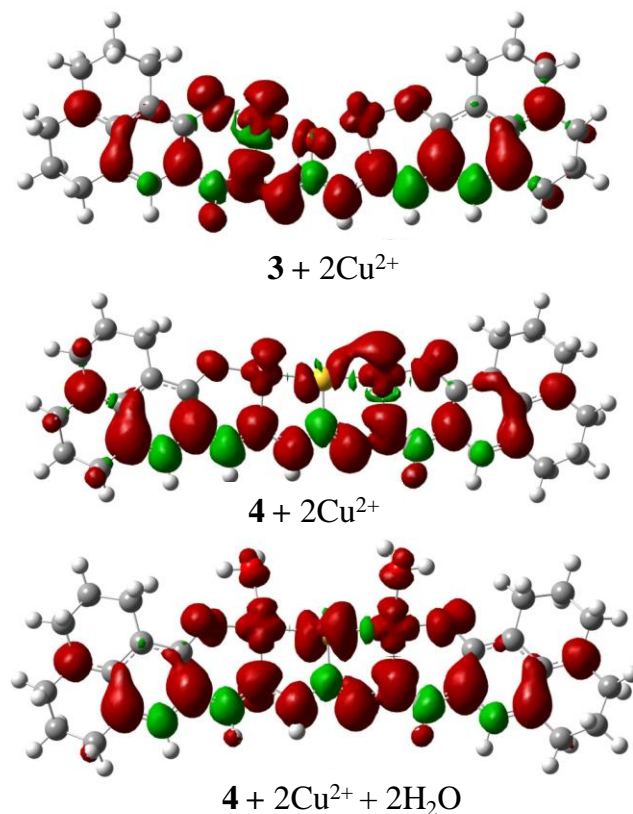


Figure 31. The spin density distribution for $3 + 2\text{Cu}^{2+}$, $4 + 2\text{Cu}^{2+}$ and $4 + 2\text{Cu}^{2+} + 2\text{H}_2\text{O}$ complexes.

The experimentally observed peaks in the visible and NIR regions of absorption spectra upon complexation with Cu^{2+} were studied using TDDFT computations on ground state optimized geometries of free ligands **3** and **4** as well as their Cu^{2+} complexes. As shown in Figure 32, the TDDFT computed excitation energies for free ligands (**3** and **4**) are in quantitative agreements with the experimental transition energies (Table 1). From an analysis of frontier molecular orbital (FMO) the lowest energy transition found to be consists of mainly promoting the electron from delocalized highest occupied molecular orbital (HOMO)

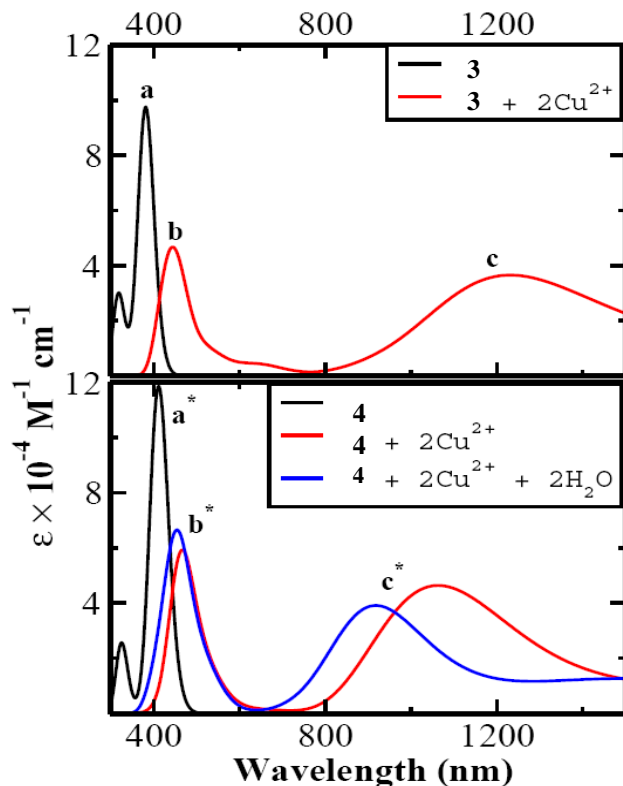


Figure 32. The calculated absorption spectra for **3** (black line, top panel), **4** (black line, bottom panel) and their Cu^{2+} complexes. The indices a ($\text{H} \rightarrow \text{L}$), b ($\text{H}-9(\beta) \rightarrow \text{L}(\beta)$), c ($\text{H}(\beta) \rightarrow \text{L}(\beta)$) and a^* ($\text{H} \rightarrow \text{L}$), b^* ($\text{H}(\alpha) \rightarrow \text{L}(\alpha)$), c^* ($\text{H}(\beta) \rightarrow \text{L}+1(\beta)$) indicate contribution from major molecular orbital transitions corresponding to the peak as shown in Figure 33.

to lowest unoccupied molecular orbital (LUMO) delocalized over the entire molecule (Figure 33). Interestingly the observed shift in absorption peak position towards near-IR in forming charge transfer complex between Cu^{2+} and ligands **3** and **4** corroborating qualitatively with the experimental findings (Figure 32). The relevant FMOs responsible for these transitions are shown in Figure 33. The β -spin orbital contributes mainly to the observed new transition of these Cu^{2+} complexes. Here, it should point out that the observed red shifting in transition energy upon Cu^{2+} chelating compared only qualitatively with the experimental results. This may be due to the consideration of the complexation of two Cu^{2+} ions with each ligands (**3** and **4**) neglecting any coordination from water molecules. To compare and contrast the effect of water coordination on photophysical properties, two water molecules have been considered, coordinating with Cu^{2+} in ligand **4**: 2Cu^{2+} complex (Figure 30).^{19,57} Interestingly,

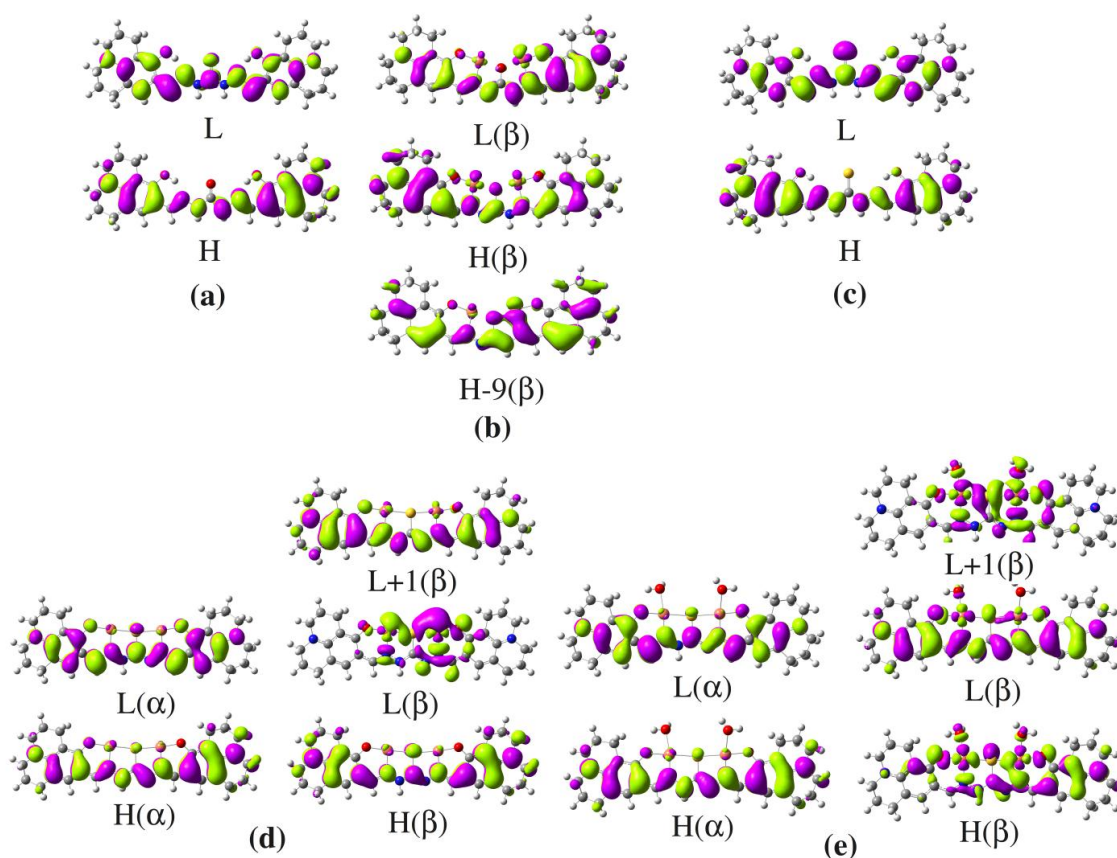


Figure 33. The relevant frontier molecular orbital (FMO) for (a) **3**, (b) **3** + 2Cu^{2+} , (c) **4**, (d) **4** + 2Cu^{2+} , and (e) **4** + 2Cu^{2+} + $2\text{H}_2\text{O}$ complexes. The symbol H and L represent highest occupied molecular orbital and lowest unoccupied molecular orbital, respectively.

the shifting of UV-Vis spectral peak position is less in comparison to the water free coordination complex (Figure 32, bottom panel) resulting in good agreement with experimentally observed shift in peak position.

In order to investigate the mechanism (energy transfer and/or charge transfer process) of fluorescence quenching behaviour upon chelating with Cu^{2+} , excited state geometry optimization and subsequent single point transition energy calculations have been performed employing TDDFT method as implemented in Gaussian suite of programs for compound **4** in presence of Cu^{2+} and two explicit water molecules. From an analysis of FMOs corresponding to the lowest energy transition the fluorescence quenching by Cu^{2+} could be rationalised in terms of the occupancy of FMOs. As shown in Figure 34, the HOMO (β) \rightarrow LUMO + 1 (β),

HOMO - 1 (β) \rightarrow LUMO + 1 (β) and HOMO - 2 (β) \rightarrow LUMO + 1 (β) electronic excitations are found to be relevant for the lowest energy fluorescence process showing predominantly ligand to metal charge transfer (LMCT) and their contributions to the lowest energy excitation are 24%, 18% and 9% respectively. The transferred charge is mainly localized on

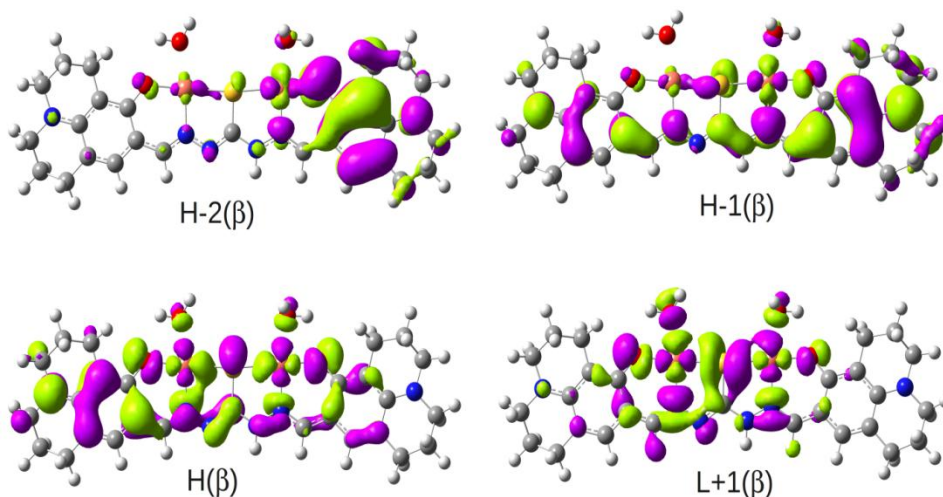


Figure 34. The relevant frontier molecular orbital (FMO) of $4 + 2\text{Cu}^{2+} + 2\text{H}_2\text{O}$ complex corresponding to the excited state charge transfer process. The symbol H and L represent highest occupied molecular orbital and lowest unoccupied molecular orbital, respectively.

the two Cu^{2+} centers as well as on its nearby regime. Note that the calculated values are comparatively small and strongly dependent on the method and basis sets used for their computations. Depending on this, the extent of excited state charge transfer may significantly alter and causes the fluorescence quenching. These excitations correspond to the charge transfer from the excited state of ligand **4** to the Cu^{2+} center (LMCT) and thus provide a pathway for the nonradiative deactivation of the excited state. Thus, fluorescence quenching behaviour can be accounted primarily due to the excited state ligand (**4**) to metal (Cu^{2+}) charge transfer (LMCT) processes.

3.8 Bioimaging

Subsequent experiments proved the ability of julolidine-thiocarbonohydrazone (**4**) to track Cu^{2+} levels in living cells using fluorescence microscopy. HEK293T cells were grown to 50% confluency in 30 mm dish with DMEM and 10% Fetal Bovine Serum (FBS) at 37°C and 5% CO_2 . The cells were washed thrice with Phosphate buffered saline (PBS) and stained using ligand **4** ($10\ \mu\text{M}$) in the growth media without FBS for 10 min. The adherent cells were washed thrice with PBS to remove excess of stain. Fluorescence emission was observed in the optical window at 450–650 nm as shown in Figure 35. The stained cells were subsequently supplemented with $10\ \mu\text{M}$ $\text{Cu}(\text{ClO}_4)_2 \cdot 6\text{H}_2\text{O}$ in DMEM without FBS at 37°C and 5% CO_2 for 10 min and then intracellular fluorescence was almost completely suppressed. Finally the excess $\text{Cu}(\text{ClO}_4)_2 \cdot 6\text{H}_2\text{O}$ was washed off with PBS and then supplemented with $10\ \mu\text{M}$ EDTA in DMEM without FBS for 10 min at 37°C to recover the fluorescence. Since the cells stained with ligand **4** showed a clear cut cytoplasmic localization. These studies clearly suggested that ligand **4** is cell-permeable and can respond to copper ions within living cells.

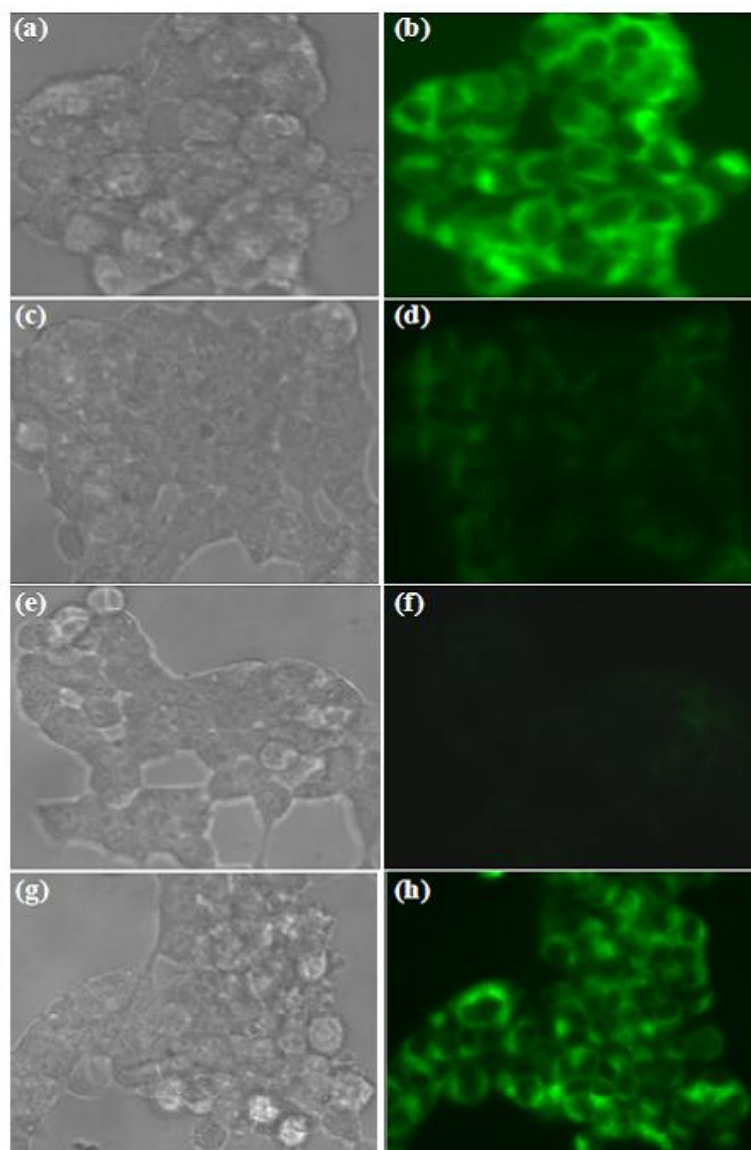


Figure 35. Fluorescence imaging of Cu^{2+} in live HEK293T cells. (a) Bright field transmission image and (b) fluorescence image of HEK293T cells incubated with $10 \mu\text{M}$ of julolidine-thiocarbonohydrazone **4** for 5 min. (c and e) Bright field transmission image and (d and f) fluorescence quenched image of julolidine-thiocarbonohydrazone **4** treated HEK293T cells incubated with $10 \mu\text{M}$ of $\text{Cu}(\text{ClO}_4)_2 \cdot 6\text{H}_2\text{O}$ for 5 and 10 minutes respectively. (g) Bright field transmission image and (h) restoration of fluorescence of ligand **4** with addition of $10 \mu\text{M}$ EDTA. (EDTA = Ethylenediaminetetraacetic acid).

4. Conclusion

Novel Vis–NIR molecular probes accessed through a highly economical, simple, and straightforward synthetic route have been developed and reported in this chapter for selective Cu²⁺ detection. The probe **1** selectively sense Cu²⁺ by colorimetry with remarkable redshifts compared with other transition-metal ions in CH₃CN. Highly conjugated carbonohydrazone and thiocarbonohydrazone (**2-4**) can independently detect Cu²⁺ with high selectivity in the presence of other metal ions with a characteristic NIR signature in aqueous medium. The colorimetric sensing of Cu²⁺ in the visible region by **2-4** was accompanied by a characteristic NIR signature in the region >800 nm. Probes **3** and **4** can be used for detection of different concentrations of Cu²⁺ with the naked eye since these exhibits distinct colors in aqueous solution and therefore one can easily assess the rough concentration levels of Cu²⁺ in analyte samples. These probes can be used for the environmental monitoring and biological detection of copper in wide pH ranges. These probes undergo 1:2 stoichiometric complexation with Cu²⁺, confirmed from absorbance study and mass spectrometry analysis. In addition, fluorescent julolidine–thiocarbonohydrazone **4** selectively senses Cu²⁺ by fluorescence quenching in the presence of all other metal ions under aqueous conditions. The quenched fluorescence emission of ligand **4** can be restored by the addition of EDTA. The utility of ligand **4** as a reversible biosensor has been demonstrated by employing it for live cell imaging of Cu²⁺ in HEK293T cells. The results obtained from theoretical calculations corroborate the experimental findings and provide a detailed microscopic understanding of the observed NIR and fluorescence properties of these probes upon Cu²⁺ chelation. These molecular probes with optical responses in the visible and NIR regions can be applied for biological imaging.

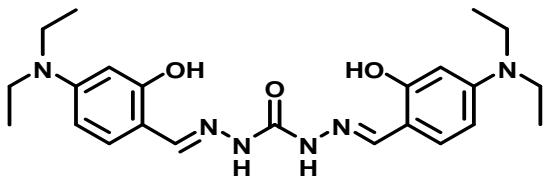
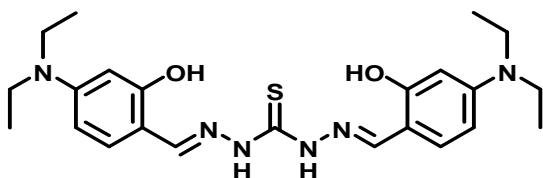
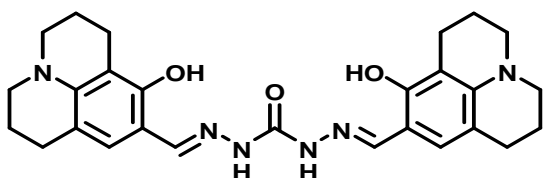
5. Experimental

5.1 General experimental procedure

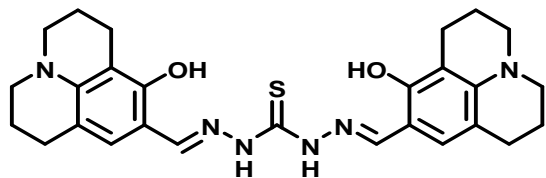
All the solvents and reagents were obtained from Sigma-Aldrich and used as received unless otherwise mentioned. The solutions of metal ions were prepared from $\text{Al}(\text{ClO}_4)_3 \cdot 9\text{H}_2\text{O}$, $\text{LiClO}_4 \cdot 3\text{H}_2\text{O}$, NaClO_4 , $\text{Mg}(\text{ClO}_4)_2$, $\text{Ca}(\text{ClO}_4)_2 \cdot 4\text{H}_2\text{O}$, $\text{Sr}(\text{NO}_3)_2$, $\text{Ba}(\text{ClO}_4)_2$, $\text{Mn}(\text{ClO}_4)_2 \cdot 6\text{H}_2\text{O}$, $\text{Fe}(\text{ClO}_4)_2 \cdot \text{H}_2\text{O}$, $\text{Co}(\text{ClO}_4)_2 \cdot 6\text{H}_2\text{O}$, $\text{Cd}(\text{ClO}_4)_2 \cdot \text{H}_2\text{O}$, $\text{Ag}(\text{ClO}_4)_2$, $\text{Hg}(\text{ClO}_4)_2$, $\text{Pb}(\text{ClO}_4)_2$, $\text{Ni}(\text{ClO}_4)_2 \cdot 6\text{H}_2\text{O}$, $\text{Cu}(\text{ClO}_4)_2 \cdot 6\text{H}_2\text{O}$ and $\text{Zn}(\text{ClO}_4)_2 \cdot 6\text{H}_2\text{O}$ respectively in CH_3CN . ^1H and ^{13}C NMR were recorded on a Bruker AV-400 spectrometer with chemical shifts reported as *ppm* (in $\text{DMSO}-d_6$, tetramethylsilane as internal standard). Mass spectra were obtained on Shimadzu 2020 LC-MS and Bruker Ultraflex II MALDI/TOF spectrometers. Elemental analysis was carried out on Thermo Scientific FLASH 2000 Organic Element Analyzer. UV-Vis spectra were recorded on a Perkin Elmer Lambda 900 spectrophotometer and fluorescence spectra were recorded on a Perkin Elmer LS 55 spectrophotometer.

5.2 General procedure for the synthesis of Schiff base ligands

A solution of different salicylaldehyde (6.0 mmol) in ethanol (40 mL) was added slowly to a solution of carbohydrazide or thiocarbohydrazide (3.0 mmol) in water (40 mL). Initially the solution turned turbid and after complete addition the solution became clear. The reaction mixture was refluxed with stirring for 24 h. Reaction mixture was cooled to room temperature and the precipitate was filtered. The precipitate was washed with ethanol and dried under vacuo to obtain biscarbonohydrazone or bithiocarbonohydrazone in quantitative yield.

1,5-Bis[[4-(N,N-diethylamino)-2-hydroxyphenyl]methylenesalicylaldehyde]**carbonohydrazide (1):** Yield 92% (yellow powder). ¹H NMR (400 MHz, DMSO-*d*₆) δ_{ppm}1.08-1.12 (12H, m), 3.31 (8H, m), 6.10 (2H, d, *J* = 2Hz), 6.21-6.24 (2H, dd, *J* = 2.4 Hz, 6.4 Hz), 7.30-7.32 (2H, d, *J* = 8Hz), 8.19 (2H, s), 10.35 (2H, s), 10.58 (2H, br). ¹³C NMR (100 MHz, DMSO-*d*₆) δ_{ppm}12.5, 43.7, 97.5, 103.5, 107.3, 129.9, 144.3, 149.6, 151.9, 158.4. MS (EI): *m/z* = 441.45 [M+ H⁺], calcd. 440.54 for C₂₃H₃₂N₆O₃. Elemental analysis: Found C, 62.56; H, 7.34; N, 19.13; Calcd. C, 62.71; H, 7.32; N, 19.08 for C₂₃H₃₂N₆O₃.**1,5-Bis[[4-(N,N-diethylamino)-2-****hydroxyphenyl]methylenesalicylaldehyde]thiocarbonohydrazide (2):** Yield 92% (yellowpowder). ¹H NMR (400 MHz, DMSO-*d*₆) δ_{ppm} 1.09-1.13 (12H, m), 3.34-3.37 (8H, m), 6.10 (2H, d, *J* = 2.4 Hz), 6.23-6.27 (2H, dd, *J* = 2.4 Hz, 6.4 Hz), 7.09 (1H, br), 7.69 (1H, br), 8.30-8.48 (2H, br), 9.57-9.61 (1H, br), 11.49 (2H, br), 11.65 (1H, br). ¹³C NMR (100MHz, DMSO-*d*₆) δ_{ppm} 12.5, 43.7, 97.5, 103.5, 107.3, 130.0, 144.3, 149.5, 151.9, 158.4. MS (EI): *m/z* = 457.4 [M+H⁺], calcd. For 456.6 C₂₃H₃₂N₆O₂S. Elemental analysis: Found C, 60.56; H, 7.08; N, 18.39; S, 7.01; Calcd. C, 60.50; H, 7.06; N, 18.41; S, 7.02 for C₂₃H₃₂N₆O₂S.**Bis[[8-hydroxyjulolidine]methylene]-carbonic dihydrazide [julolidine-****carbonohydrazone (3):** Yield 94%. ¹H NMR (400 MHz, DMSO-*d*₆) δ_{ppm} 1.76-1.82 (8H,m), 2.51-2.56 (8H, m), 3.06-3.10 (8H, m), 6.61 (2H, s), 7.98 (2H, s), 10.33 (2H, s), 10.71 (2H, br). ¹³C NMR (100 MHz, DMSO-*d*₆) δ_{ppm} 20.3, 20.8, 21.6, 26.5, 48.8, 49.3, 106.4, 106.5, 112.3,127.7, 144.6, 147.0, 151.7, 153.4. MS (EI): *m/z* = 489.3 [M+H]⁺, calcd. 488.25 for C₂₇H₃₂N₆O₃. Elemental analysis: Found C, 66.34; H, 6.61; N, 17.22; Calcd. C, 66.37; H, 6.60; N, 17.20 for C₂₇H₃₂N₆O₃.

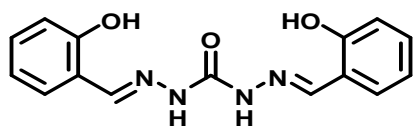
Bis[[8-hydroxyjulolidine]methylene]-carbonothioic dihydrazide [julolidine-thiocarbonohydrazone (4)]: Yield 93%. ¹H NMR (400 MHz, DMSO-*d*₆) δ_{ppm} 1.83-1.87



(8H, m), 2.59-2.64 (8H, m), 3.15-3.19 (8H, m), 6.73 (2H, s), 8.25 (2H, s), 9.43 (1H, s), 11.47-11.84 (3H, br). ¹³C NMR (100 MHz, DMSO-*d*₆) δ_{ppm} 20.3, 20.7, 21.5, 26.5, 48.8, 49.3, 106.0,

106.4, 112.6, 128.2, 145.2, 149.2, 153.7, 172.2, 191.6. MS (EI): *m/z* = 505.3 [M+H]⁺, calcd. 504.23 for C₂₇H₃₂N₆O₂S. Elemental analysis: Found C, 64.22; H, 6.40; N, 16.67; Calcd. C, 64.26; H, 6.39; N, 16.65 for C₂₇H₃₂N₆O₂S.

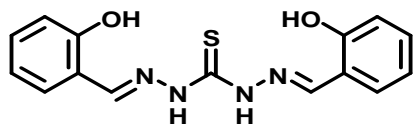
Bis[[2-hydroxyphenylmethylene]-carbonic dihydrazide (5)]: Yield 95%. ¹H NMR (400



MHz, DMSO-*d*₆) δ_{ppm} 6.86-6.90 (4H, m), 7.22-7.26 (2H, m), 7.68-7.71 (2H, m), 8.43 (2H, s), 10.84 (4H, br). ¹³C NMR (100 MHz, DMSO-*d*₆) δ_{ppm} 116.1, 119.1, 119.6,

128.1, 130.6, 142.6, 151.9, 156.6. MS (EI): *m/z* = 299.11 [M+H]⁺, calcd. 298.11 for C₁₅H₁₄N₄O₃. Elemental analysis: Found C, 60.35; H, 4.74; N, 18.79; Calcd. C, 60.40; H, 4.73; N, 18.78 for C₁₅H₁₄N₄O₃.

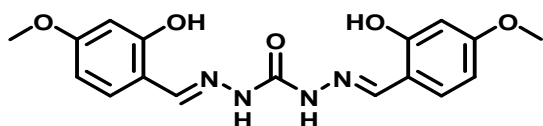
Bis[[2-hydroxyphenylmethylene]-carbonothioic dihydrazide (6)]: Yield 94%. ¹H NMR



(400 MHz, DMSO-*d*₆) δ_{ppm} 6.91-6.93 (4H, m), 7.28-7.43 (3H, m), 8.07 (1H, s), 8.52-8.76 (2H, br), 10.02 (1H, s), 11.62 (1H, s), 11.89-12.04 (2H, br). ¹³C NMR (100 MHz,

DMSO-*d*₆) δ_{ppm} 116.3, 118.1, 119.2, 120.0, 126.9, 130.4, 131.3, 141.1, 149.3, 156.9, 174.4. MS (EI): *m/z* = 315.09 [M+H]⁺, calcd. 314.08 for C₁₅H₁₄N₄O₂S. Elemental analysis: Found C, 57.29; H, 4.50; N, 17.84; Calcd. C, 57.31; H, 4.49; N, 17.82 for C₁₅H₁₄N₄O₂S.

Bis[[2-hydroxy-4-methoxyphenylmethylene]-carbonic dihydrazide (7)]: Yield 94%. ¹H

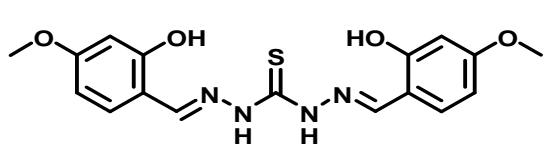


NMR (400 MHz, DMSO-*d*₆) δ_{ppm} 3.75 (6H, s), 6.45-6.50 (4H, m), 7.53-7.55 (2H, d, *J* = 8.8 Hz), 8.32 (2H, s), 10.64 (2H, s), 10.87 (2H, br). ¹³C

NMR (100 MHz, DMSO-*d*₆) δ_{ppm} 55.1, 100.9, 106.1, 112.7, 129.5, 142.8, 151.9, 158.2,

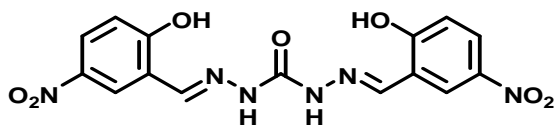
161.4. MS (EI): $m/z = 359.2$ $[M+H]^+$, calcd. 358.13 for C₁₇H₁₈N₄O₅. Elemental analysis: Found C, 56.96; H, 5.07; N, 15.65; Calcd. C, 56.98; H, 5.06; N, 15.63 for C₁₇H₁₈N₄O₅.

Bis[[2-hydroxy-4-methoxyphenylmethylene]-carbonothioic dihydrazide (8)]: Yield 94%.



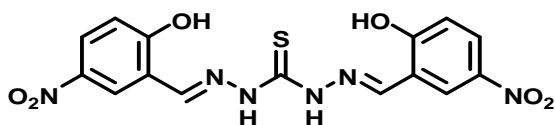
¹H NMR (400 MHz, DMSO-*d*₆) δ_{ppm} 3.77 (6H, s), 6.47-6.52 (4H, m), 7.31(1H, s), 7.96 (1H, s), 8.41-8.65 (2H, br), 10.08 (1H, s), 11.71-11.86 (3H, br). ¹³C NMR (100 MHz, DMSO-*d*₆) δ_{ppm} 55.2, 100.9, 106.3, 111.6, 112.9, 128.5, 131.6, 141.4, 149.2, 158.3, 159.2, 162.0, 173.7. MS (EI): $m/z = 375.1$ $[M+H]^+$, calcd. 374.1 for C₁₇H₁₈N₄O₄S. Elemental analysis: Found C, 54.51; H, 4.86; N, 14.97; Calcd. C, 54.53; H, 4.85; N, 14.96 for C₁₇H₁₈N₄O₄S.

Bis[[2-hydroxy-5-nitrophenylmethylene]-carbonic dihydrazide (9)]: Yield 93%. %.



¹H NMR (400 MHz, DMSO-*d*₆) δ_{ppm} 7.07 (1H, s), 7.09 (1H, s), 8.12-8.15 (2H, dd, $J = 6.4$ Hz, 2.8 Hz), 8.50 (2H, s), 8.70 (2H, s), 11.22 (2H, s), 12.02 (2H, s). ¹³C NMR (100 MHz, DMSO-*d*₆) δ_{ppm} 116.7, 120.7, 123.0, 125.9, 139.4, 140.0, 151.9, 161.9. MS (EI): $m/z = 389.1$ $[M+H]^+$, calcd. 388.09 for C₁₅H₁₂N₆O₇. Elemental analysis: Found C, 46.38; H, 3.12; N, 21.65; Calcd. C, 46.40; H, 3.11; N, 21.64 for C₁₅H₁₂N₆O₆S.

Bis[[2-hydroxy-5-nitrophenylmethylene]-carbonothioic dihydrazide (10)]: Yield 94%.



¹H NMR (400 MHz, DMSO-*d*₆) δ_{ppm} 7.12 (2H, s), 8.17-8.20 (2H, dd, $J = 6.4$ Hz, 2.8 Hz), 8.53 (2H, s), 8.89-8.94 (2H, m), 11.72 (1H, s), 12.33-12.40 (2H, m), 12.72 (1H, s). ¹³C NMR (100 MHz, DMSO-*d*₆) δ_{ppm} 116.7, 117.5, 118.7, 120.8, 122.5, 125.7, 126.7, 139.0, 139.9, 146.8, 162.5, 175.1. MS (EI): $m/z = 405.1$ $[M+H]^+$, calcd. 404.05 for C₁₅H₁₂N₆O₆S. Elemental analysis: Found C, 44.57; H, 2.98; N, 20.80; Calcd. C, 44.55; H, 2.99; N, 20.78 for C₁₅H₁₂N₆O₆S.

5.3 General method of UV-Vis titration

UV-Vis spectra were recorded on Perkin Elmer Lambda 900 spectrophotometer and fluorescence spectra were recorded on a Perkin Elmer model LS 55 spectrophotometer. 1 cm cells were used for absorption and emission titration. For UV-Vis and fluorescence titrations stock solution of ligands were prepared ($c = 2000 \mu\text{M}$) in CH₃CN. The solutions of guest cations were prepared in CH₃CN in the order of 10^{-3} M. Working solutions of ligands and metal ions were prepared from the stock solutions. Excitation was carried out at 402 and 430 nm for **3** and **4** respectively with 15 nm excitation and 5 nm emission slit widths.

5.4 Job plot by UV-Vis method

A series of solutions containing **2** and Cu(ClO₄)₂ were prepared such that the sum of the total concentration of metal ion and **2** remained constant (20 μM). The mole fraction (X) of Cu²⁺ was varied from 0.1 to 1.0. The corrected absorbance ($[A-A_0] / [A_0]$) at 940 nm was plotted against the molar fraction of the Cu²⁺ solution.

A series of solutions containing Schiff bases **3** and **4** and Cu(ClO₄)₂ were prepared such that the sum of the total concentration of metal ion and ligands **3** and **4** remained constant (50 μM). The mole fraction (X) of Cu²⁺ was varied from 0.1 to 1.0. The corrected absorbance ($[A-A_0] / [A_0]$) at 820 nm were plotted against the molar fraction of the Cu²⁺ solution.

5.5 Determination of binding constant

Tsein equation⁵⁸ is derived to the following equations that can be used in any stoichiometric ratio between the ligand and analyte.

$$[\text{M}^{n+}]^m = \frac{1}{n \cdot K} \cdot \frac{1}{[\text{L}]_T^{n-1}} \cdot \frac{1-\alpha}{\alpha^n}$$

Where K is complex equilibrium constant, M_mL_n is metal-ligand, L is ligand, [L], [Mⁿ⁺], and [M_mL_n] are the concentrations of respective species. α is the ratio between free ligand

concentration, [L], and the initial concentration of ligand, [L]. In our case, the stoichiometric ratio of the Cu²⁺ and chemosensor is 2:1. Thus, the equation can be written as

$$[\text{Cu}^{2+}]^2 = \frac{1}{2KL_T} \cdot \frac{1-\alpha}{\alpha^2}$$

5.6 Bioimaging

Fluorescence microscopy:

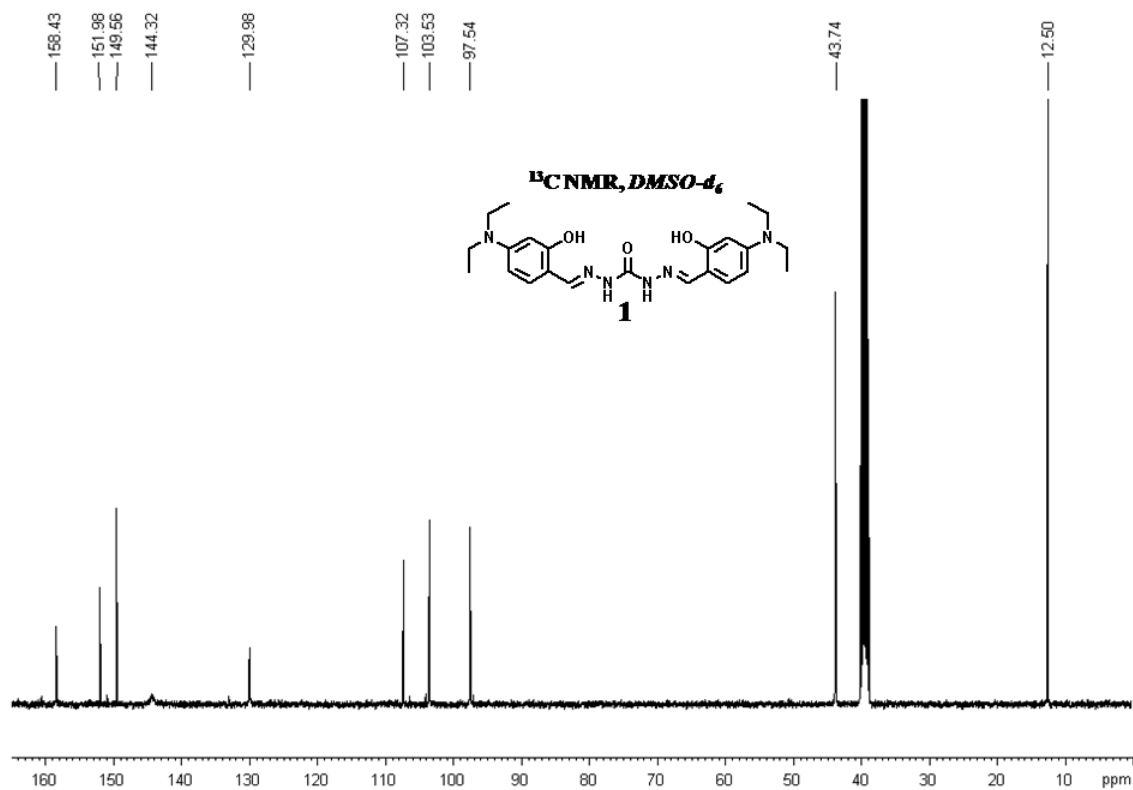
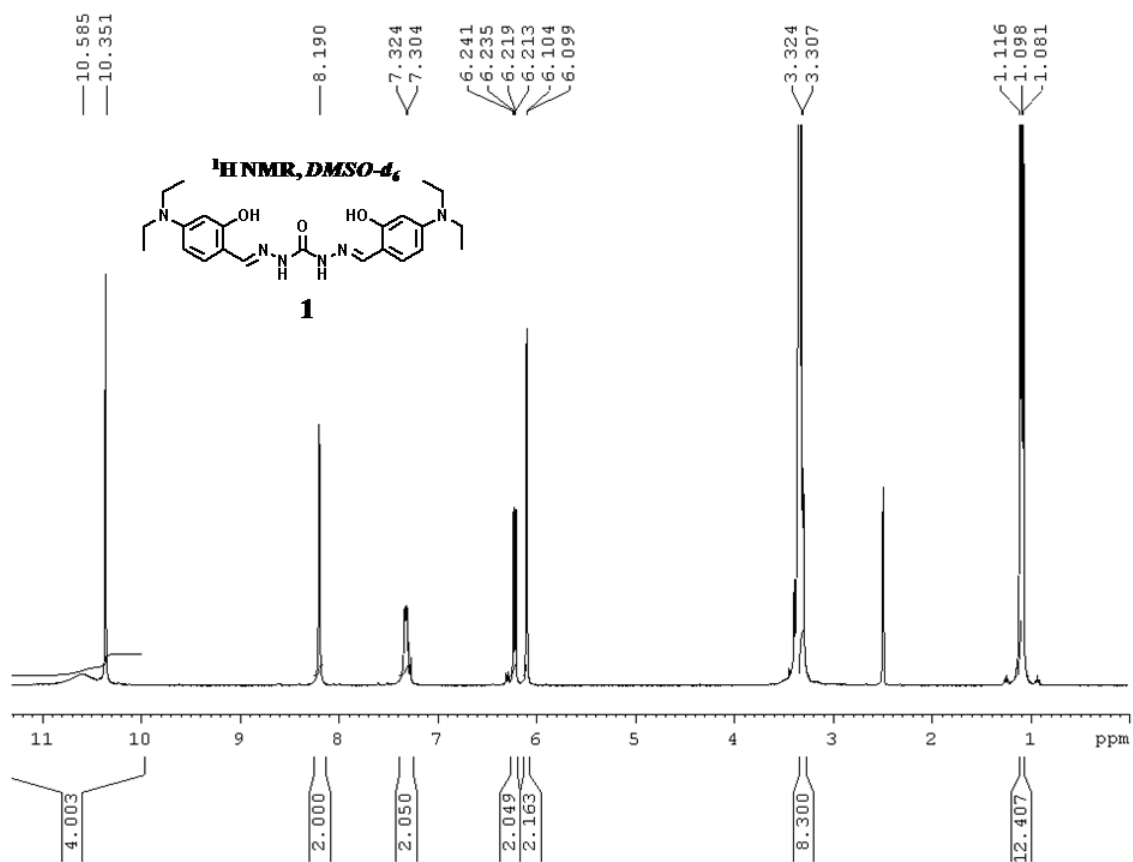
HEK293T cells stained with 10 μM thiocarbonohydrazone **4** for 10 min were captured using Axiovert 200M with an excitation at 488 nm under 40X magnification. Fluorescence emission was observed in the optical window at 450–650 nm. The stained cells were subsequently supplemented with 10 μM Cu(ClO₄)₂·6H₂O in DMEM (Dulbecco's Modified Eagle Medium) without FBS at 37°C and 5% CO₂ for 5 to 10 min. Finally the excess Cu(ClO₄)₂·6H₂O was washed off and then supplemented with 10 μM EDTA (Ethylenediaminetetraacetic acid) in DMEM without FBS for 10 min at 37°C.

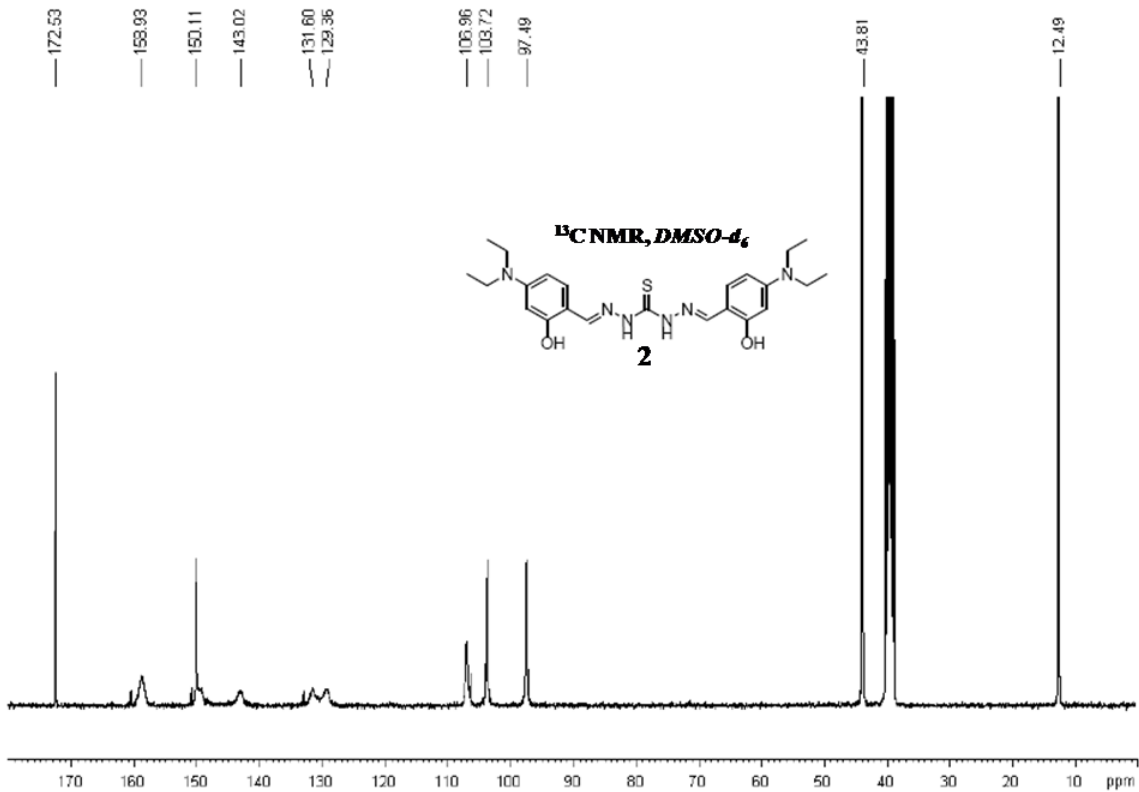
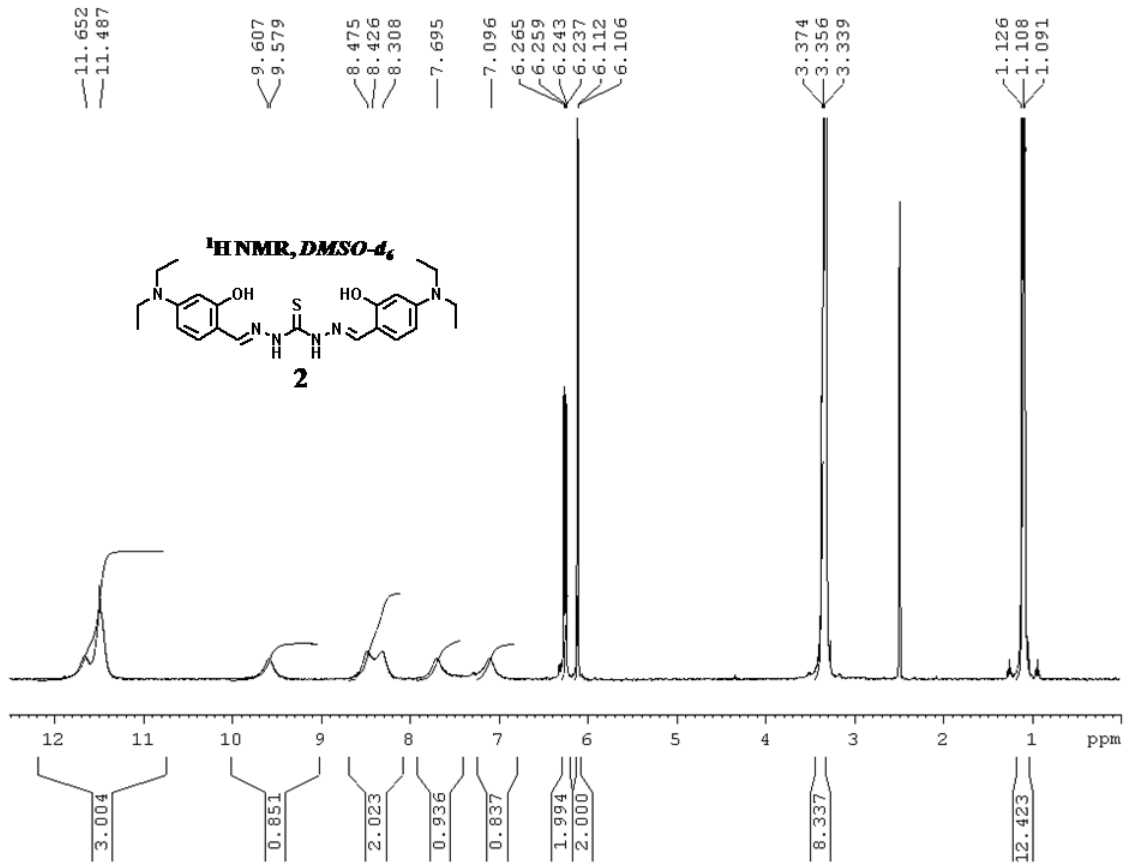
Cell culture and staining procedures:

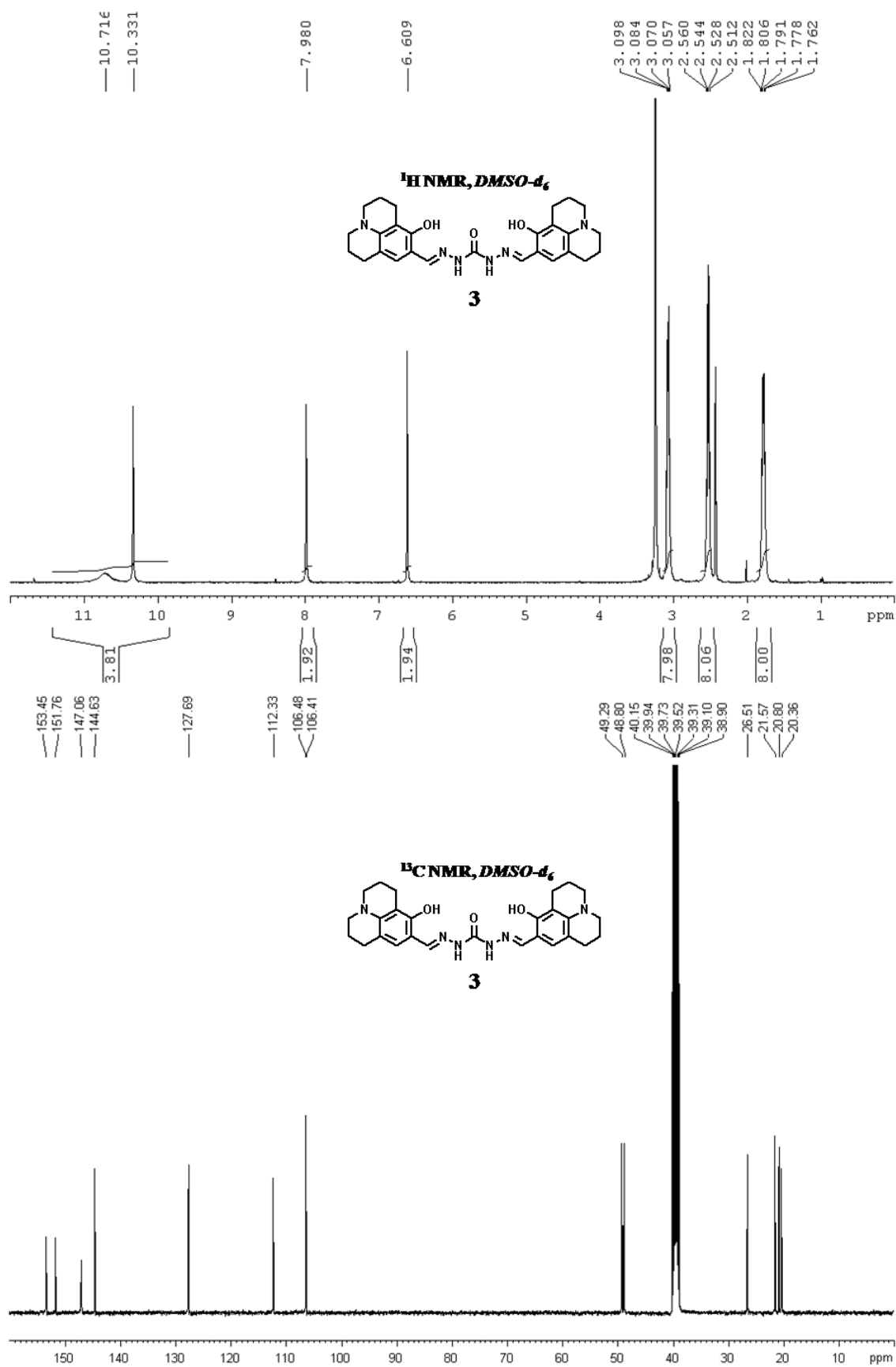
HEK293T cells were grown to 50% confluency in 30 mm dish with DMEM and 10% Fetal Bovine Serum (FBS) at 37°C and 5% CO₂. The cells were washed thrice with Phosphate-Buffered Saline (PBS) and stained using 10 μM julolidine-thiocarbonohydrazone **4** in the growth media without FBS for 10 min. The adherent cells were washed thrice with PBS to remove excess of stain and images were captured using Axiovert 200M with excitation at 488 nm under 40x magnification. The stained cells were subsequently supplemented with 10 μM Cu(ClO₄)₂·6H₂O in DMEM without FBS at 37°C and 5% CO₂ for 10 min and then the loss in fluorescence was captured. Finally the excess Cu(ClO₄)₂·6H₂O was washed off with PBS and then supplemented with 10 μM EDTA in DMEM without FBS for 10 min at 37°C. Images were captured for the reappearance of fluorescence.

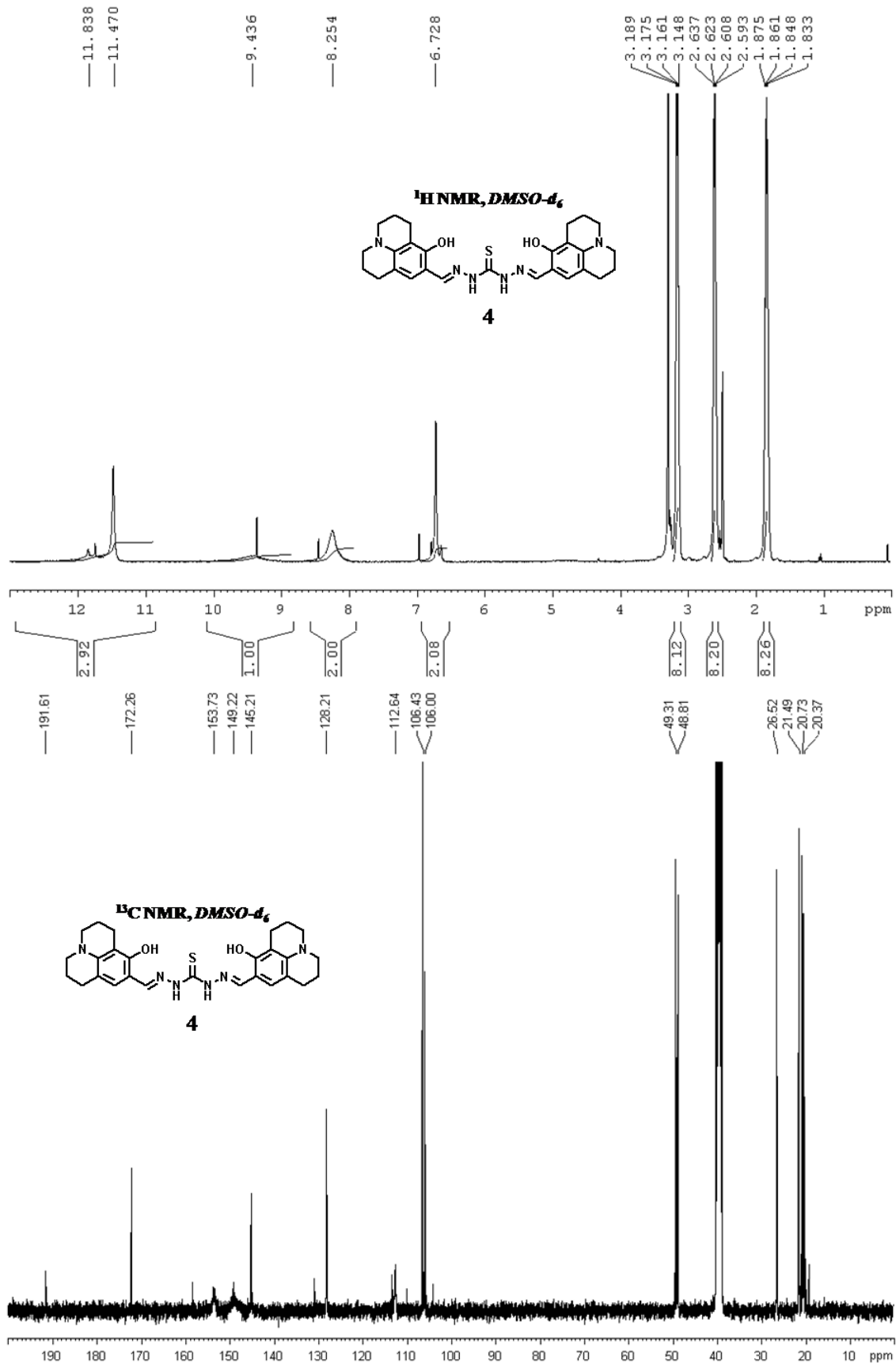
5.7 Appendix

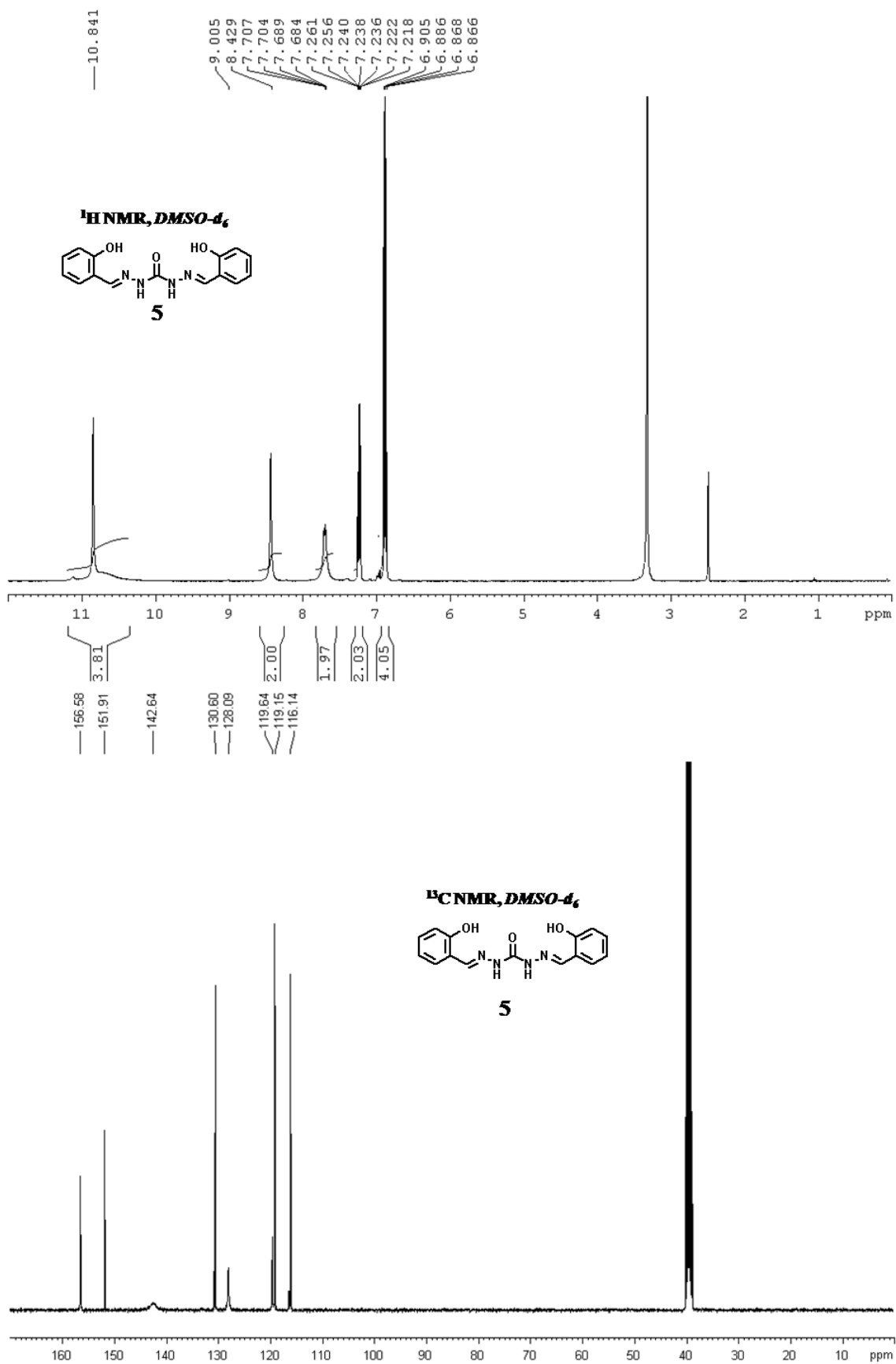
- ❖ Compound 1, ¹H and ¹³C NMR
- ❖ Compound 2, ¹H and ¹³C NMR
- ❖ Compound 3, ¹H and ¹³C NMR
- ❖ Compound 4, ¹H and ¹³C NMR
- ❖ Compound 5, ¹H and ¹³C NMR
- ❖ Compound 6, ¹H and ¹³C NMR
- ❖ Compound 7, ¹H and ¹³C NMR
- ❖ Compound 8, ¹H and ¹³C NMR
- ❖ Compound 9, ¹H and ¹³C NMR
- ❖ Compound 10, ¹H and ¹³C NMR

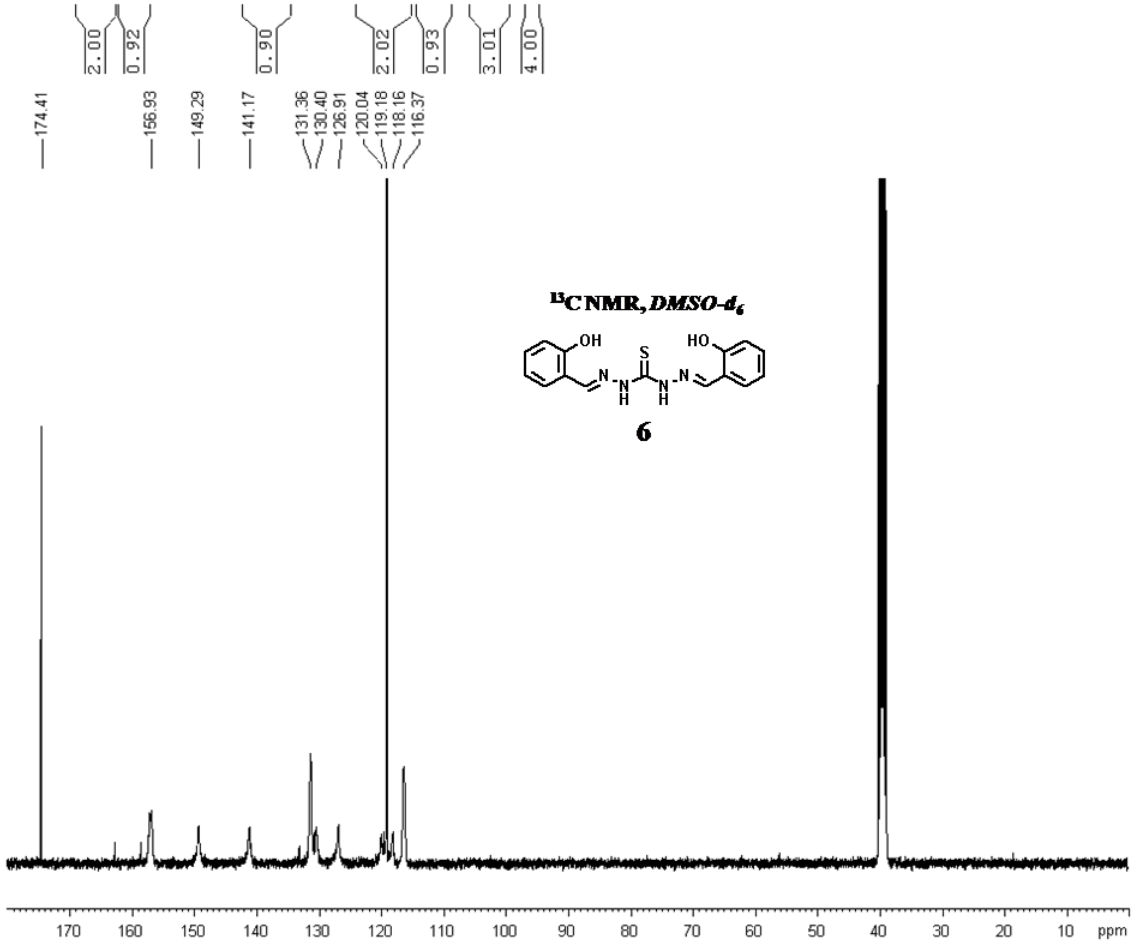
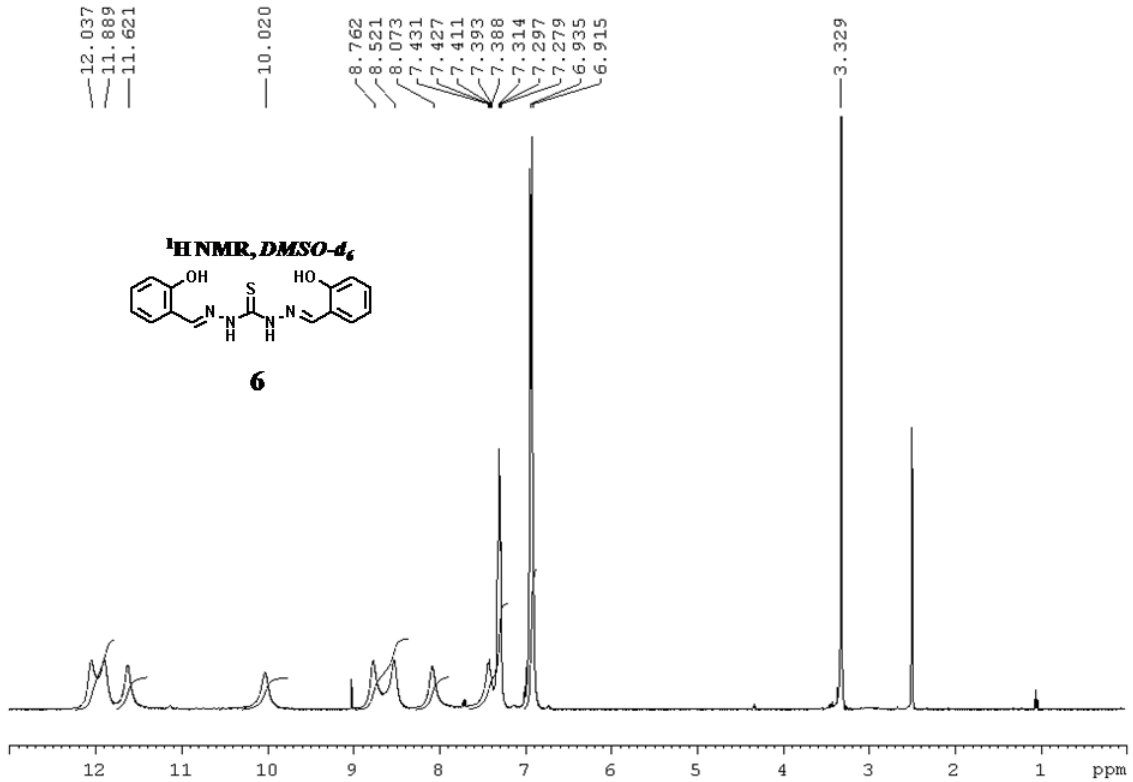


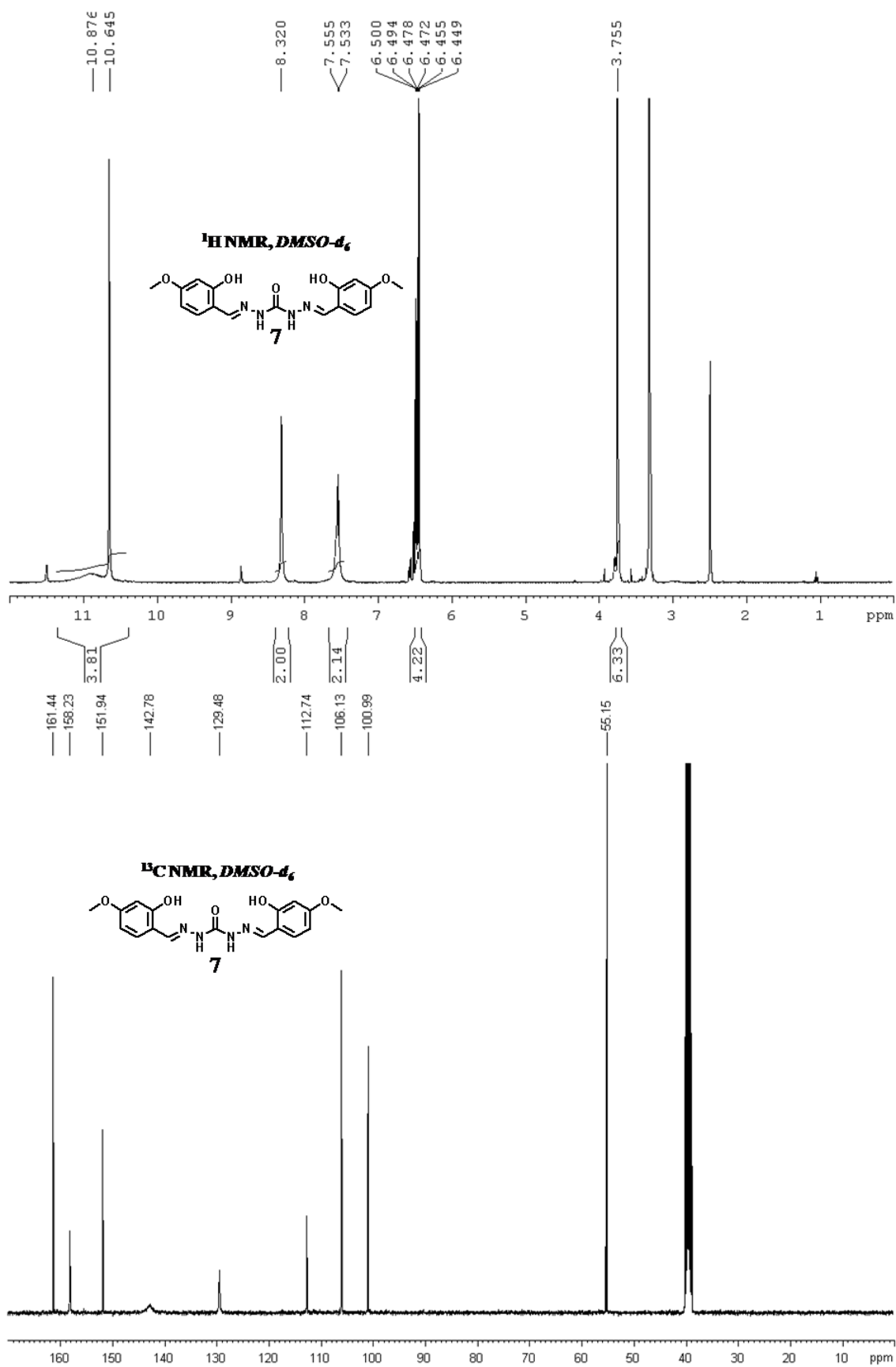


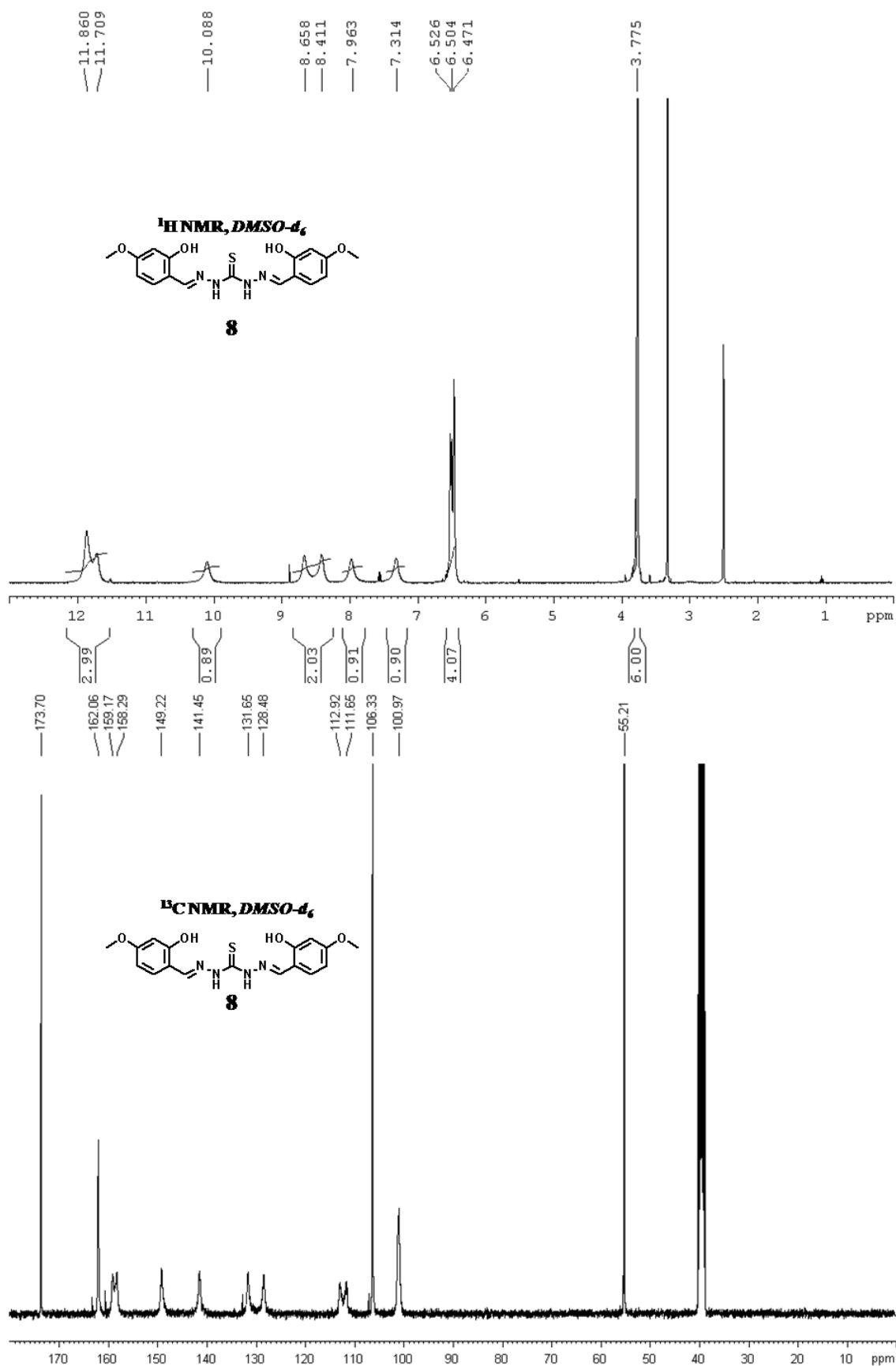


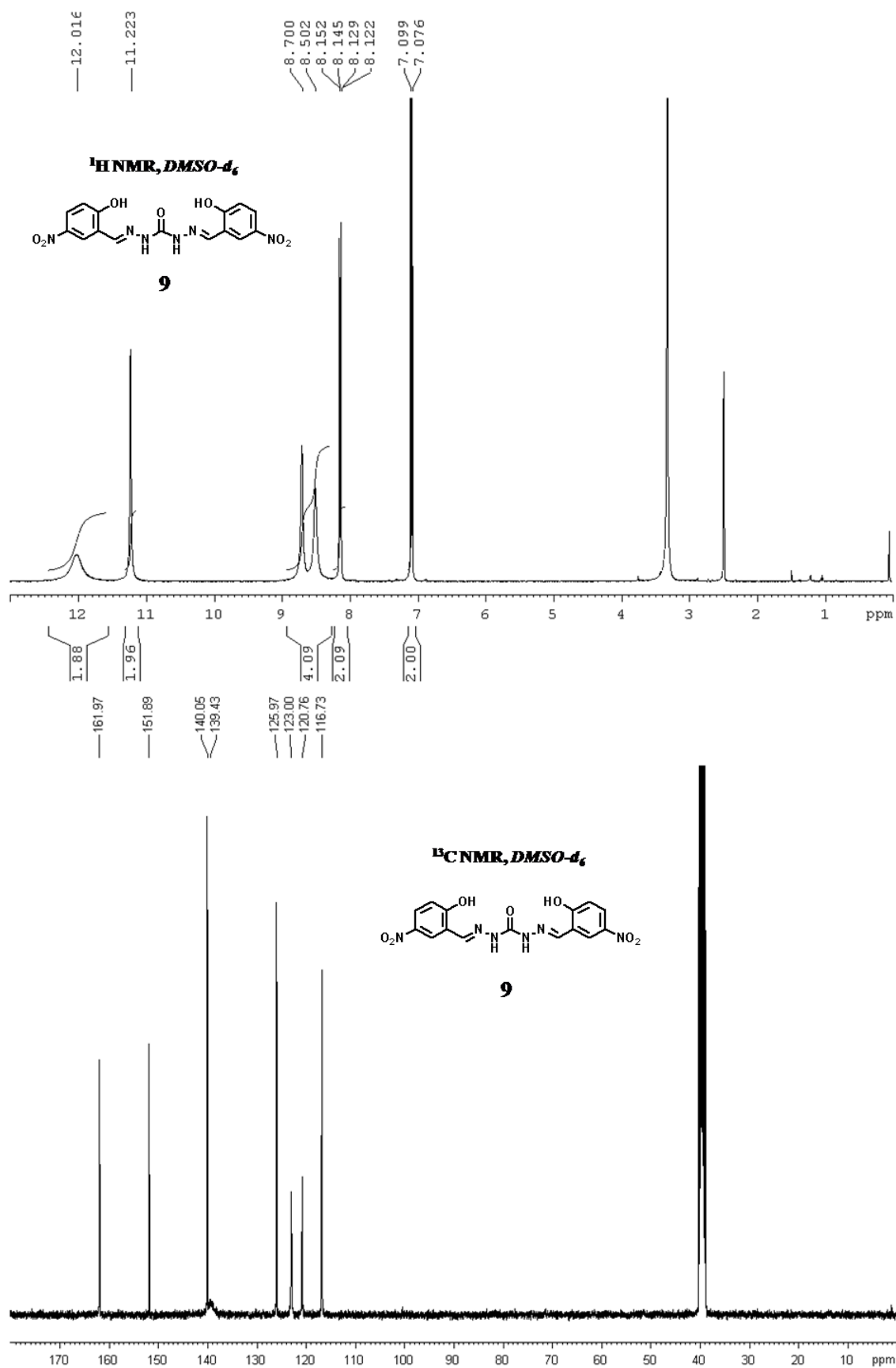


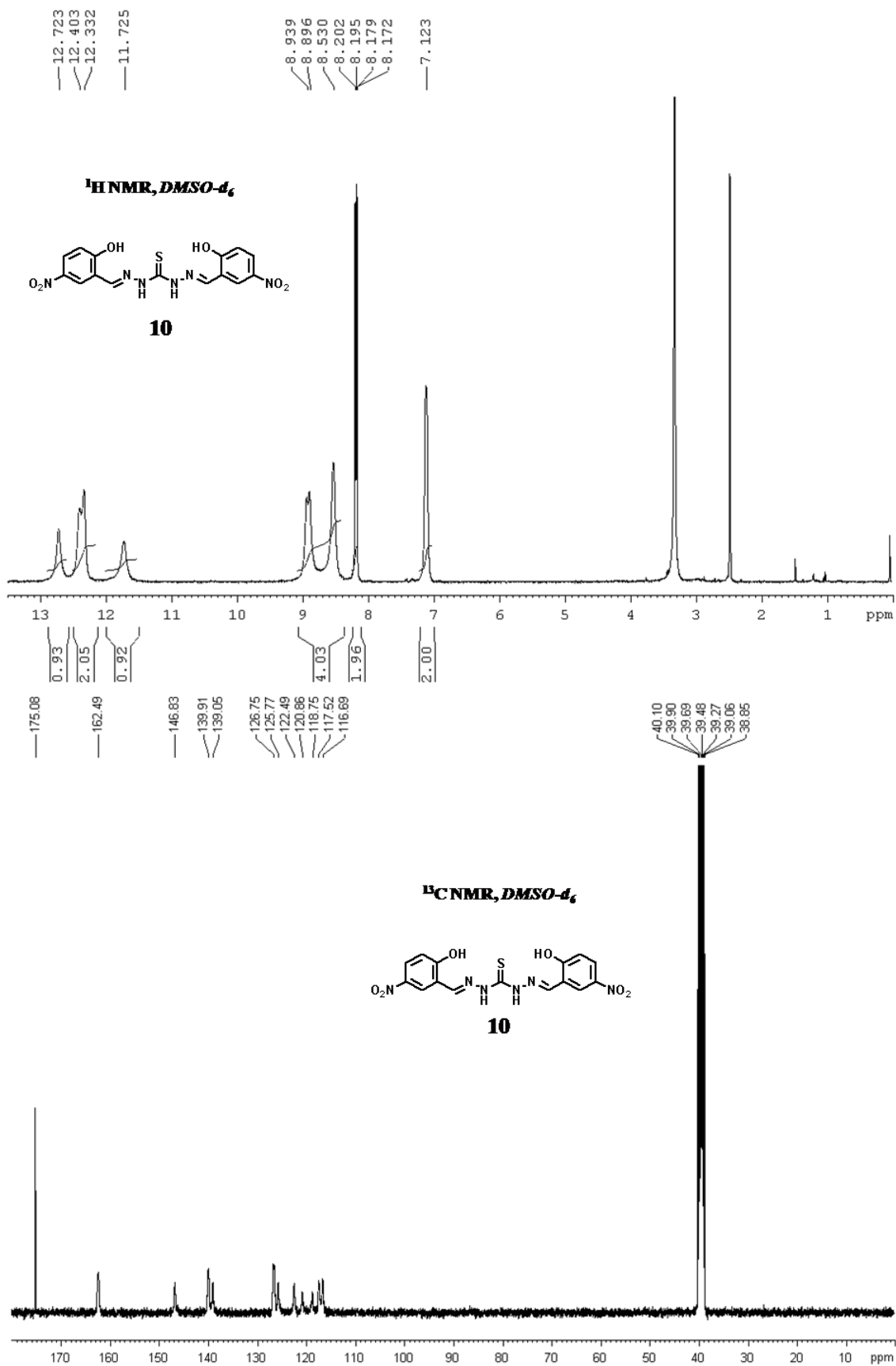












6. References

1. Gaggelli, E.; Kozłowski, H.; Valensin, D.; Valensin, G., Copper homeostasis and neurodegenerative disorders (alzheimer's, prion, and parkinson's diseases and amyotrophic lateral sclerosis). *Chem. Rev.* **2006**, *106*, 1995-2044.
2. Barceloux, D. G.; Barceloux, D., Copper. *Clin. Toxicol.* **1999**, *37*, 217-230.
3. O'Halloran, T. V.; Culotta, V. C., Metallochaperones, an intracellular shuttle service for metal ions. *J. Biol. Chem.* **2000**, *275*, 25057-25060.
4. Rosenzweig, A. C.; O'Halloran, T. V., Structure and chemistry of the copper chaperone proteins. *Curr. Opin. Chem. Biol.* **2000**, *4*, 140-147.
5. Singh, A.; Yao, Q.; Tong, L.; Clark Still, W.; Sames, D., Combinatorial approach to the development of fluorescent sensors for nanomolar aqueous copper. *Tetrahedron Lett.* **2000**, *41*, 9601-9605.
6. Puig, S.; Thiele, D. J., Molecular mechanisms of copper uptake and distribution. *Curr. Opin. Chem. Biol.* **2002**, *6*, 171-180.
7. Arnesano, F.; Banci, L.; Bertini, I.; Ciofi-Baffoni, S., Perspectives in inorganic structural genomics: a trafficking route for copper. *Eur. J. Inorg. Chem.* **2004**, *2004*, 1583-1593.
8. Sasaki, D. Y.; Shnek, D. R.; Pack, D. W.; Arnold, F. H., Metall-induzierte dispersion von lipid-aggregation. *Angew. Chem.* **1995**, *107*, 994-996.
9. Torrado, A.; Walkup, G. K.; Imperiali, B., Exploiting polypeptide motifs for the design of selective Cu(II) ion chemosensors. *J. Am. Chem. Soc.* **1998**, *120*, 609-610.
10. Valentine, J. S.; Hart, P. J., Misfolded CuZnSOD and amyotrophic lateral sclerosis. *Proc. Natl. Acad. Sci. USA* **2003**, *100*, 3617-3622.
11. Brown, D. R.; Kozłowski, H., Biological inorganic and bioinorganic chemistry of neurodegeneration based on prion and Alzheimer diseases. *Dalton Trans.* **2004**, *0*, 1907-1917.
12. Barnham, K. J.; Masters, C. L.; Bush, A. I., Neurodegenerative diseases and oxidative stress. *Nat. Rev. Drug Discov.* **2004**, *3*, 205-214.
13. Waggoner, D. J.; Bartnikas, T. B.; Gitlin, J. D., The role of copper in neurodegenerative disease. *Neurobiol. Dis.* **1999**, *6*, 221-230.
14. Herd, S. M.; Camakaris, J.; Christofferson, R.; Wookey, P.; Danks, D. M., Uptake and efflux of copper-64 in Menkes'-disease and normal continuous lymphoid cell lines. *Biochem. J.* **1987**, *247*, 341-347.
15. Shao, N.; Zhang, Y.; Cheung, S.; Yang, R.; Chan, W.; Mo, T.; Li, K.; Liu, F., Copper ion-selective fluorescent sensor based on the inner filter effect using a spiropyran derivative. *Anal. Chem.*

2005, 77, 7294-7303.

16. Yu, M.; Shi, M.; Chen, Z.; Li, F.; Li, X.; Gao, Y.; Xu, J.; Yang, H.; Zhou, Z.; Yi, T.; Huang, C., Highly sensitive and fast responsive fluorescence turn-on chemodosimeter for Cu²⁺ and its application in live cell imaging. *Chem. Eur. J.* **2008**, *14*, 6892-6900.

17. Domaille, D. W.; Que, E. L.; Chang, C. J., Synthetic fluorescent sensors for studying the cell biology of metals. *Nat. Chem. Biol.* **2008**, *4*, 168-175.

18. Swamy, K. M. K.; Ko, S.-K.; Kwon, S. K.; Lee, H. N.; Mao, C.; Kim, J.-M.; Lee, K.-H.; Kim, J.; Shin, I.; Yoon, J., Boronic acid-linked fluorescent and colorimetric probes for copper ions. *Chem. Commun.* **2008**, *0*, 5915-5917.

19. Jung, H. S.; Kwon, P. S.; Lee, J. W.; Kim, J. I.; Hong, C. S.; Kim, J. W.; Yan, S.; Lee, J. Y.; Lee, J. H.; Joo, T.; Kim, J. S., Coumarin-derived Cu²⁺-selective fluorescence sensor: synthesis, mechanisms, and applications in living cells. *J. Am. Chem. Soc.* **2009**, *131*, 2008-2012.

20. Zhou, Y.; Wang, F.; Kim, Y.; Kim, S.-J.; Yoon, J., Cu²⁺-selective ratiometric and "off-on" sensor based on the rhodamine derivative bearing pyrene group. *Org. Lett.* **2009**, *11*, 4442-4445.

21. Patonay, G.; Antoine, M. D., Near-infrared fluorogenic labels: new approach to an old problem. *Anal. Chem.* **1991**, *63* (6), 321A-327A.

22. Frangioni, J. V., In vivo near-infrared fluorescence imaging. *Curr. Opin. Chem. Biol.* **2003**, *7*, 626-634.

23. Fabian, J.; Nakazumi, H.; Matsuoka, M., Near-infrared absorbing dyes. *Chem. Rev.* **1992**, *92*, 1197-1226.

24. Kodama, M.; Kimura, E., Equilibria and kinetics of copper(II) complex formation of a linear and of 13-15-membered macrocyclic dioxo-tetra-amines. *J. Chem. Soc., Dalton Trans.* **1979**, *0*, 325-329.

25. Aldakov, D.; Anzenbacher, P., Sensing of aqueous phosphates by polymers with dual modes of signal transduction. *J. Am. Chem. Soc.* **2004**, *126*, 4752-4753.

26. Coskun, A.; Yilmaz, M. D.; Akkaya, E. U., Bis(2-pyridyl)-substituted borotriazaindacene as an NIR-emitting chemosensor for Hg(II). *Org. Lett.* **2007**, *9*, 607-609.

27. Ozmen, B.; Akkaya, E. U., Infrared fluorescence sensing of submicromolar calcium: pushing the limits of photoinduced electron transfer. *Tetrahedron Lett.* **2000**, *41*, 9185-9188.

28. Sasaki, E.; Kojima, H.; Nishimatsu, H.; Urano, Y.; Kikuchi, K.; Hirata, Y.; Nagano, T., Highly sensitive near-infrared fluorescent probes for nitric oxide and their application to isolated organs. *J. Am. Chem. Soc.* **2005**, *127*, 3684-3685.

29. Peng, X.; Song, F.; Lu, E.; Wang, Y.; Zhou, W.; Fan, J.; Gao, Y., Heptamethine cyanine dyes with a large stokes shift and strong fluorescence: a paradigm for excited-state intramolecular charge transfer. *J. Am. Chem. Soc.* **2005**, *127*, 4170-4171.

30. Kiyose, K.; Kojima, H.; Urano, Y.; Nagano, T., Development of a ratiometric fluorescent zinc ion probe in near-infrared region, based on tricarboyanine chromophore. *J. Am. Chem. Soc.* **2006**, *128*, 6548-6549.
31. Tang, B.; Huang, H.; Xu, K.; Tong, L.; Yang, G.; Liu, X.; An, L., Highly sensitive and selective near-infrared fluorescent probe for zinc and its application to macrophage cells. *Chem. Commun.* **2006**, *0*, 3609-3611.
32. Carol, P.; Sreejith, S.; Ajayaghosh, A., Ratiometric and near-infrared molecular probes for the detection and imaging of zinc ions. *Chem. Asian J.* **2007**, *2*, 338-348.
33. Bose, P.; Ghosh, P., Visible and near-infrared sensing of fluoride by indole conjugated urea/thiourea ligands. *Chem. Commun.* **2010**, *46*, 2962-2964.
34. Yin, S.; Leen, V.; Snick, S. V.; Boens, N.; Dehaen, W., A highly sensitive, selective, colorimetric and near-infrared fluorescent turn-on chemosensor for Cu²⁺ based on BODIPY. *Chem. Commun.* **2010**, *46*, 6329-6331.
35. Zhu, M.; Yuan, M.; Liu, X.; Xu, J.; Lv, J.; Huang, C.; Liu, H.; Li, Y.; Wang, S.; Zhu, D., Visible near-infrared chemosensor for mercury ion. *Org. Lett.* **2008**, *10*, 1481-1484.
36. Chen, X.; Nam, S.-W.; Kim, G.-H.; Song, N.; Jeong, Y.; Shin, I.; Kim, S. K.; Kim, J.; Park, S.; Yoon, J., A near-infrared fluorescent sensor for detection of cyanide in aqueous solution and its application for bioimaging. *Chem. Commun.* **2010**, *46*, 8953-8955.
37. Yang, Y.; Cheng, T.; Zhu, W.; Xu, Y.; Qian, X., Highly selective and sensitive near-infrared fluorescent sensors for cadmium in aqueous solution. *Org. Lett.* **2010**, *13*, 264-267.
38. Sheng, R.; Wang, P.; Gao, Y.; Wu, Y.; Liu, W.; Ma, J.; Li, H.; Wu, S., Colorimetric test kit for Cu²⁺ detection. *Org. Lett.* **2008**, *10*, 5015-5018.
39. Fabbriizzi, L.; Licchelli, M.; Pallavicini, P.; Perotti, A.; Sacchi, D., Ein Fluoreszenzsensor für Übergangsmetall-Ionen auf Anthracenbasis. *Angew. Chem.* **1994**, *106*, 2051-2053.
40. Ueno, T.; Nagano, T., Fluorescent probes for sensing and imaging. *Nat. Meth.* **2011**, *8*, 642-645.
41. de Silva, A. P.; Gunaratne, H. Q. N.; Gunlaugsson, T.; Huxley, A. J. M.; McCoy, C. P.; Rademacher, J. T.; Rice, T. E., Signaling recognition events with fluorescent sensors and switches. *Chem. Rev.* **1997**, *97*, 1515-1566.
42. Liu, Z.; He, W.; Guo, Z., Metal coordination in photoluminescent sensing. *Chem. Soc. Rev.* **2013**, *42*, 1568-1600.
43. Boiocchi, M.; Del Boca, L.; Gómez, D. E.; Fabbriizzi, L.; Licchelli, M.; Monzani, E., Nature of urea-fluoride interaction: incipient and definitive proton transfer. *J. Am. Chem. Soc.* **2004**, *126*, 16507-16514.
44. Han, F.; Bao, Y.; Yang, Z.; Fyles, T. M.; Zhao, J.; Peng, X.; Fan, J.; Wu, Y.; Sun, S., Simple

bisthiocarbonohydrazones as sensitive, selective, colorimetric, and switch-on fluorescent Chemosensors for Fluoride Anions. *Chem. Eur. J.* **2007**, *13*, 2880-2892.

45. Burdette, S. C.; Walkup, G. K.; Spingler, B.; Tsien, R. Y.; Lippard, S. J., Fluorescent sensors for Zn²⁺ based on a fluorescein platform: synthesis, properties and intracellular distribution. *J. Am. Chem. Soc.* **2001**, *123*, 7831-7841.

46. M. J. Frisch; G. W. Trucks; H. B. Schlegel; G. E. Schlegel; G. E. Scuseria; M. A. Robb; J. R. Cheeseman; J. A. Montgomery, Jr., T. V.; K. N. Kudin; J. C. Burant; J. M. Millam; S. S. Iyengar; J. Tomasi; V. Barone; B. Mennucci; M. Cossi; G. Scalmani; N. Rega; G. A. Petersson; H. Nakatsuji; M. Hada; M. Ehara; K. Toyota; R. Fukuda; J. Hasegawa; M. Ishida; T. Nakajima; Y. Honda; O. Kitao; H. Nakai; M. Klene; X. Li; J. E. Knox; H. P. Hratchian; J. B. Cross; C. Adamo; J. Jaramillo; R. Gomperts; R. E. Stratmann; O. Yazyev; A. J. Austin; R. Cammi; C. Pomelli; J. W. Ochterski; P. Y. Ayala; K. Morokuma; G. A. Voth; P. Salvador; J. J. Dannenberg; V. G. Zakrzewski; S. Dapprich; A. D. Daniels; M. C. Strain; O. Farkas; D. K. Malick; A. D. Rabuck; K. Raghavachari; J. B. Foresman; J. V. Ortiz; Q. Cui; A. G. Baboul; S. Clifford; J. Cioslowski; B. B. Stefanov; G. Liu; A. Liashenko; P. Piskorz; I. Komaromi; R. L. Martin; D. J. Fox; T. Keith; M. A. Allaham; C. Y. Peng; A. Nanayakkara; M. Challacombe; P. M. W. Gill; B. Johnson; W. Chen; M. W. Wong; C. Gonzalez; Pople, J. A., *Gaussian Inc.*, Wallingford CT **2004**.

47. Lee, C.; Yang, W.; Parr, R. G., Development of the Colle-Salvetti correlation-energy formula into a functional of the electron density. *Phys. Rev. B* **1988**, *37*, 785-789.

48. Miehlich, B.; Savin, A.; Stoll, H.; Preuss, H., Results obtained with the correlation energy density functionals of Becke and Lee, Yang and Parr. *Chem. Phys. Lett.* **1989**, *157*, 200-206.

49. Becke, A. D., Density-functional thermochemistry. III. The role of exact exchange. *J. Chem. Phys.* **1993**, *98*, 5648-5652.

50. Hay, P. J.; Wadt, W. R., Ab initio effective core potentials for molecular calculations. Potentials for the transition metal atoms Sc to Hg. *J. Chem. Phys.* **1985**, *82*, 270-283.

51. Wadt, W. R.; Hay, P. J., Ab initio effective core potentials for molecular calculations. Potentials for main group elements Na to Bi. *J. Chem. Phys.* **1985**, *82*, 284-298.

52. Hay, P. J.; Wadt, W. R., Ab initio effective core potentials for molecular calculations. Potentials for K to Au including the outermost core orbitals. *J. Chem. Phys.* **1985**, *82*, 299-310.

53. Noodleman, L., Valence bond description of antiferromagnetic coupling in transition metal dimers. *J. Chem. Phys.* **1981**, *74*, 5737-5743.

54. Noodleman, L.; Davidson, E. R., Ligand spin polarization and antiferromagnetic coupling in transition metal dimers. *Chem. Phys.* **1986**, *109*, 131-143.

55. Noodleman, L.; Peng, C. Y.; Case, D. A.; Mouesca, J. M., Orbital interactions, electron

delocalization and spin coupling in iron-sulfur clusters. *Coord. Chem. Rev.* **1995**, *144*, 199-244.

56. Ricart, J. M.; Dovesi, R.; Roetti, C.; Saunders, V. R., Electronic and magnetic structure of KNiF_3 perovskite. *Phys. Rev. B* **1995**, *52*, 2381-2389.

57. Khatua, S.; Choi, S. H.; Lee, J.; Huh, J. O.; Do, Y.; Churchill, D. G., Highly selective fluorescence detection of Cu^{2+} in water by chiral dimeric Zn^{2+} complexes through direct displacement. *Inorg. Chem.* **2009**, *48*, 1799-1801.

58. Grynkiewicz, G.; Poenie, M.; Tsien, R. Y., A new generation of Ca^{2+} indicators with greatly improved fluorescence properties. *J. Biol. Chem.* **1985**, *260*, 3440-3450.

Chapter 4

Visible–near-infrared fluorescent copper selective molecular probes

Papers based on this chapter have been published in *Chempluschem*, **2013**, DOI: 10.1002/cplu.201300089; *Org. Lett.*, **2012**, *14*, 6008-6011 ([Link](#)); *Sensor Actuat. B-Chem.*, **2013**, *176*, 831-837 ([Link](#)). Reproduced by permission of the John Wiley and Sons, American Chemical Society and Elsevier. Another two manuscripts have been submitted for publication.

1. Introduction

The redox chemistry of copper ($\text{Cu}^{2+}/\text{Cu}^{+}$) makes it crucial to biological processes but also potentially dangerous if it is not controlled properly in the cell and becomes available for Fenton-like chemistry to produce reactive oxygen species (ROS).¹ Copper is one of the trace nutrients in humans that are essential for various biological processes.² Copper has to be supplemented through daily diet and extensive regulatory mechanisms exist to maintain a its balance in human body.³ The adult human contains 1.4-2.1 mg of copper per kilogram of body weight under normal conditions.⁴ Copper-dependent enzymes are essential catalysts to provide energy for biochemical reactions, transform melanin for pigmentation of the skin and assist the formation of cross-links in collagen and elastin, thereby maintain and repair connective tissues.^{5,6} Generally most human diets contain enough copper (2–5 mg/day) to prevent a deficiency, but not sufficient to cause toxicity.⁷ Copper deficiency is important factor for developing coronary heart disease.^{1,8,9} Typically under the oxidizing extracellular environment, copper exists as Cu^{2+} but in the reducing conditions inside the cell, free copper mostly exists in the Cu^{+} oxidation state.¹⁰ Copper can be highly toxic when present in excessive amounts in human body. Copper toxicity is one of the major reasons for oxidative stress and disorders associated with neurodegenerative diseases including Alzheimer's, Parkinson's, Menkes, Wilson's, and prion diseases.^{11,12} Free solvated copper ions catalyzes the formation of ROS, including radical and nonradical species, which can also trigger oxidative damage to proteins, nucleic acids and lipids.¹³ Therefore it is crucial to develop novel methods for the detection of this redox-active cation in biological and environmental samples. In general the development of cation responsive fluorescent probes is an active research area in recent times due to wide range of applications in analytical, environmental, materials and biological sciences. Fluorescence based detection methods are more appealing due to high sensitivity and real-time monitoring of exchangeable metal ions in living cells.^{4,11,12} Confocal imaging offers an attractive platform for monitoring metal ion homeostasis in health and disease states with high spatial resolution.^{14,15}

2. Rationale for designing fluorescent molecular probes for copper

Cu^+ , which is the major oxidation state within the reducing environment of the cytosol, can readily disproportionate to Cu^{2+} and Cu^0 in water and is an effective fluorescent quencher by electron or energy transfer. Cu^{2+} also has quenching capabilities, particularly in aqueous media, because of its redox activity and unfilled d-shell. It makes very tricky to use a traditional chromophore–receptor binding scheme for selective detection of copper by emission turn on response.¹² A number of Cu^{2+} selective chemosensors have been reported based on photoinduced electron transfer (PET), internal charge transfer (ICT), excimer/exciple formation, chelation-enhanced fluorescence (CHEF), and more recently fluorescence resonance energy transfer (FRET) mechanisms¹⁶⁻²⁷ but probes for monitoring intracellular free copper i.e. Cu^+ are rare.²⁸⁻³⁶ Soft character makes Cu^+ unique among the biological metal ions, such that it has potential to be selected based on ligand donor groups. In addition, Cu^+ in d^{10} state, giving it flexibility in geometric arrangements. Cu^+ can adopt tetrahedral, trigonal, or even linear geometries that are disfavoured by other metal ions. In designing probes for Cu^+ , fluorescence quenching problem has been partially addressed by incorporating proper spacer between cation binding site and the fluorophore. These probes show cation-dependent fluorescence response based on PET mechanism. However most of the Cu^+ selective PET probes display incomplete recovery of fluorescence quantum yield compared to corresponding isolated fluorophores. Thus it is necessary to develop ideal fluorescent probe for the detection of copper in bioavailable form under physiologically reducing condition.

A modular probe was devised to visualize biological copper by means of turn on fluorescence response. It is constructed by conjugation of a dye molecule and a trigger moiety through functional group X (Figure 1). The masking of functional group reduces conjugated π -electron system of the dye and thus turns off fluorescence of the probe. Copper mediated removal of the trigger from the probe restores conjugation of functional group with π -electrons of the dye and thereby turns on fluorescent signal of the probe.

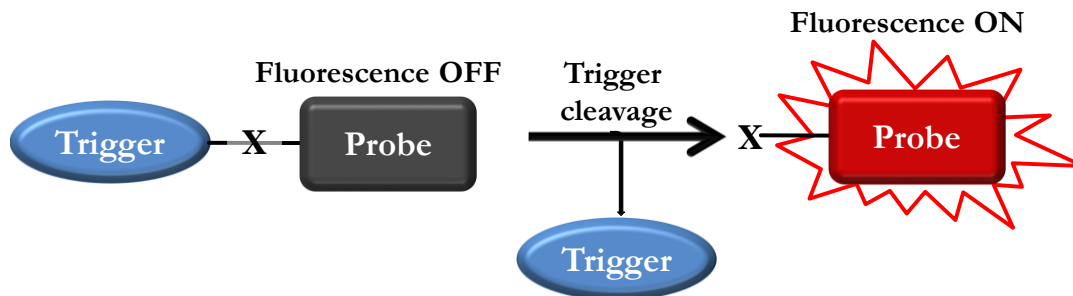


Figure 1. Mechanism of action of a modular turn on fluorescence probe.

The design strategy of the molecular probe for Cu^+ detection relies on reaction-based approach³⁷⁻⁴¹ in which a selective Cu^+ -mediated bond-cleaving reaction transforms a weakly fluorescent probe into a highly fluorescent dye, where the final product will be free of any paramagnetic metal ion. The coordination environment (trigger) was designed in such way that only Cu^+ binding would promote specific redox and/or small-molecule reactivity that other competitor metal ions would not be able to achieve. O_2 -mediated Co^{2+} reactivity was observed for biomimetic N-dealkylation of a polypyridine-based ligand as shown by McKenzie *et al.*,⁴² Taki *et al.*³³ showed turn on detection of Cu^+ ions by oxidative ether cleavage and Koide *et al.*⁴³⁻⁴⁵ demonstrated similar organometallic strategies for Pd, Pt, and Hg detection. The tetradentate ligands N_4 linked chromophore was developed as nonfluorescent caged probe for reaction-based turn on sensing of Cu^+ by Taki *et al.*³³ The metal ion mediated cleaving of benzylic ether bond in the nonfluorescent probe generates a fluorescent dye under physiologically reducing conditions.

In this chapter, the reaction based approach have been explored to expand Cu^+ selective molecular probe library for its turn on as well as ratiometric detection in the UV-Vis-near infrared (NIR) region. A two-photon excitable Cu^+ probe **XanCu** has been developed by combining a fluorescent reporter with pendant tetradentate ligand (N_4) via cleavable benzyl ether linkage. N_4 ligand is combined with excited state intramolecular proton transfer (ESIPT) based chromophore 2-(2'-hydroxyphenyl)benzothiazole (HBT) via cleavable benzylic ether bond (C–O) to generate a probe **HBTCu** for ratiometric detection of Cu^+ .⁴⁶ Cu^+ assisted benzyl ether bond cleavage releases ESIPT active HBT chromophore which undergoes enol to keto tautomeric transformation and thus large Stokes shift in the fluorescence emission was achieved.⁴⁷ Resorufin has maximal emission at 585 nm and can be

used to analyze intracellular processes without damaging the cell. The resorufin chromophore has an absorption maximum around 573 nm, was also known for colorimetric detection of fluoride, DNA hybridization, and hydrolase.⁴⁸⁻⁵⁴ The alkylation of the 7-hydroxy group of resorufin effectively weakens its intramolecular charge transfer which quenches its emission by blocking push-pull mechanism in the chromophore. In accordance with above rationale a nonfluorescent probes **ResCu** was designed by combining resorufin dye and tetradentate ligand N₄ through 7-hydroxyl functionality. Cu⁺ mediated cleaving of benzylic ether bond in nonfluorescent probe **ResCu** will release chromogenic resorufin dye which automatically shows ratiometric visible absorption (colorimetric) and ‘switch-on’ fluorometric responses for Cu⁺ under physiologically reducing conditions. Similarly tetradentate N₄ ligand masked phenolic moiety is incorporated into cyanine type dye. The Cu⁺ mediated oxidative cleavage of **TPACy** probe generates the Cyanine phenolate which rearranges itself by neutralizing the positive charge on a nitrogen atom to form stable **Cy-quinone**. This **Cy-quinone** resumes the extended π -electron conjugation pattern of the cyanine dyes to exhibit turn on NIR fluorescence. Finally, two chemosensors have been developed with coumarin as donor and rhodamine as acceptor for ratiometric fluorescent imaging of Cu²⁺ based on metal ion induced FRET off-on mechanism. Two chemosensors coumarin-rhodamine hydrazone (**CRO**) and coumarin-rhodamine thiohydrazone (**CRS**) ratiometrically detects Cu²⁺ in judiciously chosen aqueous buffer medium. Free ligands (**CRO** and **CRS**) emit green fluorescence and in presence of Cu²⁺, emission color changed to red as spirolactam ring of rhodamine opens up upon complexation with the metal ion.

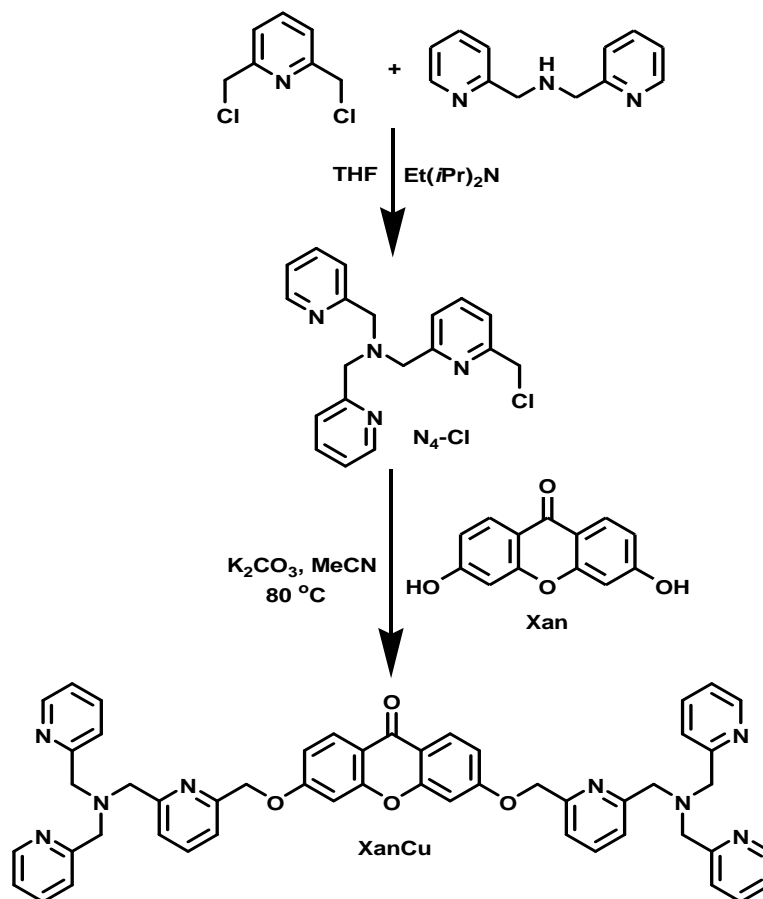
3.1 A highly selective reaction-based two-photon probe (**XanCu**) for Cu⁺ in aqueous media

The short ultraviolet excitation wavelength used in commonly employed one-photon fluorescence spectroscopy would adversely stimulate interfering absorbance, scattering and background autofluorescence generated from endogenous biomolecules. However two-photon fluorescence spectroscopy and microscopy techniques are particularly useful to overcome these drawbacks.^{39,49,55} Typically one-photon fluorescence spectroscopy uses single photon to excite a fluorophore into its excited state whereas two-photon fluorescence spectroscopy (TPS) uses two photons of much lower energy to generate a fluorophore excited state.⁵⁶⁻⁵⁸ Recently, TPS has gained much attention because it offers a number of advantages such as less photodamage of samples, low background absorption and scattering, improved spatial resolution and sensitivity, and the ability to image thicker specimens.⁵⁹⁻⁶⁶ Thus designing fluorescent probes with optional two-photon excitation capability is an added advantage. The design strategy comprised selective cation-mediated bond-cleaving reaction transforming a non-fluorescent probe into a highly fluorescent dye and detached paramagnetic metal ion bound ionophore unit. This design approach is also intent to incorporate more than one metal binding unit to enhance the sensitivity of the reaction-based probe towards the metal ion of interest.

3.1.1 Synthesis

A reaction-based two-photon excitable Cu⁺ probe **XanCu** combining a fluorescent reporter with pendant tetradentate ligands via cleavable benzyl ether linkage has been synthesized. Blue fluorescent dye xanthone as a reporter and tripicolylamine (**N₄-Cl**) ligand as metal binding units were selected for reaction-based nonfluorescent molecular probe. Tripicolylamine (**N₄-Cl**) ligand was synthesized from bis-(2-picolyl)amine and 2,6-bis-(chloromethyl)pyridine under basic condition. **N₄-Cl** ligand is known to be selective for Cu⁺ mediated benzylic ether bond cleavage reaction to generate free fluorescent reporter dye from nonfluorescent probe under aerobic conditions. The **XanCu** probe was synthesized by O-alkylation of two hydroxyl functionalities on 3,6-dihydroxyxanthone (**Xan**) with two

equivalents of tripicolylamine chloride (**N₄-Cl**) under basic condition in excellent yield (Scheme 1).



Scheme 1. Synthesis of XanCu

3.1.2 Photophysical property of molecular probe XanCu and Cu⁺ detection

The fluorescence properties of **XanCu** was studied in aqueous buffer solution (50 mM HEPES, pH 7.2) in presence of 2 mM glutathione (GSH) for mimicking the intracellular environments. The fluorometric behavior of 1.0 μM **XanCu** was investigated with the addition of several metal ions such as Li⁺, Na⁺, K⁺, Ba²⁺, Mg²⁺, Ca²⁺, Al³⁺, Mn²⁺, Fe²⁺, Co²⁺, Ni²⁺, Cu⁺, Cu²⁺, Zn²⁺, Cd²⁺, Ag⁺, Hg²⁺ and Pb²⁺ after 2 h of mixing (Figure 2). Upon 350 nm excitation **XanCu** was found to be nonfluorescent (quantum yield $\Phi = 0.0088$). The examined millimolar concentrations of alkali and alkaline earth metals had no effect on the

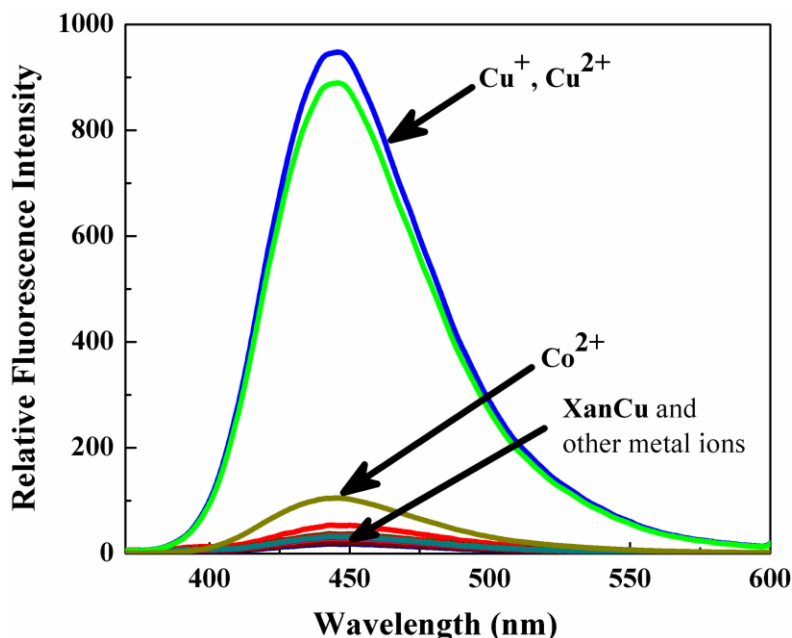


Figure 2. Fluorescence responses of **XanCu** (1.0 μM) upon addition 1 mM of Li^+ , Na^+ , K^+ , Ba^{2+} , Mg^{2+} , Ca^{2+} , Al^{3+} and 20.0 μM of Mn^{2+} , Fe^{2+} , Co^{2+} , Ni^{2+} , Cu^+ , Cu^{2+} , Zn^{2+} , Cd^{2+} , Ag^+ , Hg^{2+} and Pb^{2+} after 2 h in aqueous solution (50 mM HEPES, pH 7.2, 2 mM GSH) ($\lambda_{ex} = 350$ nm).

fluorescence behavior of **XanCu**. When tested with copper ions, it showed remarkable ~ 30 -fold enhancement in the blue fluorescence emission positioned around 445 nm (quantum yield $\Phi = 0.265$). This significant ‘switch on’ fluorescence phenomenon is identical for both Cu^+ and Cu^{2+} ions as GSH (2 mM) rapidly reduces Cu^{2+} to Cu^+ . The ‘switch on’ emission around 445 nm indicates that Cu^+ react with **XanCu** and cleaves the benzyl ether (C–O) linkages in presence of O_2 releasing blue emitting phenolic xanthone dye (**Xan**). Cu^{2+} did not show ‘switch on’ fluorescence response in the absence of GSH (Figure 3), while Cu^+ exhibited minimal response as it undergo spontaneous oxidation to Cu^{2+} in the absence of GSH. Other transition metal ions except Co^{2+} caused no significant change in the baseline fluorescence intensity (Figure 3). While Co^{2+} showed very minimal response in the emission intensity both in presence and absence of GSH. Time dependent study showed that the benzyl ether bonds cleavage reaction in **XanCu** and subsequent detection of Cu^+ is more rapid compared to previous reports (Figure 4).^{33,46} After addition of Cu^+ blue emission reaches maximum within 30 min. Concentration dependent study showed that submicromolar Cu^+ could be efficiently detected as this amount is sufficient enough to quantitatively release

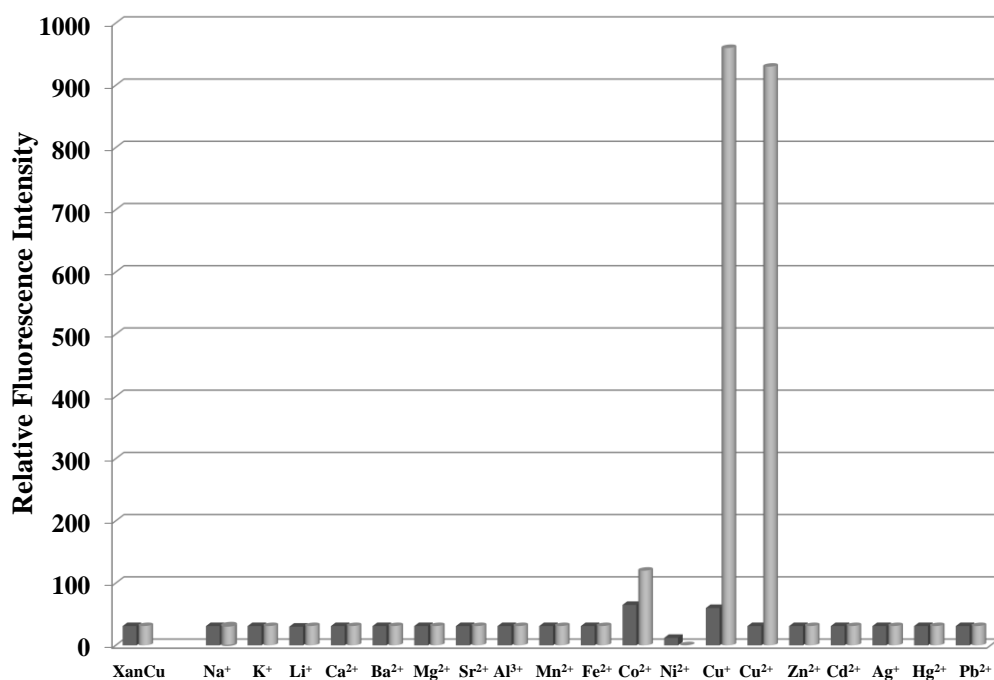


Figure 3. Fluorescent responses of **XanCu** ($1.0 \mu\text{M}$) in 50 mM HEPES buffer ($\text{pH } 7.2$). The bars represent the fluorescence intensity at 445 nm after 2 h of reaction of $1.0 \mu\text{M}$ **XanCu** with different metal ion ($20.0 \mu\text{M}$) in the absence (dark gray bars) or presence (light gray bars) of 2 mM GSH ($\lambda_{\text{ex}} = 350 \text{ nm}$).

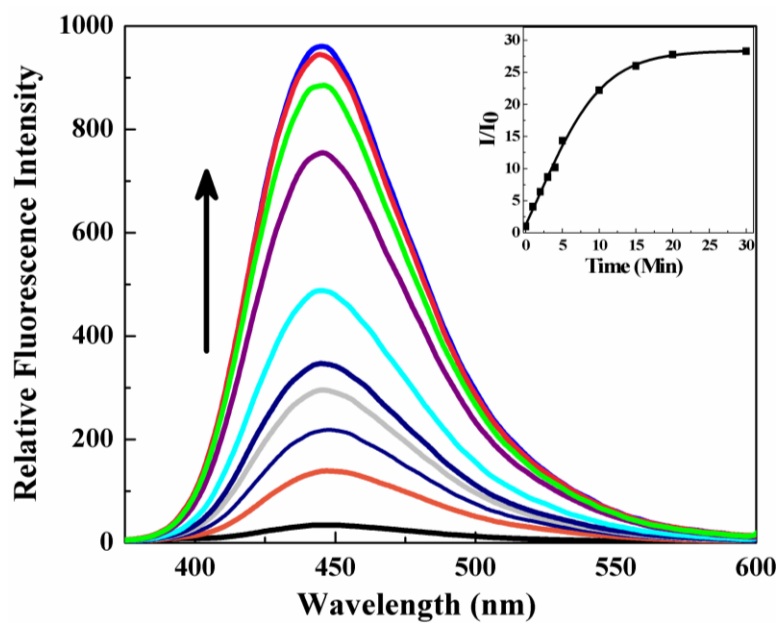


Figure 4. Time dependent fluorescence responses of **XanCu** ($1.0 \mu\text{M}$) upon addition of $20.0 \mu\text{M}$ of Cu^+ in aqueous solution (50 mM HEPES, $\text{pH } 7.2$, 2 mM GSH) ($\lambda_{\text{ex}} = 350 \text{ nm}$).

phenolic xanthone dye (**Xan**) from **XanCu** (1.0 μM) through benzyl ether bonds cleavage reaction (Figure 5). It should be noted that each molecule of **XanCu** probe contains two tripicolylamino units and therefore can react with two Cu^+ ions.

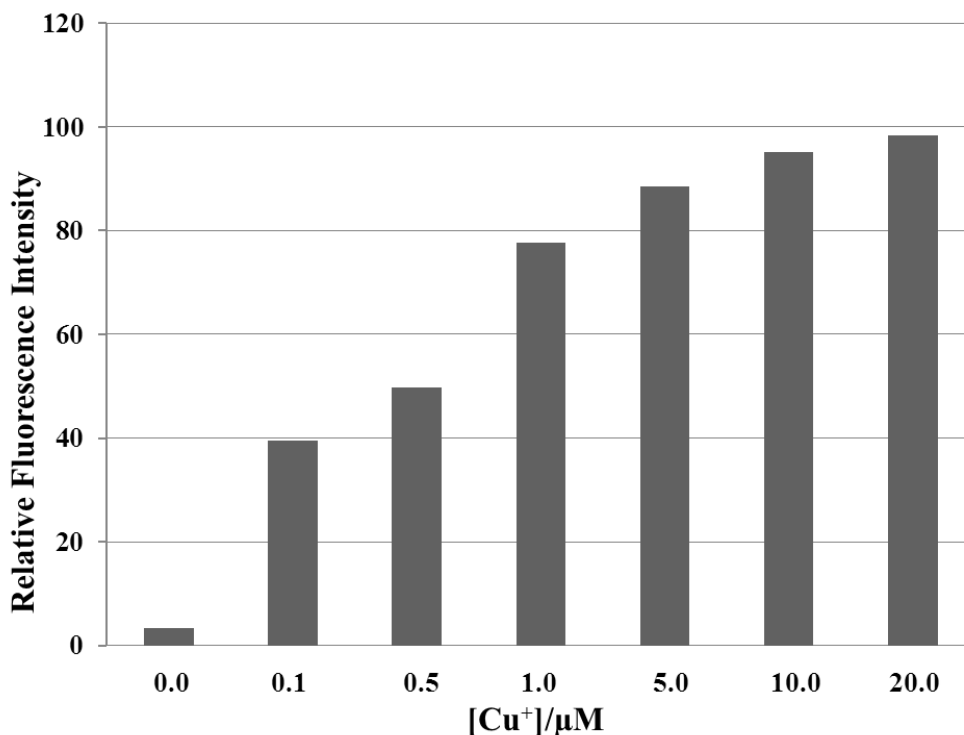


Figure 5. Fluorescence responses of **XanCu** (1.0 μM) upon addition of 0.0, 0.1, 0.5, 1.0, 5.0, 10.0 and 20.0 μM of Cu^+ after 30 min in aqueous solution (50 mM HEPES, pH 7.2, 2 mM GSH) ($\lambda_{\text{ex}} = 350 \text{ nm}$).

3.1.3 pH dependent study

The effect of pH on the Cu^+ mediated benzyl ether (C–O) bond cleavage was studied to understand utility of the probe under various pH range (Figure 6). **XanCu** reacted efficiently with Cu^+ in the biologically relevant pH range of 6.5–8.5 to release blue emitting xanthone fluorophore (**Xan**). Thus **XanCu** can be conveniently used as ‘switch on’ probe for the detection of Cu^+ without interference from pH-related effects in physiological media.

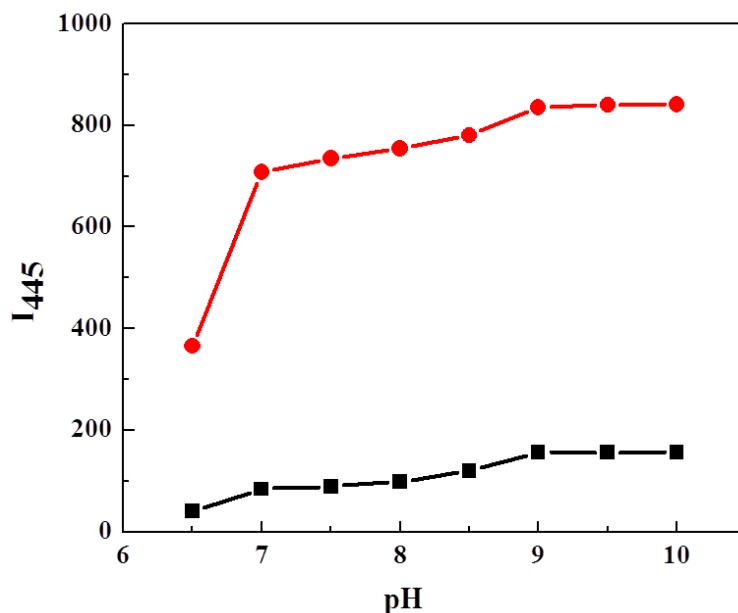
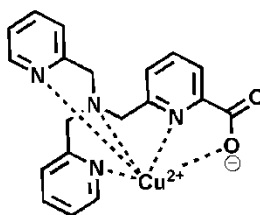
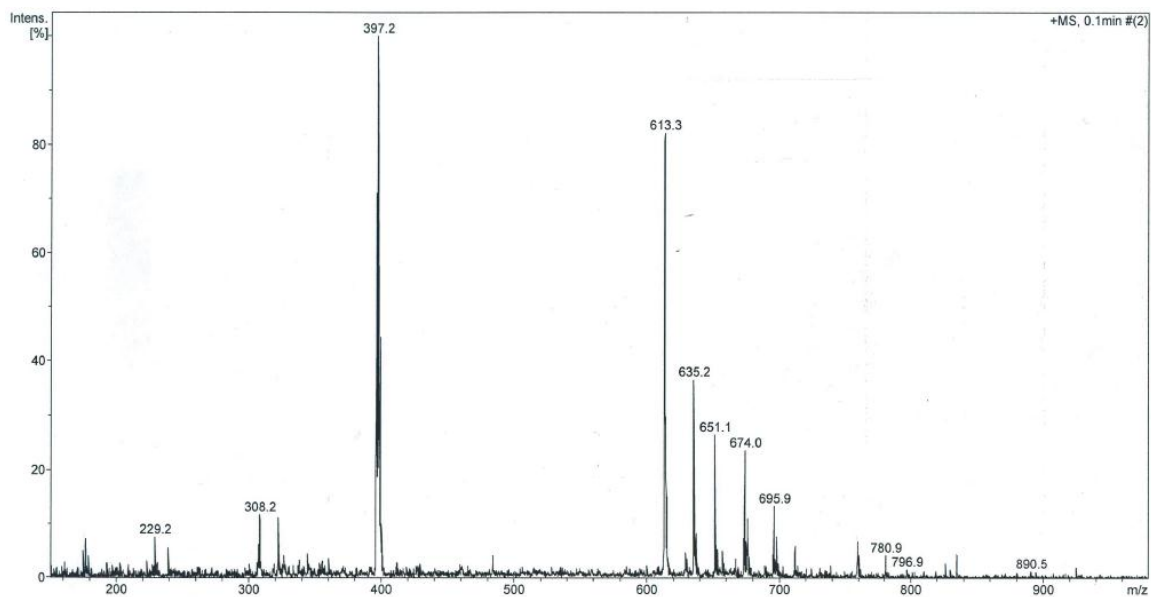


Figure 6. Effect of pH on the fluorometric property of **XanCu**. Red trace: **XanCu** (1.0 μ M) with 20.0 μ M of Cu⁺ after 30 min in aqueous solution (50 mM HEPES). Black trace: **XanCu** (1.0 μ M) in aqueous solution (50 mM HEPES).

3.1.4 Product analysis and proposed mechanism

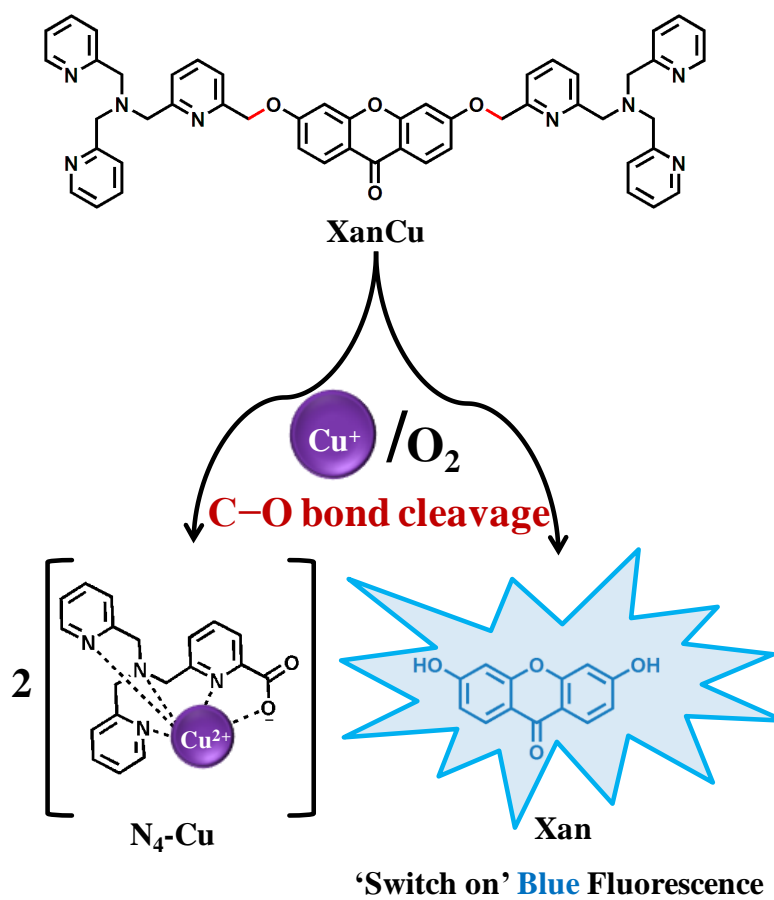
The ESI-MS data confirmed benzyl ether bonds cleavage reaction in **XanCu** to release **Xan** reporter and copper complex of oxidised **N₄** ligand (**N₄-Cu**) (Figure 7). Mass peaks found at m/z 397.2 and m/z 229.2 respectively correspond to carboxylated **N₄-Cu** complex (calcd. 396.06 for C₁₉H₁₇CuN₄O₂) and xanthone (**Xan**) fluorophore (calcd. 228.04 for C₁₃H₈O₄) released from **XanCu**. The Cu⁺ catalyzed oxidative benzyl ether bonds cleavage reaction in **XanCu** to release free **Xan** reporter dye and metal ion bound carboxylated **N₄**-ligands (**N₄-Cu**) is shown in Scheme 2. This cleavage is happening probably through a mechanism proposed based on the metal ion mediated C–N/C–O bond cleavage reactions reported in the literature.^{42,46,67} The benzylic carbons of the **N₄** ligands oxidized to benzylic radicals (**I**) in presence of Cu⁺ and activated oxygen. The bi-radical intermediate (**I**) transformed to bis-oxonium ion (**II**) which hydrolyzed to phenolic xanthone dye (**Xan**) and two equivalents of tripicolylamino-aldehyde. The tripicolylamino-aldehyde intermediate subsequently oxidized

to tripicolylamino-carboxylate by the hydroperoxide of the metal complex through a Baeyer–Villiger type reaction to form two equivalents of $\text{N}_4\text{-Cu}$ complex (Figure 8).



Calculated m/z for $\text{N}_4\text{-Cu}$ complex = 396.06 for $\text{C}_{19}\text{H}_{17}\text{CuN}_4\text{O}_2$

Figure 7. ESI mass spectra (positive ion mode) for the reaction of $10.0 \mu\text{M}$ **XanCu** with $20.0 \mu\text{M}$ Cu^+ in water in presence of $100.0 \mu\text{M}$ GSH. Mass peaks observed at 397.2 $[\text{M} + \text{H}]^+$ is corresponds to $\text{N}_4\text{-Cu}$ complex $\text{C}_{19}\text{H}_{17}\text{CuN}_4\text{O}_2$. Mass peaks observed at 229.2 $[\text{M} + \text{H}]^+$ is corresponds to 3, 6-dihydroxyxanthone. Mass peaks observed at 308.2 $[\text{M} + \text{H}]^+$ is corresponds to glutathione. Peaks at 613.3 $[\text{M} + \text{H}]^+$, 635.2 $[\text{M} + \text{Na}]^+$, 651.1 $[\text{M} + \text{K}]^+$, 674.0 $[\text{M} + \text{Na} + \text{K}]^+$ and 695.9 $[\text{M} + 2\text{Na} + \text{K}]^+$ were attributed to the oxidized form of GSH (GS–SG).



Scheme 2. Cu^+/O_2 mediated benzylic ether bond (C-O) cleavage in **XanCu** to release blue fluorescent hydroxy-xanthone (**Xan**) dye and two equivalents of $[\text{N}_4\text{-Cu}]$ complex.

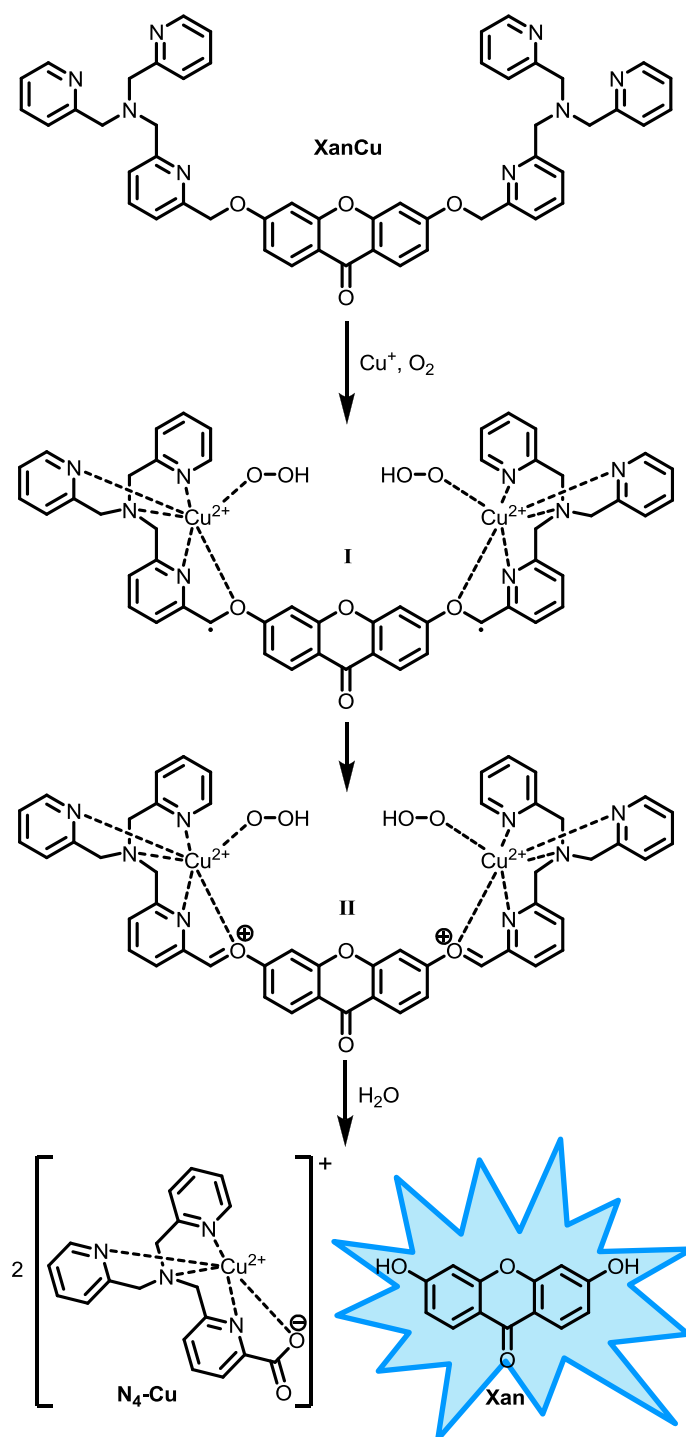


Figure 8. Proposed mechanism for Cu^+/O_2 mediated benzylic ether (C–O) bonds cleavage to release blue fluorescent hydroxy-xanthone (Xan) dye.

3.1.5 Two photon experiment for Cu⁺ detection

After establishing the utility of **XanCu** as ‘switch on’ fluorescent probe by one-photon spectroscopy, the use of **XanCu** for probing Cu⁺ by two-photon spectroscopy was explored. The two-photon action spectrum of **XanCu** in presence of Cu⁺ showed the maximum two-photon action cross section value of 2.23 GM at 700 nm in 20 mM HEPES buffer (pH 7.2) containing 2 mM GSH (Figure 9). At two photon excitation the probe showed sufficient fluorescence enhancement in presence of Cu⁺ and can be potentially used as a two-photon excitable sensor for Cu⁺. Two-photon excited fluorescence is expected to show a quadratic dependence on the excitation power. To confirm this, fluorescence was recorded for **XanCu** in presence of Cu⁺ at 690 nm varying the power from 40-200 mW at the back-aperture. Figure 10 shows the log-log plot of fluorescence obtained as a function of excitation power. The data can be fitted well by a straight line with a slope of 1.93 ± 0.04 (from first 5 points), which is close to the value of 2 expected for two-photon excitation. The deviation from linearity at higher power shows saturation and the saturation power is estimated to be ~125 mW.

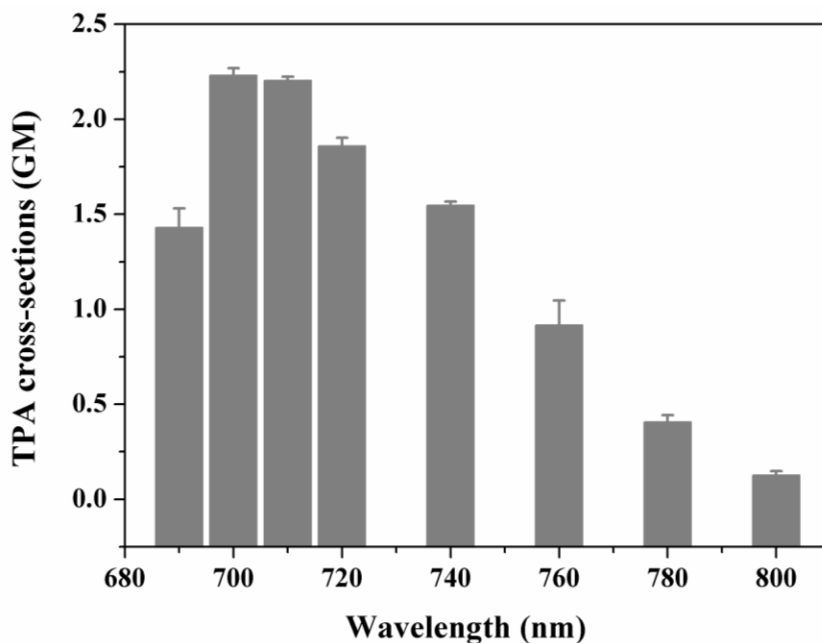


Figure 9. Two-photon action cross-sections obtained from a solution of 20 μ M **XanCu** in the presence of 400 μ M Cu⁺ using fluorescein at pH 13 as a calibrant. The values corresponds to mean \pm sem from three independent measurements.

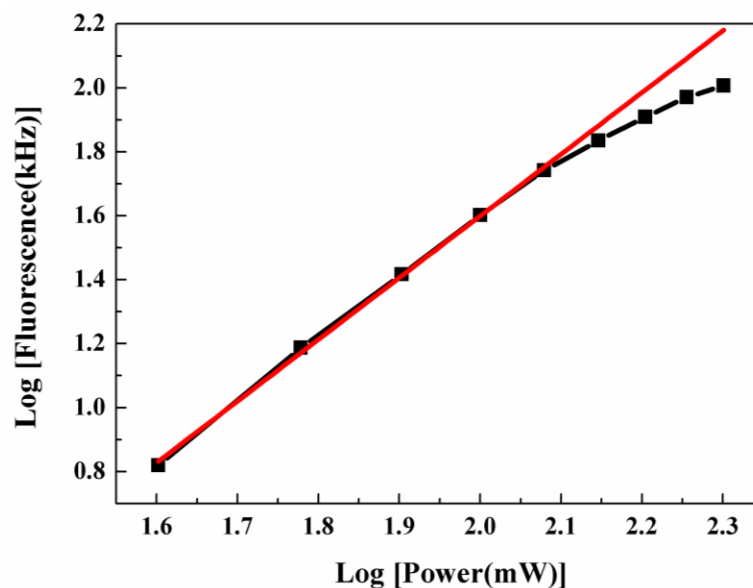


Figure 10. Fluorescence signal as a function of laser excitation power.

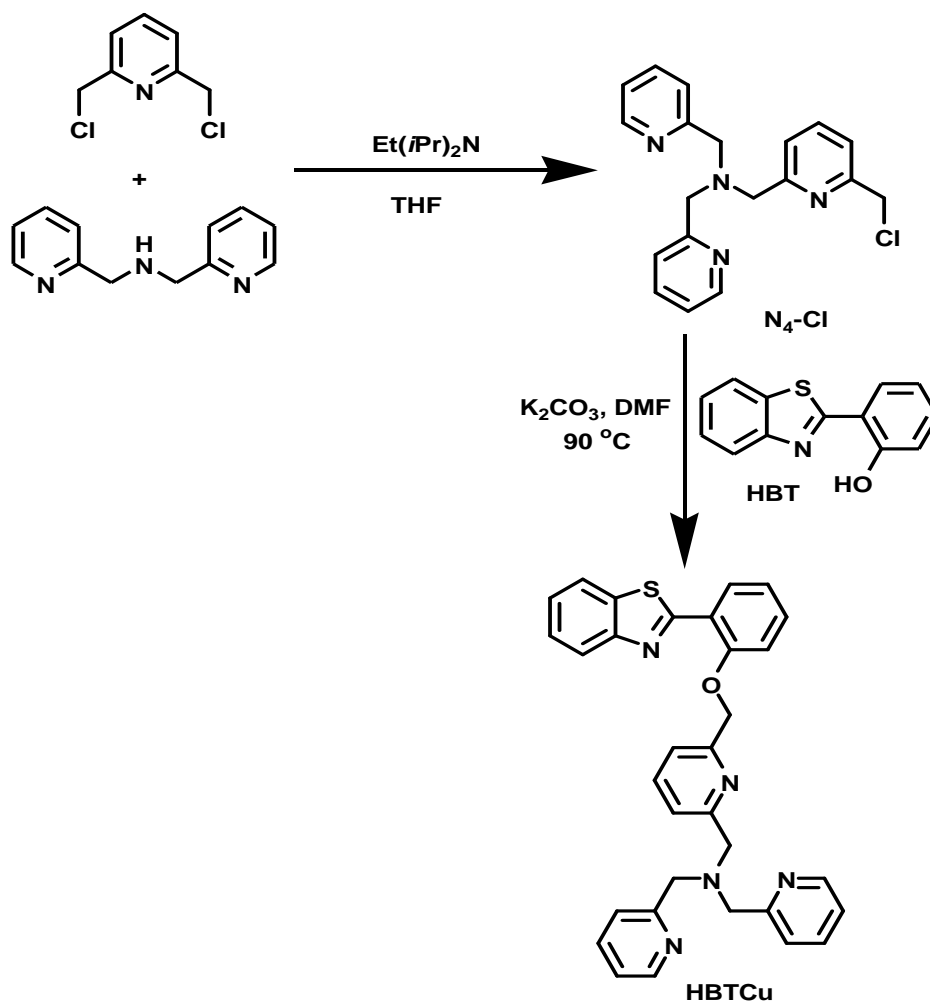
3.1.6 Conclusion

A reactive fluorescent probe **XanCu** was successfully developed for selective detection of Cu^+ under physiologically reducing conditions. Cu^+ catalyzed oxidative benzylic ether (C–O) bonds cleavage releases hydroxy-xanthone (**Xan**) reporter dye from the probe with ~ 30-fold enhancement in the fluorescence intensity. Thus **XanCu** can effectively serve as ‘switch on’ fluorometric probe for the detection of redox-active paramagnetic copper ions. Furthermore the utility of **XanCu** as two-photon fluorescent probe was also demonstrated for the detection of Cu^+ . Thus **XanCu** probe can be used to track intracellular copper ions and could inspire the development of reaction-based probes for other paramagnetic metal ions.

3.2 Reactive probe (HBTCu) for ratiometric detection of Cu⁺ based on excited-state intramolecular proton transfer mechanism

3.2.1 Synthesis

The design strategy is based on the 2-(2'-hydroxyphenyl) benzo[thiazole] (**HBT**) molecular platform as this ESIPT chromophore shows large Stokes shift and corresponding efficient ratiometric fluorescence response. A reactive ESIPT mechanism based Cu⁺ probe **HBTCu** combining **HBT** with pendant tetradentate ligand via cleavable benzyl ether linkage has been designed. Tripicolylamine (**N₄-Cl**) ligand was synthesized from bis-(2-picolyl)amine and 2,6-bis-(chloromethyl)pyridine under basic condition. **N₄-Cl** ligand is known to be selective for



Scheme 3. Synthesis of **HBTCu**

Cu^+ mediated benzylic ether bond cleavage reaction to generate free dye under aerobic conditions. The **HBTCu** probe was synthesized by the O-alkylation of 2-(2'-hydroxyphenyl) benzothiazole (**HBT**) with **N₄-Cl** under basic condition in excellent yield (Scheme 3).

3.2.2 Photophysical property of HBTCu and ratiometric detection of Cu^+

The fluorescence properties of **HBTCu** was studied in aqueous buffer solution (50 mM HEPES, pH 7.2) in presence of 2 mM glutathione (GSH) for mimicking the intracellular environment (Figure 11). Upon 350 nm excitation probe **HBTCu** emits blue fluorescence ($E_{max} = 380$ nm) correspond to **HBT** 'enol-form' emission. The fluorometric behavior of 20.0 μM probe was investigated in presence of several metal ions such as Li^+ , Na^+ , K^+ , Ba^{2+} , Mg^{2+} , Ca^{2+} , Al^{3+} , Mn^{2+} , Fe^{2+} , Co^{2+} , Ni^{2+} , Cu^+ , Cu^{2+} , Zn^{2+} , Cd^{2+} , Ag^+ , Hg^{2+} and Pb^{2+} after 2 h of mixing. The examined millimolar alkali and alkaline earth metals showed no or negligible change in fluorescence of **HBTCu**. Quenching of blue fluorescence ($E_{max} = 390$ nm) accompanied by a new intense green emission band at $E_{max} = 515$ nm was observed when

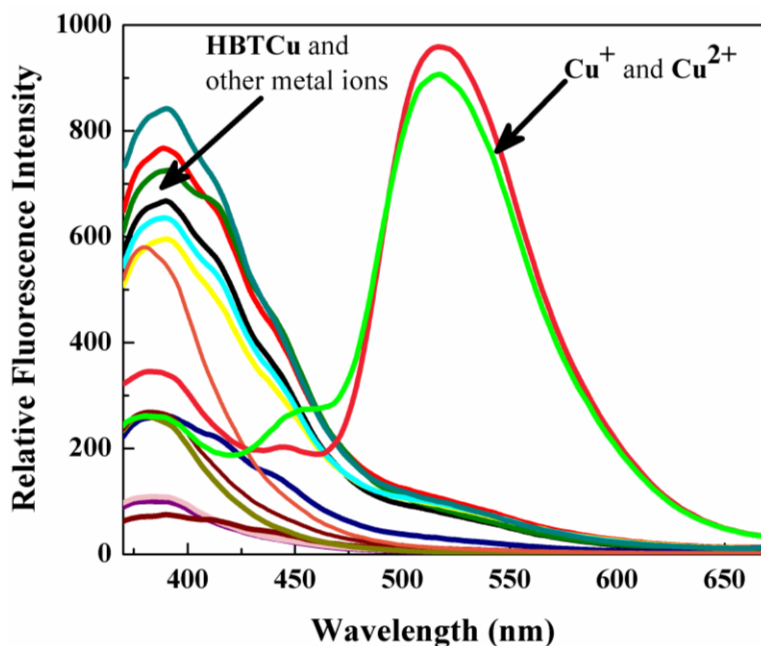


Figure 11. Fluorescence responses of **HBTCu** (20 μM) and upon adding 1 mM of Li^+ , Na^+ , K^+ , Ba^{2+} , Mg^{2+} , Ca^{2+} , Al^{3+} and 20 μM of Mn^{2+} , Fe^{2+} , Co^{2+} , Ni^{2+} , Cu^+ , Cu^{2+} , Zn^{2+} , Cd^{2+} , Ag^+ , Hg^{2+} and Pb^{2+} after 2 h in aqueous solution (50 mM HEPES, pH 7.2, 2 mM GSH) ($\lambda_{ex} = 350$ nm).

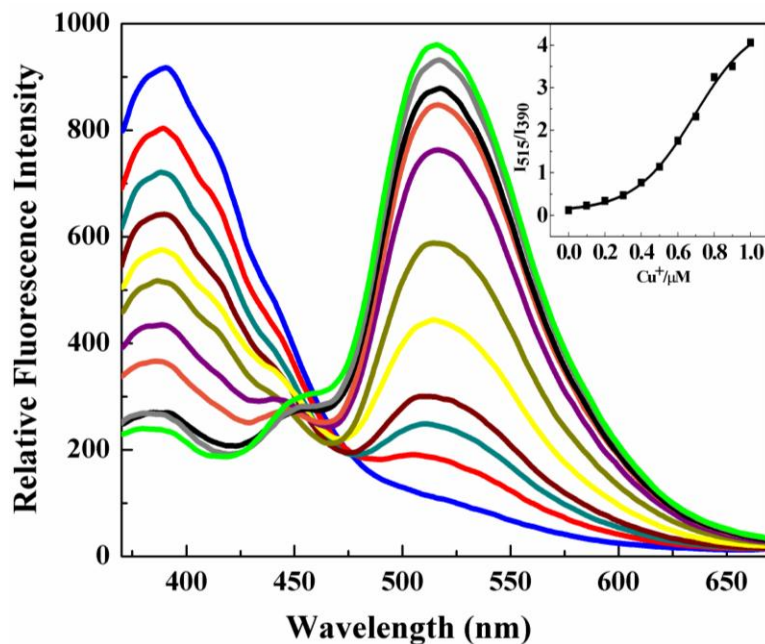


Figure 12. Fluorescence responses of **HBTCu** (20.0 μM) upon addition of 0.0, 0.1, 0.2, 0.3, 0.4, 0.5, 0.6, 0.7, 0.8, 0.9, 1.0 μM of Cu^+ after 2 h in aqueous solution (50 mM HEPES, pH 7.2, 2 mM GSH) ($\lambda_{\text{ex}} = 350 \text{ nm}$).

HBTCu treated with copper ions (Figure 11). This significant transformation in fluorescence behavior of **HBTCu** is indistinguishable for both oxidative states of copper; as GSH in the medium rapidly reduces Cu^{2+} to Cu^+ . Other control metal ions did not show blue fluorescence quenching or new emission band in the green region. The ESIPT based ratiometric emission study helped to improve the detection limit of Cu^+ down to submicromolar concentration (Figure 12). Time dependent study showed that the blue emission band around 390 nm decreases with the increase in intensity of green emission band around 515 nm upon addition of just 1.0 μM Cu^+ after a period of 1 h (Figure 13). A clear isoemissive point is found at 460 nm. As expected, Cu^+ catalyzed oxidative cleavage of benzylic ether (C–O) bond in **HBTCu** release ESIPT active **HBT** fluorophore in presence of O_2 . The phenolic **HBT** rapidly transformed to keto-form upon excitation, responsible for green fluorescence emission (ESIPT) at longer wavelength (515 nm, stokes shift = 125 nm). The reducing environment created by GSH is very much crucial as confirmed by control experiments in the absence of GSH, which did not lead to benzylic ether bond cleavage (Figure 14).

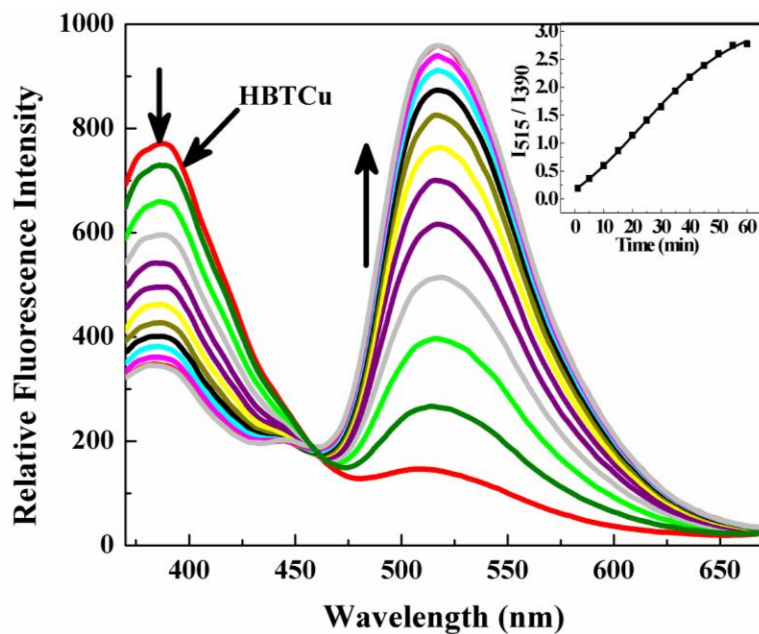


Figure 13. Time dependent fluorescence responses of **HBTCu** (20 μM) after addition of 1 μM of Cu^+ in aqueous solution (50 mM HEPES, pH 7.2, 2 mM GSH) ($\lambda_{ex} = 350$ nm).

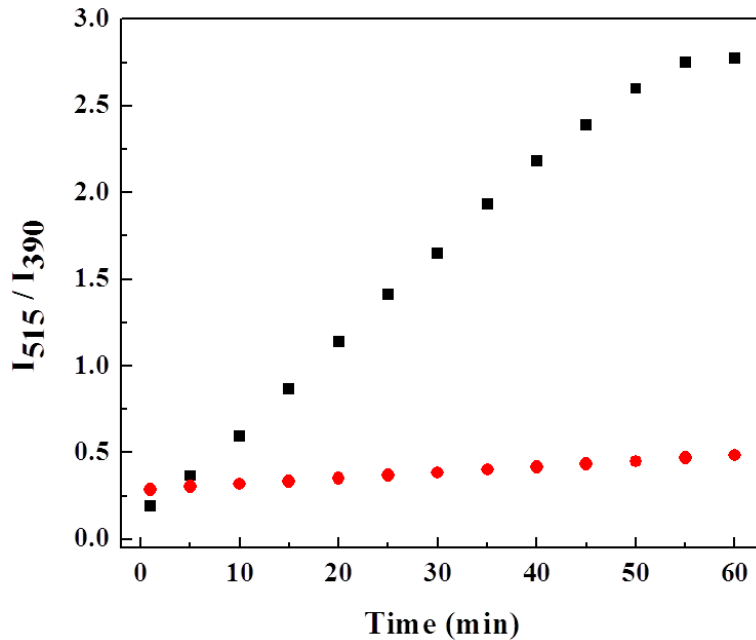


Figure 14. Time dependent ratiometric study of 20.0 μM **HBTCu** incubated with 1.0 μM of Cu^+ in aqueous solution (50 mM HEPES, pH 7.2) with (black trace) and without (red trace) 2 mM GSH.

3.2.3 Competitive study for ratiometric detection of Cu⁺

Competitive experiment suggests the molecular probe **HBTCu** can clearly detects Cu⁺ ratiometrically in presence of all other metal ions respectively (Figure 15).

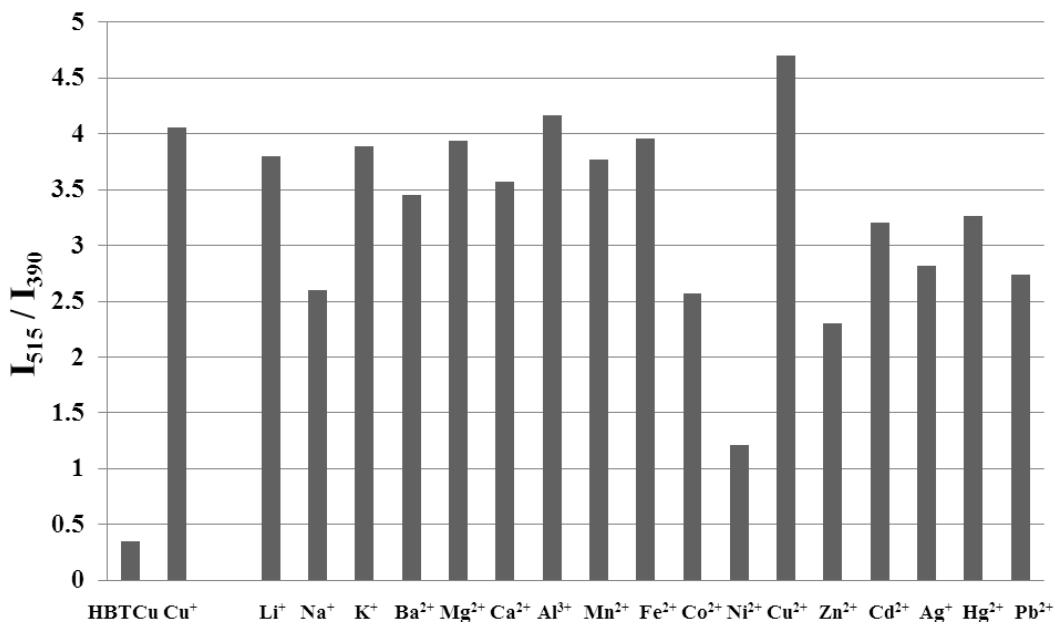


Figure 15. Competitive experiment for the detection of Cu⁺ using 20.0 μ M **HBTCu**. 100.0 μ M Cu⁺ is mixed with 100.0 μ M of corresponding metal ions. Left two bars are control response of the corresponding probe and only metal ion.

3.2.4 pH dependent effects for ratiometric detection of Cu⁺

The effect of pH on Cu⁺ mediated oxidative cleavage of benzylic ether bond was studied to understand efficiency of the process (Figure 16). **HBTCu** reacted efficiently with Cu⁺ in the biologically relevant pH range of 6.5-8.5 to release ES IPT active **HBT** fluorophore. Hence, this probe is very convenient for ratiometric detection of Cu⁺ without interference from the pH-dependent effects.

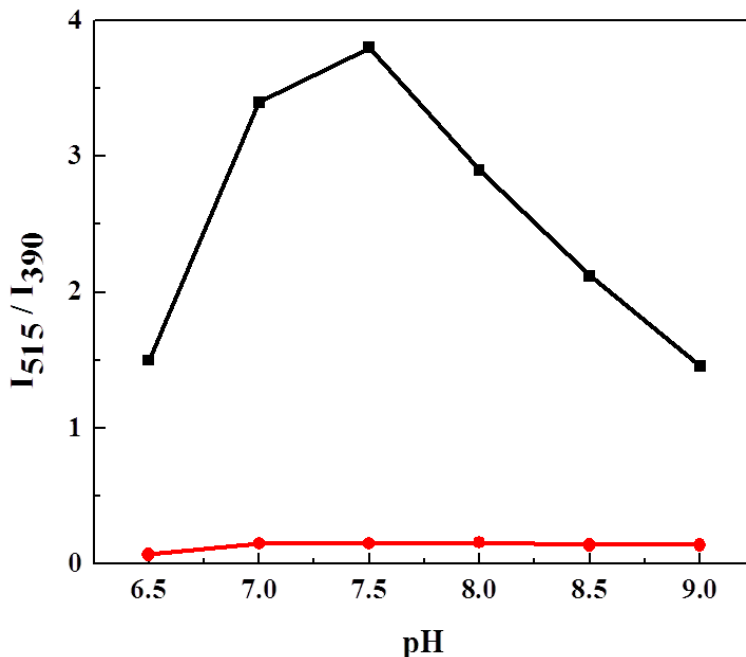
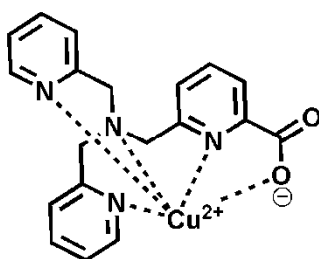
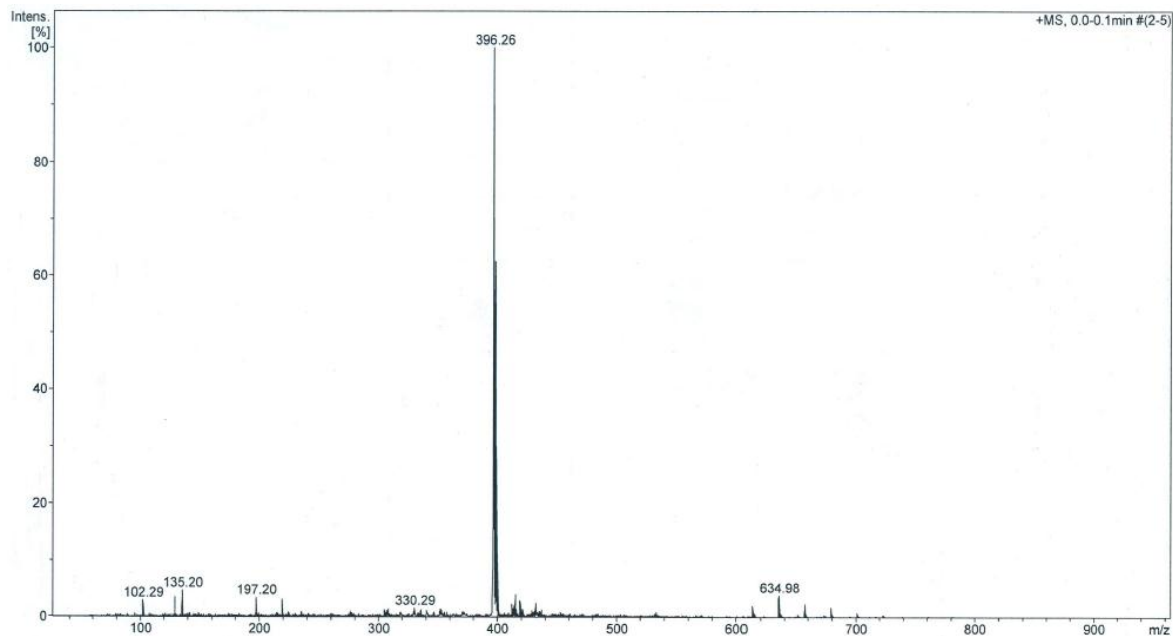


Figure 16. Effect of pH on the ratiometric emission of **HBTCu**. **HBTCu** (20.0 μM) with 1.0 μM of Cu^+ after 2 h in aqueous solution (50 mM HEPES). Black trace: with 2 mM GSH and red trace: without GSH in the buffer.

3.2.5 Proposed reaction mechanism

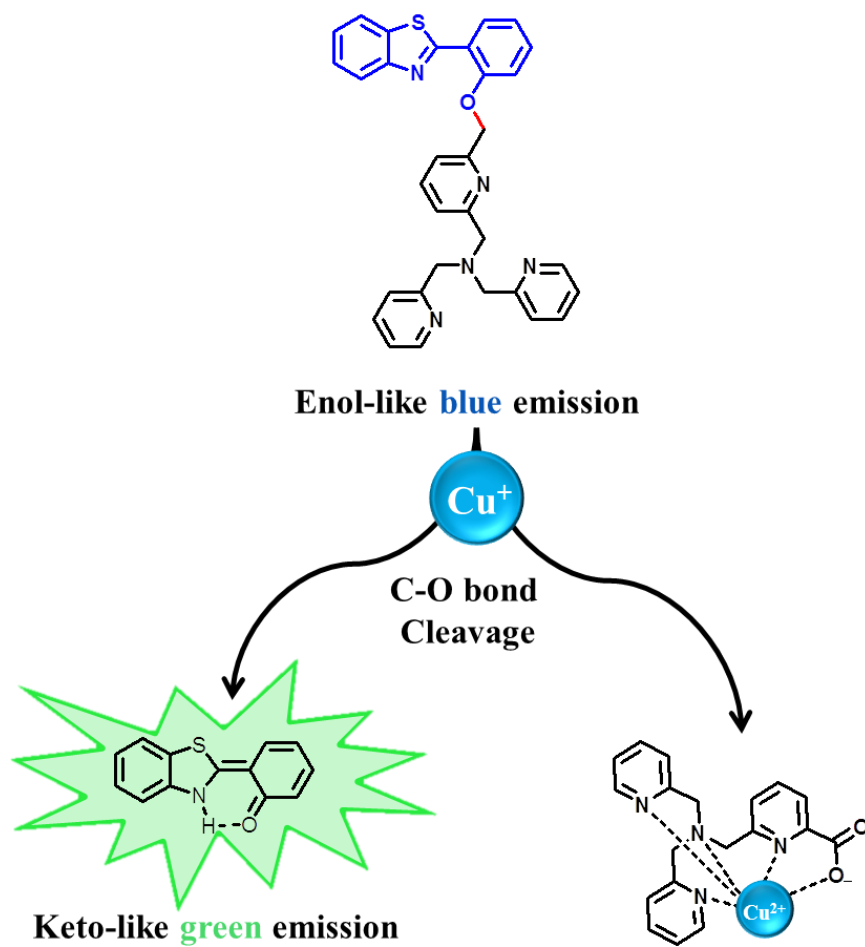
Mass peak at m/z 396.26 correspond to carboxylated $\text{N}_4\text{-Cu}$ complex (calcd. 396.06 for $\text{C}_{19}\text{H}_{17}\text{CuN}_4\text{O}_2$), in agreement with the literature data (Figure 17).^{9h,11d} The ESI-MS data confirmed the and Cu^+ mediated oxidative benzylic ether (C–O) bond cleavage reaction in **HBTCu** and formation of Cu complexes with carboxylated pentadentate ligand N_4 (Scheme 4). A tentative mechanism was proposed for the metal ion (Cu^+) catalyzed oxidative cleavage of benzylic ether (C–O) bond between the **HBT** and N_4 ligand based on the C–N bond cleavage reported by C. J. McKenzie *et al.*⁴² The benzylic carbon of the ligand (N_4) oxidized to carboxylate via benzylic radical formation in presence of activated oxygen (Figure 18). Subsequent transformation involves the formation of oxonium ion which hydrolyzed to aldehyde liberating ES IPT active **HBT**. The aldehyde further oxidized to carboxylate by the hydroperoxide of the metal complex through a Bayer–Villiger type reaction to form final $\text{N}_4\text{-Cu}$ complexes. The coordination sites played a major role by rendering differential metal ion

selectivity to the probe, as C–O bond cleavage proceeds through the formation of Cu complex with pentadentate moieties of **N₄**.



Calculated $m/z = 396.06$ for $C_{19}H_{17}CuN_4O_2$ (**N₄**-Cu complex)

Figure 17. ESI mass spectra (positive ion mode) for the reaction of 20.0 μM **HBTCu** with 10.0 μM Cu^+ in water in presence of 100.0 μM GSH. Mass peaks observed at 396.26 ($[\text{M} + \text{H}]^+$) is corresponds to **N₄**-Cu complex $C_{19}H_{17}CuN_4O_2$. Mass peaks observed at 330.29 ($[\text{M} + \text{Na}]^+$) is corresponds to GSH.



Scheme 4. Cu^+ mediated releases of ESIPT fluorophore **HBT** from **HBTcCu**.

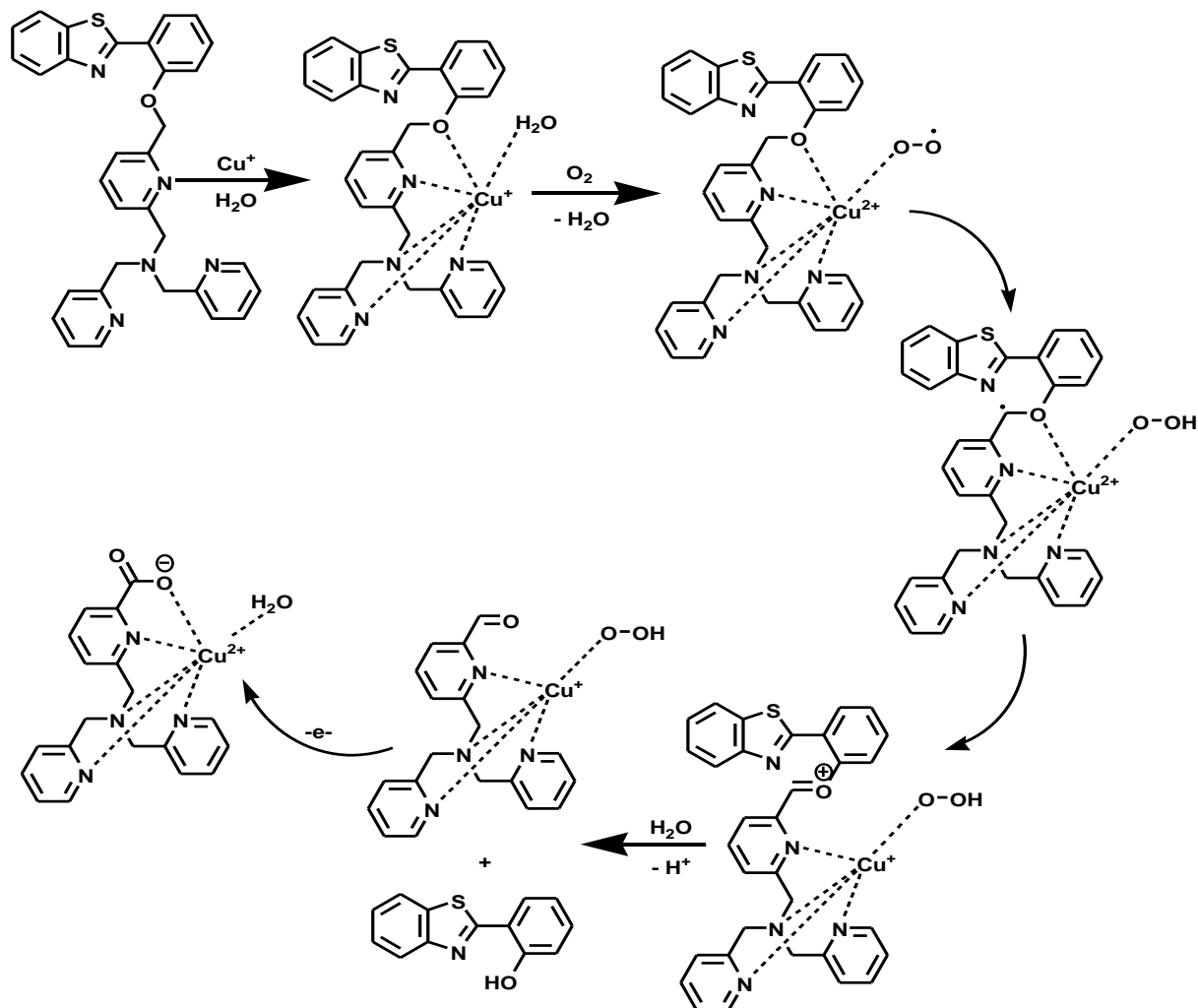


Figure 18. Proposed mechanism of Cu^+ mediated oxidative cleavage of benzylic ether (C–O) bond in ES IPT active fluorophore **HBTCu**.

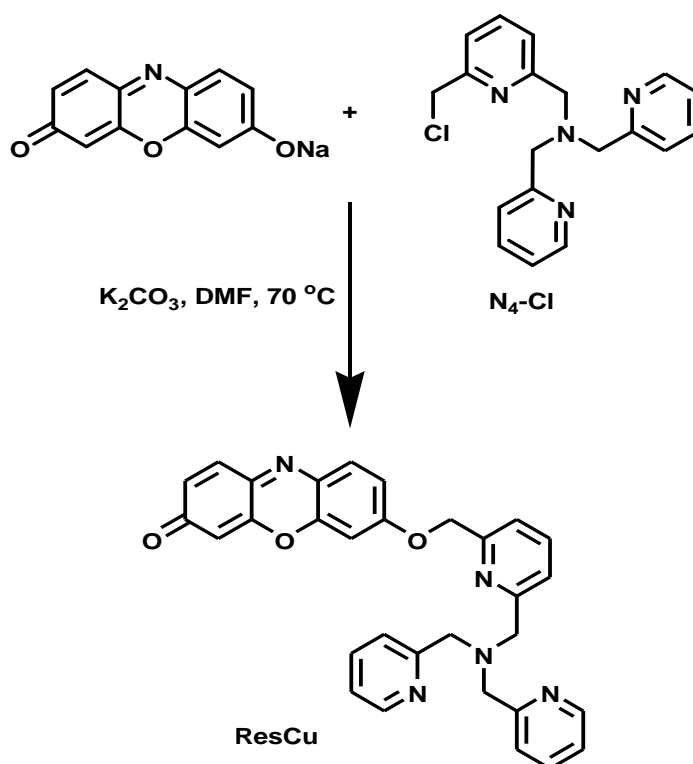
3.2.6 Conclusion

In conclusion, a novel ES IPT-based molecular probe **HBTCu** for ratiometric fluorescence detection of Cu^+ was developed under physiologically reducing conditions. The metal ion catalyzed oxidative benzylic ether bond cleavage was effectively used as switch on ES IPT in **HBT** for fluorometric detection of paramagnetic metal ions overcoming their inherently associated fluorescence quenching property. **HBTCu** reacted efficiently with Cu^+ in the biologically relevant pH range of 6.5–8.5 to release ES IPT active **HBT** fluorophore. This ratiometric probe can be efficiently used for monitoring Cu^+ in physiological and environmental samples.

3.3 Resorufin-based reactive probe (**ResCu**) for Cu^+ with dual output (colorimetric and fluorometric) modes

3.3.1 Synthesis

The alkylation of the 7-hydroxy group of resorufin effectively weakens its intramolecular charge transfer which quenches its emission by blocking push-pull mechanism in the chromophore. The tetradentate ligand N_4 is found to be selective for binding Cu^+ for its reaction-based detection under physiologically reducing conditions. In accordance with above rationale nonfluorescent probes **ResCu** for Cu^+ was designed by combining resorufin dye and tetradentate ligands N_4 through 7-hydroxyl functionality. Cu^+ mediated cleaving of benzylic ether bond in nonfluorescent probes **ResCu** will release chromogenic resorufin dye which automatically shows ratiometric visible absorption (colorimetric) and ‘switch on’ fluorometric responses for Cu^+ under physiologically reducing conditions. **ResCu** was



Scheme 5. Synthesis of **ResCu**

synthesized by the alkylation of 7- hydroxyl group of resorufin with tetradentate $\text{N}_4\text{-Cl}$ under basic conditions in excellent yield (Scheme 5). The synthesized molecular probe was characterized by NMR and mass spectrometry (MS).

3.3.2 Photophysical property of ResCu and selective colorimetric and fluorometric detection of Cu^+

Colorimetric Study of ResCu:

The photophysical properties of **ResCu** was studied in aqueous buffer (50 mM HEPES, pH 7.2) in presence of 2 mM glutathione (GSH) for mimicking the intracellular environment. **ResCu** showed absorption band centered around 470 nm (Figure 19). The absorption spectra of the probe did not exhibit any significant changes upon addition of millimolar concentration of alkali and alkaline earth metal ions and 20.0 μM of other metal ions such as Mn^{2+} , Fe^{2+} , Zn^{2+} , Cd^{2+} , Ag^+ , Hg^{2+} , and Pb^{2+} after 2 h of mixing. The absorbance band of **ResCu** at 470 nm is red-shifted to 573 nm ($\Delta\lambda = 103$ nm) and the color of the solution

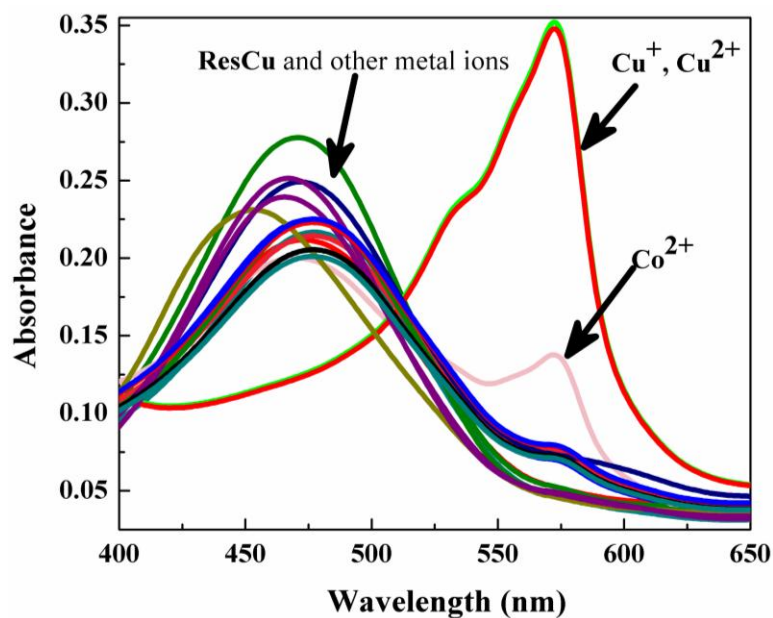


Figure 19. Absorption spectra of **ResCu** (10.0 μM) upon addition of different metal ions after 2 h in aqueous solution (50 mM HEPES, pH 7.2, 2 mM GSH).

changed from pale yellow to dark pink upon addition of 20.0 μM of Cu⁺ after 2 h of mixing (Figure 19). This significant ratiometric behavior in absorbance band of **ResCu** is indistinguishable for both oxidation states of copper, as GSH in the medium rapidly reduces Cu²⁺ to Cu⁺. Time dependent study of the reaction between Cu⁺ with **ResCu** showed decrease in the absorbance at 470 nm ($\epsilon = 1.75 \times 10^4 \text{ M}^{-1} \text{ Cm}^{-1}$) with the appearance of a strong new peak at 573 nm which reached maximum within 30 min ($\epsilon = 3.17 \times 10^4 \text{ M}^{-1} \text{ Cm}^{-1}$) of mixing the sample (Figure 20). Clear isosbestic point at 510 nm was observed, which strongly supports the formation of new product i.e., resorufin dye after Cu⁺ mediated

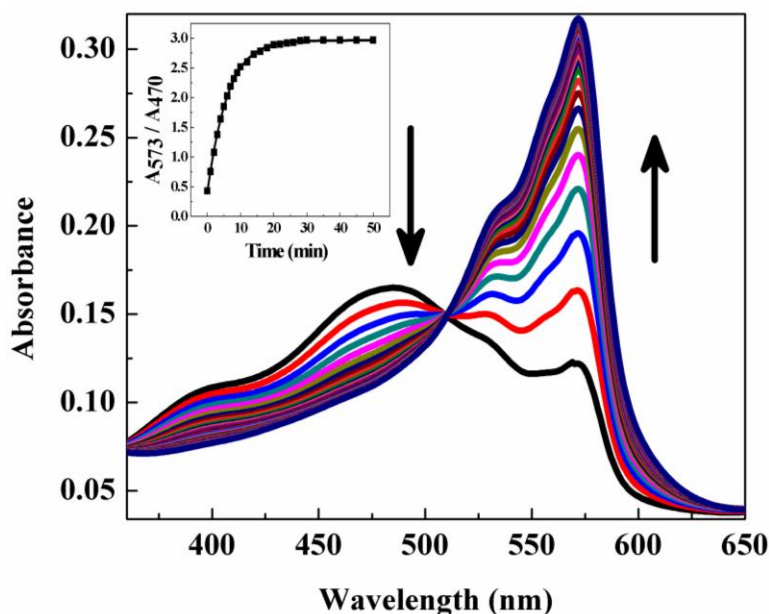


Figure 20. Time dependent absorption spectra of **ResCu** (10.0 μM) after addition of 20.0 μM of Cu⁺ in aqueous solution (50 mM HEPES, pH 7.2, 2 mM GSH) (Isobestic point = 510 nm).

oxidative benzylic ether (C–O) bond cleavage in **ResCu** in physiological reducing condition (Figure 20). **ResCu** showed slight colorimetric change with Co²⁺ (Figure 19). Submicromolar concentration of Cu⁺ can be easily detected as confirmed from the ratiometric absorption study of **ResCu** upon sequential addition of increasing concentrations of Cu⁺ (Figure 21). Moreover, this kind of ratiometric behavior of the probe **ResCu** is advantageous over normal probes as it minimizes the error arising from physical or chemical fluctuations in the sample and experimental conditions.

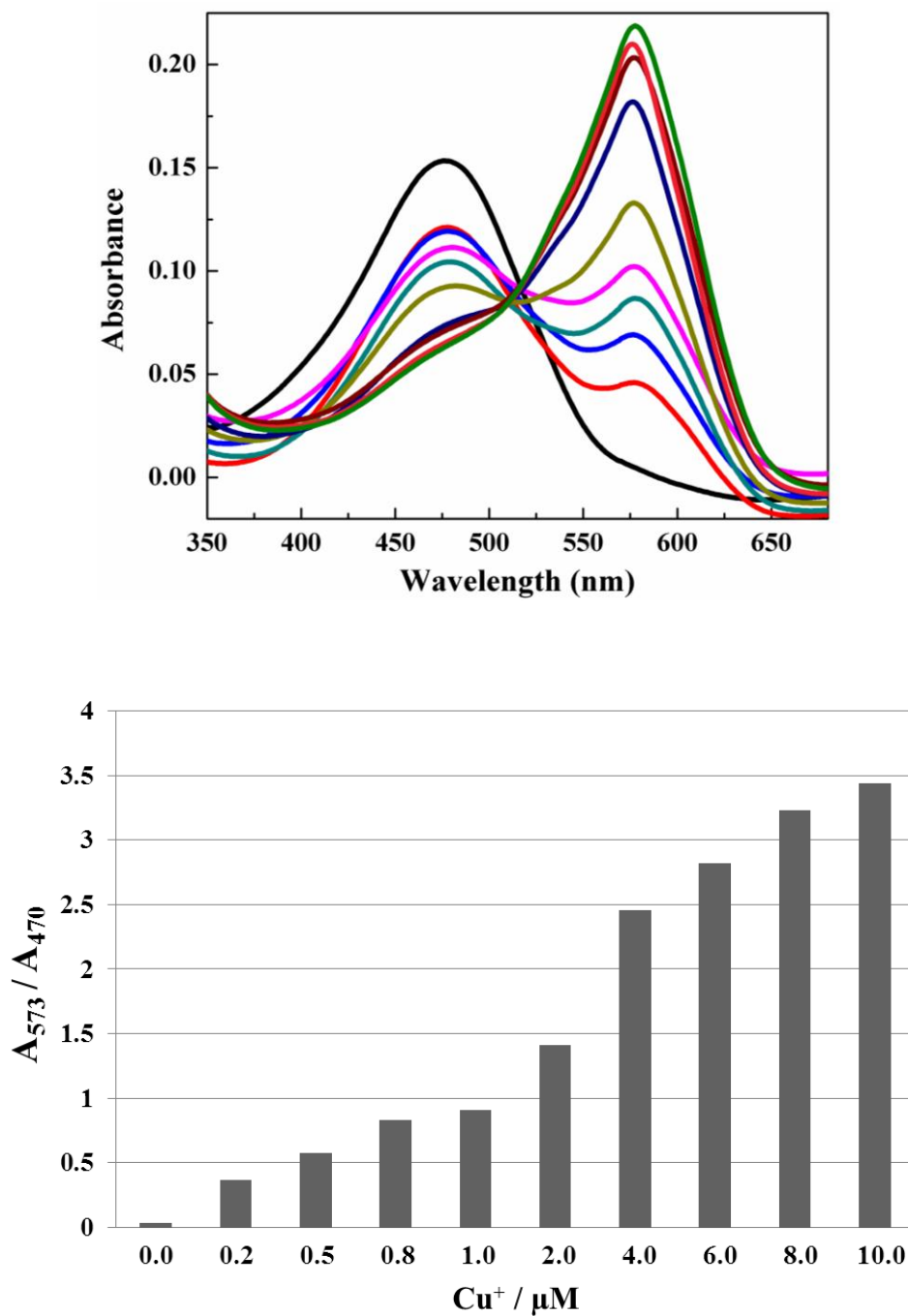


Figure 21. Absorption spectra (top) and ratiometric responses (bottom) of **ResCu** (10.0 μM) upon addition of 0.0, 0.2, 0.5, 0.8, 1.0, 2.0, 4.0, 6.0, 8.0, 10.0 μM of Cu^+ after 2 h in aqueous solution (50 mM HEPES, pH 7.2, 2 mM GSH).

Fluorometric Study of ResCu:

As expected 1.0 μM solution of **ResCu** probe exhibits very weak fluorescence upon 540 nm excitation (Figure 22). After mixing for 2h, millimolar concentrations of alkali and alkaline earth metal ions did not show significant changes in the fluorescence behavior of the probe. Next fluorometric behavior of the probe was tested upon addition 20.0 μM of several metal ions such as Mn^{2+} , Fe^{2+} , Co^{2+} , Cu^{2+} , Cu^{+} , Zn^{2+} , Cd^{2+} , Ag^{+} , Hg^{2+} , and Pb^{2+} after 2 h of mixing. As anticipated, addition of 20.0 μM of copper ions to the aqueous solution containing 1.0 μM

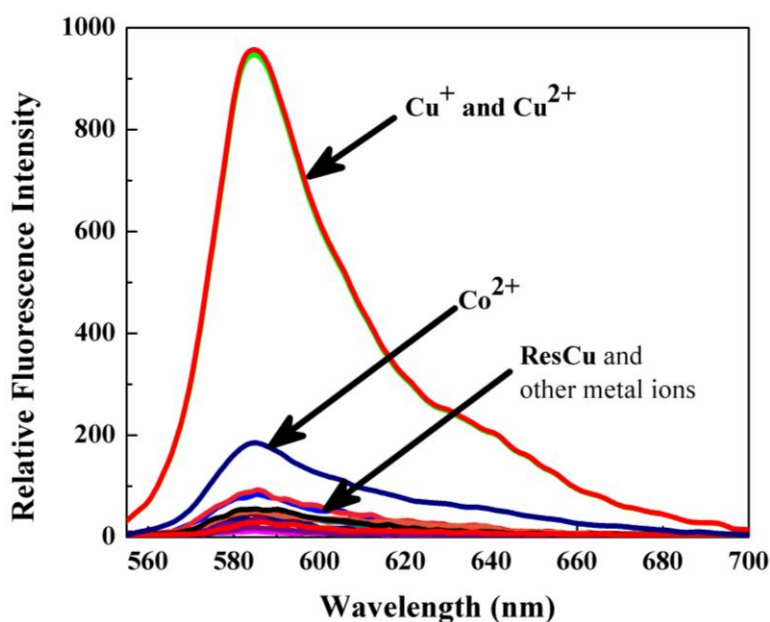


Figure 22. Fluorescence responses of **ResCu** (1.0 μM) upon addition of different metal ions after 2 h in aqueous solution (50 mM HEPES, pH 7.2, 2 mM GSH) ($\lambda_{\text{ex}} = 540 \text{ nm}$).

ResCu resulted in a *ca.* 17-fold fluorescence ($E_{\text{max}} = 586 \text{ nm}$) enhancement within 2 h (Figure 22). This significant ‘switch on’ fluorescence enhancement of **ResCu** is also indistinguishable for both oxidation states of copper, as GSH in the medium rapidly reduces Cu^{2+} to Cu^{+} . Other control metal ions tested did not show such switch on fluorescence while only Co^{2+} showed very minimal response in the emission intensity. The switch on fluorescence indicates the Cu^{+} catalyzed oxidative cleavage of benzylic ether (C–O) linkage in **ResCu** in presence of O_2 releasing highly fluorescent resorufin dye.

Time dependent study showed that Cu^+ mediated benzyl ether bond cleavage reaction in **ResCu** complete within 30 min as indicated by the fluorescence spectra (Figure 23). Concentration dependent study showed submicromolar concentration of Cu^+ is good enough to react with **ResCu** to release fluorescent resorufin dye which lead to subsequent detection of the metal ions (Figure 24). The reducing environment generated by GSH is very essential as confirmed by control experiments in the absence of GSH, which did not lead to benzylic ether (C–O) bond cleavage (Figure 25).

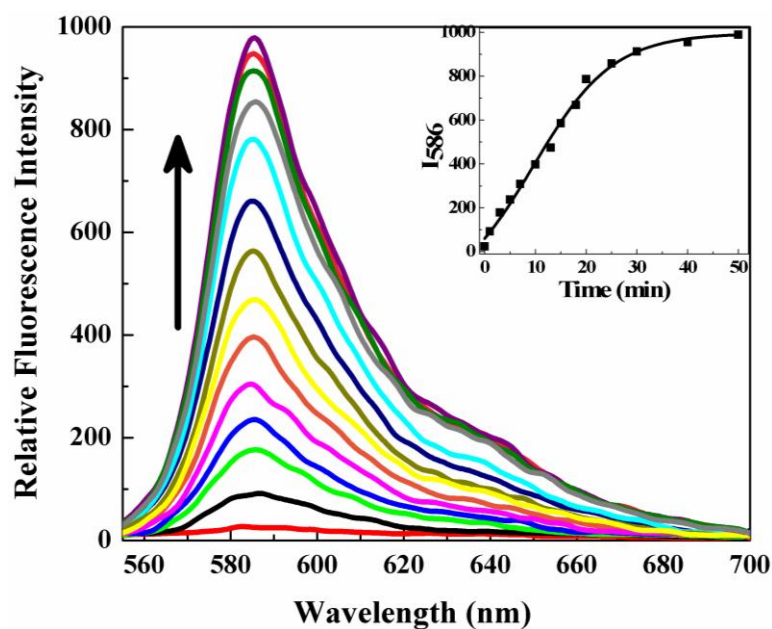


Figure 23. Time dependent fluorescence responses of **ResCu** (1.0 μM) after addition of 20.0 μM of Cu^+ in aqueous solution (50 mM HEPES, pH 7.2, 2 mM GSH) ($\lambda_{\text{ex}} = 540 \text{ nm}$).

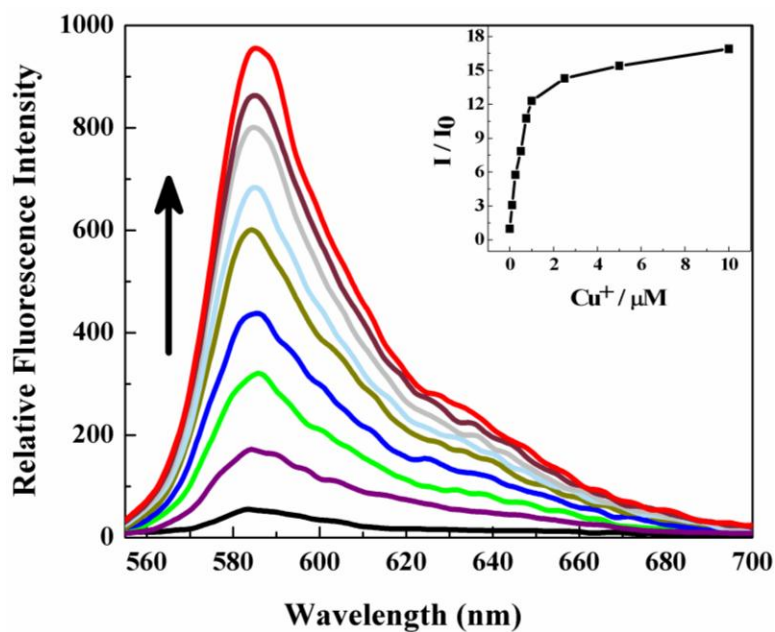


Figure 24. Fluorescence responses of **ResCu** (1.0 μM) upon addition of 0.0, 0.1, 0.25, 0.5, 0.75, 1.0, 2.5, 5.0, 10.0 μM of Cu^+ after 2 h in aqueous solution (50 mM HEPES, pH 7.2, 2 mM GSH) ($\lambda_{\text{ex}} = 540$ nm).

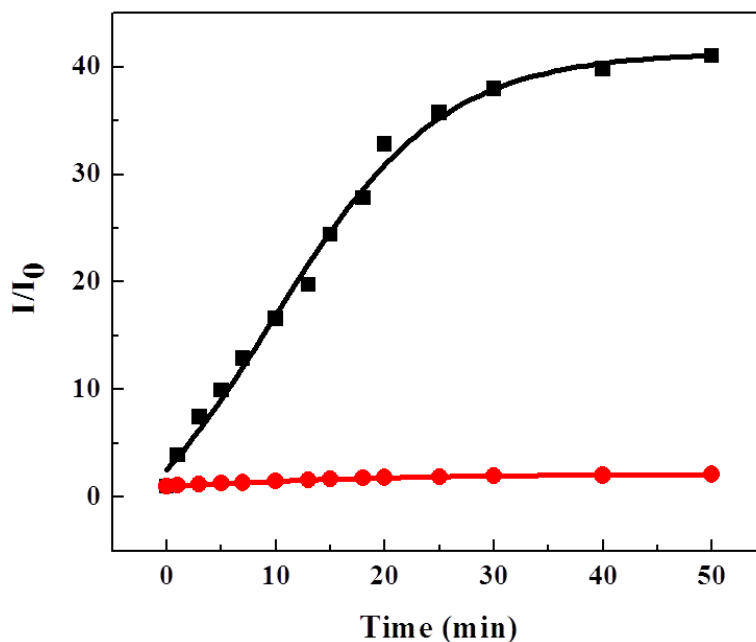


Figure 25. Time dependent fluorescence study of 1.0 μM **ResCu** incubated with 10 μM of Cu^+ in aqueous solution (50 mM HEPES, pH 7.2) with (black trace) and without (red trace) 2 mM GSH.

3.3.3 pH dependent study

The effect of pH on the Cu^+ mediated oxidative cleavage of the benzylic ether bond in **ResCu** was studied to understand the efficiency of this ‘switch on’ fluorometric method. **ResCu** reacted efficiently with Cu^+ in the biologically relevant pH range of 6.5–8.5 to release phenolic resorufin fluorophore (Figure 26). Hence, **ResCu** is very convenient for the ‘switch on’ fluorometric detection of Cu^+ without the interference from the pH-dependent effects.

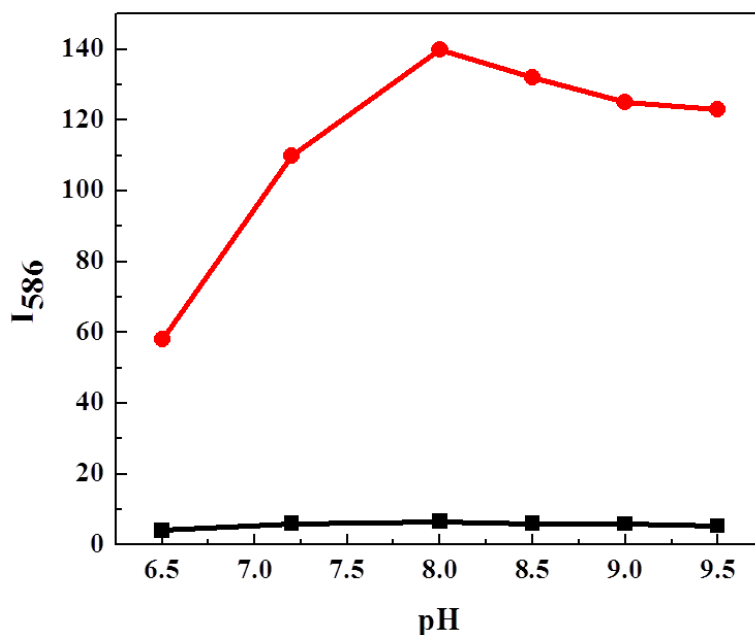


Figure 26. Effect of pH on the ‘switch on’ emission of **ResCu**. Red trace: **ResCu** (1.0 μM) with 10.0 μM of Cu^+ after 2 h in aqueous solution. Black trace: **ResCu** (1.0 μM) without Cu^+ after 2 h in aqueous solution.

3.3.4 Competitive study for detection of Cu^+

Selectivity of **ResCu** as the ‘switch on’ fluorescent probe for Cu^+ was studied in the presence of various competing metal ions. For this purpose, 1.0 μM solutions of **ResCu** were treated with 20.0 μM of Cu^+ in the presence of 20.0 μM of other metal ions. Data in Figure 27 show that there is no or very minimal interference for the detection of Cu^+ in the presence of other metal ions. This indicates the selectivity of Cu^+ mediated oxidative benzylic ether bond cleavage in **ResCu** to release fluorescent resorufin dye. Thus, **ResCu** can be used as selective

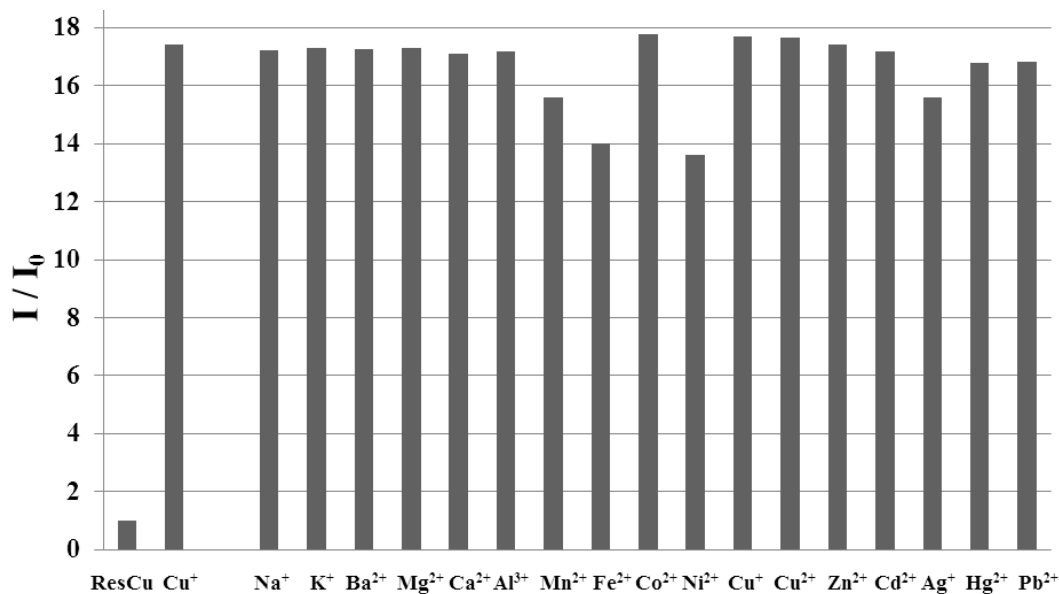
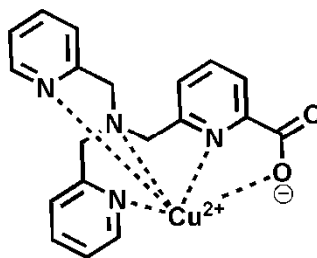
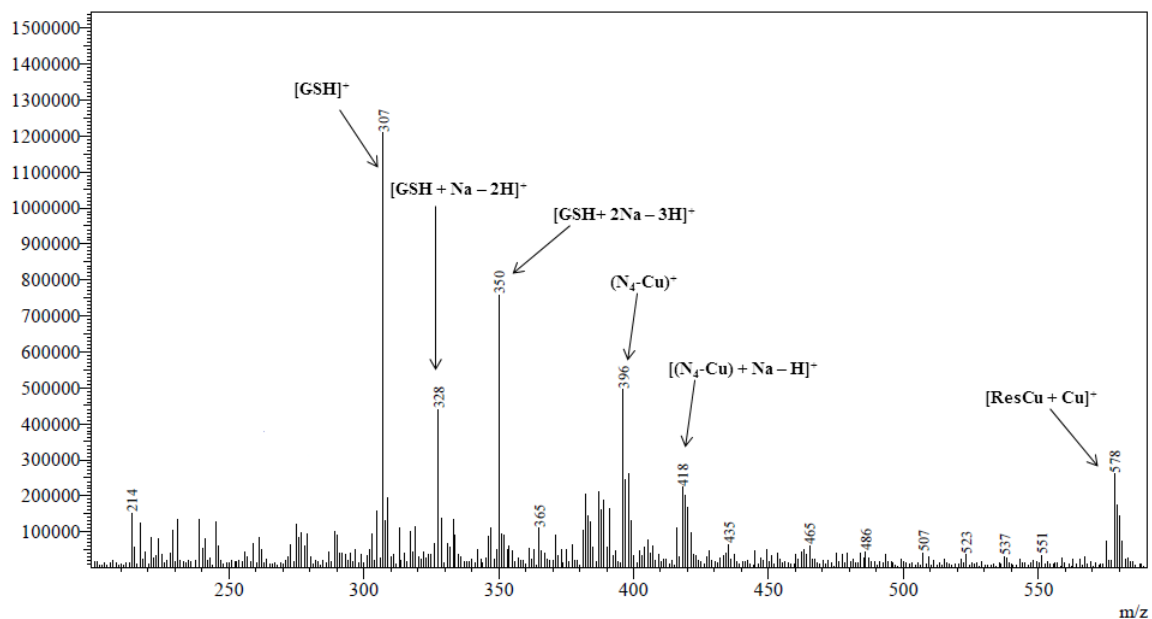


Figure 27. Competitive experiment for the detection of Cu^+ using $1.0 \mu\text{M}$ of **ResCu**. $20.0 \mu\text{M}$ Cu^+ is mixed with $20.0 \mu\text{M}$ of corresponding metal ions. Left two bars are control response of the corresponding probe and only metal ion indicated.

reaction-based switch on fluorescent probes for Cu^+ in the presence of most competing metal ions.

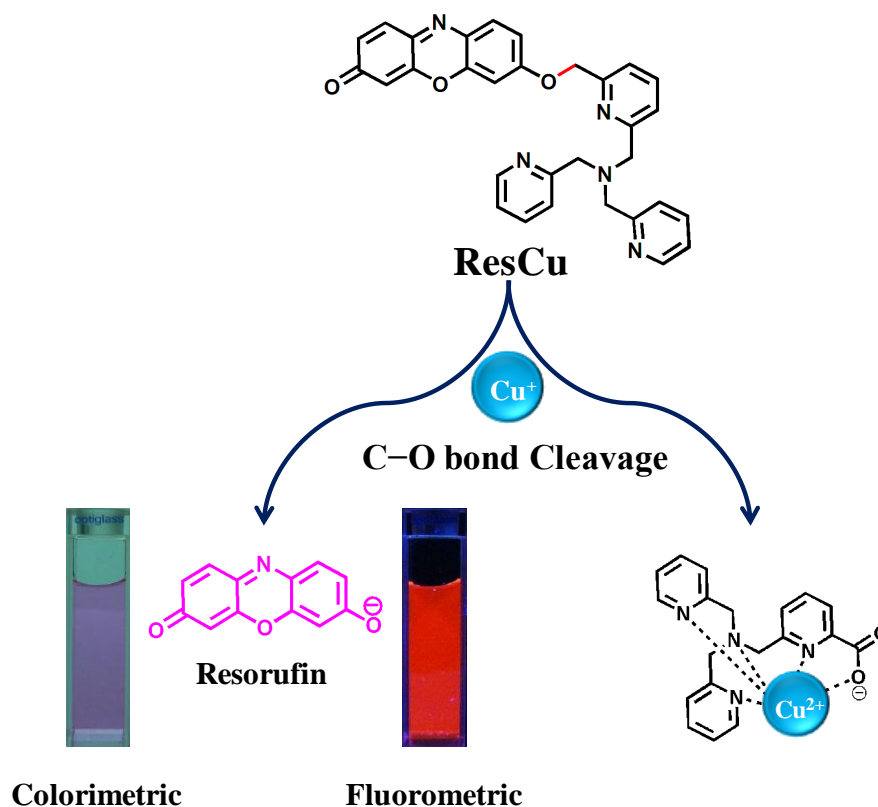
3.3.5 Product analysis

ESI-MS analysis further confirmed Cu^+ catalyzed oxidative benzylic ether (C–O) bond cleavage in **ResCu** to release fluorescence reporter dye resorufin and metal ion bound carboxylated tetradentate ligand [**N₄-Cu**]. The mass peaks at m/z 396 and 418 correspond to the carboxylated **N₄-Cu** complex (calcd 396.06 for $\text{C}_{19}\text{H}_{17}\text{CuN}_4\text{O}_2$ and 419.05 for $\text{C}_{19}\text{H}_{17}\text{CuN}_4\text{O}_2 + \text{Na}^+$) (Figure28). This mass spectroscopic data are in agreement with data reported in the literature.^{33,46,67} Thus ESI-MS data validated the Cu^+ mediated oxidative benzylic ether (C–O) bond cleavage reaction in **ResCu** and the formation of Cu complexes with carboxylated pentadentate ligands of N_4 (Scheme 6). The metal ion (Cu^+) catalyzed oxidative cleavage of the benzylic ether (C–O) bond between the resorufin and N_4 ligand is presumed to follow the mechanism proposed for C–N/C–O bond cleavage reaction reported in the literature.^{42,46,67}



Calculated $m/z = 396.06$ for $C_{19}H_{17}CuN_4O_2$ (N_4 -Cu complex)

Figure 28. ESI mass spectra (positive ion mode) for the reaction of 10.0 μM **ResCu** with 100.0 μM Cu^+ in water in presence of 100.0 μM GSH. Mass peaks observed at 396 ($[M + H]^+$) and 418 ($[M + Na - H]^+$) are correspond to N_4 -Cu complex $C_{19}H_{17}CuN_4O_2$. Mass peak observed at 578 ($[M + Cu]^+$) correspond to copper bound **ResCu** (calculated 578.12 for $C_{31}H_{25}CuN_5O_3$). Mass peaks observed at 307 ($[M]^+$), 328 ($[M + Na - 2H]^+$), 350 ($[M + 2Na - 3H]^+$) is corresponds to GSH.



Scheme 6. Cu^+/O_2 mediated benzylic ether bond (C–O) cleavage in **ResCu** to release resorufin dye and $[\text{N}_4\text{-Cu}]$ complex.

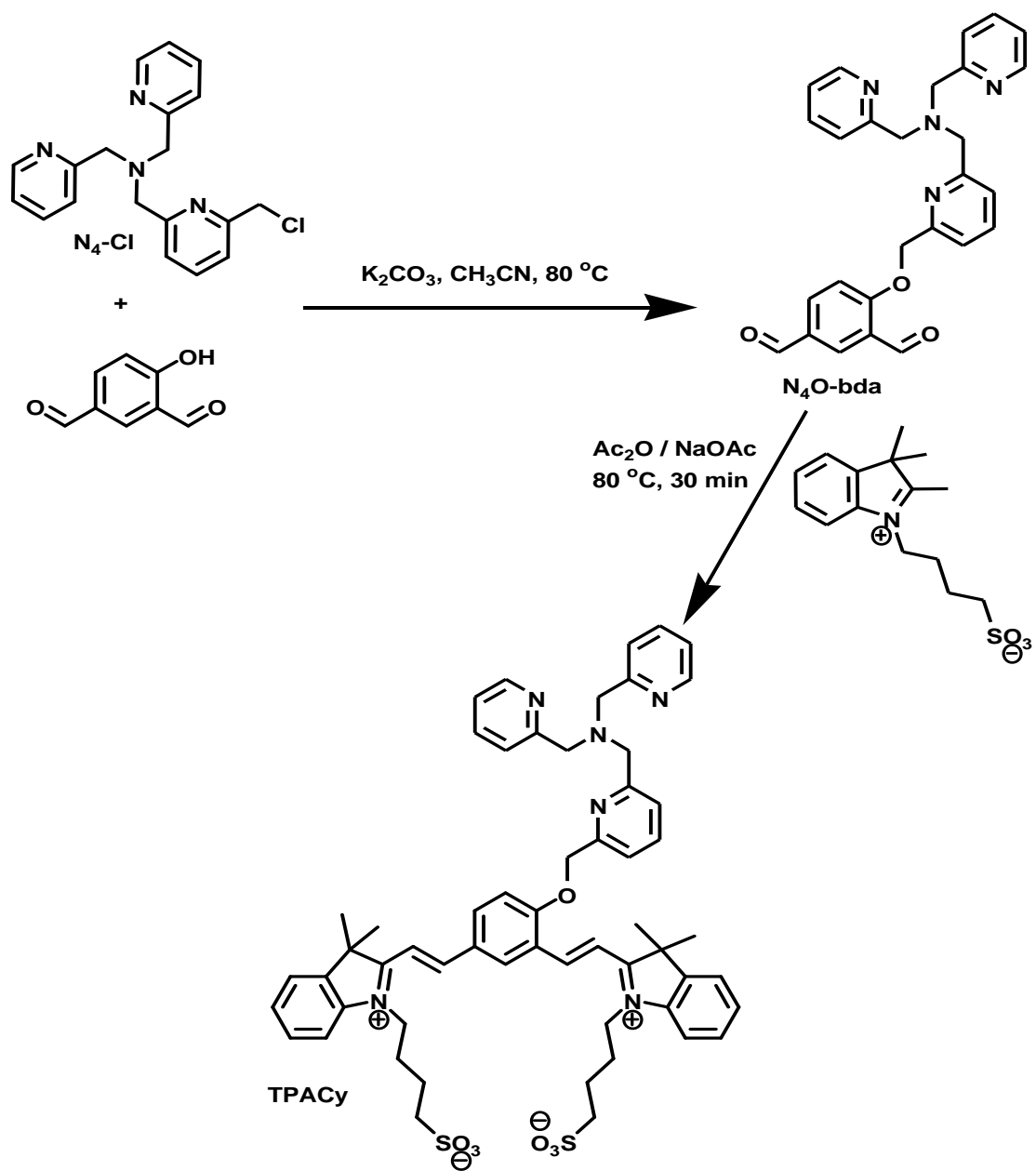
3.3.6 Conclusion

In conclusion, the design and synthesis of new type reaction-based molecular probe **ResCu** has been presented here with dual optical output for the detection of Cu^+ ion in physiological reducing media. The metal ion catalyzed oxidative benzylic ether bond cleavage was successfully established for detection of paramagnetic metal ion overcoming the inherently associated fluorescence quenching property. This molecular probe extended the scope of reaction-based molecular platform for the detection of paramagnetic metal ions by employing newer fluorescence reporter dye with emission in the longer wavelength region. Furthermore this probe offers ratiometric visible absorption (colorimetric) based second mode of optical response for the detection of Cu^+ . Thus **ResCu** probe can be efficiently used for monitoring exchangeable Cu^+ pools in analytical samples and in living cells as this probe containing fluorescence reporter resorufin dye which is not phototoxic to living cells.

3.4 Switch on near infrared fluorescent reactive probe (TPACy) for Cu⁺

3.4.1 Synthesis

Design strategy for the development of a turn on NIR fluorescence probe relied on a reaction-based approach in which Cu⁺ mediated bond-cleaving reaction converted a weak or non-fluorescence probe into a robust NIR fluorescent dye.⁶⁸ The Cu⁺ assisted removal of pendant tripicolylamine (N₄) group from phenolic moiety of a fluorophore has been found to have excellent selectivity towards Cu⁺ detection with off–on fluorescence signaling.⁴⁶ Masking phenolic group through alkylation functionality would significantly disturb the internal charge transfer (ICT) process, maximizing the fluorescence switching on–off process.⁶⁹ Heptamethine cyanine (Cy), a NIR fluorescent dye with high extinction coefficient and quantum yield, has been extensively used in NIR bioimaging.⁷⁰⁻⁷² An interesting approach has been devised by incorporating N₄-alkylated phenolic moiety onto the conjugated cyanine backbone. The N₄-phenolic moiety incorporated heptamethine cyanine (**TPACy**) was designed, however with a completely altered π -conjugation pattern and positive charges localized on both the nitrogen atoms (Scheme 7). The Cu⁺ mediated oxidative cleavage reaction on the **TPACy** probe will generate the Cy-phenolate which rearranges itself by neutralizing the positive charge on a nitrogen atom to form stable **Cy-quinone**. This **Cy-quinone** resumes the extended π -electron conjugation pattern of the cyanine dyes to exhibit turn on NIR fluorescence. To synthesize **TPACy**, first the hydroxyl group of 4-hydroxy-1,3-benzenedicarboxaldehyde was alkylated using pendant **N₄-Cl** ligand under basic condition (Scheme 7). Good yield of **TPACy** was obtained by condensing the N₄-alkylated dialdehyde (**N₄O-bda**) intermediate with 2 equiv of indolium-3-butylsulfonate. All the compounds were characterized by NMR, mass spectrometry, and elemental analysis. The indolium-3-butyl-sulfonate chains in **TPACy** are chosen to impart water solubility and to prevent aggregation of the cyanine backbone in solution.



Scheme 7. Synthesis of TPACy

3.4.2 Photophysical properties of TPACy and NIR fluorometric detection of Cu^+

The fluorescence properties of TPACy was studied in aqueous buffer solution (50 mM HEPES, pH 7.2) in presence of 2 mM glutathione (GSH) for mimicking the intracellular environments. The fluorometric behavior of 20.0 μM TPACy was investigated with the addition of several metal ions such as Li^+ , Na^+ , K^+ , Ba^{2+} , Mg^{2+} , Ca^{2+} , Al^{3+} , Mn^{2+} , Fe^{2+} , Co^{2+} , Ni^{2+} , Cu^+ , Cu^{2+} , Zn^{2+} , Cd^{2+} , Ag^+ , Hg^{2+} and Pb^{2+} after 2 h of mixing (Figure 29). As anticipated, upon 600 nm excitation TPACy was found to be weakly fluorescent. The examined millimolar concentrations of alkali and alkaline earth metals had no effect on the fluorescence behavior of TPACy. When tested with copper ions, it showed remarkable ~ 8 -fold enhancement in the blue fluorescence emission positioned around 700 nm. This significant ‘switch on’ fluorescence phenomenon is identical for both Cu^+ and Cu^{2+} ions as GSH rapidly reduces Cu^{2+} to Cu^+ . The ‘switch on’ emission around 700 nm indicates that Cu^+ react with TPACy and cleaves the benzyl ether (C–O) linkages in presence of O_2 releasing the Cy-phenolate anion. The negative charge of Cy-phenolate rearranges itself by neutralizing the positive charge on one of the nitrogen atoms to form stable **Cy-quinone**

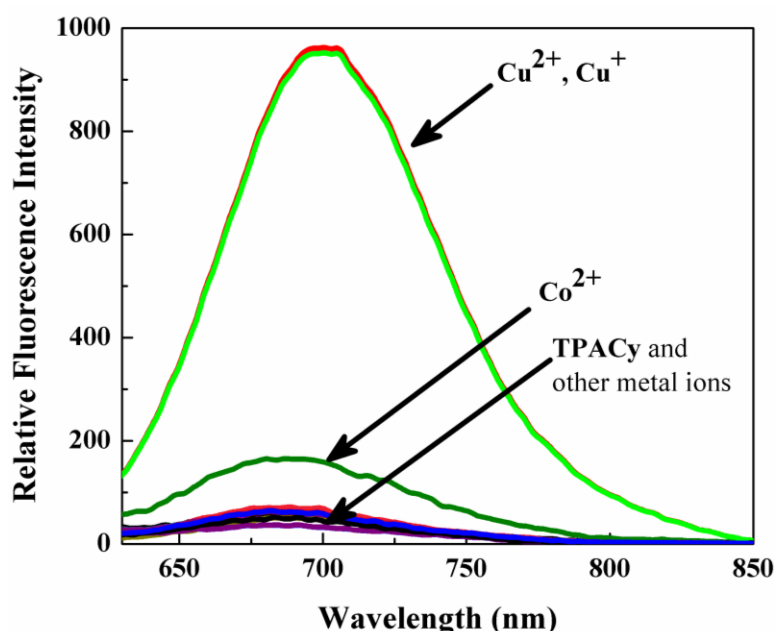
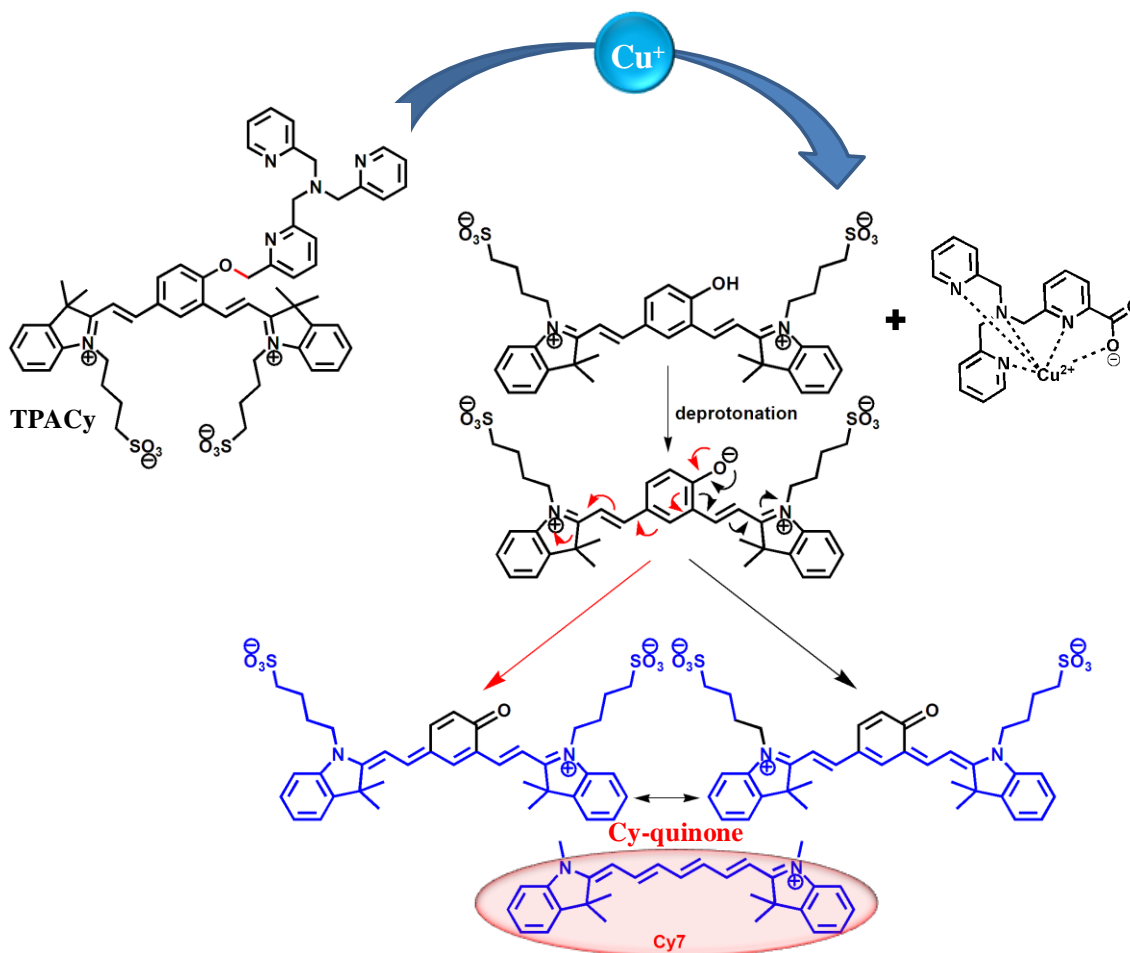


Figure 29. Fluorescence responses of TPACy (20.0 μM) upon addition 1 mM of Li^+ , Na^+ , K^+ , Ba^{2+} , Mg^{2+} , Ca^{2+} , Al^{3+} and 20.0 μM of Mn^{2+} , Fe^{2+} , Co^{2+} , Ni^{2+} , Cu^+ , Cu^{2+} , Zn^{2+} , Cd^{2+} , Ag^+ , Hg^{2+} and Pb^{2+} after 2 h in aqueous solution (50 mM HEPES, pH 7.2, 2 mM GSH) ($\lambda_{\text{ex}} = 600$ nm).



Scheme 8. Cu^+/O_2 mediated benzylic ether bond (C–O) cleavage in TPACy to release NIR emitting Cy-quinone dye.

(Scheme 8). In the process, **Cy-quinone** resumes a heptamethine cyanine-like (Cy7) extended π -electron conjugation pattern which is responsible for the observed characteristic turn on NIR fluorescence. Cu^{2+} did not show ‘switch on’ fluorescence response in the absence of GSH (Figure 30), while Cu^+ exhibited minimal response as it undergoes spontaneous oxidation to Cu^{2+} in the absence of GSH. Other transition metal ions except Co^{2+} caused no significant change in the baseline fluorescence intensity (Figure 30). While Co^{2+} showed very minimal response in the emission intensity in presence of GSH. Concentration dependent study showed that submicromolar Cu^+ could be efficiently detected as this amount is sufficient enough to react with TPACy, releasing NIR emitting **Cy-quinone** dye (Figure 31).

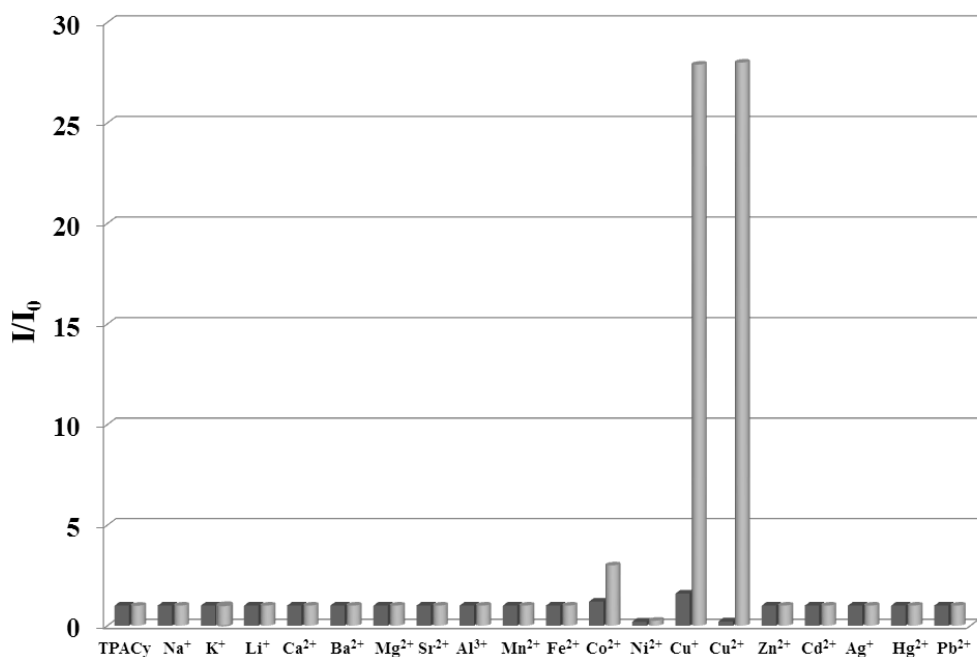


Figure 30. Fluorescent responses of TPACy (1.0 μM) in 50 mM HEPES buffer (pH 7.2). The bars represent the fluorescence intensity at 700 nm after 2 h of reaction of 20.0 μM TPACy with different metal ion (20.0 μM) in the absence (dark gray bars) or presence (light gray bars) of 2 mM GSH ($\lambda_{\text{ex}} = 600$ nm).

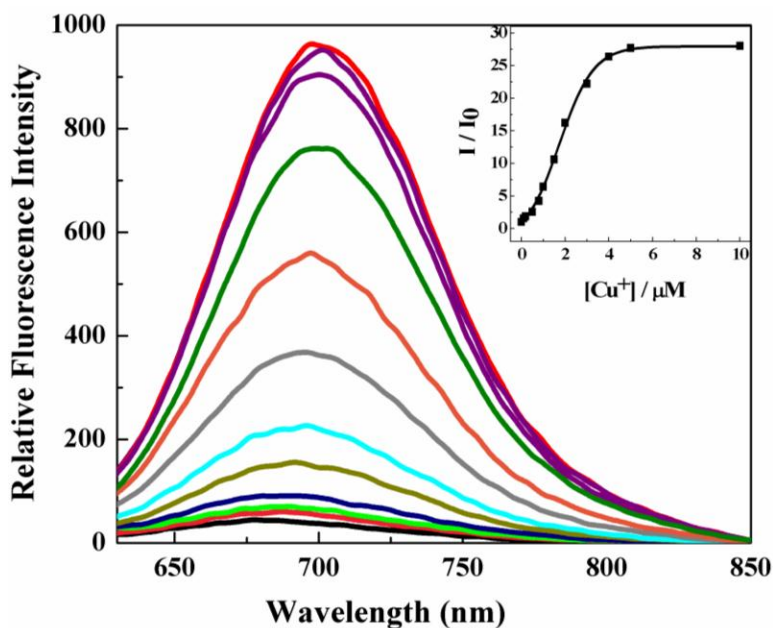


Figure 31. Fluorescence responses of TPACy (20.0 μM) upon addition of different concentration of Cu^+ after 2 h in aqueous solution (50 mM HEPES, pH 7.2, 2 mM GSH) ($\lambda_{\text{ex}} = 600$ nm).

3.4.3 pH dependent study

The effect of pH on the Cu^+ mediated benzyl ether (C–O) bond cleavage was studied to understand utility of the probe **TPACy** under various pH range (Figure 32). **TPACy** reacted efficiently with Cu^+ in the biologically relevant pH range of 6.5–8.5 to release NIR emitting **Cy-quinone** fluorophore. Thus **TPACy** can be conveniently used as ‘switch on’ probe for the detection of Cu^+ without interference from pH-related effects in physiological media.

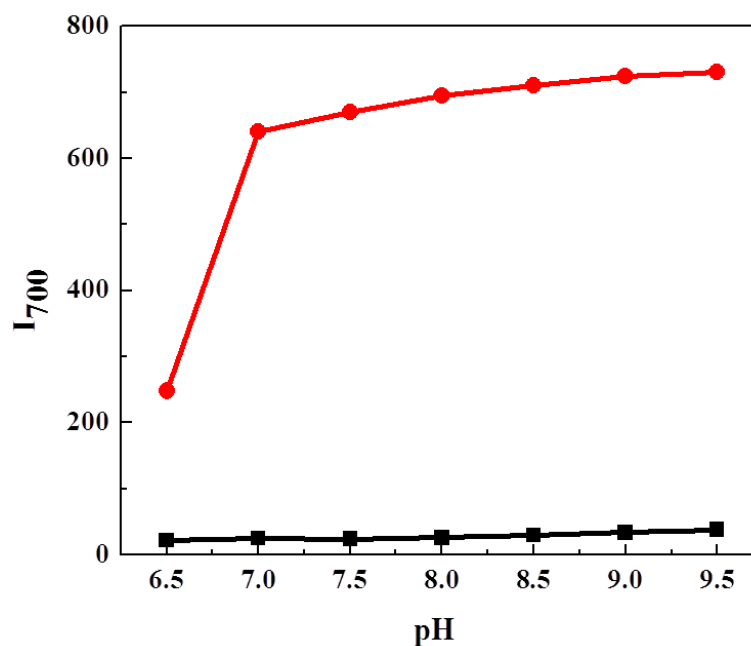


Figure 32. Effect of pH on the fluorometric property on **TPACy**. Red trace: **TPACy** (20.0 μM) with 5.0 μM of Cu^+ after 2 h in aqueous solution (50 mM HEPES). Black trace: **TPACy** (20.0 μM) in aqueous solution (50 mM HEPES).

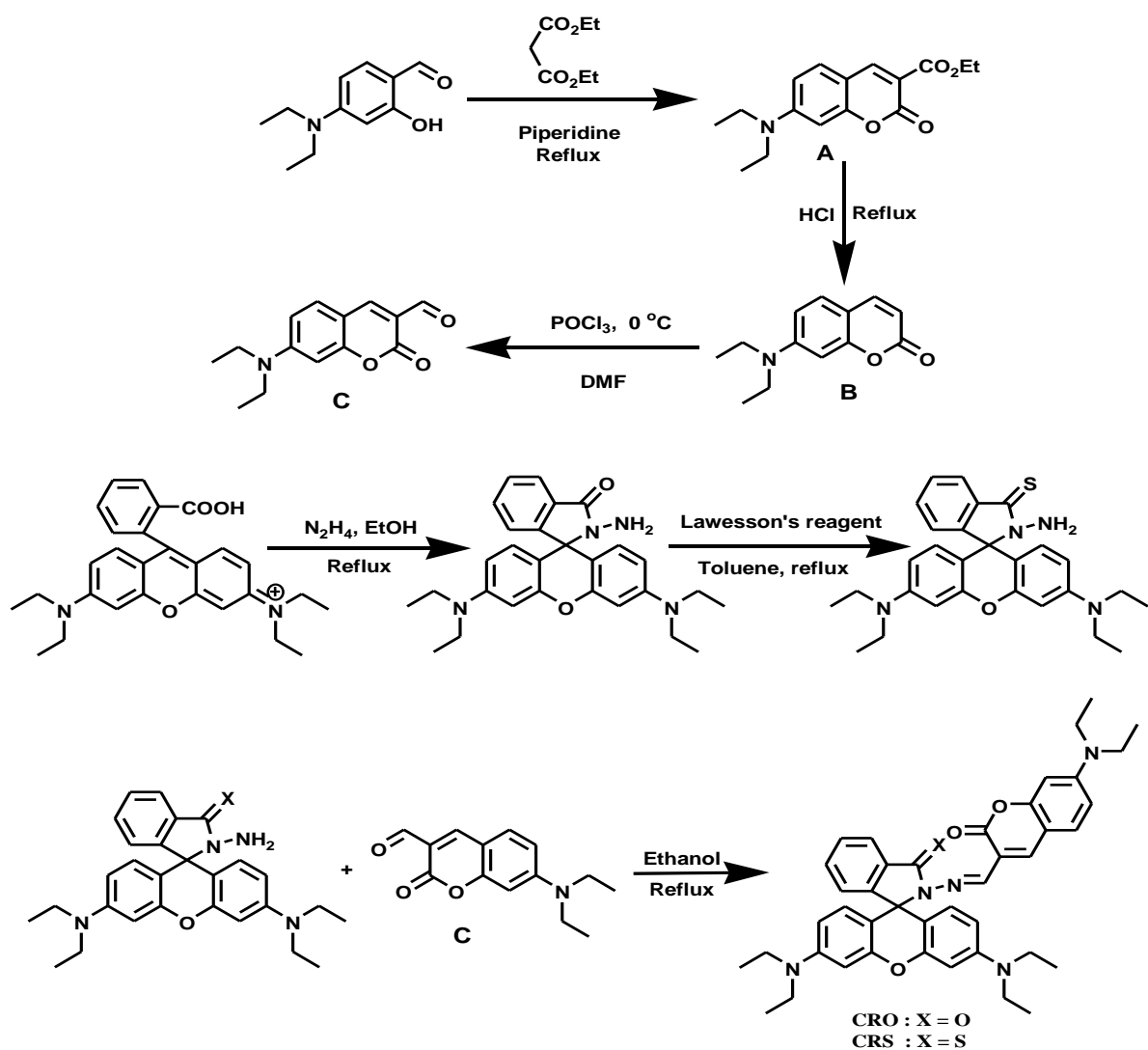
3.4.4 Conclusion

In conclusion, Cu^+ selective water soluble turn on NIR fluorescence probe **TPACy** has been successfully developed. This molecular probe readily reacts with Cu^+ to release the NIR fluorescence emitting cyanine dye over a wide pH range. Submicromolar concentration of Cu^+ can be efficiently detected as this amount is sufficient enough to react with **TPACy**, releasing NIR emitting **Cy-quinone** dye. In general, **TPACy** can be used as a non-invasive tool for the determination of Cu^+ pool in biological fluids and *in vivo* NIR fluorescence imaging applications.

3.5 FRET-based rational strategy for ratiometric detection of Cu²⁺ and live cell imaging

3.5.1 Synthesis

7-Diethylamino-2-oxo-2H-chromene-3-carboxylic acid ethyl ester (**A**) was synthesized refluxing a mixture of 4-diethylamino salicylaldehyde, diethylmalonate, and piperidine in toluene. The ester **A** undergoes acid catalyzed decarboxylation to form 7-diethylamino-



Scheme 9. Synthesis of coumarin-rhodamine hydrazone (**CRO**) and coumarin-rhodamine thiohydrazone (**CRS**).

chromene-2-one (**B**) which was further subjected to Vilsmeier–Haack reaction to obtain 7-diethylamino-2-oxo-2H-chromene-3-carboxyldehyde (**C**) in excellent yield. Rhodamine B hydrazide was synthesized by refluxing rhodamine B and hydrazine hydrate in ethanol. Rhodamine thiohydrazide was synthesized using Lawesson's reagent from Rhodamine B hydrazide. Molecular probes coumarin-rhodamine hydrazone (**CRO**) and coumarin-rhodamine thiohydrazone (**CRS**) were prepared by condensing rhodamine hydrazide and rhodamine thiohydrazide with 7-diethylamino-coumarin-3-aldehyde (**C**) respectively in ethanol (Scheme 9). These two Schiff bases were characterized by NMR and mass spectroscopy, and elemental analysis.

3.5.2 Spectral properties of **CRO**

The photophysical properties of **CRO** were investigated with absorption and fluorescence studies upon addition of several metal ions such as Li^+ , Na^+ , Ba^{2+} , Sr^{2+} , Mg^{2+} , Al^{3+} , Ca^{2+} , Mn^{2+} , Fe^{2+} , Co^{2+} , Ni^{2+} , Zn^{2+} , Ag^+ , Cd^{2+} , Hg^{2+} , Pb^{2+} , and Cu^{2+} in an aqueous buffer medium (50 mM HEPES/ CH_3CN , 6:4, v/v; pH 7.2). Rhodamine hydrazide moiety in spirolactam form of **CRO** absorbs in the UV region (Figure 33). Free **CRO** absorbs around 460 nm

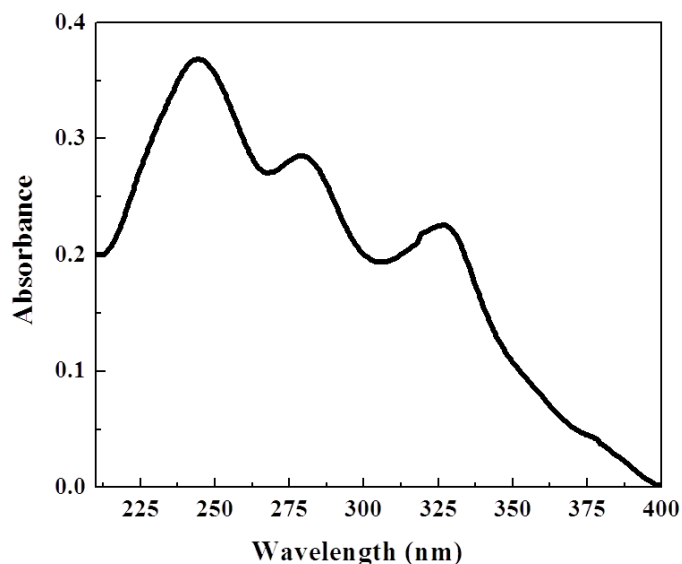


Figure 33. UV-Vis absorption spectra of rhodamine hydrazide (10.0 μM) in aqueous medium (50 mM HEPES: CH_3CN , 6:4, v/v; pH=7.2).

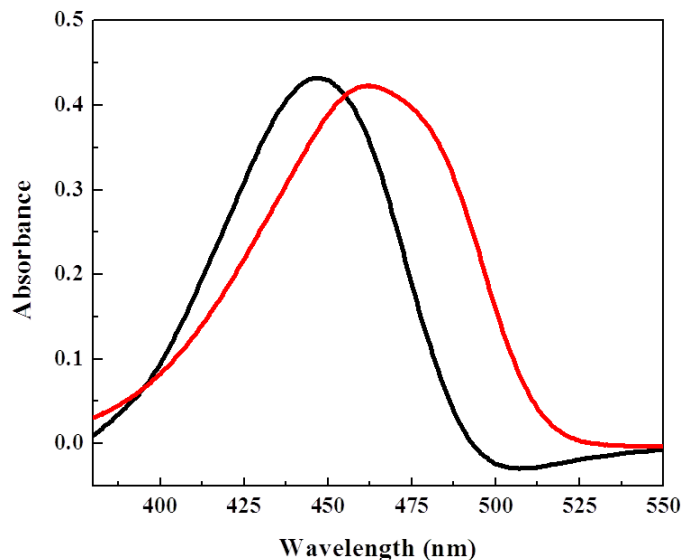


Figure 34. UV-Vis absorption spectra of 7-diethylamino-coumarin-3-aldehyde (10.0 μM) (in black) and coumarin rhodamine hydrazone (**CRO**) (10.0 μM) (in red) in aqueous medium (50 mM HEPES: CH_3CN , 6:4, v/v; pH=7.2).

which is actually the absorbance of coumarin chromophore as confirmed by the absorption study of 7-diethylamino-coumarin-3-aldehyde in aqueous media (Figure 34). The absorbance at 460 nm remained unchanged on addition of various metal ions except Cu^{2+} as shown in Figure 35. Upon addition of Cu^{2+} , the absorbance at 460 nm was decreased and slowly red shifted to 475 nm with generation of a new peak at 556 nm, which indicated the generation of rhodamine chromophore in visible region. Yellow colored probe (**CRO**) solution turned to bright red upon metal ion complexation (**CRO**- Cu^{2+}). In the Figure 36, an isosbestic point was observed at 481 nm when spectra were recorded with varying concentrations of Cu^{2+} . **CRO** can detect minimum 20 μM of Cu^{2+} ratiometrically with color change in aqueous buffer medium (50 mM HEPES/ CH_3CN , 6:4, v/v; pH 7.2). Free **CRO** emits in the green region and its fluorescence emission band positioned at 524 nm which is characteristic for N, N-diethyl coumarin moiety upon excitation at 480 nm (Figure 37). Except Cu^{2+} , addition of various other metal ions has no effect on the emission of **CRO** whereas few metal ions showed slight quenching of the fluorescence. Upon sequential addition of Cu^{2+} , the coumarin emission signal intensity at 524 nm was decreased, and strong red colored emission signal corresponding to ring-opened rhodamine appeared at 582 nm (Figure 38). A clear isosbestic

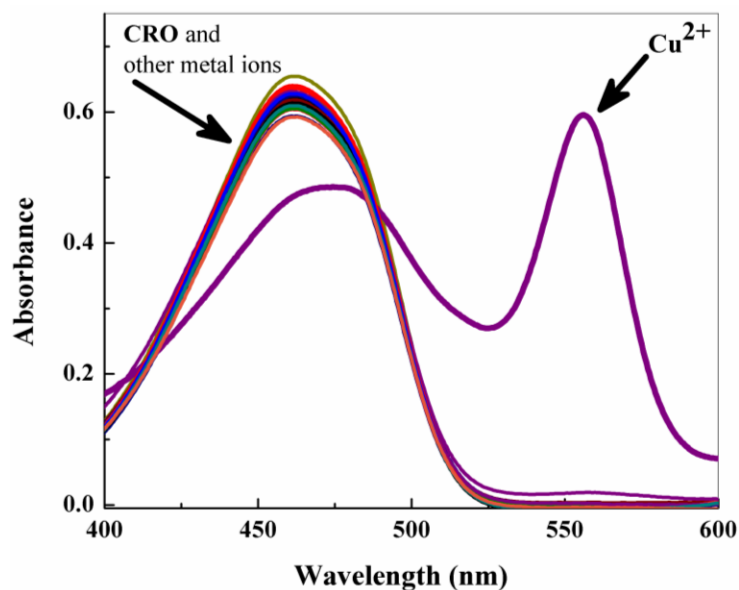


Figure 35. UV-Vis absorption spectra of **CRO** (10.0 μM) and on addition of salts (50.0 equiv) of Li^+ , Na^+ , Ba^{2+} , Sr^{2+} , Mg^{2+} , Al^{3+} , Ca^{2+} , Mn^{2+} , Fe^{2+} , Co^{2+} , Ni^{2+} , Zn^{2+} , Ag^+ , Cd^{2+} , Hg^{2+} , Pb^{2+} and Cu^{2+} in aqueous media (50 mM HEPES: CH_3CN , 6:4, v/v; pH=7.2).

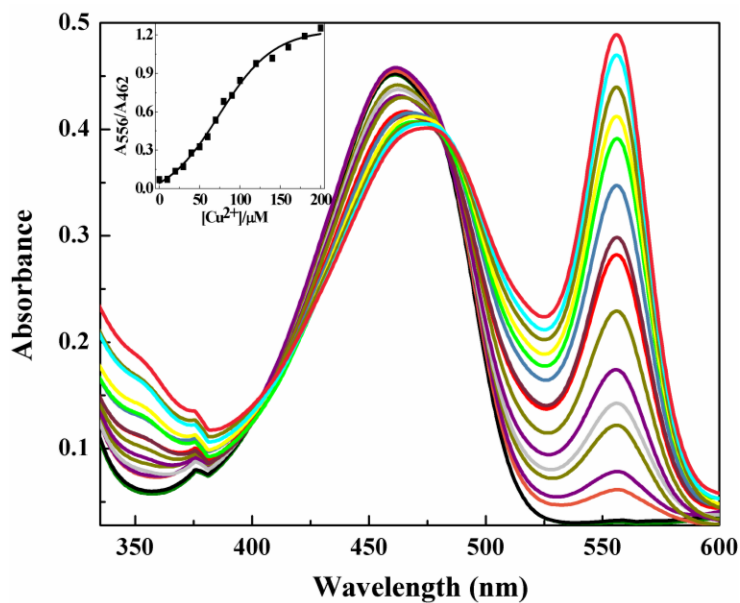


Figure 36. UV-Vis absorption spectra of **CRO** (10.0 μM) on addition of different concentrations of Cu^{2+} (0, 10, 20, 30, 40, 50, 60, 70, 80, 90, 100, 120, 140, 160, 180 and 200 μM) in aqueous media (50 mM HEPES: CH_3CN , 6:4, v/v; pH=7.2). Inset: Ratiometric absorbance $[A_{556}/A_{462}]$ as a function of $[\text{Cu}^{2+}]$.

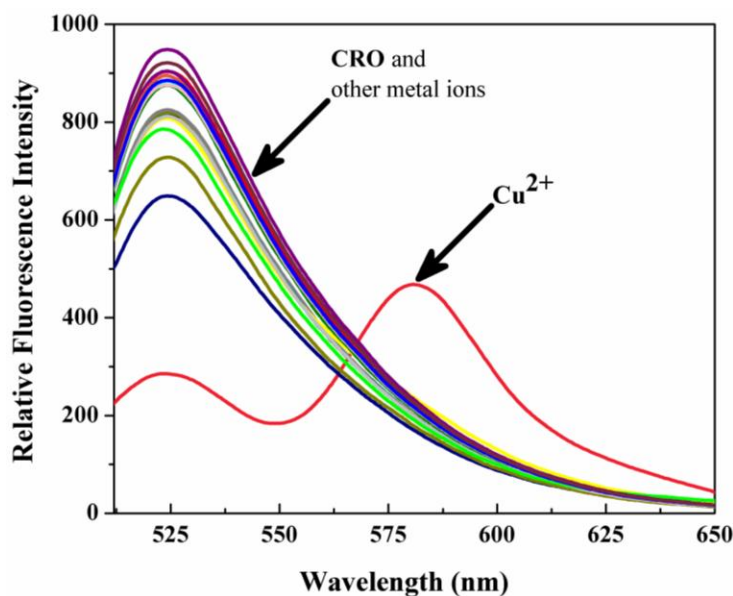


Figure 37. Fluorescence spectra of **CRO** (10.0 μM) and on addition of salts (50.0 equiv) of Li^+ , Na^+ , Ba^{2+} , Sr^{2+} , Mg^{2+} , Al^{3+} , Ca^{2+} , Mn^{2+} , Fe^{2+} , Co^{2+} , Ni^{2+} , Zn^{2+} , Ag^+ , Cd^{2+} , Hg^{2+} , Pb^{2+} and Cu^{2+} in aqueous media (50 mM HEPES: CH_3CN , 6:4, v/v; pH=7.2).

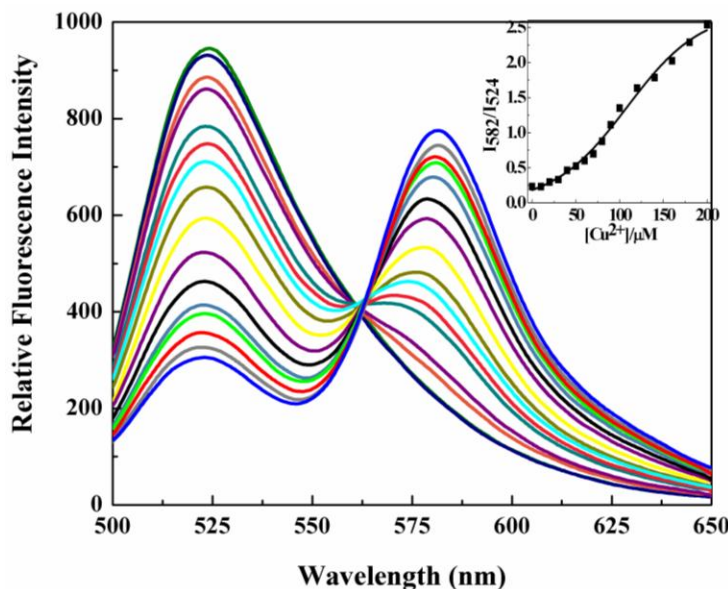


Figure 38. Fluorescence spectra of **CRO** (10.0 μM) on addition of different concentrations of Cu^{2+} (0, 10, 20, 30, 40, 50, 60, 70, 80, 90, 100, 120, 140, 160, 180 and 200 μM) in aqueous media (50 mM HEPES: CH_3CN , 6:4, v/v; pH=7.2). Inset: Ratiometric intensity [I_{582}/I_{524}] as a function of [Cu^{2+}].

point was observed at 562 nm when spectra were recorded with varying concentrations of Cu^{2+} . **CRO** can detect at least down to 20 μM of Cu^{2+} by means of ratiometric fluorescence emission in aqueous buffer medium (50 mM HEPES/ CH_3CN , 6:4, v/v; pH 7.2). The overlap integral between emission of N, N-diethyl coumarin moiety and absorption of ring-opened zwitterionic rhodamine unit as shown in Figure 39 further support the possibility of FRET mechanism in aqueous buffer medium (50 mM HEPES/ CH_3CN , 6:4, v/v; pH 7.2).

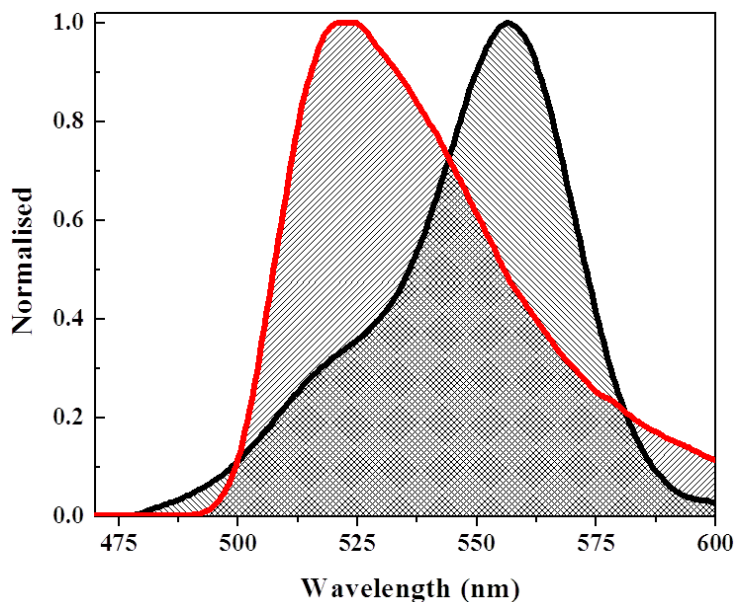


Figure 39. The spectral overlap between emission of N, N-diethyl coumarin carboxaldehyde (red) and absorbance of ring opened rhodamine unit (black) in **CRO** system.

3.5.3 Spectral properties of CRS

The photophysical properties of **CRS** were investigated by undertaking the absorption and fluorescence studies upon addition of various metal ions in an aqueous buffer medium (50 mM HEPES/ CH_3CN , 6:4, v/v; pH 7.2). Rhodamine-thiolactam hydrazide also absorbs in the UV region (Figure 40). Free **CRS** absorbs around 475 nm and spectrum is well overlapped with absorbance spectra of 7-diethylamino-coumarin-3-aldehyde in aqueous media (Figure 41). Addition of Li^+ , Na^+ , Ba^{2+} , Sr^{2+} , Mg^{2+} , Al^{3+} , Ca^{2+} , Mn^{2+} , Fe^{2+} , Ni^{2+} , Zn^{2+} , Cd^{2+} and Pb^{2+} to **CRS** solution has no effect. Upon addition of Co^{2+} , Cu^{2+} , Ag^+ and Hg^{2+} , absorption spectra

are red shifted to different extents with the generation of new peak around 560 nm indicating ring opening of rhodamine-thiolactam in presence of these metal ions (Figure 42). The fluorometric behavior of CRS was investigated upon addition of metal ions in an aqueous

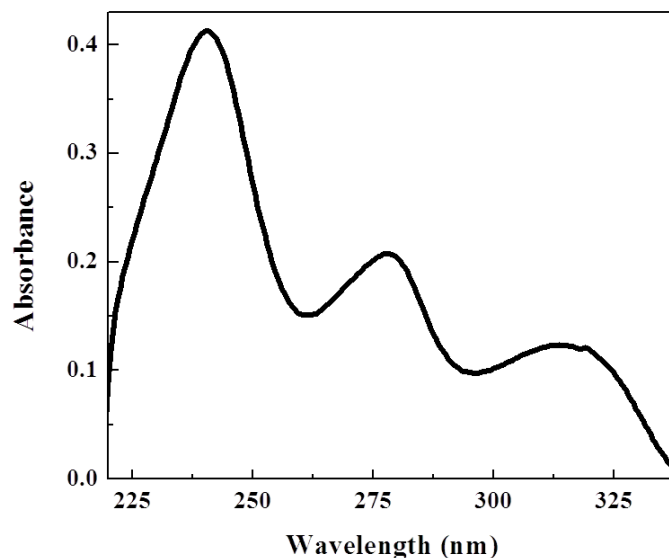


Figure 40. UV-Vis absorption spectra of rhodamine thiohydrazide (10.0 μM) in aqueous medium (50 mM HEPES:CH₃CN, 6:4, v/v; pH=7.2).

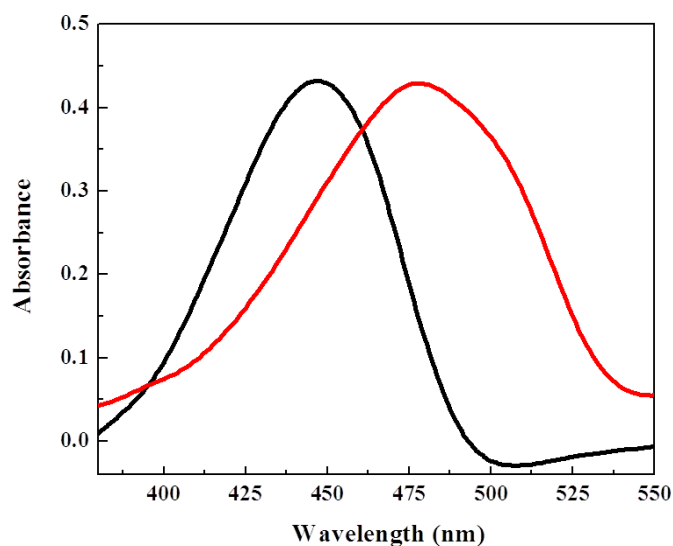


Figure 41. UV-Vis absorption spectra of 7-diethylamino-coumarin-3-aldehyde (10.0 μM) (in black) and coumarin rhodamine thiohydrazone (10.0 μM) (in red) in aqueous medium (50 mM HEPES:CH₃CN, 6:4, v/v; pH=7.2).

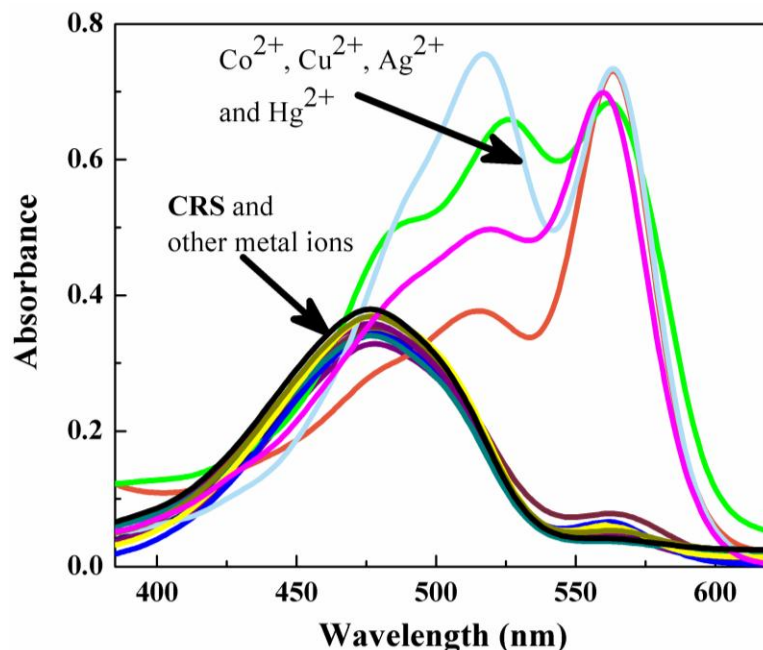


Figure 42. UV-Vis absorption spectra of coumarin-rhodamine thiohydrazone (CRS) (10.0 μM) and on addition of salts (50.0 equiv) of Li^+ , Na^+ , Ba^{2+} , Sr^{2+} , Mg^{2+} , Al^{3+} , Ca^{2+} , Mn^{2+} , Fe^{2+} , Co^{2+} , Ni^{2+} , Zn^{2+} , Ag^+ , Cd^{2+} , Hg^{2+} , Pb^{2+} and Cu^{2+} in aqueous medium (50 mM HEPES: CH_3CN , 6:4, v/v; pH=7.2).

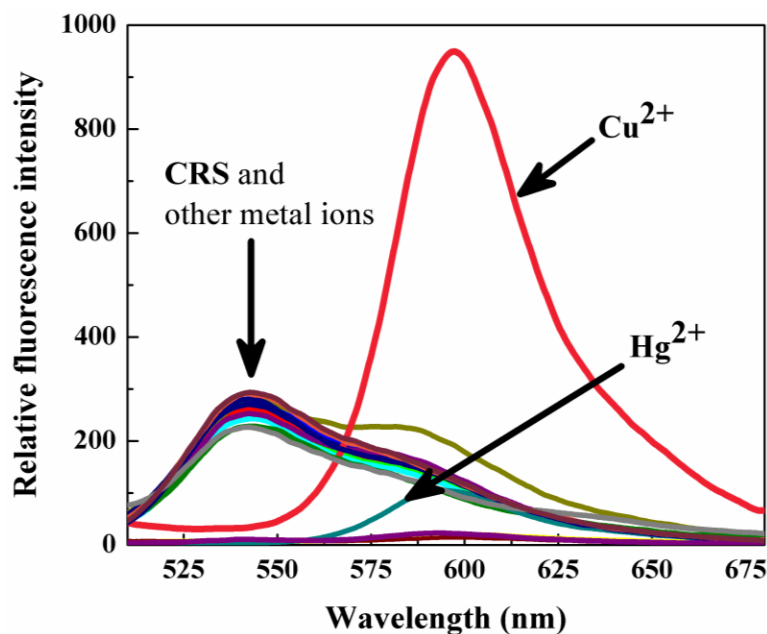


Figure 43. Fluorescence spectra of CRS (10.0 μM) and on addition of salts (50.0 equiv) of Li^+ , Na^+ , Ba^{2+} , Sr^{2+} , Mg^{2+} , Al^{3+} , Ca^{2+} , Mn^{2+} , Fe^{2+} , Co^{2+} , Ni^{2+} , Zn^{2+} , Ag^+ , Cd^{2+} , Hg^{2+} , Pb^{2+} and Cu^{2+} in aqueous media (50 mM HEPES: CH_3CN , 6:4, v/v; pH=7.2).

buffer medium (50 mM HEPES/ CH_3CN , 6:4, v/v; pH 7.2) as shown in Figure 43. **CRS** emits weak fluorescence positioned around 540 nm upon excitation at 480 nm. This emission was relatively unaffected by most of metal ions tested. However fluorescence emission was quenched by few transition and heavy transition metal ions. In case of Hg^{2+} , weak fluorescence of **CRS** was quenched with an appearance of another weak fluorescence band at 590 nm. Interestingly, addition of Cu^{2+} to the solution of **CRS**, coumarin weak emission signal at 540 nm was quenched, with the appearance of strong orange colored emission at 590 nm. The ratiometric titration of Cu^{2+} with **CRS** is shown in Figure 44. Employing ratiometric fluorescence emission property of **CRS** minimum 20 μM of Cu^{2+} can be detected in aqueous buffer medium (50 mM HEPES/ CH_3CN , 6:4, v/v; pH 7.2). The overlap integral between emission of N,N-diethyl coumarin moiety and absorption of ring-opened zwitterionic thiorhodamine unit further strengthened the existence of FRET mechanism in aqueous buffer medium (50 mM HEPES/ CH_3CN , 6:4, v/v; pH 7.2) (Figure 45).

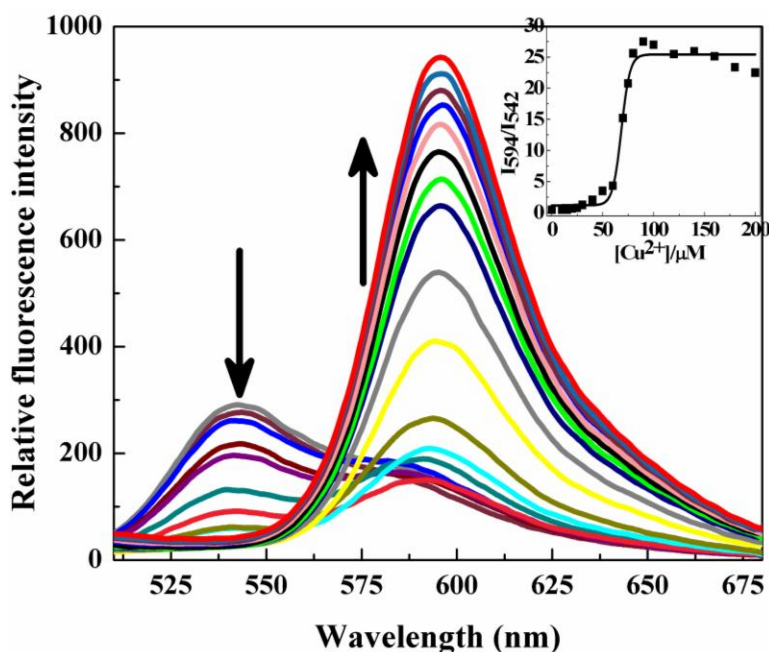


Figure 44. Fluorescence spectra of **CRS** (10.0 μM) on addition of different concentrations of Cu^{2+} (0, 10, 15, 20, 25, 30, 40, 50, 60, 70, 75, 80, 90, 100, 120, 140, 160, 180 and 200 μM) in aqueous media (50 mM HEPES: CH_3CN , 6:4, v/v; pH=7.2). Inset: Ratiometric intensity [I_{594}/I_{542}] as a function of [Cu^{2+}].

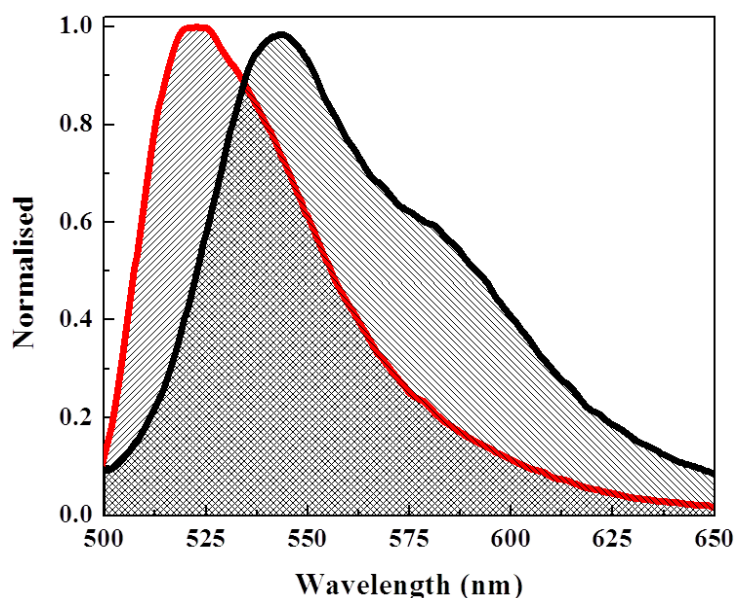


Figure 45. The spectral overlap between emission of N, N-diethyl coumarin carboxaldehyde (red) and absorbance of ring opened thiorhodamine unit (black) in **CRS** system.

3.5.4 Competitive binding experiment

Selectivity of **CRO** and **CRS** towards Cu^{2+} were studied in the presence of various competing metal ions. For these purpose ligands **CRO** and **CRS** were treated with a mixture of 10.0 equiv of Cu^{2+} and 10.0 equiv of all other metal ions. Data shown in Figure 46 confirms that using **CRO** as chemosensor there is no interference for the detection of Cu^{2+} colorimetrically as well as fluorometrically in the presence of all other metal ions tested. Thus **CRO** can be used as a selective probe for Cu^{2+} in the presence of most competing metal ions. Since Co^{2+} , Cu^{2+} , Ag^+ and Hg^{2+} ions show red coloration, **CRS** cannot be used as colorimetric chemosensor for any particular metal ion. However Cu^{2+} can be successfully detected in presence of other competing metal ions using **CRS** probe employing ratiometric fluorescence property (Figure 47).

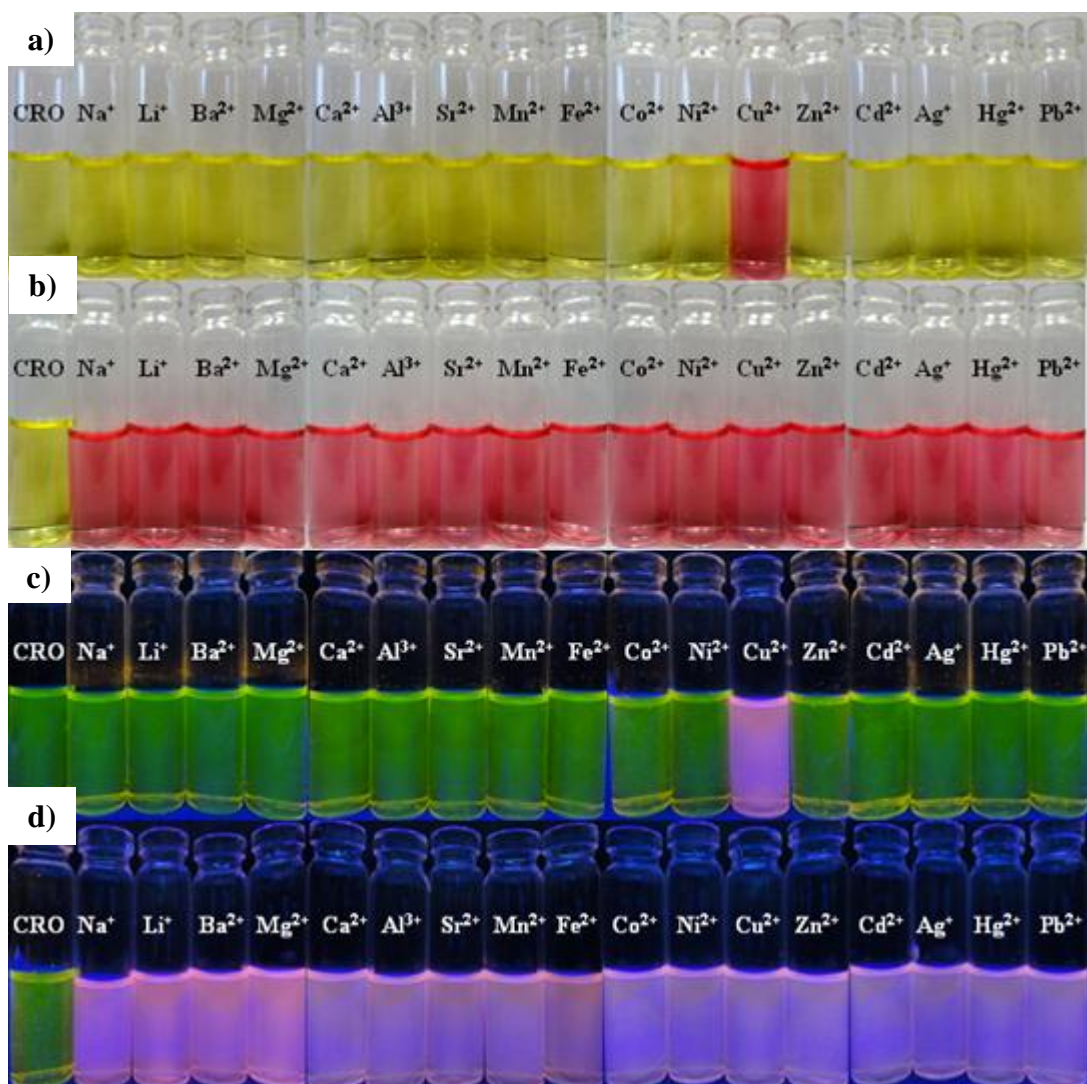


Figure 46. Competitive study of coumarin rhodamine hydrazone (**CRO**) with all metal ions for selective detection of Cu^{2+} in aqueous medium (50 mM HEPES: CH_3CN , 6:4, v/v; pH=7.2). a) Selective color change observed only for Cu^{2+} . b) Selective colorimetric detection of Cu^{2+} in presence of other metal ions. c) Selective fluorescence color change observed only for Cu^{2+} . d) Selective fluorometric detection of Cu^{2+} in presence of other metal ions. For competitive study, **CRO** (10.0 μM) was treated with 10.0 equiv of Cu^{2+} in presence of 10.0 equiv of other metal ions.

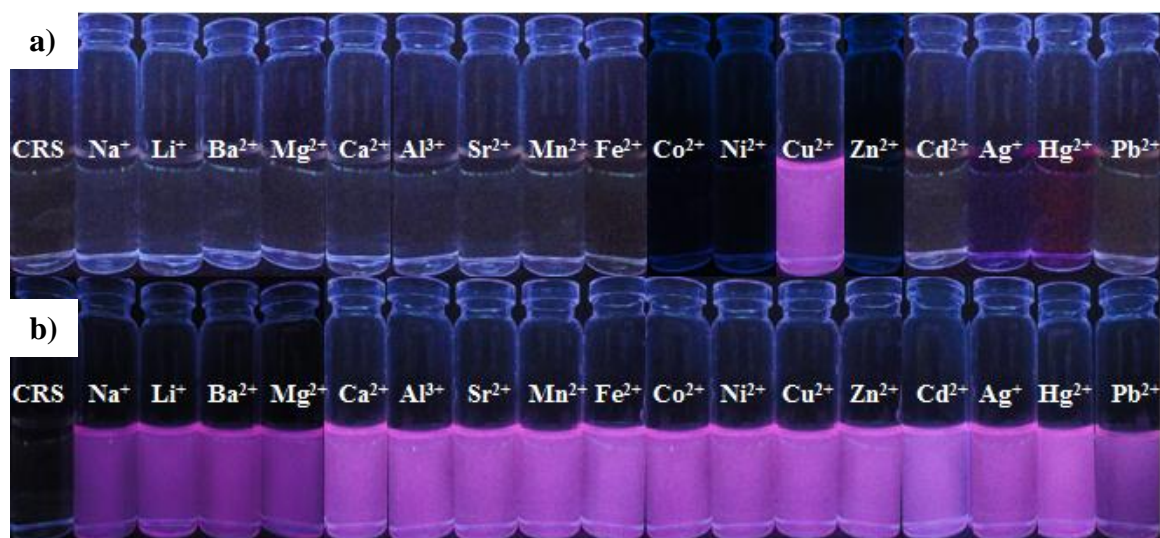


Figure 47. Competitive study of coumarin rhodamine thiohydrazone (**CRS**) with all metal ions for selective detection of Cu^{2+} in aqueous medium (50 mM HEPES: CH_3CN , 6:4, v/v; pH=7.2). a) Selective fluorescence color change observed only for Cu^{2+} . b) Selective fluorometric detection of Cu^{2+} in presence of other metal ions. For competitive study, **CRS** (10.0 μM) was treated with 10.0 equiv of Cu^{2+} in presence of 10.0 equiv of other metal ions.

3.5.5 Stoichiometry of binding, response parameter and binding constant determination

The stoichiometry of binding of Cu^{2+} to probes **CRO** and **CRS** were studied by various analytical techniques. Job's plots from UV-Vis absorbance data show 1:1 stoichiometric complexation between **CRO/CRS** with Cu^{2+} (Figure 48 and 49). This data was further supported by mass spectrometry analysis. MALDI/TOF-MS showed the formation of a complex between **CRO** and one copper ion: $[\text{C}_{42}\text{H}_{45}\text{CuN}_5\text{O}_4]^{2+}$; m/z: 746.14; calcd for $[\text{C}_{42}\text{H}_{45}\text{CuN}_5\text{O}_4]^{2+}$: 746.27. MALDI/TOF-MS also showed the formation of a complex between **CRS** and one copper ion: $[\text{C}_{42}\text{H}_{45}\text{CuN}_5\text{O}_3\text{S}]^{2+}$; m/z: 762.17; calcd for $[\text{C}_{42}\text{H}_{45}\text{CuN}_5\text{O}_3\text{S}]^{2+}$: 762.25. (Figure 50 and 51). The response parameter (α) which is defined as the ratio of free ligand concentration to the initial concentration of ligand is plotted as a function of Cu^{2+} concentration (Figure 52 and 53). This plot can serve as the calibration curve for the detection of Cu^{2+} . The association constant ($\log K_a$) of ligands **CRO** and **CRS** with Cu^{2+} was calculated to be 8.81 and 8.75 M^{-1} respectively.

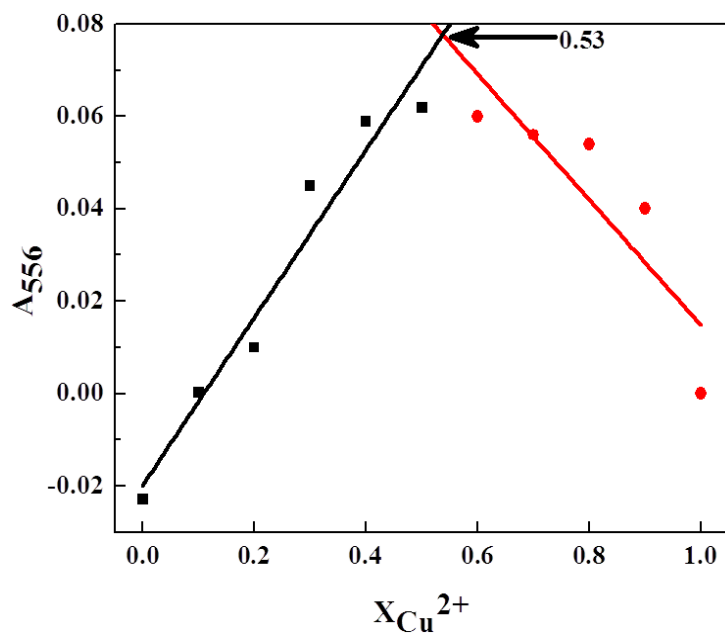


Figure 48. Absorbance at 556 nm of coumarin rhodamine hydrazone (CRO) and Cu^{2+} with a total concentration of 40 μM in aqueous medium (50 mM HEPES:CH₃CN, 6:4, v/v; pH=7.2).

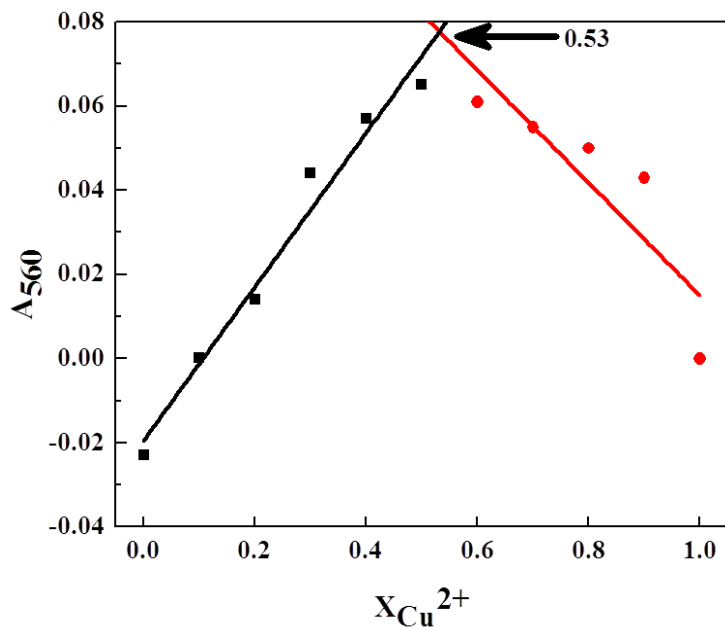


Figure 49. Absorbance at 560 nm of coumarin rhodamine hydrazone (CRS) and Cu^{2+} with a total concentration of 40 μM in aqueous medium (50 mM HEPES:CH₃CN, 6:4, v/v; pH=7.2).

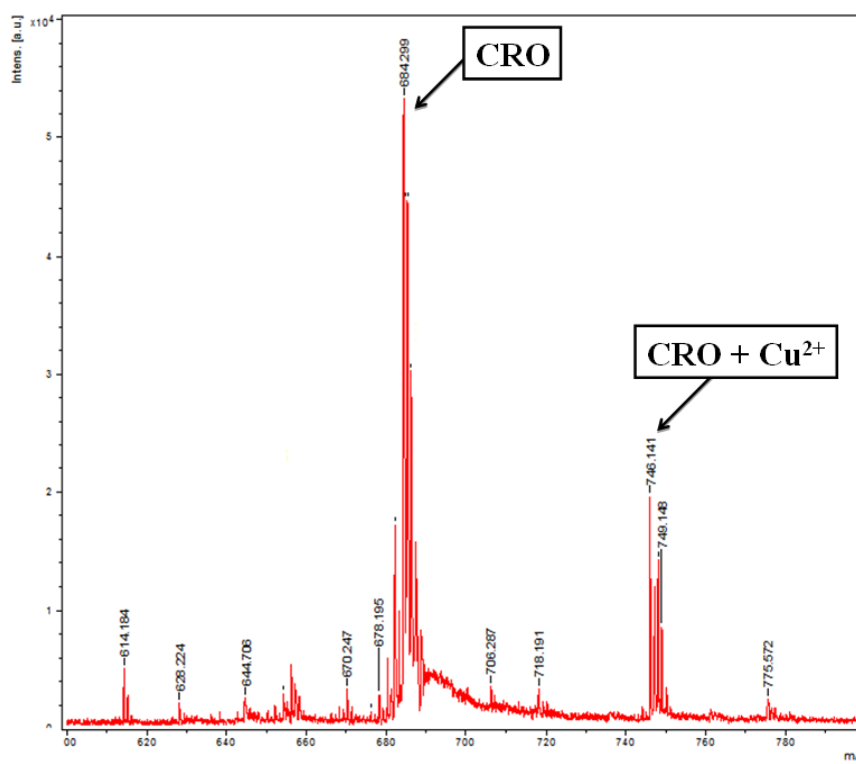


Figure 50. MALDI-TOF mass spectrum of coumarin rhodamine hydrazone [CRO-Cu²⁺] complex.

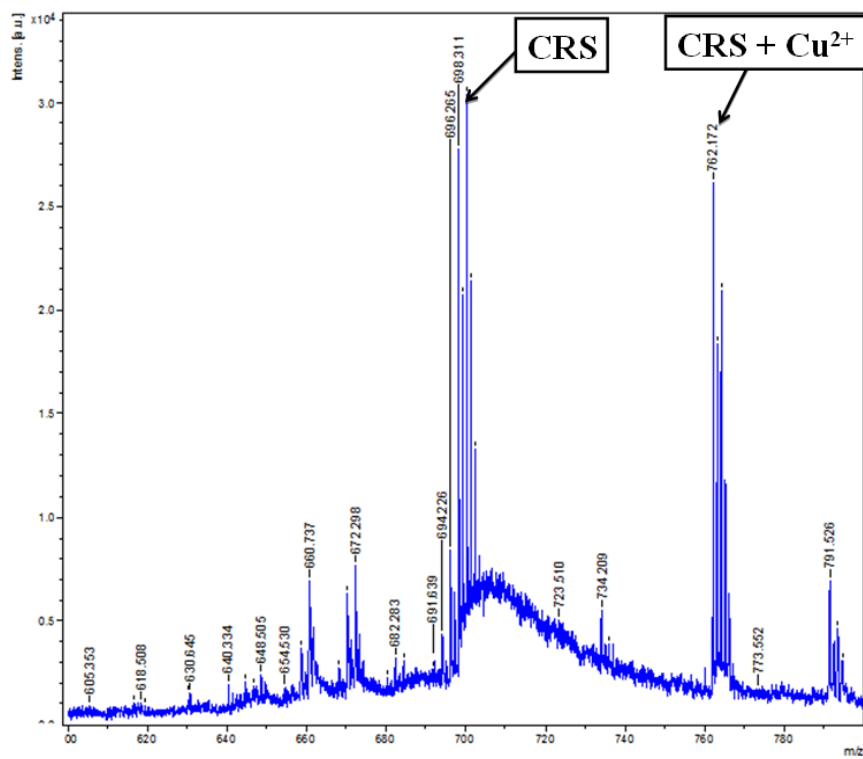


Figure 51. MALDI-TOF mass spectrum of coumarin rhodamine thiohydrazone [CRS-Cu²⁺] complex.

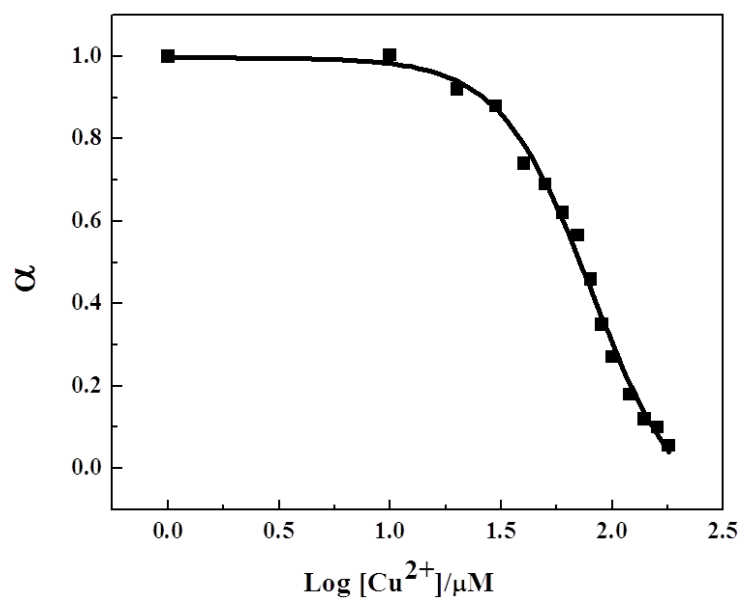


Figure 52. Response parameter values (α) of coumarin rhodamine hydrazone (CRO) as a function of the logarithm of $[\text{Cu}^{2+}]$. α is defined as the ratio between the free ligand concentration and the initial concentration of ligand.

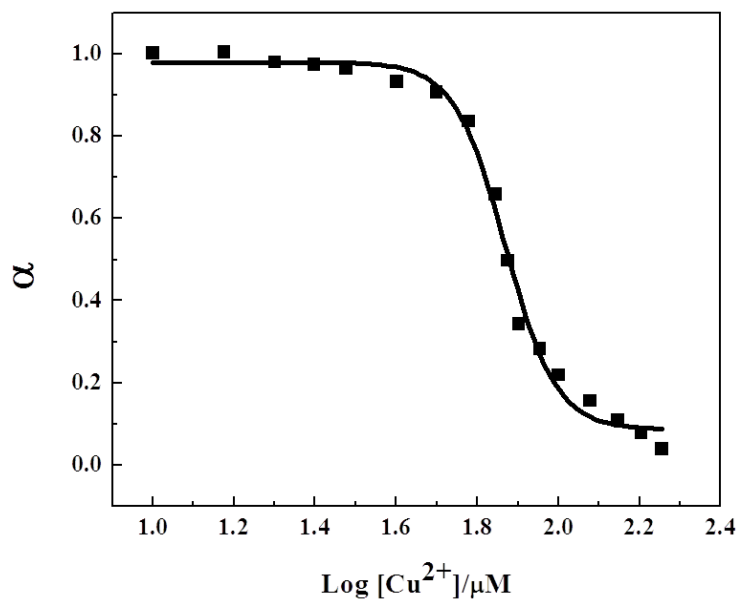


Figure 53. Response parameter values (α) of coumarin rhodamine thiohydrazone (CRS) as a function of the logarithm of $[\text{Cu}^{2+}]$. α is defined as the ratio between the free ligand concentration and the initial concentration of ligand.

3.5.6 pH dependence study

The influence of pH on the absorbance and fluorescence property of probe **CRO** upon complexation with Cu^{2+} was studied in aqueous media (50 mM HEPES/ CH_3CN , 6:4, v/v). Cu^{2+} can be clearly detected colorimetrically using **CRO** over a broad pH range of 3–9 (Figure 54). **CRO** also can be used to detect Cu^{2+} fluorometrically over a pH range of 5.5–10 (Figure 55). **CRS** detects Cu^{2+} fluorometrically in the most common physiological pH range of 6–9 (Figure 56). Therefore both probes **CRO** and **CRS** can be used for the environmental monitoring and biological detection of copper in most of commonly encountered pH ranges.

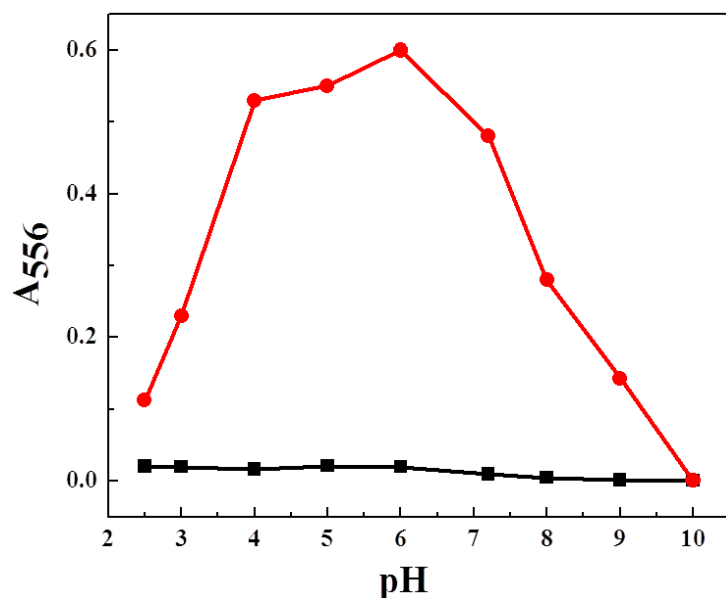


Figure 54. Dependence of the absorbance at 556 nm of coumarin rhodamine hydrazone (**CRO**) on pH. Black trace: ligand (10 μM) and red trace: ligand with 10.0 equiv of Cu^{2+} in aqueous medium (50 mM HEPES: CH_3CN , 6:4, v/v).

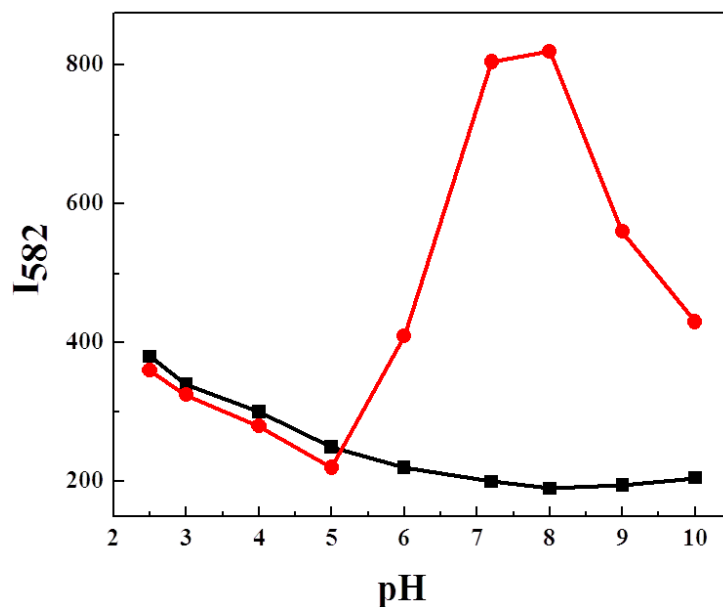


Figure 55. Dependence of the fluorescence intensity at 582 nm of coumarin rhodamine hydrazone (**CRO**) on pH. Black trace: ligand (10 μM) and red trace: ligand with 10.0 equiv of Cu^{2+} in aqueous medium (50 mM HEPES:CH₃CN, 6:4, v/v).

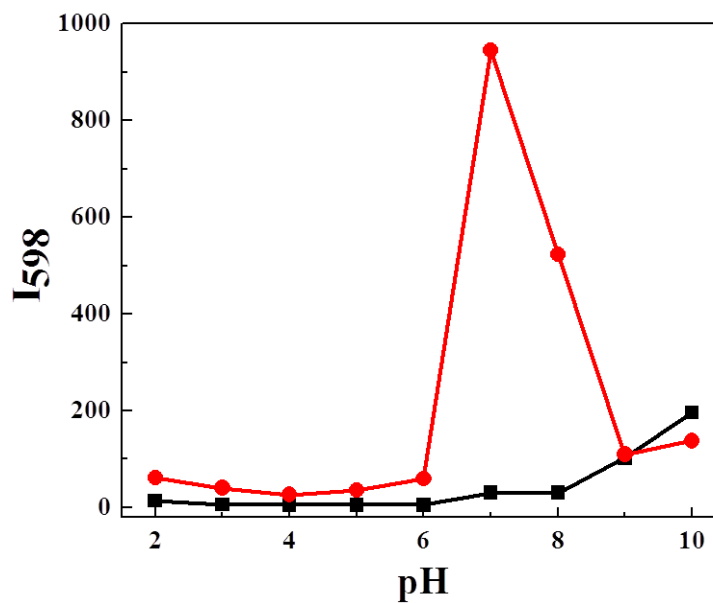


Figure 56. Dependence of the fluorescence intensity at 598 nm of coumarin rhodamine thiohydrazone (**CRS**) on pH. Black trace: ligand (10 μM) and red trace: ligand with 10.0 equiv of Cu^{2+} in aqueous medium (50 mM HEPES:CH₃CN, 6:4, v/v).

3.5.7 Bioimaging

Subsequent experiments proved the ability of **CRO** and **CRS** to track Cu^{2+} levels in living cells by using fluorescence microscopy (Figure 57 and 58). HEK293T cells were seeded in 35 mm culture dishes and grown to 40% confluence in Dulbecco's modified eagle medium (DMEM) media containing 10% Fetal bovine serum at 37°C in presence of 5% CO_2 and then supplemented with 10 μM of **CRO/CRS** for 24 h. At the end of 24 h, cells were washed with phosphate buffered saline to remove the residual compound in the media and the cells show intense fluorescence in the green channel and no fluorescence in red channel. Then cells were supplemented with DMEM containing 10% fetal bovine serum (FBS) and 20 μM Cu^{2+} and allowed to grow for 2 h. After treatment with Cu^{2+} , **CRO/CRS** loaded cells exhibit partial fluorescence in the green channel where as strong fluorescence in the red channel. These results indicate that **CRO** and **CRS** both are cell membrane permeable and could be employed for ratiometric fluorescence imaging of Cu^{2+} level in the living cells.

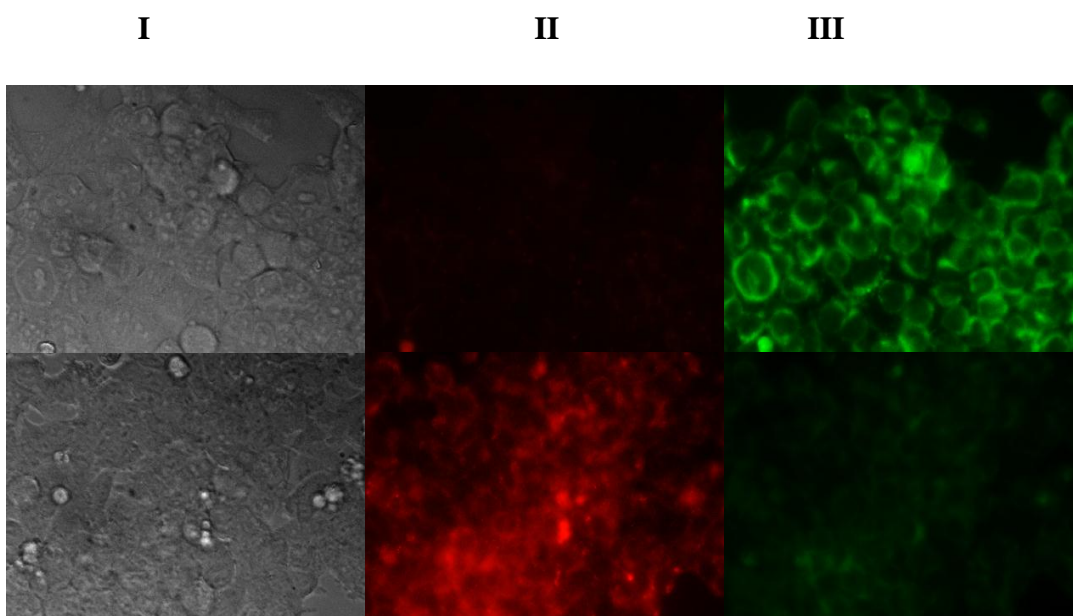


Figure 57. Top and bottom panel represents the HEK293T cells pre-incubated with 10 μM of compound **CRO** for 24 h and then subsequently treated with 20 μM Cu^{2+} for 2 h respectively. Panel I shows the bright field images, Panel II and III are the images captured in the region of red (560 nm) and green (480 nm) fluorescence respectively.

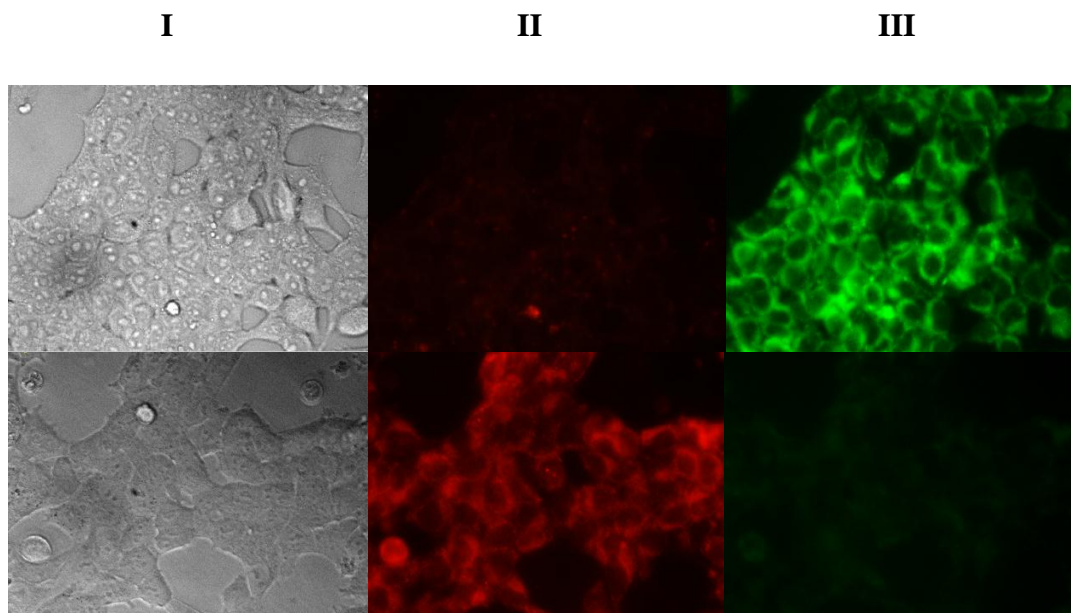


Figure 58. Top and bottom panel represents the HEK293T cells pre-incubated with 10 μM of compound **CRS** for 24 h and then subsequently treated with 20 μM Cu^{2+} for 2 h respectively. Panel I shows the bright field images, Panel II and III are the images captured in the region of red (560 nm) and green (480 nm) fluorescence respectively.

3.5.8 Conclusion

In conclusion, two probes containing coumarin as donor and rhodamine as acceptor were synthesized for ratiometric fluorescent imaging of Cu^{2+} in the living cells on the basis of Cu^{2+} induced FRET off-on mechanism. The FRET efficiency for both **CRO** and **CRS** is higher due to larger spectral overlap between acceptor and donor. These two chemosensors detect Cu^{2+} ratiometrically with two well-resolved emission peaks. The utility of **CRO** and **CRS** as ratiometric biosensor have been further demonstrated by employing them for living cell imaging of Cu^{2+} in HEK293T cells. FRET mechanism on the basis of coumarin-rhodamine platform has a great potential for the development of a wide variety of ratiometric fluorescent chemosensors due to its excellent photophysical properties.

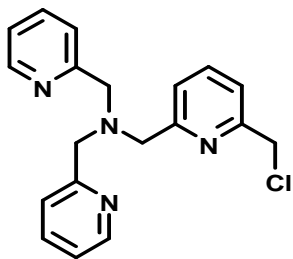
4. Experimental

4.1 General experimental procedure

All the solvents and reagents were obtained from Sigma-Aldrich and used as received unless otherwise mentioned. The solutions of metal ions were prepared from Al(ClO₄)₃·9H₂O, LiClO₄·3H₂O, NaClO₄, Mg(ClO₄)₂, Ca(ClO₄)₂·4H₂O, Sr(NO₃)₂, Ba(ClO₄)₂, Mn(ClO₄)₂·6H₂O, Fe(ClO₄)₂·H₂O, Co(ClO₄)₂·6H₂O, Cd(ClO₄)₂·H₂O, Ag(ClO₄)₂, Hg(ClO₄)₂, Pb(ClO₄)₂, Ni(ClO₄)₂·6H₂O, Cu(ClO₄)₂·6H₂O, [Cu(CH₃CN)₄]PF₆ and Zn(ClO₄)₂·6H₂O respectively in CH₃CN. ¹H and ¹³C NMR were recorded on a Bruker AV-400 spectrometer with chemical shifts reported as ppm (in CDCl₃, DMSO-*d*₆, tetramethylsilane as internal standard). Mass spectra were measured on Shimadzu 2020 LC-MS and BrukerUltraflex II MALDI/TOF spectrometers. Elemental analysis was carried out on ThermoScientific FLASH 2000 Organic Element Analyzer. UV-Vis spectra were recorded on a Perkin Elmer Model Lambda 900 spectrophotometer. HRMS were recorded on Agilent 6538 UHD Accurate-Mass Q-TOF LC/MS analyzer. Fluorescence spectra were recorded on a Perkin Elmer LS 55 spectrophotometer.

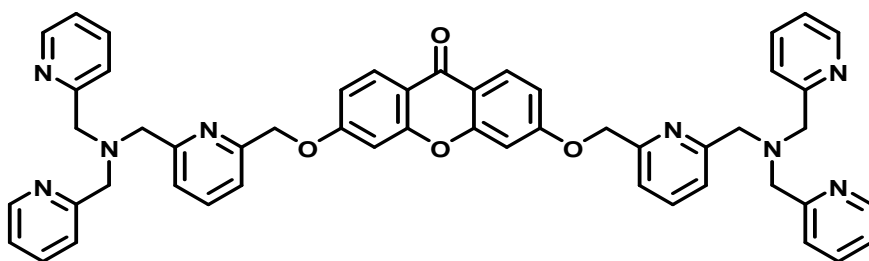
4.2 Detailed synthetic procedure

Tripicolylamine-chloride (N₄-Cl): Bis-(2-picolyl)amine (4 g, 20.0 mmol) and 2,6-bis-(chloromethyl)pyridine (3.4 g, 19.3 mmol) were dissolved in 50mL of THF and placed in a round-bottom flask. N,N-diisopropylethylamine (20 mL, 114.8 mmol) was then added to the THF solution and the reaction mixture was stirred at room temperature for 7 days. The pale yellow solution changed over time to an increasingly dark orange. A white powdery precipitate started to appear within the next few days. It was filtered and washed thoroughly with THF. The filtrate, combined with the THF solution used to wash the precipitate, was concentrated under reduced pressure to give a reddish brown oily mixture. This was purified by column chromatography over alumina using ethyl acetate/hexane (3:7) as eluent to afford the white solid (2.6 g, 40% yield). ¹H



NMR (400 MHz, *CDCl*₃) δ_{ppm} 3.89 (4H, s), 3.90 (2H, s), 4.64 (2H, s), 7.12-7.15 (2H, m), 7.31 (1H, d, *J* = 7.6 Hz), 7.52-7.58 (3H, m), 7.62-7.69 (3H, m), 8.52-8.53 (2H, m). MS (EI): *m/z* = 339.9 [M+H]⁺ for C₁₉H₁₉ClN₄. Elemental analysis: Found C, 67.33; H, 5.66; N, 16.56; Calcd. C, 67.35; H, 5.65; N, 16.54 for C₁₉H₁₉ClN₄.

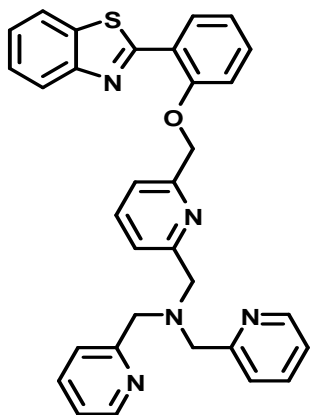
XanCu: A mixture of 3, 6-dihydroxyxanthone (50 mg, 0.22 mmol) and tripicolylamine-



chloride (**N₄-Cl**) (149 mg, 0.44 mmol) was dissolved in acetonitrile (15 mL). K₂CO₃ (600 mg, 4.4

mmol) was added and the resulting mixture was refluxed at 90°C for overnight. After cooling to room temperature, solvent was evaporated in vacuo. The residue in 50 mL of water was extracted with 3×20 mL of CH₂Cl₂. This organic layer was washed with brine, dried over Na₂SO₄, solvent was evaporated in vacuo and the residue was purified on basic alumina column (solvent. CH₂Cl₂/MeOH: 95/5) to obtain the product as light brown oil (164 mg, yield 90 %). ¹H NMR (400 MHz, *CDCl*₃) δ_{ppm} 3.92 (8H, s), 3.93 (4H, s), 5.27 (4H, s), 6.92 (1H, s), 6.93 (1H, s), 7.00 (2H, dd, *J* = 6.52 Hz, 2.36 Hz), 7.12-7.16 (4H, m), 7.35 (2H, d, *J* = 7.64 Hz), 7.53-7.58 (6H, m), 7.62-7.72 (6H, m), 8.20 (2H, d, *J* = 8.88 Hz), 8.53 (4H, m). ¹³C NMR (100 MHz, *CDCl*₃) δ_{ppm} 60.1, 71.0, 77.2, 101.4, 113.4, 116.0, 119.6, 122.1, 122.2, 123.0, 128.2, 136.5, 137.4, 149.0, 155.2, 157.8, 159.1, 159.2, 163.4, 175.4. Elemental analysis: Found: C, 73.49; H, 5.32; N, 13.46, Calcd: C, 73.54; H, 5.32; N, 13.45 for C₂₂H₂₆N₆O₂.

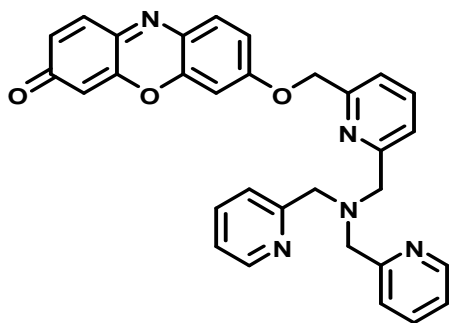
HBTCu: A mixture of 2-hydroxybenzothiazole (80 mg, 0.35mmol) and tripicolylamine-chloride (**N₄-Cl**) (143 mg, 0.42mmol) was dissolved in DMF (10 mL). K₂CO₃ (490 mg, 3.5 mmol) was added and the resulting mixture was heated at 90°C for overnight. After cooling to room temperature, the solvent was evaporated in vacuo. The residue in water (50 mL) was extracted with of CH₂Cl₂ (3×20 mL). This organic layer was washed with brine, dried over Na₂SO₄, evaporated in vacuo and the residue was purified on neutral alumina column (solvent. ethyl acetate) to obtain the product as light yellow oil (168 mg, yield 90%). ¹H



NMR (400 MHz, $CDCl_3$) δ_{ppm} 3.92 (4H, s), 3.93 (2H, s), 5.46 (2H, s), 7.08-7.16 (4H, m), 7.33-7.39 (2H, m), 7.46-7.49 (2H, m), 7.50-7.70 (6H, m), 7.86 (1H, d, $J = 7.6$ Hz), 8.08 (1H, d, $J = 8$ Hz), 8.50 (1H, dd, $J = 6.4$ Hz, 1.6 Hz), 8.53 (2H, d, $J = 4.4$ Hz). ^{13}C NMR (100MHz, $CDCl_3$) δ_{ppm} 59.0, 59.2, 70.6, 76.1, 112.0, 119.0, 120.2, 120.5, 121.0, 121.1, 121.6, 121.8, 121.9, 123.6, 124.9, 128.8, 130.7, 135.0, 135.4, 136.3, 148.1, 151.2, 154.7, 154.9, 158.1, 158.3, 162.0. HRMS: observed $m/z = 530.2014$ $[M + H]^+$ and

calculated $m/z = 530.2015$ for $C_{32}H_{28}N_5OS$.

ResCu: A mixture of resorufin sodium salt (100 mg, 0.42 mmol) and **N₄-Cl** ligand (158 mg,

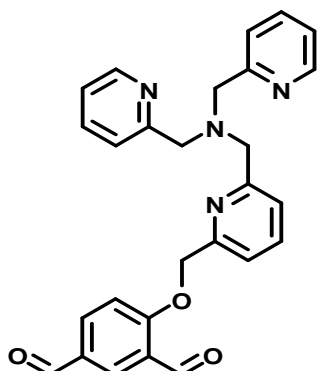


0.47 mmol) was dissolved in DMF (10 mL). K_2CO_3 (88 mg, 0.63 mmol) was added and the resulting mixture was heated at 90°C for overnight. After cooling to room temperature, the solvent was evaporated in vacuo. The residue in 50 mL of water was extracted with 3×20 mL of CH_2Cl_2 . This organic layer was washed with brine,

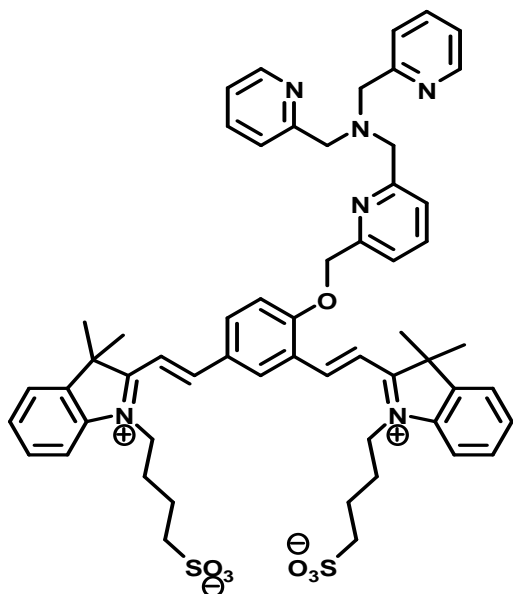
dried over Na_2SO_4 , evaporated in vacuo and the residue was purified on neutral alumina column (solvent = $CH_2Cl_2/MeOH$: 90/10) to obtain the product as red colored powder (197 mg, yield 90 %). 1H NMR (400 MHz, $CDCl_3$) δ_{ppm} 3.90 (4H, s), 3.93 (2H, s), 5.27 (2H, s), 6.27 (1H, d, $J = 2$ Hz), 6.81 (1H, dd, $J = 7.6$ Hz, 2 Hz), 6.90 (1H, d, $J = 2.4$ Hz), 7.01 (1H, dd, $J = 6.4$ Hz, 2.4 Hz), 7.13-7.16 (2H, m), 7.33 (1H, d, $J = 7.6$ Hz), 7.39 (1H, d, $J = 10$ Hz), 7.55-7.57 (3H, m), 7.62-7.72 (4H, m), 8.53 (2H, d, $J = 4$ Hz). ^{13}C NMR (100 MHz, $CDCl_3$) δ_{ppm} 58.9, 59.1, 70.5, 100.3, 105.7, 113.0, 118.7, 121.0, 121.4, 121.9, 127.5, 130.6, 133.2, 133.6, 135.3, 136.3, 144.5, 144.8, 148.1, 148.7, 153.8, 158.2, 158.4, 161.3, 185.2. HRMS: observed $m/z = 516.2022$ $[M + H]^+$ and calculated $m/z = 516.2036$ for $C_{31}H_{26}N_5O_3$.

N₄O-bda: A mixture of 4-hydroxy-1,3-benzenedicarboxaldehyde (221 mg, 1.48 mmol), **N₄-Cl** ligand (500 mg, 1.48 mmol) was dissolved in CH_3CN (80 mL). K_2CO_3 (2 g, 14.76 mmol) was added and the resulting mixture was refluxed at 90°C for overnight. After cooling to room temperature, the mixture was filtered. The residue was washed thoroughly with

CH₃CN. Then total filtrate was evaporated in vacuo to obtain residue. This residue was dissolved in 50 mL of CH₂Cl₂ was extracted with 3×20 mL of brine solution. Finally the organic layer was washed with 2×20 mL water, dried over Na₂SO₄, evaporated in vacuo and the residue was purified on neutral alumina column (solvent = CH₂Cl₂/MeOH: 90/10) to obtain the product (600 mg, yield 90 %). ¹H NMR (400 MHz, CDCl₃) δ_{ppm} 3.97 (6H, s), 5.39 (2H, s), 7.16-7.19 (2H, t, *J* = 6.4 Hz), 7.24 (1H, d, *J* = 8.8 Hz), 7.36 (1H, d, *J* = 7.6 Hz), 7.56-7.59 (3H, m), 7.65-7.75 (3H, m), 8.05-8.08 (1H, dd, *J* = 2 Hz, 6.8 Hz), 8.35 (1H, d, *J* = 2.4 Hz), 8.54 (2H, d, *J* = 4 Hz), 9.94 (1H, s), 10.59 (1H, s). ¹³C NMR (100 MHz, CDCl₃) δ_{ppm} 29.6, 59.9, 71.5, 113.8, 119.7, 122.2, 122.6, 123.1, 125.0, 129.8, 131.6, 135.9, 136.7, 137.5, 148.7, 154.4, 158.8, 159.1, 164.5, 188.3, 190.0. MS (EI): *m/z* = 453.6 [M+H]⁺ for C₂₇H₂₄N₄O₃. Elemental analysis: Found C, 71.65; H, 5.36; N, 12.40; Calcd. C, 71.67; H, 5.35; N, 12.38 for C₂₇H₂₄N₄O₃.

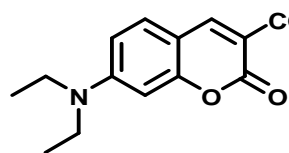


TPACy: A mixture of **N₄O-bda** (100 mg, 0.263 mmol), indolium-3-butyl-sulfonate (140 mg, 0.473 mmol) and NaOAc (39 mg, 0.473 mmol) was dissolved in 3 mL Ac₂O. The reaction mixture was stirred for 30 min at 80 °C under an argon atmosphere. After completion, the reaction mixture was concentrated by evaporation under reduced pressure. The crude product was diluted with 3.0 mL water, 3.0 mL CH₃CN, 300 μL AcOH, and purified by preparative RP-HPLC (grad. 10–90% CH₃CN in water, 20 min) to obtain the probe **TPACy** (185 mg, 70%) as a yellow powder. ¹H NMR (400 MHz, DMSO-*d*₆) δ_{ppm} 1.71 (6H, s), 1.82 (12H, s), 2.63-2.68 (4H, dd, *J* = 6.4 Hz, 7.2 Hz), 4.28 (2H, s), 4.38 (4H, s), 4.70-4.74 (4H, m), 5.57 (2H, s), 7.47-7.49 (2H, d *J* = 7.6 Hz), 7.54-7.68 (11H, m), 7.81-7.85 (3H, m), 7.90-7.94 (1H, m), 7.98-8.07 (5H, m), 8.41-8.54 (3H, m), 8.64-8.65 (2H, d, *J* = 4.8 Hz), 8.99 (1H, s). ¹³C NMR (100 MHz, DMSO-*d*₆) δ_{ppm} 21.8, 24.0, 25.5, 25.7, 25.8, 26.5, 46.4, 46.8,



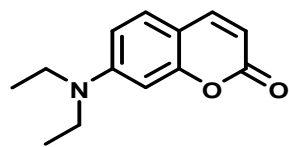
49.6, 49.7, 52.2, 56.6, 58.6, 71.2, 112.1, 114.4, 114.5, 115.1, 115.4, 117.3, 121.3, 122.9, 123.5, 123.8, 124.8, 125.5, 128.1, 129.2, 129.3, 129.5, 129.8, 133.1, 137.5, 138.3, 140.4, 140.5, 142.2, 143.5, 143.7, 144.7, 146.5, 148.9, 152.1, 153.0, 154.7, 158.3, 158.6, 159.0, 161.3, 181.6, 181.8. MS (EI): $m/z = 1008.3$ $[M+H]^+$ for C₅₇H₆₂N₆O₇S₂. Elemental analysis: Found C, 66.95; H, 6.20; N, 8.35; Calcd. C, 67.97; H, 6.20; N, 8.34 for C₅₇H₆₂N₆O₇S₂.

7-Diethylamino-2-oxo-2H-chromene-3-carboxylic acid ethyl ester (A): 7-Diethylamino



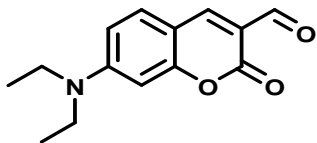
salicylaldehyde (2.66 g, 13.8 mmol) and diethyl malonate (3.31 g, 20.7 mmol) were dissolved in toluene-acetonitrile (150 mL, 1:2). Piperidine (3.53 g, 41.5 mmol) was added and the mixture was refluxed for 12 h. After cooling, the solvent was evaporated and the residue was purified by silica gel chromatography (methylene chloride/ethyl acetate; 8:2) to obtain the product **A** as yellow oil (2.39 g, 60% yield). ¹H NMR (400 MHz, CDCl₃) δ_{ppm} 1.21-1.25 (6H, m), 1.37-1.41 (3H, m), 3.42-3.47 (4H, dd, $J = 7.6$ Hz, 6.8 Hz), 4.34-4.40 (2H, m), 6.47 (1H, s), 6.59 (1H, d, $J = 9.2$ Hz), 7.34 (1H, dd, $J = 1.2$ Hz, 8 Hz), 8.42 (1H, s). ¹³C NMR (100 MHz, CDCl₃) δ_{ppm} 12.4, 14.3, 45.0, 61.1, 96.7, 107.7, 109.1, 109.4, 130.9, 149.1, 152.8, 158.2, 158.4, 164.2. MS (EI): $m/z = 290.4$ $[M+H]^+$ for C₁₆H₁₉NO₄. Elemental analysis: Found C, 66.40; H, 6.62; N, 4.85; Calcd. C, 66.42; H, 6.62; N, 4.84 for C₁₆H₁₉NO₄.

7-Diethylamino-chromene-2-one (B): 7-Diethylamino-coumaric-3-carboxylic acid ethyl



ester (1 g) in 60 mL of 18% strength hydrochloric acid was heated for 5 h to the boil under reflux. After cooling, saturated sodium acetate solution was added and the pH was adjusted to 4-5 with 45% strength sodium hydroxide, whilst cooling. The crystalline precipitate was filtered off, thoroughly washed with water and dried in vacuum at 50 °C, which afforded product **(B)** as light yellow solid (0.6 g, 80% yield). ¹H NMR (400 MHz, CDCl₃) δ_{ppm} 1.24 (6H, t, $J = 7.2$ Hz), 3.41-3.47 (4H, q, $J = 7.2$ Hz), 6.05 (1H, d, $J = 9.6$ Hz), 6.52 (1H, d, $J = 2$ Hz), 6.57-6.60 (1H, dd, $J = 2.4$ Hz, 6.4 Hz), 7.29 (1H, s), 7.54 (1H, d, $J = 9.2$ Hz). ¹³C NMR (100 MHz, CDCl₃) δ_{ppm} 12.4, 44.7, 97.6, 108.3, 108.6, 109.2, 128.7, 143.6, 150.7, 156.7, 162.2. MS (EI): $m/z = 218.3$ $[M+H]^+$ for C₁₃H₁₅NO₂. Elemental analysis: Found C, 71.85; H, 6.97; N, 6.47; Calcd. C, 71.87; H, 6.96; N, 6.45 for C₁₃H₁₅NO₂.

7-Diethylamino-2-oxo-2H-chromene-3-carboxyldehyde (C): DMF (4 mL) was added



dropwise to POCl₃ (0.4 mL) at 20-50 °C. The mixture was stirred for 45 min at 50 °C under N₂ atmosphere. A suspension of 7-diethylamino coumarin (0.65 g, 3 mmol) in DMF (3 mL) was then

added, the mixture was warmed to 60 °C for 2 h and poured out onto ice water, and stirred for 2 h. The crystalline precipitate was filtered off, thoroughly washed with water and dried in vacuum at 50 °C, which afforded product **C** as orange solid. (0.47 g, 66% yield). ¹H NMR (400 MHz, CDCl₃) δ_{ppm} 1.23 (6H, t, *J* = 6.8 Hz), 3.44 (4H, dd, *J* = 7.2 Hz, 6.8 Hz), 6.47 (1H, d, *J* = 2 Hz), 6.61 (1H, dd, *J* = 2.4 Hz, 6.8 Hz), 7.39 (1H, d, *J* = 9.2 Hz), 8.24 (1H, s), 10.11 (1H, s). ¹³C NMR (100 MHz, CDCl₃) δ_{ppm} 12.4, 45.3, 97.2, 108.2, 110.2, 114.4, 132.5, 145.3, 153.4, 158.9, 161.8. MS (EI): *m/z* = 246.3 [M+H]⁺ for C₁₄H₁₅NO₃. Elemental analysis: Found C, 68.54; H, 6.17; N, 5.72; Calcd. C, 68.56; H, 6.16; N, 5.71 for C₁₄H₁₅NO₃.

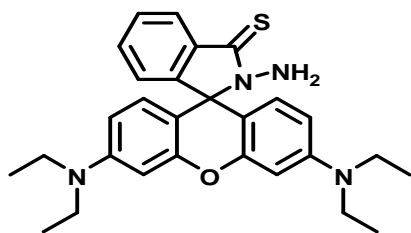
Rhodamine hydrazide: To a 100 mL flask, rhodamine B (1.2 g, 2.5 mmol) dissolved in 30



mL ethanol was added. 85% Hydrazine hydrate (3.0 mL, excess) was then added dropwise with vigorous stirring at room temperature. After the addition, the stirred mixture was heated to reflux for 2 h. The solution changed from dark purple to light orange and became clear. Then the

mixture was cooled and solvent was removed under reduced pressure. 1 M HCl (50 mL) was added to the solid in the flask to generate a clear red solution. After that, 1 M NaOH (70 mL) was added slowly with stirring until the pH of the solution reached 9~10. The resulting precipitate was filtered and washed with water (3 × 15 mL). After drying, the reaction afforded 0.83 g of rhodamine hydrazide (75%) as pink solid. ¹H NMR (400 MHz, DMSO-*d*₆) δ_{ppm} 1.06 (12H, t, *J* = 7.2 Hz), 3.30 (8H, q, *J* = 6.4 Hz), 4.24 (2H, s), 6.32-6.37 (6H, m), 6.97-6.99 (1H, m), 7.45-7.48 (2H, m), 7.74-7.76 (1H, m). MS (EI): *m/z* = 457.6 [M+H]⁺ for C₂₈H₃₂N₄O₂. Elemental analysis: Found C, 73.64; H, 7.06; N, 12.28; Calcd. C, 73.66; H, 7.06; N, 12.27 for C₂₈H₃₂N₄O₂.

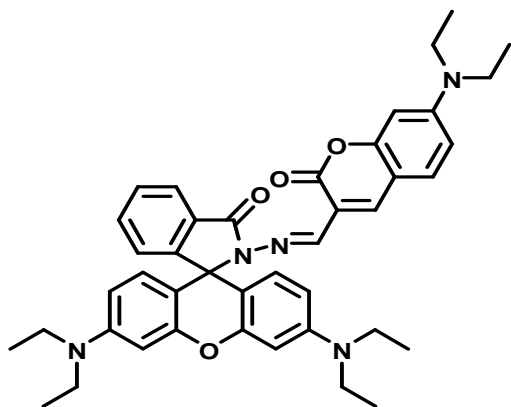
Rhodamine thiohydrazide: Rhodamine B hydrazide (0.6g, 1.3mmol) and Lawesson's



Reagent (0.52 g, 1.3 mmol) were dissolved in benzene, and the reaction mixture was refluxed for 4 h under nitrogen atmosphere, after removal of benzene, the residue was purified by flash chromatography with CH₂Cl₂/petroleum (3/4) as eluent to afford rhodamine thiohydrazide (0.12 g,

yield: 19%). ¹H NMR (400 MHz, DMSO-*d*₆) δ_{ppm} 1.06-1.10 (12H, t, *J* = 7.2 Hz), 3.33 (8H, q, *J* = 7.2 Hz), 5.35 (2H, s), 6.16 (2H, d, *J* = 8.8 Hz), 6.34-6.40 (4H, m), 7.03-7.05 (1H, m), 7.50-7.53 (2H, m), 7.87-7.88 (1H, m). MS (EI): *m/z* = 473.7 [M+H]⁺ for C₂₈H₃₂N₄OS. Elemental analysis: Found C, 71.16; H, 6.83; N, 11.86; Calcd. C, 71.15; H, 6.82; N, 11.85 for C₂₈H₃₂N₄OS.

CRO: In 25 mL of ethanol, 7-diethylamino-2-oxo-2H-chromene-3-carboxyldehyde (C)

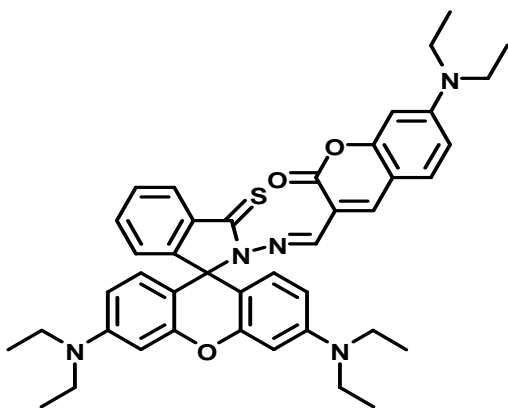


(0.245 g, 1.0 mmol) and rhodamine thiohydrazide (0.457 g, 1.0 mmol) were dissolved to form a mixture. The reaction mixture was stirred and refluxed for 12 h under nitrogen atmosphere. Yellow precipitate obtained was filtered, washed with cold ethanol and dried under vacuum. (0.52 g, 76% yield). ¹H NMR (400 MHz, CDCl₃) δ_{ppm} 1.10-1.17 (18H, m), 3.26-3.38 (12H, ddd, *J* = 5.6 Hz,

6.8 Hz, 7.2 Hz, 7.2 Hz), 6.20-6.23 (2H, dd, *J* = 6.4 Hz, 2.4 Hz), 6.36 (1H, d, *J* = 2.4 Hz), 6.44-6.50 (5H, m), 7.06 (1H, m), 7.23 (1H, s), 7.39-7.46 (2H, m), 7.96-7.98 (1H, m), 8.17 (1H, s), 8.34 (1H, s). ¹³C NMR (400 MHz, CDCl₃) δ_{ppm} 12.4, 12.6, 44.3, 44.8, 65.8, 97.1, 98.3, 105.5, 108.0, 108.8, 109.1, 115.0, 123.3, 123.6, 127.7, 128.1, 128.4, 130.1, 133.3, 138.2, 141.2, 149.0, 151.0, 152.5, 152.9, 156.8, 161.3, 165.0. MS (EI): *m/z* = 684.3 (M+H)⁺, calcd. 683.3 for C₄₂H₄₅N₅O₄. Elemental analysis: Found C, 73.76; H, 6.63; N, 10.26; Calcd. C, 73.77; H, 6.63; N, 10.24 for C₄₂H₄₅N₅O₄.

CRS: In 25 mL of ethanol, 7-diethylamino-2-oxo-2H-chromene-3-carboxyldehyde (C) (0.245 g, 1.0 mmol) and rhodamine thiohydrazide (0.473 g, 1.0 mmol) were dissolved to

form a mixture. The reaction mixture was stirred and refluxed for 12 h under nitrogen



atmosphere. Orange-red precipitate obtained was filtered, washed with cold ethanol and dried under vacuum. (0.433 g, 62% yield). ¹H NMR (400 MHz, CDCl₃) δ_{ppm} 1.13-1.23 (18H, m), 3.29-3.35 (8H, dd, *J* = 6.8 Hz, 7.2 Hz), 3.39-3.44 (4H, dd, *J* = 7.2 Hz, 6.8 Hz), 6.28-6.32 (4H, m), 6.46 (1H, d, *J* = 2.4 Hz), 6.54-6.57 (1H, dd, *J* = 6.4 Hz, 2.4 Hz), 6.78 (2H, d, *J* = 8.8 Hz), 7.11-7.13 (1H, m), 7.24

(1H, s), 7.41-7.43 (2H, ddd, *J* = 2 Hz, 0.8 Hz, 2.8 Hz), 8.11-8.13 (1H, m), 8.37 (1H, s), 8.76 (1H, s). ¹³C NMR (400 MHz, CDCl₃) δ_{ppm} 12.4, 12.6, 44.3, 44.9, 63.0, 77.21, 97.2, 97.5, 108.3, 108.9, 109.5, 110.6, 113.8, 122.4, 127.0, 127.8, 130.2, 130.5, 132.1, 135.3, 140.4, 148.2, 151.6, 151.8, 153.5, 155.0, 157.4, 161.5, 170.8. MS (EI): *m/z* = 700.4 (M+H)⁺, calcd. 699.3 for C₄₂H₄₅N₅O₃S. Elemental analysis: Found C, 72.05; H, 6.49; N, 10.03; Calcd. C, 72.07; H, 6.48; N, 10.01 for C₄₂H₄₅N₅O₃S.

4.3 General method for measurements of photophysical properties

UV-Vis spectra were recorded on a Perkin Elmer Model Lambda 900 spectrophotometer. Fluorescence spectra were recorded on a Perkin Elmer model LS 55 spectrophotometer. 1 cm cells were used for titration. For UV-Vis titrations, stock solutions of probe were prepared (*c* = 2000 μM) in acetonitrile. For fluorescence titrations stock solution of ligands **XanCu**, **ResCu**, **TPACu**, **CRO** and **CRS** was prepared (*c* = 2000 μM) in DMSO. For titrations stock solution of ligand **HBTCu** was prepared (*c* = 2000 μM) in CH₃CN. The solutions of guest cations were prepared in acetonitrile/water/DMSO in the order of 10⁻³ M. Working solutions were prepared from the stock solutions. 10 nm excitation and 10 nm emission slit widths were used.

4.4 Job plot by UV-Vis method

A series of solutions containing **CRO/CRS** and $\text{Cu}(\text{ClO}_4)_2$ were prepared such that the sum of the total concentration of metal ion and **CRO/CRS** remained constant (40 μM). The mole fraction (X) of Cu^{2+} was varied from 0.1 to 1.0.

4.5 Determination of binding constant

The response parameter α is defined as the ratio of the free ligand concentration to the initial concentration of the ligand. α defined as the ratio between the free ligand concentration ($[\text{L}]$) and the total concentration of ligand $[\text{L}_T]$:

$$\alpha = \frac{[\text{L}]}{[\text{L}_T]}$$

α can be determined from the emission changes in the presence of different concentrations of M^{n+} :

$$\alpha = \frac{[I - I_0]}{[I_1 - I_0]}$$

where I_1 and I_0 are the limiting emission values for $\alpha = 1$ (in the absence of M^{n+}) and $\alpha = 0$ (probe is completely complexes with M^{n+}), respectively.

The Tsein equation⁷³ to the following equations that can be used in any stoichiometric ratio between the ligand and analyte.

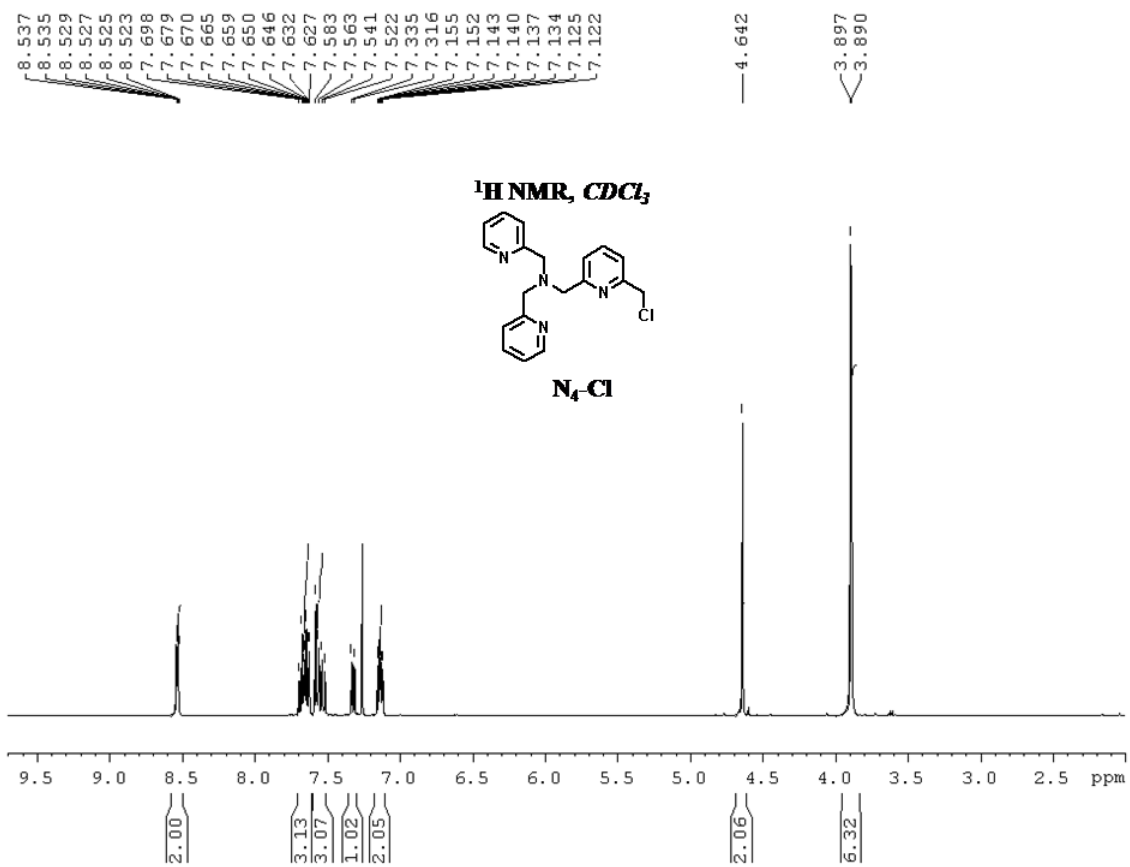
$$[\text{M}^{n+}]^m = \frac{1}{n \cdot K} \cdot \frac{1}{[\text{L}]_T^{n-1}} \cdot \frac{1-\alpha}{\alpha^n}$$

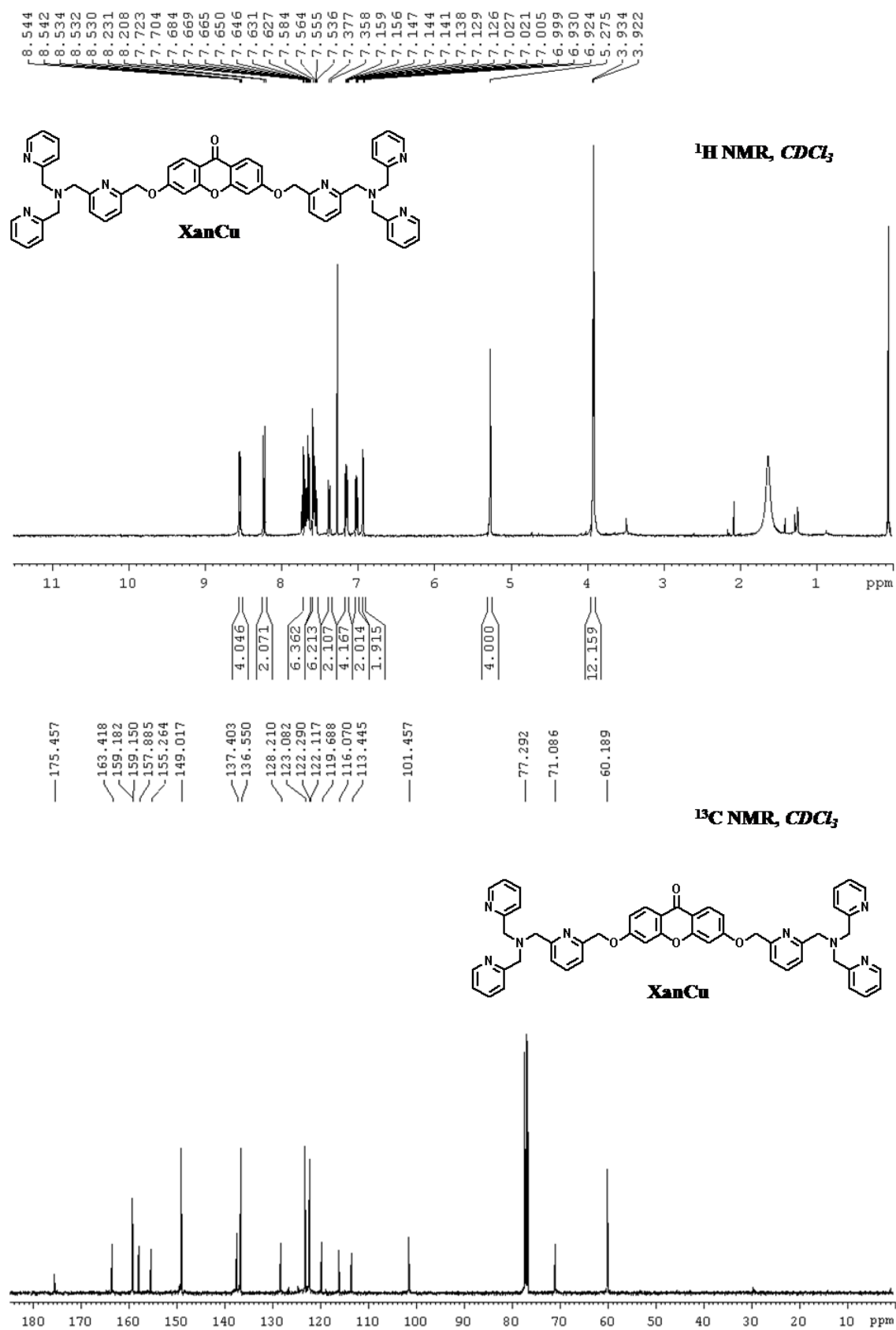
Where K is complex equilibrium constant, M_mL_n is metal-ligand, L is ligand, $[\text{L}]$, $[\text{M}^{n+}]$, and $[\text{M}_m\text{L}_n]$ are the concentrations of respective species. α is the ratio between free ligand concentration, $[\text{L}]$, and the initial concentration of ligand, $[\text{L}]$. In this case, the stoichiometric ratio of the Cu^{2+} : fluoroionophore is 1:1. So, this equation can be written as

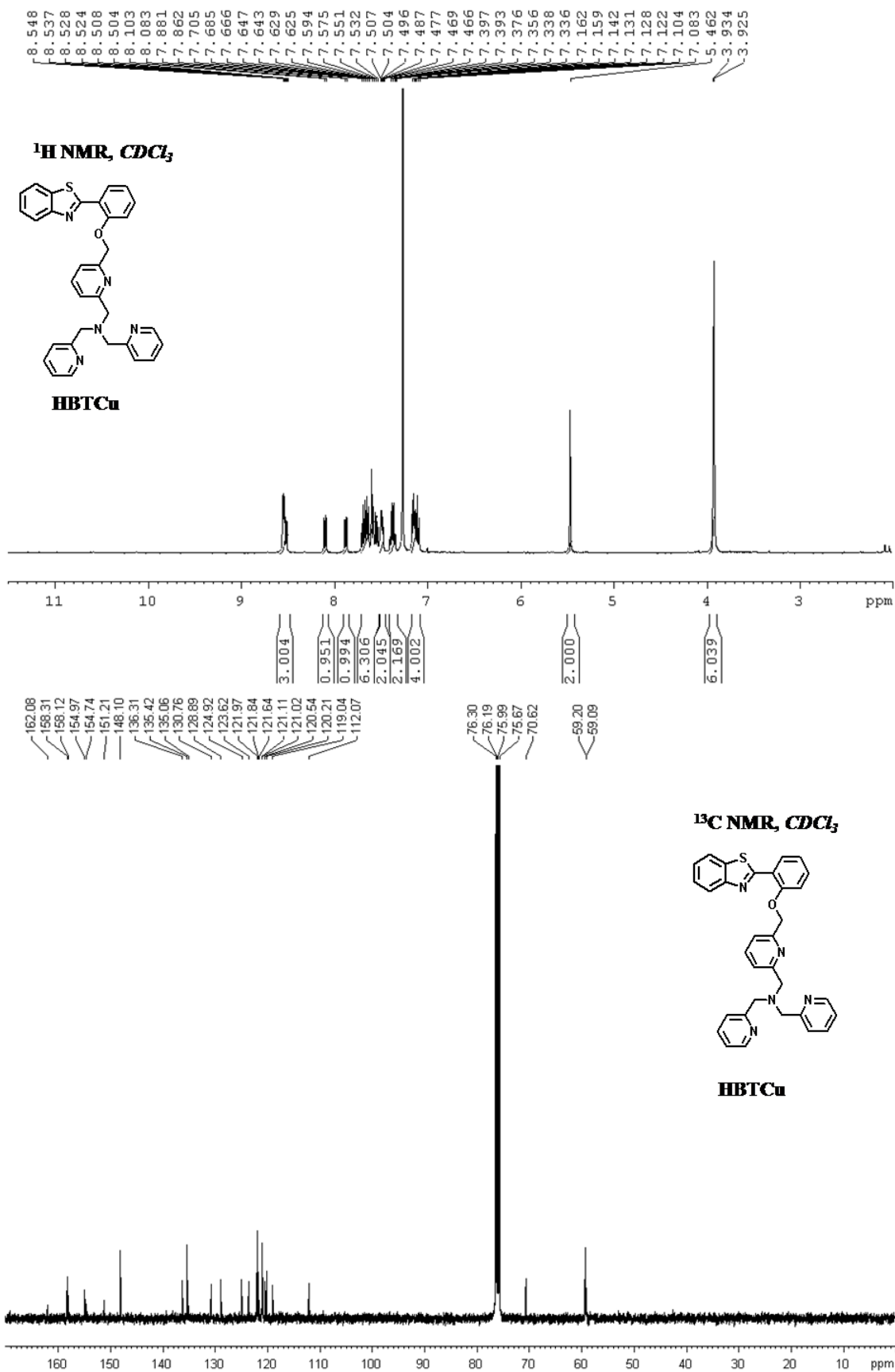
$$[\text{Cu}^{2+}] = \frac{1}{2KL_T} \times \frac{1-\alpha}{\alpha^2}$$

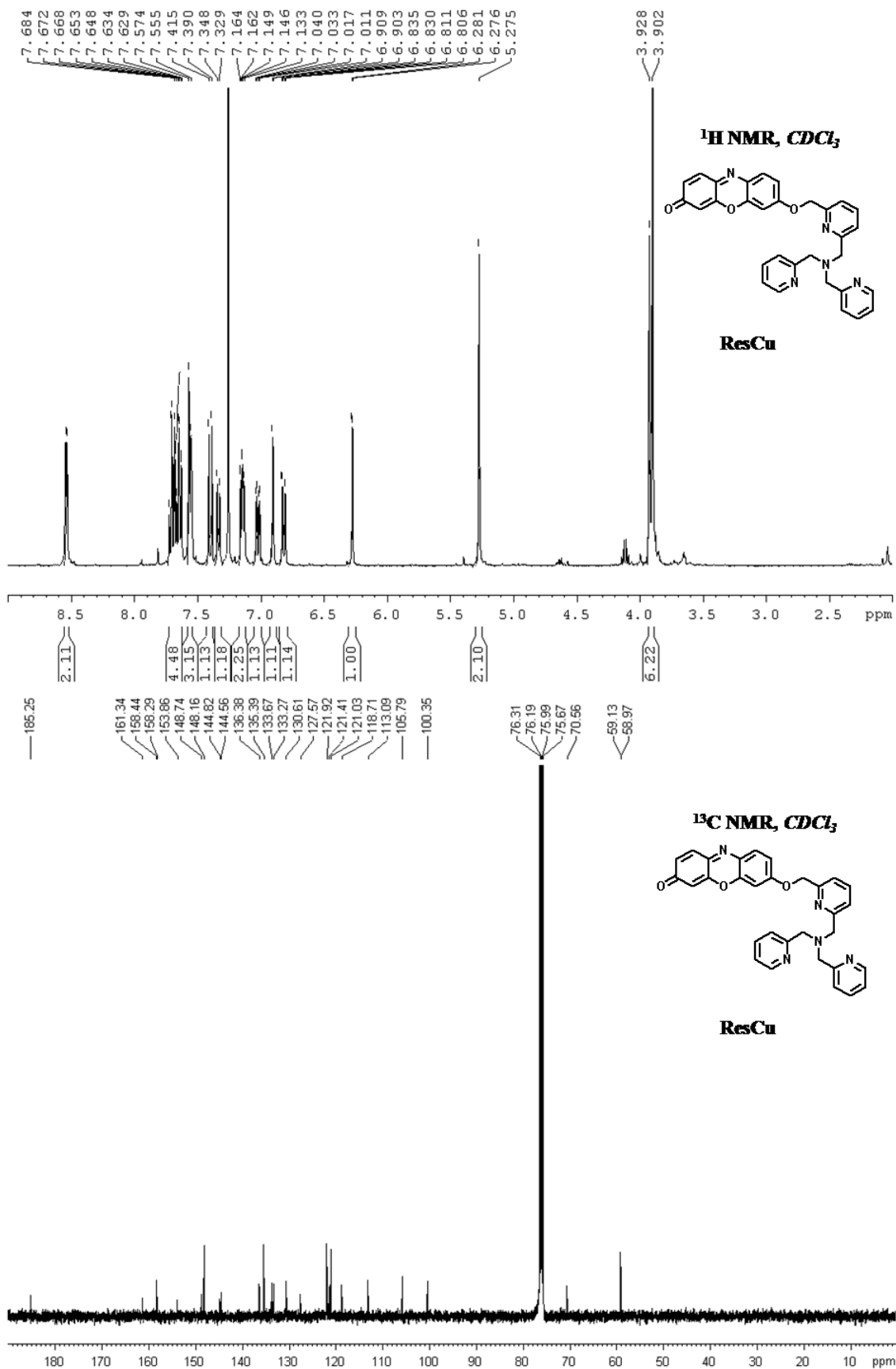
4.6 Appendix

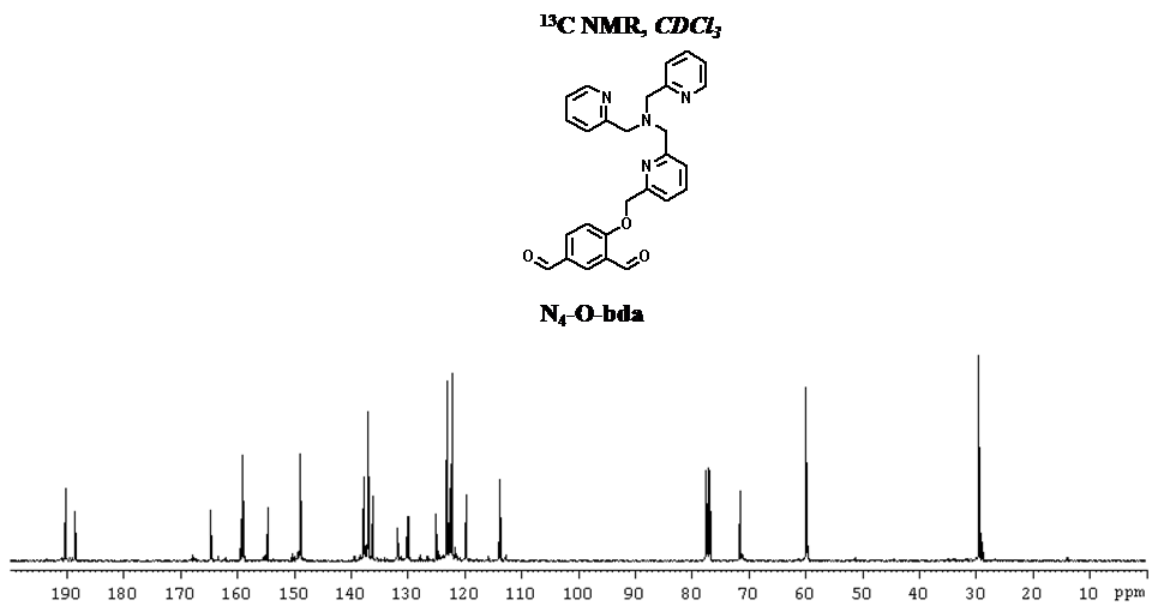
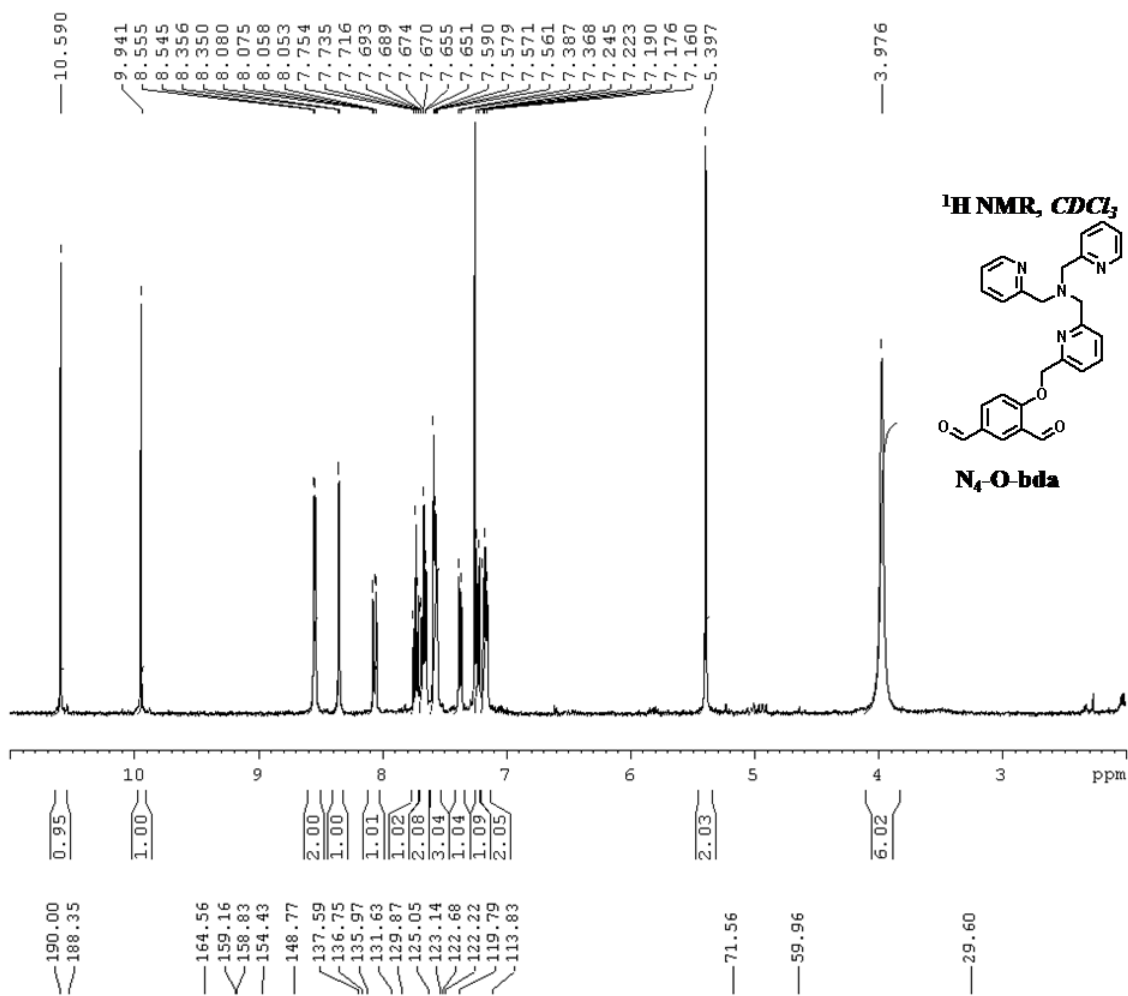
- ❖ Compound N₄-Cl, ¹H NMR
- ❖ Compound XanCu, ¹H and ¹³C NMR
- ❖ Compound HBTCu, ¹H and ¹³C NMR
- ❖ Compound ResCu, ¹H and ¹³C NMR
- ❖ Compound N₄-O-bda, ¹H and ¹³C NMR
- ❖ Compound TPACy, ¹H and ¹³C NMR
- ❖ Compound A, ¹H and ¹³C NMR
- ❖ Compound B, ¹H and ¹³C NMR
- ❖ Compound C, ¹H and ¹³C NMR
- ❖ Compound rhodamine hydrazide and rhodamine thiohydrazide, ¹H NMR
- ❖ Compound CRO, ¹H and ¹³C NMR
- ❖ Compound CRS, ¹H and ¹³C NMR

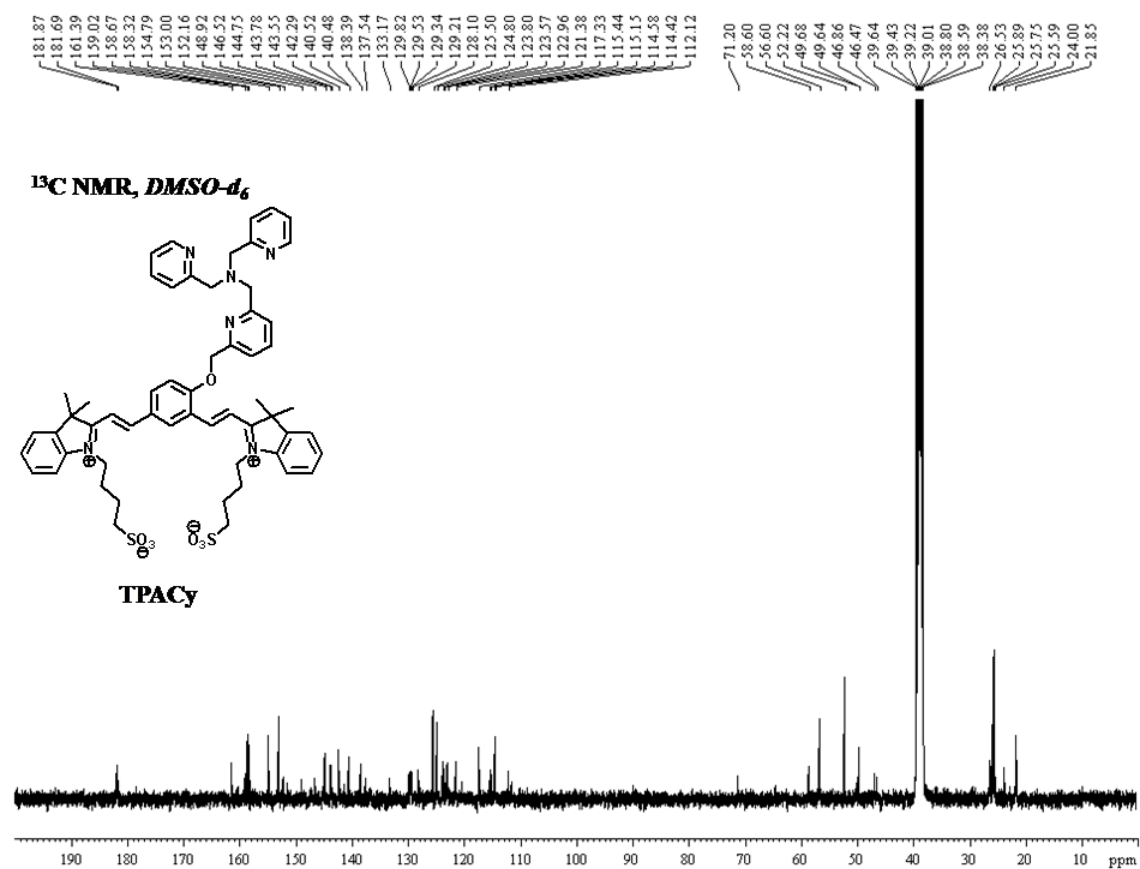
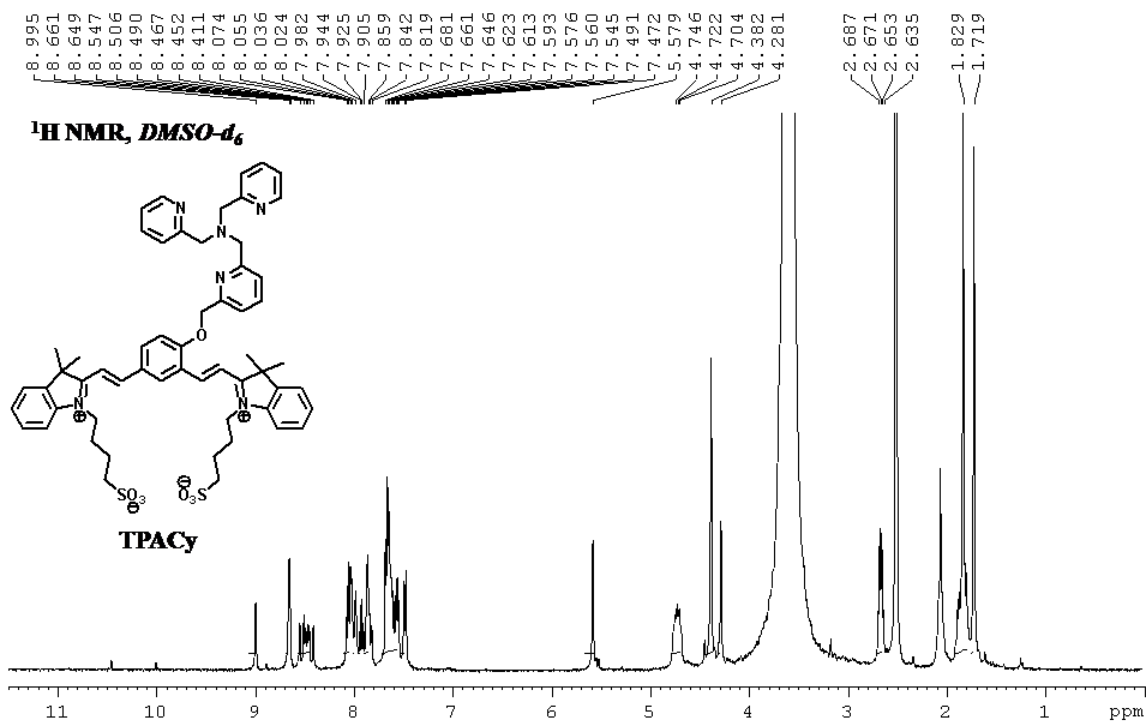


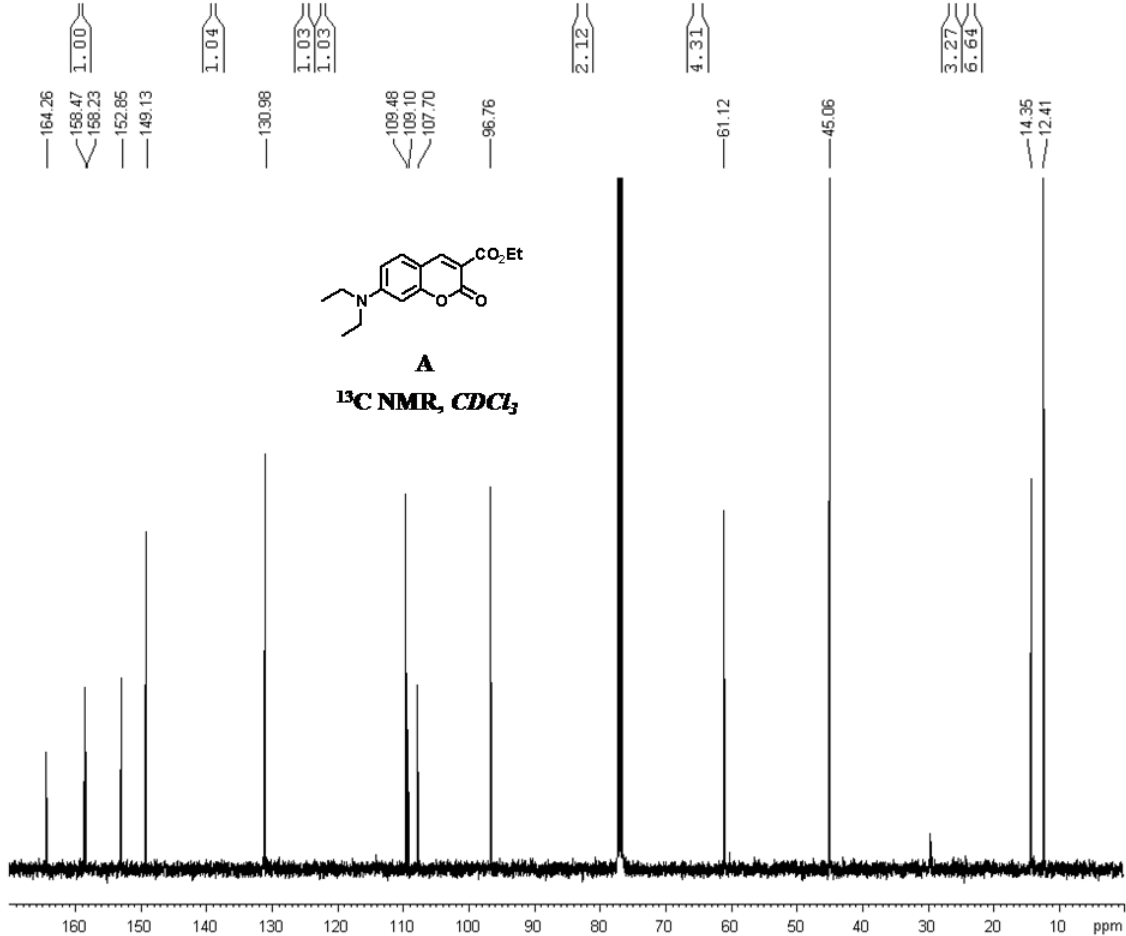
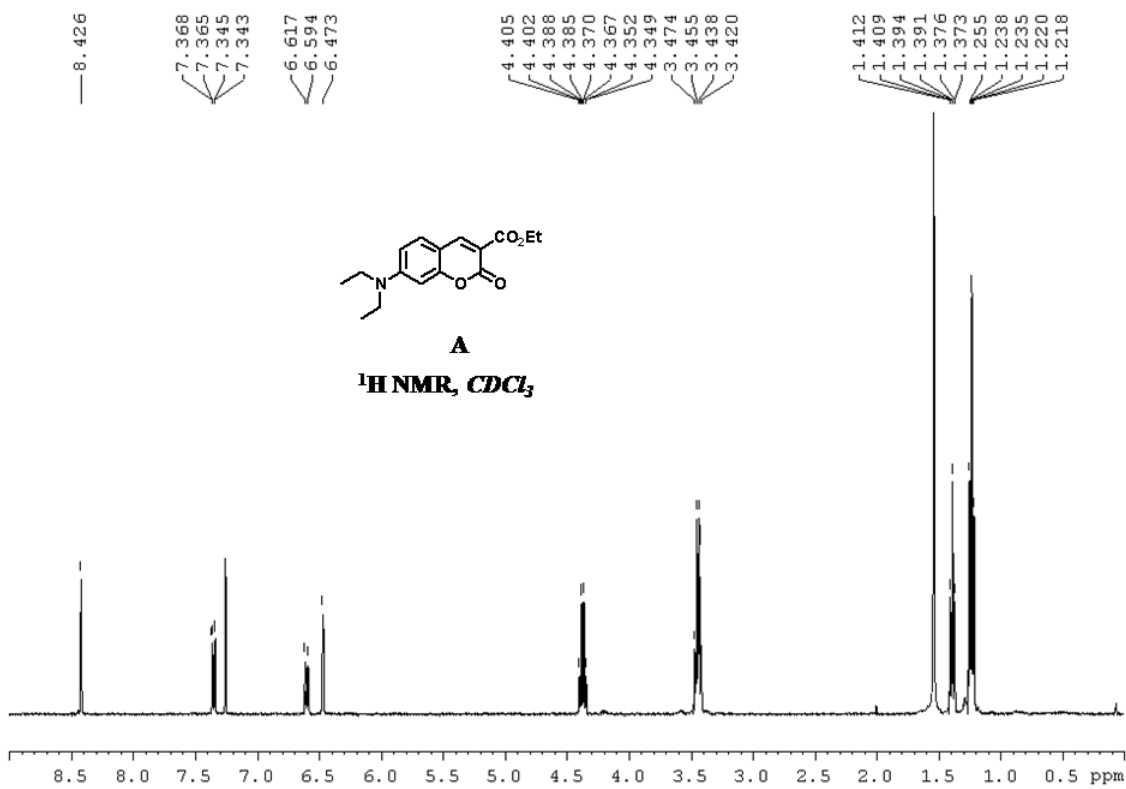


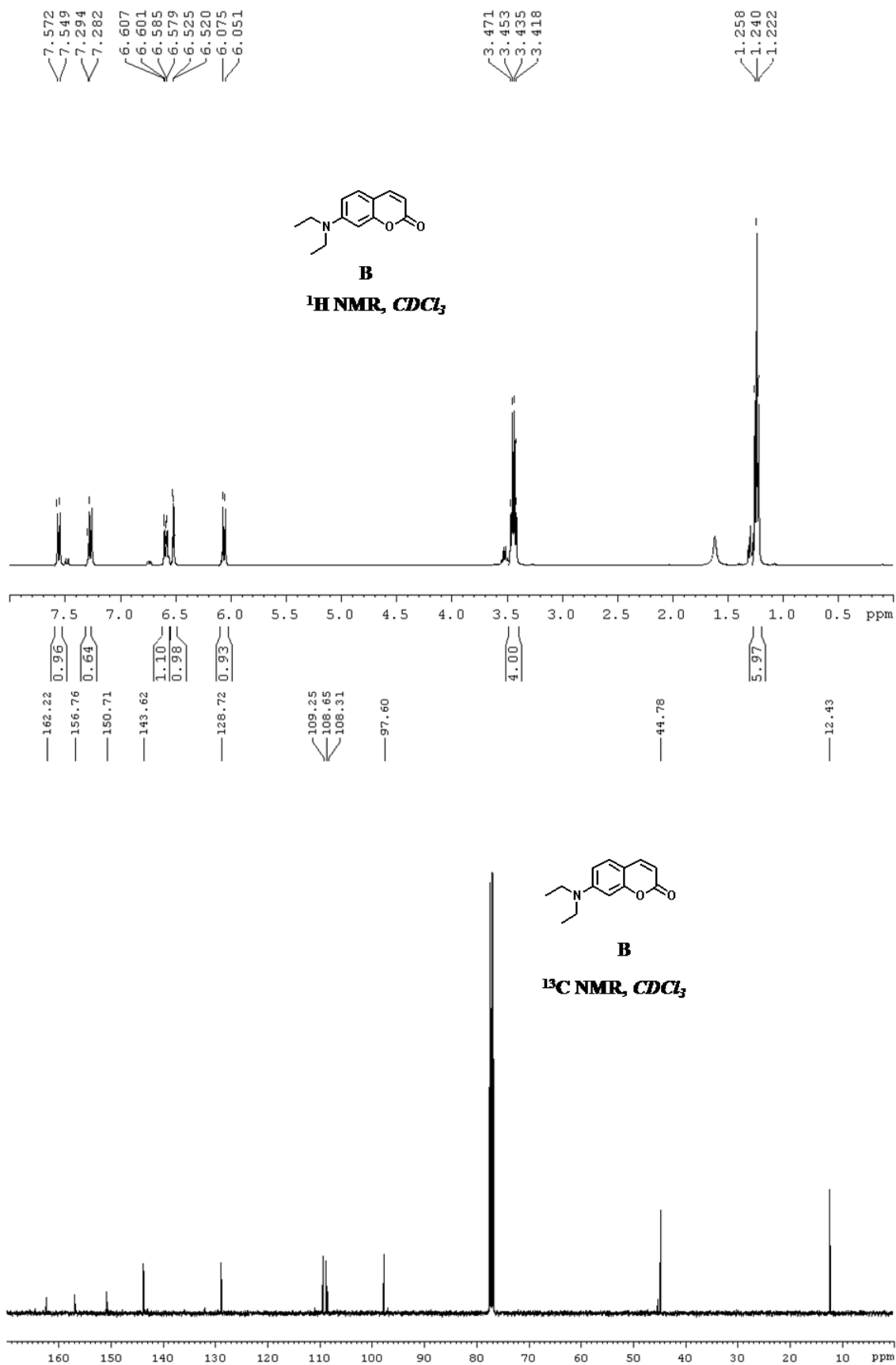


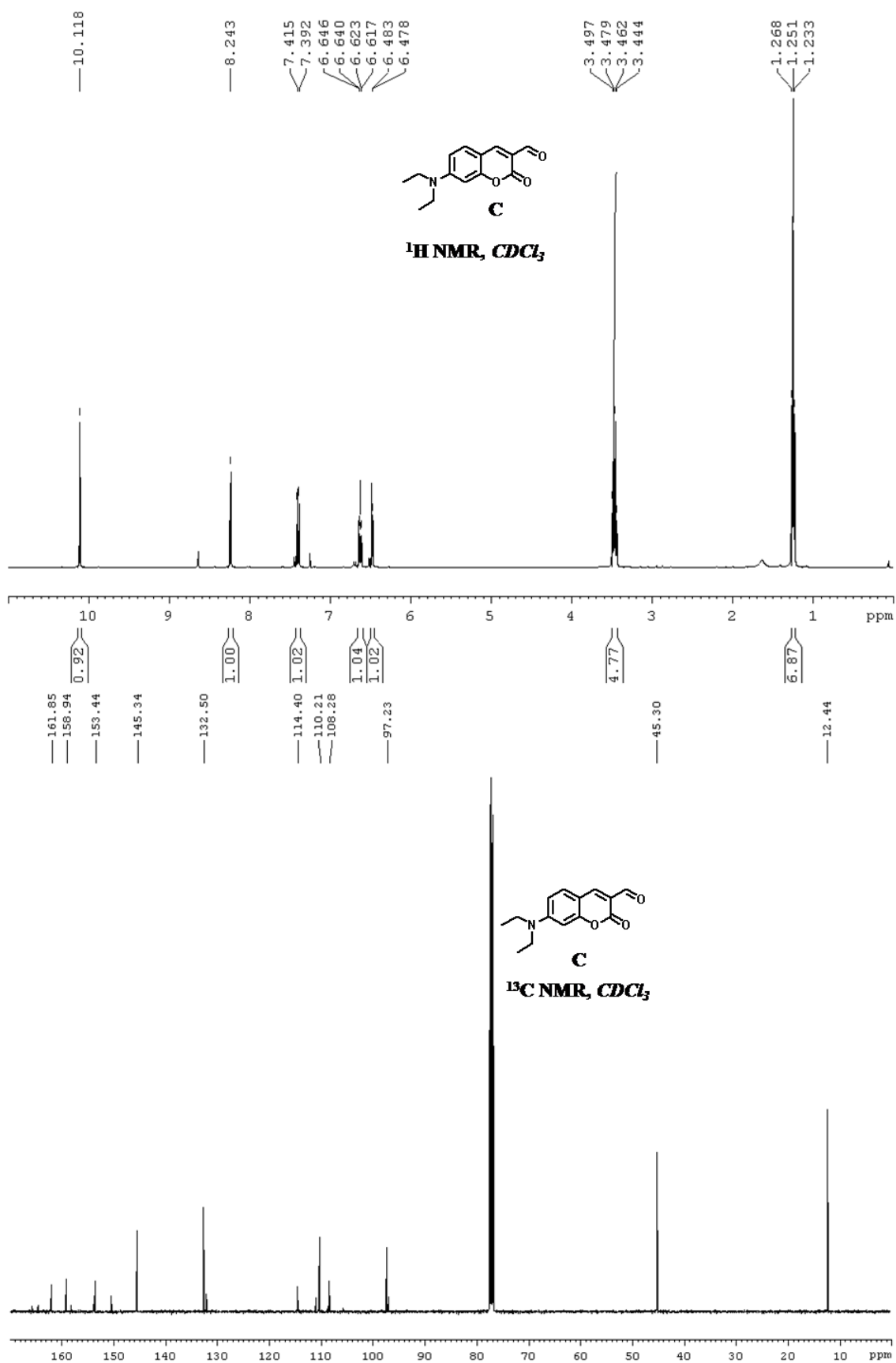


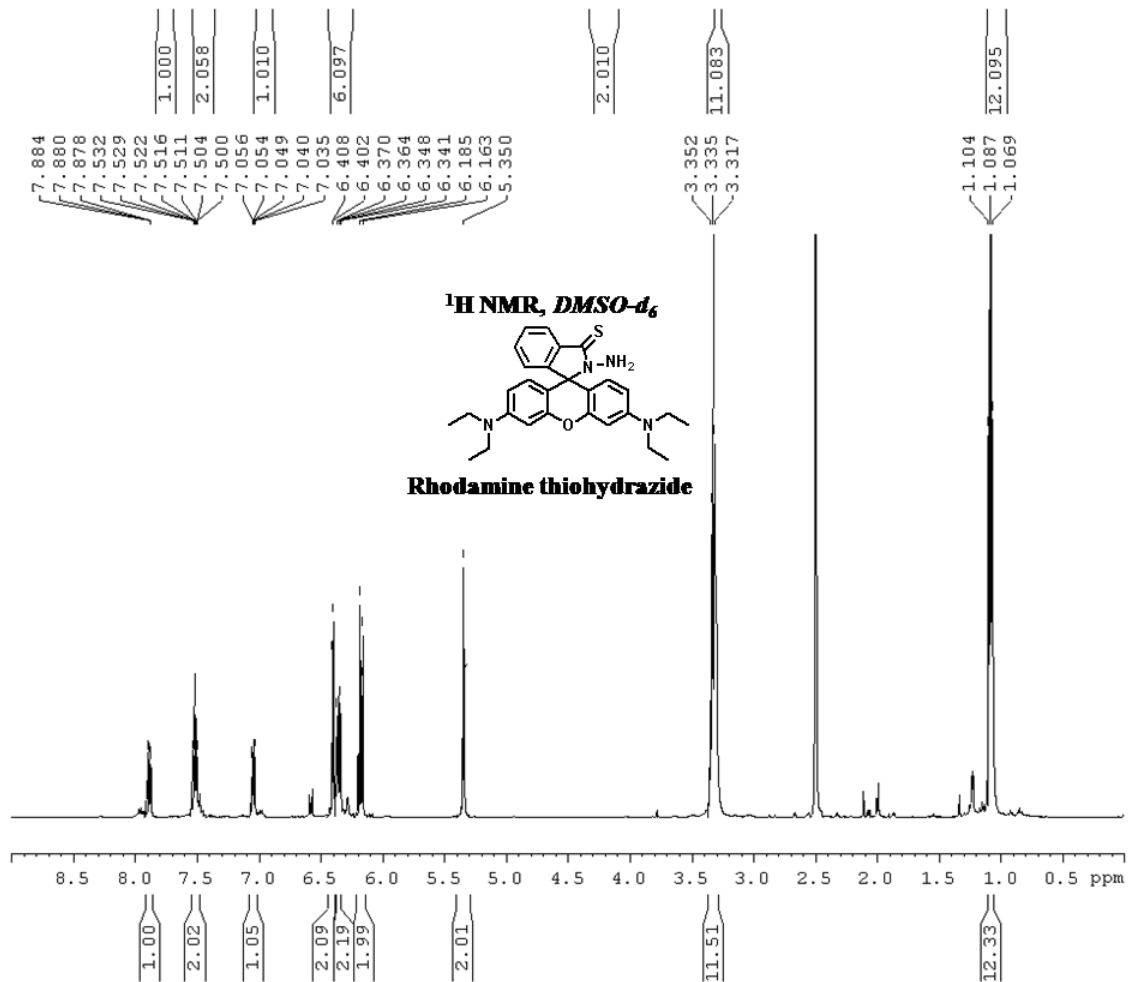
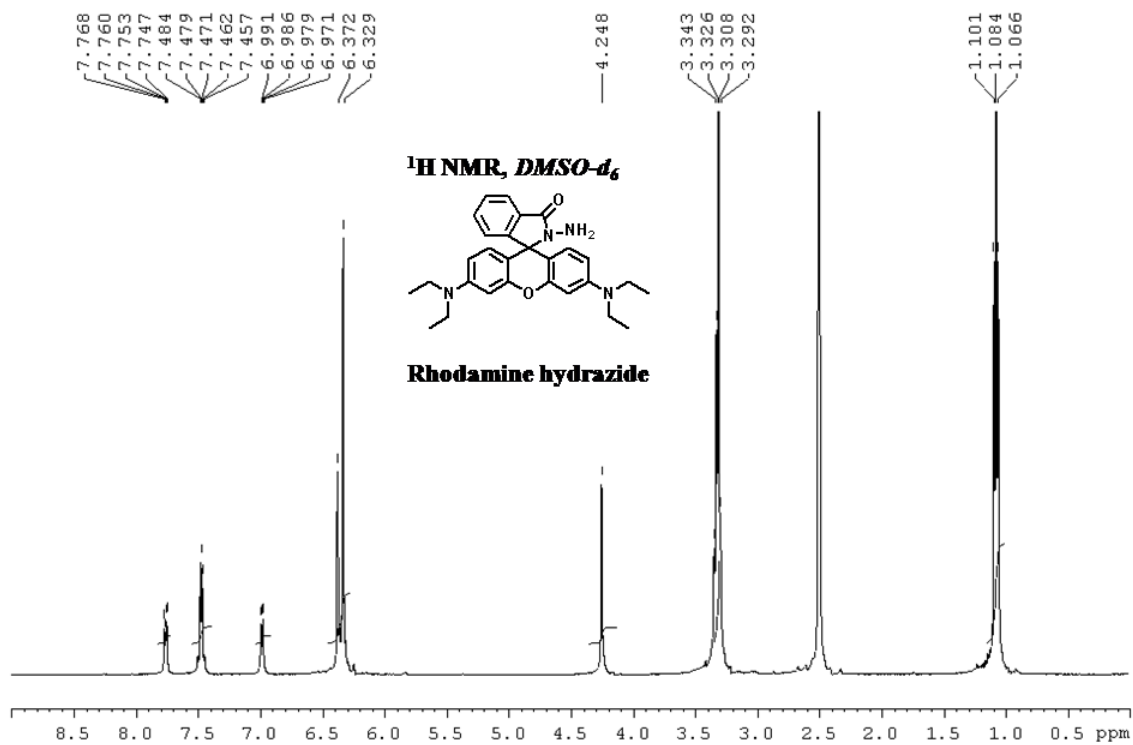


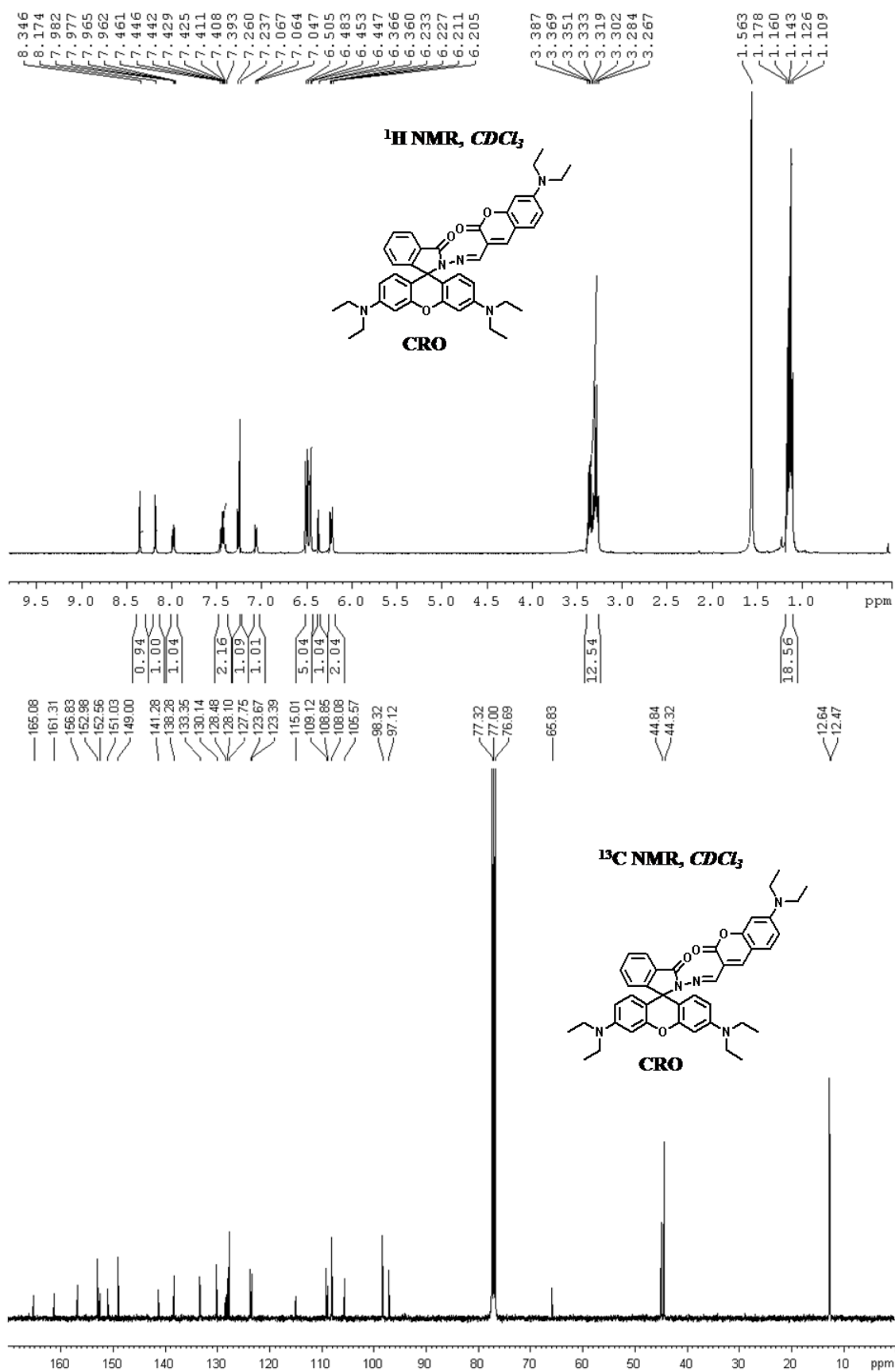


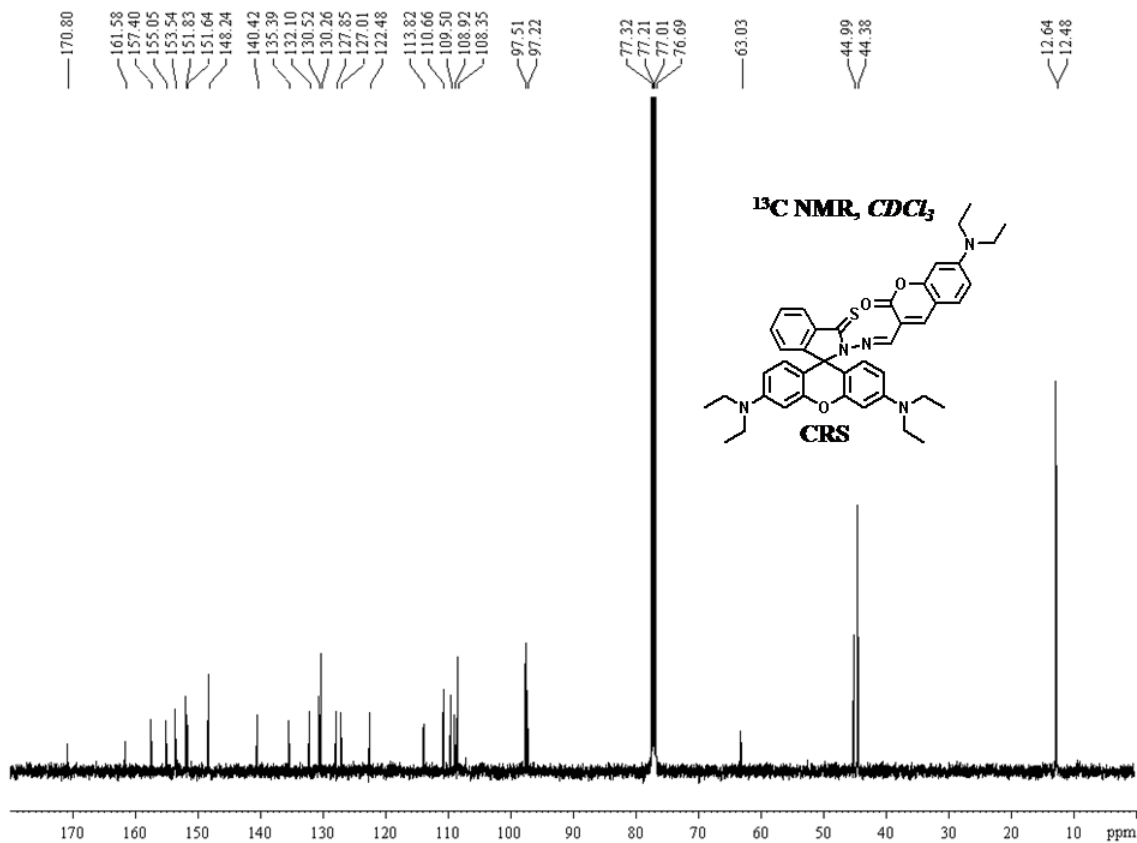
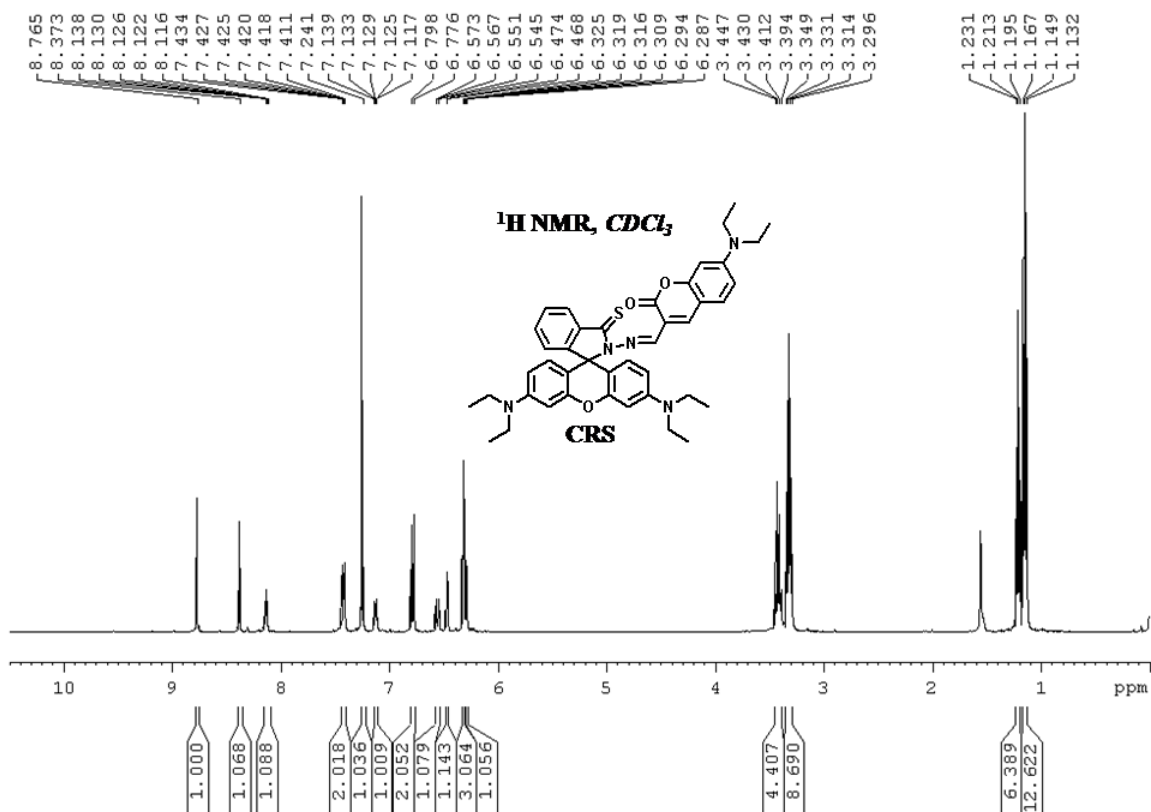












5. References

1. Waggoner, D. J.; Bartnikas, T. B.; Gitlin, J. D., The role of copper in neurodegenerative disease. *Neurobiol. Dis.* **1999**, *6*, 221-230.
2. Barceloux, D. G.; Barceloux, D., Copper. *Clin. Toxicol.* **1999**, *37*, 217-230.
3. Fabbri, L.; Poggi, A., Sensors and switches from supramolecular chemistry. *Chem. Soc. Rev.* **1995**, *24*, 197-202.
4. Prodi, L.; Bolletta, F.; Montalti, M.; Zaccheroni, N., Luminescent chemosensors for transition metal ions. *Coord. Chem. Rev.* **2000**, *205*, 59-83.
5. Herd, S. M.; Camakaris, J.; Christofferson, R.; Wookey, P.; Danks, D. M., Uptake and efflux of copper-64 in Menkes'-disease and normal continuous lymphoid cell lines. *Biochem. J.* **1987**, *247*, 341-347.
6. Millhauser, G. L., Copper Binding in the Prion Protein. *Acc. Chem. Res.* **2004**, *37*, 79-85.
7. Brewer, G. J., Copper in medicine. *Curr. Opin. Chem. Biol.* **2003**, *7*, 207-212.
8. Barnham, K. J.; Masters, C. L.; Bush, A. I., Neurodegenerative diseases and oxidative stress. *Nat. Rev. Drug Discov.* **2004**, *3*, 205-214.
9. Valentine, J. S.; Hart, P. J., Misfolded CuZnSOD and amyotrophic lateral sclerosis. *Proc. Natl. Acad. Sci. USA* **2003**, *100*, 3617-3622.
10. Arnesano, F.; Banci, L.; Bertini, I.; Ciofi-Baffoni, S., Perspectives in Inorganic Structural Genomics: A Trafficking Route for Copper. *Eur. J. Inorg. Chem.* **2004**, *2004*, 1583-1593.
11. Valeur, B.; Leray, I., Design principles of fluorescent molecular sensors for cation recognition. *Coord. Chem. Rev.* **2000**, *205*, 3-40.
12. Domaille, D. W.; Que, E. L.; Chang, C. J., Synthetic fluorescent sensors for studying the cell biology of metals. *Nat. Chem. Biol.* **2008**, *4*, 168-175.
13. Crichton, R. R.; Dexter, D. T.; Ward, R. J., Metal based neurodegenerative diseases—From molecular mechanisms to therapeutic strategies. *Coord. Chem. Rev.* **2008**, *252*, 1189-1199.
14. Ueno, T.; Nagano, T., Fluorescent probes for sensing and imaging. *Nat. Meth.* **2011**, *8*, 642-645.
15. Que, E. L.; Domaille, D. W.; Chang, C. J., Metals in Neurobiology: Probing Their Chemistry and Biology with Molecular Imaging. *Chem. Rev.* **2008**, *108*, 1517-1549.
16. Shao, N.; Zhang, Y.; Cheung, S.; Yang, R.; Chan, W.; Mo, T.; Li, K.; Liu, F., Copper Ion-Selective Fluorescent Sensor Based on the Inner Filter Effect Using a Spiropyran Derivative. *Anal. Chem.* **2005**, *77*, 7294-7303.

17. Swamy, K. M. K.; Ko, S.-K.; Kwon, S. K.; Lee, H. N.; Mao, C.; Kim, J.-M.; Lee, K.-H.; Kim, J.; Shin, I.; Yoon, J., Boronic acid-linked fluorescent and colorimetric probes for copper ions. *Chem. Commun.* **2008**, *0*, 5915-5917.
18. Zhou, Z.; Fahrni, C. J., A fluorogenic probe for the copper(I)-catalyzed azide–alkyne ligation reaction: modulation of the fluorescence emission via 3(n,π*)–1(π,π*) inversion. *J. Am. Chem. Soc.* **2004**, *126*, 8862-8863.
19. Zhou, Y.; Wang, F.; Kim, Y.; Kim, S.-J.; Yoon, J., Cu²⁺-selective ratiometric and “off-on” sensor based on the rhodamine derivative bearing pyrene group. *Org. Lett.* **2009**, *11*, 4442-4445.
20. Qi, X.; Jun, E. J.; Xu, L.; Kim, S.-J.; Joong Hong, J. S.; Yoon, Y. J.; Yoon, J., New BODIPY derivatives as OFF–ON fluorescent chemosensor and fluorescent chemodosimeter for Cu²⁺: cooperative selectivity enhancement toward Cu²⁺. *J. Org. Chem.* **2006**, *71*, 2881-2884.
21. Xiang, Y.; Tong, A.; Jin, P.; Ju, Y., New fluorescent rhodamine hydrazone chemosensor for Cu(II) with high selectivity and sensitivity. *Org. Lett.* **2006**, *8*, 2863-2866.
22. Li, G.-K.; Xu, Z.-X.; Chen, C.-F.; Huang, Z.-T., A highly efficient and selective turn-on fluorescent sensor for Cu²⁺ ion based on calix[4]arene bearing four iminoquinoline subunits on the upper rim. *Chem. Commun.* **2008**, *0*, 1774-1776.
23. Lee, M. H.; Kim, H. J.; Yoon, S.; Park, N.; Kim, J. S., Metal ion induced FRET OFF–ON in tren/dansyl-appended rhodamine. *Org. Lett.* **2007**, *10*, 213-216.
24. Yu, M.; Shi, M.; Chen, Z.; Li, F.; Li, X.; Gao, Y.; Xu, J.; Yang, H.; Zhou, Z.; Yi, T.; Huang, C., Highly sensitive and fast responsive fluorescence turn-on chemodosimeter for Cu²⁺ and its application in live cell imaging. *Chem. Eur. J.* **2008**, *14*, 6892-6900.
25. Goswami, S.; Sen, D.; Das, N. K., A new highly selective, ratiometric and colorimetric fluorescence sensor for Cu²⁺ with a remarkable red shift in absorption and emission spectra based on internal charge transfer. *Org. Lett.* **2010**, *12*, 856-859.
26. Xu, Z.; Yoon, J.; Spring, D. R., A selective and ratiometric Cu²⁺ fluorescent probe based on naphthalimide excimer-monomer switching. *Chem. Commun.* **2010**, *46*, 2563-2565.
27. Ko, K. C.; Wu, J.-S.; Kim, H. J.; Kwon, P. S.; Kim, J. W.; Bartsch, R. A.; Lee, J. Y.; Kim, J. S., Rationally designed fluorescence 'turn-on' sensor for Cu²⁺. *Chem. Commun.* **2011**, *47*, 3165-3167.
28. Cao, X.; Lin, W.; Wan, W., Development of a near-infrared fluorescent probe for imaging of endogenous Cu⁺ in live cells. *Chem. Commun.* **2012**, *48*, 6247-6249.
29. Hirayama, T.; Van de Bittner, G. C.; Gray, L. W.; Lutsenko, S.; Chang, C. J., Near-infrared fluorescent sensor for in vivo copper imaging in a murine Wilson disease model. *Proc. Natl. Acad. Sci. USA* **2012**, *109*, 2228-2233.

30. Morgan, M. T.; Bagchi, P.; Fahrni, C. J., Designed To dissolve: suppression of colloidal aggregation of Cu(I)-selective fluorescent probes in aqueous buffer and in-gel detection of a metallochaperone. *J. Am. Chem. Soc.* **2011**, *133*, 15906-15909.
31. Dodani, S. C.; Leary, S. C.; Cobine, P. A.; Winge, D. R.; Chang, C. J., A targetable fluorescent sensor reveals that copper-deficient SCO1 and SCO2 patient cells prioritize mitochondrial copper Homeostasis. *J. Am. Chem. Soc.* **2011**, *133*, 8606-8616.
32. Chaudhry, A. F.; Verma, M.; Morgan, M. T.; Henary, M. M.; Siegel, N.; Hales, J. M.; Perry, J. W.; Fahrni, C. J., Kinetically controlled photoinduced electron transfer switching in Cu(I)-responsive fluorescent probes. *J. Am. Chem. Soc.* **2009**, *132*, 737-747.
33. Taki, M.; Iyoshi, S.; Ojida, A.; Hamachi, I.; Yamamoto, Y., Development of highly sensitive fluorescent probes for detection of intracellular copper(I) in living systems. *J. Am. Chem. Soc.* **2010**, *132*, 5938-5939.
34. Verma, M.; Chaudhry, A. F.; Morgan, M. T.; Fahrni, C. J., Electronically tuned 1,3,5-triarylpyrazolines as Cu(i)-selective fluorescent probes. *Org. Biomol. Chem.* **2010**, *8*, 363-370.
35. Viguiet, R. F. H.; Hulme, A. N., A Sensitized europium complex generated by micromolar concentrations of copper(I): toward the detection of copper(I) in biology. *J. Am. Chem. Soc.* **2006**, *128*, 11370-11371.
36. Zeng, L.; Miller, E. W.; Pralle, A.; Isacoff, E. Y.; Chang, C. J., A selective turn-on fluorescent sensor for imaging copper in living cells. *J. Am. Chem. Soc.* **2005**, *128*, 10-11.
37. Lippert, A. R.; Van de Bittner, G. C.; Chang, C. J., Boronate oxidation as a bioorthogonal reaction approach for studying the chemistry of hydrogen peroxide in living systems. *Acc. Chem. Res.* **2011**, *44*, 793-804.
38. Lippert, A. R.; New, E. J.; Chang, C. J., Reaction-based fluorescent probes for selective imaging of hydrogen sulfide in living cells. *J. Am. Chem. Soc.* **2011**, *133*, 10078-10080.
39. Kim, H. M.; Cho, B. R., Two-photon probes for intracellular free metal ions, acidic vesicles, and lipid rafts in live tissues. *Acc. Chem. Res.* **2009**, *42*, 863-872.
40. Quang, D. T.; Kim, J. S., Fluoro- and chromogenic chemodosimeters for heavy metal ion detection in solution and biospecimens. *Chem. Rev.* **2010**, *110*, 6280-6301.
41. Cho, D.-G.; Sessler, J. L., Modern reaction-based indicator systems. *Chem. Soc. Rev.* **2009**, *38*, 1647-1662.
42. Vad, M. S.; Nielsen, A.; Lennartson, A.; Bond, A. D.; McGrady, J. E.; McKenzie, C. J., Switching on oxygen activation by cobalt complexes of pentadentate ligands. *Dalton Trans.* **2011**, *40*, 10698-10707.

43. Garner, A. L.; Koide, K., Oxidation state-specific fluorescent method for palladium(II) and platinum(IV) based on the catalyzed aromatic claisen rearrangement. *J. Am. Chem. Soc.* **2008**, *130*, 16472-16473.
44. Song, F.; Watanabe, S.; Floreancig, P. E.; Koide, K., Oxidation-resistant fluorogenic probe for mercury based on alkyne oxymercuration. *J. Am. Chem. Soc.* **2008**, *130*, 16460-16461.
45. Song, F.; Garner, A. L.; Koide, K., A highly sensitive fluorescent sensor for palladium based on the allylic oxidative insertion mechanism. *J. Am. Chem. Soc.* **2007**, *129*, 12354-12355.
46. Maity, D.; Kumar, V.; Govindaraju, T., Reactive probes for ratiometric detection of Co²⁺ and Cu⁺ based on excited-state intramolecular proton transfer mechanism. *Org. Lett.* **2012**, *14*, 6008-6011.
47. Zhao, J.; Ji, S.; Chen, Y.; Guo, H.; Yang, P., Excited state intramolecular proton transfer (ESIPT): from principal photophysics to the development of new chromophores and applications in fluorescent molecular probes and luminescent materials. *PCCP* **2012**, *14*, 8803-8817.
48. Janes, L. E.; Cimpoia, A.; Kazlauskas, R. J., Protease-mediated separation of Cis and Trans diastereomers of 2(R,S)-benzyloxymethyl-4(S)-carboxylic acid 1,3-dioxolane methyl ester: intermediates for the synthesis of dioxolane nucleosides. *J. Org. Chem.* **1999**, *64*, 9019-9029.
49. Miller, E. W.; Albers, A. E.; Pralle, A.; Isacoff, E. Y.; Chang, C. J., Boronate-based fluorescent probes for imaging cellular hydrogen peroxide. *J. Am. Chem. Soc.* **2005**, *127*, 16652-16659.
50. Li, Z.; Hayman, R. B.; Walt, D. R., Detection of single-molecule DNA hybridization using enzymatic amplification in an array of femtoliter-sized reaction vessels. *J. Am. Chem. Soc.* **2008**, *130*, 12622-12623.
51. Kim, S. Y.; Hong, J.-I., Chromogenic and fluorescent chemodosimeter for detection of fluoride in aqueous solution. *Org. Lett.* **2007**, *9*, 3109-3112.
52. Choi, M. G.; Hwang, J.; Eor, S.; Chang, S.-K., Chromogenic and fluorogenic signaling of sulfite by selective deprotection of resorufin levulinate. *Org. Lett.* **2010**, *12*, 5624-5627.
53. Chen, W.; Li, Z.; Shi, W.; Ma, H., A new resorufin-based spectroscopic probe for simple and sensitive detection of benzoyl peroxide via deboronation. *Chem. Commun.* **2012**, *48*, 2809-2811.
54. Apfel, U.-P.; Buccella, D.; Wilson, J. J.; Lippard, S. J., Detection of nitric oxide and nitroxyl with benzo-resorufin-based fluorescent sensors. *Inorg. Chem.* **2013**, *52*, 3285-3294.
55. Sumalekshmy, S.; Fahrni, C. J., Metal-ion-responsive fluorescent probes for two-photon excitation microscopy. *Chem. Mater.* **2010**, *23*, 483-500.
56. So, P. T. C.; Dong, C. Y.; Masters, B. R.; Berland, K. M., Two-photon excitation fluorescence microscopy. *Annu. Rev. Biomed. Eng.* **2000**, *2*, 399-429.
57. Zipfel, W. R.; Williams, R. M.; Webb, W. W., Nonlinear magic: multiphoton microscopy in the biosciences. *Nat. Biotech.* **2003**, *21*, 1369-1377.

58. Helmchen, F.; Denk, W., Deep tissue two-photon microscopy. *Nat. Meth.* **2005**, *2* (12), 932-940.
59. Sumalekshmy, S.; Henary, M. M.; Siegel, N.; Lawson, P. V.; Wu; Schmidt, K.; Brédas, J.-L.; Perry, J. W.; Fahrni, C. J., Design of emission ratiometric metal-ion sensors with enhanced two-photon cross section and brightness. *J. Am. Chem. Soc.* **2007**, *129*, 11888-11889.
60. Lee, J. H.; Lim, C. S.; Tian, Y. S.; Han, J. H.; Cho, B. R., A two-photon fluorescent probe for thiols in live cells and tissues. *J. Am. Chem. Soc.* **2010**, *132*, 1216-1217.
61. Kim, H. N.; Lee, M. H.; Kim, H. J.; Kim, J. S.; Yoon, J., A new trend in rhodamine-based chemosensors: application of spirolactam ring-opening to sensing ions. *Chem. Soc. Rev.* **2008**, *37*, 1465-1472.
62. Park, H. J.; Lim, C. S.; Kim, E. S.; Han, J. H.; Lee, T. H.; Chun, H. J.; Cho, B. R., Measurement of pH Values in Human Tissues by Two-Photon Microscopy. *Angew. Chem. Int. Ed.* **2012**, *51*, 2673-2676.
63. Mohan, P. S.; Lim, C. S.; Tian, Y. S.; Roh, W. Y.; Lee, J. H.; Cho, B. R., A two-photon fluorescent probe for near-membrane calcium ions in live cells and tissues. *Chem. Commun.* **2009**, *0*, 5365-5367.
64. Kim, D.; Singha, S.; Wang, T.; Seo, E.; Lee, J. H.; Lee, S.-J.; Kim, K. H.; Ahn, K. H., In vivo two-photon fluorescent imaging of fluoride with a desilylation-based reactive probe. *Chem. Commun.* **2012**, *48*, 10243-10245.
65. Kim, D.; Sambasivan, S.; Nam, H.; Hean Kim, K.; Yong Kim, J.; Joo, T.; Lee, K.-H.; Kim, K.-T.; Han Ahn, K., Reaction-based two-photon probes for in vitro analysis and cellular imaging of monoamine oxidase activity. *Chem. Commun.* **2012**, *48*, 6833-6835.
66. Sreenivasa Rao, A.; Kim, D.; Nam, H.; Jo, H.; Kim, K. H.; Ban, C.; Ahn, K. H., A turn-on two-photon fluorescent probe for ATP and ADP. *Chem. Commun.* **2012**, *48*, 3206-3208.
67. Au-Yeung, H. Y.; New, E. J.; Chang, C. J., A selective reaction-based fluorescent probe for detecting cobalt in living cells. *Chem. Commun.* **2012**, *48*, 5268-5270.
68. Karton-Lifshin, N.; Segal, E.; Omer, L.; Portnoy, M.; Satchi-Fainaro, R.; Shabat, D., A unique paradigm for a Turn-ON near-infrared cyanine-based probe: noninvasive intravital optical imaging of hydrogen peroxide. *J. Am. Chem. Soc.* **2011**, *133*, 10960-10965.
69. Maity, D.; Govindaraju, T., A turn-on NIR fluorescence and colourimetric cyanine probe for monitoring the thiol content in serum and the glutathione reductase assisted glutathione redox process. *Org. Biomol. Chem.* **2013**, *11*, 2098-2104.
70. Leevy, W. M.; Gammon, S. T.; Jiang, H.; Johnson, J. R.; Maxwell, D. J.; Jackson, E. N.; Marquez, M.; Piwnicka-Worms, D.; Smith, B. D., Optical imaging of bacterial infection in living mice using a fluorescent near-infrared molecular probe. *J. Am. Chem. Soc.* **2006**, *128*, 16476-16477.

71. Atilgan, S.; Ozdemir, T.; Akkaya, E. U., A sensitive and selective ratiometric near IR fluorescent probe for zinc ions based on the distyryl–Bodipy fluorophore. *Org. Lett.* **2008**, *10*, 4065-4067.
72. Chen, X.; Nam, S.-W.; Kim, G.-H.; Song, N.; Jeong, Y.; Shin, I.; Kim, S. K.; Kim, J.; Park, S.; Yoon, J., A near-infrared fluorescent sensor for detection of cyanide in aqueous solution and its application for bioimaging. *Chem. Commun.* **2010**, *46*, 8953-8955.
73. Grynkiewicz, G.; Poenie, M.; Tsien, R. Y., A new generation of Ca²⁺ indicators with greatly improved fluorescence properties. *J. Biol. Chem.* **1985**, *260*, 3440-3450.

Chapter 5

Colorimetric and fluorometric molecular probes for Co^{2+}

Papers based on this chapter have been published in *Inorg. Chem.*, **2011**, *50*, 11282-11284 ([Link](#)) and *Org. Lett.*, **2012**, *14*, 6008-6011 ([Link](#)). Reproduced by permission of the American Chemical Society. Another one manuscript has been submitted for publication.

1. Introduction

Cobalt is an important element for all multicellular organisms present in minute amounts as a part of cobalamin.¹⁻³ Cobalamin is necessary for myelin formation—an insulating layer found around nerves, to supports red blood cell production, for the metabolism of fats, carbohydrates and synthesis of proteins.⁴ The deficiency of Co^{2+} leads to anemia, retarded growth, and loss of appetite. Apart from its biological role, exposure to high levels of cobalt can cause health effects like decreased cardiac output, cardiac and thyroid enlargements, heart disease, elevated red blood cells accompanied by increased cells in the bone marrow, increased blood volume, and vasodilation and flushing.^{5,6} Cobalt is also responsible for allergic contact dermatitis and possibly carcinogenic to humans.⁷ The maximum tolerable level of Co^{2+} is ca. 10 ppm (170 μM). Major sources of cobalt in the atmosphere are soil, dust, seawater, forest fires and volcanic eruptions. Cobalt is also released to the environment from burning coal and oil, truck and airplane exhausts, and diamond polishing, porcelain, chemical and hard metal industry.⁸ Therefore, it is crucial to detect trace amounts of cobalt samples in the environment for maintaining good human health. Many analytical techniques such as flame atomic absorption and flow injection detect low levels of Co^{2+} , but require either tedious sample pretreatments or expensive instrumentation. Despite the patent contributions of cobalt homeostasis to physiology and pathology, the underlying mechanisms of how its signal/stress dichotomy can affect healthy and disease states remain insufficiently understood. Fluorometric detection is practically difficult because of the fluorescence quenching nature of paramagnetic Co^{2+} .⁹ However, it is possible to develop novel new methods for real-time monitoring of cobalt in biological and environmental samples, particularly in bioavailable forms, offer potentially useful tools to help elucidate its physiological and pathological effects. There have been only a few sensors reported for the detection for Co^{2+} with moderate success.¹⁰⁻¹²

2. Rationale for designing colorimetric and fluorometric molecular probes for cobalt

Metal-responsive colorimetric and fluorometric indicators provide a convenient and effective approach for studying the chemistry of exchangeable metal pools in live biological samples.¹³⁻¹⁸ Two major practical challenges for biological cobalt detection stem from the fact that (i) its dominant oxidation state in biological systems, Co^{2+} , is paramagnetic and thus a potent free radical quencher in all coordination environments, and (ii) biologically relevant divalent metal ion competitors like Ni^{2+} , Cu^{2+} , and Zn^{2+} typically bind more tightly to common ligand scaffolds over Co^{2+} owing to Irving-Williams series considerations.¹⁹ As such, these two critical issues make it difficult to use a traditional chromophore–receptor binding scheme for selective detection of metal ions like Co^{2+} by colorimetric as well as emission turn on response.¹⁶

The development of sensitive chromogenic chemosensors has been gaining momentum in recent years because of the potential application in medical biochemistry and simplicity of the approach. Colorimetric chemosensors of cations can be generated based on right combination of a receptor and chromophore. Compared to fluorometric sensors, colorimetric sensors have attracted much attention for allowing “naked-eye” detection in an uncomplicated and inexpensive manner, offering qualitative and quantitative information.²⁰⁻²³ Colorimetric chemosensors of cations can be generated based on the right combination of receptor and chromophore. One such combination would be a conjugate of an amine and an aldehyde carrying thioamides formed through Schiff base linkages.²⁴⁻²⁶ Coumarin and its derivatives have been used as excellent chromogenic and fluorogenic chromophores because of their tunable photophysical properties in the visible region. A simple approach has been undertaken by conjugating thiourea with coumarin-3-carboxaldehyde derivative to form bisthiocarbonohydrazone system as efficient colorimetric sensor that can selectively detect Co^{2+} by visible color change in aqueous medium. 7-(diethylamino)coumarin serves as a chromophoric core. The π -conjugation and stronger electron-withdrawing ability of the thioketone group have enhanced charge transfer within the molecule. The imine and thioketo groups can act as chelating sites of the metal cations, in particular, transition- and post

transition-metal cations. Tautomerized thioamide can easily coordinates to Co^{2+} after deprotonation, which will lead to a red shift in the absorbance band in the visible region.

Next, a modular fluorescence probe was devised to visualize biological cobalt by turn on response. It is constructed of a dye molecule with a conjugated functional group (X) linked to a trigger moiety (Figure 1). The masking of functional group suppresses conjugated π -electron system of the dye and thus turns off fluorescence of the probe. Cobalt assisted

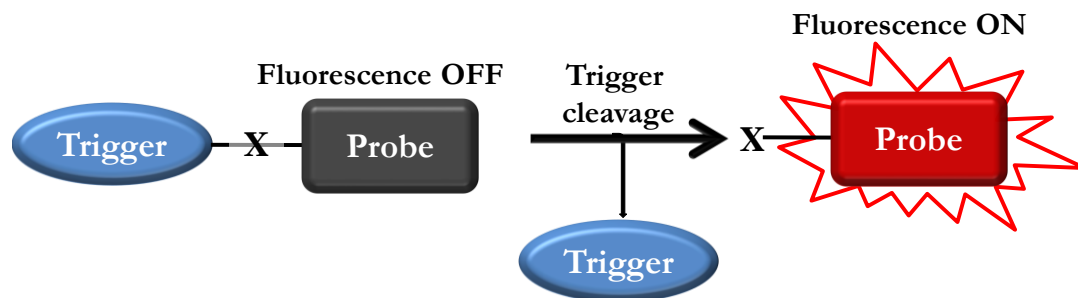


Figure 1. Classic mechanism for a modular turn on fluorescence probe.

removal of the trigger restore conjugation of lone pair electrons on functional group with π -electrons of the dye and thereby turns on fluorescent signal of the probe.

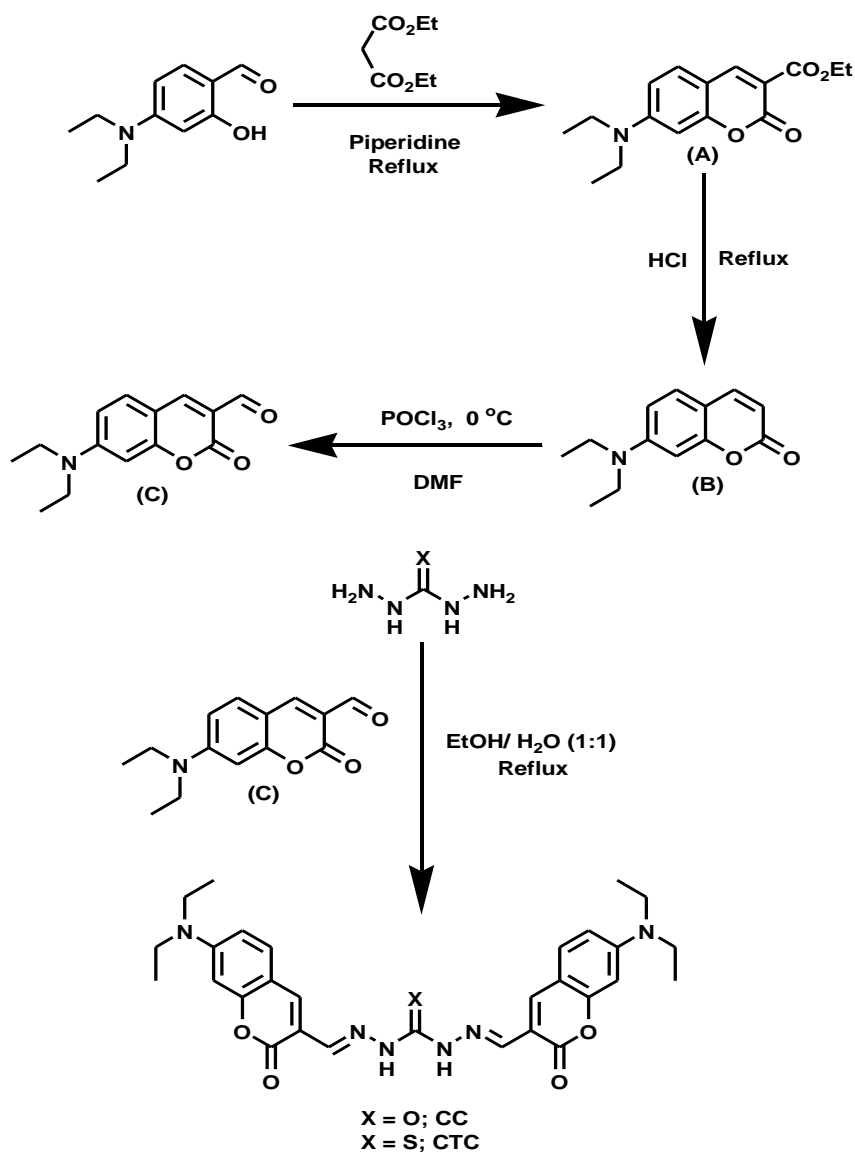
As the paramagnetic Co^{2+} has tendency to quench fluorescence, the design strategy for its turn on detection relies on reaction-based approach²⁷⁻³¹ in which a selective but transient Co^{2+} -mediated bond-cleaving reaction transforms a weakly fluorescent probe into a highly fluorescent dye, where the final product will be free of paramagnetic metal center. As a secondary selectivity filter to overcome thermodynamic biases due to Irving-Williams series considerations, the coordination environment (trigger) was designed in such way that only Co^{2+} binding would promote specific redox and/or small-molecule reactivity while other competitor metal ions would not be able to achieve. O_2 -mediated Co^{2+} reactivity was observed for biomimetic N-dealkylation of a polypyridine-based ligand shown by McKenzie *et al.*,³² a report by Taki *et al.*³³ on turn-on detection of Cu^+ ions by oxidative ether cleavage and Koide's organometallic strategies for Pd, Pt, and Hg detection.³⁴⁻³⁶ The tetradentate ligands N_3O linked chromophore was developed as nonfluorescent probe for reaction-based turn on sensing of Co^{2+} by Chang *et al.*³⁷ The metal ion mediated cleaving of the benzylic ether bond in the nonfluorescent probes generates a fluorescent dye under physiologically reducing conditions. Excited state intramolecular proton transfer (ESIPT) based chromophore

2-(2'-hydroxyphenyl)benzothiazole (**HBT**) shows a large Stokes shift and corresponding efficient ratiometric fluorescence response.³⁸⁻⁴⁰ In this chapter, Co^{2+} reactive tetradentate N_3O ligand is combined with ESIPT active chromophore HBT to generate a molecular probe **HBTCo** is presented. Co^{2+} assisted benzyl ether bond (C–O) cleavage releases an ESIPT active **HBT** fluorophore. The released **HBT** fluorophore undergoes enol to keto tautomeric transformation as a result of ESIPT, and thus a large Stokes shift in the fluorescence emission was achieved. Resorufin has maximal emission at 585 nm upon excitation at 550 nm and can be used to analyze intracellular processes without damaging the cell. The resorufin chromophore has an absorption maximum around 573 nm was also known for colorimetric detection of fluoride, DNA hybridization, and hydrolase.⁴¹⁻⁴⁷ The alkylation of the 7-hydroxy group of resorufin effectively weakens its intramolecular charge transfer which quenches its emission by blocking push-pull mechanism in the chromophore. In accordance with above rationale a nonfluorescent probes **ResCo** was designed for Co^{2+} by combining resorufin dye and tetradentate ligands N_3O through 7-hydroxyl functionality. Co^{2+} mediated cleaving of benzylic ether bond in nonfluorescent probe **ResCo** will release chromogenic resorufin dye which automatically shows ratiometric visible absorption (colorimetric) and 'switch-on' fluorometric responses for Co^{2+} under physiologically reducing conditions.

3.1 Highly selective colorimetric molecular probe (CTC) for Co^{2+}

3.1.1 Synthesis

7-Diethylamino-2-oxo-2H-chromene-3-carboxylic acid ethyl ester (**A**) was synthesized refluxing a mixture of 4-diethylamino salicylaldehyde, diethylmalonate, and piperidine in toluene. The ester (**A**) undergoes acid catalyzed decarboxylation to form 7-diethylamino-



Scheme 1. Synthesis of coumarin-carbonohydrazone (CC) and coumarin-thiocarbonohydrazone (CTC).

chromene-2-one (**B**) which was further subjected to Vilsmeier–Haack reaction to obtain 7-diethylamino-2-oxo-2H-chromene-3-carboxyldehyde (**C**) in excellent yield. 7-Diethylamino-2-oxo-2H-chromene-3-carboxyldehyde (**C**) was treated with carbonylhydrazone/thiocarbonylhydrazone in an ethanol/water (1:1) mixture under reflux condition to form Schiff base derivatives coumarin-carbonohydrazone (**CC**) and coumarin-thiocarbonohydrazone (**CTC**) respectively (Scheme 1) in quantitative yield. These ligands were characterized by NMR, mass spectrometry and elemental analysis.

3.1.2 Photophysical property of coumarin-thiocarbonylhydrazone (**CTC**) and colorimetric detection of Co^{2+}

The photophysical properties of **CC** and **CTC** were investigated by monitoring the absorption spectral behavior upon addition of several metal ions such as Li^+ , Na^+ , K^+ , Ba^{2+} , Sr^{2+} , Mg^{2+} , Al^{3+} , Ca^{2+} , Mn^{2+} , Fe^{2+} , Ni^{2+} , Cu^{2+} , Zn^{2+} , Ag^+ , Cd^{2+} , Hg^{2+} , Pb^{2+} and Co^{2+} in aqueous medium (0.05 mM HEPES, $\text{pH}=7.2/\text{CH}_3\text{CN} = 60:40$). **CC** shows an absorption band centered around 455 nm and there was no specific selectivity for various metal ions

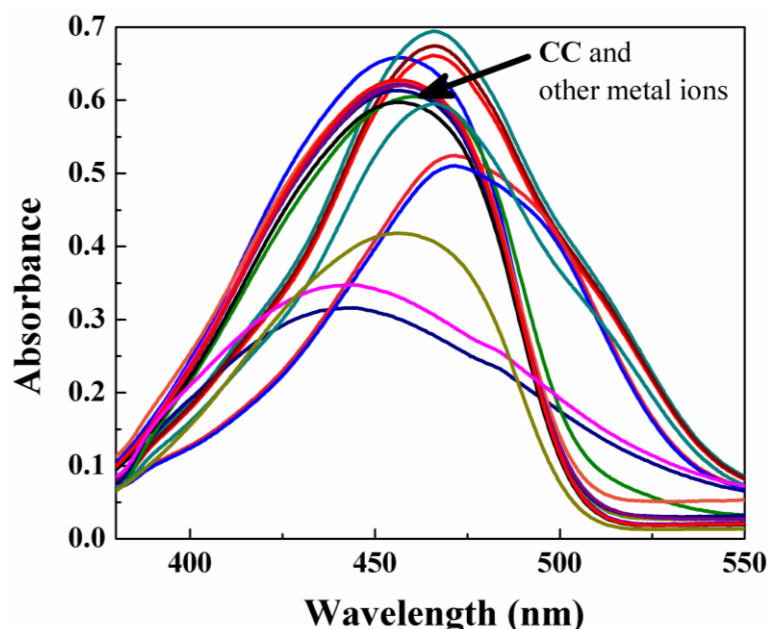


Figure 2. UV-Vis absorbance spectra of **CC** (10.0 μM) and on addition of salts of Li^+ , Na^+ , K^+ , Ca^{2+} , Mg^{2+} , Al^{3+} , Ba^{2+} , Sr^{2+} , Mn^{2+} , Fe^{2+} , Ni^{2+} , Cu^{2+} , Zn^{2+} , Cd^{2+} , Ag^+ , Hg^{2+} , Pb^{2+} , and Co^{2+} (50.0 equiv) in aqueous medium (0.05 mM HEPES, $\text{pH}=7.2/\text{CH}_3\text{CN} = 60:40$).

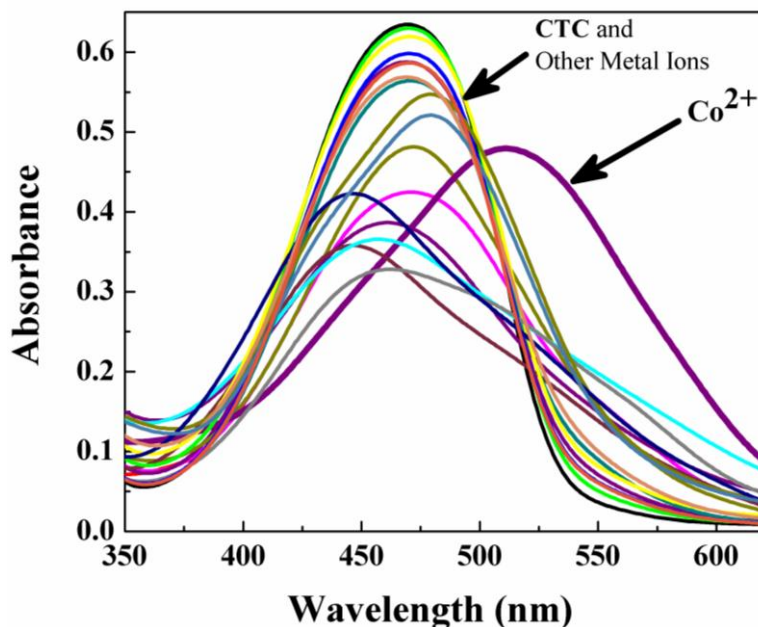


Figure 3. UV-Vis absorption spectra of CTC (10.0 μM) and on addition of salts of Li^+ , Na^+ , K^+ , Ca^{2+} , Mg^{2+} , Al^{3+} , Ba^{2+} , Sr^{2+} , Mn^{2+} , Fe^{2+} , Ni^{2+} , Cu^{2+} , Zn^{2+} , Cd^{2+} , Ag^+ , Hg^{2+} , Pb^{2+} , and Co^{2+} (50.0 equiv) in aqueous medium (0.05 mM HEPES, $\text{pH}=7.2$ / $\text{CH}_3\text{CN} = 60:40$).

tested (Figure 2). As shown in Figure 3, CTC exhibited an absorption band centered around 470 nm with extinction coefficient (ϵ) of $6.8 \times 10^4 \text{ M}^{-1} \text{ cm}^{-1}$, which remains unchanged upon addition of 50.0 equiv of Li^+ , Na^+ , K^+ , Ba^{2+} , Mg^{2+} , Al^{3+} and Ca^{2+} . Upon addition of 50.0 equiv of Mn^{2+} , Fe^{2+} , Cu^{2+} , Ag^+ and Hg^{2+} absorbance intensity decreases and band slightly blue shifted to different extents. The absorption band slightly red shifted upon addition of 50.0 equiv of Sr^{2+} , Ni^{2+} , Zn^{2+} , Cd^{2+} and Pb^{2+} and no color changes in the CTC solution was observed. In case of Co^{2+} , the absorbance band at 470 nm red shifted to 510 nm ($\Delta\lambda = 40 \text{ nm}$) and color of the solution has changed from yellow to deep pink. Absorption study of CTC with sequential addition of increasing concentrations of Co^{2+} (0 – 3.0 μM) is shown in Figure 4. The absorbance is slowly decreased and band at 470 nm red shifted to 490 nm upon addition of 1.5 μM of Co^{2+} . After reaching 2.2 μM , the absorbance started increasing and absorbance maxima overall red shifted to 510 nm. The absorbance attains saturation with addition of 3.0 μM of Co^{2+} ($\epsilon = 6 \times 10^4 \text{ M}^{-1} \text{ cm}^{-1}$).

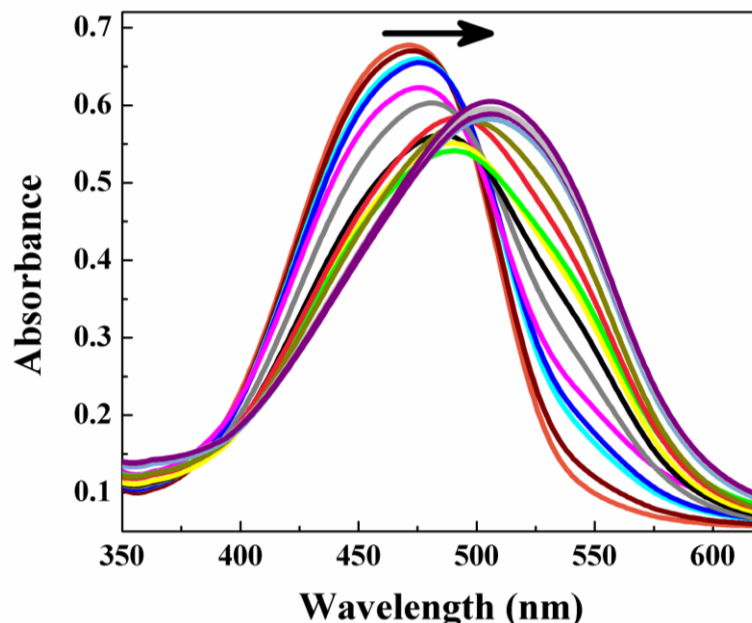


Figure 4. UV-Vis absorption spectra of CTC (10.0 μM) upon additions of Co^{2+} (0.0, 0.2, 0.4, 0.6, 0.8, 1.0, 1.2, 1.4, 1.6, 1.8, 2.0, 2.2, 2.4, 2.6, 2.8 and 3.0 μM) in aqueous medium.

3.1.3 Competitive study for colorimetric detection of Co^{2+} using CTC

The preferential selectivity of CTC as colorimetric chemosensor for the detection of Co^{2+} was studied in presence of various competing metal ions. CTC exhibited a distinct color change from yellow to deep pink upon addition of Co^{2+} (Figure 5a). For competition studies, CTC was treated with 1.0 equiv of Co^{2+} in the presence of 5.0 equiv of other metal ions as indicated in Figure 5b. There was no interference for the detection of Co^{2+} in presence of Li^+ , Na^+ , K^+ , Ba^{2+} , Sr^{2+} , Ca^{2+} , Mg^{2+} , Mn^{2+} , Fe^{2+} , Ni^{2+} , Cu^{2+} , Zn^{2+} , Cd^{2+} , Hg^{2+} and Pb^{2+} , except Ag^+ . In case of Ag^+ , a relatively diminished, but detectable color change was observed for Co^{2+} . Thus, CTC can be used as a selective colorimetric sensor for Co^{2+} in the presence of most competing metal ions.

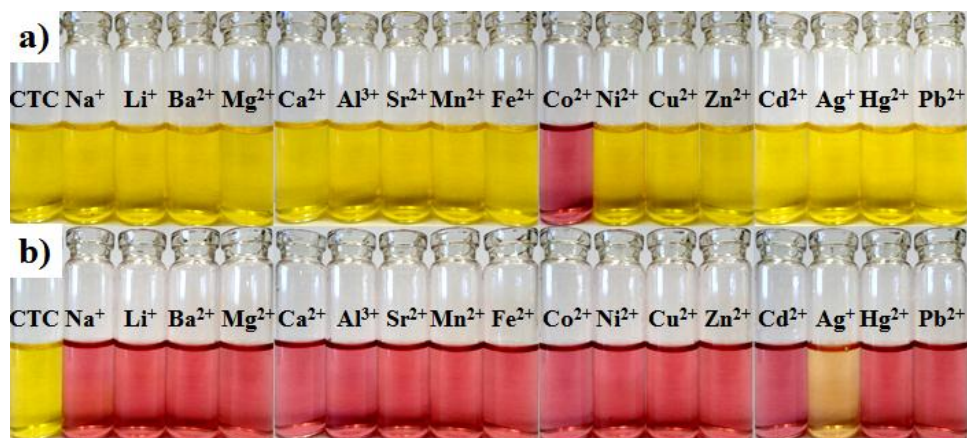


Figure 5. a) The observed color changes of CTC solution (10.0 μM) upon adding 5.0 equiv of different metal ions in aqueous media. b) The color changes of CTC solution (10.0 μM) containing Co^{2+} (1.0 equiv) in the presence of different metal ions (5.0 equiv) in aqueous media.

3.1.4 Determination of binding stoichiometry of CTC with Co^{2+} and pH dependent study

Job's plot obtained from absorbance spectral studies showed 2:1 stoichiometric complexation between CTC and Co^{2+} (Figure 6). This data was further supported by mass spectrometric

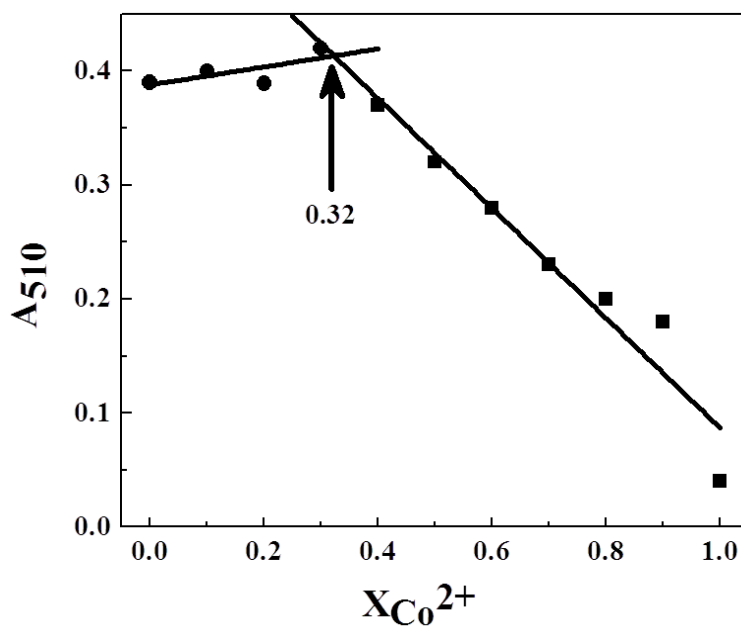


Figure 6. Job plot for the determination of the stoichiometry of CTC and Co^{2+} complex formation.

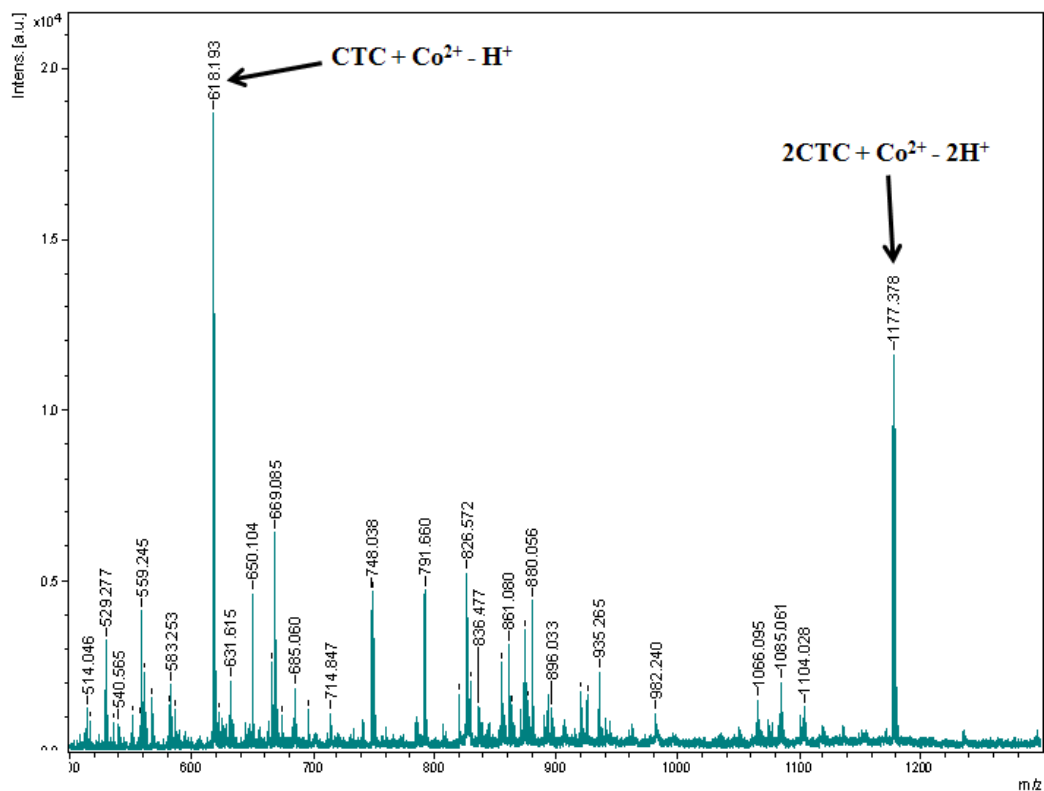


Figure 7. MALDI-TOF mass spectrum of $2\text{CTC}:\text{Co}^{2+}$ complex.

analysis of $\text{CTC}-\text{Co}^{2+}$ complex formation. MALDI/TOF-MS shows the formation of complex between two molecules of deprotonated CTC and a cobalt ion [m/z : 1177.38 ($2\text{CTC} + \text{Co}^{2+} - 2\text{H}^+$); calcd for $\text{C}_{58}\text{H}_{64}\text{CoN}_{12}\text{O}_8\text{S}_2$: 1179.37] (Figure 7). The response parameter α , which is defined as the ratio of free ligand concentration to the initial concentration of ligand, was plotted as a function of the Co^{2+} concentration. This plot can serve as the calibration curve for the detection of Co^{2+} (Figure 8). The association constant ($\log K_a$) for the complexation of CTC and Co^{2+} was found to be 7.95 M^{-2} .

In colorimetric sensor **CTC**, binding and signaling subunits are electronically conjugated to each other to effectively induce color changes. Sulphur analogues ($\text{C}=\text{S}$) are less stable because of the poor overlap between the 2sp^2 orbital on carbon and 3sp^2 orbital on sulphur. In **CTC**, thioamide undergoes conjugation with nitrogen to stabilize the weak $\text{C}=\text{S}$ bond.¹⁰ Tautomerized thioamide coordinate to Co^{2+} after deprotonation which leads to red shift in the absorbance band in visible region (Figure 9).

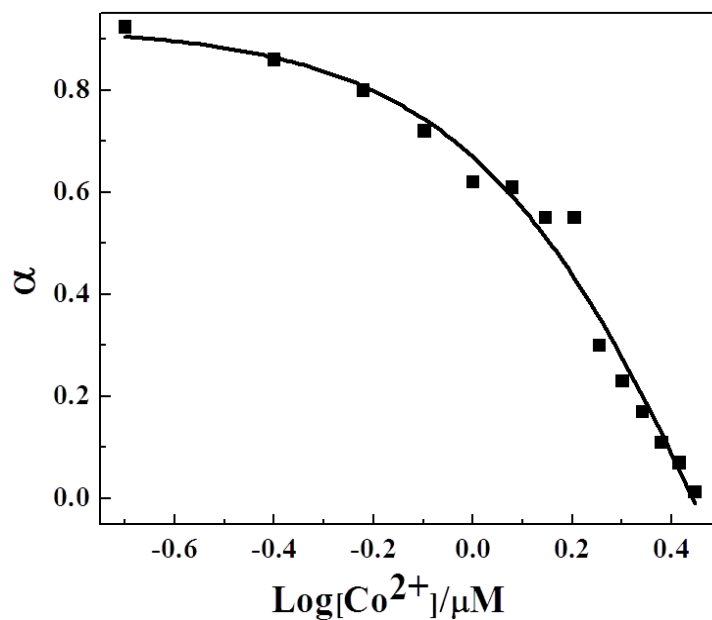


Figure 8. Response parameter values (α) as a function of the logarithm of Co^{2+} concentration. α is defined as the ratio between the free ligand concentration and the initial concentration of ligand.

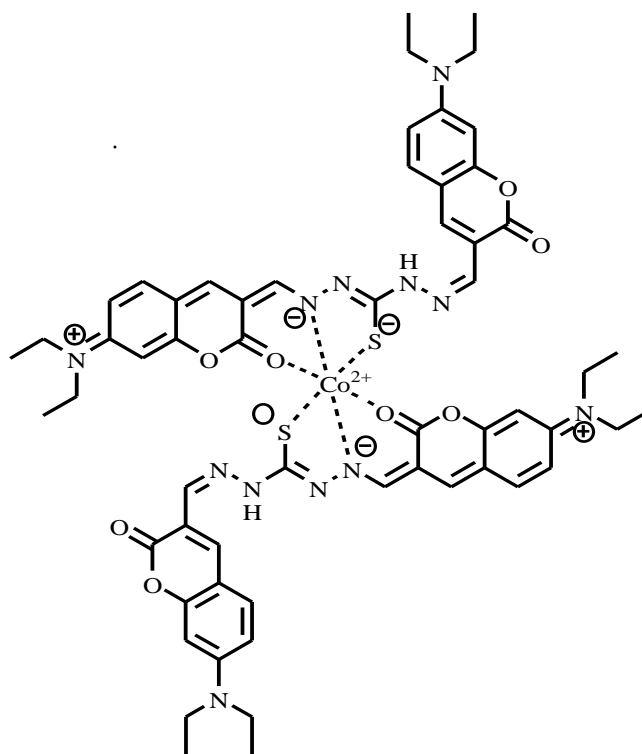


Figure 9. Proposed structure of CTC- Co^{2+} complex.

The absorbance of $[\text{2CTC}:\text{Co}^{2+}]$ complex have been recorded as a function of pH. The absorbance intensity at 510 nm was found to increase gradually from pH 2.0–12.5 (Figure 10). Co^{2+} can be clearly detected by naked eye or UV/Vis absorption measurements using CTC over a wide pH range of 2.0–12.5.

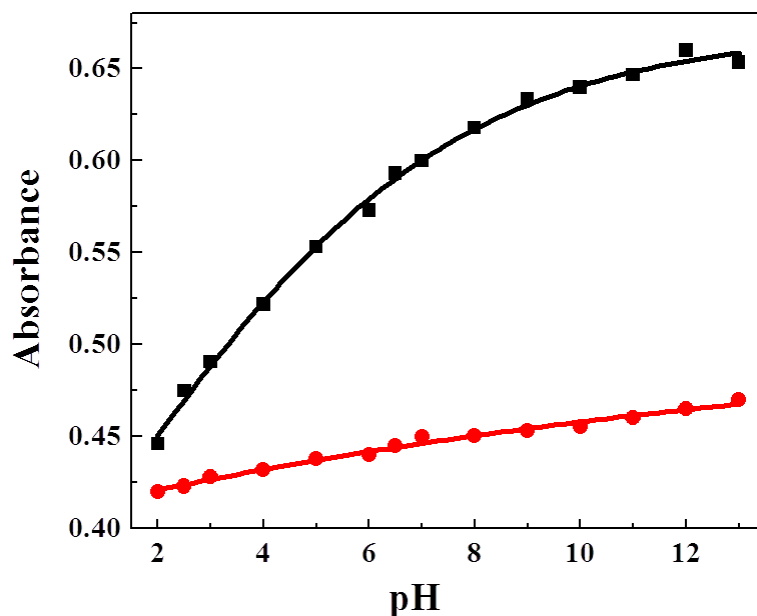


Figure 10. Absorbance at 510 nm of CTC as function of pH. Red trace: absorbance intensity of a solution of CTC and black trace: absorbance intensity of a solution of CTC and Co^{2+} (1 equiv) are plotted against pH in aqueous medium (50 mM HEPES, 40% CH_3CN).

3.1.5 Colorimetric kit for Co^{2+} detection

For practical applications, a colorimetric test kit has been developed. The test kit uses ligand coated filter paper strips which were prepared by immersing them into CTC solution (2.0 mM). The aqueous solutions of different metal ions were sprayed onto these strips and yellow colored strip changed its color to deep pink exclusively when Co^{2+} solution was sprayed (Figure 11). In addition, intensity of the colored strips can be used to estimate different concentrations range of Co^{2+} . This experiment exhibits steady colorimetric changes for increasing concentrations of Co^{2+} with at least down to 1.0 μM detection limit.

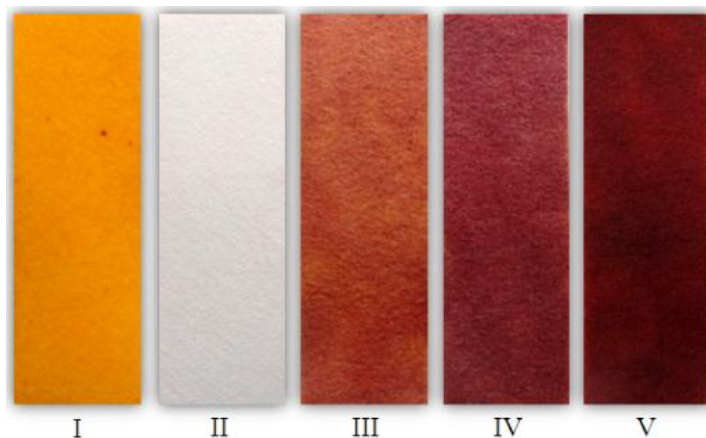


Figure 11. Colorimetric test kit. Photographs of the filter paper coated with **CTC** ($10.0 \mu\text{M}$) used for detecting different concentrations of Co^{2+} in aqueous solutions. I: **CTC** (control), II: Co^{2+} ($500 \mu\text{M}$, control), III-V: **CTC** filter paper sprayed with 1.0 , 2.0 and $3.0 \mu\text{M}$ Co^{2+} respectively.

3.1.6 **CTC** as colorimetric reagent for the detection of Co^{2+} in microbes

The use of **CTC** has been further demonstrated as colorimetric reagent for the detection of Co^{2+} in microbes. The *E. coli* strain DH5 α were grown overnight in LB media (HIMEDIA) at 37°C incubation. The cells were harvested and vortexed for making the homogeneous suspension in sterile distilled water. The cultured cells were first exposed to Co^{2+} ($5.0 \mu\text{M}$) in a 50 mM HEPES/ CH_3CN buffer (v/v, 3:2; pH 7.2) for 30 min at 25°C . The excess Co^{2+} present in the cultured media was removed through centrifugation. This process was repeated after adding $\sim 5 \text{ mL}$ of 50 mM HEPES/ CH_3CN buffer to remove traces of Co^{2+} that may present on the microorganism surfaces in order to avoid the background color while recording optical microscope images. The centrifuged bacterial cells were finally exposed to **CTC** ($10.0 \mu\text{M}$) in 50 mM HEPES/ CH_3CN buffer. The treated bacterial cells were examined at $100\times$ magnification on a confocal laser scanning microscope (LSM 510 META, Carl Zeiss), and captured using LSM5 Image Examiner (Figure 12). The microscopy images of bacterial cells in the absence and presence of Co^{2+} were observed for comparison. The *E. coli* exposed to Co^{2+} followed by **CTC** developed deep pink color as shown in light microscope image (Figure 12d). This clearly revealed that the detection and staining of Co^{2+} in cell is possible using colorimetric reagent **CTC**.

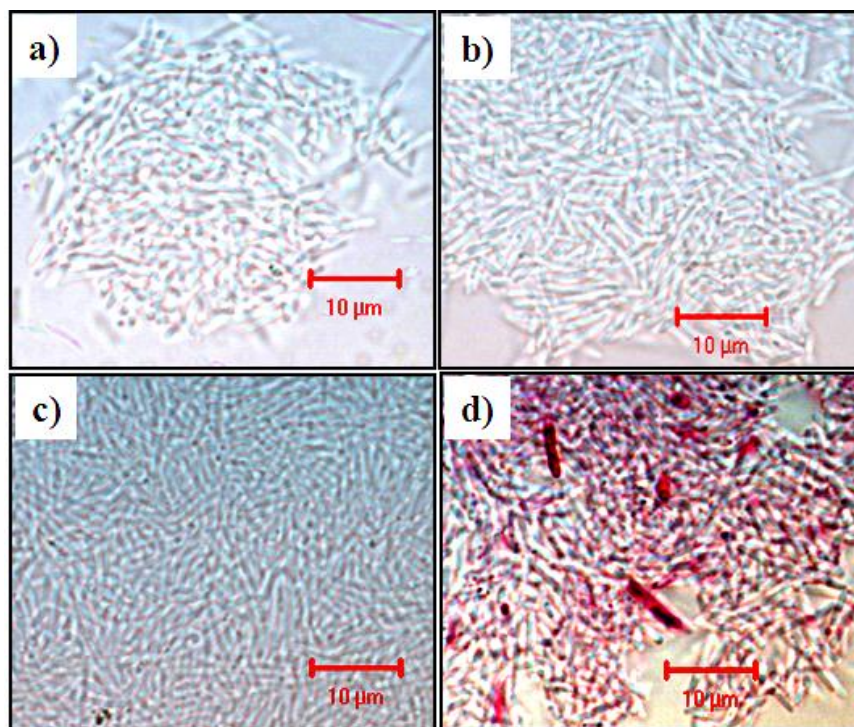


Figure 12. Light microscope images of a) control cells of *E. Coli*, b) cells exposed to only Co^{2+} (5.0 μM), c) cells exposed to only CTC (10.0 μM), d) cells exposed to Co^{2+} (5.0 μM) and CTC (10.0 μM).

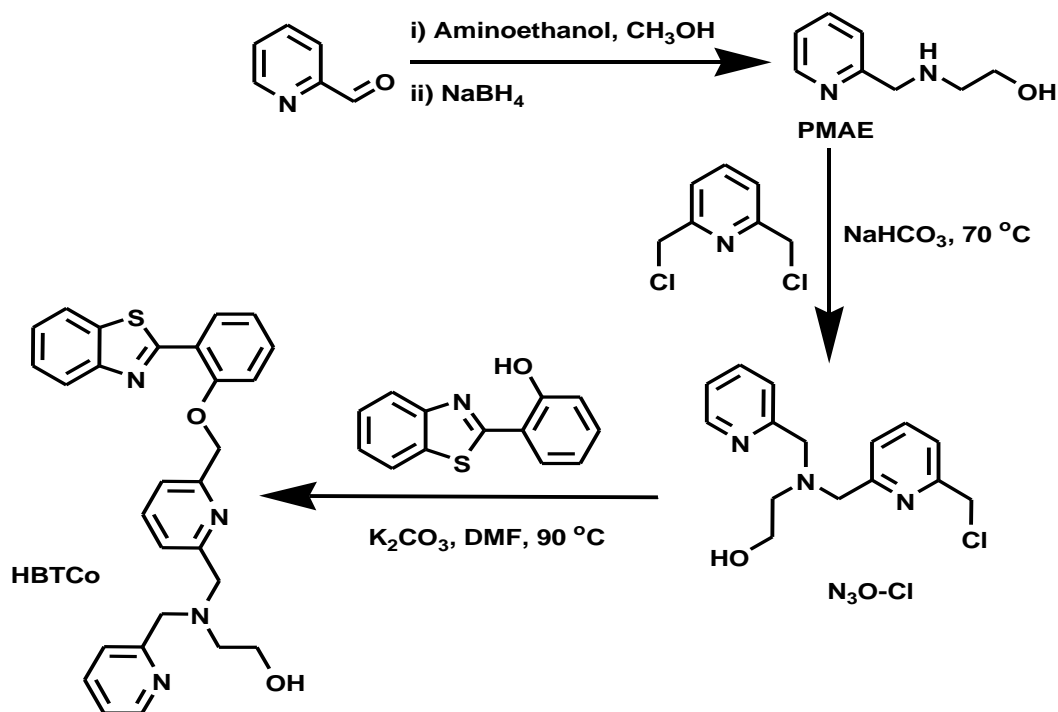
3.1.7 Conclusion

In summary, a new colorimetric chemosensor **CTC** was designed and synthesized. The sensitivity and selectivity of **CTC** to Co^{2+} over other metal ions in aqueous media were demonstrated by its optical response, ascribed to the formation of push-pull Co^{2+} Schiff base complex. The main strength of the work presented herein is the ability to access Co^{2+} chromogenic sensor through a highly economical, simple and straightforward synthetic route. **CTC** based colorimetric kit was developed for Co^{2+} detection and demonstrated as staining agent for Co^{2+} in cellular microorganisms. Therefore molecular sensor **CTC** with optical responses in the visible region can be used as a practically viable probe for environmental and biological sensing of cobalt ions.

3.2 Reactive probe (HBTCo) for ratiometric fluorescence detection of Co^{2+} based on excited-state intramolecular proton transfer (ESIPT) mechanism

3.2.1 Synthesis

The design strategy is based on the 2-(2'-hydroxyphenyl) benzothiazole (HBT) molecular platform as this ESIPT chromophore shows large Stokes shift and corresponding efficient ratiometric fluorescence response. Intermediate amino ligand 2-[(pyridin-2-ylmethyl)amino] ethanol (PMAE) was prepared in a one-pot synthesis. Typically, pyridine-2-carbaldehyde was reacted with aminoethanol, subsequent reduction with sodium tetrahydridoborate, gave the amino ligand (Scheme 2). This amino ligand was treated with 2,6-dichloromethylpyridine under basic condition to obtain receptor $\text{N}_3\text{O-Cl}$. HBTCo was synthesized by linking HBT with tetradentate $\text{N}_3\text{O-Cl}$ under basic condition in excellent yield.



Scheme 2. Synthesis of HBTCo.

3.2.2 Photophysical property of **HBTCo** and ratiometric detection of Co^{2+}

The fluorescence properties of **HBTCo** was studied in aqueous buffer solution (50 mM HEPES, pH 7.2) in presence of 2 mM glutathione (GSH) for mimicking the intracellular environment (Figure 13). Upon 350 nm excitation probe **HBTCo** emit blue fluorescence ($E_{max} = 380$ nm) correspond to **HBT** 'enol-form' emission. The fluorometric behavior of 20.0 μM probe was investigated in presence of several metal ions such as Li^+ , Na^+ , K^+ , Ba^{2+} , Mg^{2+} , Ca^{2+} , Al^{3+} , Mn^{2+} , Fe^{2+} , Co^{2+} , Ni^{2+} , Cu^+ , Cu^{2+} , Zn^{2+} , Cd^{2+} , Ag^+ , Hg^{2+} and Pb^{2+} after 2 h of mixing. The examined millimolar alkali and alkaline earth metals shown no or negligible change in fluorescence of **HBTCo**. While addition of Co^{2+} to **HBTCo** solution led to quenching of blue emission ($E_{max} = 380$ nm) and subsequent appearance of a new intense emission band in the green region ($E_{max} = 510$ nm). Other metal ions tested quench the blue fluorescence of **HBTCo** to different extent but there was no new emission band in the green region. The observed large red shift (130 nm) in emission indicate the Co^{2+} catalyzed oxidative cleavage of benzylic ether (C–O) linkage in presence of O_2 releasing ES IPT active

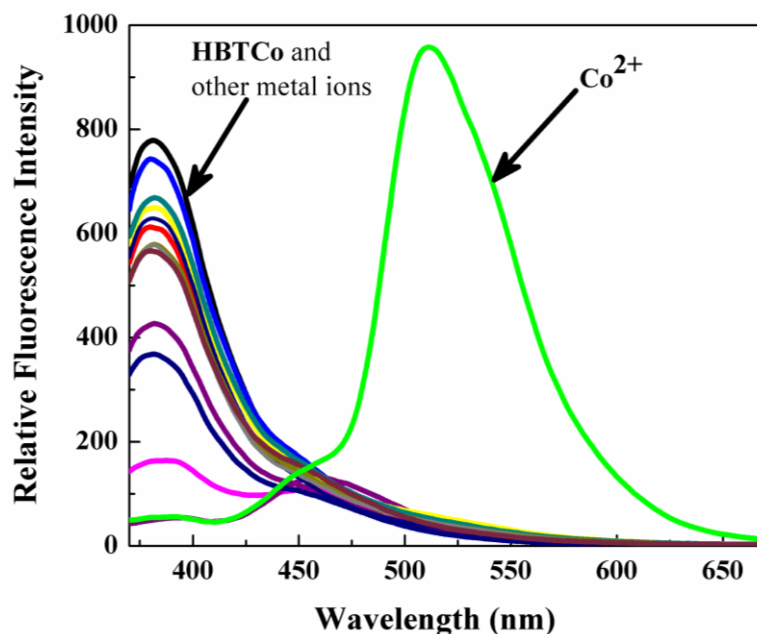


Figure 13. Fluorescence responses of **HBTCo** (20 μM) upon addition 1 mM of Li^+ , Na^+ , K^+ , Ba^{2+} , Mg^{2+} , Ca^{2+} , Al^{3+} and 20 μM of Mn^{2+} , Fe^{2+} , Co^{2+} , Ni^{2+} , Cu^+ , Cu^{2+} , Zn^{2+} , Cd^{2+} , Ag^+ , Hg^{2+} and Pb^{2+} after 2 h in aqueous solution (50 mM HEPES, pH 7.2, 2 mM GSH) ($\lambda_{ex} = 350$ nm).

phenolic **HB**T. The decrease in blue emission and corresponding increase in green emission band was also observed during sequential addition of Co^{2+} in a titration experiment. Minimum 20.0 μM Co^{2+} can be easily detected by this ratiometric study employing **HBTC**o (Figure 14). Time dependent study showed that the addition of Co^{2+} quenches **HBTC**o

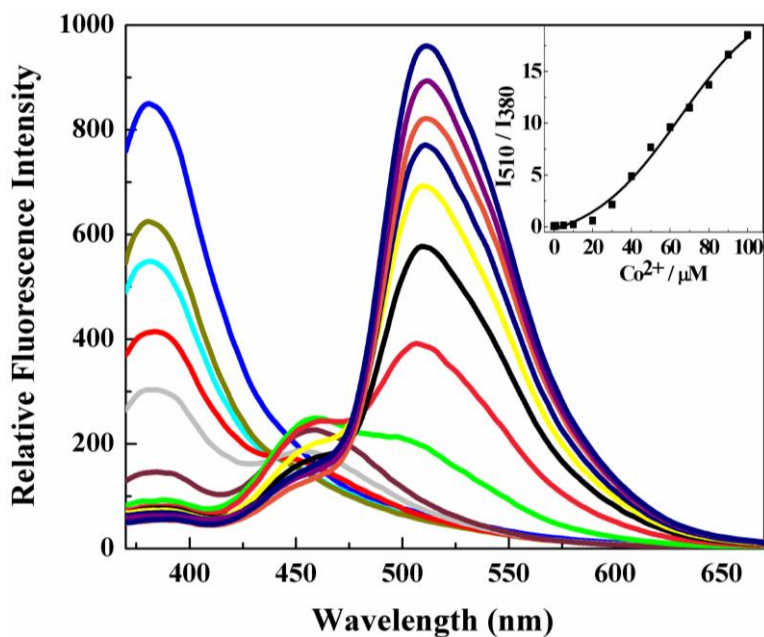


Figure 14. Fluorescence responses of **HBTC**o (20.0 μM) upon addition of 0.0, 5.0, 10.0, 20.0, 30.0, 40.0, 50.0, 60.0, 70.0, 80.0, 90.0, 100.0 μM of Co^{2+} after 2h in aqueous solution (50 mM HEPES, pH 7.2, 2 mM GSH) ($\lambda_{\text{ex}} = 350$ nm).

blue fluorescence ($E_{\text{max}} = 380$ nm) rapidly with appearance of a new peak around 460 nm (Figure 15). The rapid fluorescence quenching of probe is due to binding of paramagnetic Co^{2+} . Subsequent Co^{2+} catalyzed oxidative cleavage of benzyl ether bond releases **HB**T. The weak emission band at 460 nm is due to enolic rotamer,⁴⁰ as the Co^{2+} coordination with phenolic ($-\text{OH}$) moiety seems to initially stabilize the enol rotamer. Thus weak emission band at 460 nm may be viewed as the evidence for the existence of enolic intermediate. Then, the enol form slowly converts to keto tautomer upon excitation to emit bright green fluorescence at longer wavelength ($E_{\text{max}} = 510$ nm). The reducing environment created by GSH is very much crucial as confirmed by control experiments in the absence of GSH, which did not lead to benzylic ether bond cleavage (Figure 16).

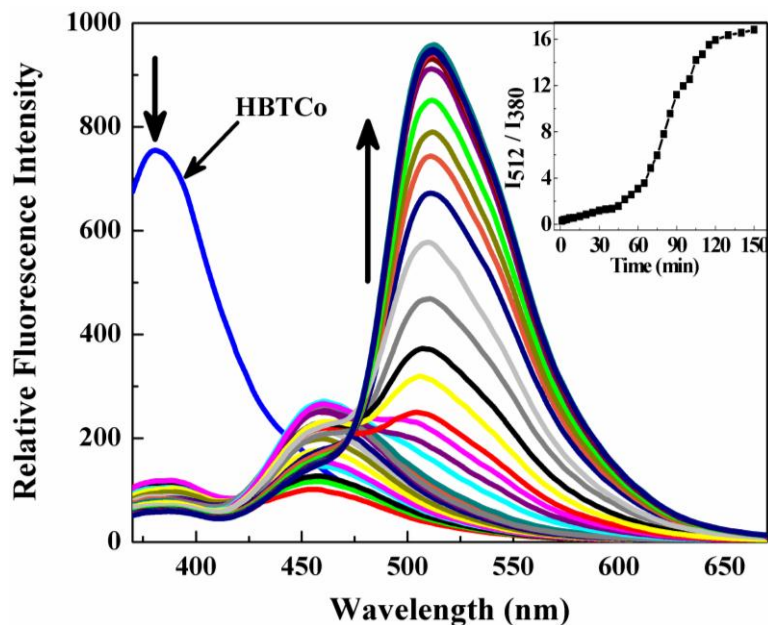


Figure 15. Time dependent fluorescence responses of **HBTCO** (20 μM) after addition of 100 μM of Co^{2+} in aqueous solution (50 mM HEPES, pH 7.2, 2 mM GSH) ($\lambda_{\text{ex}} = 350$ nm).

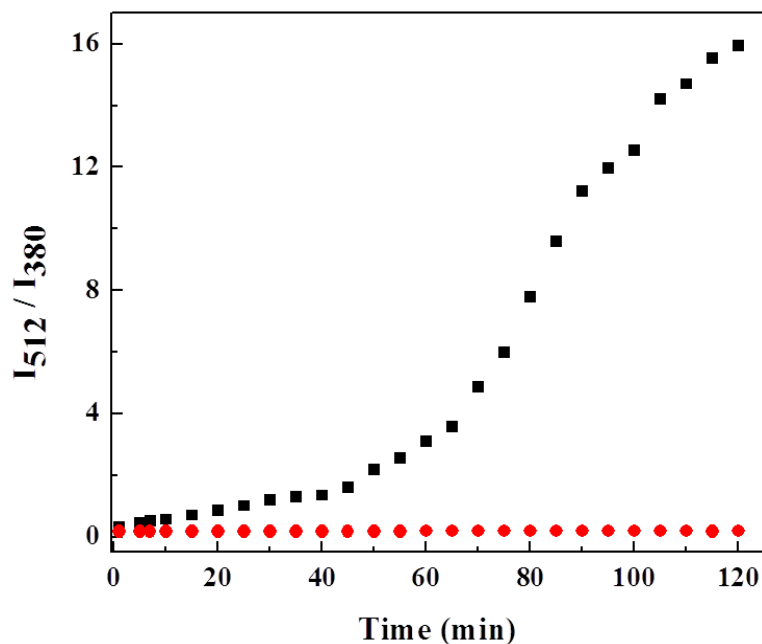


Figure 16. Time dependent ratiometric study of 20.0 μM **HBTCO** incubated with 100 μM of Co^{2+} in aqueous solution (50 mM HEPES, pH 7.2) with (**black trace**) and without (**red trace**) 2 mM GSH.

3.2.3 Competitive study for ratiometric detection of Co^{2+}

Competitive experiment suggest that the ratiometric probe **HBTCo** can clearly detects Co^{2+} in presence of all other metal ions respectively (Figure 17).

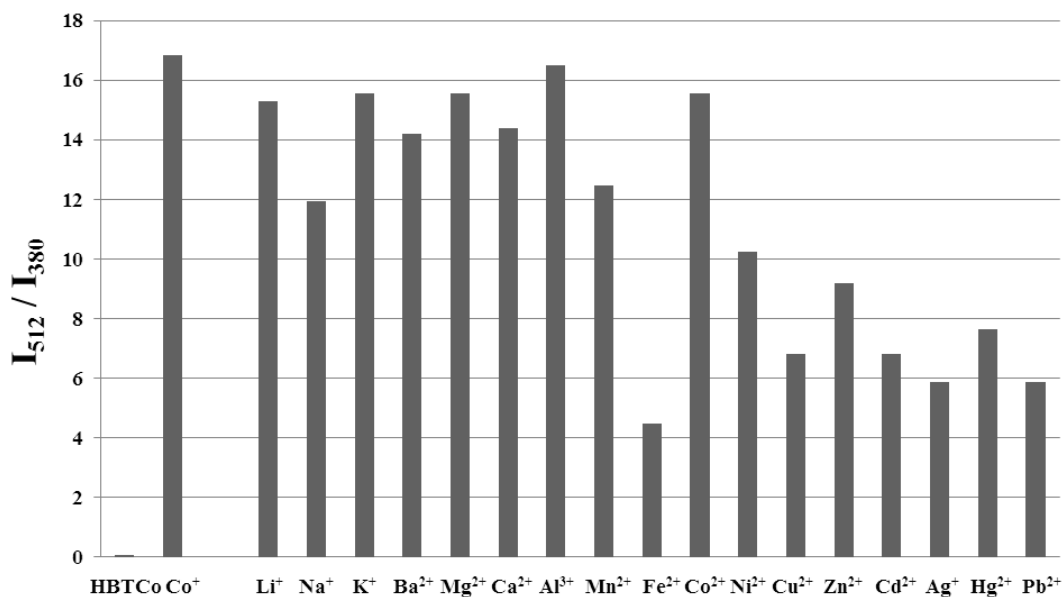


Figure 17. Competitive experiment for the detection of Co^{2+} using $20.0 \mu\text{M}$ **HBTCo**. $100.0 \mu\text{M}$ Co^{2+} is mixed with $100.0 \mu\text{M}$ of corresponding metal ions. Left two bars are control response of the corresponding probe and only metal ion.

3.2.4 pH dependent effects for ratiometric detection of Co^{2+}

The effect of pH on Co^{2+} mediated oxidative cleavage of benzylic ether bond was studied to understand efficiency of the process (Figure 18). **HBTCo** reacted efficiently with Co^{2+} in the biologically relevant pH range of 6.5-8.5 to release ES IPT active **HBT** fluorophore. Hence, this probe is very convenient for ratiometric detection of Co^{2+} without the interference from pH-dependent effects.

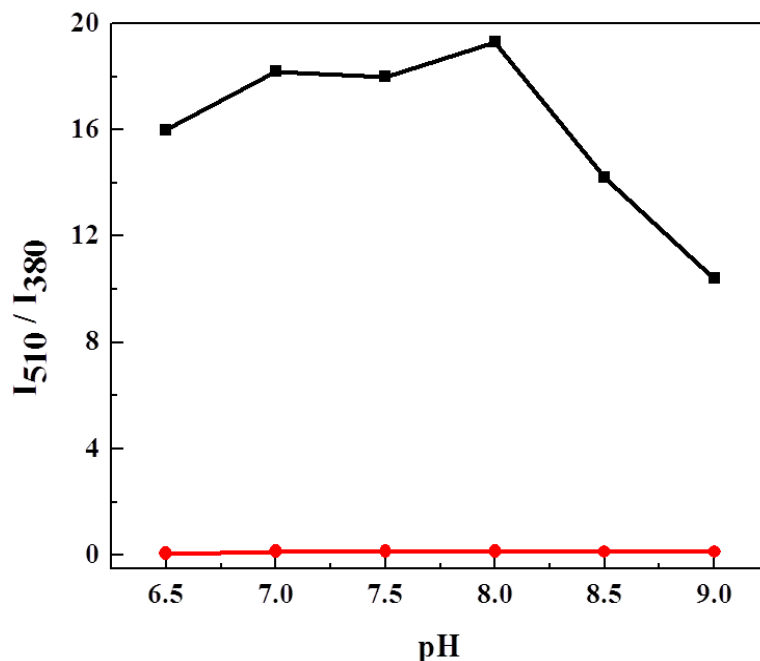
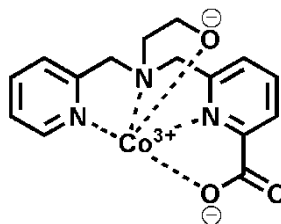
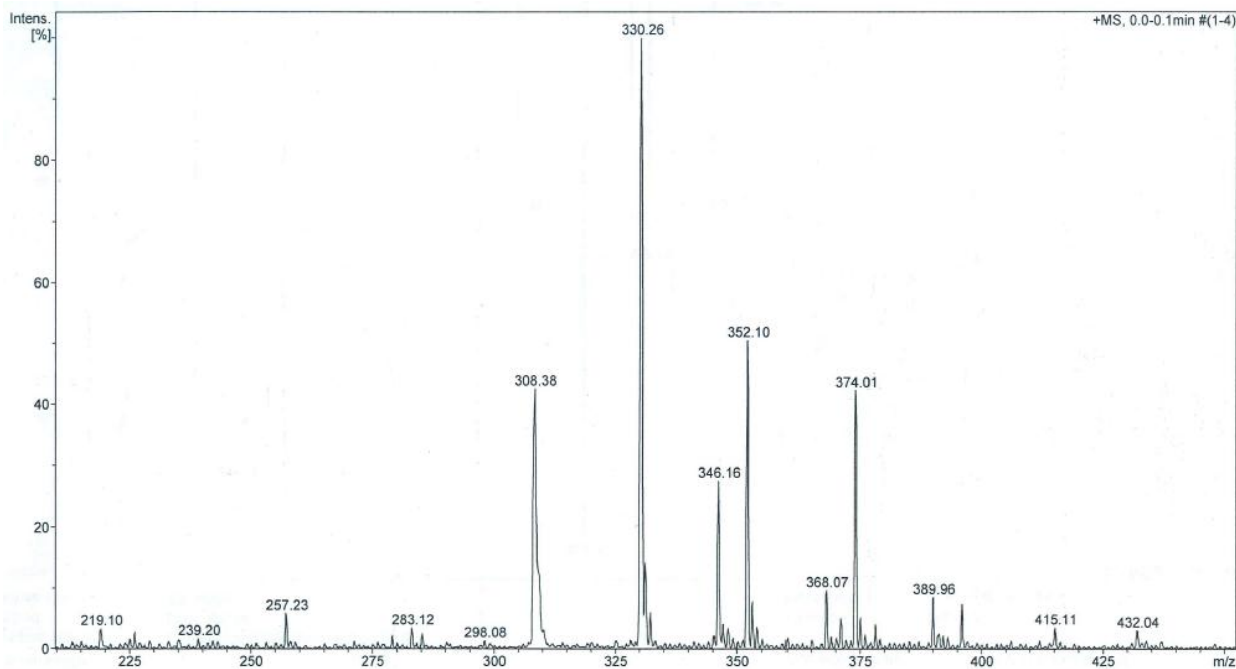


Figure 18. Effect of pH on the ratiometric fluorescence emission of **HBTCo**. **HBTCo** (20.0 μM) with 100.0 μM of Co^{2+} after 2h in aqueous solution (50 mM HEPES). Black trace: with 2 mM GSH and red trace: without GSH in the buffer.

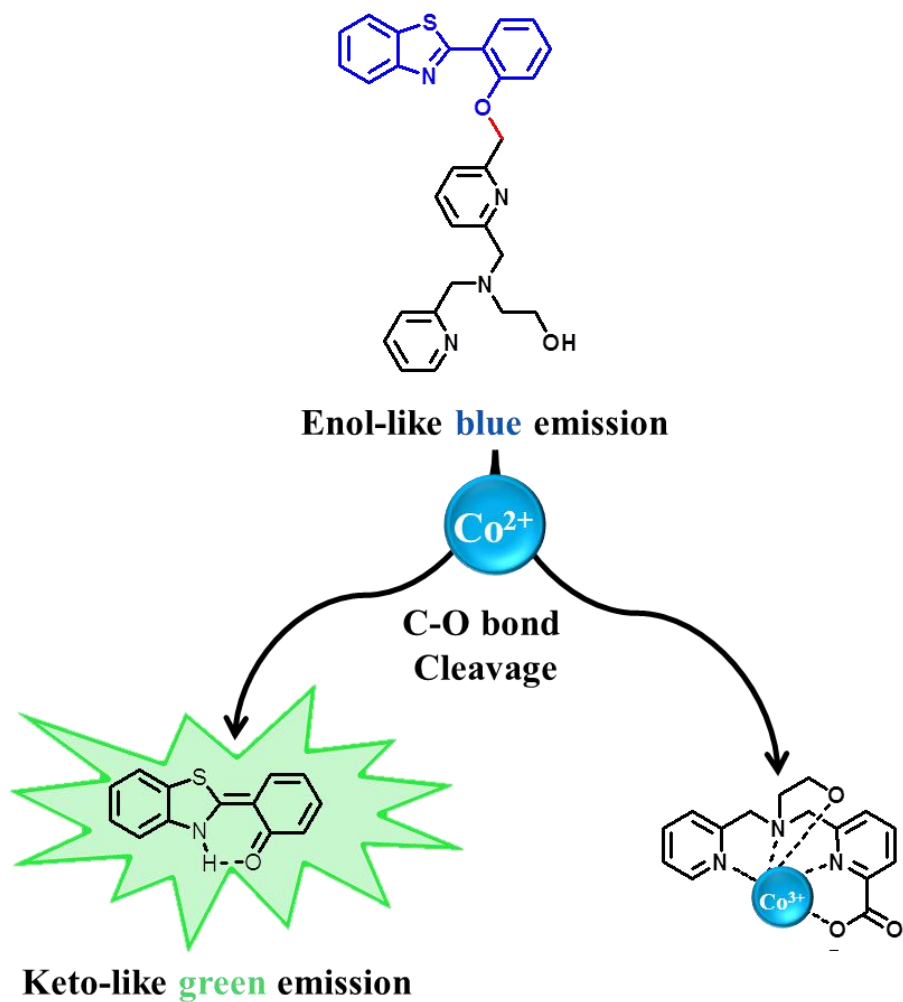
3.2.5 Proposed reaction mechanism

Mass peak at m/z 346.16 in ESI-MS spectrum is correspond to carboxylated $\text{N}_3\text{O-Co}$ complex (calcd. 346.06 for $\text{C}_{15}\text{H}_{15}\text{CoN}_3\text{O}_3$), in agreement with the literature data (Figure 19).³⁷ The ESI-MS data confirmed the Co^{2+} mediated oxidative benzylic ether (C–O) bond cleavage reaction in **HBTCo** and formation of Co complexes with carboxylate dpentadentate ligand N_3O (Scheme 3). A tentative mechanism was proposed for the metal ion (Co^{2+}) catalyzed oxidative cleavage of benzylic ether (C–O) bond between the **HBT** and N_3O ligand based on the C–N bond cleavage reported by McKenzie *et al.*³² The benzylic carbon of the ligand (N_3O) oxidized to carboxylate via benzylic radical formation in presence of activated oxygen (Figure 20). Subsequent transformation involves the formation of oxonium ion which hydrolyzed to aldehyde liberating ESIPT active **HBT**. The aldehyde further oxidized to carboxylate by the hydroperoxide of the metal complex through a Bayer–Villiger type reaction to form final $\text{N}_3\text{O-Co}$ complexes (Scheme 3).



Calculated $m/z = 344:04$ for $\text{C}_{15}\text{H}_{16}\text{CoN}_3\text{O}_3$ ($\text{N}_3\text{O-Co}$ complex)

Figure 19. ESI mass spectra (positive ion mode) for the reaction of $20.0 \mu\text{M}$ **HBTCo** with $100.0 \mu\text{M}$ Co^{2+} in water in presence of $100.0 \mu\text{M}$ GSH. Mass peaks observed at 346.16 ($[\text{M} + 2\text{H}]^+$), 368.07 ($[\text{M} + \text{H} + \text{Na}]^+$) and 389.96 ($[\text{M} + 2\text{Na}]^+$) are corresponds to $\text{N}_3\text{O-Co}$ complex $\text{C}_{15}\text{H}_{16}\text{CoN}_3\text{O}_3$. Mass peaks observed at 308.38 ($[\text{M} + \text{H}]^+$), 330.26 ($[\text{M} + \text{Na}]^+$), 352.10 ($[\text{M} + 2\text{Na} - \text{H}]^+$) and 374.01 ($[\text{M} + 3\text{Na} - 2\text{H}]^+$) are corresponds to GSH.



Scheme 3. Co^{2+} catalyzed releases of ESIPT fluorophore **HBT** from **HBTCO**.

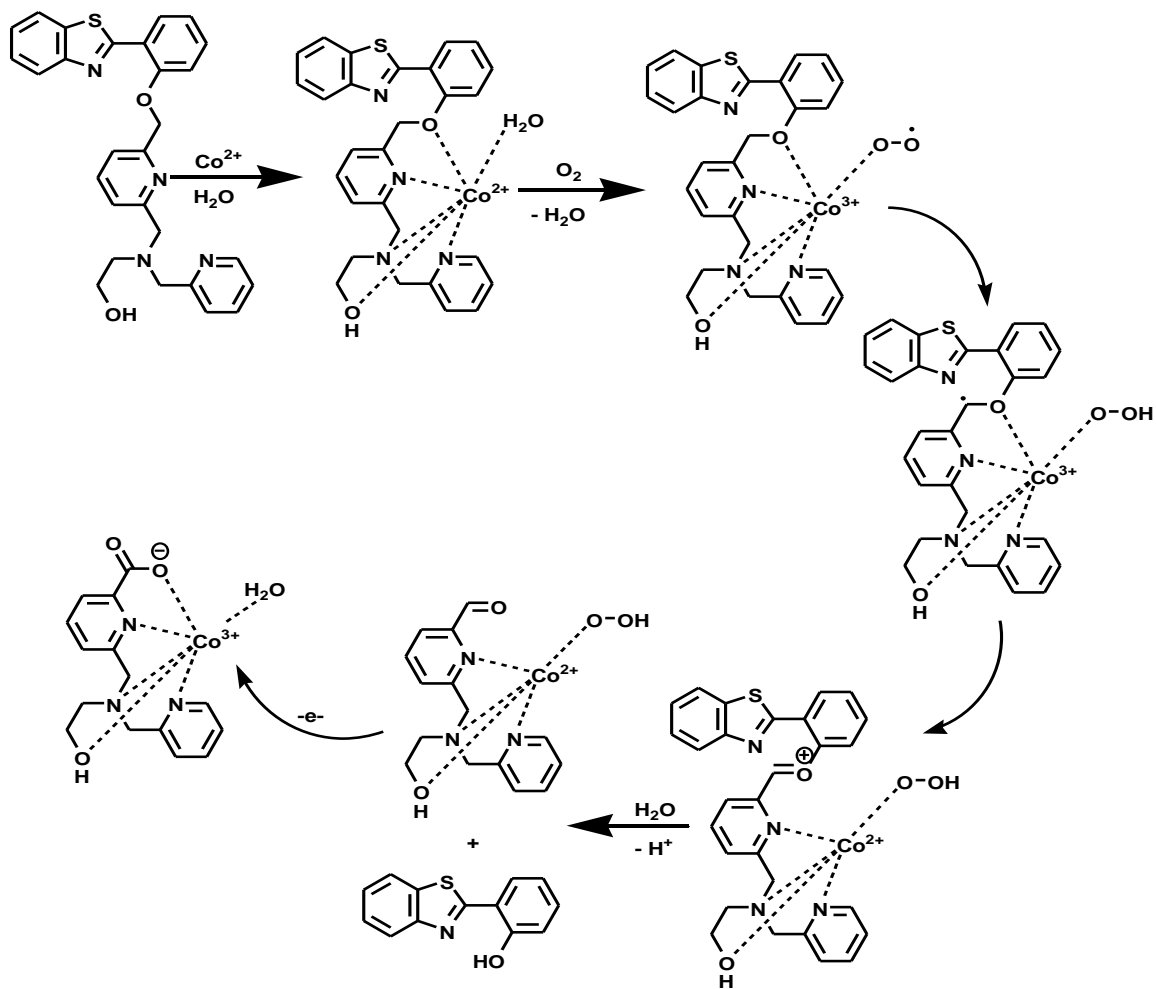


Figure 20. Proposed mechanism of Co^{2+} catalyzed oxidative cleavage of benzylic ether (C-O) bond in ESIPT active fluorophore HBTCO.

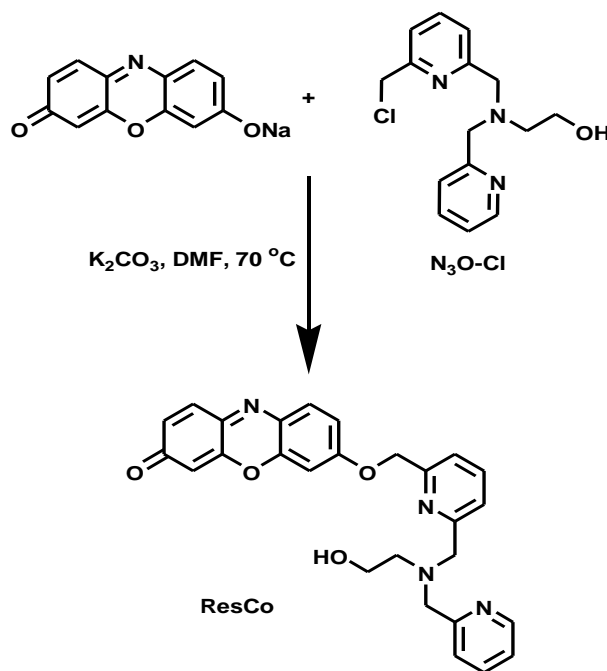
3.2.6 Conclusion

In conclusion, a novel ESIPT-based molecular probe **HBTCo** for ratiometric fluorescence detection of Co^{2+} under physiologically reducing conditions is demonstrated. The metal ion catalyzed oxidative benzylic ether bond cleavage was effectively used as switch-on ESIPT in **HBT** for fluorometric detection of paramagnetic metal ions overcoming their inherently associated fluorescence quenching property. **HBTCo** reacted efficiently with Co^{2+} in the biologically relevant pH range of 6.5-8.5 to release ESIPT active **HBT** fluorophore. This ratiometric probe can be efficiently used for monitoring Co^{2+} in physiological and environmental samples.

3.3 Resorufin-based reactive probe (ResCo) for Co^{2+} with dual output (colorimetric and fluorometric) modes

3.3.1 Synthesis

The alkylation of the 7-hydroxy group of resorufin effectively weakens its intramolecular charge transfer which quenches its emission by blocking push-pull mechanism in the chromophore. The tetradentate ligand N_3O is found to be selective for binding Co^{2+} for its reaction-based detection under physiologically reducing conditions. In accordance with above rationale nonfluorescent probe **ResCo** for Co^{2+} was designed by combining resorufin dye and tetradentate ligands N_3O through 7-hydroxyl functionality. Co^{2+} mediated cleaving of benzylic ether bond in nonfluorescent probe **ResCo** will release chromogenic resorufin dye which automatically show ratiometric visible absorption (colorimetric) and ‘switch-on’ fluorometric responses for Co^{2+} under physiologically reducing conditions. **ResCo** was synthesized by the alkylation of 7- hydroxyl group of resorufin with tetradentate $\text{N}_3\text{O-Cl}$ under basic conditions in excellent yield (Scheme 4). The synthesized molecular probe was characterized by NMR and mass spectrometry.



Scheme 4. Synthesis of **ResCo**.

3.3.2 Photophysical property of ResCo and selective colorimetric and fluorometric detection of Co^{2+}

Colorimetric Study of ResCo

The photophysical property of **ResCo** was studied in aqueous buffer (50 mM HEPES, pH 7.2) in presence of 2 mM glutathione (GSH) for mimicking the intracellular environment. **ResCo** probe showed absorption band centered around 470 nm (Figure 21). The absorption spectra of the probes did not exhibit any significant changes upon addition of millimolar concentration of alkali and alkaline earth metal ions and 20.0 μM of other metal ions such as Mn^{2+} , Fe^{2+} , Zn^{2+} , Cd^{2+} , Ag^+ , Hg^{2+} , and Pb^{2+} after 2 h of mixing. When tested with 20.0 μM Co^{2+} , the absorbance band of **ResCo** at 470 nm is red-shifted to 573 nm ($\Delta\lambda = 103$ nm) and the color of the solution changed from pale yellow to pink (Figure 21). Submicromolar concentration of Co^{2+} can be easily detected as confirmed from the ratiometric absorption study of **ResCo** upon sequential addition of increasing concentrations of Co^{2+} (Figure 22). Time dependent study showed that the absorbance at 470 nm ($\epsilon = 1.70 \times 10^4 \text{ M}^{-1} \text{ Cm}^{-1}$)

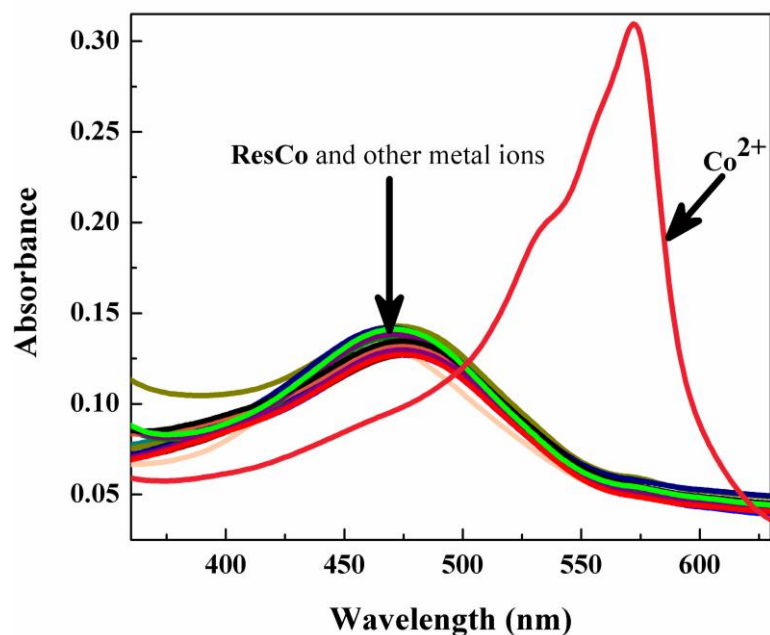


Figure 21. UV-Vis absorption spectra of **ResCo** (10.0 μM) upon addition of different metal ions after 2h in aqueous solution (50 mM HEPES, pH 7.2, 2 mM GSH).

decreased slowly with concomitant appearance of a new prominent peak at 573 nm which reaches maximum ($\epsilon = 2.98 \times 10^4 \text{ M}^{-1} \text{ Cm}^{-1}$) within 30 min after mixing of Co^{2+} and **ResCo** (Figure 23). Clear isosbestic point at 510 nm was observed, which strongly supports the formation of new product i.e., resorufin dye after the Co^{2+} mediated oxidative benzylic

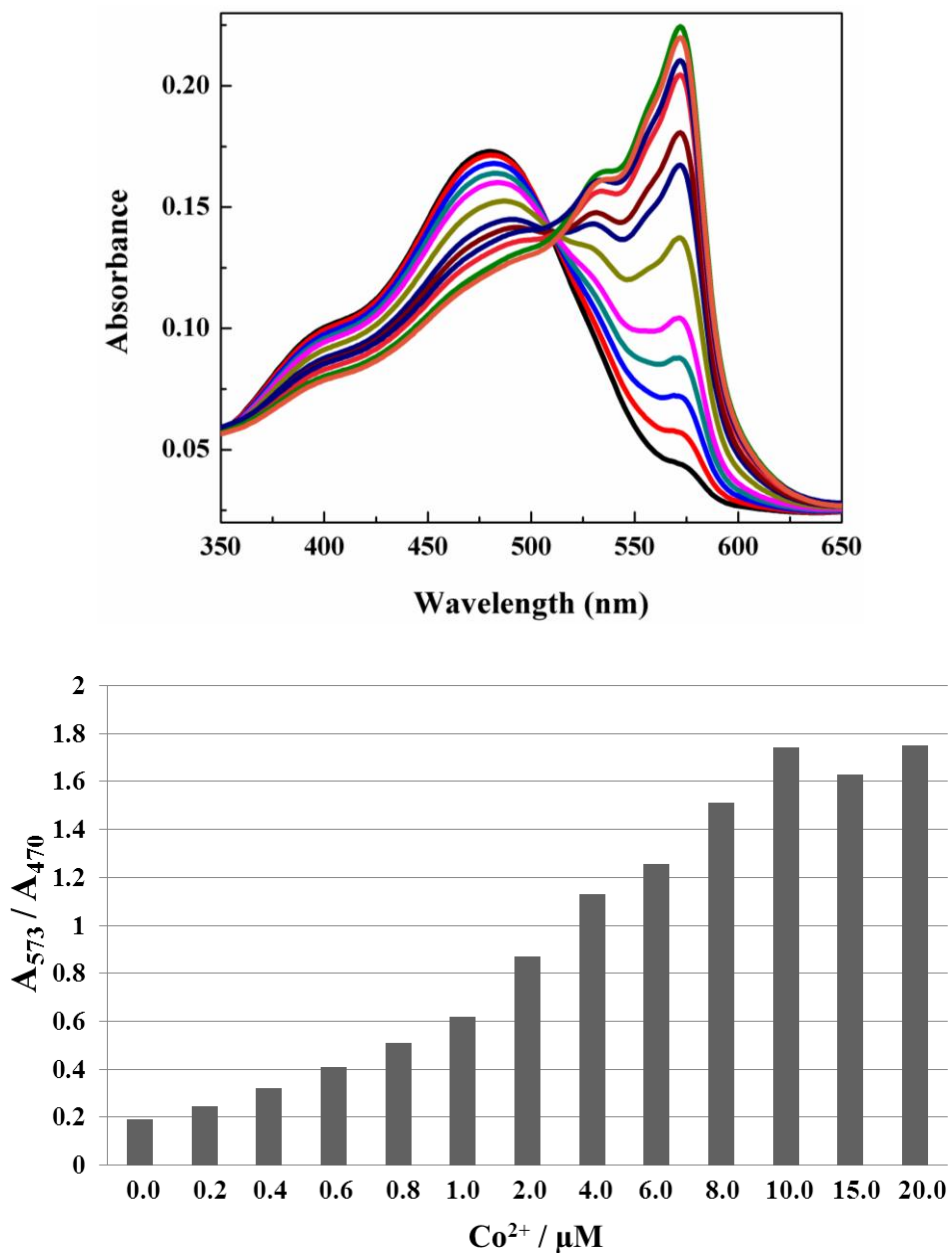


Figure 22. UV-Vis absorption spectra (top) and ratiometric response (bottom) of **ResCo** (10.0 μM) upon addition of 0.0, 0.2, 0.4, 0.6, 0.8, 1.0, 2.0, 4.0, 6.0, 8.0, 10.0, 15.0, 20.0 μM of Co^{2+} after 2h in aqueous solution (50 mM HEPES, pH 7.2, 2 mM GSH).

ether (C–O) bond cleavage in **ResCo** probe in physiological reducing condition (Figure 23). Moreover, this kind of ratiometric behavior of the probe **ResCo** is advantageous over normal probes as it minimizes the error arising from physical or chemical fluctuations in the sample and experimental conditions.

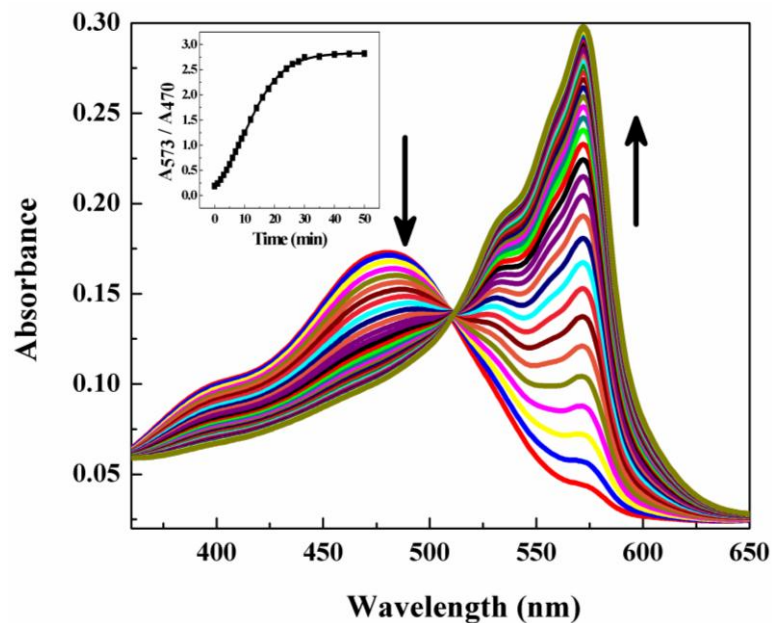


Figure 23. Time dependent absorption spectra of **ResCo** ($10.0 \mu\text{M}$) after addition of $20.0 \mu\text{M}$ of Co^{2+} in aqueous solution (50 mM HEPES , $\text{pH } 7.2$, 2 mM GSH) (Isobestic point = 510 nm).

Fluorometric study of ResCo

As expected, 1.0 μM solution of **ResCo** probe exhibited very weak fluorescence upon 540 nm excitation (Figure 24). After mixing for 2h, millimolar concentrations of alkali and alkaline earth metal ions did not show significant changes in the fluorescence behavior of the probe. Next we have tested fluorometric behavior of the probe upon addition 20.0 μM of several metal ions such as Mn^{2+} , Fe^{2+} , Co^{2+} , Cu^{2+} , Cu^+ , Zn^{2+} , Cd^{2+} , Ag^+ , Hg^{2+} , and Pb^{2+} after 2 h of mixing. As anticipated, treating 1.0 μM **ResCo** with 20.0 μM of Co^{2+} switched on a *ca.* 7-fold fluorescence ($E_{\text{max}} = 586 \text{ nm}$) enhancement within 2 h (Figure 24). While **ResCo** did not exhibit switch on fluorescence phenomena with other metal ions tested. The switch on fluorescence from the probe clearly indicate the Co^{2+} catalyzed oxidative cleavage of benzylic ether (C–O) linkage in **ResCo** in the presence of O_2 releasing highly fluorescent resorufin dye. Time dependent study showed that the Co^{2+} mediated benzyl ether bond cleavage reaction in **ResCo** complete within 30 min respectively as indicated by the fluorescence spectra (Figure 25). Concentration dependent study showed submicromolar concentration of Co^{2+} is good enough to react with **ResCo** to release fluorescent resorufin dye which leads to subsequent detection of the metal ions (Figure 26).

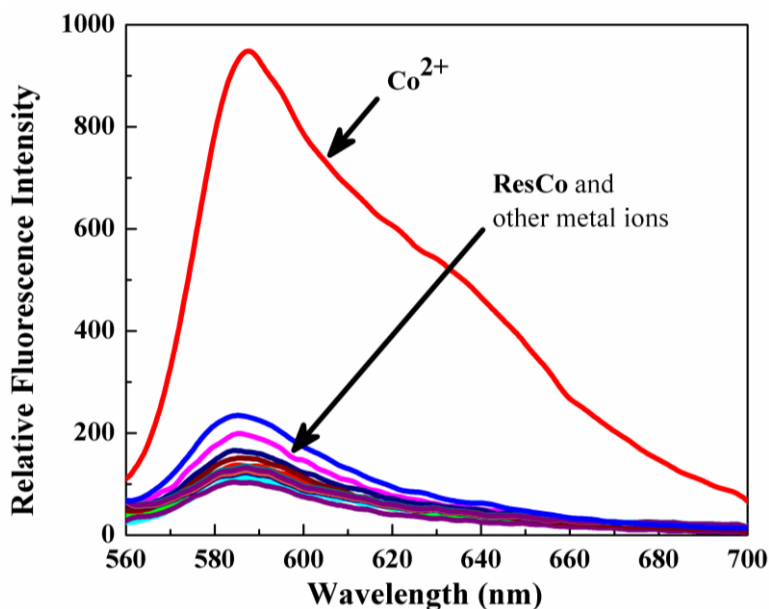


Figure 24. Fluorescence response of **ResCo** (1.0 μM) upon addition of different metal ions after 2h in aqueous solution (50 mM HEPES, pH 7.2, 2 mM GSH) ($\lambda_{\text{ex}} = 540 \text{ nm}$).

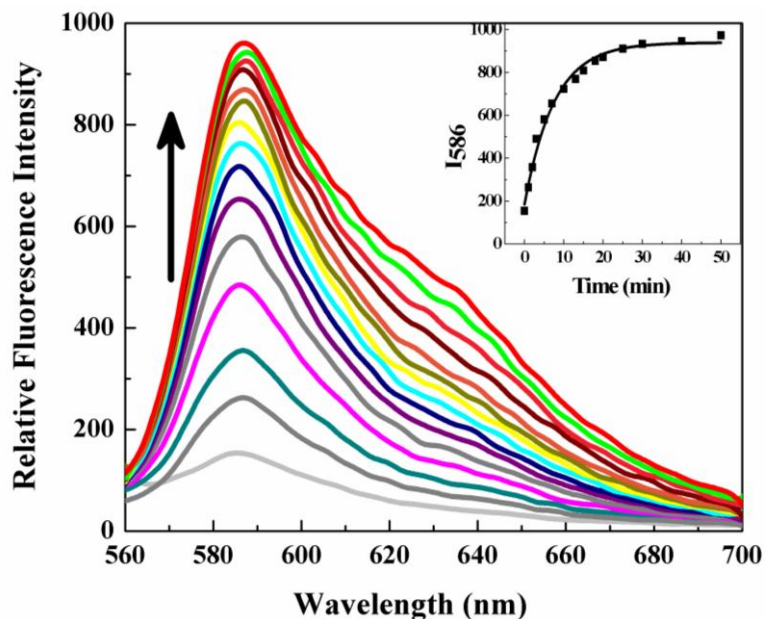


Figure 25. Time dependent fluorescence response of **ResCo** ($1.0 \mu\text{M}$) after addition of $20.0 \mu\text{M}$ of Co^{2+} in aqueous solution (50 mM HEPES , $\text{pH } 7.2$, 2 mM GSH) ($\lambda_{\text{ex}} = 540 \text{ nm}$).

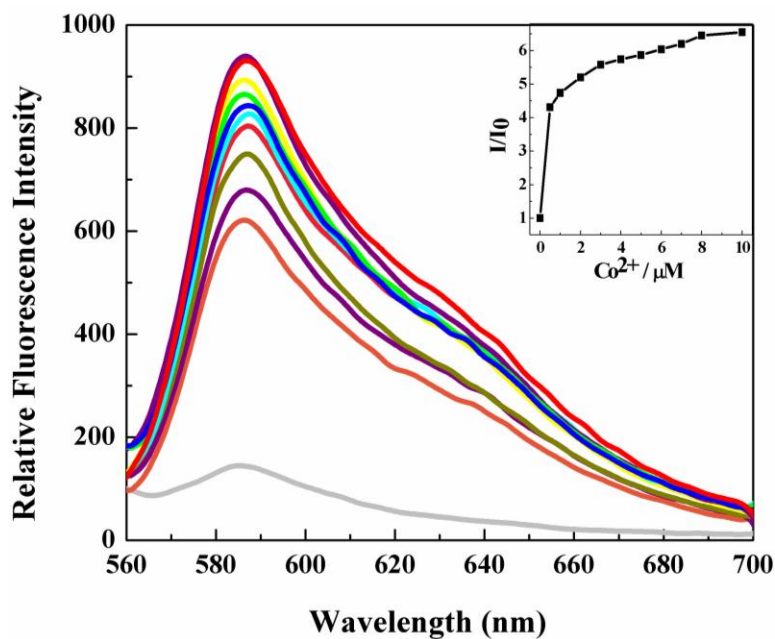


Figure 26. Fluorescence response of **ResCo** ($1.0 \mu\text{M}$) upon addition of $0.0, 0.5, 1.0, 2.0, 3.0, 4.0, 5.0, 6.0, 7.0, 8.0, 10.0 \mu\text{M}$ of Co^{2+} after 2 h in aqueous solution (50 mM HEPES , $\text{pH } 7.2$, 2 mM GSH) ($\lambda_{\text{ex}} = 540 \text{ nm}$).

The reducing environment generated by GSH is very essential as confirmed by control experiment in the absence of GSH, which did not lead to benzylic ether (C–O) bond cleavage (Figure 27).

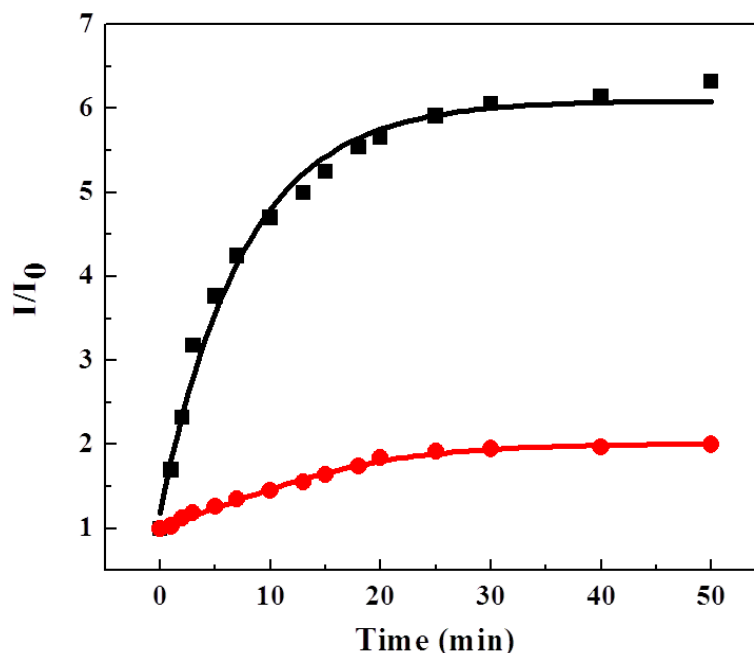


Figure 27. Time dependent fluorescence study of 1.0 μM ResCo incubated with 10 μM of Co^{2+} in aqueous solution (50 mM HEPES, pH 7.2) with (black trace) and without (red trace) 2 mM GSH.

3.3.3 pH dependent study

The effect of pH on the Co^{2+} mediated oxidative cleavage of the benzylic ether bond in ResCo was studied to understand the efficiency of this ‘switch-on’ fluorometric method. ResCo reacted efficiently with Co^{2+} in the biologically relevant pH range of 6.5–8.5 to release phenolic resorufin fluorophore (Figure 28). Hence, ResCo is very convenient for the ‘switch-on’ fluorometric detection of Co^{2+} without the interference from the pH-dependent effects.

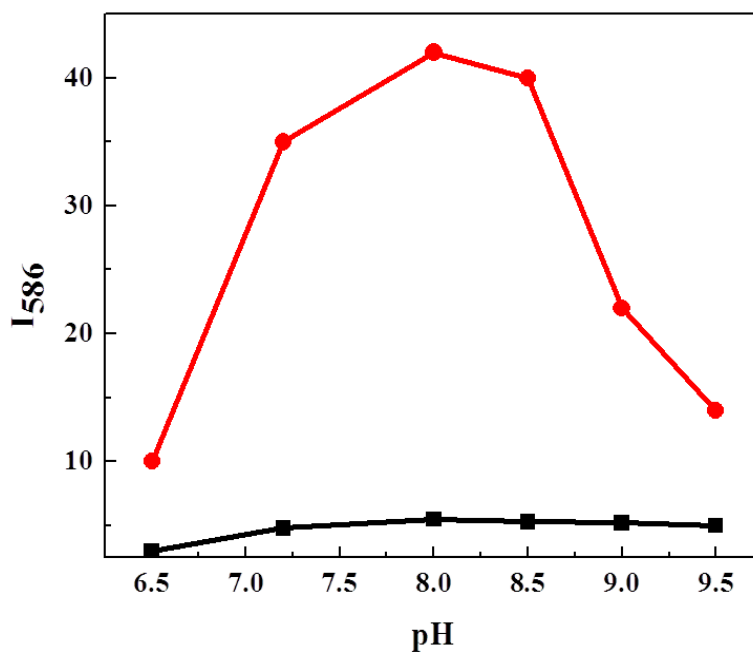


Figure 28. Effect of pH on the ‘switch on’ emission of **ResCo**. Red trace: **ResCo** (1.0 μM) with 10.0 μM of Co^{2+} after 2 h in aqueous solution. Black trace: **ResCo** (1.0 μM) without Co^{2+} after 2 h in aqueous solution.

3.3.4 Competitive study for detection of Co^{2+}

Selectivity of **ResCo** as the ‘switch-on’ fluorescent probe for Co^{2+} was studied in the presence of various competing metal ions. For this purpose, 1.0 μM solutions of **ResCo** were treated with 20.0 μM of Co^{2+} in the presence of 20.0 μM of other metal ions. Data in Figure 29 show that there is no or very minimal interference for the detection of Co^{2+} in the presence of other metal ions. This indicates the selectivity of Co^{2+} mediated oxidative benzylic ether bond cleavage in **ResCo** to release fluorescent resorufin dye. Thus, **ResCo** can be used as selective reaction-based switch on fluorescent probe for Co^{2+} in the presence of most competing metal ions.

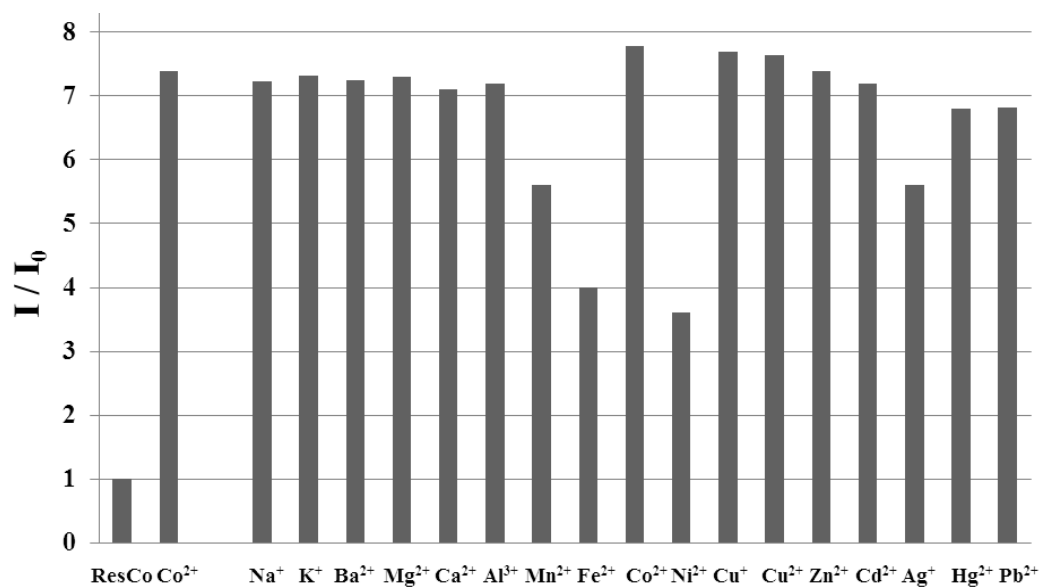
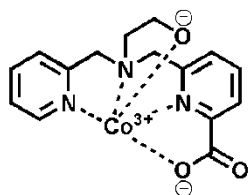
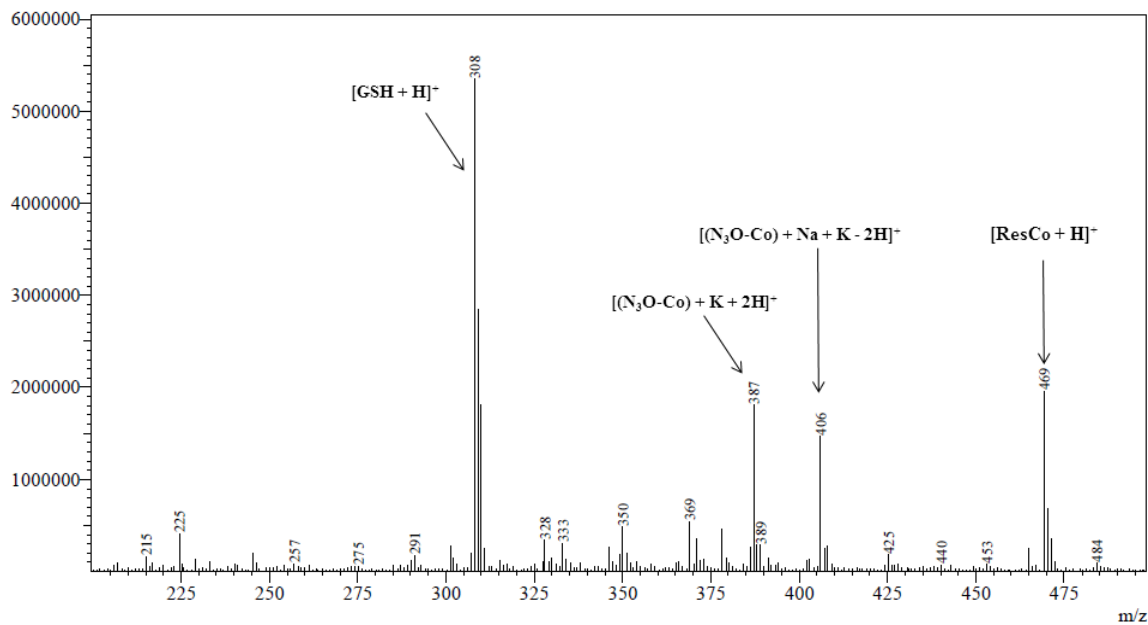


Figure 29. Competitive experiment for the detection of Co^{2+} using 1.0 μM of **ResCo**. Top: 20.0 μM Co^{2+} is mixed with 20.0 μM of corresponding metal ions. Left two bars are control response of the corresponding probe and only metal ion indicated.

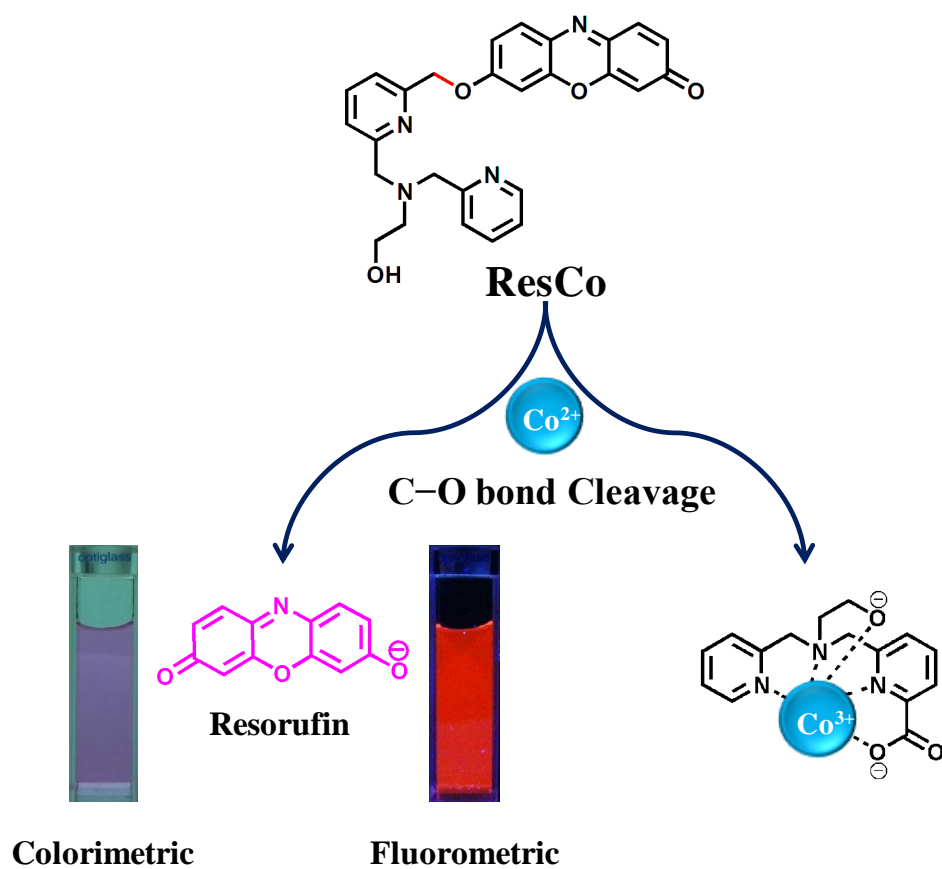
3.3.5 Product analysis

ESI-MS analysis further confirmed the Co^{2+} catalyzed oxidative benzylic ether (C–O) bond cleavage in **ResCo** to release fluorescence reporter dye resorufin and metal ion bound carboxylated tetradentate ligands $\text{N}_3\text{O-Co}$. The mass peaks at m/z 387 and 406 correspond to carboxylated $\text{N}_3\text{O-Co}$ complex (calcd 387.03 for $\text{C}_{15}\text{H}_{17}\text{CoN}_3\text{O}_3 + \text{K}^+ + 2\text{H}^+$ and 405.99 for $\text{C}_{15}\text{H}_{15}\text{CoN}_3\text{O}_3 + \text{K}^+ + \text{Na}^+$) (Figure 30). This mass spectroscopic data are in agreement with data reported in the literature.^{37,48} Thus ESI-MS data validated the Co^{2+} mediated oxidative benzylic ether (C–O) bond cleavage reaction in **ResCo** and the formation of Co complex with carboxylated pentadentate ligands of N_3O (Scheme 5). The metal ion (Co^{2+}) catalyzed oxidative cleavage of the benzylic ether (C–O) bond between the resorufin and N_3O ligand is presumed to follow the mechanism proposed for C–N/C–O bond cleavage reaction reported in the literature.^{32,37,48} Notably single cation coordination (hydroxyl) site in **ResCo** played a crucial role by introducing differential selectivity of metal ions (Co^{2+}), as the C–O bond cleavage regulated through the formation of the Co complex with pentadentate moieties of N_3O in the probes.



Calculated $m/z = 387.04$ for $\text{C}_{15}\text{H}_{17}\text{CoN}_3\text{O}_3 + \text{K}^+ + 2\text{H}^+$ ($\text{N}_3\text{O-Co}$ complex)

Figure 30. ESI mass spectra (positive ion mode) for the reaction of $10.0 \mu\text{M}$ **ResCo** with $100.0 \mu\text{M}$ Co^{2+} in water in presence of $100.0 \mu\text{M}$ GSH. Mass peaks observed at 387 ($[\text{M} + \text{K} + 2\text{H}]^+$) and 406 ($[\text{M} + \text{Na} + \text{K} - 2\text{H}]^+$) are corresponds to $\text{N}_3\text{O-Co}$ complex $\text{C}_{15}\text{H}_{17}\text{CoN}_3\text{O}_3$. Mass peak observed at 469 ($[\text{M} + \text{H}]^+$) correspond to **ResCo** (calculated 468.18 for $\text{C}_{27}\text{H}_{24}\text{N}_4\text{O}_4$). Mass peak observed at 308 ($[\text{M} + \text{H}]^+$) correspond to GSH.



Scheme 5. $\text{Co}^{2+}/\text{O}_2$ mediated benzylic ether bond (C-O) cleavage in **ResCo** to release resorufin dye and $[\text{N}_3\text{O-Co}]$ complex.

3.3.6 Conclusion

In conclusion, the design and synthesis of new type reaction-based molecular probe **ResCo** has been presented here, with dual optical output (colorimetric and switch on fluorometric) for the detection of Co^{2+} ion in physiological reducing media. The metal ion catalyzed oxidative benzylic ether bond cleavage was successfully established for detection of the paramagnetic metal ion overcoming the inherently associated fluorescence quenching property. This molecular probe extended the scope of reaction-based molecular platform for the detection of paramagnetic metal ions by employing newer fluorescence reporter dye with emission in the longer wavelength region. Furthermore this probe offer ratiometric visible absorption (colorimetric) based second mode of optical response for the detection of Co^{2+} . Thus **ResCo** probe can be efficiently used for monitoring exchangeable Co^{2+} pools in analytical samples and in living cells as these probes containing fluorescence reporter resorufin dye which is not phototoxic to living cells.

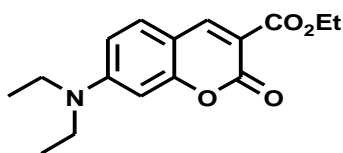
4. Experimental

4.1 General experimental procedure

All the solvents and reagents were obtained from Sigma-Aldrich and used as received unless otherwise mentioned. The solutions of metal ions were prepared from $\text{Al}(\text{ClO}_4)_3 \cdot 9\text{H}_2\text{O}$, $\text{LiClO}_4 \cdot 3\text{H}_2\text{O}$, NaClO_4 , $\text{Mg}(\text{ClO}_4)_2$, $\text{Ca}(\text{ClO}_4)_2 \cdot 4\text{H}_2\text{O}$, $\text{Sr}(\text{NO}_3)_2$, $\text{Ba}(\text{ClO}_4)_2$, $\text{Mn}(\text{ClO}_4)_2 \cdot 6\text{H}_2\text{O}$, $\text{Fe}(\text{ClO}_4)_2 \cdot \text{H}_2\text{O}$, $\text{Co}(\text{ClO}_4)_2 \cdot 6\text{H}_2\text{O}$, $\text{Cd}(\text{ClO}_4)_2 \cdot \text{H}_2\text{O}$, $\text{Ag}(\text{ClO}_4)_2$, $\text{Hg}(\text{ClO}_4)_2$, $\text{Pb}(\text{ClO}_4)_2$, $\text{Ni}(\text{ClO}_4)_2 \cdot 6\text{H}_2\text{O}$, $\text{Cu}(\text{ClO}_4)_2 \cdot 6\text{H}_2\text{O}$, $[\text{Cu}(\text{CH}_3\text{CN})_4]\text{PF}_6$ and $\text{Zn}(\text{ClO}_4)_2 \cdot 6\text{H}_2\text{O}$ respectively in CH_3CN . ^1H and ^{13}C NMR were recorded on a Bruker AV-400 spectrometer with chemical shifts reported as ppm (in CDCl_3 , $\text{DMSO}-d_6$, tetramethylsilane as internal standard). Mass spectra were measured on Shimadzu 2020 LC-MS and BrukerUltraflex II MALDI/TOF spectrometers. Elemental analysis was carried out on ThermoScientific FLASH 2000 Organic Element Analyzer. UV-Vis spectra were recorded on a Perkin Elmer Model Lambda 900 spectrophotometer. HRMS were recorded on Agilent 6538 UHD Accurate-Mass Q-TOF LC/MS analyzer. Fluorescence spectra were recorded on a Perkin Elmer LS 55 spectrophotometer.

4.2 Detailed synthetic procedure

7-Diethylamino-2-oxo-2H-chromene-3-carboxylic acid ethyl ester (A): 7-Diethylamino

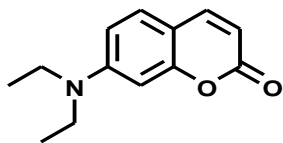


salicylaldehyde (2.66 g, 13.8 mmol) and diethyl malonate (3.31 g, 20.7 mmol) were dissolved in (1:2) toluene-acetonitrile (150 mL). Piperidine (3.53 g, 41.5 mmol) was added and the mixture

was refluxed for 12 h. After cooling, the solvent was evaporated and the residue was purified by silica gel chromatography (methylene chloride/ethyl acetate; 8:2) to obtain the product **A** as yellow oil (2.39 g, 60% yield). ^1H NMR (400 MHz, CDCl_3) δ_{ppm} 1.21-1.25 (6H, m), 1.37-1.41 (3H, m), 3.42-3.47 (4H, dd, $J = 7.6$ Hz, 6.8 Hz), 4.34-4.40 (2H, m), 6.47 (1H, s), 6.59 (1H, d, $J = 9.2$ Hz), 7.34 (1H, dd, $J = 1.2$ Hz, 8 Hz), 8.42 (1H, s). ^{13}C NMR (100 MHz, CDCl_3) δ_{ppm} 12.4, 14.3, 45.0, 61.1, 96.7, 107.7, 109.1, 109.4, 130.9, 149.1, 152.8, 158.2,

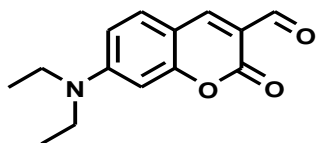
158.4, 164.2. MS (EI): $m/z = 290.4$ $[\text{M}+\text{H}]^+$ for $\text{C}_{16}\text{H}_{19}\text{NO}_4$. Elemental analysis: Found C, 66.40; H, 6.62; N, 4.85; Calcd. C, 66.42; H, 6.62; N, 4.84 for $\text{C}_{16}\text{H}_{19}\text{NO}_4$.

7-Diethylamino-chromene-2-one (B): 1 g of 7-diethylamino-coumaric-3-carboxylic acid



ethyl ester in 60 mL of 18% strength hydrochloric acid was heated for 5 h to the boil under reflux. After cooling, saturated sodium acetate solution was added and the pH value adjusted to 4-5 with 45% strength sodium hydroxide, whilst cooling. The crystalline precipitate was filtered off, thoroughly washed with water and dried in vacuum at 50 °C, which afforded product (B) as light yellow solid (0.6 g, 80% yield). ^1H NMR (400 MHz, CDCl_3) δ_{ppm} 1.24 (6H, t, $J = 7.2$ Hz), 3.41-3.47 (4H, q, $J = 7.2$ Hz), 6.05 (1H, d, $J = 9.6$ Hz), 6.52 (1H, d, $J = 2$ Hz), 6.57-6.60 (1H, dd, $J = 2.4$ Hz, 6.4 Hz), 7.29 (1H, s), 7.54 (1H, d, $J = 9.2$ Hz). ^{13}C NMR (100 MHz, CDCl_3) δ_{ppm} 12.4, 44.7, 97.6, 108.3, 108.6, 109.2, 128.7, 143.6, 150.7, 156.7, 162.2. MS (EI): $m/z = 218.3$ $[\text{M}+\text{H}]^+$ for $\text{C}_{13}\text{H}_{15}\text{NO}_2$. Elemental analysis: Found C, 71.85; H, 6.97; N, 6.47; Calcd. C, 71.87; H, 6.96; N, 6.45 for $\text{C}_{13}\text{H}_{15}\text{NO}_2$.

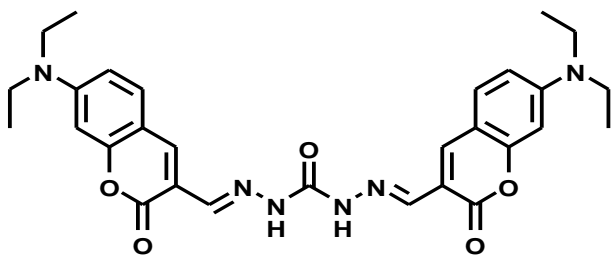
7-Diethylamino-2-oxo-2H-chromene-3-carboxyldehyde (C): 4 mL of dry DMF are added



dropwise to 0.4 mL of POCl_3 at 20-50 °C. The mixture was stirred for 45 min at 50 °C under N_2 atmosphere. A suspension of 0.65 g of 7-diethylamino coumarin in 3 mL of dry DMF was then added; the mixture was warmed to 60 °C for 2 h and poured out onto ice water, and stirred for 2 h. The crystalline precipitate was filtered off, thoroughly washed with water and dried in vacuum at 50 °C, which afforded product (C) as orange solid. (0.47 g, 66% yield). ^1H NMR (400 MHz, CDCl_3) δ_{ppm} 1.23 (6H, t, $J = 6.8$ Hz), 3.44 (4H, dd, $J = 7.2$ Hz, 6.8 Hz), 6.47 (1H, d, $J = 2$ Hz), 6.61 (1H, dd, $J = 2.4$ Hz, 6.8 Hz), 7.39 (1H, d, $J = 9.2$ Hz), 8.24 (1H, s), 10.11 (1H, s). ^{13}C NMR (100 MHz, CDCl_3) δ_{ppm} 12.4, 45.3, 97.2, 108.2, 110.2, 114.4, 132.5, 145.3, 153.4, 158.9, 161.8. MS (EI): $m/z = 246.3$ $[\text{M}+\text{H}]^+$ for $\text{C}_{14}\text{H}_{15}\text{NO}_3$. Elemental analysis: Found C, 68.54; H, 6.17; N, 5.72; Calcd. C, 68.56; H, 6.16; N, 5.71 for $\text{C}_{14}\text{H}_{15}\text{NO}_3$.

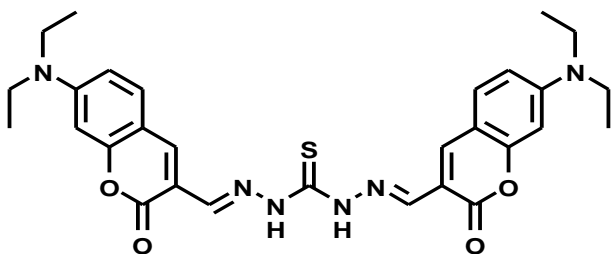
General synthetic procedure for CC and CTC

A solution of 7-diethylamino-2-oxo-2H-chromene-3-carboxyldehyde (0.40 g, 1.63 mmol) in ethanol (20 mL) was added slowly to a solution of carbohydrazide or thiocarbohydrazide (0.81 mmol) in water (20 mL). Initially the solution turn turbid and after complete addition the solution became clear. The reaction mixture was refluxed with stirring for 24 h. The precipitate formed was cooled and filtered. The precipitate was washed with ethanol and dried under vacuo to obtain biscarbonohydrazone **CC** or bistiocarbohydrazone **CTC** in quantitative yield.

Bis[[7-(diethylamino)-2-oxo-2H-chromene]methylene]-carbonic dihydrazide (CC):

Yield 92% (orange powder). ^1H NMR (400 MHz, $\text{DMSO}-d_6$) δ_{ppm} 1.14 (12H, t, $J = 6.8$ Hz), 3.46 (8H, dd, $J = 6.8$ Hz, 7.2 Hz), 6.57 (2H, d, $J = 2.4$ Hz), 6.77 (2H, dd, $J = 2.4$ Hz, 6.8 Hz), 7.57 (2H, d, $J = 8.8$ Hz), 8.22

(2H, s), 8.45 (2H, s), 10.78 (2H, s). ^{13}C NMR (100 MHz, $\text{DMSO}-d_6$) δ_{ppm} 12.3, 44.2, 96.5, 108.1, 109.7, 113.2, 130.3, 137.2, 137.9, 150.9, 151.7, 156.2, 160.8. MS (EI): $m/z = 545.3$ $[\text{M}+\text{H}]^+$, calcd. 544.2 for $\text{C}_{29}\text{H}_{32}\text{N}_6\text{O}_5$. Elemental analysis: Found C, 63.92; H, 5.93; N, 15.44; Calcd. C, 63.96; H, 5.92; N, 15.43 for $\text{C}_{29}\text{H}_{32}\text{N}_6\text{O}_5$.

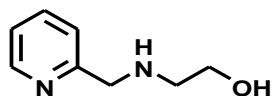
Bis[[7-(diethylamino)-2-oxo-2H-chromene]methylene]-carbonothioic dihydrazide (CTC):

Yield 92% (brick red powder). ^1H NMR (400 MHz, $\text{DMSO}-d_6$) δ_{ppm} 1.12-1.16 (12H, m), 3.45-3.50 (8H, m), 6.56-6.59 (2H, dd, $J = 2$ Hz, 6.4 Hz), 6.77-6.79 (2H, d, $J = 8.4$ Hz), 7.57-7.59 (2H, d, $J = 6.4$

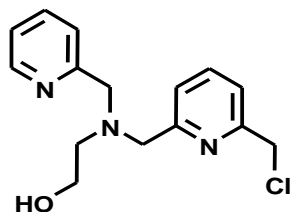
Hz), 8.18 (1H, br), 8.30 (1H, br), 8.67 (2H, br), 11.67 (1H, br), 11.94 (1H, br). ^{13}C NMR (100 MHz, $\text{DMSO}-d_6$) δ_{ppm} 12.3, 44.2, 96.5, 108.1, 109.8, 112.5, 130.6, 136.3, 138.8, 151.3, 156.5, 160.7, 173.9. MS (EI): $m/z = 561.2$ $[\text{M}+\text{H}]^+$, calcd. For 560.2 $\text{C}_{29}\text{H}_{32}\text{N}_6\text{O}_4\text{S}$. Elemental

analysis: Found C, 62.08; H, 5.76; N, 15.02; S, 5.71; Calcd. C, 62.12; H, 5.75; N, 14.99; S, 5.72 for $\text{C}_{29}\text{H}_{32}\text{N}_6\text{O}_4\text{S}$.

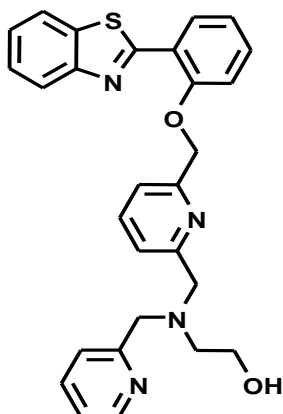
2-[(Pyridin-2-ylmethyl)amino]ethanol: Pyridine-2-carbaldehyde (2.14 g, 0.02 mol) was added slowly to an ice-cooled solution of aminoethanol (1.22 g, 0.02 mol) in 30 mL of methanol. The resulting solution was stirred at ambient temperature for 2 h and subsequently treated with sodium tetrahydridoborate (1.89 g, 0.05 mol) in small portions. After additional 2 h, water (30 mL) was added and the reaction mixture was concentrated to about 20 mL using a rotavap. The remaining solution was extracted with dichloromethane (2×20 mL), and the organic layer was separated and subsequently dried with sodium sulfate. Filtration and evaporation of the solvent gave the amino ligand (1.92 g, 63%) as orange oil, which was used without further purification for the synthesis of $\text{N}_3\text{O-Cl}$. $^1\text{H NMR}$ (400 MHz, $\text{DMSO-}d_6$) δ_{ppm} 2.60-2.64 (2H, br, s), 2.81 (2H, t, $J = 4.8$ Hz), 3.62 (2H, t, $J = 5.2$ Hz), 3.91 (2H, s), 7.12-7.16 (1H, m), 7.23 (1H, d, $J = 8.4$ Hz), 7.59-7.64 (1H, m), 8.51 (1H, d, $J = 4.8$ Hz). MS (EI): $m/z = 153.2$ $[\text{M}+\text{H}]^+$ for $\text{C}_8\text{H}_{12}\text{N}_2\text{O}$. Elemental analysis: Found C, 63.16; H, 7.96; N, 18.41; Calcd. C, 63.13; H, 7.95; N, 18.41 for $\text{C}_8\text{H}_{12}\text{N}_2\text{O}$.



Synthesis of receptor $\text{N}_3\text{O-Cl}$: To a mixture of 2,6-dichloromethylpyridine (352 mg, 2 mmol) and NaHCO_3 (84 mg, 1 mmol) in CH_3CN (30 mL) heated at 70°C , a solution of compound **2** (152 mg, 1 mmol, 15 mL) in the same solvent was added slowly. The resulting mixture was stirred at 70°C for overnight and cooled to room temperature. Insoluble materials were removed by filtration. The filtrate was concentrated and purified by basic alumina column (ethyl acetate/MeOH; 9:1). The product was obtained as pale yellow oil. Yield = 106 mg, 36%. $^1\text{H NMR}$ (400 MHz, CDCl_3) δ_{ppm} 2.86 (2H, t, $J = 4.8$ Hz), 3.66 (2H, t, $J = 5.2$ Hz), 3.92 (2H, s), 3.93 (2H, s), 4.65 (2H, s), 7.12-7.15 (1H, m), 7.27-7.32 (3H, m), 7.56-7.64 (2H, m), 8.52-8.54 (1H, m). MS (EI): $m/z = 292.8$ $[\text{M}+\text{H}]^+$ for $\text{C}_{15}\text{H}_{18}\text{ClN}_3\text{O}$. Elemental analysis: Found C, 61.76; H, 6.21; N, 14.41; Calcd. C, 61.75; H, 6.22; N, 14.4 for $\text{C}_{15}\text{H}_{18}\text{ClN}_3\text{O}$.



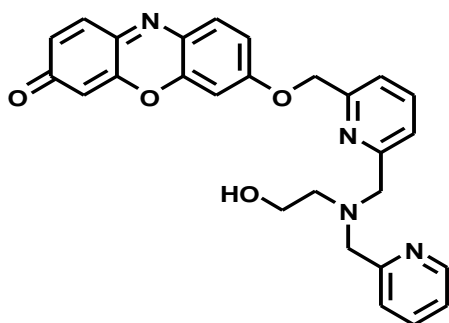
Synthesis of HBTCo: A mixture of 2-hydroxybenzothiazole (65 mg, 0.28 mmol) and **N₃O-Cl**



Cl ligand (100 mg, 0.34 mmol) was dissolved in DMF (10 mL). K_2CO_3 (400 mg, 2.8 mmol) was added and the resulting mixture was heated at 90°C for overnight. After cooling to room temperature, solvent was evaporated in vacuo. The residue in H_2O (50 mL) was extracted with of CH_2Cl_2 (3×20 mL). This organic layer was washed with brine, dried over Na_2SO_4 , solvent was evaporated in vacuo and the residue was purified on basic alumina column (solvent. $\text{CH}_2\text{Cl}_2/\text{MeOH}$: 95/5) to obtain the product as light yellow oil (121

mg, yield 88%). ^1H NMR (400 MHz, CDCl_3) δ_{ppm} 2.90 (2H, t, $J = 5.2$ Hz), 3.69 (2H, t, $J = 5.2$ Hz), 3.96 (4H, d, $J = 4$ Hz), 5.47 (2H, s), 7.11-7.16 (3H, m), 7.27-7.31 (2H, m), 7.34-7.43 (2H, m), 7.47-7.51 (2H, m), 7.54-7.58 (1H, td, $J = 6$ Hz, 1.6 Hz), 7.63 (1H, t, $J = 7.6$ Hz), 7.88 (1H, d, $J = 8$ Hz), 8.09 (1H, d, $J = 8$ Hz), 8.51-8.55 (2H, m). ^{13}C NMR (100MHz, CDCl_3) δ_{ppm} 56.8, 59.7, 60.0, 60.1, 71.4, 113.1, 120.2, 121.2, 121.6, 122.1, 122.2, 122.7, 122.8, 123.0, 124.6, 125.9, 129.9, 131.8, 136.0, 136.5, 137.4, 149.0, 152.2, 155.8, 155.9, 159.1, 159.2, 163.0. HRMS: observed $m/z = 505.1667$ [$\text{M} + \text{Na}$] $^+$ and calculated $m/z = 505.1674$ for $\text{C}_{28}\text{H}_{26}\text{N}_4\text{NaO}_2\text{S}$.

Synthesis of ResCo: A mixture of resorufin sodium salt (84 mg, 0.35 mmol) and **N₃O-Cl** ligand (125 mg, 0.43 mmol) was dissolved in DMF (10 mL). K_2CO_3 (72 mg, 0.53 mmol) was



added and the resulting mixture was heated at 90°C for overnight. After cooling to room temperature, solvent was evaporated in vacuo. The residue in 50 mL of H_2O was extracted with 3×20 mL of CH_2Cl_2 . This organic layer was washed with brine, dried over Na_2SO_4 , solvent was evaporated in vacuo and the residue was purified on basic alumina column (solvent.

$\text{CH}_2\text{Cl}_2/\text{MeOH}$: 90/10) to obtain the product as red colored powder (142 mg, yield 85 %). ^1H NMR (400 MHz, CD_3OD) δ_{ppm} 2.77 (2H, t, $J = 5.6$ Hz), 3.67 (2H, t, $J = 5.6$ Hz), 3.88 (2H, s), 3.91 (2H, s), 5.32 (2H, s), 6.30 (1H, d, $J = 2$ Hz), 6.84 (1H, dd, $J = 8$ Hz, 2Hz), 7.12-7.18 (2H, m), 7.23-7.27 (1H, m), 7.44 (1H, d, $J = 7.2$ Hz), 7.51-7.58 (3H, m), 7.72-7.82 (3H, m),

8.42 (1H, m). ¹³C NMR (100 MHz, DMSO-*d*₆) δ_{ppm} 56.1, 59.0, 60.0, 60.1, 71.2, 101.2, 105.6, 114.1, 120.2, 121.9, 122.5, 127.9, 131.2, 133.6, 134.8, 136.3, 137.4, 137.6, 145.0, 145.2, 148.6, 149.5, 154.6, 159.4, 159.5, 162.0, 185.2. HRMS: observed m/z = 469.1855 [M + H]⁺ and calculated m/z = 469.1876 for C₂₇H₂₅N₄O₄.

4.3 General method for measurements of photophysical properties

UV-Vis spectra were recorded on a Perkin Elmer Model Lambda 900 spectrophotometer. Fluorescence spectra were recorded on a Perkin Elmer model LS 55 spectrophotometer. 1 cm cells were used for titration. For UV-Vis titrations, stock solutions of **CC** and **CTC** were prepared (c = 2000 μM) in acetonitrile. For fluorescence titrations stock solution of ligand **HBTCo** was prepared (c = 2000 μM) in CH₃CN. For titrations stock solution of ligand **ResCo** was prepared (c = 2000 μM) in DMSO. The solutions of guest cations were prepared in acetonitrile/water/DMSO in the order of 10⁻³ M. Working solutions of **CC**, **CTC**, **HBTCo** and **ResCo** and metal ions were prepared from the stock solutions. 10 nm excitation and 10 nm emission slit widths were used.

4.4 Job plot by UV-Vis method

A series of solutions containing **CTC** and Co(ClO₄)₂ were prepared such that the sum of the total concentration of metal ion and **CTC** remained constant (10 μM). The mole fraction (X) of Co²⁺ was varied from 0.1 to 1.0. The corrected absorbance ([A-A₀] / [A₀]) at 510 nm was plotted against the molar fraction of the Co²⁺ solution.

4.5 Determination of binding constant

Tsein equation⁴⁹ is derived to the following equations that can be used in any stoichiometric ratio between the ligand and analyte.

$$[M^{n+}]^m = \frac{1}{n \cdot K} \cdot \frac{1}{[L]_T^{m-1}} \cdot \frac{1-\alpha}{\alpha^n}$$

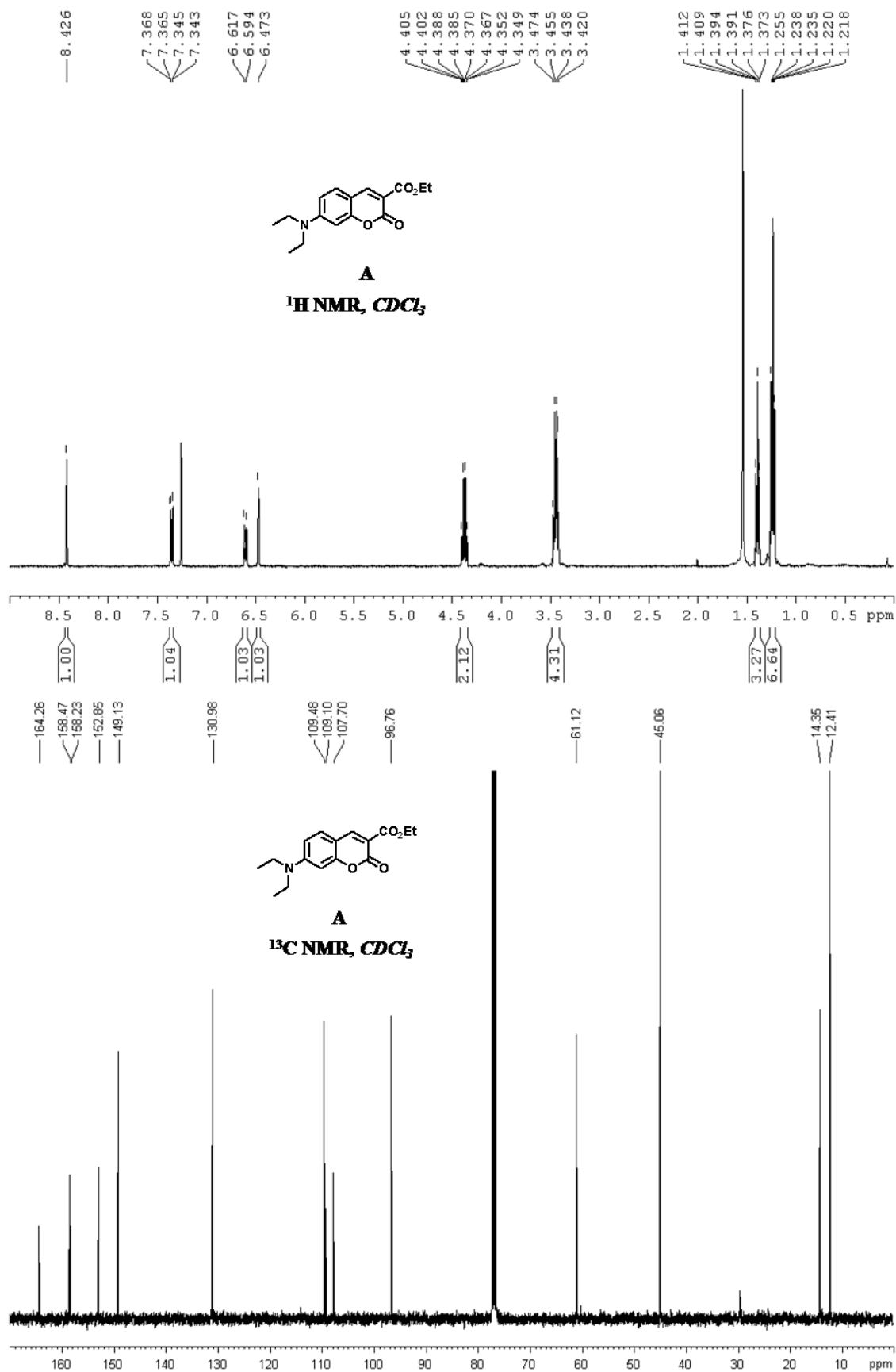
Where K is complex equilibrium constant, M_mL_n is metal-ligand, L is ligand, $[L]$, $[\text{M}^{n+}]$, and $[\text{M}_m\text{L}_n]$ are the concentrations of respective species. α is the ratio between free ligand concentration, $[L]$, and the initial concentration of ligand, $[L]_T$. In this case, the stoichiometric ratio of the CTC and Co^{2+} is 2:1. So, this equation can be written as

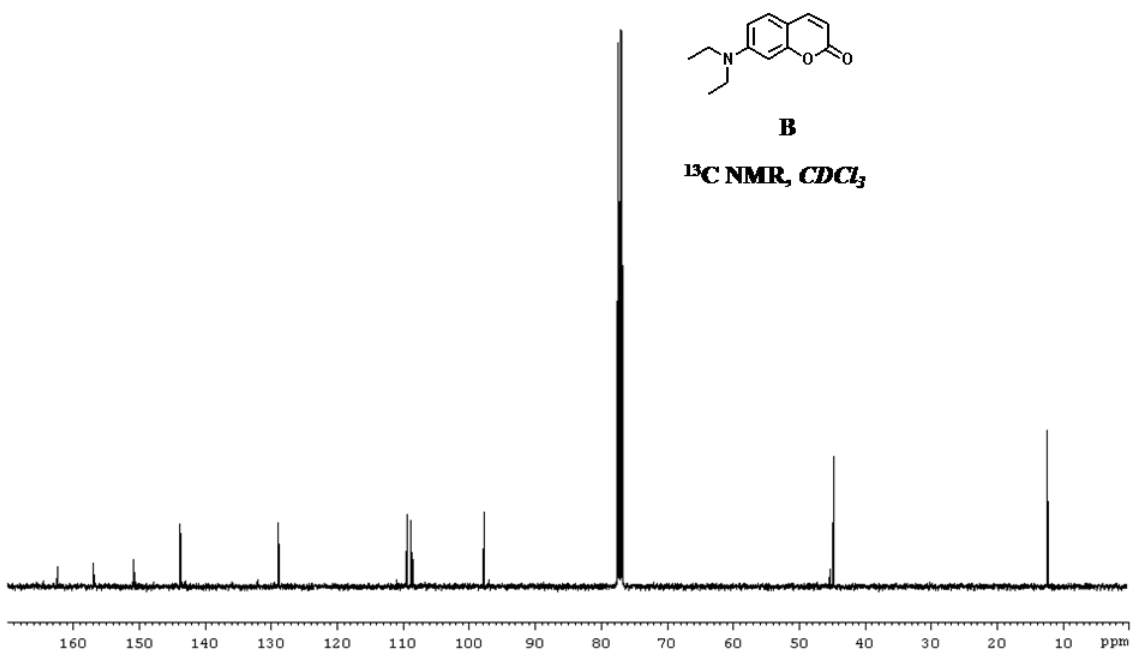
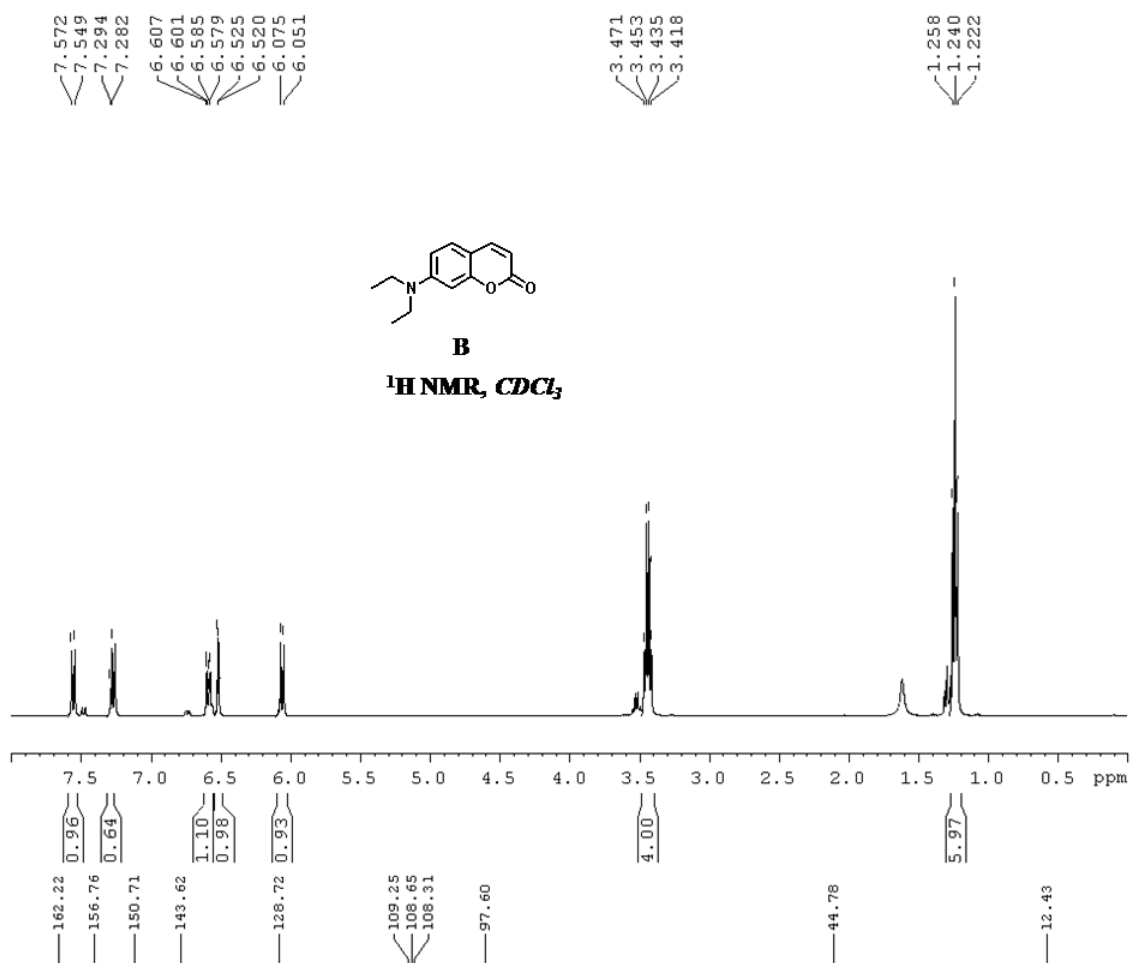
$$[\text{Co}^{2+}]^{0.5} = \frac{1}{2KL_T} \cdot \frac{1-\alpha}{\alpha^2}$$

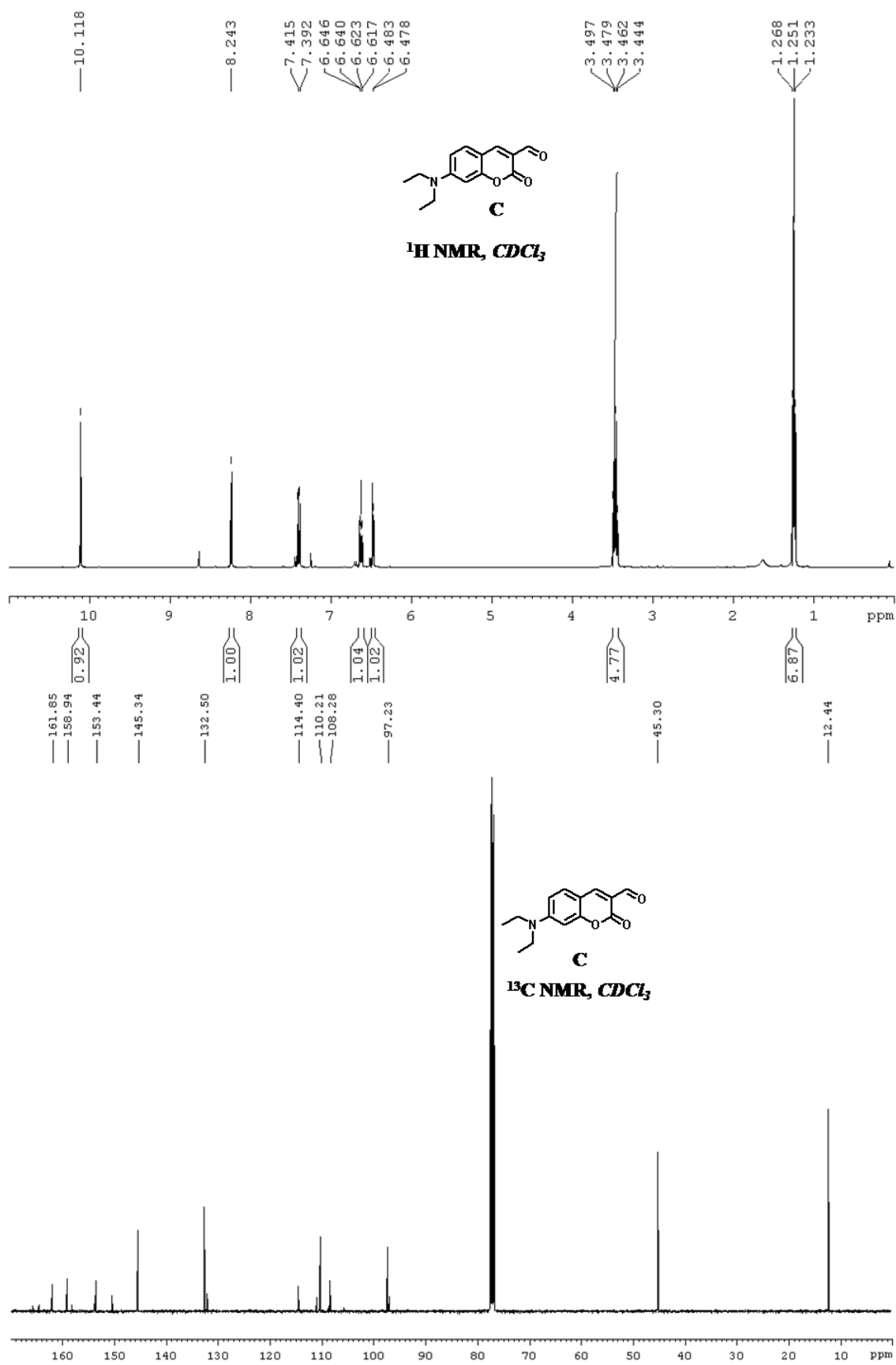
The curve fitting experimental data points were calculated from this equation with $\log K_a = 7.95 \text{ M}^{-2}$.

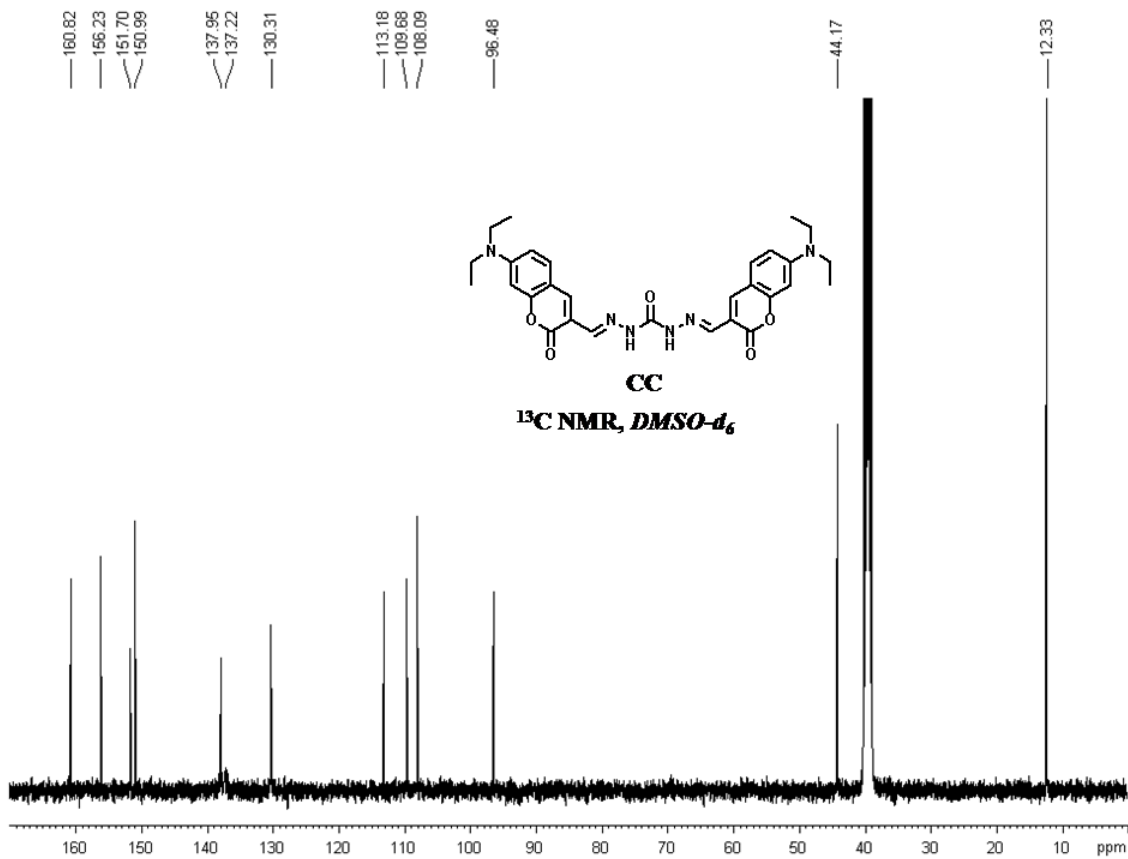
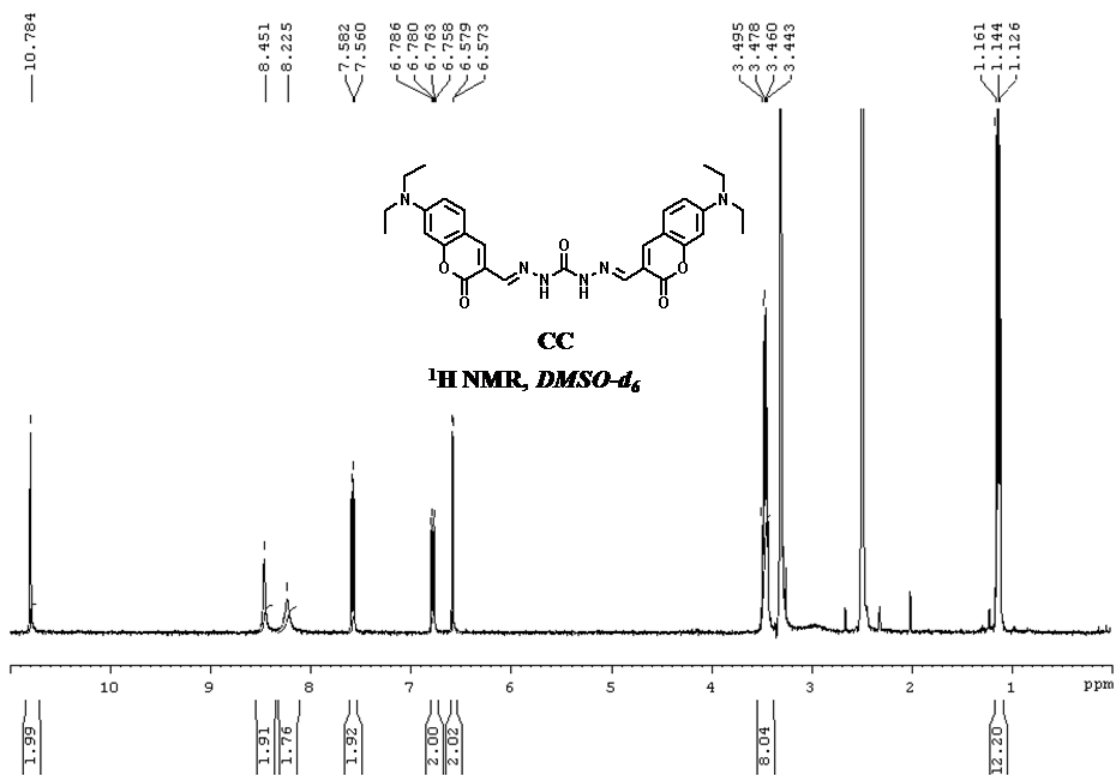
4.6 Appendix

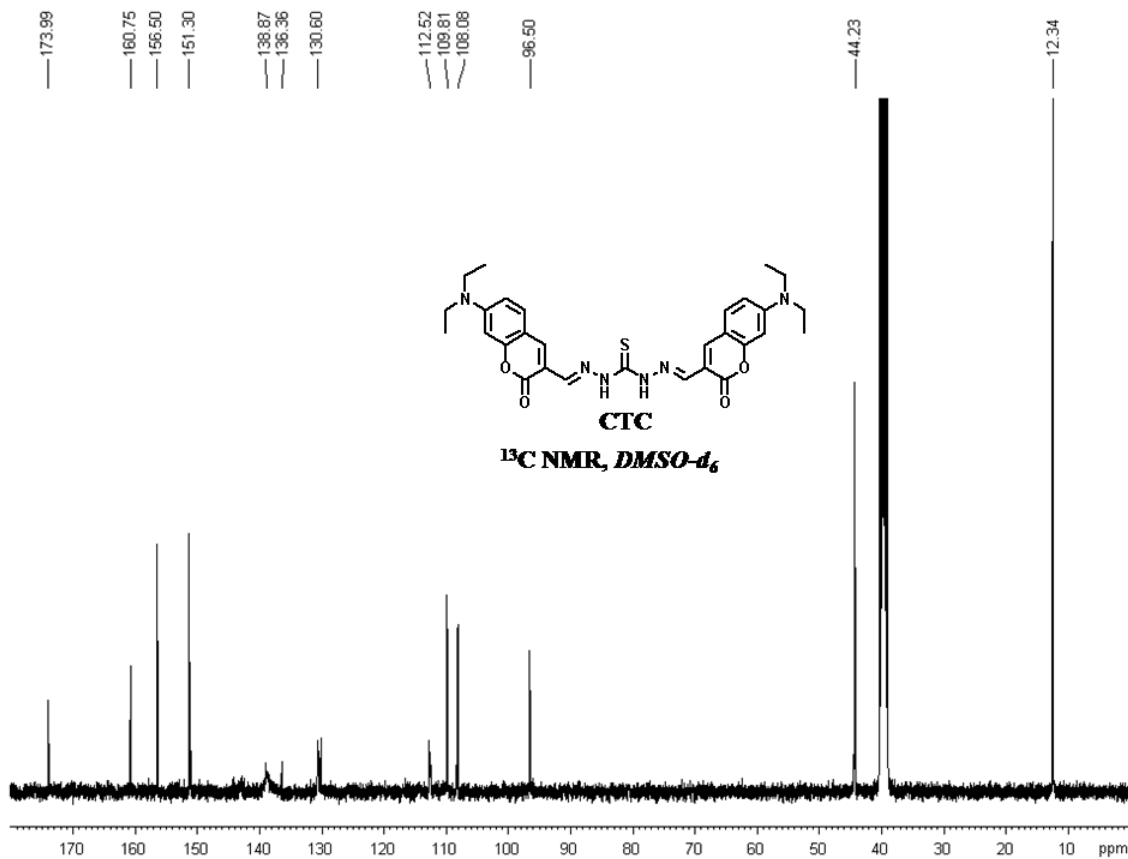
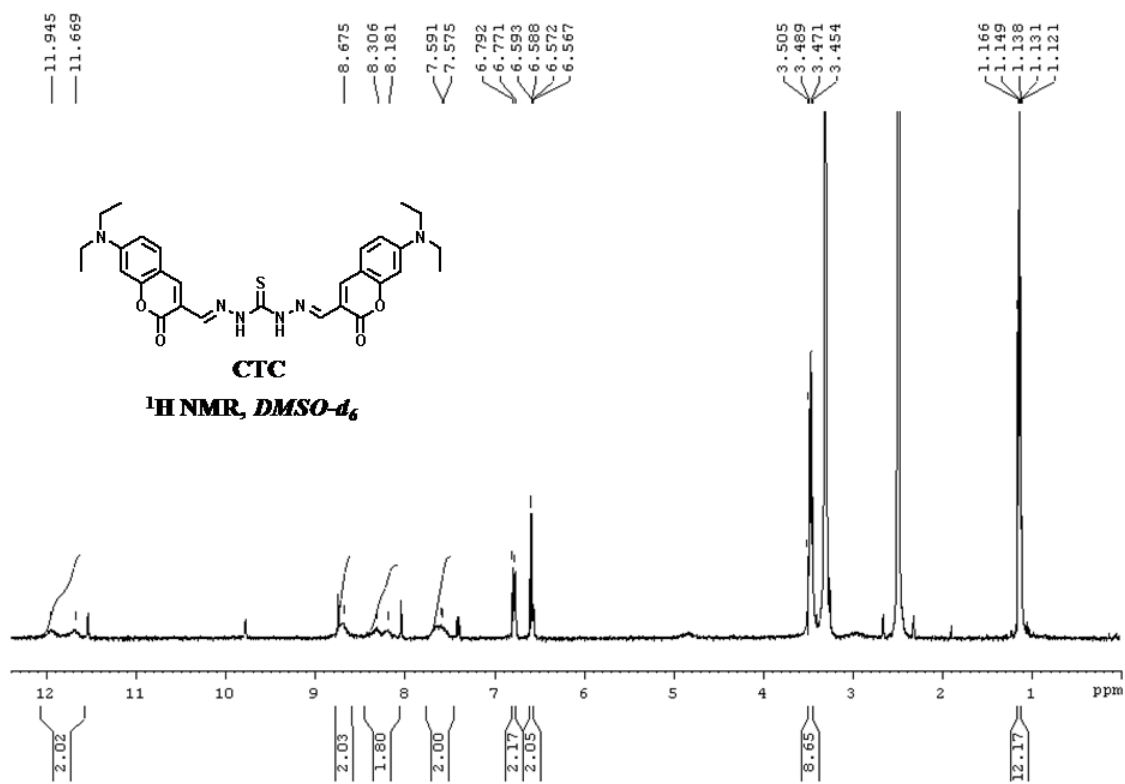
- ❖ Compound A, ^1H and ^{13}C NMR
- ❖ Compound B, ^1H and ^{13}C NMR
- ❖ Compound C, ^1H and ^{13}C NMR
- ❖ Compound CC, ^1H and ^{13}C NMR
- ❖ Compound CTC, ^1H and ^{13}C NMR
- ❖ Compound PMAE and $\text{N}_3\text{O-Cl}$, ^1H NMR
- ❖ Compound HBTCO, ^1H and ^{13}C NMR
- ❖ Compound ResCo, ^1H and ^{13}C NMR

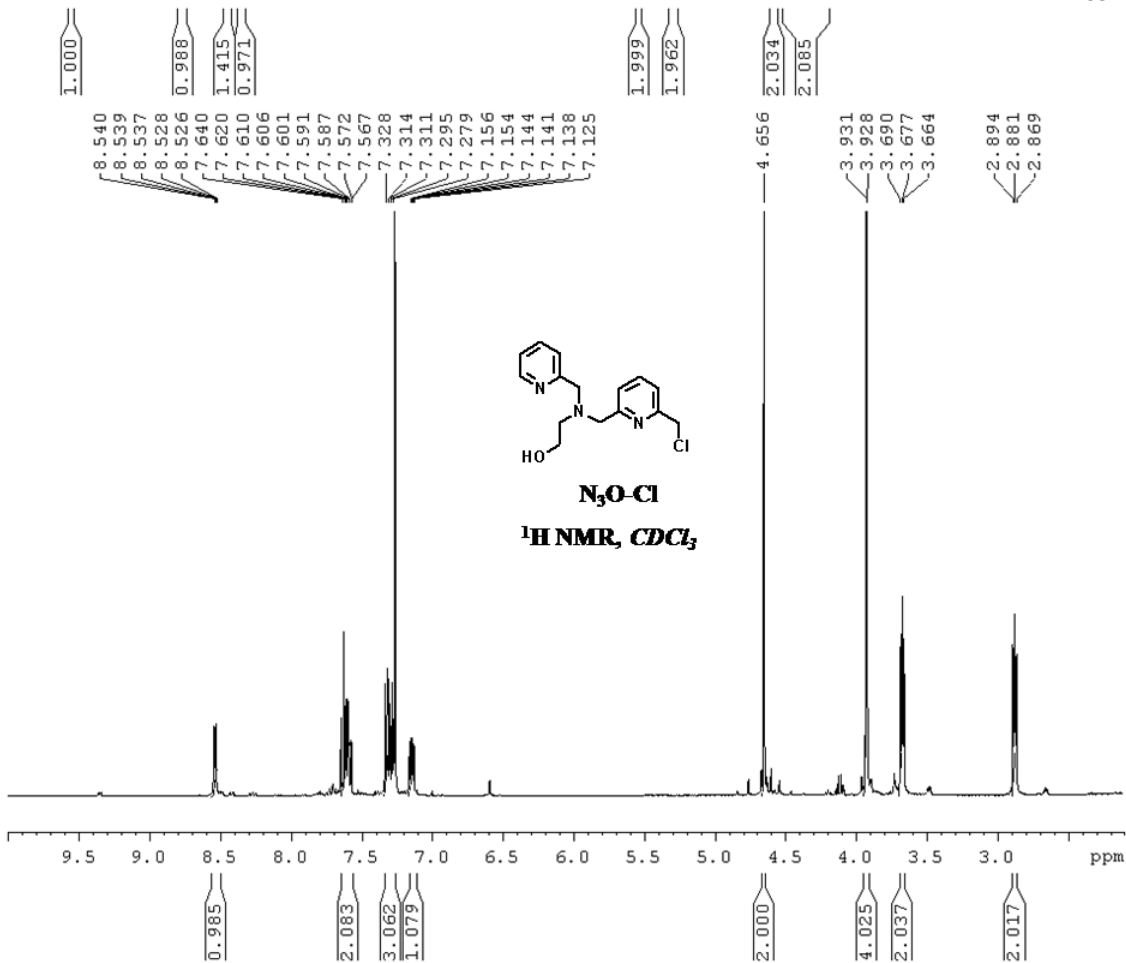
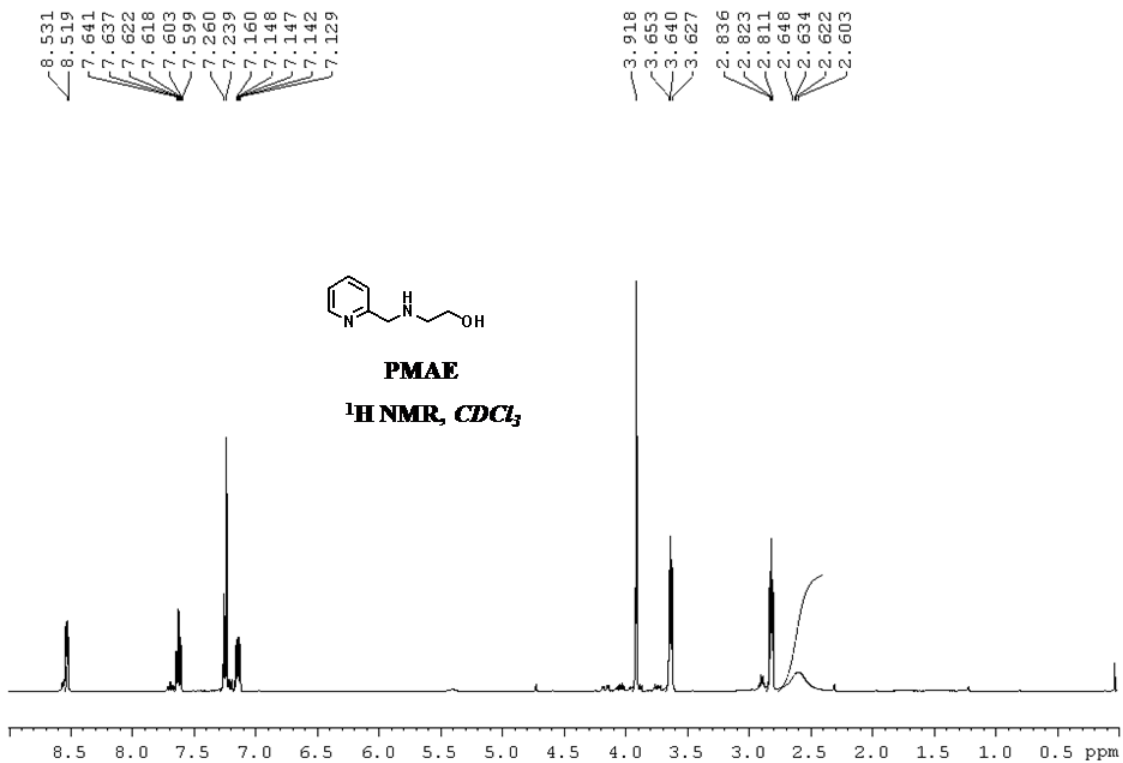


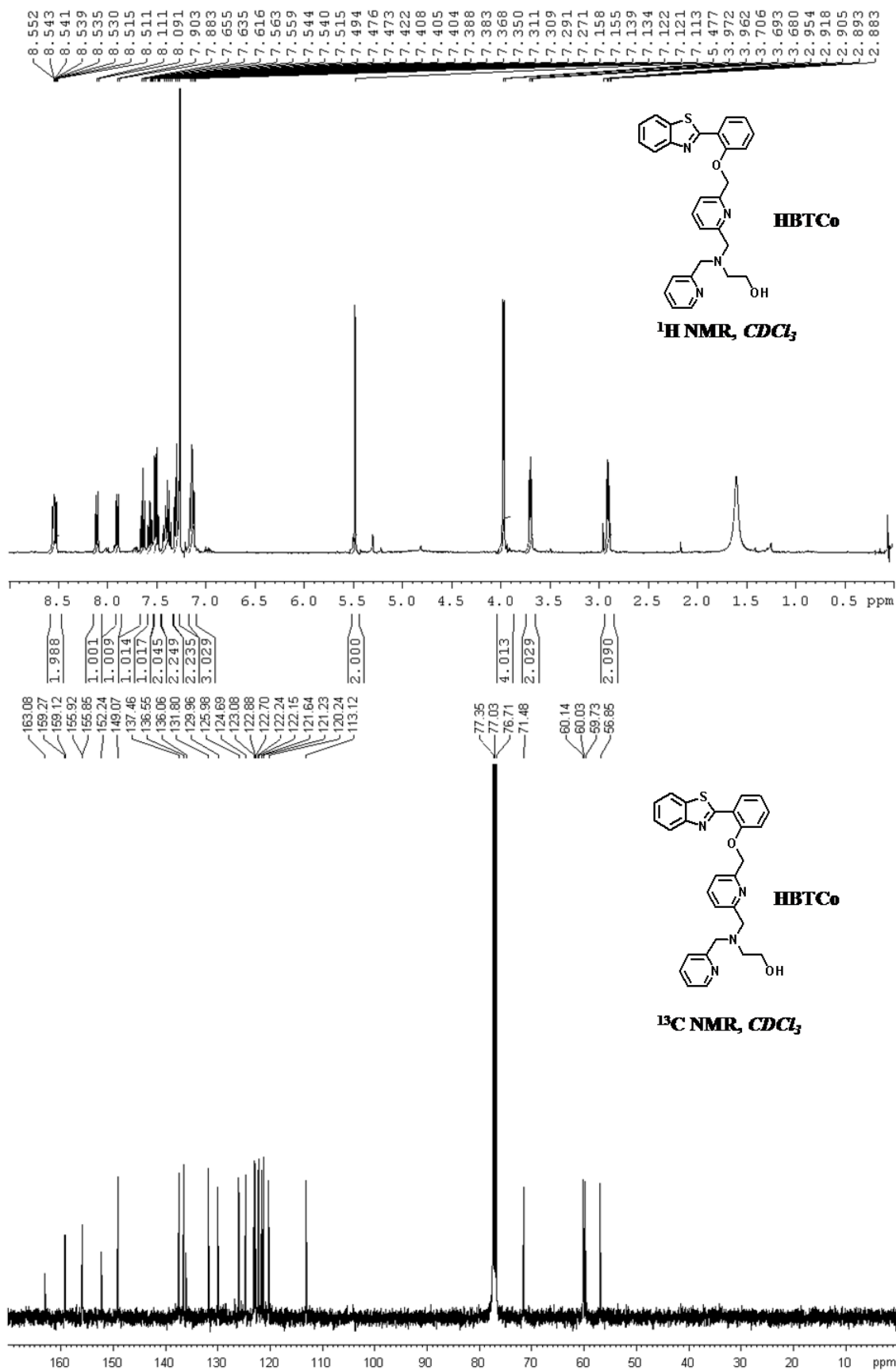


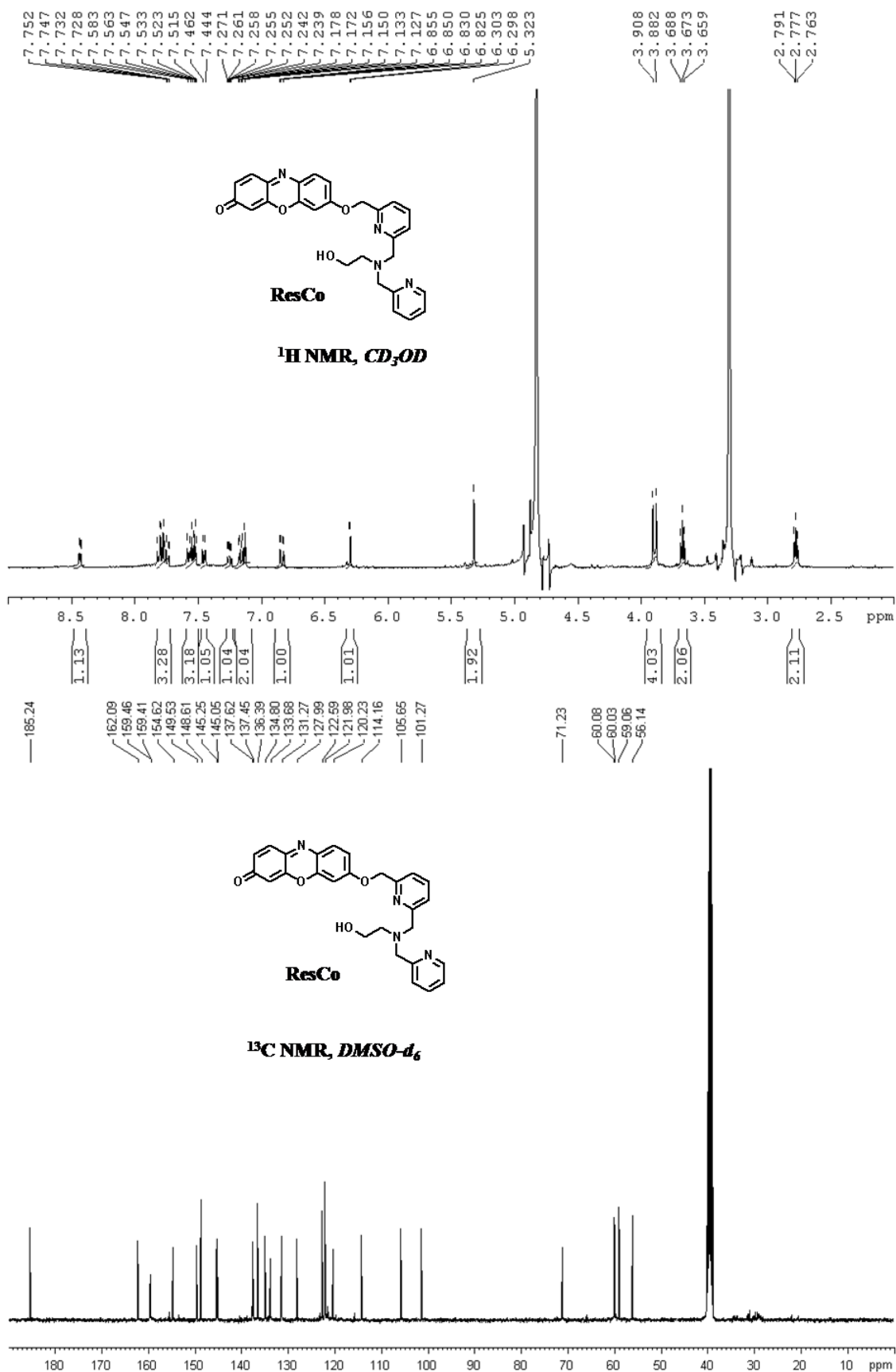












4.7 HRMS data

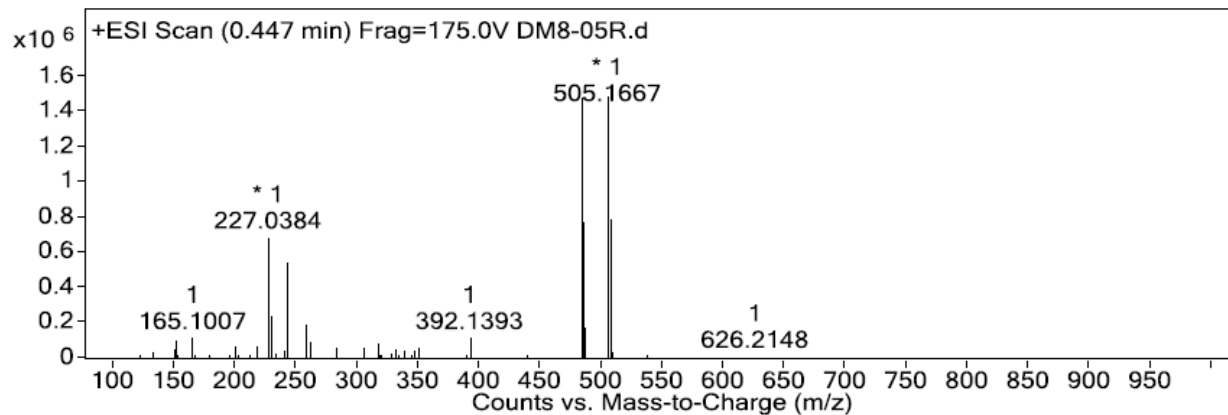


Figure 31. HRMS spectra of **HBTCo**. Observed $m/z = 505.1667$ $[\text{M} + \text{Na}]^+$ and calculated $m/z = 505.1674$ for $\text{C}_{28}\text{H}_{26}\text{N}_4\text{NaO}_2\text{S}$.

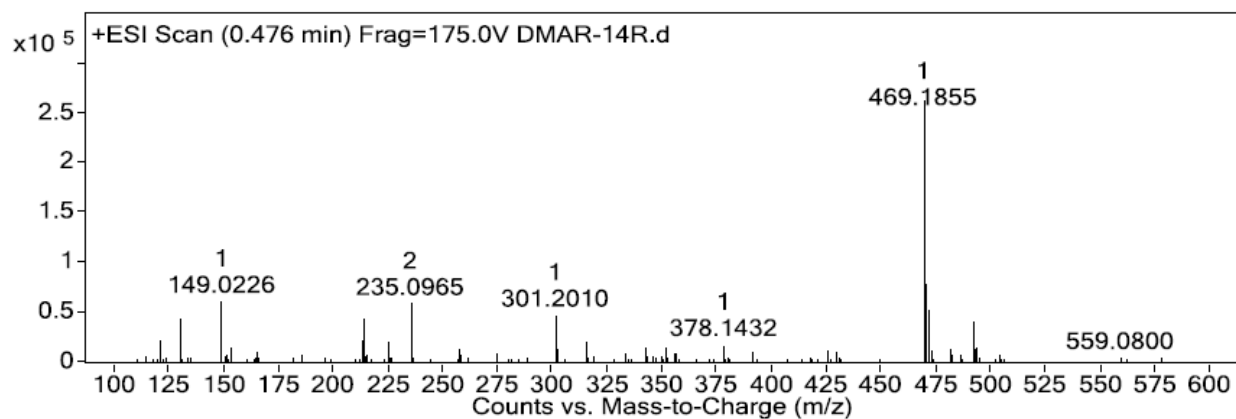


Figure 31. HRMS spectra of **ResCo**. Observed $m/z = 469.1855$ $[\text{M} + \text{H}]^+$ and calculated $m/z = 469.1876$ for $\text{C}_{27}\text{H}_{25}\text{N}_4\text{O}_4$.

5. References

1. Dennis, M.; Kolattukudy, P. E., A cobalt-porphyrin enzyme converts a fatty aldehyde to a hydrocarbon and CO. *Proc. Natl. Acad. Sci. USA* **1992**, *89*, 5306-5310.
2. Vallee, W. M. B. L., Cobalt as probe and label of proteins. In *Methods Enzymol.*, James, F. R.; Bert, L. V., Eds. Academic Press: 1993; Vol. 226, pp 52-71.
3. Walker, K. W.; Bradshaw, R. A., Yeast methionine aminopeptidase I can utilize either Zn^{2+} or Co^{2+} as a cofactor: A case of mistaken identity? *Protein Sci.* **1998**, *7*, 2684-2687.
4. Okamoto, S.; Eltis, L. D., The biological occurrence and trafficking of cobalt. *Metallomics* **2011**, *3*, 963-970.
5. Seldén, A. I.; Norberg, C.; Karlson-Stiber, C.; Hellström-Lindberg, E., Cobalt release from glazed earthenware: Observations in a case of lead poisoning. *Environ. Toxicol. Pharmacol.* **2007**, *23*, 129-131.
6. Barceloux, D. G.; Barceloux, D., Cobalt. *Clin. Toxicol.* **1999**, *37*, 201-216.
7. Basketter, D. A.; Angelini, G.; Ingber, A.; Kern, P. S.; Menné, T., Nickel, chromium and cobalt in consumer products: revisiting safe levels in the new millennium. *Contact Dermatitis* **2003**, *49*, 1-7.
8. El-Safty, S., Functionalized hexagonal mesoporous silica monoliths with hydrophobic azo-chromophore for enhanced Co(II) ion monitoring. *Adsorption* **2009**, *15*, 227-239.
9. Zeng, Z.; A. Jewsbury, R., The synthesis and applications of a new chromogenic and fluorescence reagent for cobalt(II). *Analyst* **1998**, *123*, 2845-2850.
10. Lin, W.; Yuan, L.; Long, L.; Guo, C.; Feng, J., A fluorescent cobalt probe with a large ratiometric fluorescence response via modulation of energy acceptor molar absorptivity on metal ion binding. *Adv. Funct. Mater.* **2008**, *18*, 2366-2372.
11. Yao, Y.; Tian, D.; Li, H., Cooperative binding of bifunctionalized and click-synthesized silver nanoparticles for colorimetric Co^{2+} sensing. *ACS Appl. Mater. Interfaces* **2010**, *2*, 684-690.
12. Zhen, S. J.; Guo, F. L.; Chen, L. Q.; Li, Y. F.; Zhang, Q.; Huang, C. Z., Visual detection of cobalt(ii) ion in vitro and tissue with a new type of leaf-like molecular microcrystal. *Chem. Commun.* **2011**, *47*, 2562-2564.
13. Que, E. L.; Chang, C. J., Responsive magnetic resonance imaging contrast agents as chemical sensors for metals in biology and medicine. *Chem. Soc. Rev.* **2010**, *39*, 51-60.
14. McRae, R.; Bagchi, P.; Sumalekshmy, S.; Fahrni, C. J., In situ imaging of metals in cells and tissues. *Chem. Rev.* **2009**, *109*, 4780-4827.
15. Haas, K. L.; Franz, K. J., Application of metal coordination chemistry to explore and manipulate

- cell biology. *Chem. Rev.* **2009**, *109*, 4921-4960.
16. Domaille, D. W.; Que, E. L.; Chang, C. J., Synthetic fluorescent sensors for studying the cell biology of metals. *Nat. Chem. Biol.* **2008**, *4*, 168-175.
17. Pluth, M. D.; Tomat, E.; Lippard, S. J., Biochemistry of mobile zinc and nitric oxide revealed by fluorescent sensors. *Annu. Rev. Biochem.* **2011**, *80*, 333-355.
18. Terai, T.; Nagano, T., Fluorescent probes for bioimaging applications. *Curr. Opin. Chem. Biol.* **2008**, *12*, 515-521.
19. Irving, H.; Williams, R. J. P., 637. The stability of transition-metal complexes. *J. Chem. Soc.* **1953**, *0*, 3192-3210.
20. Gunnlaugsson, T.; Leonard, J. P.; Murray, N. S., Highly selective colorimetric naked-eye Cu(II) detection using an azobenzene chemosensor. *Org. Lett.* **2004**, *6*, 1557-1560.
21. Zhou, Y.; Won, J.; Lee, J. Y.; Yoon, J., Studies leading to the development of a highly selective colorimetric and fluorescent chemosensor for lysine. *Chem. Commun.* **2011**, *47*, 1997-1999.
22. Maity, D.; Govindaraju, T., Pyrrolidine constrained bipyridyl-dansyl click fluoroionophore as selective Al^{3+} sensor. *Chem. Commun.* **2010**, *46*, 4499-4501.
23. Quinlan, E.; Matthews, S. E.; Gunnlaugsson, T., Colorimetric recognition of anions using preorganized tetra-amidourea derived calix[4]arene sensors. *J. Org. Chem.* **2007**, *72*, 7497-7503.
24. Sessler, J. L.; Tomat, E.; Lynch, V. M., Positive homotropic allosteric binding of silver(I) cations in a Schiff base oligopyrrolic macrocycle. *J. Am. Chem. Soc.* **2006**, *128*, 4184-4185.
25. Katsiaouni, S.; Dechert, S.; Briñas, R. P.; Brückner, C.; Meyer, F., Schiff base macrocycles containing pyrroles and pyrazoles. *Chem. Eur. J.* **2008**, *14*, 4823-4835.
26. Devoille, A. M. J.; Richardson, P.; Bill, N. L.; Sessler, J. L.; Love, J. B., Selective anion binding by a cofacial binuclear zinc complex of a Schiff-base pyrrole macrocycle. *Inorg. Chem.* **2011**, *50*, 3116-3126.
27. Lippert, A. R.; New, E. J.; Chang, C. J., Reaction-based fluorescent probes for selective imaging of hydrogen sulfide in living cells. *J. Am. Chem. Soc.* **2011**, *133*, 10078-10080.
28. Lippert, A. R.; Van de Bittner, G. C.; Chang, C. J., Boronate oxidation as a bioorthogonal reaction approach for studying the chemistry of hydrogen peroxide in living systems. *Acc. Chem. Res.* **2011**, *44* (9), 793-804.
29. Kim, H. M.; Cho, B. R., Two-photon probes for intracellular free metal ions, acidic vesicles, And lipid rafts in live tissues. *Acc. Chem. Res.* **2009**, *42*, 863-872.
30. Quang, D. T.; Kim, J. S., Fluoro- and chromogenic chemodosimeters for heavy metal ion detection in solution and biospecimens. *Chem. Rev.* **2010**, *110*, 6280-6301.
31. Cho, D.-G.; Sessler, J. L., Modern reaction-based indicator systems. *Chem. Soc. Rev.* **2009**, *38*,

1647-1662.

32. Vad, M. S.; Nielsen, A.; Lennartson, A.; Bond, A. D.; McGrady, J. E.; McKenzie, C. J., Switching on oxygen activation by cobalt complexes of pentadentate ligands. *Dalton Trans.* **2011**, *40*, 10698-10707.

33. Taki, M.; Iyoshi, S.; Ojida, A.; Hamachi, I.; Yamamoto, Y., Development of highly sensitive fluorescent probes for detection of intracellular copper(I) in living systems. *J. Am. Chem. Soc.* **2010**, *132*, 5938-5939.

34. Garner, A. L.; Koide, K., Oxidation state-specific fluorescent method for Palladium(II) and Platinum(IV) based on the catalyzed aromatic claisen rearrangement. *J. Am. Chem. Soc.* **2008**, *130*, 16472-16473.

35. Song, F.; Watanabe, S.; Floreancig, P. E.; Koide, K., Oxidation-resistant fluorogenic probe for mercury based on alkyne oxymercuration. *J. Am. Chem. Soc.* **2008**, *130*, 16460-16461.

36. Song, F.; Garner, A. L.; Koide, K., A highly sensitive fluorescent sensor for palladium based on the allylic oxidative insertion mechanism. *J. Am. Chem. Soc.* **2007**, *129*, 12354-12355.

37. Au-Yeung, H. Y.; New, E. J.; Chang, C. J., A selective reaction-based fluorescent probe for detecting cobalt in living cells. *Chem. Commun.* **2012**, *48*, 5268-5270.

38. Taki, M.; Wolford, J. L.; O'Halloran, T. V., Emission ratiometric imaging of intracellular zinc: design of a benzoxazole fluorescent sensor and Its application in two-photon microscopy. *J. Am. Chem. Soc.* **2003**, *126*, 712-713.

39. Seo, J.; Kim, S.; Park, S. Y., Strong solvatochromic fluorescence from the intramolecular charge-transfer state created by excited-state intramolecular proton transfer. *J. Am. Chem. Soc.* **2004**, *126*, 11154-11155.

40. Zhao, J.; Ji, S.; Chen, Y.; Guo, H.; Yang, P., Excited state intramolecular proton transfer (ESIPT): from principal photophysics to the development of new chromophores and applications in fluorescent molecular probes and luminescent materials. *PCCP* **2012**, *14*, 8803-8817.

41. Janes, L. E.; Cimpoia, A.; Kazlauskas, R. J., Protease-mediated separation of Cis and Trans diastereomers of 2(R,S)-benzyloxymethyl-4(S)-carboxylic acid 1,3-dioxolane methyl ester: intermediates for the synthesis of dioxolane nucleosides. *J. Org. Chem.* **1999**, *64*, 9019-9029.

42. Miller, E. W.; Albers, A. E.; Pralle, A.; Isacoff, E. Y.; Chang, C. J., Boronate-based fluorescent probes for imaging cellular hydrogen peroxide. *J. Am. Chem. Soc.* **2005**, *127*, 16652-16659.

43. Li, Z.; Hayman, R. B.; Walt, D. R., Detection of single-molecule DNA hybridization using enzymatic amplification in an array of femtoliter-sized reaction vessels. *J. Am. Chem. Soc.* **2008**, *130*, 12622-12623.

44. Kim, S. Y.; Hong, J.-I., Chromogenic and fluorescent chemodosimeter for detection of fluoride in

- aqueous solution. *Org. Lett.* **2007**, *9*, 3109-3112.
45. Choi, M. G.; Hwang, J.; Eor, S.; Chang, S.-K., Chromogenic and fluorogenic signaling of sulfite by selective deprotection of resorufin levulinate. *Org. Lett.* **2010**, *12*, 5624-5627.
46. Chen, W.; Li, Z.; Shi, W.; Ma, H., A new resorufin-based spectroscopic probe for simple and sensitive detection of benzoyl peroxide via deboronation. *Chem. Commun.* **2012**, *48*, 2809-2811.
47. Apfel, U.-P.; Buccella, D.; Wilson, J. J.; Lippard, S. J., Detection of nitric oxide and nitroxyl with benzoresorufin-based fluorescent sensors. *Inorg. Chem.* **2013**, *52*, 3285-3294.
48. Maity, D.; Kumar, V.; Govindaraju, T., Reactive probes for ratiometric detection of Co^{2+} and Cu^{+} based on excited-state intramolecular proton transfer mechanism. *Org. Lett.* **2012**, *14*, 6008-6011.
49. Grynkiewicz, G.; Poenie, M.; Tsien, R. Y., A new generation of Ca^{2+} indicators with greatly improved fluorescence properties. *J. Biol. Chem.* **1985**, *260*, 3440-3450.

Chapter 6

Near-infrared fluorometric and colorimetric molecular probes for thiol and H₂S

Paper based on this chapter have been published in *Org. Biomol. Chem.*, **2013**, *11*, 2098-2104. ([Inside Cover Page](#)) ([Link](#)). Reproduced by permission of the Royal Society of Chemistry. Another one manuscript has been submitted for publication.

Part A

1. Turn on NIR fluorescence and colorimetric cyanine probe (DNBSCy) for thiol

1.1 Introduction

The optical monitoring of thiols such as glutathione (GSH), cysteine (Cys) and homocysteine (Hcy) is of significant interest due to their crucial roles in maintaining the biological redox homeostasis through the equilibrium of free thiols and oxidized disulfides in biological systems.¹⁻⁴ These low molecular weight thiols (LMWTs) are essential for the growth of cells and tissues in living organisms.⁵⁻⁸ Dramatic changes in the intracellular thiol concentrations in biological fluids are implicated in a number of diseases including liver damage, heart disease, cancer, AIDS, inflammatory bowel disease, osteoporosis, Alzheimer's and cardiovascular diseases.⁹⁻¹¹ Among these LMWTs, GSH is a major endogenous antioxidant produced in the cell (0.5–10 mM).¹² GSH protects the cells from oxidative stress by trapping free radicals and reactive oxygen species (ROS); it also maintains exogenous antioxidants in their reduced forms.⁵ The abnormal ratio of reduced GSH to oxidized glutathione is one of the potential reasons for oxidative stress.¹³⁻¹⁸ In cells, the enzyme glutathione reductase catalyses the reduction of GSSG to free GSH, thus preventing the occurrence of oxidative stress. Hence, it is very crucial to monitor the concentration of GSH and the activity of glutathione reductase in physiological media. Although several strategies have been developed to detect these mercapto-biomolecules, fluorescence detection has been recognized as the most convenient method due to its simplicity and low detection limit. In the past few years, researchers have developed thiol-selective fluorescence probes exploiting the strong nucleophilicity of the thiol group and their cation binding affinity.¹⁹ However, the existing fluorescence probes for thiols are plagued by certain serious limitations like excitation and emission in the UV-visible region, relatively time consuming procedures, and the use of organic–water mixed media.

NIR molecular probes have gained special interest in the recent years due to several inherent advantages over the UV-visible probes.²⁰⁻²³ Deeper penetration of the NIR radiation

(650-900 nm) enables the assessment of molecular and physiological events several layers deep inside the analyte samples and tissues. Moreover, optical response in the NIR region is not affected by the autofluorescence generated from chromophores and macromolecules present in the analyte or tissue samples.²⁴⁻²⁶ A few research groups have taken the initiative in designing thiol-selective NIR sensors.²⁷⁻³⁰ However, many of these thiol sensors work by means of reduction in NIR fluorescence. Therefore, a turn on NIR fluorescence probe based on the extended π -electron conjugated system that could instantly monitor thiol in complete physiological media is necessary.

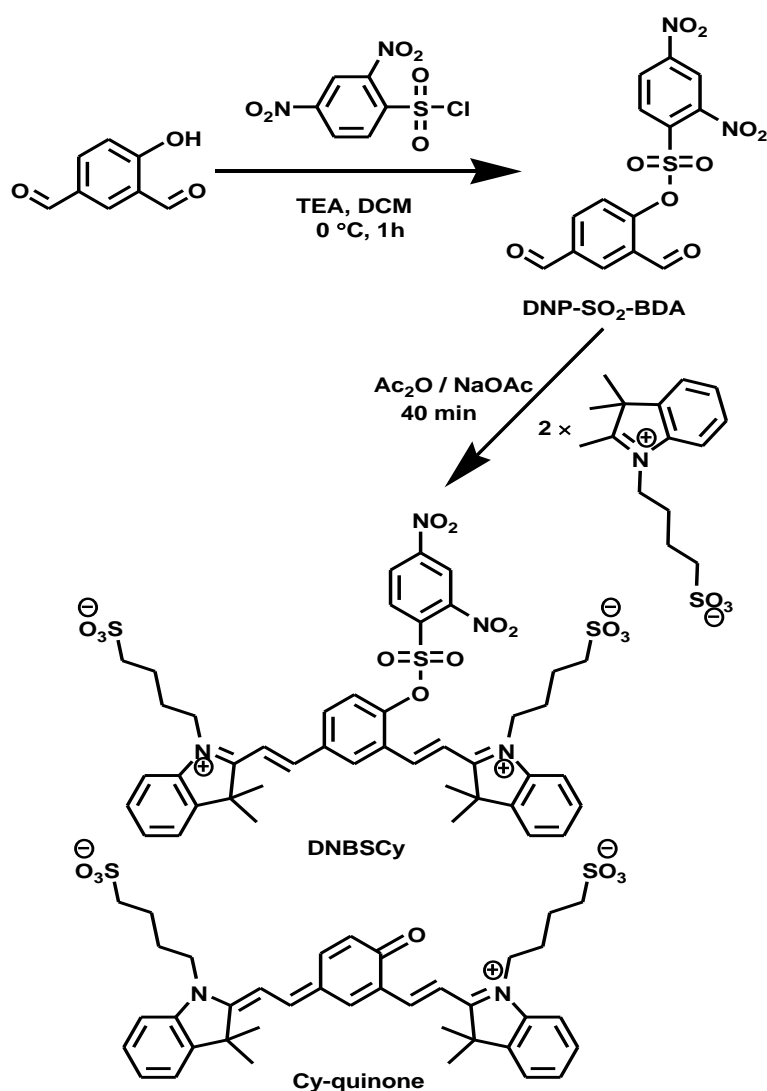
1.2 Design strategy

The design strategy for the development of a turn on NIR fluorescence probe relied on a reaction-based approach in which a thiol mediated bond-cleaving reaction converted a weak or non-fluorescence probe into a robust NIR fluorescent dye.³¹⁻³⁷ In this chapter a highly sensitive turn on NIR fluorescence and colorimetric probe is discussed for monitoring thiols, especially GSH, over GSSG in physiological media. The thiol assisted removal of 2,4-dibenzenesulfonyl (DNBS) from the hydroxyl group moiety of a fluorophore has been found to have excellent selectivity towards thiol detection with off-on fluorescence signaling.³⁸⁻⁴³ Strong electron withdrawing DNBS functionality would significantly disturb the ICT process, maximising the fluorescence switching on-off process. Heptamethine cyanine (Cy), a NIR fluorescent dye with high extinction coefficient and quantum yield has been extensively used in NIR bioimaging.¹³ An interesting approach has been devised by incorporating the DNBS protected phenolic moiety onto the conjugated cyanine backbone.⁴⁴ The DNBS-phenolic moiety incorporated heptamethine cyanine (**DNBSCy**) was designed, however, with a completely altered π -conjugation pattern and positive charges localised on both the nitrogen atoms (Scheme 1). The thiol mediated nucleophilic reaction on the **DNBSCy** probe releases thiol-dinitrobenzene by-product, generating the Cy-phenolate which rearranges itself by neutralising the positive charge on a nitrogen atom to form stable **Cy-quinone**. This **Cy-quinone** resumes the extended π -electron conjugation pattern of the cyanine dyes. Similar to parent heptamethine cyanine (Cy), the **Cy-quinone** has an odd number of carbon atoms between two nitrogen atoms to facilitate conjugation along the

polymethine chain. It was thus expected to exhibit turn on NIR fluorescence besides showing unique visible color changes due to the conjugated π -electron push-pull character.

1.3 Synthesis of molecular probe DNBSCy

A two-step straightforward synthetic route was developed for the preparation of the DNBSCy probe as outlined in Scheme 1. The arenosulfonate ester moiety (DNP-SO₂-BDA) was synthesized by sulfonating the hydroxyl group of 4-hydroxy-1,3-benzenedicarboxaldehyde with 2,4-dinitrobenzenesulfonyl chloride. Good yields of



Scheme 1. Synthesis of DNBSCy and molecular structure of Cy-quinone.

DNBSCy were obtained by condensing this dialdehyde-arenesulfonate ester intermediate with 2 equiv of indolium-3-butyl-sulfonate. All the compounds were characterized by NMR, mass spectrometry, and elemental analysis. The arenesulfonate ester moiety in the **DNBSCy** probe is highly reactive towards thiolate, which releases the hydroxyl group of the cyanine fluorophore backbone in the presence of free thiols. The indolium-3-butyl-sulfonate chains in **DNBSCy** are chosen to impart water solubility and to prevent aggregation of the cyanine backbone in solution.

1.4 Photophysical studies of DNBSCy in presence of thiol

DNBSCy is a yellow powder and readily dissolves in water to form a light green solution. **DNBSCy** exhibits an absorption band centred around 390 nm with an extinction coefficient (ϵ) of $2.6 \times 10^4 \text{ M}^{-1}\text{cm}^{-1}$ in 10 mM PBS buffer (pH = 7.4) (Figure 1). The probe itself is almost non-fluorescent, displaying a very weak emission band around 700 nm (Figure 2). In the presence of GSH, the absorbance at 390 nm decreased drastically while two new absorption bands appeared at 476 nm and 581 nm (Figure 1). Concurrently, the color of the

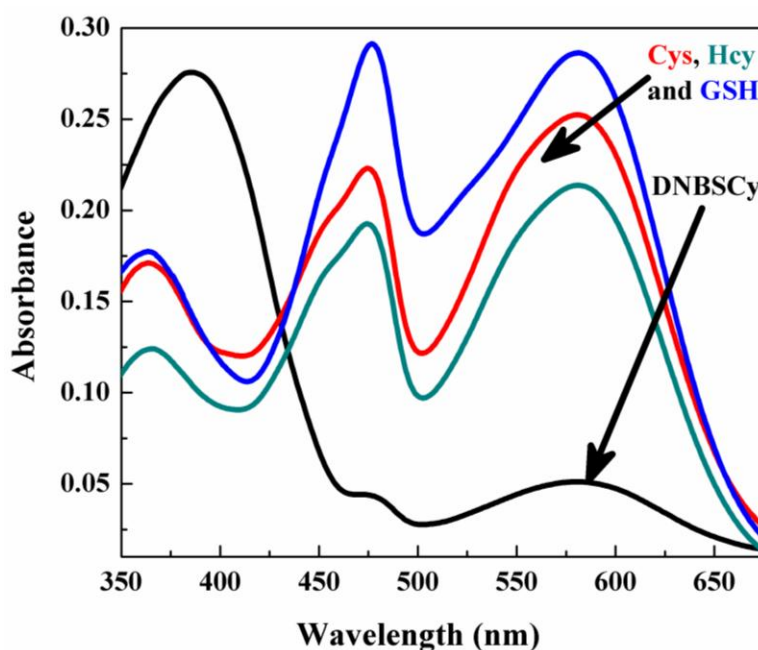


Figure 1. UV-Vis absorption spectra of **DNBSCy** (10.0 μM) and on addition of 10.0 equiv of Cys, Hcy and GSH in 10 mM PBS buffer medium (pH = 7.4).

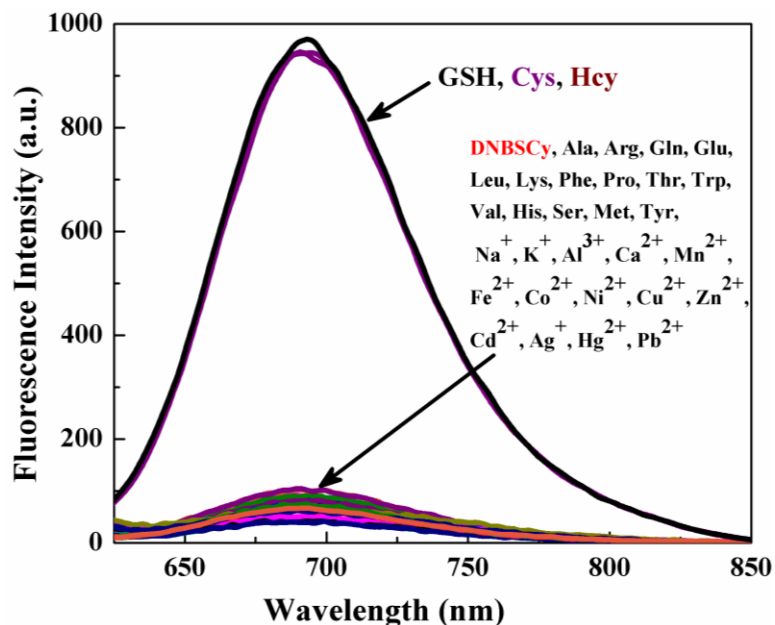


Figure 2. Fluorescence response of **DNBSy** probe (10.0 μM) towards various amino acids (1.0 mM) and metal ions (1.0 mM). Each spectrum was acquired after 30 min. incubation of the probe with analyte in 10 mM PBS buffer (pH 7.4) with $\lambda_{\text{ex}} = 600$ nm.

solution changed from light green to blue. As anticipated upon 600 nm excitation (λ_{ex}), the fluorescence emission spectra displayed a switchon peak around 700 nm in the NIR region (Figure 2). This large Stokes shift (~ 119 nm) between the absorbance and emission peaks is a highly desirable characteristic feature of a fluorescence probe that assists in increasing the signal-to-noise ratio. Other free thiol containing amino acids like Cys and Hcy showed similar absorption and emission spectral changes. However, the presence of amino acids with no thiol functionality or biologically relevant metal ions did not show any significant spectral changes with **DNBSy** (Figure 2). Though thiols are present in millimolar concentration inside cells, only 5.0 μM GSH was found to be enough to display significant NIR fluorescence response within two minutes after reacting with the arenesulfonate ester moiety of the **DNBSy** probe (10 μM) (Figure 3). This clearly emphasised the sensitivity of the probe, as **DNBSy** respond quickly towards the detection of GSH as low as three orders of magnitude less than the actual concentration present in normal cells. On addition of GSH to the **DNBSy** solution, NIR fluorescence emission intensity at $E_{\text{max}} = 695$ nm increased rapidly in the initial stage and reached the maximum (> 25 fold) over a period of 20 min. The

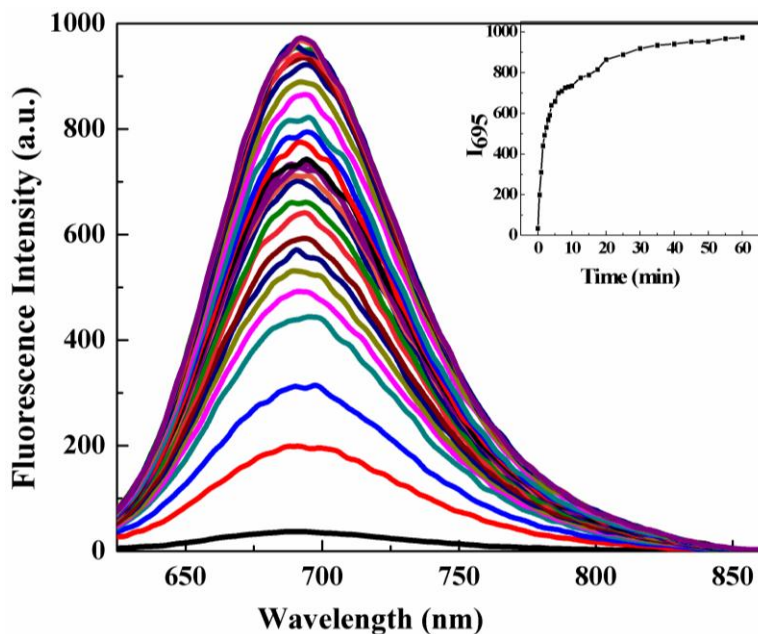


Figure 3. Time-dependent NIR fluorescence spectra recorded when probe **DNBSy** (10.0 μM) was treated with GSH (5.0 μM) in 10 mM PBS buffer (pH 7.4) with $\lambda_{\text{ex}} = 600$ nm. Inset: Fluorescence intensity changes at 695 nm recorded as a function of time.

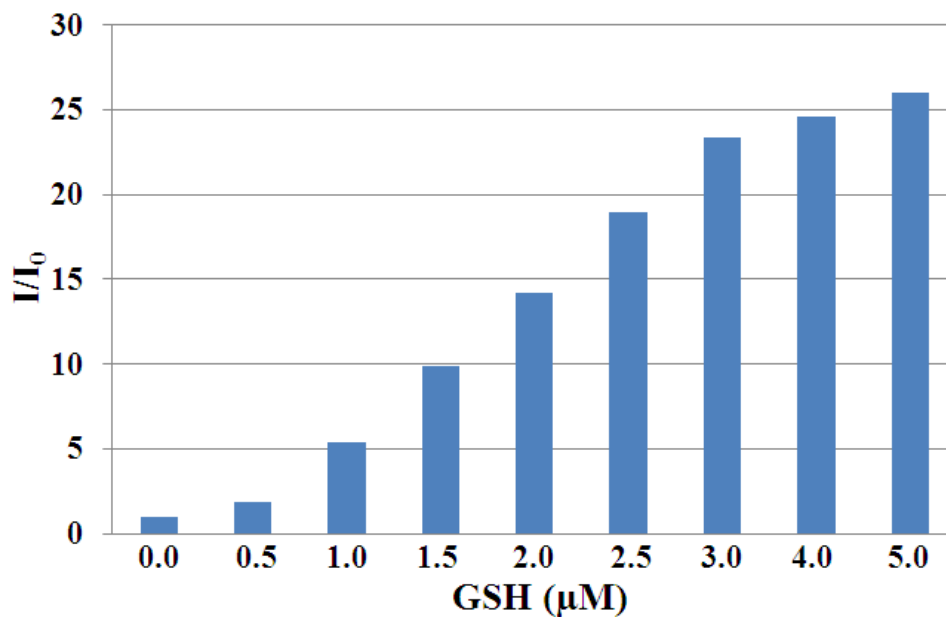


Figure 4. Relative fluorescence response of **DNBSy** (10.0 μM) on addition of different concentrations of GSH in 10 mM PBS buffer medium (pH = 7.4).

GSH titration study showed that **DNBSCy** could detect submicromolar concentration of GSH efficiently (Figure 4). GSH mediated rapid nucleophilic reaction with the electron withdrawing sulfonyl ester moiety of **DNBSCy** probe releases the Cy-phenolate anion. The negative charge of Cy-phenolate rearranges itself by neutralizing the positive charge on one of the nitrogen atoms to form stable **Cy-quinone** (Scheme 1). In the process, **Cy-quinone** resumes heptamethine cyanine-like extended π -electron conjugation pattern which is responsible for the observed characteristic turnon NIR fluorescence. The conjugated π -electron push-pull character is also generated in the **Cy-quinone** system that lends a unique blue color to the solution.

1.5 Competitive study

Further, **DNBSCy** was also found to be highly selective for GSH over other competing non-thiol amino acids in the buffer solution (Figure 5).

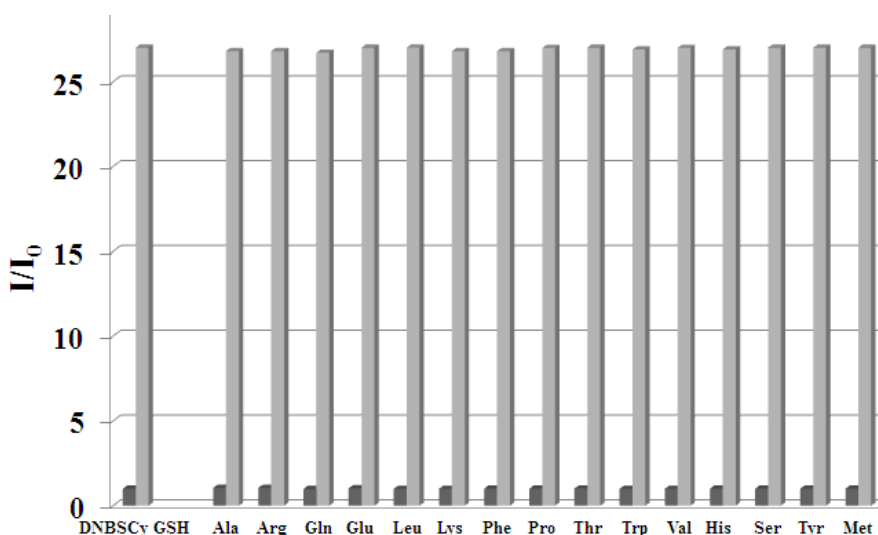


Figure 5. Relative fluorescence intensities of **DNBSCy** with GSH in the presence of various other amino acids. Dark grey bar: **DNBSCy** (10.0 μ M) with 10 equiv of amino acid stated. Light grey bar: 10.0 μ M of **DNBSCy** and 5 equiv of GSH with 10 equiv of amino acid stated. ($E_{\lambda} = 695$ nm). The responses of the **DNBSCy** to GSH, in the absence of amino acids, is included as controls, dark grey bar, no amino acid added, light grey bar, 10.0 μ M of **DNBSCy** with 5 equiv of GSH in 10 mM PBS buffer medium (pH = 7.4).

1.6 Product analysis after reaction with GSH

Mass spectroscopic analysis confirmed that **DNBSCy** was converted to the **Cy-quinone** dye under the experimental conditions used for GSH detection (Figure 6). The ESI-mass spectra showed peaks at $m/z = 705.2$ (calculated for $C_{38}H_{43}N_2O_7S_2 + H^+$) corresponding to **Cy-quinone** and at $m/z = 474.0$ (calculated for $C_{16}H_{19}N_5O_{10}S$) corresponding to the by-product γ -glutamyl-S-(2,4-dinitrophenyl)cysteinylglycine.

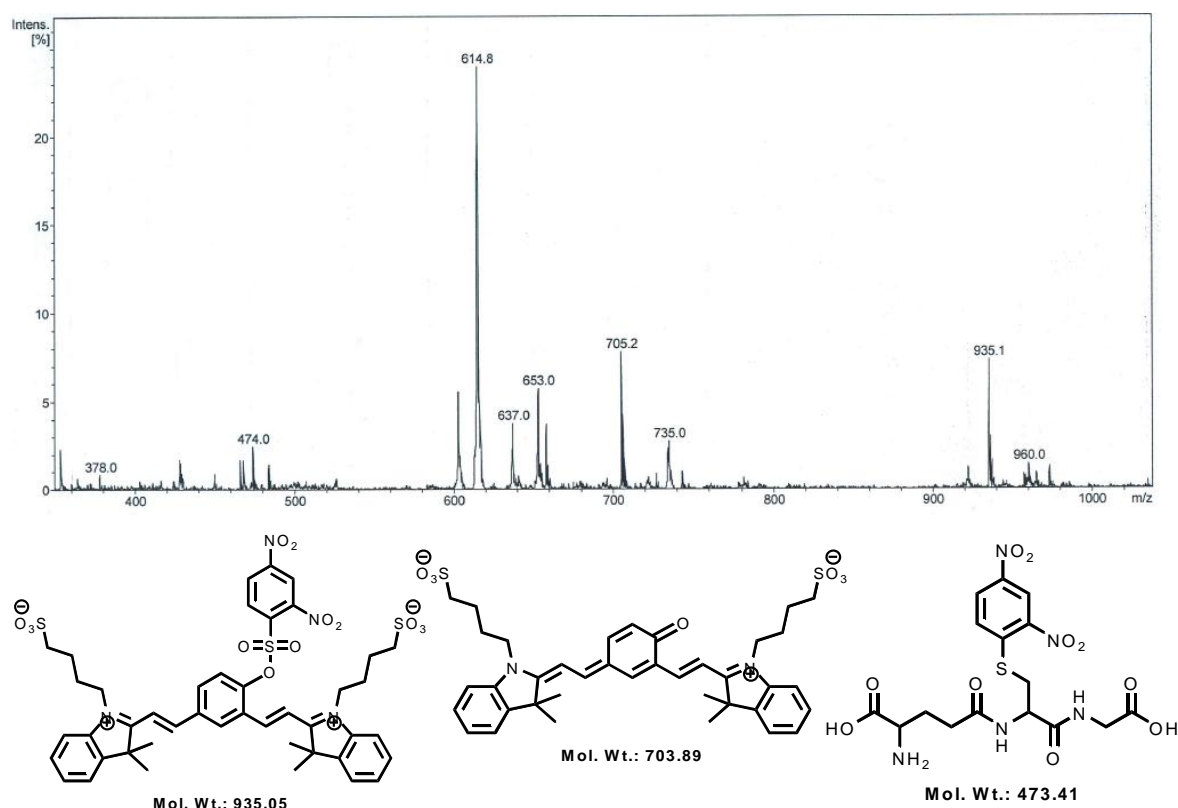


Figure 6. ESI mass spectra (positive ion mode) for the reaction of 10.0 μM **DNBSCy** with GSH (10.0 μM) in water. Mass peak observed at 935.1 was attributed to unreacted **DNBSCy**, peak at $m/z = 705.2$, (calculated for $[C_{38}H_{43}N_2O_7S_2^- + H]^+$) corresponding to this cyanine dye (**Cy-quinone**); peaks at 614.8 ($[M + 2H]^+$), 637.0 ($[M + H + Na]^+$) and 653 ($[M + H + K]^+$) were attributed to the oxidized form of GSH (GS-SG). Peak at $m/z = 474.0$ corresponding to the side product γ -glutamyl-S-(2,4-dinitrophenyl)cysteinylglycine (calculated for $C_{16}H_{19}N_5O_{10}S$).

1.7 pH dependent study

The effect of pH on the GSH mediated arenesulfonate ester bond cleavage was studied to understand the efficiency of the process. **DNBSCy** alone was stable within the pH range of 5-8 while small changes were observed in the pH range of 8-10 (Figure 7). However, the **DNBSCy** probe reacted selectively with GSH in the biologically relevant pH range of 6-10 to form the NIR fluorescence emitting **Cy-quinone** dye. The optimum NIR fluorescence emission was observed in the commonly used physiological pH range of 6.5-8.5, which makes the **DNBSCy** probe convenient for the detection and monitoring of thiols without interference from the pH-dependent effects of the physiological media.

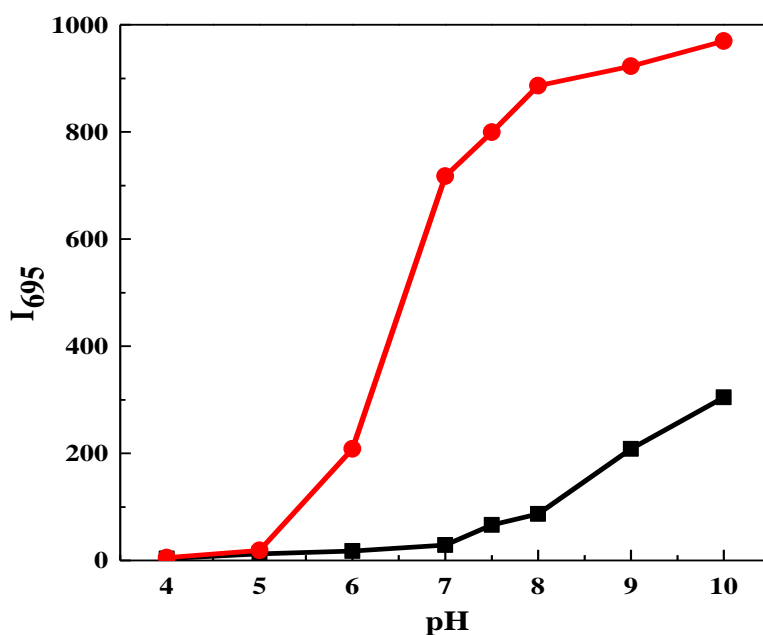


Figure 7. Effect of pH on the NIR emission of **DNBSCy** monitored at 695 nm. Black trace: **DNBSCy** (10 μM) and red trace: **DNBSCy** (10.0 μM) with 5.0 μM of GSH in 10 mM PBS buffer.

1.8 Reduced thiol detection in fetal bovine serum (FBS)

To ascertain the practical applicability of our turn on NIR fluorescence probe, thiol content in the fetal bovine serum (FBS) sample was studied. Thiol containing amino acids generally occur in the disulfide form in blood serum. Estimation of the thiol pool in blood serum is crucial for understanding the role of thiols in the pathogenesis of cardiovascular diseases. The plasma (FBS) was treated with a reducing agent triphenylphosphine to reduce all the oxidized disulfide to free thiols.⁴⁵ Different aliquots of the reduced FBS were added to **DNBSCy** in buffer solution (2 mL, 10 mM PBS, pH 7.4) at ambient temperature. Figure 8 shows the turn on NIR fluorescence signal and linear increase in the intensity of the signal with the addition of reduced FBS. These data clearly suggest the presence of free thiols that react rapidly with the **DNBSCy** probe to form the NIR emitting **Cy-quinone** dye. In addition, spontaneous colorimetric changes were observed in the absorption spectra (Figure 9). The visible light greenish color of the solution gradually changed to blue as the amount of reduced FBS was increased in the analysis mixture under study. This experiment demonstrates that **DNBSCy** is capable of monitoring thiols in the serum sample by means of characteristic turn on NIR fluorescence as well as colorimetric optical responses.

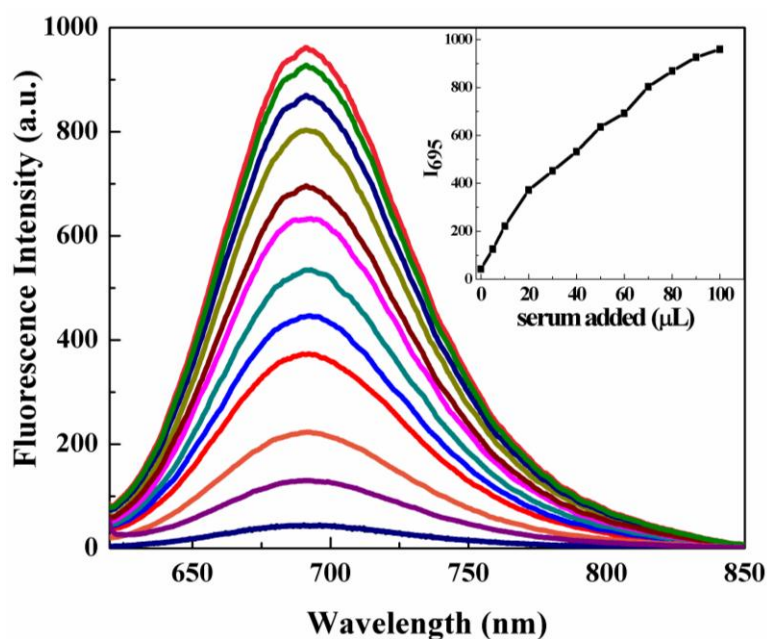


Figure 8. NIR fluorescence spectra of **DNBSCy** (10.0 μM) upon addition of aliquots (0, 5, 10, 20, 30, 40, 50, 60, 70, 80, 90, 100 μL) of reduced fetal bovine serum ($\lambda_{\text{ex}} = 600$ nm; $E_{\text{max}} = 695$ nm).

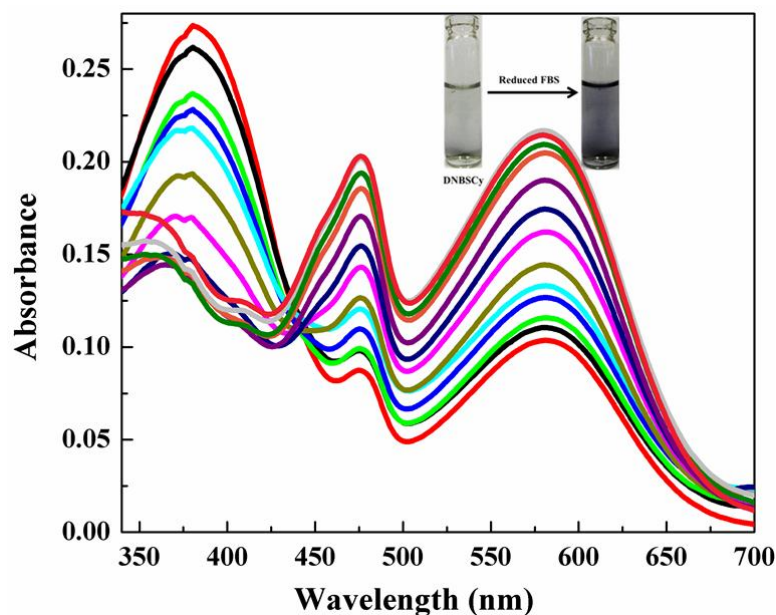
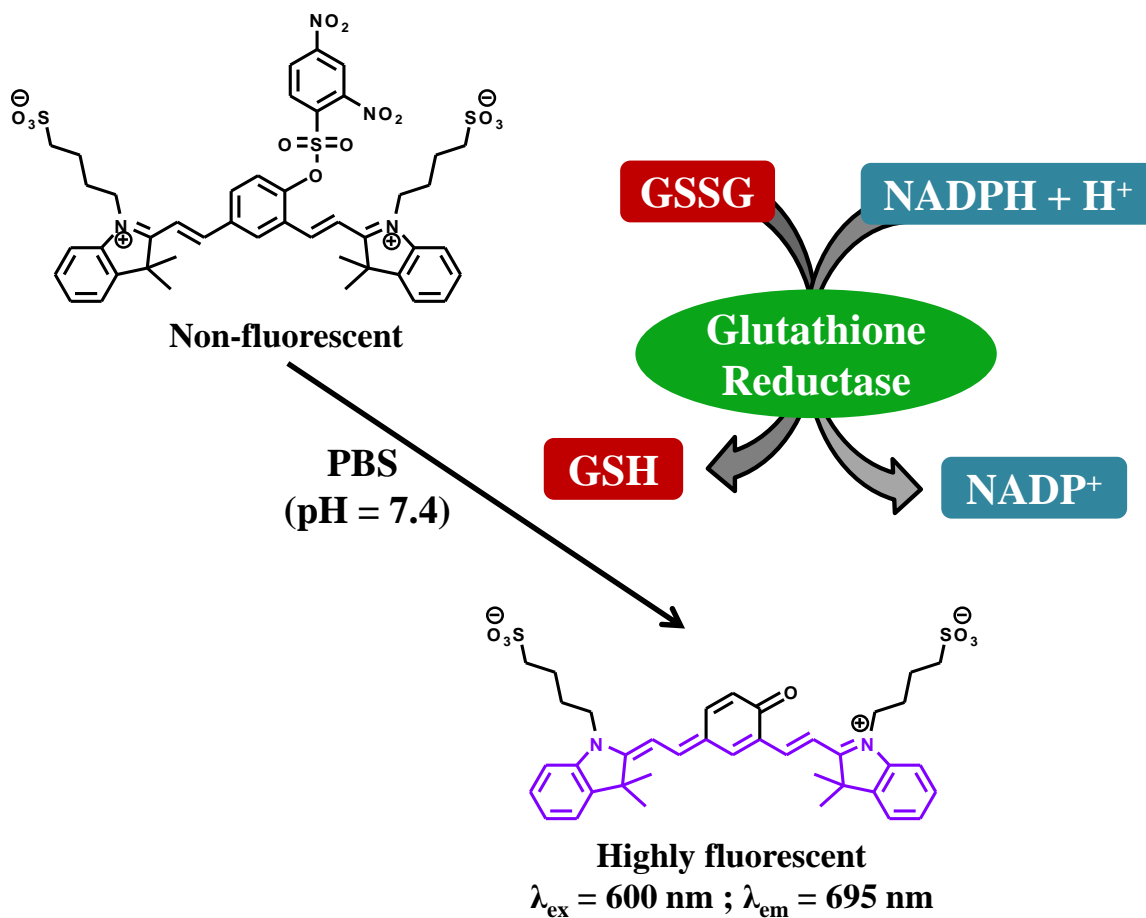


Figure 9. UV-Vis absorption spectra of probe **DNBSy** (10.0 μM) upon addition of various amounts (0, 5, 10, 15, 20, 30, 40, 50, 60, 70, 80, 90, 100 μL) of reduced fetal bovine serum solution to the 10 mM PBS buffer solution (pH 7.4).

1.9 Selective detection of the reduced GSH over oxidized GSSG using a combination of glutathione reductase and DNBSy

Significant imbalance in the GSH/GSSG ratio is responsible for oxidative stress and has direct implications for human health. Therefore, the measure of glutathione reductase activity serves as an indicator for the assessment of oxidative stress. The enzyme glutathione reductase catalyzes the reduction of GSSG to GSH in the presence of the reducing agent nicotinamide adenine dinucleotide phosphate (NADPH) under physiological conditions.⁴⁶ Thus, the formation of GSH by reducing the oxidized GSSG was monitored in the presence of glutathione reductase by coupling our free thiol responsive **DNBSy/Cy-quinone** transformation with enzyme catalyzed GSSG/GSH conversion (Scheme 2). **DNBSy** reacted instantaneously with the free GSH generated from GSSG under the assay conditions (10 mM PBS buffer, 1 unit/mL glutathione



Scheme 2. Efficient monitoring of free thiol generated from glutathione reductase (in presence of NADPH) catalyzed GSSG/GSH conversion by coupling the thiol responsive DNBSCy/Cy-quinone transformation with unique turn on NIR fluorescence and colorimetric optical response.

reductase, 0.4 mM NADPH) as indicated by the enhanced NIR emission (> 11 fold) within 2 min of adding the enzyme (Figure 10). This preliminary experiment motivated us to study the kinetic effect of the reduction of GSSG to GSH at different concentrations of the enzyme. This experiment revealed that higher concentrations of glutathione reductase lowered the time required for completion of the GSSG/GSH redox process and its subsequent detection (Figure 11). Maximum NIR emission signal was achieved within 20 min when 10 mU/mL of glutathione reductase was employed. However, more time (double) was required to reach the maximum intensity when half the concentration of glutathione reductase was used. In the absorption spectra, the DNBSCy absorbance band at 385 nm decreased while new bands

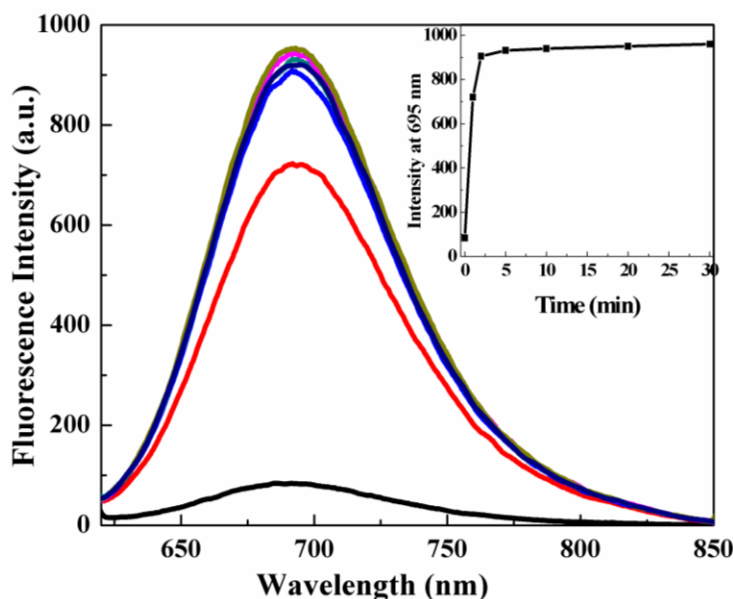


Figure 10. Fluorescence spectra of probe **DNBSCy** (10.0 μM) in response to enzymatic conversion of GSSG (2 mM) to free GSH using glutathione reductase (1 unit/mL) and 0.4 mM of NADPH in the 10 mM PBS buffer solution (pH 7.4).

appeared at 475 and 582 nm with the addition of NADPH and glutathione reductase (Figure 12). A clear isobestic point at 440 nm indicated the formation of **Cy-quinone** dye by the reaction of free GSH on **DNBSCy**. The solution color changed from light green to blue as a result of formation of the cyanine dye with extended conjugation.

Normally, the glutathione reductase activity is monitored with NADPH consumption by recording the decreased absorbance at 340 nm or the free GSH generated can be visualized from the increased absorbance at 412 nm using Ellman's reagent. **DNBSCy** probe, with dual optical response (turn on NIR fluorescence and colorimetric response), provides a sophisticated, non-invasive and accurate way of monitoring the activity of glutathione reductase which in turn can be a parameter for measuring oxidative stress. As an added advantage, this probe allows the naked eye detection of GSSG to GSH conversion in the presence of glutathione reductase without the need for expensive instrumentation. To the best of our knowledge, dual responsive **DNBSCy** is the first probe with an excellent combination of turn on NIR fluorescence and colorimetric optical response to detect free thiol content in serum and to measure the activity of glutathione reductase in the GSSG/GSH redox process (Scheme 2).

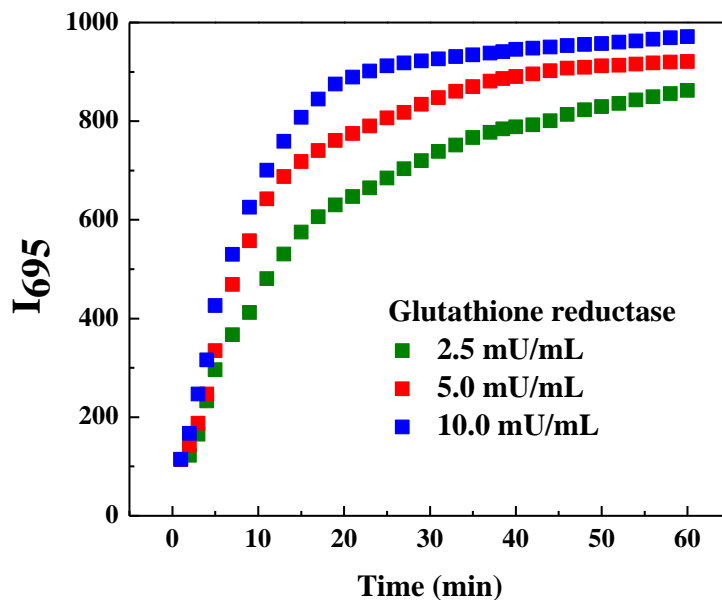


Figure 11. Glutathione reductase activity assay. NIR fluorescence response of DNBSy (10.0 μ M) at 695 nm ($\lambda_{\text{ex}} = 600$ nm) monitored as a function of time. In the assay mixture glutathione reductase reduces GSSG to reduced free GSH form using a reducing agent NADPH (100.0 μ M). The activity of enzyme glutathione reductase was measured at three different concentrations (2.5, 5.0 and 10.0 mU/mL) in 10 mM PBS buffer (pH 7.4).

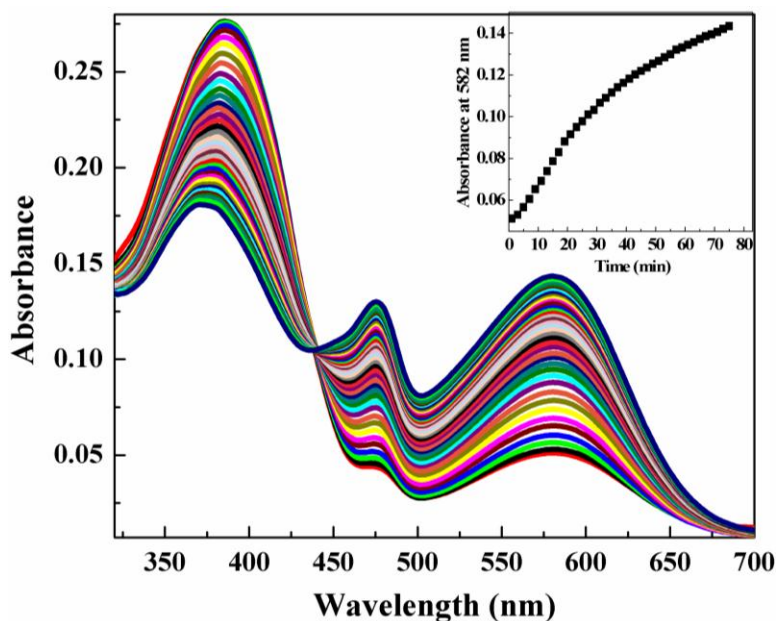


Figure 12. Time-dependent UV-Vis absorption spectra of DNBSy (10.0 μ M). Assay conditions: 10 mM PBS buffer (pH = 7.4), GSSG, NADPH (10.0 μ M), glutathione reductase (10 mU/mL). Inset: Absorbance changes at 582 nm recorded as a function of time.

1.10 Conclusion

In conclusion, a thiol selective water soluble turn on NIR fluorescence probe **DNBSCy** has been successfully developed. This molecular probe readily reacts with thiols, in particular GSH, to release NIR fluorescence emitting cyanine dye over a wide pH range. The probe was used effectively for the turn on NIR fluorescence and colorimetric monitoring of thiols in fetal bovine serum (FBS). For the first time, we also demonstrated the ability of the **DNBSCy** probe to be used in monitoring the GSSG/GSH redox process in the presence of glutathione reductase enzyme and the reducing agent NADPH with the unique combination of NIR turn on fluorescence and colorimetric optical response. Therefore, this probe is capable of monitoring the activity of glutathione reductase which in turn serves as a tool to assess the levels of oxidative stress. In general, **DNBSCy** can be used as a non-invasive tool for the determination of thiol content in biological fluids, measuring the activities of the enzymes involved in thiol coupled redox processes and *in vivo* NIR fluorescence imaging applications.

Part B

2. Ratiometric NIR fluorescence and colorimetric cyanine (DNPOCy) probe for H₂S

2.1 Introduction

Hydrogen sulfide (H₂S) is also known as “sewer gas” has strong odor similar to rotten eggs at lower concentration levels. H₂S has emerged as the third endogenous gaseous signaling compound (gasotransmitter) after nitric oxide (NO) and carbon monoxide (CO). The typical concentration of H₂S in blood is found to be in the range 10–100 μM.⁴⁷ H₂S plays important physiological role in many biological processes including regulation of cell growth, vasodilation and angiogenesis, mediation of neurotransmission, inhibition of insulin signaling, and regulation of inflammation.⁴⁸⁻⁵¹ Unlike NO, H₂S does not generate the toxic reactive oxygen species (ROS) and moreover it acts as an antioxidant or scavenger of ROS. There are three enzymes: cystathionine-β-synthase (CBS), cystathionine-γ-lyase (CSE), and 3-mercaptopyruvate sulfur transferase (3MST) catalyze the cysteine or cysteine derivatives to H₂S within different organs and tissues.⁵² It was reported that mitochondrial sulfide quinone oxidoreductase (SQOR) and persulfidedioxygenase (ETHE1) inactivate H₂S by oxidizing it, which emphasizes the importance of H₂S homeostasis.⁵³ In humans, altered levels of H₂S have been correlated with central nervous system diseases such as Down syndrome, Alzheimer’s disease, and other diseases of mental deficiency.⁵⁴⁻⁵⁶ Furthermore, the abnormal production of H₂S has been associated with diseases such as chronic kidney disease, liver cirrhosis and diabetes.⁵⁷ Thus, it is crucial to understand the chemistry and properties of H₂S in biosystems. Though there are several methods reported for H₂S detection, fluorometric technique is now one of the most attractive molecular imaging tools for the *in vivo* detection of biomolecules owing to its high sensitivity/selectivity, non-invasiveness, and aptness for living cells, tissues, and small animals. In recent years, several fluorescent molecular probes have been reported for H₂S detection *in vitro* as well as *in vivo*. They are developed by taking advantages of several significant characteristic properties of H₂S, such as good reducing power towards azide, nitro and hydroxy-amine groups, dual nucleophilicity, high binding

affinity towards copper ion, and efficient thiolysis of dinitrophenyl ether.⁴⁷ Though these molecular probes are shown to be useful for H₂S detection, they have some major drawbacks which restricted their actual purposes. The major drawbacks of existing probes include (i) the concentration of H₂S is 10–100 μM in blood and much lower (submicromolar range) in living cells. Most of probes detects H₂S at higher concentration, (ii) almost all probes sense H₂S in fluorescence on–off manner which is not absolute perfect for quantitative analysis of H₂S in living systems. These techniques can be easily influenced by photobleaching, local probe concentration, microenvironment etc, (iii) some of the reported probes trap this H₂S only in aqueous-organic mixture, (iv) these existing fluorescence probes for H₂S are plagued by a serious limitation i.e. high energy absorption and emission of the dyes, (v) Most of the reported H₂S probes display response time between 20 min to two hours, except for dansylazide and HSip-1 (within seconds) reported by Wang *et. al.*⁵⁸ and Nagano *et. al.*,⁵⁹ these probes, however, are not suitable for real-time determination of the fluctuations in H₂S concentration in biological systems. The drawbacks discussed above can be addressed by developing ratiometric and NIR fluorescent probes. Ratiometric analysis means the changes in ratio of intensities of absorption or emission at two wavelengths which minimize the error arise from the physical or chemical fluctuations in the sample. Ratiometric fluorescent probes can do signal rationing to increase the dynamic range and provide built-in-correction for aforementioned interferences. Near-infrared (NIR) dyes have the unique advantages of tracing molecular activity *in vivo* because deeper penetration of the NIR radiation (650–900 nm) enables the assessment of molecular and physiological events several layers deep inside the analyte samples and tissues.⁶⁰ Moreover, NIR optical response is not affected by the autofluorescence generated from chromophores and macromolecules present in the analyte or tissue samples. The first ratiometric probe reported is Cy-N₃, but it responds to H₂S in 20 min with only 40 nm redshift in the NIR region.⁶¹ The second probe known is nitro derivatized probe, which works only in pure organic solvent (DMF).⁶² The third probe is disulfide-containing probe excited-state intramolecular proton transfer (ESIPT) based fluorescent probe E1, whose excitation and emission wavelengths are comparatively short for biological applications.⁶³ The cresyl violet-based probe is developed with excellent ratiometric fluorescent response in the visible region but the reaction time is about 40 min.⁶⁴ Flavylium derivative is reported with quick ratiometric fluorescent response within 10 sec but in

organic-aqueous mixture which contains 30% acetonitrile.⁶⁵ Hybrid fluorophore of coumarin and merocyanine, CouMC also displays very quick ratiometric fluorescent response in aqueous media but with fluorescence quenching in the NIR region.⁶⁶ Therefore it is necessary to design a highly sensitive molecular probe which can detect H₂S from other competing species at lower concentration levels by immediately displaying remarkable Stokes shift and ratiometric response in the NIR region, in pure aqueous media.

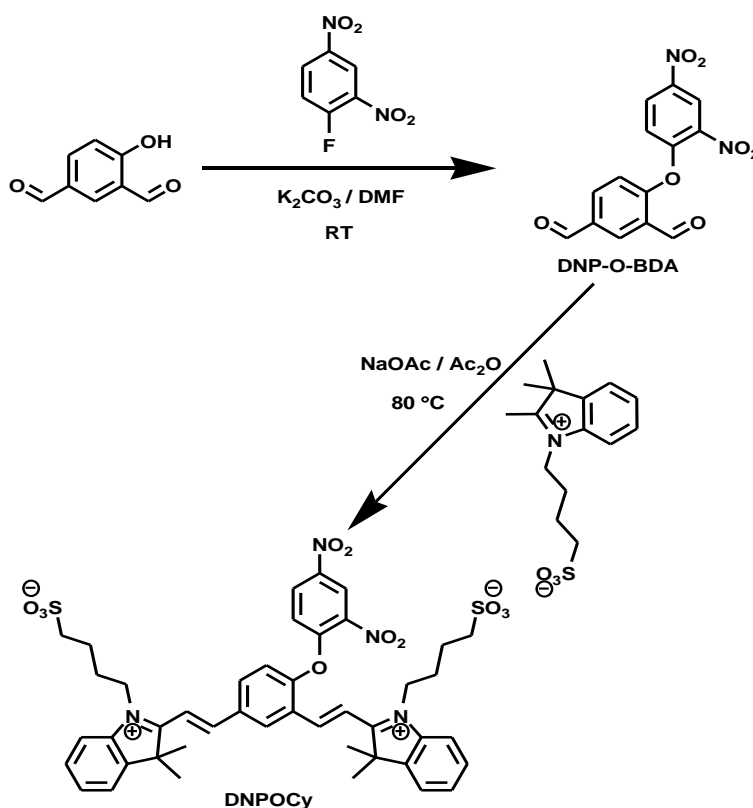
2.2 Design strategy

Shabat and coworkers developed NIR cyanine-based dye QCy7 in which a phenolic moiety is incorporated as donor in conjugation with two acceptors.⁴⁴ This phenolate donor moiety can be protected either by single proton or by a trigger moiety specific for a particular analyte of interest. The removal of the protecting group upon reaction with target analyte releases the single donor with double acceptor π -electron system that can undergo an intramolecular charge transfer to generate a resonance species with a π -electron pattern similar to that of Cy7. This has provided a very efficient approach for designing NIR turn on probe. We set out to design a H₂S selective NIR probe by incorporating a specific trigger moiety with the phenolic cyanine scaffold QCy7. Selection of specific trigger moiety for H₂S is tricky as it should be reactive for only H₂S not for other biothiols present inside the cells. We realize that H₂S has a pKa of 6.9 while biothiols like cysteine, glutathione etc. have higher pKa values. Due to this significant difference in pKa values, it is expected that H₂S should be a better nucleophile than biothiols in physiological condition. Based on this differential nucleophilicity, researchers have developed several molecular probes selective for H₂S over biologically abundant thiols. Recently, Lin *et. al.* developed a probe selective for only H₂S over biothiols based on the thiolysis of the dinitrophenyl ether reaction.⁶⁷ Based on these observations and facts we have designed a H₂S selective reaction-based NIR probe by incorporating a dinitrophenyl (DNP) group as a functional trigger moiety within cyanine backbone (Scheme 3). The DNPO-phenolic moiety incorporated heptamethine cyanine (**DNPOCy**) has completely altered π -conjugation pattern and positive charges localized on both nitrogen atoms. H₂S mediated nucleophilic reaction on the **DNPOCy** probe cleaves phenolic ether bond to generate the Cy-phenolate which rearranges itself by neutralizing one

of the positive charge on nitrogen atom to form stable quinone embedded **Cy-quinone**.⁶⁸ It was thus expected to exhibit turn on NIR fluorescence due to restoration of extended π -electron conjugation pattern of the cyanine dyes like QCy7. This NIR probe also features unique colorimetric response for H₂S due to the conjugated π -electron push-pull character in aqueous environments.

2.3 Synthesis

DNPOCy probe was synthesized in two-step straightforward synthetic route as outlined in Scheme 3. The 2,4-dinitrophenyl phenyl ether moiety (**DNP-O-BDA**) was synthesized via nucleophilic substitution of 1-fluoro-2,4-dinitrobenzene by treating the 4-hydroxy-1,3-benzenedicarboxaldehyde under the basic conditions. Good yield of **DNPOCy** was obtained by condensing the bisaldehyde (**DNP-O-BDA**) functionalized ether intermediate with 2 equiv of indolium-3-butylsulfonate. All the compounds were characterized by NMR and mass spectrometry.



Scheme 3. Synthesis of **DNPOCy**

2.4 Photophysical studies of DNPOCy and H₂S detection

DNPOCy readily dissolves in water to form greenish yellow colored solution. **DNPOCy** (10.0 μM) exhibits an absorption band located around 400 nm with an extinction coefficient (ϵ) of $3.9 \times 10^4 \text{ M}^{-1} \text{ cm}^{-1}$ in PBS buffer (pH = 7.4) (Figure 13). This peak in the absorption spectra can be attributed to the masking of the phenolic group which disrupts the conjugated π -electron system of cyanine chromophore. Consequently, the removal of the trigger moiety by H₂S can restore the conjugation π -electrons of the cyanine dye. As expected, **DNPOCy** displayed an obvious spectral change when incubated with 20.0 μM of NaSH (common source for H₂S) in PBS buffer (pH = 7.4) (Figure 13). The absorbance at 400 nm decreased while two new absorption bands appeared at longer wavelength i.e. 475 nm and 583 nm, exactly matched with the spectroscopic behavior of **Cy-quinone**. Concurrently, the color of the solution changed from greenish yellow to characteristic blue. The H₂S reacts with the electron withdrawing dinitrophenyl ether moiety of the **DNPOCy** probe to release the Cy-phenolate anion which rearranges itself by neutralizing the positive charge on one of the

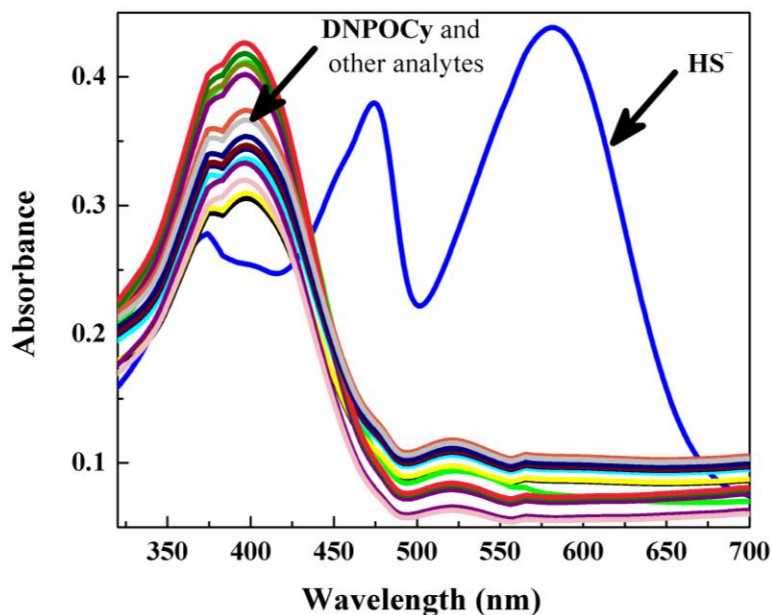


Figure 13. UV-Vis absorption spectra of **DNPOCy** probe (10.0 μM) in presence of 20.0 μM of NaSH, different anions (Cl^- , Br^- , I^- , AcO^- , N_3^- , CN^- , CO_3^{2-} , NO_2^-) at 1 mM, metal ions (K^+ , Mg^{2+} , Ca^{2+} , Zn^{2+}) at 1 mM, 5 equiv of reactive oxygen species (H_2O_2 , OCl^-), and reducing agents (ascorbic acid, $\text{S}_2\text{O}_3^{2-}$, SO_3^{2-}). Each spectrum was acquired after 2 min. incubation of the probe with analyte in 10 mM PBS buffer (pH 7.4).

nitrogen atoms to form stable extended π -electron conjugated **Cy-quinone**. Moreover, the intensity of absorption peak at 400 nm decreased ($\epsilon = 2.6 \times 10^4 \text{ M}^{-1} \text{ cm}^{-1}$) while that of two new band at 475 and 583 increased and attained saturation ($\epsilon = 3.8 \times 10^4 \text{ M}^{-1} \text{ cm}^{-1}$ and $\epsilon = 4.3 \times 10^4 \text{ M}^{-1} \text{ cm}^{-1}$ respectively) after addition of 20.0 μM of H₂S during the titration experiment with **DNPOCy** (10.0 μM) (Figure 14). These facts indicate that **DNPOCy** could serve as a ‘‘naked-eye’’ probe for H₂S.

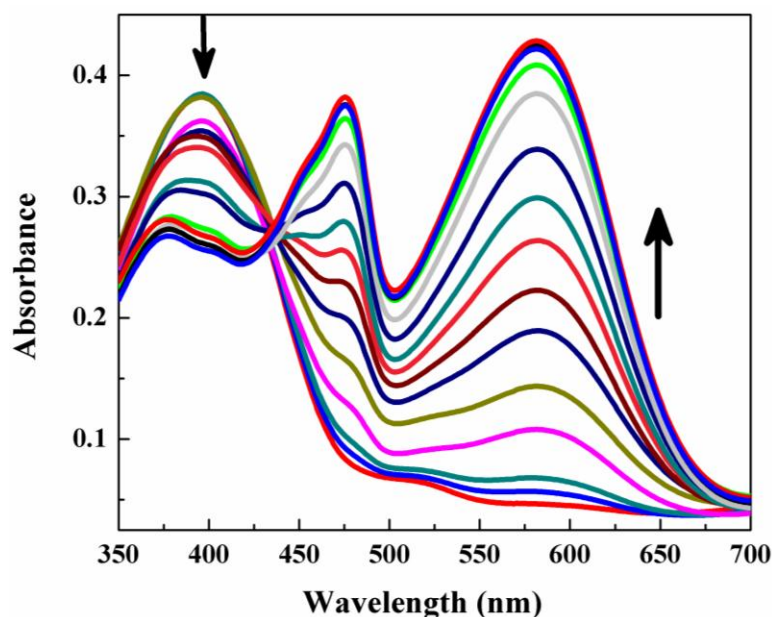


Figure 14. UV-Vis absorption spectra of **DNPOCy** probe (10.0 μM) upon addition of NaSH (0-20.0 μM). Each spectrum was acquired after 2 min incubation of the probe with analyte in 10 mM PBS buffer (pH 7.4).

Fluorometric behavior of **DNPOCy** probe has been tested varying the excitation wavelength after the addition of NaSH. At 600 nm excitation, nonfluorescent **DNPOCy** probe gave a very quick fluorescence switch on (~ 90 fold) band around 695 nm in presence of NaSH (Figure 15). The NIR emission intensity increased linearly with increasing concentration of NaSH to 10.0 μM (Figure 16). This switch on fluorescence response of **DNPOCy** was not observed for other tested bioanalytes (Figure 15). Biothiols like glutathione and cysteine show very minimal fluorescence response. **DNPOCy** exhibits an emission peak around 555 nm upon excitation at 510 nm in PBS buffer (pH = 7.4) (Figure 17). Addition of 20.0 μM NaSH decreases the fluorescence intensity at 556 nm while a new band appeared around 695 nm corresponding to trigger removed product **Cy-quinone** in the NIR region. This

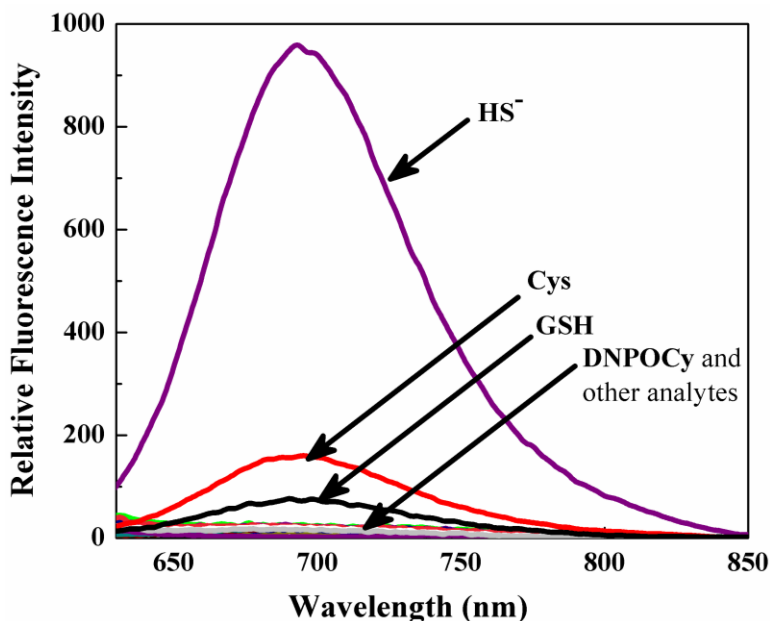


Figure 15. Fluorescence spectra of **DNPOCy** probe ($10.0 \mu\text{M}$) in presence of $20.0 \mu\text{M}$ of NaSH , different anions (Cl^- , Br^- , I^- , AcO^- , N_3^- , CN^- , CO_3^{2-} , NO_2^-) at 1 mM , metal ions (K^+ , Mg^{2+} , Ca^{2+} , Zn^{2+}) at 1 mM , 5 equiv of reactive oxygen species (H_2O_2 , OCl^-), and reducing agents (ascorbic acid, $\text{S}_2\text{O}_3^{2-}$, SO_3^{2-}). Each spectrum was acquired after 2 min. incubation of the probe with analyte in 10 mM PBS buffer ($\text{pH } 7.4$). $\lambda_{\text{ex}} = 600 \text{ nm}$.

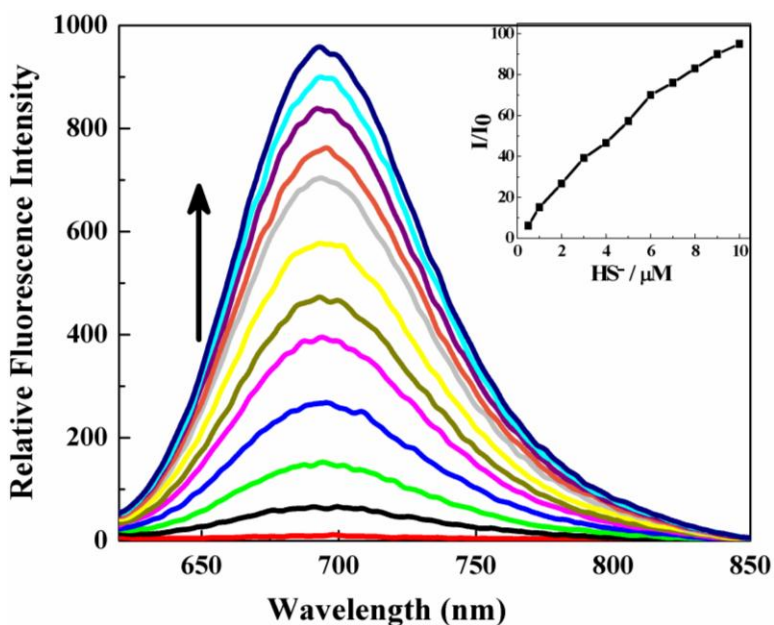


Figure 16. Fluorescence spectra of **DNPOCy** probe ($10.0 \mu\text{M}$) upon addition of NaSH (0 - $10.0 \mu\text{M}$). Each spectrum was acquired after 2 min. incubation of the probe with analyte in 10 mM PBS buffer ($\text{pH } 7.4$). $\lambda_{\text{ex}} = 600 \text{ nm}$.

remarkable large Stokes shift (~140 nm) is a highly desirable characteristic feature of a fluorescence probe that assists in increasing the signal-to-noise ratio. As we know, ratiometric analysis involves monitoring two signals at different wavelength. These signals changes differentially with analyte concentration and the ratio of the signals are independent of the probe concentration and environment which makes the ratiometric measurement to be more accurate and quantitative.

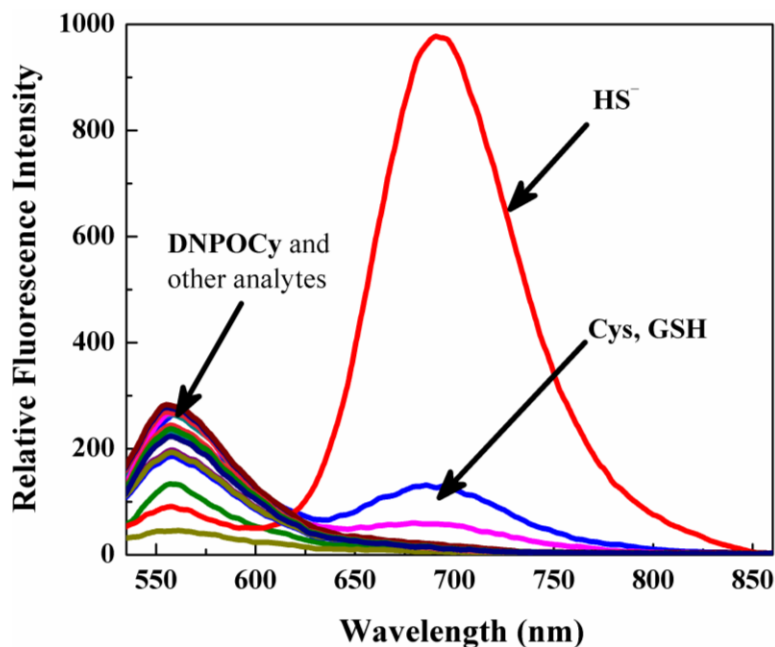


Figure 17. Fluorescence spectra of **DNPOCy** probe (10.0 μM) ($\lambda_{\text{ex}} = 510 \text{ nm}$) in presence of 20.0 μM of NaSH, different anions (Cl^- , Br^- , I^- , AcO^- , N_3^- , CN^- , CO_3^{2-} , NO_2^-) at 1 mM, metal ions (K^+ , Mg^{2+} , Ca^{2+} , Zn^{2+}) at 1 mM, 5 equiv of reactive oxygen species (H_2O_2 , OCl^-), and reducing agents (ascorbic acid, $\text{S}_2\text{O}_3^{2-}$, SO_3^{2-}). Each spectrum was acquired after 2 min. incubation of the probe with analyte in 10 mM PBS buffer (pH 7.4).

The fluorescence ratio ($I_{695\text{nm}}/I_{555 \text{ nm}}$) increased linearly as the concentration of H₂S was increased from 0 to 30 μM (Figure 18). Minimum 1.0 μM concentration of H₂S can be detected using this ratiometric study (Figure 19). This switch on as well as ratiometric fluorescent response and colorimetric changes were not observed upon addition of different anions (Cl^- , Br^- , I^- , AcO^- , N_3^- , CN^- , CO_3^{2-} , NO_2^-) at 1 mM, metal ions (K^+ , Mg^{2+} , Ca^{2+} , Zn^{2+}) at 1 mM, 5 equiv of reactive oxygen species (H_2O_2 , OCl^-), and reducing agents (ascorbic acid, $\text{S}_2\text{O}_3^{2-}$, SO_3^{2-}) (Figure 13, 15, and 17). The small molecule thiols such as GSH and Cys at 1 mM showed only very minimal fluorescence response.

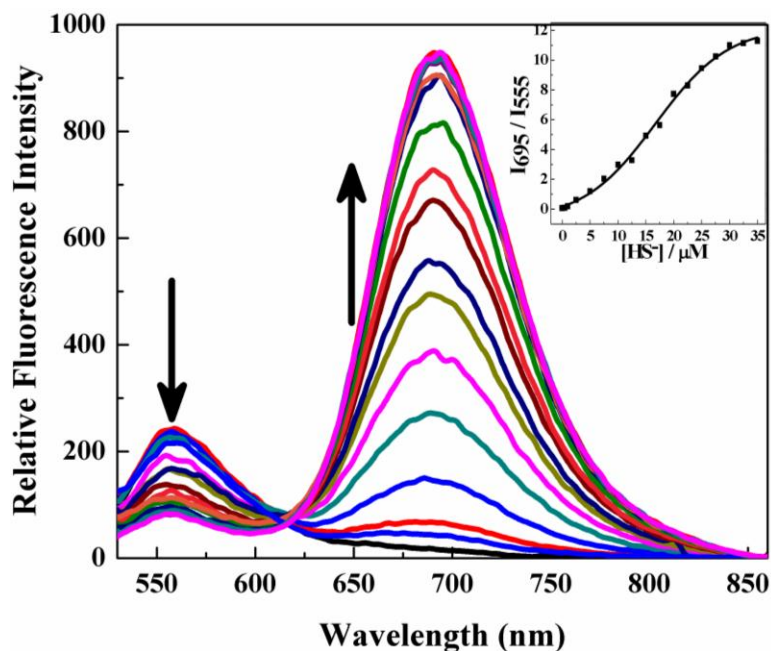


Figure 18. Fluorescence spectra of **DNPOCy** probe (10.0 μM) upon addition of NaSH (0-35.0 μM). Each spectrum was acquired after 2 min. incubation of the probe with NaSH in 10 mM PBS buffer (pH 7.4). λ_{ex} = 510 nm.

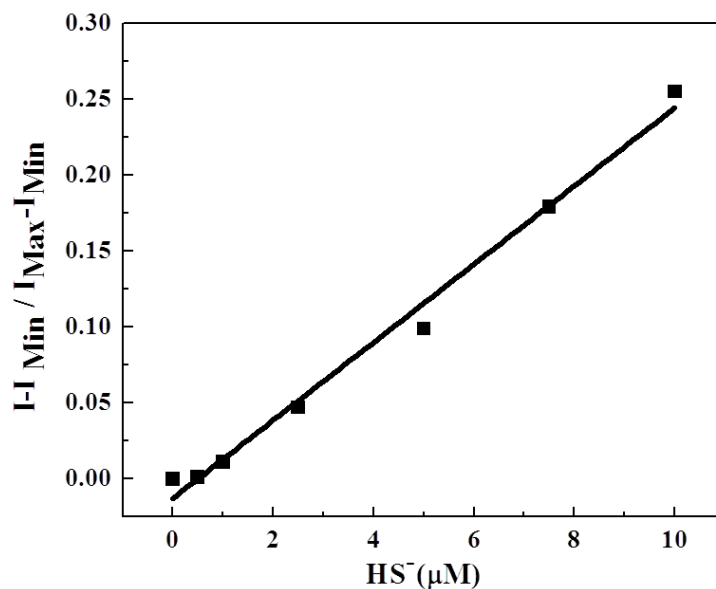


Figure 19. Ratiometric study of **DNPOCy** at different concentrations of NaSH (0.0, 0.5, 1.0, 2.5, 5.0, 7.5, 10.0 μM) added, normalized between the minimum (0.0 μM of NaSH) to maximum ratiometric response. The detection limit was determined to be 1×10^{-6} μM .

2.5 pH dependent study

The effect of pH on the H₂S mediated dinitrophenyl phenyl ether bond cleavage was studied to understand the efficiency of the ratiometric fluorometric method (Figure 20). **DNPOCy** reacted efficiently with H₂S in the biologically relevant pH range of 6.5–8.5 to release NIR fluorescence emitting **Cy-quinone** dye. Hence, this probe is very convenient for the detection and monitoring of H₂S without interference from the pH dependent effects of the physiological media.

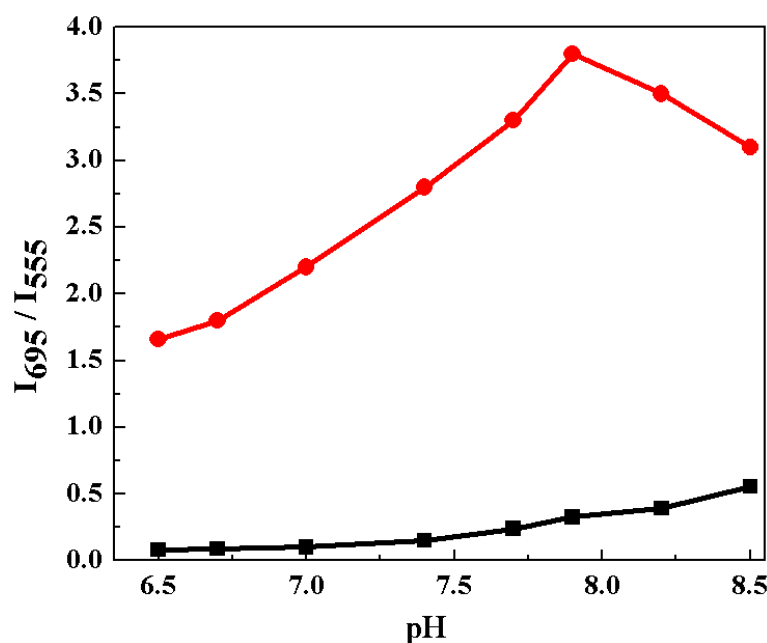


Figure 20. Effect of pH on the ratiometric emission of **DNPOCy** monitored at 695 and 555 nm. Black trace: **DNPOCy** (10 μ M) and red trace: **DNPOCy** (10.0 μ M) with 2.0 μ M of NaSH in 10 mM PBS buffer.

2.5 Product analysis

The H₂S mediated transformation from **DNPOCy** to **Cy-quinone** dye under the experimental conditions was confirmed by mass spectroscopic analysis (Figure 21). The ESI-mass spectrum showed peaks at $m/z = 705$ (calculated for $C_{38}H_{43}N_2O_7S_2 + H^+$) corresponding to **Cy-quinone** and at $m/z = 224.0$ (calculated for $C_6H_4N_2O_4S + Na^+ + H^+$) corresponding to the by-product 2,4-dinitrothiophenol. The H₂S triggered rapid nucleophilic reaction with the

electron withdrawing dinitrophenyl ether moiety of the **DNPOCy** probe releases the Cy-phenolate anion which rearranges itself by neutralizing the positive charge on one of the nitrogen atoms to form stable **Cy-quinone** dye. In the process, this dye resumes a heptamethine **Cy7**-like extended π -electron conjugation pattern which is responsible for the observed characteristic fluorescence in the NIR region.

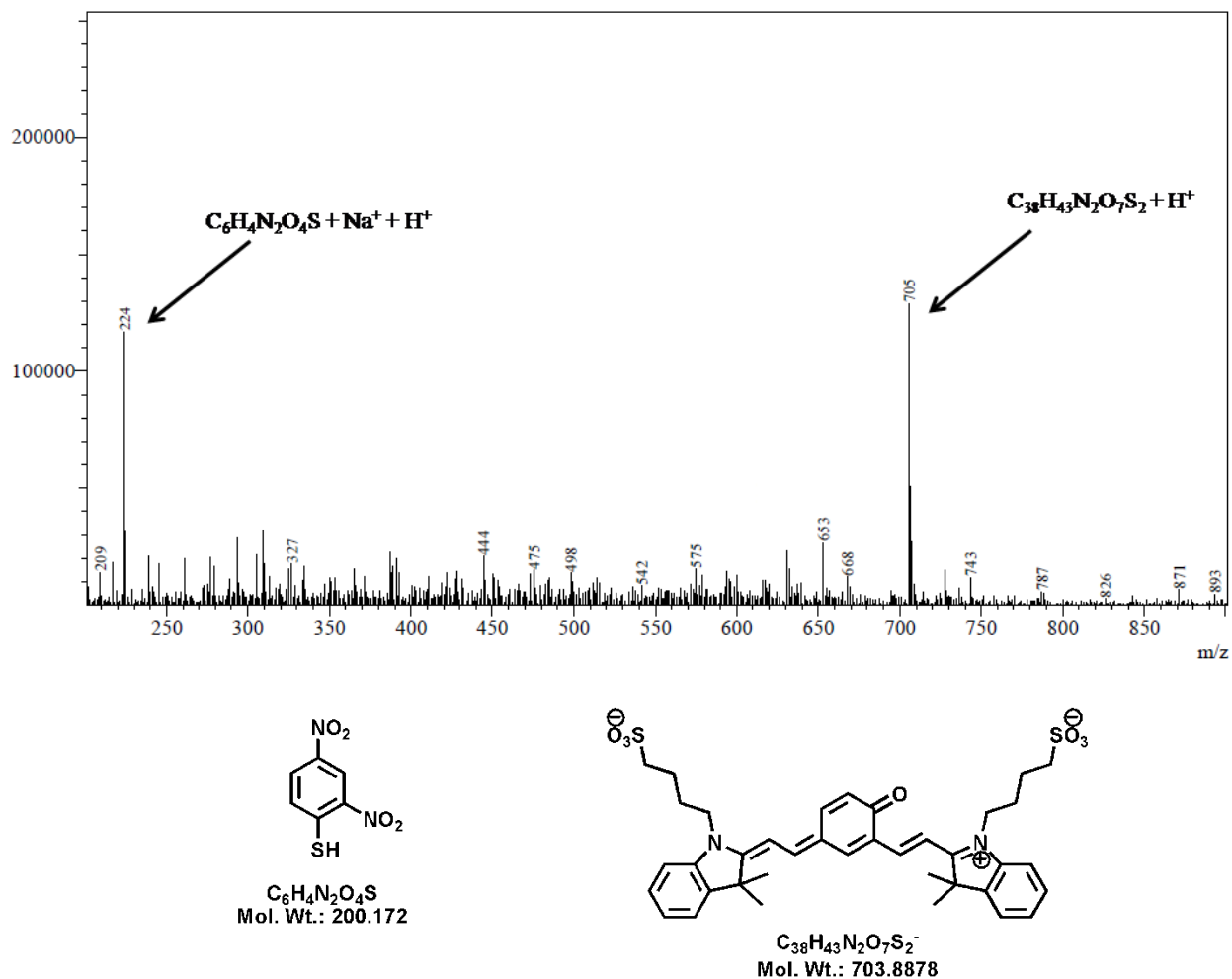


Figure 21. ESI-mass spectrum (positive ion mode) for the reaction of 10.0 μM **DNPOCy** with NaSH (50.0 μM) in water. Mass peak observed at 705 was attributed to cyanine dye (**Cy-quinone**) (calculated for $[\text{C}_{38}\text{H}_{43}\text{N}_2\text{O}_7\text{S}_2^- + \text{H}]^+$). Peak at $m/z = 224.0$ corresponding to the side product 2,4-dinitrothiophenol (calculated for $\text{C}_6\text{H}_4\text{N}_2\text{O}_4\text{S} + \text{Na}^+ + \text{H}^+$).

2.6 Theoretical investigation

Doron Shabat *et al.* have performed computational study to understand the molecular mechanism for near infrared fluorescence of **Cy-quinone**.⁶⁹ Further, we have investigated the molecular mechanism underlying experimentally observed band around 555 nm in the emission spectra for **DNPOCy**. The computations data is well matched with the observed experimental spectra for **DNPOCy**. We have considered the molecules in gas phase for our theoretical study. In our calculation the structure **DNPOCy** and **Cy-quinone** were simplified with structure **A** and **B** respectively by replacing long chain sulphonic acid group with methyl groups. Each molecule was optimized with the help of *ab initio* density functional theory (DFT) combined with time-dependent density functional theory (TDDFT) as implemented in Gaussian 09 package.⁷⁰ For the DFT and TDDFT calculations we use B3LYP⁷¹⁻⁷³ exchange and correlation functional with 6-31g(d) basis set for all atoms. The optimized structures are shown in the Figure 22. The absorbance spectra was calculated using optimized ground state (S₀) geometry and the emission spectra was calculated using optimized first excited state (S₁) geometry. The TDDFT calculation provides excitation energies and oscillator strengths to the lowest singlet states (Table 1). We found lowering in energy for absorption and emission transition in **Cy-quinone** than **DNPOCy**. This is because of the extended delocalization of electron over **Cy-quinone**. Thus, though **Cy-quinone** (**B**) emits in the near infrared region, the model compound of **DNPOCy** (**A**) emits in the shorter

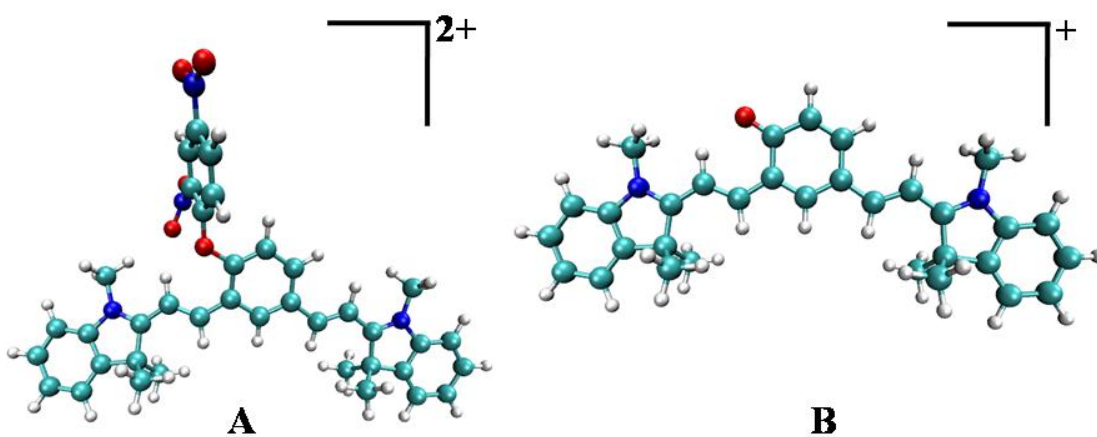
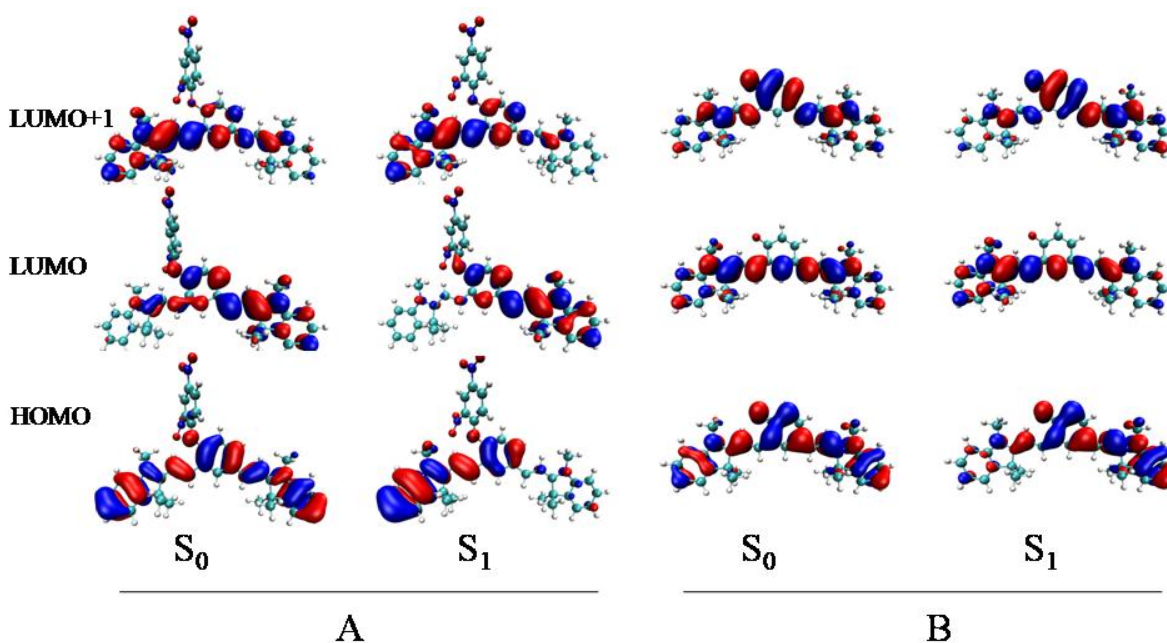


Figure 22. The optimized structures of the model compounds of **DNPOCy** (**A**) and **Cy-quinone** (**B**).

Table 1. Calculated absorption/emission transition with corresponding oscillator strength of **A** and **B** in gas phase.

Compound	Transition	Excitation energy (nm)	Oscillator Strength
A	S ₀ →S ₁ (abs)	458.55	0.71
	S ₁ →S ₀ (fluo)	503.72	1.40
B	S ₀ →S ₁ (abs)	562.81	1.53
	S ₁ →S ₀ (fluo)	629.08	1.02

(homo→lumo) + 0.5121 (homo→lumo+1) for **A** and 0.6995 (homo→lumo) + 0.1055 (homo→lumo+1) for **Cy-quinone**. The emission is approximately describes 0.3277 (lumo→homo-1)-0.6098 (lumo+1→homo) for **A** and 0.7021 (lumo→homo) for **B**. The frontier molecular orbital of **DNPOCy (A)** and **Cy-quinone (B)** are included in Figure 23.

**Figure 23.** Frontier molecular orbital of the optimized ground state (S₀) and optimized excited state (S₁) of the model compounds of **DNPOCy (A)** and **Cy-quinone (B)**.

2.7 Conclusion

In conclusion, a hydrogen sulfide (H₂S) selective water soluble ratiometric NIR fluorescence probe **DNPOCy** has been successfully developed. This molecular probe readily reacts with H₂S to release NIR fluorescence emitting cyanine dye over a wide pH range. The probe was used effectively for colorimetric monitoring of H₂S. In general, **DNPOCy** can be used as a non-invasive tool for *in vitro* detection and *in vivo* NIR fluorescence imaging of H₂S. Results obtained from theoretical calculations corroborate the experimental findings and provide us with a detailed microscopic understanding of the observed fluorescence properties of **DNPOCy**.

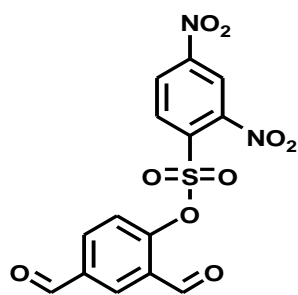
3. Experimental

3.1 General experimental procedure

All the solvents and reagents were obtained from Sigma-Aldrich and used as received unless otherwise mentioned. ¹H and ¹³C NMR were recorded on a Bruker AV-400 spectrometer with chemical shifts reported as ppm (in CDCl₃, DMSO-*d*₆, tetramethylsilane as internal standard). Mass spectra were obtained on Shimadzu 2020 LC-MS. Elemental analysis was carried out on ThermoScientific FLASH 2000 Organic Element Analyzer. UV-Vis spectra were recorded on a Perkin Elmer Lambda 900 spectrophotometer and fluorescence spectra were recorded on a Perkin Elmer LS 55 spectrophotometer.

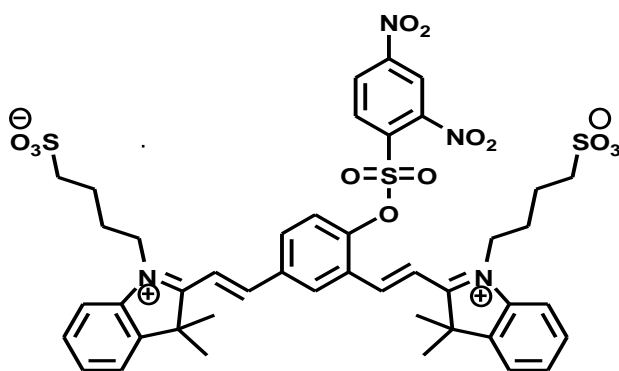
3.2 Detailed synthetic procedure

2,4-Dinitrophenyl 2,4-diformylphenyl sulphate (DNP-SO₂-BDA): A mixture of 4-hydroxy-1,3-benzenedicarboxaldehyde (150 mg, 1 mmol), 2,4-dinitrobenzenesulfonyl chloride (292 mg, 1.1 mmol) and triethylamine (0.15 mL, 1.1 mmol) in dichloromethane (10 mL) was stirred at 0°C for 1 h. under inert atmosphere. The reaction mixture was washed with water. The organic phase was dried over Na₂SO₄ and solvent was evaporated to dryness. The crude product was



purified by column chromatography on silica gel using chloroform as an eluent to obtain **DNP-SO₂-BDA** as yellow solid (68%). ¹H NMR (400 MHz, DMSO-*d*₆) δ_{ppm} 7.50 (1H, d, *J* = 8.4 Hz), 8.23 (1H, dd, *J* = 6.4 Hz, 2 Hz), 8.37 (1H, d, *J* = 8.8 Hz), 8.46 (1H, d, *J* = 2.0 Hz), 8.65 (1H, dd, *J* = 6.4 Hz, 2.0 Hz), 9.14 (1H, d, *J* = 2.4 Hz), 10.11 (1H, s), 10.16 (1H, s). ¹³C NMR (100 MHz, DMSO-*d*₆) δ_{ppm} 121.2, 124.2, 127.7, 129.3, 130.3, 131.4, 133.8, 135.6, 135.8, 148.0, 151.7, 152.0, 187.4, 191.5. LCMS: *m/z* = 381.2 [M + H]⁺ for C₁₄H₈N₂O₉S. Elemental analysis: Found: C, 44.19; H, 2.12; N, 7.38, Calcd: C, 44.22; H, 2.12; N, 7.37 for C₁₄H₈N₂O₉S.

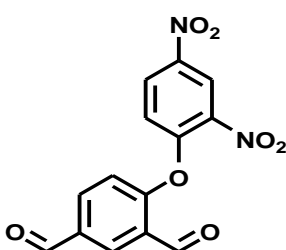
Dinitrobenzenesulfonyl-cyanine (DNBSCy) probe: A mixture of 2,4-dinitrophenyl-2,4-



diformylphenyl sulfate (**DNP-SO₂-BDA**) (76 mg, 0.2 mmol), indolium-3-butylsulfonate (118 mg, 0.4 mmol) and NaOAc (32 mg, 0.4 mmol) was dissolved in 3 mL Ac₂O. The reaction mixture was stirred for 30 min at 80°C under an argon atmosphere. After completion, the

reaction mixture was concentrated by evaporation under reduced pressure. The crude product was diluted with 3.0 mL H₂O, 3.0 mL ACN, 300 μL AcOH, and purified by preparative RP-HPLC (grad. 10%-90 ACN in water, 20 min) to obtain the probe **DNBSCy** (130 mg, 70%) as yellow powder. ¹H NMR (400 MHz, DMSO-*d*₆) δ_{ppm} 1.79 (6H, s), 1.84 (6H, s), 1.86-1.91 (4H, m), 2.04-2.11 (4H, m), 2.62 (2H, t, *J* = 6.8 Hz), 2.69 (2H, t, *J* = 6.7 Hz), 4.80-4.87 (4H, m), 7.41 (1H, d, *J* = 8.5 Hz), 7.65-7.69 (4H, m), 7.89-7.93 (2H, m), 8.03-8.12 (3H, m), 8.21-8.35 (3H, m), 8.48-8.53 (2H, m), 8.68 (1H, dd, *J* = 6.4 Hz, 2.2 Hz), 9.18 (1H, d, *J* = 2.2 Hz), 9.35 (1H, d, *J* = 1.5 Hz). ¹³C NMR (100 MHz, DMSO-*d*₆) δ_{ppm} 22.0, 22.1, 25.3, 26.4, 26.6, 47.1, 47.4, 49.2, 49.4, 52.5, 53.0, 115.7, 115.9, 116.5, 118.1, 121.5, 123.1, 127.9, 129.0, 129.1, 129.3, 129.9, 130.1, 130.7, 131.1, 133.9, 135.1, 136.0, 140.6, 140.7, 142.4, 144.1, 144.2, 148.0, 149.4, 149.6, 151.7, 157.9, 158.3, 181.5, 181.9. LCMS: *m/z* = 935.1 [M]⁺ for C₄₄H₄₆N₄O₁₃S₃. Elemental analysis: Found: C, 56.51; H, 4.95; N, 6.01, Calcd: C, 56.52; H, 4.96; N, 5.99 for C₄₄H₄₆N₄O₁₃S₃.

2,4-dinitrophenyl 2,4-diformylphenyl ether (DNP-O-BDA): A mixture of 4-hydroxy-1,3-

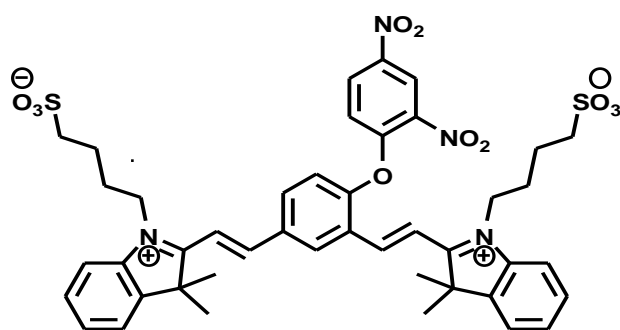


benzenedicarboxaldehyde (100 mg, 0.67 mmol), 1-fluoro-2,4-dinitrobenzene (619 mg, 3.3 mmol) and K₂CO₃ (920 mg, 6.66 mmol) in anhydrous DMF (4 mL) was stirred at room temperature for overnight under inert atmosphere. After completion, the reaction mixture was concentrated by evaporation under reduced pressure.

The reaction mixture was dissolved in dichloromethane. The organic phase was washed with water. Finally it was dried over Na₂SO₄ and evaporated to dryness. The crude product was purified by flash column chromatography (hexane/ethyl acetate = 7/3) as eluent to obtain

DNP-O-BDA as light yellow solid (148 mg, 70%). ¹H NMR (400 MHz, CDCl₃) δ_{ppm} 7.09 (1H, d, *J* = 8.4 Hz), 7.29 (1H, d, *J* = 8.8 Hz), 8.16 (1H, dd, *J* = 2 Hz, 6.4 Hz), 8.50 (2H, m), 8.98 (1H, d, *J* = 2.8 Hz), 10.08 (1H, s), 10.45 (1H, s). ¹³C NMR (100 MHz, CDCl₃) δ_{ppm} 119.1, 121.8, 122.6, 127.3, 129.4, 132.8, 133.7, 135.5, 140.9, 143.7, 153.0, 160.2, 186.7, 189.4. LCMS: *m/z* = 316.3 [M]⁺ for C₁₄H₈N₂O₇. Elemental analysis: Found: C, 53.15; H, 2.55; N, 8.87, Calcd: C, 53.17; H, 2.55; N, 8.86 for C₁₄H₈N₂O₇.

Dinitrophenyl-ether-cyanine (DNPOCy) probe: A mixture of 2,4-dinitrophenyl 2,4-diformylphenyl ether (**DNP-O-BDA**) (50 mg, 0.16 mmol), indolium-3-butylsulfonate (84 mg, 0.28 mmol) and NaOAc (23 mg, 0.28 mmol) was dissolved in Ac₂O (3 mL). The reaction mixture was stirred for 30 min at 80°C under an argon atmosphere. After completion, the reaction



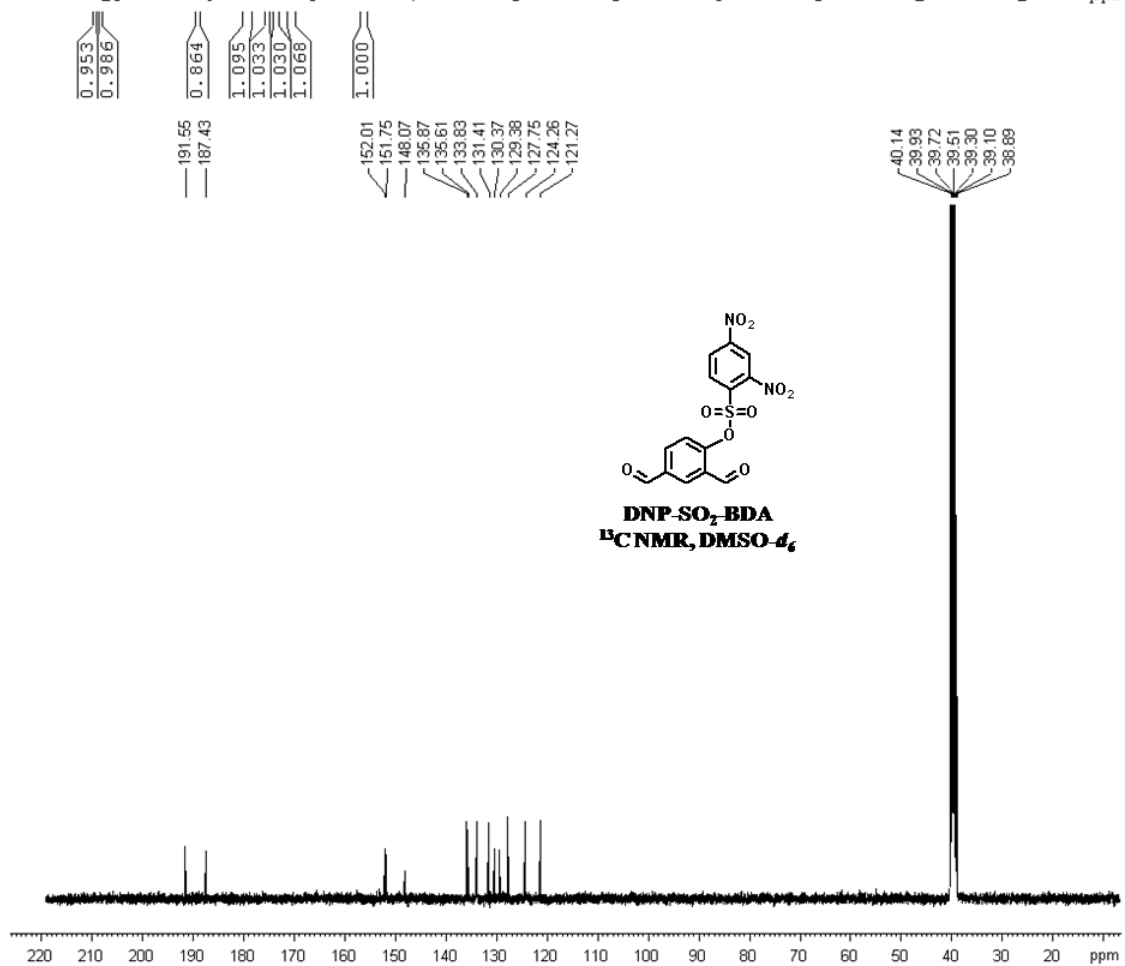
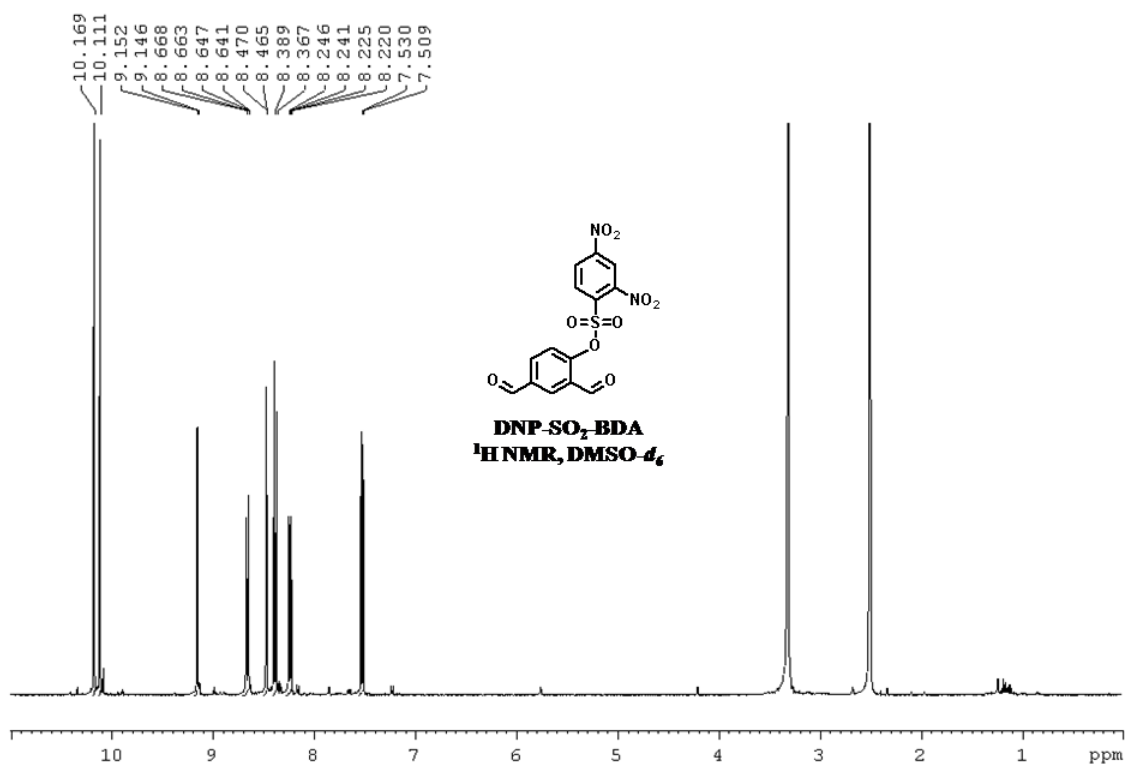
mixture was concentrated by evaporation under reduced pressure. The crude product was diluted with 3.0 mL H₂O, 3.0 mL ACN, 300 μL AcOH, and purified by preparative RP-HPLC (grad. 10%-90 ACN in water, 20 min) to obtain the probe **DNPOCy** (115 mg, 82%) as yellow powder. ¹H NMR (400 MHz, DMSO-*d*₆) δ_{ppm} 1.72 (6H, s), 1.86-1.89 (10H, m), 2.07-2.10 (4H, m), 2.62-2.70 (4H, m), 4.80-4.85 (4H, m), 7.49 (1H, d, *J* = 8.8 Hz), 7.64-7.67 (5H, m), 7.87-7.91 (2H, m), 8.01-8.21 (4H, m), 8.39-8.43 (1H, m), 8.53-8.60 (3H, m), 8.99 (1H, d, *J* = 2.4 Hz), 9.34 (1H, m). ¹³C NMR (100 MHz, DMSO-*d*₆) δ_{ppm} 22.1, 25.5, 25.6, 26.5, 26.6, 46.9, 47.2, 49.3, 49.5, 52.4, 52.5, 114.9, 115.5, 115.8, 117.1, 119.6, 121.6, 122.1, 123.0, 126.6, 129.1, 129.2, 129.7, 129.9, 132.0, 132.6, 136.4, 140.1, 140.6, 140.7, 142.8, 143.3, 143.9, 144.1, 150.7, 152.6, 156.1, 158.0, 158.4, 181.5, 181.9. LCMS: *m/z* = 870.3 [M]⁺ for C₄₄H₄₆N₄O₁₁S₂. Elemental analysis: Found: C, 60.65; H, 5.32; N, 6.44, Calcd: C, 60.67; H, 5.32; N, 6.43 for C₄₄H₄₆N₄O₁₁S₂.

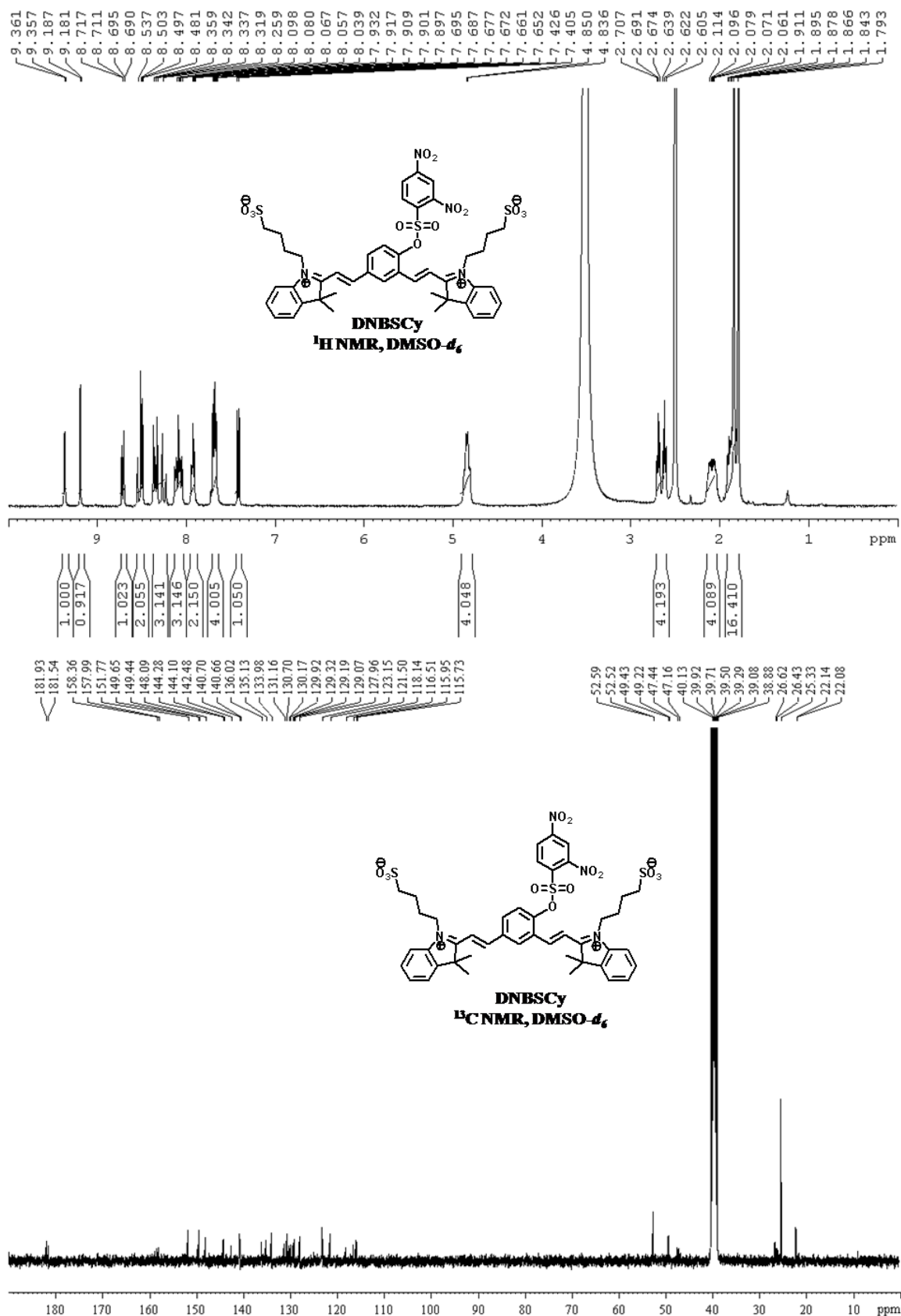
3.3 General method for measurements of photophysical properties

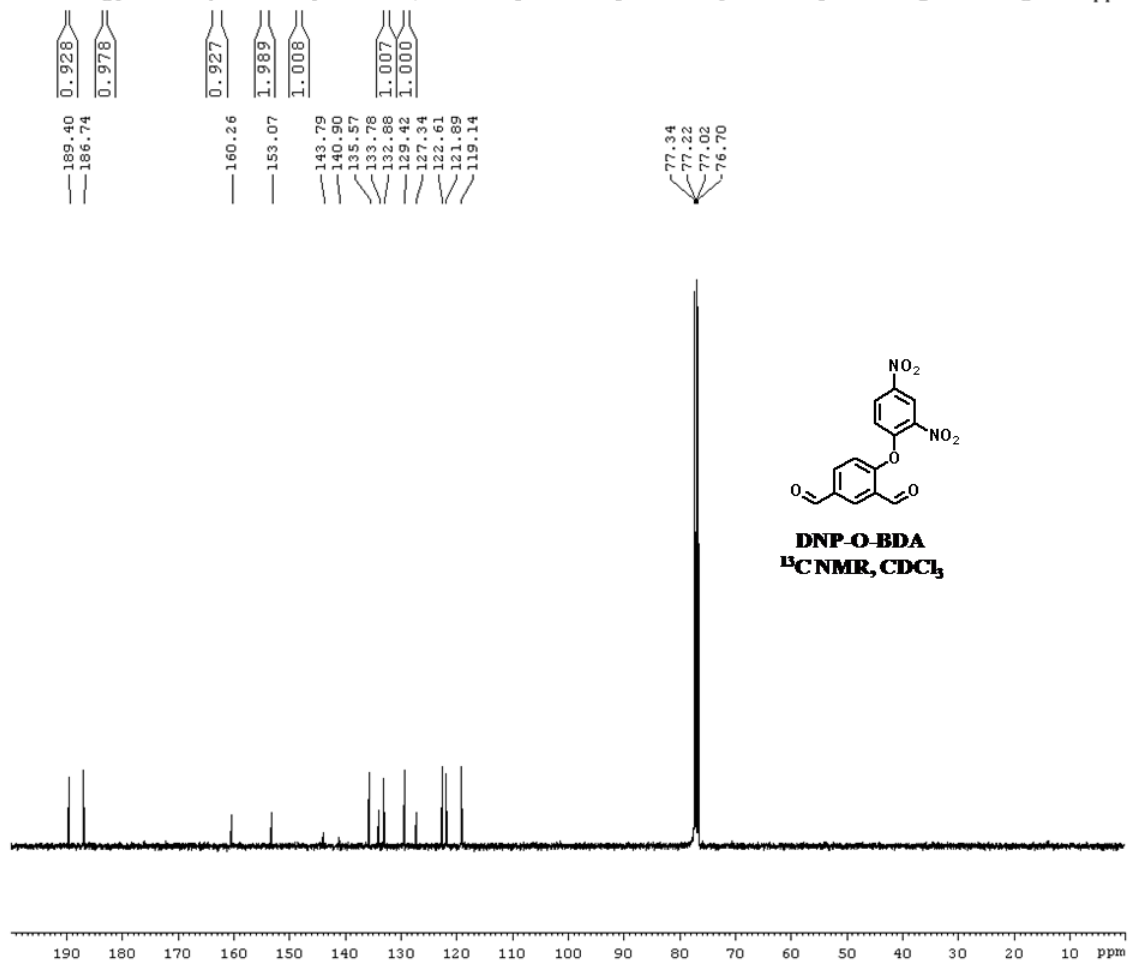
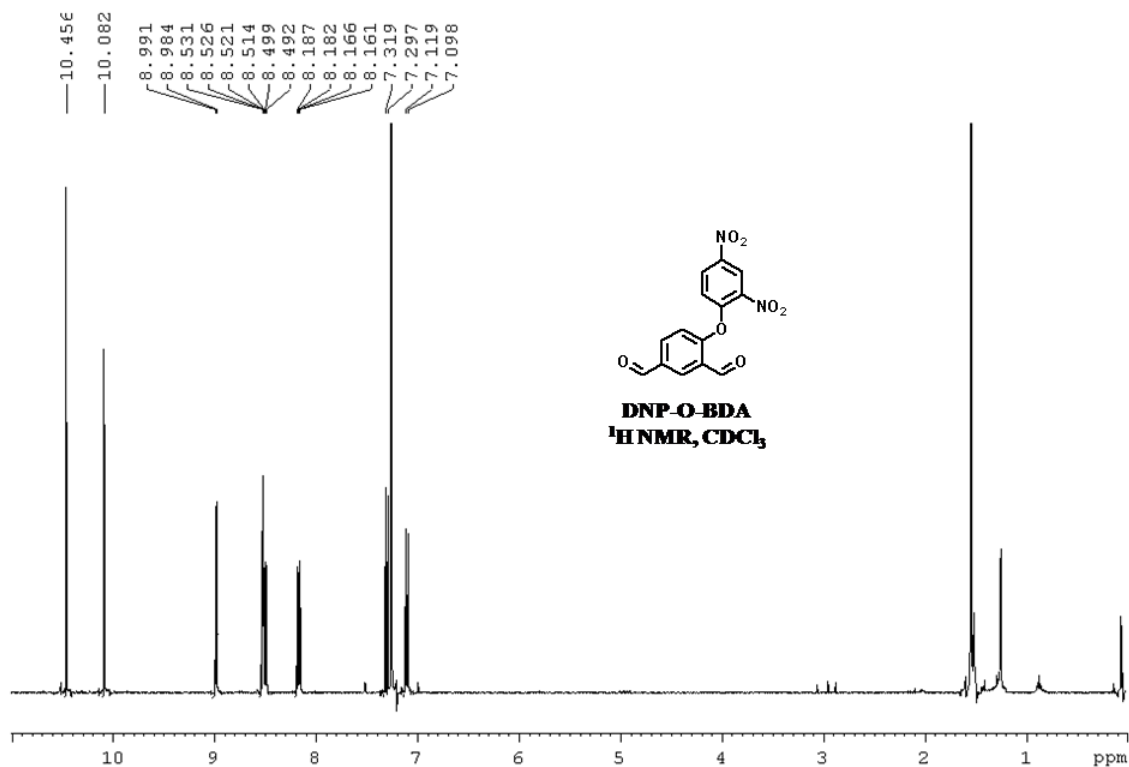
UV-Vis spectra were recorded on Perkin Elmer Lambda 900 spectrophotometer and fluorescence spectra were recorded on a Perkin Elmer model LS 55 spectrophotometer. 1 cm cells were used for absorption and emission titration. For UV-Vis and fluorescence titrations stock solution of probes were prepared ($c = 2000 \mu\text{M}$) in 10 mM PBS buffer ($\text{pH} = 7.4$). The solutions of guest cations and amino acids were prepared in buffer solution in the order of 10^{-3} M. Working solutions of the probe and metal ions were prepared from the stock solutions. 10 nm emission slit widths were used.

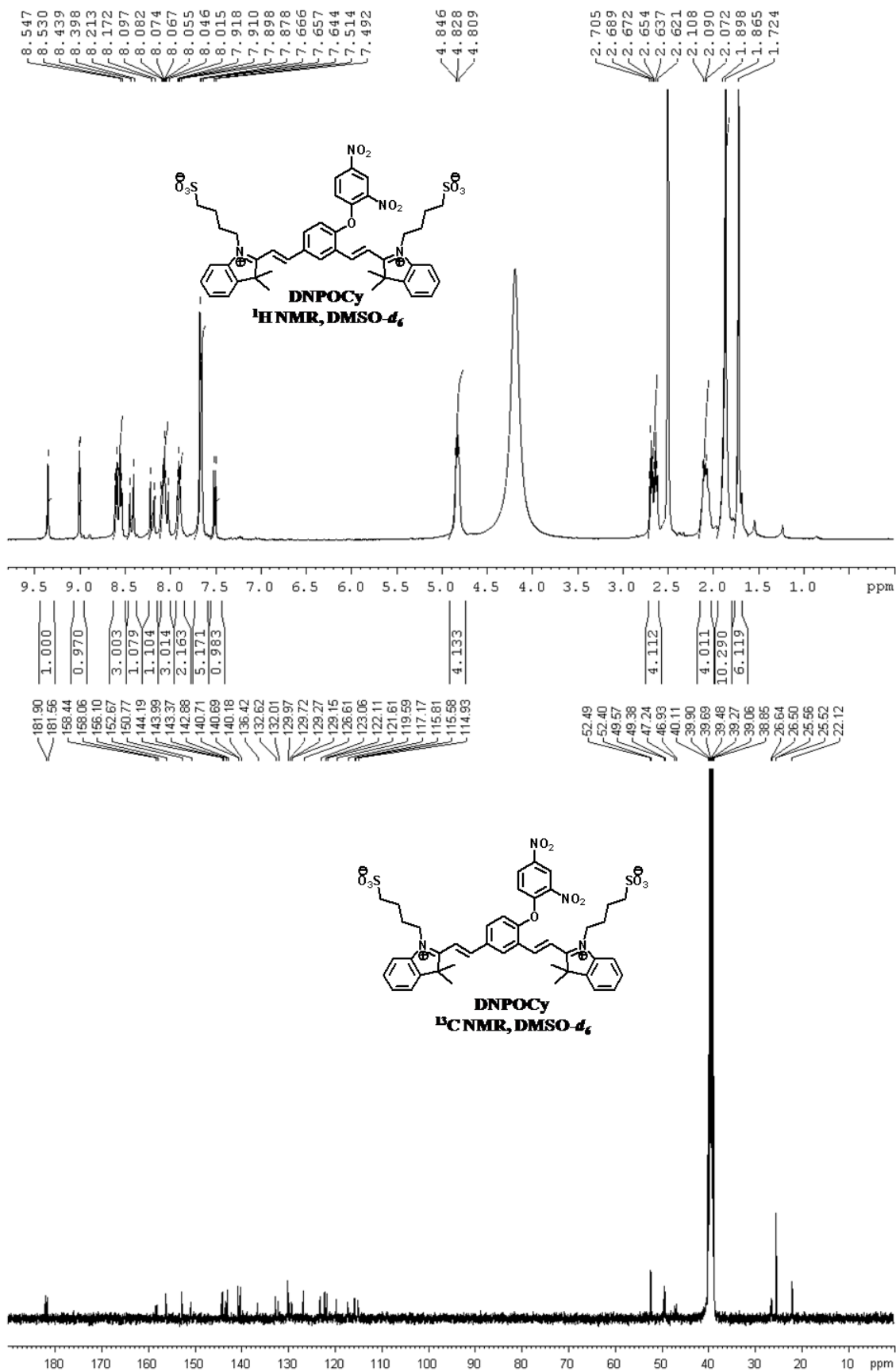
3.4 Appendix

- ❖ Compound **DNP-SO₂-BDA**, ¹H and ¹³C NMR
- ❖ Compound **DNBSCy**, ¹H and ¹³C NMR
- ❖ Compound **DNP-O-BDA**, ¹H and ¹³C NMR
- ❖ Compound **DNPOCy**, ¹H and ¹³C NMR









Optimized Cartesian coordinate (in Å) of model compound **DNPOCy (A)** in ground state

(S₀): Total Energy: SCF Done: E(RB3LYP) = -2064.16330023 Hartree

C	5.53762807	-3.62980890	0.19053002
C	4.64755607	-4.56687992	-0.33264896
C	5.09152708	-5.85389792	-0.60671494
C	6.43247908	-6.16430191	-0.34919294
C	7.31019108	-5.20589690	0.17413804
C	6.87541507	-3.90946189	0.45704902
C	3.56819207	-2.49383291	-0.00575299
C	3.28305107	-3.92397692	-0.48716096
H	4.42431908	-6.60817393	-1.01341792
H	6.79897508	-7.16407291	-0.55926493
H	8.34511308	-5.47180489	0.36308304
H	7.55911107	-3.16960188	0.85842901
C	5.54134306	-1.24065089	0.93656899
H	6.07600907	-1.56408888	1.83235099
H	6.26188406	-0.86969190	0.20179298
H	4.84658006	-0.45226489	1.21197398
C	2.25953008	-4.64277591	0.43440005
H	2.20450108	-5.69631192	0.14567007
H	2.56573008	-4.59626790	1.48358005
H	1.25552407	-4.21991892	0.34723405
C	2.68593306	-1.36134892	0.02329300
H	3.11527406	-0.40795191	0.29503198
N	4.84060307	-2.40422190	0.37758001
C	2.83031406	-3.94741095	-1.96930596
H	2.74254707	-4.98616895	-2.30074294
H	1.85900206	-3.46484196	-2.10677496
H	3.55814006	-3.44810796	-2.61568397
C	1.35140306	-1.41637893	-0.24736499

H	0.90593006	-2.38011793	-0.46946098
C	-8.14416895	0.11119004	0.18738102
C	-7.85002194	-1.24062997	0.00926904
C	-8.88592994	-2.16174397	-0.07447294
C	-10.20261694	-1.69414798	0.01685906
C	-10.47551594	-0.33103697	0.18783604
C	-9.44293595	0.60496503	0.27705902
C	-5.86311595	0.02798104	0.09243601
C	-6.34560694	-1.42125696	-0.05845096
H	-8.69057393	-3.22138297	-0.21036992
H	-11.02552794	-2.39875798	-0.04830593
H	-11.50461394	0.00724702	0.25062104
H	-9.66364095	1.65945903	0.40054001
C	-6.90422795	2.28429305	0.44669998
H	-7.02126896	2.79532403	-0.51362102
H	-7.73424195	2.54999605	1.10168198
H	-5.97902295	2.59593506	0.92764498
C	-5.93628394	-2.02046398	-1.42893695
H	-6.39757694	-3.00612698	-1.53923994
H	-6.27977195	-1.39328499	-2.25681996
H	-4.85360794	-2.14393498	-1.51531396
C	-4.52537295	0.53314905	0.05722100
H	-4.41711695	1.61088205	0.10595198
N	-6.91740095	0.83030604	0.24856301
C	-5.85966093	-2.30728194	1.12009605
H	-6.33599393	-3.28896894	1.04457407
H	-4.77697693	-2.45757693	1.10363705
H	-6.13446993	-1.87270493	2.08564905
C	-3.39548694	-0.22545895	-0.04826199
H	-3.49446694	-1.30447295	-0.09975297
C	-1.66597195	1.61924306	-0.04931903

C	-2.02563195	0.25413206	-0.09566100
C	-0.98412694	-0.68472994	-0.18606899
C	0.37564805	-0.33235293	-0.21837801
C	0.67961505	1.05737407	-0.21127903
C	-0.33995096	2.01304307	-0.11209804
H	-2.42568596	2.38944106	0.03218696
H	-1.23570794	-1.74216094	-0.21192698
H	-0.09005496	3.06695107	-0.08403006
O	1.99569505	1.39023507	-0.30405104
C	2.42574504	2.70110607	-0.39813806
C	2.22523303	3.41158005	-1.58251407
C	3.12907804	3.29947009	0.66175693
C	2.71278003	4.70956405	-1.71287009
H	1.69645703	2.93486304	-2.40126706
C	3.60452404	4.60382109	0.54880390
C	3.39150303	5.28397307	-0.64131010
H	2.57923102	5.27686204	-2.62640110
H	4.13142704	5.07451111	1.36980390
N	3.40362405	2.59146411	1.92385194
N	3.90706402	6.66728107	-0.77242813
O	4.51907002	7.12385209	0.18553986
O	3.67623501	7.24271206	-1.82984414
O	3.50550806	1.36071711	1.88696096
O	3.53161205	3.27480013	2.92827093

Optimized Cartesian coordinate (in Å) of model compound **Cy-quinone (B)** in ground state (S₀): Total Energy: SCF Done: E(RB3LYP) = -1423.81487058 Hartree

C	-7.07731294	-0.19714294	0.00248000
C	-6.49194795	-1.46553194	-0.00096501
C	-7.29689096	-2.59641793	-0.00713902

C	-8.68788696	-2.43369092	-0.01133403
C	-9.25583695	-1.15625992	-0.01010802
C	-8.45613094	-0.00930392	-0.00355901
C	-4.82205694	0.20498405	0.00540702
C	-4.97948595	-1.32179795	0.00217400
H	-6.86345897	-3.59278894	-0.00941403
H	-9.33129197	-3.30794192	-0.01652205
H	-10.33589595	-1.04725791	-0.01509403
H	-8.91106493	0.97517408	-0.00575600
C	-6.27967592	2.21796506	0.02040403
H	-5.90682491	2.66954806	-0.90340396
H	-7.34826692	2.40485807	0.10426003
H	-5.77100392	2.67683204	0.87204804
C	-4.37421395	-1.95279094	-1.27665700
H	-4.60193095	-3.02320994	-1.29551501
H	-4.79664794	-1.50074493	-2.17900900
H	-3.28777294	-1.83587995	-1.31125399
C	-3.66061993	0.99824704	-0.00012096
H	-3.77152392	2.07525404	-0.00884695
N	-6.04377493	0.77405106	0.01150102
C	-4.37868796	-1.95712697	1.28117900
H	-4.60728097	-3.02743497	1.29595799
H	-3.29224796	-1.84122598	1.31961701
H	-4.80375797	-1.50757398	2.18354800
C	-2.35927494	0.52972903	0.00276504
H	-2.18493494	-0.54388397	0.00921203
C	7.21674106	-0.09703205	-0.00052290
C	6.62795305	-1.36335604	0.00111108
C	7.42842804	-2.49727705	0.00176608
C	8.82033804	-2.34153106	0.00063309
C	9.39231205	-1.06645407	-0.00117289

C	8.59653106	0.08372494	-0.00181189
C	4.95787606	0.31106497	0.00015909
C	5.11475705	-1.21866403	0.00174708
H	6.99037903	-3.49170305	0.00308106
H	9.45993204	-3.21853907	0.00109508
H	10.47277005	-0.96079207	-0.00215389
H	9.05685907	1.06585694	-0.00343487
C	6.43122808	2.31670696	-0.00184888
H	5.99345908	2.77851395	0.88866812
H	7.50373908	2.50046595	0.00227913
H	6.00039609	2.77624897	-0.89695688
C	4.51684704	-1.85388504	1.28170606
H	4.75095203	-2.92297104	1.29923705
H	4.94058303	-1.40033105	2.18271407
H	3.42969104	-1.74522803	1.32267206
C	3.79254507	1.08492398	-0.00091391
H	3.92596108	2.16108898	-0.00338190
N	6.18824807	0.87837196	-0.00068590
C	4.51561305	-1.85639401	-1.27641594
H	4.74931605	-2.92560102	-1.29192395
H	3.42846606	-1.74734901	-1.31669694
H	4.93879406	-1.40484801	-2.17868993
C	2.48759407	0.59731999	0.00055308
H	2.34565306	-0.47915401	0.00326806
C	1.26163608	2.80384700	-0.00537391
C	1.29708507	1.35598200	-0.00121692
C	0.05991707	0.67945301	0.00106706
C	-1.17880193	1.32676302	-0.00086194
C	-1.21277192	2.81639102	-0.00525793
C	0.09111109	3.48462401	-0.00708791
H	2.19616309	3.35731599	-0.00724590

H	0.07272006	-0.41026499	0.00434905
H	0.06245710	4.56972601	-0.01021190
O	-2.26214991	3.47430803	-0.00711293

4. References

1. Zhang, M.; Yu, M.; Li, F.; Zhu, M.; Li, M.; Gao, Y.; Li, L.; Liu, Z.; Zhang, J.; Zhang, D.; Yi, T.; Huang, C., A highly selective fluorescence turn-on sensor for cysteine/homocysteine and its application in bioimaging. *J. Am. Chem. Soc.* **2007**, *129*, 10322-10323.
2. Wang, S.-P.; Deng, W.-J.; Sun, D.; Yan, M.; Zheng, H.; Xu, J.-G., A colorimetric and fluorescent merocyanine-based probe for biological thiols. *Org. Biomol. Chem.* **2009**, *7*, 4017-4020.
3. Hong, V.; Kislukhin, A. A.; Finn, M. G., Thiol-selective fluorogenic probes for labeling and release. *J. Am. Chem. Soc.* **2009**, *131*, 9986-9994.
4. Yang, X.; Guo, Y.; Strongin, R. M., Conjugate addition/cyclization sequence enables selective and simultaneous fluorescence detection of cysteine and homocysteine. *Angew. Chem. Int. Ed.* **2011**, *50*, 10690-10693.
5. Prasanna de Silva, A.; Nimal Gunaratne, H. Q.; Gunnlaugsson, T., Fluorescent PET(Photoinduced Electron Transfer) reagents for thiols. *Tetrahedron Lett.* **1998**, *39*, 5077-5080.
6. Matsumoto, T.; Urano, Y.; Shoda, T.; Kojima, H.; Nagano, T., A thiol-reactive fluorescence probe based on donor-excited photoinduced electron transfer: key role of ortho substitution. *Org. Lett.* **2007**, *9*, 3375-3377.
7. Jiang, W.; Cao, Y.; Liu, Y.; Wang, W., Rational design of a highly selective and sensitive fluorescent PET probe for discrimination of thiophenols and aliphatic thiols. *Chem. Commun.* **2010**, *46*, 1944-1946.
8. Jung, H. S.; Han, J. H.; Pradhan, T.; Kim, S.; Lee, S. W.; Sessler, J. L.; Kim, T. W.; Kang, C.; Kim, J. S., A cysteine-selective fluorescent probe for the cellular detection of cysteine. *Biomaterials* **2012**, *33*, 945-953.
9. Herzenberg, L. A.; De Rosa, S. C.; Dubs, J. G.; Roederer, M.; Anderson, M. T.; Ela, S. W.; Deresinski, S. C.; Herzenberg, L. A., Glutathione deficiency is associated with impaired survival in HIV disease. *Proc. Natl. Acad. Sci. USA* **1997**, *94*, 1967-1972.
10. Shahrokhian, S., Lead phthalocyanine as a selective carrier for preparation of a cysteine-selective Electrode. *Anal. Chem.* **2001**, *73*, 5972-5978.
11. Townsend, D. M.; Tew, K. D.; Tapiero, H., The importance of glutathione in human disease. *Biomedicine & Pharmacotherapy* **2003**, *57*, 145-155.
12. Meister, A.; Anderson, M. E., Glutathione. *Annu. Rev. Biochem* **1983**, *52*, 711-760.
13. Dalton, T. P.; Shertzer, H. G.; Puga, A., Regulation of gene expression by reactive oxygen. *Annu. Rev. Pharmacool. Toxicol.* **1999**, *39*, 67-101.

14. Kanzok, S. M.; Schirmer, R. H.; Türbachova, I.; Iozef, R.; Becker, K., The Thioredoxin System of the Malaria Parasite *Plasmodium falciparum* : glutathione reduction revisited. *J. Biol. Chem.* **2000**, *275*, 40180-40186.
15. Krauth-Siegel, R. L.; Bauer, H.; Schirmer, R. H., Dithiol proteins as guardians of the intracellular redox milieu in parasites: old and new drug targets in trypanosomes and malaria-causing Plasmodia. *Angew. Chem. Int. Ed.* **2005**, *44*, 690-715.
16. Ścibior, D.; Skrzycki, M.; Podsiad, M.; Czczot, H., Glutathione level and glutathione-dependent enzyme activities in blood serum of patients with gastrointestinal tract tumors. *Clin. Biochem.* **2008**, *41*, 852-858.
17. Jung, H. S.; Ko, K. C.; Kim, G.-H.; Lee, A.-R.; Na, Y.-C.; Kang, C.; Lee, J. Y.; Kim, J. S., Coumarin-based thiol chemosensor: synthesis, turn-on mechanism, and its biological application. *Org. Lett.* **2011**, *13*, 1498-1501.
18. McMahon, B. K.; Gunnlaugsson, T., Selective detection of the reduced form of glutathione (GSH) over the oxidized (GSSG) form using a combination of glutathione reductase and a Tb(III)-cyclen maleimide based lanthanide luminescent 'switch on' assay. *J. Am. Chem. Soc.* **2012**, *134*, 10725-10728.
19. Chen, X.; Zhou, Y.; Peng, X.; Yoon, J., Fluorescent and colorimetric probes for detection of thiols. *Chem. Soc. Rev.* **2010**, *39*, 2120-2135.
20. Patonay, G.; Antoine, M. D., Near-infrared fluorogenic labels: new approach to an old problem. *Anal. Chem.* **1991**, *63*, 321A-327A.
21. Leevy, W. M.; Gammon, S. T.; Johnson, J. R.; Lampkins, A. J.; Jiang, H.; Marquez, M.; Piwnicka-Worms, D.; Suckow, M. A.; Smith, B. D., Noninvasive optical imaging of staphylococcus aureus bacterial infection in living mice using a bis-dipicolylamine-zinc(II) affinity group conjugated to a near-infrared fluorophore. *Bioconjugate Chem.* **2008**, *19*, 686-692.
22. Maity, D.; Govindaraju, T., Highly selective visible and near-IR sensing of Cu²⁺ based on thiourea-salicylaldehyde coordination in aqueous media. *Chem. Eur. J.* **2011**, *17*, 1410-1414.
23. Maity, D.; Manna, A. K.; Karthigeyan, D.; Kundu, T. K.; Pati, S. K.; Govindaraju, T., Visible-near-infrared and fluorescent copper sensors based on julolidine conjugates: selective detection and Fluorescence Imaging in Living Cells. *Chem. Eur. J.* **2011**, *17*, 11152-11161.
24. Fabian, J.; Nakazumi, H.; Matsuoka, M., Near-infrared absorbing dyes. *Chem. Rev.* **1992**, *92*, 1197-1226.
25. Frangioni, J. V., In vivo near-infrared fluorescence imaging. *Curr. Opin. Chem. Biol.* **2003**, *7*, 626-634.

26. Baumes, J. M.; Gassensmith, J. J.; Giblin, J.; Lee, J.-J.; White, A. G.; Culligan, W. J.; Leevy, W. M.; Kuno, M.; Smith, B. D., Storable, thermally activated, near-infrared chemiluminescent dyes and dye-stained microparticles for optical imaging. *Nat. Chem.* **2010**, *2*, 1025-1030.
27. Sreejith, S.; Divya, K. P.; Ajayaghosh, A., A near-infrared squaraine dye as a latent ratiometric fluorophore for the detection of aminothiols in blood plasma. *Angew. Chem. Int. Ed.* **2008**, *47*, 7883-7887.
28. Hewage, H. S.; Anslyn, E. V., Pattern-based recognition of thiols and metals using a single squaraine indicator. *J. Am. Chem. Soc.* **2009**, *131*, 13099-13106.
29. Guo, Z.; Nam, S.; Park, S.; Yoon, J., A highly selective ratiometric near-infrared fluorescent cyanine sensor for cysteine with remarkable shift and its application in bioimaging. *Chem. Sci.* **2012**, *3*, 2760-2765.
30. Wang, R.; Chen, L.; Liu, P.; Zhang, Q.; Wang, Y., Sensitive near-infrared fluorescent probes for thiols based on Se-N Bond cleavage: imaging in living cells and tissues. *Chem. Eur. J.* **2012**, *18*, 11343-11349.
31. Tang, B.; Xing, Y.; Li, P.; Zhang, N.; Yu, F.; Yang, G., A rhodamine-based fluorescent probe containing a Se-N bond for detecting thiols and Its application in living cells. *J. Am. Chem. Soc.* **2007**, *129*, 11666-11667.
32. Lee, J. H.; Lim, C. S.; Tian, Y. S.; Han, J. H.; Cho, B. R., A two-photon fluorescent probe for thiols in live cells and tissues. *J. Am. Chem. Soc.* **2010**, *132*, 1216-1217.
33. Lim, C. S.; Masanta, G.; Kim, H. J.; Han, J. H.; Kim, H. M.; Cho, B. R., Ratiometric detection of mitochondrial thiols with a two-photon fluorescent probe. *J. Am. Chem. Soc.* **2011**, *133*, 11132-11135.
34. Lin, Q.; Bao, C.; Cheng, S.; Yang, Y.; Ji, W.; Zhu, L., Target-activated coumarin phototriggers specifically switch on fluorescence and photocleavage upon bonding to thiol-bearing protein. *J. Am. Chem. Soc.* **2012**, *134*, 5052-5055.
35. Pires, M. M.; Chmielewski, J., Fluorescence imaging of cellular glutathione using a latent rhodamine. *Org. Lett.* **2008**, *10*, 837-840.
36. Li, X.; Qian, S.; He, Q.; Yang, B.; Li, J.; Hu, Y., Design and synthesis of a highly selective fluorescent turn-on probe for thiol bioimaging in living cells. *Org. Biomol. Chem.* **2010**, *8*, 3627-3630.
37. Zhu, B.; Zhang, X.; Li, Y.; Wang, P.; Zhang, H.; Zhuang, X., A colorimetric and ratiometric fluorescent probe for thiols and its bioimaging applications. *Chem. Commun.* **2010**, *46*, 5710-5712.

38. Maeda, H.; Matsuno, H.; Ushida, M.; Katayama, K.; Saeki, K.; Itoh, N., 2,4-Dinitrobenzenesulfonyl fluoresceins as fluorescent alternatives to ellman's reagent in thiol-quantification enzyme assays. *Angew. Chem. Int. Ed.* **2005**, *44*, 2922-2925.
39. Maeda, H.; Katayama, K.; Matsuno, H.; Uno, T., 3'-(2,4-Dinitrobenzenesulfonyl)-2',7'-dimethylfluorescein as a fluorescent probe for selenols. *Angew. Chem. Int. Ed.* **2006**, *45*, 1810-1813.
40. Jiang, W.; Fu, Q.; Fan, H.; Ho, J.; Wang, W., A highly selective fluorescent probe for thiophenols. *Angew. Chem. Int. Ed.* **2007**, *46*, 8445-8448.
41. Bouffard, J.; Kim, Y.; Swager, T. M.; Weissleder, R.; Hilderbrand, S. A., A highly selective fluorescent probe for thiol bioimaging. *Org. Lett.* **2007**, *10*, 37-40.
42. Shibata, A.; Furukawa, K.; Abe, H.; Tsuneda, S.; Ito, Y., Rhodamine-based fluorogenic probe for imaging biological thiol. *Bioorg. Med. Chem. Lett.* **2008**, *18*, 2246-2249.
43. Shao, J.; Sun, H.; Guo, H.; Ji, S.; Zhao, J.; Wu, W.; Yuan, X.; Zhang, C.; James, T. D., A highly selective red-emitting FRET fluorescent molecular probe derived from BODIPY for the detection of cysteine and homocysteine: an experimental and theoretical study. *Chem. Sci.* **2012**, *3*, 1049-1061.
44. Karton-Lifshin, N.; Segal, E.; Omer, L.; Portnoy, M.; Satchi-Fainaro, R.; Shabat, D., A unique paradigm for a turn-on near-infrared cyanine-based probe: noninvasive intravital optical imaging of hydrogen peroxide. *J. Am. Chem. Soc.* **2011**, *133*, 10960-10965.
45. Lin, W.; Yuan, L.; Cao, Z.; Feng, Y.; Long, L., A sensitive and selective fluorescent thiol probe in water based on the conjugate 1,4-addition of thiols to α,β -unsaturated ketones. *Chem. Eur. J.* **2009**, *15*, 5096-5103.
46. Yi, L.; Li, H.; Sun, L.; Liu, L.; Zhang, C.; Xi, Z., A highly sensitive fluorescence probe for fast thiol-quantification assay of glutathione reductase. *Angew. Chem. Int. Ed.* **2009**, *48*, 4034-4037.
47. Lin, V. S.; Chang, C. J., Fluorescent probes for sensing and imaging biological hydrogen sulfide. *Curr. Opin. Chem. Biol.* **2012**, *16*, 595-601.
48. Papapetropoulos, A.; Pyriochou, A.; Altaany, Z.; Yang, G.; Marazioti, A.; Zhou, Z.; Jeschke, M. G.; Branski, L. K.; Herndon, D. N.; Wang, R.; Szabó, C., Hydrogen sulfide is an endogenous stimulator of angiogenesis. *Proc. Natl. Acad. Sci. USA* **2009**, *106*, 21972-21977.
49. Peng, Y.-J.; Nanduri, J.; Raghuraman, G.; Souvannakitti, D.; Gadalla, M. M.; Kumar, G. K.; Snyder, S. H.; Prabhakar, N. R., H₂S mediates O₂ sensing in the carotid body. *Proc. Natl. Acad. Sci. USA* **2010**, *107*, 10719-10724.
50. Yang, G.; Wu, L.; Wang, R., Pro-apoptotic effect of endogenous H₂S on human aorta smooth muscle cells. *FASEB J.* **2006**, *20*, 553-555.

51. Li, L.; Bhatia, M.; Zhu, Y. Z.; Zhu, Y. C.; Ramnath, R. D.; Wang, Z. J.; Anuar, F. B. M.; Whiteman, M.; Salto-Tellez, M.; Moore, P. K., Hydrogen sulfide is a novel mediator of lipopolysaccharide-induced inflammation in the mouse. *FASEB J.* **2005**, *19*, 1196-1198.
52. Singh, S.; Padovani, D.; Leslie, R. A.; Chiku, T.; Banerjee, R., The relative contributions of cystathionine beta-synthase and gamma-cystathionase to H₂S biogenesis via alternative transsulfuration reactions. *J. Biol. Chem.* **2009**.
53. Kabil, O.; Banerjee, R., Redox Biochemistry of Hydrogen Sulfide. *J. Biol. Chem.* **2010**, *285*, 21903-21907.
54. Eto, K.; Asada, T.; Arima, K.; Makifuchi, T.; Kimura, H., Brain hydrogen sulfide is severely decreased in Alzheimer's disease. *Biochem. Biophys. Res. Commun.* **2002**, *293*, 1485-1488.
55. Yang, G.; Wu, L.; Jiang, B.; Yang, W.; Qi, J.; Cao, K.; Meng, Q.; Mustafa, A. K.; Mu, W.; Zhang, S.; Snyder, S. H.; Wang, R., H₂S as a physiologic vasorelaxant: hypertension in mice with deletion of cystathionine γ -Lyase. *Science* **2008**, *322*, 587-590.
56. Yang, W.; Yang, G.; Jia, X.; Wu, L.; Wang, R., Activation of KATP channels by H₂S in rat insulin-secreting cells and the underlying mechanisms. *J Physiol* **2005**, *569*, 519-531.
57. Fiorucci, S.; Antonelli, E.; Mencarelli, A.; Orlandi, S.; Renga, B.; Rizzo, G.; Distrutti, E.; Shah, V.; Morelli, A., The third gas: H₂S regulates perfusion pressure in both the isolated and perfused normal rat liver and in cirrhosis. *Hepatology* **2005**, *42*, 539-548.
58. Peng, H.; Cheng, Y.; Dai, C.; King, A. L.; Predmore, B. L.; Lefer, D. J.; Wang, B., A fluorescent probe for fast and quantitative detection of hydrogen Sulfide in Blood. *Angew. Chem. Int. Ed.* **2011**, *50*, 9672-9675.
59. Sasakura, K.; Hanaoka, K.; Shibuya, N.; Mikami, Y.; Kimura, Y.; Komatsu, T.; Ueno, T.; Terai, T.; Kimura, H.; Nagano, T., Development of a highly selective fluorescence probe for hydrogen sulfide. *J. Am. Chem. Soc.* **2011**, *133*, 18003-18005.
60. Yuan, L.; Lin, W.; Zheng, K.; He, L.; Huang, W., Far-red to near infrared analyte-responsive fluorescent probes based on organic fluorophore platforms for fluorescence imaging. *Chem. Soc. Rev.* **2013**, *42*, 622-661.
61. Yu, F.; Li, P.; Song, P.; Wang, B.; Zhao, J.; Han, K., An ICT-based strategy to a colorimetric and ratiometric fluorescence probe for hydrogen sulfide in living cells. *Chem. Commun.* **2012**, *48*, 2852-2854.
62. Wu, M.-Y.; Li, K.; Hou, J.-T.; Huang, Z.; Yu, X.-Q., A selective colorimetric and ratiometric fluorescent probe for hydrogen sulfide. *Org. Biomol. Chem.* **2012**, *10*, 8342-8347.

63. Xu, Z.; Xu, L.; Zhou, J.; Xu, Y.; Zhu, W.; Qian, X., A highly selective fluorescent probe for fast detection of hydrogen sulfide in aqueous solution and living cells. *Chem. Commun.* **2012**, *48*, 10871-10873.
64. Wan, Q.; Song, Y.; Li, Z.; Gao, X.; Ma, H., In vivo monitoring of hydrogen sulfide using a cresyl violet-based ratiometric fluorescence probe. *Chem. Commun.* **2013**, *49*, 502-504.
65. Liu, J.; Sun, Y.-Q.; Zhang, J.; Yang, T.; Cao, J.; Zhang, L.; Guo, W., A ratiometric fluorescent probe for biological signaling molecule H₂S: fast response and high selectivity. *Chem. Eur. J.* **2013**, *19*, 4717-4722.
66. Chen, Y.; Zhu, C.; Yang, Z.; Chen, J.; He, Y.; Jiao, Y.; He, W.; Qiu, L.; Cen, J.; Guo, Z., A ratiometric fluorescent probe for rapid detection of hydrogen sulfide in mitochondria. *Angew. Chem. Int. Ed.* **2013**, *52*, 1688-1691.
67. Cao, X.; Lin, W.; Zheng, K.; He, L., A near-infrared fluorescent turn-on probe for fluorescence imaging of hydrogen sulfide in living cells based on thiolysis of dinitrophenyl ether. *Chem. Commun.* **2012**, *48*, 10529-10531.
68. Maity, D.; Govindaraju, T., A turn-on NIR fluorescence and colourimetric cyanine probe for monitoring the thiol content in serum and the glutathione reductase assisted glutathione redox process. *Org. Biomol. Chem.* **2013**, *11*, 2098-2104.
69. Karton-Lifshin, N.; Albertazzi, L.; Bendikov, M.; Baran, P. S.; Shabat, D., "Donor-two-acceptor" dye design: a distinct gateway to NIR fluorescence. *J. Am. Chem. Soc.* **2012**, *134*, 20412-20420.
70. M. J. Frisch; G. W. Trucks; H. B. Schlegel; G. E. Schlegel; G. E. Scuseria; M. A. Robb; J. R. Cheeseman; J. A. Montgomery, Jr., T. V.; K. N. Kudin; J. C. Burant; J. M. Millam; S. S. Iyengar; J. Tomasi; V. Barone; B. Mennucci; M. Cossi; G. Scalmani; N. Rega; G. A. Petersson; H. Nakatsuji; M. Hada; M. Ehara; K. Toyota; R. Fukuda; J. Hasegawa; M. Ishida; T. Nakajima; Y. Honda; O. Kitao; H. Nakai; M. Klene; X. Li; J. E. Knox; H. P. Hratchian; J. B. Cross; C. Adamo; J. Jaramillo; R. Gomperts; R. E. Stratmann; O. Yazyev; A. J. Austin; R. Cammi; C. Pomelli; J. W. Ochterski; P. Y. Ayala; K. Morokuma; G. A. Voth; P. Salvador; J. J. Dannenberg; V. G. Zakrzewski; S. Dapprich; A. D. Daniels; M. C. Strain; O. Farkas; D. K. Malick; A. D. Rabuck; K. Raghavachari; J. B. Foresman; J. V. Ortiz; Q. Cui; A. G. Baboul; S. Clifford; J. Cioslowski; B. B. Stefanov; G. Liu; A. Liashenko; P. Piskorz; I. Komaromi; R. L. Martin; D. J. Fox; T. Keith; M. A. Allaham; C. Y. Peng; A. Nanayakkara; M. Challacombe; P. M. W. Gill; B. Johnson; W. Chen; M. W. Wong; C. Gonzalez; Pople, J. A., *Gaussian Inc.*, Wallingford CT **2004**.
71. Becke, A. D., Density-functional thermochemistry. III. The role of exact exchange. *J. Chem. Phys.* **1993**, *98*, 5648-5652.

72. Lee, C.; Yang, W.; Parr, R. G., Development of the Colle-Salvetti correlation-energy formula into a functional of the electron density. *Phys. Rev. B* **1988**, *37*, 785-789.
73. Miehlich, B.; Savin, A.; Stoll, H.; Preuss, H., Results obtained with the correlation energy density functionals of becke and Lee, Yang and Parr. *Chem. Phys. Lett.* **1989**, *157*, 200-206.

List of Publications

1. A highly selective reaction-based two-photon probe for Cu⁺ in aqueous media
D. Maity, B. Sarkar, S. Maiti and T. Govindaraju, *Chempluschem*, 2013, DOI: 10.1002/cplu.201300089
2. Turn-on NIR fluorescence and colourimetric cyanine probe for monitoring thiol content in serum and glutathione reductase assisted glutathione redox process
D. Maity and T. Govindaraju, *Org. Biomol. Chem.* **2013**, *11*, 2098-2104. ([Inside Cover Page](#))
3. FRET-based rational strategy for ratiometric detection of Cu²⁺ and live cell imaging
D. Maity, D. Karthigeyan, T. K. Kundu and T. Govindaraju, *Sensor Actuat. B-Chem.*, **2013**, *176*, 831-837.
4. Reactive probes for ratiometric detection of Co²⁺ and Cu⁺ based on excited-state intramolecular proton transfer mechanism
D. Maity, V. Kumar and T. Govindaraju, *Org. Lett.*, **2012**, *14*, 6008-6011.
5. A differentially selective sensor with fluorescence turn-on response to Zn²⁺ and dual-mode ratiometric response to Al³⁺ in aqueous media
D. Maity and T. Govindaraju, *Chem. Commun.*, **2012**, *48*, 1039-1041.
6. Naphthaldehyde-urea/thiourea conjugates as turn-on fluorescent probes for Al³⁺ based on restricted C=N isomerization
D. Maity and T. Govindaraju, *Eur. J. Inorg. Chem.*, **2011**, 5479-5489.
7. Highly selective colorimetric chemosensor for Co²⁺
D. Maity and T. Govindaraju, *Inorg. Chem.*, **2011**, *50*, 11282-11284.
8. Visible-near-infrared and fluorescent copper sensors based on julolidine conjugates: selective detection and fluorescence imaging in living cells
D. Maity, A. K. Manna, D. Karthigeyan, T. K. Kundu, S. K. Pati and T. Govindaraju, *Chem. Eur. J.*, **2011**, *17*, 11152-11161. ([Frontispiece](#))
9. Highly selective visible and near-IR sensing of Cu²⁺ based on thiourea-salicylaldehyde coordination in aqueous media
D. Maity and T. Govindaraju, *Chem. Eur. J.*, **2011**, *17*, 1410-1414.

10. Conformationally constrained (coumarin-triazolyl-bipyridyl) click fluoroionophore as a selective Al³⁺ sensor
D. Maity and T. Govindaraju, *Inorg. Chem.*, **2010**, *49*, 7229-7231.
11. Pyrrolidine constrained bipyridyl-dansyl click fluoroionophore as selective Al³⁺ sensor
D. Maity and T. Govindaraju, *Chem. Commun.*, **2010**, *46*, 4499-4501.
12. Reversible fluorescence sensing of Zn²⁺ based on pyridine-constrained bis (triazole-linked hydroxyquinoline) sensor
N. Narayanaswamy, **D. Maity**, T. Govindaraju, *Supramol. Chem.*, **2011**, *23*, 703-709. (Non-thesis publication)

Manuscripts submitted (Thesis):

13. Reaction-based probes for Co²⁺ and Cu⁺ with dual output modes
D. Maity, A. Raj and T. Govindaraju
14. Highly selective cyanine-based colorimetric and ratiometric near-infrared fluorescent reactive probe for rapid detection of hydrogen sulfide with significant shift in living cells
D. Maity and T. Govindaraju
15. Near-infrared switch-on fluorescent cyanine based reactive probes for Cu⁺
D. Maity and T. Govindaraju